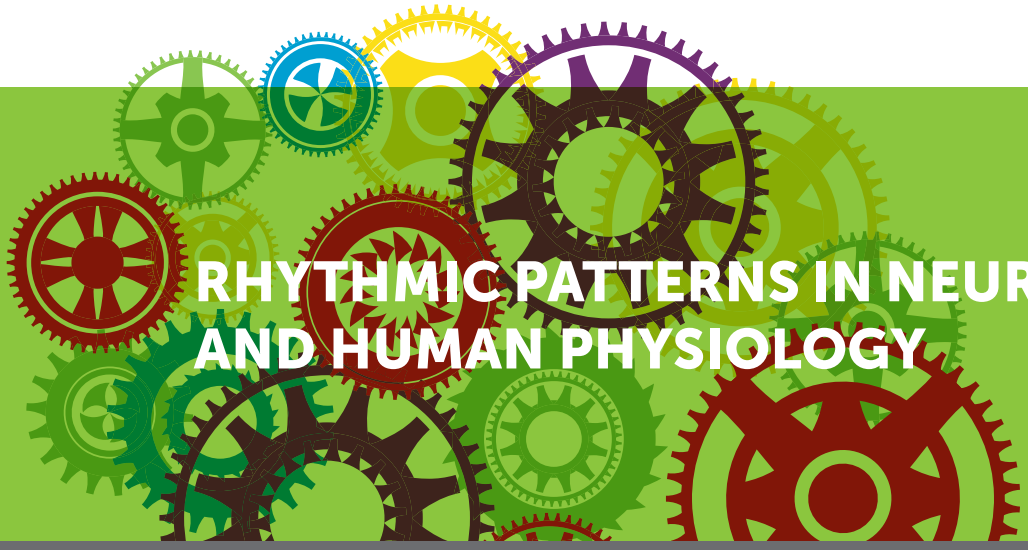

RHYTHMIC PATTERNS IN NEUROSCIENCE AND HUMAN PHYSIOLOGY

EDITED BY: Daniela De Bartolo, Marco Iosa, Giuseppe Vannozzi and Nadia Dominici

PUBLISHED IN: Frontiers in Human Neuroscience

frontiers Research Topics

ISSN 1664-8714
ISBN 978-2-88976-577-5
DOI 10.3389/978-2-88976-577-5

About Frontiers

Frontiers is more than just an open-access publisher of scholarly articles: it is a pioneering approach to the world of academia, radically improving the way scholarly research is managed. The grand vision of Frontiers is a world where all people have an equal opportunity to seek, share and generate knowledge. Frontiers provides immediate and permanent online open access to all its publications, but this alone is not enough to realize our grand goals.

Frontiers Journal Series

The Frontiers Journal Series is a multi-tier and interdisciplinary set of open-access, online journals, promising a paradigm shift from the current review, selection and dissemination processes in academic publishing. All Frontiers journals are driven by researchers for researchers; therefore, they constitute a service to the scholarly community. At the same time, the Frontiers Journal Series operates on a revolutionary invention, the tiered publishing system, initially addressing specific communities of scholars, and gradually climbing up to broader public understanding, thus serving the interests of the lay society, too.

Dedication to Quality

Each Frontiers article is a landmark of the highest quality, thanks to genuinely collaborative interactions between authors and review editors, who include some of the world's best academicians. Research must be certified by peers before entering a stream of knowledge that may eventually reach the public - and shape society; therefore, Frontiers only applies the most rigorous and unbiased reviews.
Frontiers revolutionizes research publishing by freely delivering the most outstanding research, evaluated with no bias from both the academic and social point of view. By applying the most advanced information technologies, Frontiers is catapulting scholarly publishing into a new generation.

What are Frontiers Research Topics?

Frontiers Research Topics are very popular trademarks of the Frontiers Journals Series: they are collections of at least ten articles, all centered on a particular subject. With their unique mix of varied contributions from Original Research to Review Articles, Frontiers Research Topics unify the most influential researchers, the latest key findings and historical advances in a hot research area! Find out more on how to host your own Frontiers Research Topic or contribute to one as an author by contacting the Frontiers Editorial Office: frontiersin.org/about/contact

RHYTHMIC PATTERNS IN NEUROSCIENCE AND HUMAN PHYSIOLOGY

Topic Editors:
Daniela De Bartolo, Santa Lucia Foundation (IRCCS), Italy
Marco Iosa, Sapienza University of Rome, Italy
Giuseppe Vannozzi, Foro Italico University of Rome, Italy
Nadia Dominici, Department of Human Movement Sciences, Faculty of Behavioural and Movement Sciences, VU Amsterdam, Netherlands

Citation: De Bartolo, D., Iosa, M., Vannozzi, G., Dominici, N., eds. (2022). Rhythmic Patterns in Neuroscience and Human Physiology. Lausanne: Frontiers Media SA. doi: 10.3389/978-2-88976-577-5

Table of Contents

frontiers | Frontiers in Human Neuroscience

EDITORIAL
published: 25 May 2022
doi: 10.3389/fnhum.2022.936090

Editorial: Rhythmic Patterns in Neuroscience and Human Physiology

Nadia Dominici[1], *Marco Iosa*[2,3], *Giuseppe Vannozzi*[3,4] *and Daniela De Bartolo*[2,3]*

[1] Department of Human Movement Sciences, Amsterdam Movement Sciences, Institute Brain and Behavior Amsterdam, Vrije Universiteit Amsterdam, Amsterdam, Netherlands, [2] Department of Psychology, Sapienza University of Rome, Rome, Italy, [3] IRCCS Santa Lucia Foundation, Rome, Italy, [4] Interuniversity Centre of Bioengineering of the Human Neuromusculoskeletal System, Department of Movement, Human and Health Sciences, University of Rome "Foro Italico", Rome, Italy

Keywords: motor neuroscience, rhythm, coordination dynamics, periodic movements, spatio temporal analysis, harmony

Editorial on the Research Topic

Rhythmic Patterns in Neuroscience and Human Physiology

Human movement, as it happens for some other natural phenomena, is characterized by periodicity, with patterns and harmonic structures repeated over time and space. Several mental processes and behaviors have already been described in these terms, that is, through the activation of interconnected neural populations that gives rise to global dynamic states, at the basis of human perception and cognition. Although much research has been directed in this regard, it is still unclear how anatomical connectivity interacts with the neuronal dynamics, from which complex human behavior emerges as rhythmic motor activity.

Accordingly, this Research Topic aimed to collect scientific contributions concerning advances in complex models of brain cells (Rodríguez-Collado and Cristina Rueda) up to motor-behavior control models (Verrelli et al.; Hiraoka; Lindén and Berg; Ulloa), the investigation of coordinated-rhythmic (Benedetto and Baud-Bovy; Bekius et al.; Leach et al.; Pakniyat and Namazi; Dewolf et al.; Den Hartigh et al.; Janzen et al.) and synchronized behaviors (Rosso et al.; Zamm et al.), also including studies conducted on targeted clinical populations of scientific interest (Salesse et al.; Zhao et al.; Rosso et al.).

A total of 16 papers have been accepted including 11 Original Research papers, 2 Mini-Reviews, 1 Review, 1 Case Report, and 1 Hypothesis and Theory.

We have collected scientific contributions that focused on the dynamic systems underlying complex human movements having the property of harmonic spatial and/or temporal structures, such as coordinated and/or synchronized movements.

The ability to produce stable but, at the same time, adaptive behavior raises two constitutive questions. On one hand, it implies the investigation of the mechanisms that are responsible for coordinated actions of the neuromusculoskeletal components of the body that organize themselves temporally and spatially in an ordered and coherent movement pattern. On the other hand, it involves the analysis of cognitive factors such as perceptual processes that guarantee constant feedback on a body in motion and interacting with an environment, in order to select appropriate actions suited to environmental conditions.

In this regard, the paper by Den Hartigh et al. analyzed the concept of resilient motor action providing empirical support between complexity and resilience, and that differential learning supports complexity. Following in the footsteps of Gibson (1979), an alternative approach was that of Leach et al. who investigated what happens to the perception-action dynamics responsible for bimanual coordinated rhythmic movement after differential learning conditions. In this study, although the results differ from predictions, the ecological aspect of the task would seem to guide

OPEN ACCESS

Edited and reviewed by:
Julie Duque,
Catholic University of Louvain, Belgium

***Correspondence:**
Daniela De Bartolo
d.debartolo@hsantalucia.it

Specialty section:
This article was submitted to Motor Neuroscience, a section of the journal Frontiers in Human Neuroscience

Received: *04 May 2022*
Accepted: *13 May 2022*
Published: *25 May 2022*

Citation:
Dominici N, Iosa M, Vannozzi G and De Bartolo D (2022) Editorial: Rhythmic Patterns in Neuroscience and Human Physiology. Front. Hum. Neurosci. 16:936090. doi: 10.3389/fnhum.2022.936090

the transfer. In this regard, in Benedetto and Baud-Bovy a rhythmic tapping task was used to assess the role of perception in the organization of motor representation of the rhythm. These authors found a general effect of rhythm complexity on sensorimotor precision and accuracy speculating that simple rhythms facilitate prediction, requiring less attentional and mnemonical resources.

COMPLEX BEHAVIORS AND NEURONAL DYNAMICS

The review of Ulloa outlined that perception and action are intertwined, at a lower level of organization of the motor system, with feedforward and feedback circuits essential for motor control. This reciprocal interaction is replicated at the highest levels of the organization of the motor system. This entails an assumption of complexity following the hypothesis that the organization observed in human behavior could *ipso facto* imply the existence of a controller, a Central Pattern Generator (CPG), action plan, or internal model that is responsible for its organization and regulation. Usually, the CPG is assumed to be located in the spinal cord and the medulla. Lindén and Berg propose a reinterpretation of this model, focusing on the distribution of firing rates across the spinal neurons population, also suggesting the idea that recurrent inhibition should be considered as embedded in each CPG module (Haghpanah et al., 2017). In the Mini-Review, Hiraoka discussed crossed inhibition during bilateral movement and the anti-phase coordination in rhythmic movements like gait.

Generally speaking, when studying the interlimb coordination dynamics one cannot ignore the investigation of the physiological attractors of movement (Zanone and Kelso, 1997) defined as "attraction of stable movements to maintain robust performance against variability" (Yamamoto et al., 2020). This characteristic is typical of complex dynamic systems such as rhythmic coordinated movements like gait.

In Dewolf et al., neuromuscular control and underlying age-related adjustments were investigated during a level, uphill, and downhill walking as well as stair ascending and descending. Their findings showed subtle age-related differences in all conditions that may potentially reflect systematic age-related adjustments of the neuromuscular control of locomotion across various support surfaces.

In different walking conditions, the foot-off timing undergoes a low variability (Riener et al., 2002), suggesting the possibility that the proportion between stance and swing (60–62% vs. 40–38%) is largely unaffected by external conditions (Lythgo et al., 2011; Iosa et al., 2019). It is interesting that the proportion between the phases of the gait cycle (stride/stance, stance/swing, swing/double support) is stable and coincides with the value of the golden section (Iosa et al., 2013) which has recently been also found in toddlers learning to walk (De Bartolo et al., 2022). In the framework of this temporal point of view, Verrelli et al. proposed a new model of human locomotion, that is based on recursivity, self-similarity, and symmetry of gait assessed through the introduction of a new gait index the *Φ-bonacci gait number*. As hypothesized in Serrao et al. (2017), the golden ratio could allow not only to investigate the harmony of walking but could also represent a physiological attractor of movement.

This concept is not new in the field of neuroscience. (Luria, 1976) wrote about kinetic melodies referring to coordinated and fluid movements, which today are often investigated through the analysis of the coupling of physiological signals to deepen motor control starting from sensorimotor integration (De Bartolo et al., 2020, 2021) (Pakniyat and Namazi; Rosso et al.; Zamm et al.).

Pakniyat and Namazi investigated the variations of the brain and muscle activations while subjects are exposed to different perturbations to walking and standing balance. They found an inverse correlation between changes in brain reactions and muscle activations in standing and walking tasks showing that coordinated behavior such as walking requires greater cerebral but not muscular complexity (Pakniyat and Namazi). These results are in line with the literature on muscle synergies, suggesting that muscle activity may be tailored to task-specific biomechanical needs (Zandvoort et al., 2019).

Recently the literature on the coupling of physiological signals during motor tasks has focused on the phenomenon of auditory-motor (Rosso et al.) and interpersonal synchronization tasks (Zamm et al., 2022). Both of these rely on the physical phenomenon of entrainment firstly reported by Thaut et al. (2015) concerning the frequency locking of two oscillating bodies that can move independently in stable, periodic, or rhythmic cycles (Thaut et al., 2015), but when interacting each other they may assume a common period.

In the study by Zamm et al. (2022) the ability of motor synchronization entrained by music inexperienced musicians performing at spontaneous (uncued) rates was investigated. The authors provided evidence that the dynamics of oscillator coupling are reflected in both behavioral and neural measures of temporal coordination during musical joint action.

Today, this phenomenon of entrainment is the basis of many rehabilitation protocols that use music for motor facilitation, as outlined in the review by Janzen et al. They reported studies using different rehabilitation techniques like rhythmic auditory stimulation, music-supported therapy, therapeutic instrumental music performance, and patterned sensory enhancement and the effectiveness of rhythm and music in restoring motor function in patients with movement-related disorders. In this regard, Rosso et al. proposed a neural outcome measure of auditory-motor coupling that may be useful for rehabilitation purposes.

INTEGRATED APPROACHES TO UNDERSTAND HARMONIC MOVEMENT PATTERNS

Finally, in this Research Topic, we also selected three papers providing interesting clinical implications.

In a case report, Bekius et al. investigated the development of locomotor patterns and neuromotor control during walking in three very young children with early brain lesions, at risk for developing cerebral palsy (CP). The exploratory longitudinal study reported novel observations by following

the children within a period of 1–2 years, presenting different developmental trajectories. The findings revealed differences in maturation of locomotor patterns between children with divergent developmental trajectories.

Zhao et al. reported a study on how restrictedness is manifested in motor behavior. The authors presented an interesting new method by means of entropy analysis to obtain objective behavioral markers of autism spectrum disorder (ASD). This method revealed a lower level of variance in the velocity distribution of participants with ASD, suggesting that children with ASD displayed a more restricted movement compared to typically developing children.

Salesse et al. focused on socio-motor improvisation in individuals with schizophrenia. Using the mirror game paradigm, they recorded hand motions of two people mirroring each other. Results showed that patients exhibited significantly higher difficulties to be synchronized with someone they have to follow, but not when they were leaders of the joint improvisation game.

In light of all these findings, cyclic human movements seem to emerge as a compromise between reliability and adaptable, non-stereotyped patterns. In these terms, human movements should be considered as an orchestrated unique phenomenon, impossible to observe or replicate twice in the same identical way (Stergiou et al., 2006). For this reason, it is essential that the investigation methods are innovative as those proposed in this Research Topic, integrating different techniques in order to characterize the movement in all its complexity.

AUTHOR CONTRIBUTIONS

DD: conceptualization. DD and ND: wrote the first draft. GV and MI: revision of the manuscript draft. All authors contributed to manuscript revision, read, and approved the final version.

REFERENCES

De Bartolo, D., Belluscio, V., Vannozzi, G., Morone, G., Antonucci, G., Giordani, G., et al. (2020). Sensorized assessment of dynamic locomotor imagery in people with stroke and healthy subjects. *Sensors* 20, 4545. doi: 10.3390/s20164545

De Bartolo, D., De Giorgi, C., Compagnucci, L., Betti, V., Antonucci, G., Morone, G., et al. (2021). Effects of cognitive workload on heart and locomotor rhythms coupling. *Neurosci. Lett.* 762, 136140. doi: 10.1016/j.neulet.2021.136140

De Bartolo, D., Zandvoort, C. S., Goudriaan, M., Kerkman, J. N., Iosa, M., and Dominici, N. (2022). The role of walking experience in the emergence of gait harmony in typically developing toddlers. *Brain Sci.* 12, 155. doi: 10.3390/brainsci12020155

Gibson, J. J. (1979). *The Ecological Approach to Visual Perception*. Boston, MA: Houghton Mifflin.

Haghpanah, S. A., Farahmand, F., and Zohoor, H. (2017). Modular neuromuscular control of human locomotion by central pattern generator. *J. Biomech.* 53, 154–162. doi: 10.1016/j.jbiomech.2017.01.020

Iosa, M., De Bartolo, D., Morone, G., Boffi, T., Mammucari, E., Vannozzi, G., et al. (2019). Gait phase proportions in different locomotion tasks: the pivot role of golden ratio. *Neurosci. Lett.* 699, 127–133. doi: 10.1016/j.neulet.2019.01.052

Iosa, M., Fusco, A., Marchetti, F., Morone, G., Caltagirone, C., Paolucci, S., et al. (2013). The golden ratio of gait harmony: repetitive proportions of repetitive gait phases. *Biomed. Res. Int.* 2013, 918642. doi: 10.1155/2013/918642

Luria, A. R. (1976). *The Working Brain: An Introduction to Neuropsychology, 1st Edn*. Middle Sex: Penguin. p. 198.

Lythgo, N., Wilson, C., and Galea, M. (2011). Basic gait and symmetry measures for primary school-aged children and young adults. II. Walking at slow, free and fast speed. *Gait Posture* 33, 29–35. doi: 10.1016/j.gaitpost.2010.09.017

Riener, R., Rabuffetti, M., and Frigo, C. (2002). Stair ascent and descent at different inclinations. *Gait Posture* 15, 32–44. doi: 10.1016/S0966-6362(01)00162-X

Serrao, M., Chini, G., Iosa, M., Casali, C., Morone, G., Conte, C., et al. (2017). Harmony as a convergence attractor that minimizes the energy expenditure and variability in physiological gait and the loss of harmony in cerebellar ataxia. *Clin. Biomech.* 48, 15–23. doi: 10.1016/j.clinbiomech.2017.07.001

Stergiou, N., Harbourne, R. T., and Cavanaugh, J. T. (2006). Optimal movement variability: a new theoretical perspective for neurologic physical therapy. *J. Neurol. Phys. Ther.* 30, 120–129. doi: 10.1097/01.NPT.0000281949.48193.d9

Thaut, M. H., McIntosh, G. C., and Hoemberg, V. (2015). Neurobiological foundations of neurologic music therapy: rhythmic entrainment and the motor system. *Front. Psychol.* 5, 1185. doi: 10.3389/fpsyg.2014.01185

Yamamoto, K., Shinya, M., and Kudo, K. (2020). The influence of attractor stability of intrinsic coordination patterns on the adaptation to new constraints. *Sci. Rep.* 10, 1–12. doi: 10.1038/s41598-020-60066-7

Zandvoort, C. S., van Dieën, J. H., Dominici, N., and Daffertshofer, A. (2019). The human sensorimotor cortex fosters muscle synergies through cortico-synergy coherence. *Neuroimage* 199, 30–37. doi: 10.1016/j.neuroimage.2019.05.041

Zanone, P. G., and Kelso, J. S. (1997). Coordination dynamics of learning and transfer: collective and component levels. *J. Exp. Psychol. Hum. Percept. Perform.* 23, 1454. doi: 10.1037/0096-1523.23.5.1454

Conflict of Interest: The authors declare that the research was conducted in the absence of any commercial or financial relationships that could be construed as a potential conflict of interest.

frontiers in Human Neuroscience

ORIGINAL RESEARCH
published: 22 April 2021
doi: 10.3389/fnhum.2021.633956

Tapping Force Encodes Metrical Aspects of Rhythm

Alessandro Benedetto[1]* *and Gabriel Baud-Bovy*[2,3]

[1] Department of Translational Research, University of Pisa, Pisa, Italy, [2] Robotics, Brain and Cognitive Science Unit, Italian Institute of Technology, Genoa, Italy, [3] Faculty of Psychology, Vita-Salute San Raffaele University, Milan, Italy

Humans possess the ability to extract highly organized perceptual structures from sequences of temporal stimuli. For instance, we can organize specific rhythmical patterns into hierarchical, or metrical, systems. Despite the evidence of a fundamental influence of the motor system in achieving this skill, few studies have attempted to investigate the organization of our motor representation of rhythm. To this aim, we studied—in musicians and non-musicians—the ability to perceive and reproduce different rhythms. In a first experiment participants performed a temporal order-judgment task, for rhythmical sequences presented via auditory or tactile modality. In a second experiment, they were asked to reproduce the same rhythmic sequences, while their tapping force and timing were recorded. We demonstrate that tapping force encodes the metrical aspect of the rhythm, and the strength of the coding correlates with the individual's perceptual accuracy. We suggest that the similarity between perception and tapping-force organization indicates a common representation of rhythm, shared between the perceptual and motor systems.

Keywords: beat perception, metrical coding, rhythm perception and production, music perception, action and perception, force

OPEN ACCESS

Edited by:
Daniela De Bartolo,
Sapienza University of Rome, Italy

Reviewed by:
Manuel Varlet,
Western Sydney University, Australia
Daniel J. Cameron,
McMaster University, Canada

***Correspondence:**
Alessandro Benedetto
alessandro.benedetto@med.unipi.it

Specialty section:
This article was submitted to Motor Neuroscience, a section of the journal Frontiers in Human Neuroscience

Received: *26 November 2020*
Accepted: *26 March 2021*
Published: *22 April 2021*

Citation:
Benedetto A and Baud-Bovy G (2021) Tapping Force Encodes Metrical Aspects of Rhythm. Front. Hum. Neurosci. 15:633956. doi: 10.3389/fnhum.2021.633956

INTRODUCTION

When listening to music, people often perceive a certain regularity in the auditory temporal pattern, emerging from the presence of perceptual accents at specific intervals known as "beats." Our ability to extract rhythmic patterns from temporal events crucially depends on several factors, including the temporal context (Lenc et al., 2020) and cultural environment (Jacoby and McDermott, 2017; London et al., 2017; van der Weij et al., 2017), and this has been widely explored over the years (Grondin, 2010; McAuley, 2010). One of the most influential ideas in time perception research is that humans possess an internal clock mechanism by which we measure and represent time (Treisman, 1963; Treisman et al., 1990). It has been proposed that this clock can synchronize with external events (e.g., sounds) and generates perceptual accents according to a specific set of rules (Povel and Okkerman, 1981; Essens and Povel, 1985). Based on these perceptual rules we can generate *simple rhythms* (i.e., sequences with equally spaced perceptual accents); alternatively, we can generate *complex rhythms* (i.e., sequences with unequally spaced perceptual accents (London, 1995)). The ability to extract a temporal meter from rhythms relies on musical training and on musical exposure to those rhythms (Cameron et al., 2015; London et al., 2017; van der Weij et al., 2017; Bouwer et al., 2018; Nave-Blodgett et al., 2021). This means that certain rhythms may induce, or favor (particularly in participants not previously exposed to those rhythms), perceptual strategies

based on non-metrical rules, such as chunking and serial grouping rules (non-metrical coding) (Grahn and Brett, 2007; Grube and Griffiths, 2009; Bouwer et al., 2018).

Hierarchical (metrical) percepts show a vertical organization, with inequalities between the elements of the structure; conversely, non-hierarchical (non-metrical) percepts possess a horizontal organization, with perceptual equalities between the members of the structure. Interestingly, metrical encoding of rhythm is generally accompanied by better performance in both discrimination/perceptual and reproduction/motor tasks than non-metrical encoding (Semjen and Vos, 2002; Patel et al., 2005; Phillips-Silver and Trainor, 2005; Grube and Griffiths, 2009), suggesting that meter perception is a sensorimotor phenomenon (Todd and Lee, 2015). Indeed, moving with the beat improves time perception (Manning and Schutz, 2013), metrical encoding of rhythm can be biased by movements (Phillips-Silver and Trainor, 2005, 2008), and specific activations from the motor system (including basal ganglia, premotor cortex, and supplementary motor area) have been reported during perception of metrical rhythms (Zatorre et al., 2007; Chen et al., 2008a,b; Bengtsson et al., 2009; Grahn and Rowe, 2009; Patel and Iversen, 2014). Furthermore, several studies involving transcranial magnetic stimulation (TMS) demonstrated that motor cortex excitability is directly influenced by the groove of the music. For instance, high-groove music (i.e., music easily inducing a metric encoding) modules corticospinal excitability (Stupacher et al., 2013), and TMS pulses delivered synchronously with the beat for metrically strong sequences generates greater motor-evoked potential responses than for metrically weak sequences (Cameron et al., 2012). In addition, it has been suggested that musicians might possess an effective and automatic internal motor simulation related to beat perception (Su and Poppel, 2012), directly modulating primary motor cortex excitability (Stupacher et al., 2013).

Crucially, beat perception is known to generate a spontaneous synchronization between the perceptual pulses and our movements (Drake et al., 2000; Grahn and Brett, 2007; Repp and Su, 2013; Burger et al., 2014), and different metrical levels are embodied within the whole body (Burger et al., 2014, 2018), suggesting the presence of a common hierarchical organization of the sensory and the motor system during metrical encoding of rhythmic sequences. This sensorimotor link is consistent with the hypothesis of a common encoding strategy shared between the motor and the perceptual systems, or a shared sensorimotor representation of time (Morillon et al., 2014; Morillon and Baillet, 2017; Benedetto et al., 2020). However, this view is challenged by the evidence of a strong auditory vs. visual advantage in sensorimotor synchronization and beat perception (Bartlett and Bartlett, 1959; Patel et al., 2005; Grahn, 2012b), leading to the hypothesis of a special auditory-motor specialization. Tactile modality is certainly the best candidate to compare with auditory: not only do both auditory and tactile information consist of vibrations, but there are profound and early interferences between the two systems (Von Bekesy, 1959; Caetano and Jousmaki, 2006). Nevertheless, only a few studies have investigated rhythm perception and sensorimotor synchronization in the tactile modality, reporting the emergence of beat perception also for this modality (Brochard et al., 2008; Ammirante et al., 2016; Gilmore et al., 2018). However, the hypothesis of an enhanced auditory-motor coupling for rhythmic processing cannot be dismissed (Ammirante et al., 2016).

Grahn (2009) previously investigated finger-tap velocity (an indirect measure of tapping force) during the reproduction of simple rhythms, auditorily presented. The author found that mean velocity was higher on taps presented on the beat than on other taps (Grahn, 2009), suggesting that participants spontaneously organize their motor output according to the metric structure of the percept. However, the internal hierarchy of a metrical sequence might reveal additional levels, and the extent to which force organization mimics this highly structured perceptual hierarchy is currently unknown.

We aimed, here, to provide a clearer picture of the tapping-force organization during rhythm reproduction. First, we assessed the individual perceptual abilities in estimating the temporal order judgments of rhythms varying in complexity in a group of musicians and non-musicians. Secondly, we investigated the fine internal motor representation of the rhythmic sequences (tapping force) during the reproduction of these sequences. To test for the generalizability of the results, rhythms were presented through auditory or tactile modality. The rationale was to investigate if metrical organization of forces (if any) could be driven only by auditory stimulation (as hypothesized by the auditory-motor enhancement hypothesis), or if it generalizes for a different modality.

To summarize the results, we found that the perceptual organization of the rhythm fits the force profile of the finger-taps during its reproduction, irrespective of the modality of stimulation: (*i*) we confirmed the presence of a generalized difference in force for taps presented on the beat vs. other taps; (*ii*) we found that this difference was not modality specific, being present also following a tactile stimulation; (*iii*) we found that the tapping force profile showed a difference between the metrical elements falling on the strong vs. medium elements of the sequence, indicating the presence of a fine-graded and hierarchical motor representation of the rhythm; (*iv*) finally, we show that the amount of *metricality* in the tapping-force, correlates with the perceptual precision, corroborating the idea of a shared and a-modal sensorimotor representation of rhythm.

MATERIALS AND METHODS

Participants

17 volunteers (including one author; age mean ± standard deviation: 23.3 ± 1.6, three women) participated in the study (15 right-handed). We selected participants on the basis of their years of institutional western musical training (music high school and/or conservatory of music in Italy), resulting in eight musicians (age: 22.5 ± 2.2; with at least 5 years of musical training: 7 ± 2; one woman) and nine non-musicians (age 23.9 ± 0.8; no institutional musical training; two women). Musicians played piano (1), bass (1), percussion (2), clarinet (2), trumpet (1), bassoon (1). All the participants performed the temporal-order task (experiment 1), 15 of those were additionally

tested for the reproduction task (including one author; eight musicians, seven non-musicians; experiment 2). The studies were reviewed and approved by the local ethics committee (Comitato Etico per la Sperimentazione con l'Essere Umano della ASL 3 di Genova).

Experimental Setup

The experimental setup was composed of headphones, a tactile stimulator, and a flat piezo-transducer to record finger taps. All devices were connected to a DAQ card (NI DAQ USB-6211) which was controlled through custom C# software run on a PC. The tension of the DAQ analogical output ports controlling the audio or tactile stimuli was updated at a high sampling rate (20 kHz). Note that the output vector that defined the stimulus was computed and loaded in memory using the DAQ dedicated driver and API beforehand so that the timing would be exact. In the reproduction task, one analog input port of the DAQ was used to record the tension produced by the flat piezo-transducer that was fixed on the top of a box. Piezoelectric sensors have the characteristic of transforming mechanical energy into electrical energy and are sensitive to the mechanical force applied. For this reason, the piezo-sensor recorded both the timing of the tap and the force applied by the participants for their finger-tapping. The output tension of the piezo was adjusted by mounting a resistor (22 kΩ) in parallel and sampled at 1000 Hz. The synchronization between output and input signals was ensured by using DAQ hardware synchronization mechanisms. The tactile stimulator was based on a speaker from which the cone had been removed. A light custom-designed 3D printed plastic pin was fixed on the voice coil. To deliver the tactile stimulation, the pin moved vertically through a small hole on the top of the box containing the speaker, where the participants rested their finger. The position of the pin was controlled by setting the tension of the DAQ analogical output port ($\pm$10 V), which was amplified through a custom-designed current amplifier. The ability of the device to change position quickly and to apply a constant force on the fingertip was checked with a 6 DOF force sensor (Nano 17, ATI) placed just above the tip of the pin.

Stimuli and Procedures

The present study comprised two experiments. In experiment 1, participants performed a temporal-order judgment task; in experiment 2 they completed a non-isochronous continuous finger-tapping (reproduction task). The stimuli consisted of six sequences; half of the stimuli were simple sequences and the other half complex sequences. Simple rhythms were defined as sequences with equally spaced perceptual accents in time (e.g., a perceptual accent every 400 ms), and complex rhythms as sequences with unequally spaced perceptual accents in time (e.g., the delay between accents varied between 400 and 600 ms) (Povel and Okkerman, 1981; Essens and Povel, 1985). Each stimulus was composed of five elements, that could have either a single (1) or double (2) unit duration (determining the *speed* of the sequence), and the same intensity. The unit duration varied between 200, 223, 246, and 269 ms. The three simple sequences were: 21122, 22112, 22211 (*simple rhythm*). The three complex sequences were: 11122, 21112, 22111 (*complex rhythm*). The intervals between each element of the sequence were obtained by shortening each element by 50 ms. Within each session, the duration of the unit varied randomly across trials to avoid learning effects and keep participants attentive to each rhythm. The auditory and tactile rhythmic sequences were presented block-wise. The auditory rhythmic elements were pure tone of 440 Hz (output tension amplitude: $\pm$ 0.05 V). The tactile sequences consisted of stimulation of the index fingertip of the non-dominant hand by a custom tactile stimulator. For both conditions, an auditory white noise (0.03 V) was superimposed onto the signal during the whole trial duration to assure acoustic isolation from the tactile stimulator and from the finger tapping.

Experiment 1: Temporal-Order Task

Each trial started with a rhythmic sequence (auditory or tactile) presented in a continuous loop for a total of three times. Participants were asked to imagine two following repetitions and to decide whether the beginning of the last repetition preceded or followed a probe (200 ms of duration) that occurred around the time of its ideal onset (**Figure 1B**). The probe preceded or followed the ideal onset of the last repetition by a 5, 10, 20, or 40% of the global duration of the sequence. After each trial, participants verbally reported whether the probe preceded or followed the ideal onset of the sequence. The probe consisted of an 800 Hz pure tone for the auditory condition and a tactile stimulation for the tactile condition. Each modality (auditory or tactile) and rhythm complexity (simple or complex) was tested in separate blocks. Each sequence was combined with the four possible speeds (determined by the unit duration), and all the possible time lags, which yielded 96 trials per condition. The order of presentation of the rhythmic sequences and tempi within each condition was randomized. The experiment lasted approximately 80 min and was divided in two separate sessions.

Experiment 2: Reproduction Task

Experiment 2 used the same stimuli as in experiment 1. A sequence was presented in a continuous loop for a total of three times. Participants were instructed to start the reproduction of the perceived rhythm after the end of the last repetition, and to reproduce the sequence until the end of the trial, which lasted 25 s (**Figure 1C**). The end of the trial was signaled by the stop of the white noise delivered via headphones. Participants were asked to tap with the index fingertip of their dominant hand on a piezoelectric transducer. Each modality (auditory or tactile) and rhythm complexity (simple or complex) was tested in separate blocks. Each stimulus was presented once for each speed (unit duration), which yielded 12 trials per condition. All four conditions were acquired during a unique recording session.

Data Analysis

Experiment 1: Temporal-Order Task

A cumulative gaussian function was fitted to the participants' responses as a function of the probe delay expressed as a percentage of the rhythm duration. For each participant, sensory modality (auditory or tactile) and rhythm complexity (simple or complex), we estimated the point-of-subjective-simultaneity (PSS) and the just-notable-difference (JND). PSS

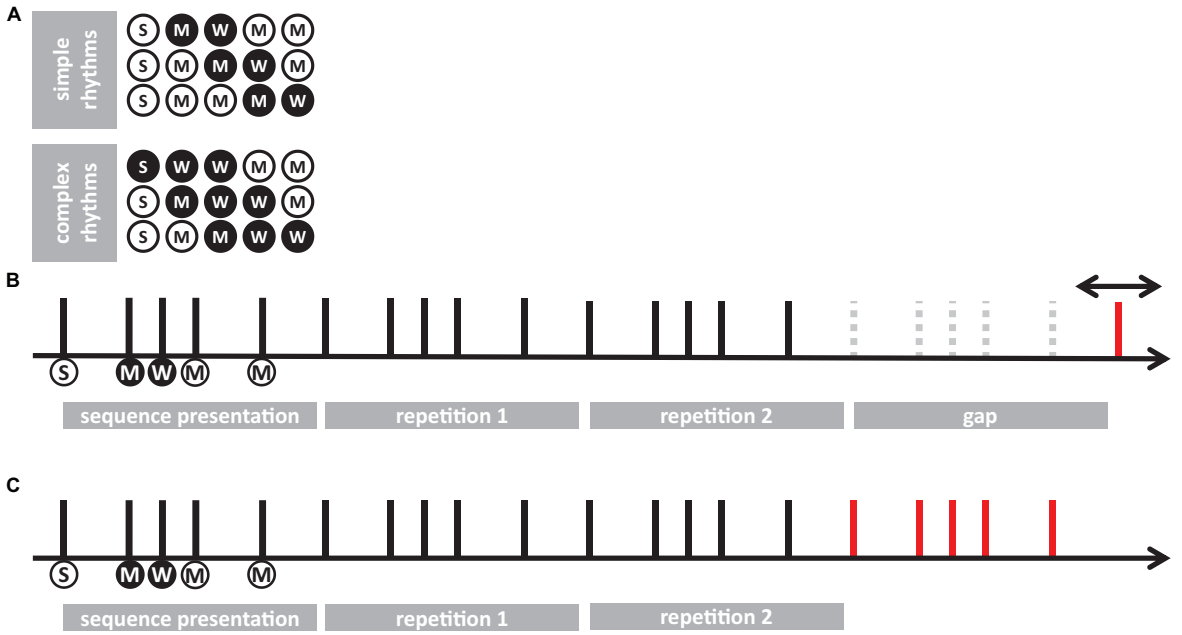

FIGURE 1 | A schematic of the experimental procedures. **(A)** representation of simple and complex rhythms adopted in the present study. Each circle represents a unit of the sequence. White and black circles denote long and short elements, respectively. Letters in the circles indicate the predicted level of perceptual accent for each element: "S" for strong, "M" for medium; "W" for weak. **(B)** trial example from temporal-order task (experiment 1). Each vertical line represents the onset of the element for a given sequence (e.g., 21122). Circles below the lines report the length and the perceptual accent for each element (following the symbol conventions from **A**). The sequence was presented 3 times in succession, then—after an interval gap of the duration of the sequence plus a random jitter—a probe was presented (red line). Participants had to report whether the probe was presented before or after the predicted onset of the imagined 5th sequence. **(C)** Example of reproduction task (experiment 2). After presenting the sequence three times, participants were asked to continue the reproduction (red line) for about 20 s, by tapping with their finger on a piezo-electric sensor.

measures a possible temporal shift of the perceived rhythm onset while JND measures the temporal variability of the perceived onset. Mixed-design repeated measure ANOVA on PSS and JND was run to estimate the main effects and the interaction of a full model (2 rhythm complexities × 2 modalities × 2 expertise, with rhythm complexity and modality as within factors, and expertise as between-subject effect). To satisfy the conditions of the ANOVA and power analysis (homoscedasticity and homogeneity of variance between groups), PSS and JND were transformed with a cubic-root transformation. For all statistically significant effects, we reported the generalized eta-squared η^2_G with expertise as a measured variable (Olejnik and Algina, 2003).

For all analyses, we conducted a power analysis that combined elements of *a priori* and *post hoc* analysis. For all tests, the unstandardized effect size was determined on *a priori* ground, as the smallest effect that we considered to be meaningful or interesting. The variance-covariance structure was determined from the results of the experiments. In particular, we retained that a difference of 5% for the PSS and the JND was a meaningful difference for all effects and used the results of the experiments to estimate all relevant sources of variance. Given the sample sizes of this study, the probability of detecting a 5% temporal shift difference between the two groups was 51% for the PSS and 44% for the JND analysis. However, the power of detecting such a 5% difference was above 86% for all other effects in the PSS analysis, including interactions with the between-subject group factor, and above 99% for all effects in the JND analysis.

To deal with the unbalance between the two groups, all power analyses were conducted in R with simulations (Arnold et al., 2011). First, we used linear mixed-effect models to identify the variance-covariance structure for each variable (Bates et al., 2015; Matuschek et al., 2017). In general, the identified variance-covariance structure included a random intercept for the subject and, in several cases, an uncorrelated random slope for one within-subject factor. More complex variance-covariance structures were not supported by the data. Note that the linear mixed-effect model (LME) included the same fixed effects as the corresponding mixed-effect repeated-measure ANOVA and that the *p*-values of both analyses were very similar in all cases. Second, we used the LME model with the variance-covariance structure identified in the previous step to simulate datasets. The fixed effects of these LME models were defined so that all main effects and interactions would include a meaningful difference (see above). Finally, we estimated the power by analyzing each simulated dataset with a mixed-effect repeated-measure ANOVA as described above and by tallying the number of times each effect was statistically significant. In general, these analyses indicated that the sample size was sufficient to detect reliably a meaningful difference if it existed with the exception of the expertise main effect. This result reflects the fact that the power for the main effect corresponding to a between-subject factor

in a split-plot design is markedly lower than the power of the within-subject factors and/or all their interactions (including the interactions between between-subject and within-subject factors) (Bradley and Russell, 1998). Note that this approach is different from standard *post hoc* power analysis where the effect size is determined by the actual results. Provided that the power is large enough, it ensures that a meaningful effect would be statistically significant. Accordingly, it also ensures that a non-statistically significant test is not due to lack of power but to an effect size that is of little interest. Still, the results of the simulations should be interpreted cautiously as it is not possible to exclude the possibility that the simulated datasets underestimate or misrepresent the variance in the actual populations given the limited sample size of the study.

In addition to frequentist statistics, we also implemented a Bayesian analysis for the repeated measure ANOVA (JASP version 0.9.1.0), and for *t*-tests. Bayesian analysis of effects in the ANOVA were computed across matched models. We report the change from prior to posterior inclusion odds ($BF_{inclusion}$). The JZS Bayes Factor (BF10) was estimated for paired *t*-tests with a default scale factor of 0.707 (Liang et al., 2008; Rouder et al., 2009).

Experiment 2: Reproduction Task

Reproduction Quality

Given the circular nature of the tapping behavior, the tapping performance was assessed using circular measures (Della Bella et al., 2017). For each trial, we defined an expected sequence to be reproduced (i.e., the presented sequence), that we compared with the observed one. Each recorded tap was categorized as long (double duration) or short (single duration), according to the expected order of long and short elements. Within each category, we discarded outliers, defined as taps farther away than 2 standard deviations from the average observed delay (about 4% of total taps). We transformed each tap-delay into a phase (φ_k), according to its expected delay with the formula:

$$\varphi_k = 2\pi \frac{x_k}{\widehat{x}_k} \tag{1}$$

where x_k is the observed, and $\widehat{x}_k$ is the expected delay for the tap k. We computed the vector length (*R*, synchronization precision) and the angle (Ψ, synchronization accuracy) of the resulting distribution as:

$$R = \frac{\left|\sum_{k=1}^{N} e^{i\varphi_k}\right|}{N} \tag{2}$$

and

$$\Psi = \arg\left(\sum_{k=1}^{N} e^{i\varphi_k}\right) \tag{3}$$

In order to compensate for possible missing taps, the procedure was run for each possible expected sequence obtainable from the original one (e.g., from the sequence "22112": "22112," "21122," "11222," "12221," "22211"). Thus, for each trial we ended up with five couples of measures (two for each tested sequence). The measures referring to the sequence with the higher synchronization precision were kept for further analysis. Trials with a poor synchronization precision (below 0.5) were discarded from further analysis (about 5% of trials). The procedure resulted in two indexes of reproduction quality: (i) synchronization precision (*R*), and (ii) synchronization accuracy (Ψ). Synchronization precision measured the participants' precision in reproducing the sequence, and its values were bounded between 0 (minimal precision) to 1 (maximal precision). To meet the ANOVA assumptions about the normal distribution of residuals, the synchronization precision was Fisher-transformed (*z*) using the inverse hyperbolic tangent of the vector length (*R*), as:

$$R_z = \frac{1}{2} \ln\left(\frac{1+R}{1-R}\right) \tag{4}$$

Synchronization accuracy measured the participants' accuracy in reproducing the sequence, with values reported in radians and bounded between $-\pi$ and π, where values closer to 0 indicate maximal accuracy and closer to π indicate minimal accuracy. For the two indexes, we evaluated the effects of rhythm complexity, expertise and modality by a mixed-design repeated measure ANOVA (2 rhythm complexities × 2 modalities × 2 expertise, with rhythm complexity and modality as within factors, and expertise as between-subjects effect). Power was computed similarly as in experiment 1, with the smallest meaningful effect size set as 0.1 for synchronization precision, and 0.15° for synchronization accuracy. The probability of detecting a meaningful difference between the two groups was only 9% for synchronization precision and 23% for the synchronization accuracy analysis. For the synchronization precision analysis, power was also low for rhythm complexity (21%) and the interaction between group and rhythm complexity (22%). The power of detecting a meaningful difference in synchronization precision or accuracy was above 87 and 77%, respectively, for all other effects and interactions.

Reproduction Force

For each element of each sequence, we predicted—according to metrical encoding rules (Povel and Okkerman, 1981; Essens and Povel, 1985)—the strength of its perceptual accent (corresponding to the hierarchical level of the element in the sequence). This prediction led to a categorization of each element as strong (S), medium (M), and weak (W) (see **Figure 1A**). Strong elements (S) were defined as those elements falling on the perceptual beat and starting the sequence (i.e., the elements with the higher hierarchical position). Medium elements (M) were defined as elements falling on a perceptual beat but not in a starting position. Finally, weak elements (W) were defined as those elements that did not fall on a perceptual beat.

The reproduction force of each tap was estimated by computing the maximal voltage generated around the time of each tap by the piezo-sensor (within −10 to 50 ms from tap onset). In order to directly compare forces across trials and conditions, they were standardized (z-scored) within each trial, and a repeated measure ANOVA was run to investigate the main effects of modality, rhythm complexity and element (2 modalities × 2 rhythm complexities × 3 elements). The test

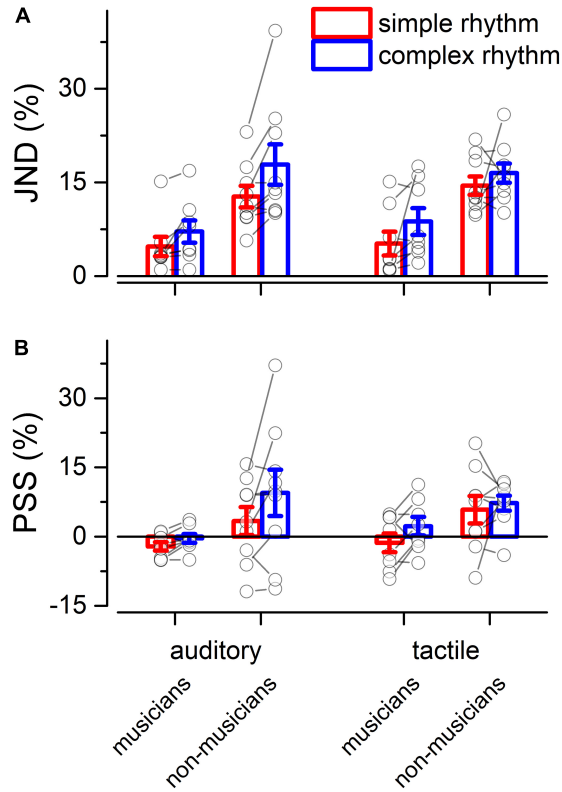

FIGURE 2 | Experiment 1: temporal order judgment task. **(A)** Grand-average just-noticeable-difference (JND) for simple (red) and complex rhythms (blue) for all the modality conditions and expertise. Dots indicate individual data, error bar indicates ± 1 S.E.M. **(B)** Same as **(A)** but for point-of-subjective-simultaneity (PSS).

of Maunchly revealed a violation of sphericity for the factor "element" (Maunchly's $W = 0.514$; $p = 0.018$). Consequently, a Greenhouse-Geisser sphericity correction was applied to the degrees of freedom of the ANOVA. Power was computed similarly as in experiment 1, with the smallest meaningful effect size set as 0.1. Power was above 94% for all the effects and interactions, except for the element main effect (19%).

We defined an index of metrical coding resulting in the difference between the mean force generated to reproduce the strong and the medium elements of each sequence (*metrical coding index*). This comparison allowed us to investigate further the hierarchical organization of the forces, i.e. the dissimilarities between elements presented on the perceptual beat (note that weak elements were not presented on the perceptual beat).

RESULTS

Experiment 1: Temporal-Order Task

Separated repeated measure ANOVA analyses were conducted on the transformed JND and PSS to investigate the main effect of rhythm complexity (simple vs. complex), expertise (non-musicians vs. musicians), and modality (auditory vs. tactile).

As shown in **Figure 2A**, the analysis on JND revealed an effect of expertise [$F(1, 15) = 17.97$, $p < 0.001$, $\eta^2_G = 0.43$; $BF10_{inclusion} = 39.41$] and rhythm complexity [$F(1, 15) = 17.31$, $p < 0.001$, $\eta^2_G = 0.05$; $BF10_{inclusion} = 227.56$]. No other effects or interactions were statistically significant ($p > 0.05$, see **Table 1**). The PSS revealed a statistically significant effect of expertise [$F(1, 15) = 5.51$, $p = 0.033$, $\eta^2_G = 0.17$; $BF10_{inclusion} = 2.32$] and rhythm complexity [$F(1, 15) = 7.30$, $p = 0.01$, $\eta^2_G = 0.034$; $BF10_{inclusion} = 2.38$; see **Figure 2B**]. No other main effects or interactions were statistically significant ($p > 0.05$, see **Table 2**). Overall, these results indicate a higher perceptual precision and accuracy for musicians compared to non-musicians, as well as a general perceptual advantage in temporal order judgments for simple sequences compared to complex sequences, independent of the modality of stimulation.

Experiment 2: Reproduction Task

Reproduction Quality

We evaluated two indexes of reproduction quality: *i*) synchronization precision, and *ii*) synchronization accuracy (see section "Materials and Methods" for details). Repeated measure ANOVA on synchronization precision revealed a significant effect of expertise [$F(1, 13) = 6.99$, $p = 0.02$, $\eta^2_G = 0.23$; $BF10_{inclusion} = 3.28$], modality [$F(1, 13) = 6.20$, $p = 0.027$, $\eta^2_G = 0.009$; $BF10_{inclusion} = 0.64$] and rhythm complexity [$F(1, 13) = 13.15$, $p = 0.003$, $\eta^2_G = 0.13$; $BF10_{inclusion} = 9532.69$], and no significant interactions ($p > 0.05$, see **Table 3** and **Figure 3A**). The same analysis performed on the synchronization accuracy revealed a main effect of rhythm complexity [$F(1, 13) = 5.50$, $p = 0.036$, $\eta^2_G = 0.054$; $BF10_{inclusion} = 8.97$], and no other

TABLE 1 | Repeated measure ANOVA—JND (experiment 1).

Effect	Df num.	DF den.	MSE	*F*	η^2_G	*P*-value
Expertise	1	15	0.488	17.975	0.469	**<0.001**
Modality	1	15	0.055	0.818	0.005	0.380
Expertise:modality	1	15	0.055	0.006	<0.001	0.938
Complexity	1	15	0.062	17.312	0.098	**<0.001**
Expertise:complexity	1	15	0.062	1.354	0.008	0.263
Modality:complexity	1	15	0.057	0.005	<0.001	0.943
Expertise:modality:complexity	1	15	0.057	1.680	0.009	0.214

Transformation: $x^{1/3}$. Bold highlights the statistically significant results ($p < 0.05$).

TABLE 2 | Repeated measure ANOVA—PSS (experiment 1).

Effect	Df num.	DF den.	MSE	*F*	η^2_G	*P*-value
Expertise	1	15	1.78	5.51	0.175	**0.033**
Modality	1	15	0.75	1.22	0.016	0.286
Expertise:modality	1	15	0.75	0.06	<0.001	0.804
Complexity	1	15	0.27	7.30	0.034	**0.016**
Expertise:complexity	1	15	0.27	0.01	<0.001	0.911
Modality:complexity	1	15	0.27	0.00	<0.001	0.976
Expertise:modality:complexity	1	15	0.27	0.30	0.001	0.590

Transformation: $sign(x)((|x| + 1)^{1/3} - 1)$. Bold highlights the statistically significant results ($p < 0.05$).

significant effects or interactions ($p > 0.05$) (see **Table 4** and **Figure 3B**). Overall, the results confirm that complex sequences were generally reproduced with less precision and accuracy then simple sequences.

Reproduction Force

With the goal of investigating the internal motor organization of rhythm, we focused on the force aspects of the reproduction (see **Figure 4**). Repeated measure ANOVA on the applied force revealed a main effect of the element [$F(1.25, 17.52) = 52.70$, $p < 0.001$, $\eta^2_G = 0.70$; $BF_{inclusion} = 2.874e+43$], rhythm complexity [$F(1, 14) = 45.77$, $p < 0.001$, $\eta^2_G = 0.06$; $BF_{inclusion} = 43.36$], and a significant triple interaction between modality, rhythm complexity and element [$F(1.46, 20.48) = 4.70$, $p = 0.029$, $\eta^2_G = 0.02$; $BF_{inclusion} = 0.81$; see **Table 5**]. Importantly, Bayesian repeated measure ANOVA revealed that the best model was the one including only rhythm complexity and element ($BF_{model} = 47.78$). *Post hoc* comparisons revealed that weak elements were reproduced with less force than medium [$t(14) = -7.46$, $p_{holm} < 0.01$, Cohen's $d = -1.92$, BF10 = 1.075e+13] and strong elements [$t(14) = -9.83$, $p_{holm} < 0.001$, Cohen's $d = -2.54$, BF10 = 1.135e+17], and medium elements were reproduced with less force than strong elements [$t(14) = -2.37$, $p_{holm} = 0.025$, Cohen's $d = -0.61$, BF10 = 2.588e+6]. To summarize, results revealed that rhythm complexity and element modulated the force of the tap. Crucially, a force difference was evident not only between elements presented on the beat (strong and medium elements) vs. elements presented off the beat (weak elements), but also between strong and medium elements (i.e., both elements presented on the perceptual beat but differing in the hierarchy of the sequence; see **Figures 4A,B**). Although expertise was not included in the ANOVA for sake of simplification, the average force for each musician and non-musician are indicated in **Figure 4**.

To assure that the reported differences in force were not simply due to a physical constraint imposed by the duration of the current element to be reproduced, we replicated the analysis by focusing on strong and medium elements with double unit durations (i.e., the double elements presented on the

TABLE 3 | Repeated measure ANOVA—synchronization precision (experiment 2).

Effect	Df num.	DF den.	MSE	*F*	η^2_G	*P*-value
Expertise	1	13	0.35	6.99	0.281	**0.020**
Modality	1	13	0.01	6.20	0.015	**0.027**
Expertise:modality	1	13	0.01	0.11	0.000	0.740
Complexity	1	13	0.10	13.15	0.183	**0.003**
Expertise:complexity	1	13	0.10	0.84	0.014	0.374
Modality:complexity	1	13	0.01	2.19	0.003	0.162
Expertise:modality:complexity	1	13	0.01	0.00	0.000	0.958

Transformation: atanh(x). Bold highlights the statistically significant results (p < 0.05).

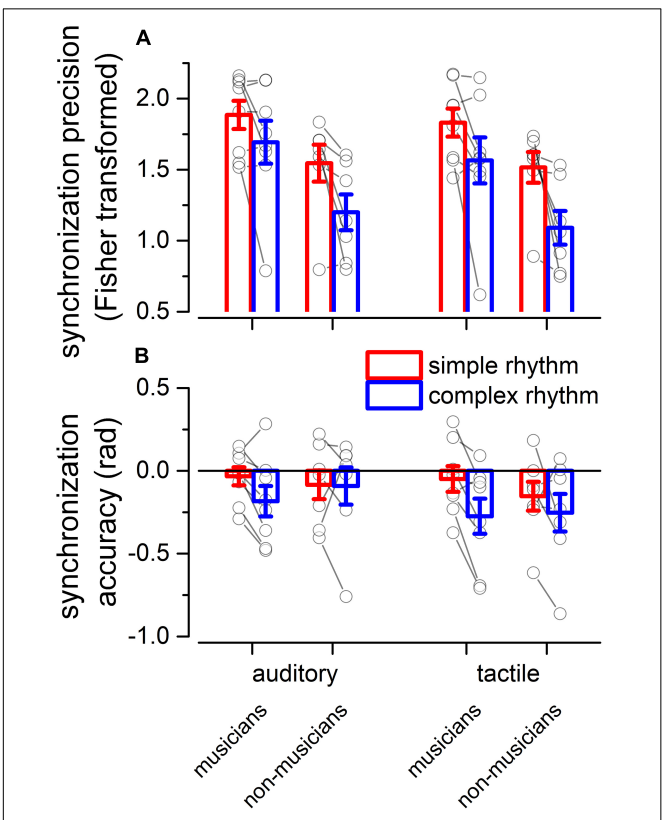

FIGURE 3 | Experiment 2: reproduction quality. **(A)** grand-average synchronization precision for simple (red) and complex rhythms (blue) for all the modality conditions and expertise. Dots indicate individual data, error bar indicates ± 1 S.E.M. **(B)** Same as **(A)** but for synchronization accuracy.

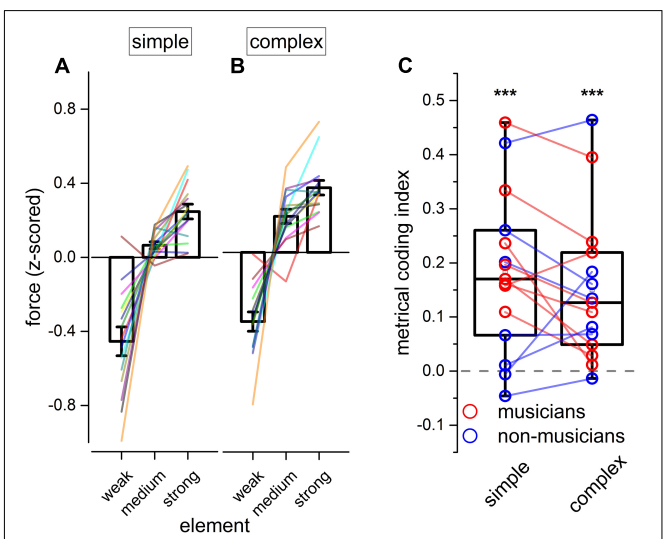

FIGURE 4 | Experiment 2: reproduction force. **(A,B)** Grand-average force profile of the finger-tapping for the different elements of a simple **(A)** and complex sequence **(B)**. Error bar indicates ± 1 S.E.M. Colored lines show single participants. **(C)** Boxplot showing the metrical coding index distribution for both simple and complex sequences. Dots indicate individual data (musicians are marked in red, and non-musicians in blue); error bar indicates confidence intervals (95 %ile). Asterisks mark the statistical significance (*p*-value): *** < 0.001.

perceptual beat but differing in the hierarchy of the sequence. The sequence "11122" was discarded from this analysis because of the short duration of the strong element). Results revealed significant effects of rhythm complexity [$F(1, 14) = 25.59$, $p < 0.001$, $\eta^2_G = 0.17$; $BF_{inclusion} = 8033.50$] and element [$F(1, 14) = 6.01$, $p = 0.028$, $\eta^2_G = 0.1$; $BF_{inclusion} = 78.99$], indicating that participants used more force in reproducing the strong element of the sequence as compared to the medium one, and this effect cannot be attributed to the duration of the element that was reproduced.

The temporal gaps between taps might influence the applied force. In order to control for this possibility, we ran a repeated-measure ANOVA on the speed of the sequences (unit duration). If the level of force depends on the temporal gap between taps, we expect an effect of speed (e.g., lower force for faster rhythms, where the gaps are shorter than for slower rhythms). The ANOVA revealed no significant effects or interactions [speed: $F(3, 42) = 1.06$, $p = 0.374$, $\eta^2_G = 0.07$; $BF_{inclusion} = 0.26$], suggesting that the reported effect was driven by the position of the element in the sequence and not by physical constraints.

To summarize the previous findings, we measured the force difference between the strong and the medium elements of each sequence (*metrical coding index*, see **Figure 4C**). Values above 0 would indicate that the strong element was reproduced with more force than the medium one. In other words, a value above 0 would indicate a coherence between the predicted metrical hierarchy of the element and the force applied in reproducing it and, hence, the presence of metrical coding in the force. Conversely, values around 0 would indicate that tapping force was not coding the metrical aspects of the rhythm. Two-tail paired t-tests were run for simple and complex sequences. Results demonstrated that participants encoded metrical information in force for both simple and complex sequences [simple rhythm: $t(14) = 4.79$, $p_{holm} < 0.001$, BF10 = 114.39; complex rhythm: $t(14) = 4.29$, $p_{holm} < 0.001$, BF10 = 50.32].

It is known that metrical coding favors both rhythm perception and reproduction (Semjen and Vos, 2002; Phillips-Silver and Trainor, 2005; Grahn and Brett, 2007; Chen et al., 2008a; Grube and Griffiths, 2009; Cameron and Grahn, 2014). To investigate this aspect further, we correlated the perceptual performance from experiment 1 (for both JND and PSS) with the *metrical coding index*. To account for possible spurious correlations introduced by differences in experimental conditions and expertise, all the indexes to-be-correlated were mean-centered (*ipsitized*) for rhythm complexity and expertise (e.g., the distribution of the JNDs pertaining to musicians in complex rhythms was centered at 0). Results revealed that the PSS correlated with metrical coding abilities (Pearson's $r = -0.56$; $p = 0.001$), while JND did not (Pearson's $r = 0.002$; $p = 0.99$, see **Figures 5A,B**).

Finally, we found that JND (not shown), PSS, and metrical coding index within participants strongly correlated across rhythm complexities [JND: $F(1, 13) = 72.4$, $p < 0.001$, $r(15) = 0.92$; PSS: $F(1, 13) = 27.9$, $p < 0.001$, $r(15) = 0.82$; metrical coding index: $F(1, 13) = 17.1$, $p = 0.001$, $r(15) = 0.75$; see **Figures 5C,D**).

TABLE 4 | Repeated measure ANOVA—synchronization accuracy (experiment 2).

Effect	Df num.	DF den.	MSE	*F*	η^2_G	*P*-value
Expertise	1	13	0.19	0.00	0.000	0.928
Modality	1	13	0.02	4.34	0.028	0.057
Expertise:modality	1	13	0.02	0.58	0.003	0.457
Complexity	1	13	0.03	5.49	0.057	**0.035**
Expertise:complexity	1	13	0.03	1.70	0.018	0.213
Modality:complexity	1	13	0.01	2.32	0.007	0.151
Expertise:modality:complexity	1	13	0.01	0.02	0.000	0.873

Bold highlights the statistically significant results ($p < 0.05$).

TABLE 5 | Repeated measure ANOVA—force (experiment 2).

Effect	Df num.	DF den.	MSE	*F*	η^2_G	*P*-value
Modality	1	14	0.00	0.25	0.000	0.618
Complexity	1	14	0.01	45.77	0.067	**<0.001**
Element	1.25	17.52	0.24	52.70	0.707	**<0.001**
Modality:complexity	1	14	0.00	0.04	0.000	0.840
Modality:element	1.91	26.84	0.03	0.49	0.004	0.604
Complexity: element	1.19	16.74	0.04	0.11	0.000	0.779
Modality:complexity:element	1.46	20.48	0.02	4.70	0.022	**0.029**

Bold highlights the statistically significant results ($p < 0.05$).

DISCUSSION

Volunteers (musicians and non-musicians) were asked to separately perform an auditory and a tactile temporal-order judgment task (experiment 1), where the experimenter manipulated the complexity of the rhythm. In a second experiment, volunteers were asked to reproduce the same rhythms, and the timing and force of their reproduction was analyzed (experiment 2).

Our results revealed that (*i*) rhythm complexity affects precision and accuracy for both perceptual and reproduction tasks; (*ii*) tapping force was higher for elements presented on the beat than for elements falling outside the beat (or on the weak beat); (*iii*) metrical elements falling on the strong vs. medium beat of the sequence were further differentiated, indicating the presence of a complex hierarchical motor organization; (*iv*) this force difference was not modality specific; (*v*) the sensorimotor organization of rhythms was the same for different modalities of rhythm presentation (auditory or tactile); and finally, (*vi*) the amount of *metricality* in the tapping-force correlates with the individual perceptual accuracy.

Overall, results from experiment 1 and 2 revealed the presence of a general effect of rhythm complexity on sensorimotor precision and accuracy: simple rhythms were perceived and reproduced with more accuracy and precision compared to complex rhythms. There is currently no consensus about the key factors making a rhythm "complex" or "simple" (Grahn, 2012a). We speculate that a main difference between the two types of rhythm might be linked to the number of clocks (or oscillators) needed to univocally predict the pulses generated by

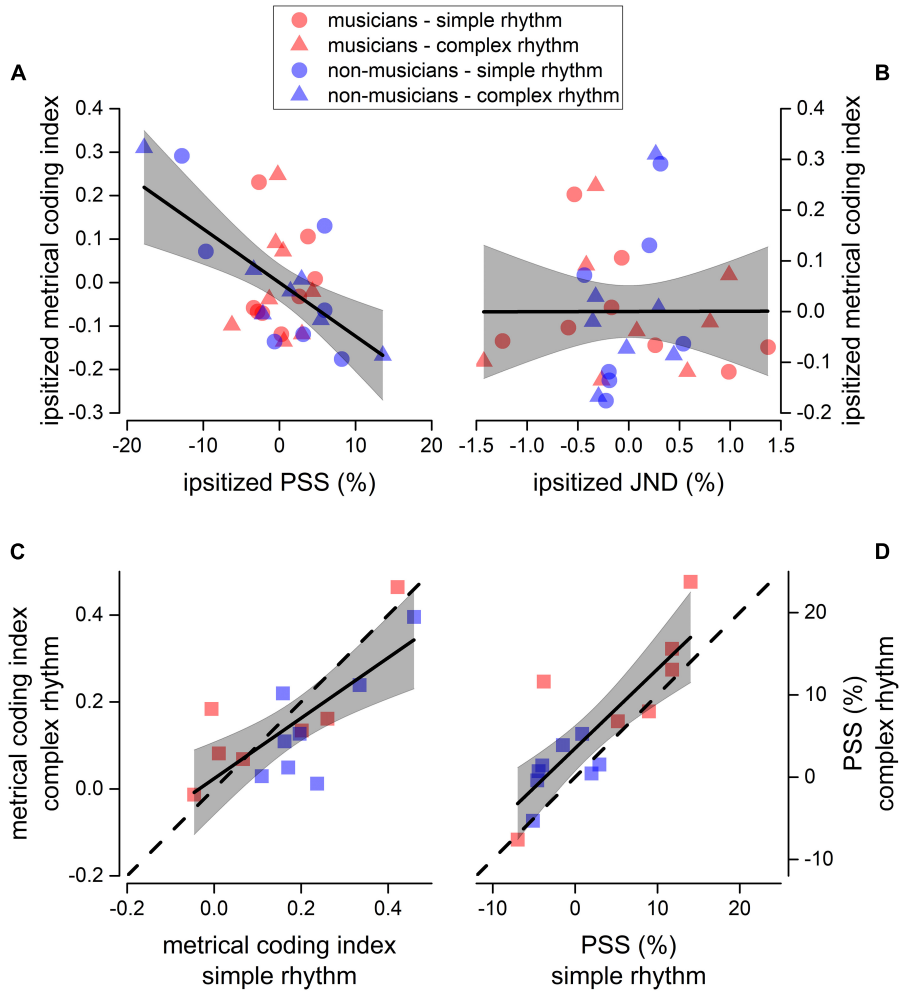

FIGURE 5 | . Sensorimotor correlation. Linear regression between ipsitized metrical coding index and ipsitized PSS **(A)**, and between ipsitized metrical coding index and ipsitized JND **(B)**. We plotted a value for each participant (musicians in red, and non-musicians in blue) and rhythm complexity (simple as circles, complex as triangles). Thick lines show the best linear regression of data, gray areas show 95% confidence band. The linear regression revealed a significant negative correlation between metrical coding index and PSS ($p < 0.05$, see section "Materials and Methods for details). **(C,D)** Correlation between metrical coding index for simple (*x*-axis) and complex (*y*-axis) rhythms **(C)** and between PSS for simple (*x*-axis) and complex (*y*-axis) rhythms **(D)**. Dashed lines report the equality line, thick lines show the best linear regression of data, gray areas show 95% confidence band. Red and blue squares indicate musicians and non-musicians, respectively.

the rhythm itself (i.e., the complexity of the predictive model). Subsequent pulses in simple rhythms are perceived at fixed and equal temporal intervals, and a single oscillator could easily model the perceptual distribution of pulses. On the other hand, complex rhythms generate un-equally spaced pulses, that cannot be modeled by a single oscillator, implicating the presence of multiple phase-locked oscillators working together to predict the timing of the perceptual pulses. In this sense, simple predictive models might be advantageous for perception and sensorimotor synchronization as they generally might require less attentional and mnemonic (and generally neuronal) resources, as compared to complex models of prediction.

Although the facilitatory effect of simple rhythms was clearly visible for both groups, we also found that musicians perceived and, to some extent, reproduced complex rhythms better than non-musicians. It is noteworthy that musicians received an institutional western musical training in Italy, which includes the exposure to complex rhythms. For this reason, complex rhythms are considered metrical by most musicians. In contrast, the impact of the subjective experience in shaping rhythm perception is intrinsically more problematic for non-musicians (reporting no institutional music training) despite possible exposure to rhythms and music that might have included complex rhythms. In this respect, it should be noted that the perception of metrical structures in a rhythm strongly relies on subjective experiences and culture (Cameron et al., 2015; London et al., 2017; van der Weij et al., 2017; Bouwer et al., 2018; Nave-Blodgett et al., 2021) and could be shaped by passive exposure to music (Jacoby and McDermott, 2017). For instance, some of the complex rhythms adopted here are common in certain folk music from Balkan, east European, or in jazz music, but almost absent in other cultures (e.g., they are almost absent in the Italian folk music, the state

where participants were recruited and tested). Unfortunately, we could not investigate this aspect further, as non-musicians reported no institutional training in music, and we did not evaluate their degree of musical expertise with any other scale.

Grahn (2009) demonstrated that tap velocity (an indirect measure of tapping force) during the reproduction of simple rhythms was higher on taps presented on the beat than on other taps (Grahn, 2009). We replicated this effect showing that the weak elements of a sequence (i.e., those elements not falling on the beat, or falling on sub-division of it) are reproduced with less force than medium and strong elements. Importantly, we extended this result by showing that the strong and medium elements (i.e., elements falling on the beat, but pertaining to different hierarchical levels) were further reproduced with different intensities, indicating the presence of a complex hierarchical coding.

We found here the presence of a comparable hierarchical organization of forces for both simple and complex rhythms. Indeed, a close look at the metrical coding index, revealed that—across participants—it strongly correlated for the different rhythm complexities. This suggests that, irrespective of a general sensorimotor facilitation for simple vs. complex rhythms, participants were able to code both simple and complex sequences adopting a hierarchical organization. Importantly, the correlation between perceptual accuracy and metrical coding suggests the presence of a continuous gradient in which participants with a stronger metrical coding were also more accurate in the perceptual task. It would be interesting, for future research, to investigate the organization of forces on different rhythms (e.g., rhythms with different integer ratios, or purely non-metrical sequences) and directly comparing it for musicians, non-musicians, and cross-culturally.

Metrical coding has been mostly reported in auditory modality, suggesting that this ability might be specific to the auditory system (Bartlett and Bartlett, 1959; Patel et al., 2005; Grahn, 2012b). In line with this hypothesis, a close link between sensorimotor brain activity and auditory temporal predictions or musical imagery has been demonstrated (Morillon et al., 2014; Morillon and Baillet, 2017; Gelding et al., 2019). Motor cortex excitability and coordination is directly influenced by the groove of the auditory stimulation (Wilson and Davey, 2002; Stupacher et al., 2013); however, metrical coding has been recently shown in tactile perception (Brochard et al., 2008; Ammirante et al., 2016; Gilmore et al., 2018), questioning the existence of a special link between beat perception and auditory modality (Ammirante et al., 2016).

Current results revealed no effect of modality in the perceptual task (for both perceptual accuracy and precision) and in reproduction accuracy, but a significant (although weak) effect of modality for reproduction precision. Crucially, the analysis on forces revealed no effect of the modality of stimulation, indicating the presence of a similar hierarchical organization of forces under both stimulation conditions, and further questioning the hypothesis of specific auditory-motor processes for rhythm perception and reproduction.

How might this shared temporal rhythm be orchestrated in the brain? The synchrony between different perceptual systems (or between perception and action) is challenged by the evidence that different processes elaborate the information at different speeds: for instance, time has been shown to vary across sensory modalities and features of the sensory stimulation (Johnston et al., 2006; Kanai et al., 2006; Burr et al., 2011; Harrington et al., 2011; Tomassini et al., 2011). It has been suggested that motor system might play a key role in shaping a unitary sense of time, possibly by synchronizing the dynamics of local processing (Hommel et al., 2001; Benedetto et al., 2018, 2020). This hypothesis is in line with the evidence that time perception and motor timing rely on similar cerebral structures (Schubotz et al., 2000; Nobre and O'Reilly, 2004).

Passive perception of metrical rhythms is known to elicit the activity of several motor areas (Zatorre et al., 2007; Chen et al., 2008a,b; Bengtsson et al., 2009; Grahn and Rowe, 2009; Patel and Iversen, 2014), and it has been suggested that it might involve an internal motor simulation, phase-locked with the pulse of the rhythm (Wilson and Davey, 2002; Su and Poppel, 2012). Manning and Schutz (H2013) demonstrated that timekeeping is improved when participants move along with a rhythm. In their study, participants heard a series of isochronous sounds followed by a short silence and a probe beat, and they were asked to judge whether the timing of the probe was consistent with the timing of the preceding sequence. The authors found an improvement in the perceptual performance when participants tapped along with the beat, remarking on the presence of a beneficial crosstalk between the sensory and the motor system (Manning and Schutz, 2013) and suggesting that perceptual contents and action plans are coded in a common representational medium (Hommel et al., 2001). In line with this hypothesis, our results demonstrated further that the organization of the rhythm is directly encoded in the force profile of the finger-taps, and this effect is independent of the modality of stimulation.

CONCLUSION

To sum up, our results show the presence of a hierarchical organization of the forces during finger-tapping to reproduce a rhythm, and this organization mimics the perceptual hierarchical organization of the rhythm itself. We speculate that this effect reflects the presence of a shared representation of rhythm between the motor and the sensory systems, i.e., a supra-modal representation of time shared within the sensorimotor circuit that facilitates both the perception and the reproduction of the temporal sequences.

DATA AVAILABILITY STATEMENT

Experimental data are downloadable at Zenodo repository: https://doi.org/10.5281/zenodo.4637676.

ETHICS STATEMENT

The study followed a protocol approved by the Local Ethics Committee, Comitato Etico per la Sperimentazione con l'Essere

Umano della ASL 3 di Genova, in accordance with institutional requirements and national legislation. A written informed consent was obtained for the participation.

AUTHOR CONTRIBUTIONS

AB and GB-B conceived, designed the experiment, performed the analysis, and wrote the manuscript. AB collected the data. Both authors contributed to the article and approved the submitted version.

FUNDING

This project was supported by the European Research Council (ERC) under the European Union's Horizon 2020 program (Grant Agreement Nos. 832813-GENPERCEPT and 801715-PUPILTRAITS) and by MIUR—PRIN 2017—grant No. 2017SBCPZY_02.

ACKNOWLEDGMENTS

We thank Eleanor Reynolds for proofreading the manuscript.

REFERENCES

Ammirante, P., Patel, A. D., and Russo, F. A. (2016). Synchronizing to auditory and tactile metronomes: a test of the auditory-motor enhancement hypothesis. *Psychon. Bull. Rev.* 23, 1882–1890. doi: 10.3758/s13423-016-1067-9

Arnold, B. F., Hogan, D. R., Colford, J. M. Jr., and Hubbard, A. E. (2011). Simulation methods to estimate design power: an overview for applied research. *BMC Med. Res. Methodol.* 11:94. doi: 10.1186/1471-2288-11-94

Bartlett, N. R., and Bartlett, S. C. (1959). Synchronization of a motor response with an anticipated sensory event. *Psychol. Rev.* 66, 203–218. doi: 10.1037/h0046490

Bates, D., Kliegl, R., Vasishth, S., and Baayen, H. (2015). Parsimonious mixed models. *arXiv* [Preprint] arXiv:1506.04967,

Benedetto, A., Burr, D. C., and Morrone, M. C. (2018). Perceptual oscillation of audiovisual time simultaneity. *eNeuro* 5, ENEURO.0047-18.2018.

Benedetto, A., Morrone, M. C., and Tomassini, A. (2020). The common rhythm of action and perception. *J. Cogn. Neurosci.* 32, 187–200. doi: 10.1162/jocn_a_01436

Bengtsson, S. L., Ullen, F., Ehrsson, H. H., Hashimoto, T., Kito, T., Naito, E., et al. (2009). Listening to rhythms activates motor and premotor cortices. *Cortex* 45, 62–71. doi: 10.1016/j.cortex.2008.07.002

Bouwer, F. L., Burgoyne, J. A., Odijk, D., Honing, H., and Grahn, J. A. (2018). What makes a rhythm complex? The influence of musical training and accent type on beat perception. *PLoS One* 13:e0190322. doi: 10.1371/journal.pone.0190322

Bradley, D. R., and Russell, R. L. (1998). Some cautions regarding statistical power in split-plot designs. *Behav. Res. Methods Instrum. Comput.* 30, 462–477. doi: 10.3758/bf03200681

Brochard, R., Touzalin, P., Despres, O., and Dufour, A. (2008). Evidence of beat perception via purely tactile stimulation. *Brain Res.* 1223, 59–64. doi: 10.1016/j.brainres.2008.05.050

Burger, B., London, J., Thompson, M. R., and Toiviainen, P. (2018). Synchronization to metrical levels in music depends on low-frequency spectral components and tempo. *Psychol. Res.* 82, 1195–1211. doi: 10.1007/s00426-017-0894-2

Burger, B., Thompson, M. R., Luck, G., Saarikallio, S. H., and Toiviainen, P. (2014). Hunting for the beat in the body: on period and phase locking in music-induced movement. *Front. Hum. Neurosci.* 8:903. doi: 10.3389/fnhum.2014.00903

Burr, D. C., Cicchini, G. M., Arrighi, R., and Morrone, M. C. (2011). Spatiotopic selectivity of adaptation-based compression of event duration. *J. Vis.* 11, 21; author reply 21a.

Caetano, G., and Jousmaki, V. (2006). Evidence of vibrotactile input to human auditory cortex. *Neuroimage* 29, 15–28. doi: 10.1016/j.neuroimage.2005.07.023

Cameron, D. J., Bentley, J., and Grahn, J. A. (2015). Cross-cultural influences on rhythm processing: reproduction, discrimination, and beat tapping. *Front. Psychol.* 6:366. doi: 10.3389/fpsyg.2015.00366

Cameron, D. J., and Grahn, J. A. (2014). Enhanced timing abilities in percussionists generalize to rhythms without a musical beat. *Front. Hum. Neurosci.* 8:1003. doi: 10.3389/fnhum.2014.01003

Cameron, D. J., Stewart, L., Pearce, M. T., Grube, M., and Muggleton, N. G. (2012). Modulation of motor excitability by metricality of tone sequences. *Psychomusicology* 22, 122–128. doi: 10.1037/a0031229

Chen, J. L., Penhune, V. B., and Zatorre, R. J. (2008a). Listening to musical rhythms recruits motor regions of the brain. *Cereb. Cortex* 18, 2844–2854. doi: 10.1093/cercor/bhn042

Chen, J. L., Penhune, V. B., and Zatorre, R. J. (2008b). Moving on time: brain network for auditory-motor synchronization is modulated by rhythm complexity and musical training. *J. Cogn. Neurosci.* 20, 226–239. doi: 10.1162/jocn.2008.20018

Della Bella, S., Farrugia, N., Benoit, C. E., Begel, V., Verga, L., Harding, E., et al. (2017). BAASTA: battery for the assessment of auditory sensorimotor and timing abilities. *Behav. Res. Methods* 49, 1128–1145. doi: 10.3758/s13428-016-0773-6

Drake, C., Penel, A., and Bigand, E. (2000). Tapping in time with mechanically and expressively performed music. *Music Percept.* 18, 1–23. doi: 10.2307/40285899

Essens, P. J., and Povel, D. J. (1985). Metrical and nonmetrical representations of temporal patterns. *Percept. Psychophys.* 37, 1–7. doi: 10.3758/bf03207132

Gelding, R. W., Thompson, W. F., and Johnson, B. W. (2019). Musical imagery depends upon coordination of auditory and sensorimotor brain activity. *Sci. Rep. U. K.* 9:16823.

Gilmore, S. A., Nespoli, G., and Russo, F. A. (2018). Neural correlates of beat perception in vibro-tactile modalities. *J. Acoust. Soc. Am.* 144, 1838–1838. doi: 10.1121/1.5068102

Grahn, J. A. (2009). The role of the basal ganglia in beat perception: neuroimaging and neuropsychological investigations. *Ann. N. Y. Acad. Sci.* 1169, 35–45. doi: 10.1111/j.1749-6632.2009.04553.x

Grahn, J. A. (2012a). Neural mechanisms of rhythm perception: current findings and future perspectives. *Top. Cogn. Sci.* 4, 585–606. doi: 10.1111/j.1756-8765.2012.01213.x

Grahn, J. A. (2012b). See what I hear? Beat perception in auditory and visual rhythms. *Exp. Brain Res.* 220, 51–61. doi: 10.1007/s00221-012-3114-8

Grahn, J. A., and Brett, M. (2007). Rhythm and beat perception in motor areas of the brain. *Journal of cognitive neuroscience* 19, 893–906. doi: 10.1162/jocn.2007.19.5.893

Grahn, J. A., and Rowe, J. B. (2009). Feeling the beat: premotor and striatal interactions in musicians and nonmusicians during beat perception. *J. Neurosci.* 29, 7540–7548. doi: 10.1523/jneurosci.2018-08.2009

Grondin, S. (2010). Timing and time perception: a review of recent behavioral and neuroscience findings and theoretical directions. *Atten. Percept. Psycho.* 72, 561–582. doi: 10.3758/app.72.3.561

Grube, M., and Griffiths, T. D. (2009). Metricality-enhanced temporal encoding and the subjective perception of rhythmic sequences. *Cortex* 45, 72–79. doi: 10.1016/j.cortex.2008.01.006

Harrington, D. L., Castillo, G. N., Fong, C. H., and Reed, J. D. (2011). Neural underpinnings of distortions in the experience of time across senses. *Front. Integr. Neurosci.* 5:32. doi: 10.3389/fnint.2011.00032

Hommel, B., Musseler, J., Aschersleben, G., and Prinz, W. (2001). The theory of event coding (TEC): a framework for perception and action planning. *Behav. Brain Sci.* 24, 849–878; discussion 878–937.

Jacoby, N., and McDermott, J. H. (2017). Integer ratio priors on musical rhythm revealed cross-culturally by iterated reproduction. *Curr. Biol.* 27, 359–370. doi: 10.1016/j.cub.2016.12.031

Johnston, A., Arnold, D. H., and Nishida, S. (2006). Spatially localized distortions of event time. *Curr. Biol.* 16, 472–479. doi: 10.1016/j.cub.2006.01.032

Kanai, R., Paffen, C. L. E., Hogendoorn, H., and Verstraten, F. A. J. (2006). Time dilation in dynamic visual display. *J. Vis.* 6, 1421–1430.

Lenc, T., Keller, P. E., Varlet, M., and Nozaradan, S. (2020). Neural and behavioral evidence for frequency-selective context effects in rhythm processing in humans. *Cereb. Cortex Commun.* 1:tgaa037.

Liang, F., Paulo, R., Molina, G., Clyde, M. A., and Berger, J. O. (2008). Mixtures of g priors for Bayesian variable selection. *J. Am. Stat. Assoc.* 103, 410–423.

London, J. (1995). Some examples of complex meters and their implications for models of metric perception. *Music Percept.* 13, 59–77. doi: 10.2307/40285685

London, J., Polak, R., and Jacoby, N. (2017). Rhythm histograms and musical meter: a corpus study of Malian percussion music. *Psychon. Bull. Rev.* 24, 474–480. doi: 10.3758/s13423-016-1093-7

Manning, F., and Schutz, M. (2013). "Moving to the beat" improves timing perception. *Psychon. Bull. Rev.* 20, 1133–1139. doi: 10.3758/s13423-013-0439-7

Matuschek, H., Kliegl, R., Vasishth, S., Baayen, H., and Bates, D. (2017). Balancing type I error and power in linear mixed models. *J. Mem. Lang.* 94, 305–315. doi: 10.1016/j.jml.2017.01.001

McAuley, J. D. (2010). "Tempo and Rhythm",in *Springer Handbook of Auditory Research: Music Percept*, Vol. 36, eds M. R. Jones, R. R. Fay and A. N. Popper (New York, NY: Springer), 165–199.

Morillon, B., and Baillet, S. (2017). Motor origin of temporal predictions in auditory attention. *Proc. Natl. Acad. Sci. U.S.A.* 114, E8913–E8921.

Morillon, B., Schroeder, C. E., and Wyart, V. (2014). Motor contributions to the temporal precision of auditory attention. *Nat. Commun.* 5:5255.

Nave-Blodgett, J. E., Snyder, J. S., and Hannon, E. E. (2021). Hierarchical beat perception develops throughout childhood and adolescence and is enhanced in those with musical training. *J. Exp. Psychol. Gen.* 150, 314–339. doi: 10.1037/xge0000903

Nobre, A. C., and O'Reilly, J. (2004). Time is of the essence. *Trends Cogn. Sci.* 8, 387–389.

Olejnik, S., and Algina, J. (2003). Generalized eta and omega squared statistics: measures of effect size for some common research designs. *Psychol. Methods* 8, 434–447. doi: 10.1037/1082-989x.8.4.434

Patel, A. D., and Iversen, J. R. (2014). The evolutionary neuroscience of musical beat perception: the action simulation for auditory prediction (ASAP) hypothesis. *Front. Syst. Neurosci.* 8:57. doi: 10.3389/fnsys.2014.00057

Patel, A. D., Iversen, J. R., Chen, Y. Q., and Repp, B. H. (2005). The influence of metricality and modality on synchronization with a beat. *Exp. Brain Res.* 163, 226–238. doi: 10.1007/s00221-004-2159-8

Phillips-Silver, J., and Trainor, L. J. (2005). Feeling the beat: movement influences infant rhythm perception. *Science* 308, 1430–1430. doi: 10.1126/science.1110922

Phillips-Silver, J., and Trainor, L. J. (2008). Vestibular influence on auditory metrical interpretation. *Brain Cogn.* 67, 94–102. doi: 10.1016/j.bandc.2007.11.007

Povel, D. J., and Okkerman, H. (1981). Accents in equitone sequences. *Percept. Psychophys.* 30, 565–572. doi: 10.3758/bf03202011

Repp, B. H., and Su, Y. H. (2013). Sensorimotor synchronization: a review of recent research (2006-2012). *Psychon. B Rev.* 20, 403–452. doi: 10.3758/s13423-012-0371-2

Rouder, J. N., Speckman, P. L., Sun, D. C., Morey, R. D., and Iverson, G. (2009). Bayesian t tests for accepting and rejecting the null hypothesis. *Psychon. B Rev.* 16, 225–237. doi: 10.3758/pbr.16.2.225

Schubotz, R. I., Friederici, A. D., and von Cramon, D. Y. (2000). Time perception and motor timing: A common cortical and subcortical basis revealed by fMRI. *Neuroimage* 11, 1–12. doi: 10.1006/nimg.1999.0514

Semjen, A., and Vos, P. G. (2002). The impact of metrical structure on performance stability in bimanual 1 : 3 tapping. *Psychol. Res.Psych. Fo* 66, 50–59. doi: 10.1007/s004260100073

Stupacher, J., Hove, M. J., Novembre, G., Schütz-Bosbach, S., and Keller, P. E. (2013). Musical groove modulates motor cortex excitability: a TMS investigation. *Brain Cogn.* 82, 127–136. doi: 10.1016/j.bandc.2013.03.003

Su, Y. H., and Poppel, E. (2012). Body movement enhances the extraction of temporal structures in auditory sequences. *Psychol. Res.* 76, 373–382. doi: 10.1007/s00426-011-0346-3

Todd, N. P., and Lee, C. S. (2015). The sensory-motor theory of rhythm and beat induction 20 years on: a new synthesis and future perspectives. *Front. Hum. Neurosci.* 9:444. doi: 10.3389/fnhum.2015.00444

Tomassini, A., Gori, M., Burr, D., Sandini, G., and Morrone, M. C. (2011). Perceived duration of visual and tactile stimuli depends on perceived speed. *Front. Integr. Neurosci.* 5:51.

Treisman, M. (1963). Temporal discrimination and the indifference interval: Implications for a model of the "internal clock". *Psychol. Monogr.* 77, 1–31. doi: 10.1037/h0093864

Treisman, M., Faulkner, A., Naish, P. L. N., and Brogan, D. (1990). The internal clock - evidence for a temporal oscillator underlying time perception with some estimates of its characteristic frequency. *Perception* 19, 705–743. doi: 10.1068/p190705

van der Weij, B., Pearce, M. T., and Honing, H. (2017). A probabilistic model of meter perception: simulating enculturation. *Front. Psychol.* 8:824. doi: 10.3389/fpsyg.2017.00824

Von Bekesy, G. (1959). Similarities between hearing and skin sensations. *Psychol. Rev.* 66, 1–22. doi: 10.1037/h0046967

Wilson, E. M., and Davey, N. J. (2002). Musical beat influences corticospinal drive to ankle flexor and extensor muscles in man. *Int. J. Psychophysiol.* 44, 177–184. doi: 10.1016/s0167-8760(01)00203-3

Zatorre, R. J., Chen, J. L., and Penhune, V. B. (2007). When the brain plays music: auditory-motor interactions in music perception and production. *Nat. Rev. Neurosci.* 8, 547–558. doi: 10.1038/nrn2152

Conflict of Interest: The authors declare that the research was conducted in the absence of any commercial or financial relationships that could be construed as a potential conflict of interest.

frontiers in Human Neuroscience

MINI REVIEW
published: 06 May 2021
doi: 10.3389/fnhum.2021.668442

Phase-Dependent Crossed Inhibition Mediating Coordination of Anti-phase Bilateral Rhythmic Movement: A Mini Review

*Koichi Hiraoka**

College of Health and Human Sciences, Osaka Prefecture University, Habikino, Japan

The activity of the left and right central pattern generators (CPGs) is efficiently coordinated during locomotion. To achieve this coordination, the interplay between the CPG controlling one leg and that controlling another must be present. Previous findings in aquatic vertebrates and mammalians suggest that the alternate activation of the left and right CPGs is mediated by the commissural interneurons crossing the midline of the spinal cord. Especially, V0 commissural interneurons mediate crossed inhibition during the alternative activity of the left and right CPGs. Even in humans, phase-dependent modulation of the crossed afferent inhibition during gait has been reported. Based on those previous findings, crossed inhibition of the CPG in one leg side caused by the activation of the contralateral CPG is a possible mechanism underlying the coordination of the anti-phase rhythmic movement of the legs. It has been hypothesized that the activity of the flexor half center in the CPG inhibits the contralateral flexor half center, but crossed inhibition of the extensor half center is not present because of the existence of the double limb support during gait. Nevertheless, previous findings on the phase-dependent crossed inhibition during anti-phase bilateral movement of the legs are not in line with this hypothesis. For example, extensor activity caused crossed inhibition of the flexor half center during bilateral cycling of the legs. In another study, the ankle extensor was inhibited at the period switching from extension to flexion during anti-phase rhythmic movement of the ankles. In this review article, I provide a critical discussion about crossed inhibition mediating the coordination of the anti-phase bilateral rhythmic movement of the legs.

Keywords: rhythmic movement, bilateral coordination, locomotion, central pattern generator, extensor half center, flexor half center, half center model, crossed inhibition

OPEN ACCESS

Edited by:
Marco Iosa,
Sapienza University of Rome, Italy

Reviewed by:
Simon M. Danner,
Drexel University, United States
Renato Moraes,
University of São Paulo, Brazil

***Correspondence:**
Koichi Hiraoka
hiraoka@rehab.osakafu-u.a.jp

Specialty section:
This article was submitted to Motor Neuroscience, a section of the journal Frontiers in Human Neuroscience

Received: *16 February 2021*
Accepted: *12 April 2021*
Published: *06 May 2021*

Citation:
Hiraoka K (2021) Phase-Dependent Crossed Inhibition Mediating Coordination of Anti-phase Bilateral Rhythmic Movement: A Mini Review. Front. Hum. Neurosci. 15:668442. doi: 10.3389/fnhum.2021.668442

INTRODUCTION

Anti-phase bilateral rhythmic movement is produced during locomotion in mammals. The central pattern generators (CPGs) produce the rhythmic movement of the limbs (Guertin, 2009). Previous studies using a split belt treadmill suggested that the CPG in each side produces rhythmic movement of the ipsilateral leg during locomotion (Dietz et al., 1994; Prokop et al., 1995; Yang et al., 2005; Choi and Bastian, 2007). An experiment on animals has shown that V0 commissural interneurons crossing the midline of the spinal cord play a role in the left-right alternate

activity of the locomotion (Talpalar et al., 2013). Those interneurons contribute to crossed inhibition of the contralateral motor output (Rybak et al., 2015; Danner et al., 2017). Even in humans, crossed afferent inhibition is present (Stubbs and Mrachacz-Kersting, 2009; Stubbs et al., 2011a), and is modulated during gait (Stubbs et al., 2011b; Hanna-Boutros et al., 2014). There are several important findings indicating that the phase-dependent crossed inhibition occurs during the anti-phase bilateral movement in humans (Ting et al., 1998; Hiraoka et al., 2014). In this review, I introduce important previous findings on this issue, and discuss crossed inhibition mediating the coordination of the anti-phase rhythmic movement of the legs.

Left and Right CPGs

The CPGs in the spinal cord produce locomotion in mammals (Brown, 1911, 1914; Frigon, 2012). Even in humans, the existence of the CPG in the spinal cord has been suggested by a previous finding in patients with complete spinal cord injury (Dimitrijevic et al., 1998). The activity of the CPG is explained by the half center model in which the flexor and extensor half centers are alternatively activated during rhythmic movement (McCrea and Rybak, 2008; Guertin, 2009).

In rats, locomotor activity in each side of the limb was produced even the spinal cord was separated with a midline cut (Kudo and Yamada, 1987). This finding indicates that the neural networks responsible for producing rhythmic movement of the leg (i.e., CPG) are located on each side of the spinal cord. Even in humans, this view seems to be true, according to previous findings that different patterns of the stepping movements are produced in the legs when humans gait over the split-belt treadmill in which each of the two belts under each leg runs at a different speed or direction. For example, the stance phase of one leg on the faster moving belt was shortened relative to the contralateral leg on the slower moving belt (Dietz et al., 1994; Prokop et al., 1995). Moreover, even in infant humans, the extra step was produced for the leg on the faster moving belt (Yang et al., 2005). In addition, when the split belts ran in the opposite directions, the infants produced forward stepping in one leg and backward stepping in the contralateral leg. Such opposite stepping between the legs during the opposite running of the moving belts has been observed in adult humans as well (Choi and Bastian, 2007).

Crossed Pathways

Even though the CPG on each side of the spinal cord is possible to produce rhythmic movement in each leg separately, activity of the left and right CPGs must be coordinated during locomotion in humans, according to an observation that humans move the legs coordinately during gait (Perry, 1992). Previous studies in mammals have reported the existence of the pathways crossing the midline of the spinal cord ventral commissure, namely commissural interneurons, and those neurons mediate the coordination of the left and right motor activities (Kjaerulff and Kiehn, 1996, 1997; Butt et al., 2002; Kiehn, 2006; Goulding, 2009). In some aquatic vertebrates, there are three populations of the commissural interneurons; class 1, 2, and 3 (Butt et al., 2002). Importantly, the class 1 population of the commissural interneurons inhibits the contralateral motor output of the CPG. In the other words, the class 1 population of the commissural interneurons, acting for crossed inhibition, plays a role in the coordination of the alternate activity of the left and right motor systems at least in those animals.

V0–V3 commissural interneurons represent the classes of the postmitotic spinal interneurons based on the transcription factor expression (Butt et al., 2002; Kiehn et al., 2010). Especially, V0 interneurons play a role in the left-right alternation of the motor output during locomotion (Talpalar et al., 2013). V0 commissural interneurons are the major class of neurons in the ventral spinal cord. There are subdivisions of the V0 commissural interneurons; excitatory $V0_V$ interneurons, and inhibitory $V0_D$ interneurons. The role of the V0 commissural interneurons on the left-right alternation of the motor output is dependent on the frequency of the locomotion cycle (Talpalar et al., 2013; Bellardita and Kiehn, 2015). Ablation of the excitatory $V0_V$ interneurons maintained an alternate activity at low-frequency cycle of locomotion, but switched to a synchronized activity at high-frequency cycle of locomotion (Talpalar et al., 2013). Ablation of the V0v commissural interneurons eliminated expression of the trot, but the walk was still present (Bellardita and Kiehn, 2015). The cycle frequency of the trot was faster than that of the walk (Bellardita and Kiehn, 2015). Thus, the findings indicate that $V0_V$ commissural interneurons play a role in the left-right alternation during the high-frequency cycle of the locomotion. In contrast, ablation of the inhibitory $V0_D$ interneurons eliminated the left-right alternation at low-frequency cycle of the locomotion, but maintained it at high-frequency cycle of the locomotion (Talpalar et al., 2013). Thus, the inhibitory $V0_D$ interneurons play a role in the low-left-right coordination of the low-frequency locomotion.

The pathways mediating the alternate activity of the half centers during locomotion have been proposed by a computational model (Rybak et al., 2015; Danner et al., 2017). On the one hand, inhibitory $V0_D$ interneurons receive exaction from the ipsilateral flexor centers and inhibit the contralateral flexor half center (**Figure 1A**). On the other hand, $V0_V$ commissural interneurons are involved in two possible connections. One is that the excitatory V2a interneurons receive excitation from the ipsilateral flexor center and excite $V0_V$ interneurons but inhibit contralateral flexor half center through the inhibitory interneurons (**Figure 1B**). Another is that the excitatory V2a interneurons receive excitation from the ipsilateral extensor half center and excite $V0_V$ interneurons, and then, $V0_V$ interneurons excite the contralateral flexor half center (**Figure 1C**). Taken together, crossed inhibition mediated by the V0 commissural interneurons plays a role in the crossed inhibition mediating the left-right alternate activity of the half centers.

Crossed Inhibition During Unilateral Movement

According to the discussion above, the alternate activity of the left and right CPGs is likely mediated by crossed inhibition between the CPGs; activity of the half center on one side inhibits the contralateral half center. Crossed inhibition induced by the activity of the CPG in one leg has been examined by observing

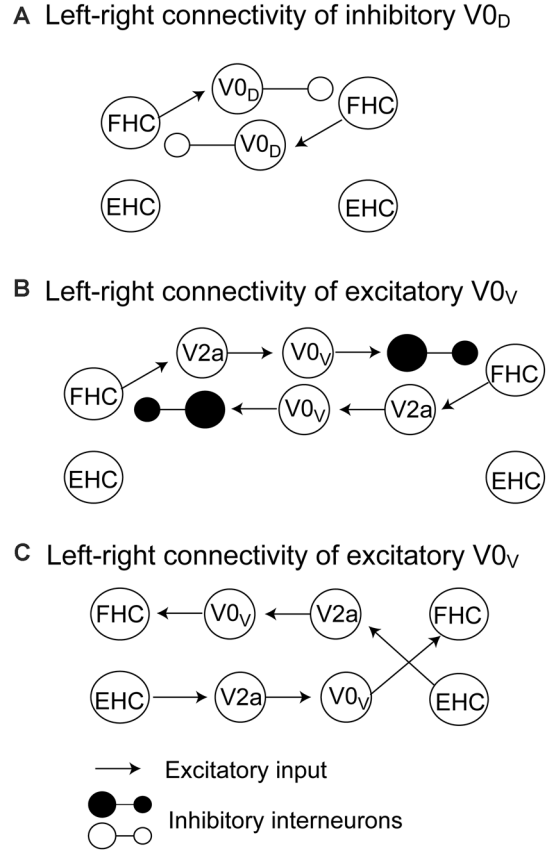

FIGURE 1 | The pathways mediating crossed inhibition between the left and right half centers proposed by Rybak et al. (2015) and Danner et al. (2017). The crossed inhibitory pathway involving $V0_D$ commissural interneurons is shown in panel **(A)**. The crossed inhibitory pathways involving $V0_V$ commissural interneurons are shown in panels **(B)** and **(C)**. The detailed explanation is presented in the text. FHC, flexor half center; EHC, extensor half center.

the effect of the rhythmic movement of one leg on the soleus H-reflex in the contralateral leg at rest in humans. The soleus H-reflex at rest was suppressed by the contralateral leg cycling in the flexion phase and the end of the extension phase (McIllroy et al., 1992). In another study by Mori and colleagues, active rhythmic movement of the ankle caused tonic suppression of the contralateral soleus H-reflex at rest throughout the whole movement phases (Mori et al., 2015). Those findings indicate that the unilateral activation of the CPG on one leg side induces suppression of the H-reflex pathway in the contralateral ankle extensor.

However, those previous findings on the unilateral rhythmic movement are not direct evidences indicating the mechanism underlying the coordination of the leg movements during the anti-phase bilateral rhythmic movement during which both left and right half centers are alternately activated. In addition, we have to note supraspinal influence on crossed inhibition during unilateral movement. Unimanual activation of one finger muscle increases interhemispheric inhibition from the active hemisphere to the resting hemisphere (Vercauteren et al., 2008). This interhemispheric inhibition is to prevent unwanted motor output of the limb at rest (mirror activity) during the activity of the contralateral limb (Vercauteren et al., 2008). Such interhemispheric inhibition may be a possible mechanism underlying the unilateral rhythmic movement-induced suppression of the contralateral soleus H-reflex.

Crossed Afferent Inhibition

In humans, one important neural event indicating the existence of the inhibitory pathways crossing the midline of the spinal cord is crossed afferent inhibition. The soleus H-reflex in the leg at rest was suppressed by the conditioning stimulation of the tibial nerve in the contralateral leg given 3–33 ms after the test stimulus (Stubbs et al., 2011a). This finding indicates that the activation of the pathways crossing the midline of the spinal cord induced by the afferent input suppresses the contralateral soleus H-reflex pathway. The central delay of this crossed inhibition was 3 ms, indicating that crossed inhibition is mediated by the crossed pathway in the spinal cord, and the commissural interneurons are likely involved in this process (Hanna-Boutros et al., 2014). Moreover, crossed inhibition was modulated by transcranial magnetic stimulation over the primary motor cortex, indicating that the pathways mediating the crossed afferent inhibition receive descending input (Hanna-Boutros et al., 2014).

Soleus H-reflex amplitude is suppressed by the contralateral cutaneous stimulation of the dorsum of the foot in the early stance phase of gait (Suzuki et al., 2014). The late stance phase of the soleus muscle activity is inhibited by electrical stimulation to the contralateral leg in the late phase of the swing leg (Stubbs et al., 2011b). Group II crossed afferent inhibition was reduced especially in the stance phase of the gait cycle (Hanna-Boutros et al., 2014). Those findings indicate that the crossed afferent inhibition is phase-dependently modulated during gait.

Such crossed afferent inhibition is possible to be induced by passive movement of the contralateral leg. For example, passive rhythmic movement of one leg suppressed the contralateral soleus H-reflex at rest (McIllroy et al., 1992; Collins et al., 1993; Cheng et al., 1998; Misiaszek et al., 1998). Either in-phase or anti-phase rhythmic passive movement of both hips or unilateral rhythmic passive movement of the hip contralateral to the tested side suppressed the soleus H-reflex (Stanislaus et al., 2010). During passive movement, the descending motor drive is absent, but the somatosensation induced by the movement is present. Thus, suppression of the soleus H-reflex induced by the passive movement of the contralateral leg is likely mediated by the afferent discharge induced by the somatosensation. This means that the suppression of the soleus H-reflex induced by the passive rhythmic movement of the contralateral leg reflects the crossed afferent inhibition.

Based on those findings, the activity of one half center is inhibited not only by the active rhythmic movement of the contralateral leg, but also by the passive rhythmic movement of that. The somatosensation is induced, but the CPG is inactive during passive movement. It has been stated that the CPG is capable of reorganizing the sensory input to reconfigure itself to evoke the appropriate pattern (Frigon, 2012). Accordingly, one hypothetical explanation for the crossed afferent inhibition

is that the activity of the CPG in one leg side induces afferent discharge, and this inhibits the contralateral half center. One previous finding against this hypothesis is that the interlimb coordination of the air stepping in cats was not changed by sensory perturbations (Giuliani and Smith, 1985). In future studies, the hypothesis must be tested in humans. Investigation of the crossed inhibition without somatosensation may be possible if one uses ischemic nerve block (Hayashi et al., 2019) or local anesthesia. Further studies on the patients with diabetic polyneuropathy in which the proprioception is selectively impaired (Bloem et al., 2000) may also be a nice idea for investigating crossed inhibition without somatosensation.

Crossed Inhibition During Bilateral Movement

As discussed above, crossed inhibition of the contralateral CPG is a possible mechanism underlying the anti-phase bilateral rhythmic movement. Crossed inhibition is supposed to be achieved through mutual inhibition between the extensor half centers, between the flexor half centers, or between the extensor half center and contralateral flexor half center (see "Crossed Pathways" section and **Figure 1**). As shown in **Figure 2A**, Dietz (2002) hypothesized that the neural circuits coordinating the leg flexor activity of both sides during the swing phase of locomotion (i.e., flexor half center) mutually inhibit one another (Dietz, 2002). By contrast, the extensor half-centers on each side have no crossed inhibitory connections, agreeing with the coexistence of the stance phase on the two sides.

This hypothesis by Dietz was supported by a previous finding on the split-treadmill gait (Yang et al., 2005). When infants walk on the split-belt treadmill with different speeds of belts under the legs, coactivation of the left and right extensors was greater than that of the left and right flexors. Accordingly, the authors of this study speculated that the mutual inhibition between the left and right flexor half centers is greater, compared to the extensor half centers. Moreover, the hypothesis by Dietz is in line with the computational model of the $V0_D$ commissure interneurons proposed by Rybak et al. and Danner et al. (Rybak et al., 2015; Danner et al., 2017; see "Crossed Pathways" section and **Figure 1** in the present review), shown in **Figure 1A**. In contrast, short-latency crossed inhibitory response, followed by the long-latency excitatory response, on the extensors was observed in the stance phase during locomotion in cat (Frigon and Rossignol, 2008). This indicates that the extensor half center in the stance phase side of the limb receives crossed inhibition from the contralateral flexor half center during locomotion (**Figure 2B**). This finding conflicts with the hypothesis by Dietz.

Phase-Dependent Crossed Inhibition During Bilateral Movement

In human experiments, crossed inhibition of the CPG during activity of the contralateral CPG has been examined by comparing the motor output between the unilateral and bilateral rhythmic movements. For example, peak power during unilateral cycling was greater than that during the anti-phase bilateral cycling (Dunstheimer et al., 2001). This finding indicates that the activity level of the rhythmically moving one leg is less when the contralateral side moves rhythmically with an anti-phase fashion.

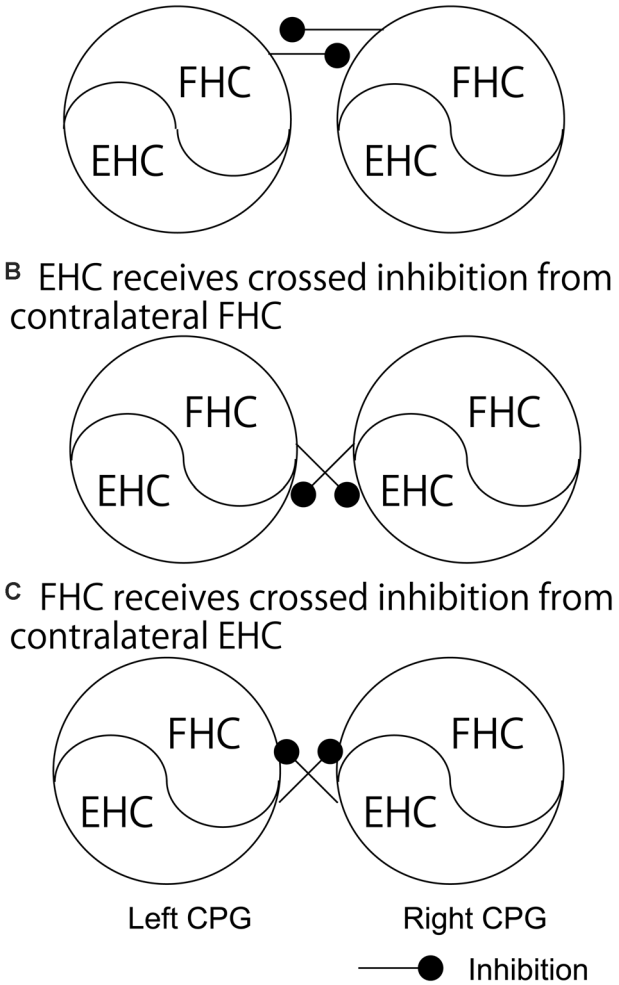

FIGURE 2 | The pathways regarding the phase-dependent crossed inhibition between the left and right half centers. A model proposed by Dietz **(A)**, a model indicated by the finding in the study by Frigon and colleagues **(B)**, and a model proposed by Ting and colleagues **(C)** are shown. Those pathways are discussed in the text. FHC, flexor half center; EHC, extensor half center.

Previous findings on the phase-dependent inhibition of the rhythmically moving one leg induced by the rhythmic movement of the contralateral leg were not in line with the hypothesis proposed by Dietz. For example, during bilateral anti-phase cycling, the activity of the tibialis anterior, biceps femoris, and rectus femoris muscles in the flexion phase was less than that during the unilateral cycling of the tested leg (Ting et al., 1998). This finding indicates that the activation of the extensors in the extension phase of one leg decreases the activity of the contralateral leg muscles in the flexion phase in which the flexor half center is active. Based on this finding, Ting and colleagues hypothesized that the activity of the extensor half center inhibits the activity of the contralateral

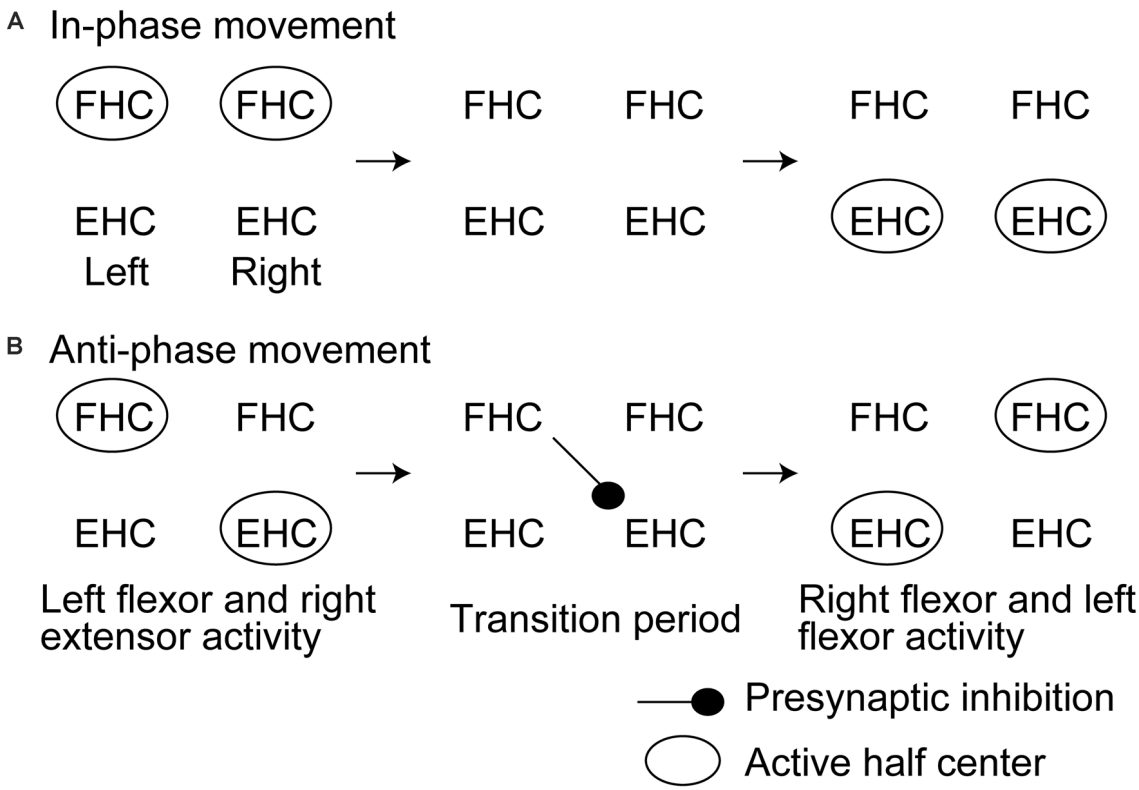

FIGURE 3 | Hypothesized time course of the half center activities and crossed inhibition during in-phase **(A)** and anti-phase bilateral rhythmic ankle movement **(B)** proposed by Hiraoka and colleagues. This model is discussed in the text. FHC, flexor half center; EHC, extensor half center.

flexor half center (**Figure 2C**). This view is in line with the proposed model regarding crossed inhibition mediated by $V0_V$ commissural interneurons (**Figure 1C**). However, this view may not be applicable for the explanation of the anti-phase bilateral coordination. That is, the activation of the extensor half center inhibits the contralateral flexor half center which is active at this moment during the anti-phase bilateral movement based on this view, but this is not functionally meaningful for the anti-phase bilateral movement.

Another previous study had tested the soleus H-reflex of the rhythmically moving ankle with and without rhythmic movement of the contralateral ankle (Hiraoka et al., 2014). The soleus H-reflex during the anti-phase bilateral ankle movement at the period switching the movement from the extension to the flexion of the tested ankle while switching the contralateral ankle movement from the flexion to the extension was smaller than that at the same period of the tested ankle during the unilateral movement of the tested ankle. This finding supports a view that crossed inhibition of the extensor half center is produced at the period switching the activity from the extensor to flexor half center while the contralateral side is at the period switching the activity from the flexor to extensor half center (**Figure 3**). A previous study reported that the activity of the bifunctional thigh muscle increased at the transition period between the extension and flexion of bilateral anti-phase cycling (Kautz et al., 2002). The authors of this previous study speculated that the mutual modulation of the left and right motor systems in the legs is produced at the switching phase between the flexion and extension to ensure the smooth switching of the flexor and extensor half center activity. The finding by Hiraoka and colleagues mentioned above supports this view.

A previous study reported that the soleus H-reflex during bilateral leg cycling was not significantly different from that during the unilateral cycling of the leg contralateral to the tested side (McIllroy et al., 1992). This finding was inconsistent with the previous finding by Hiraoka and colleagues. In the study by McIlroy and colleagues, both ankles were fixed, but the hip and knee were moved during the cycling movement. In contrast, in the study by Hiraoka and colleagues, the ankle, in which the soleus muscle was the prime mover of the extension movement, was actively moved. Based on this, those conflicting findings indicate that crossed inhibition targeting the different segmental levels of the spinal cord is different from the inhibition targeting the same segmental level of the spinal cord. Accordingly, phase-dependent suppression of the soleus H-reflex during the anti-phase bilateral movement of the ankles observed in the study by Hiraoka and colleagues is well explained by a view that crossed inhibition of the soleus H-reflex during the anti-phase bilateral movement occurs within the intrasegmental level of the spinal cord.

An important finding in the previous study by Hiraoka and colleagues is that such phase-dependent inhibition was not present during the in-phase movement of the ankles. This finding suggests that crossed inhibition during the switching period of bilateral rhythmic movement is particularly present during the anti-phase bilateral movement. It has been suggested that the control process of the in-phase bilateral movement of the hands is different from that of the anti-phase movement (Shih et al., 2019). As shown in previous studies on the aquatic vertebrates, the population of the pathways crossing the midline of the spine to mediating the synchronous motor activity of the left and right motor systems is different from that mediating the alternate motor output of those (Butt et al., 2002). There is a hypothetical view that the inhibitory commissural interneurons are active during the alternate activity of the left and right motor systems during walking whereas the excitatory commissural interneurons are active during the synchronous activity of those during galloping or hopping (Kiehn, 2006). More recently, it has been reported that crossed inhibition between the left and right half centers mediated by V0 or V2a commissural interneurons particularly contributes to the left-right alternation of the motor output during locomotion in animals (Crone et al., 2009; Talpalar et al., 2013; Bellardita and Kiehn, 2015). According to those previous findings, phase-dependent crossed inhibition particularly during the anti-phase bilateral movement observed in the study by Hiraoka and colleagues may reflect a fact that crossed inhibition is mediated by such class-specific activity of the commissural interneurons.

Presynaptic Origin of Crossed Inhibition

Because pre-stimulus background muscle activity level was equivalent between the conditions in this previous study by Hiraoka and colleagues, suppression of the soleus H-reflex during bilateral rhythmic movement observed is likely presynaptic origin. In humans, rhythmic leg activation during gait was greatly controlled by presynaptic inhibition (Stein and Capaday, 1988; Stein, 1995). The force at the toe contact of the stance phase influenced the presynaptic inhibition of the contralateral limb during locomotion in rat (Hayes et al., 2012). Crossed inhibition during locomotion was induced without change in the electromyographic activity, indicating that crossed inhibition is presynaptic origin (Suzuki et al., 2014). Those previous findings indirectly support a view that crossed inhibition at the switching period of the extensor and flexor half center activities during the anti-phase bilateral movement observed in the previous study by Hiraoka and colleagues is mediated by the presynaptic inhibition. Some commissural interneurons directly project to the contralateral motoneurons, but others provide indirect influence on the motoneurons through the inhibitory interneurons (Kiehn et al., 2010). The presynaptic origin of the phase-dependent crossed inhibition found in the study by Hiraoka and colleagues may be related to this indirect influence mediated by the pathway that involves the commissural interneurons.

The conflict between the finding by Hiraoka and colleagues and the finding by Ting and colleagues may be due to the difference in the measurement of the motor status. The experiment by Ting and colleagues observed the EMG and force. Thus, the finding indicates the direct inhibition of the motoneurons causing the decrease in the motor output. In contrast, the experiment by Hiraoka and colleagues observed the suppression of the H-reflex with equal EMG activity. Thus, the finding in the study by Hiraoka and colleagues indicates the inhibition of the excitatory synaptic transmission to the motoneurons. This process is not direct inhibition of the motoneurons, and thus, does not indicate the change in the motor output. Such difference may be related to the conflicting findings between the studies.

Remained Issues on Phase-Dependent Crossed Inhibition

In the studies on bilateral coordination in humans, as introduced in the present study, actual locomotion is not performed; pedaling movement (Ting et al., 1998) or ankle movement (Hiraoka et al., 2014) was performed. Thus, the findings in those studies are not direct evidences indicating crossed inhibition during locomotion. In future studies, crossed inhibition during actual locomotion (i.e., gait) must be tested. Studies using a split-belt treadmill, as investigated to observe the CPGs in previous studies (Dietz et al., 1994; Prokop et al., 1995; Yang et al., 2005; Choi and Bastian, 2007), might be useful to investigate this issue. Another issue that remains to be investigated is whether such crossed inhibition actually contributes to bilateral coordination. The decrease in the EMG activity, force, or H-reflex excitability does not indicate the change in bilateral coordination. Coordination of the two limbs has been studied through observing stability, accuracy, or transition of the relative phase between the two-limb movements (Kelso and Schöner, 1988; Abe et al., 2003; Asai et al., 2003; Nomura et al., 2016). Such measurements are the direct evidence indicating bilateral coordination. Thus, further studies observing those measurements with testing crossed inhibition must be conducted to test a view that crossed inhibition contributes to bilateral coordination in humans.

Descending Motor Drive

The mesencephalic locomotor region and the lateral hypothalamus project to the reticulospinal neurons, and those neurons project to the spinal cord for activating the CPGs (Jordan et al., 2008; Frigon, 2012). Accordingly, the CPGs are under the control of the descending pathways. At least in the upper extremities, the supraspinal pathways crossing the midline are likely involved in bilateral coordination (Carson, 2005). Selective ablation of the descending spinal neurons perturbed interlimb coordination during high-speed stepping in mice (Ruder et al., 2016). In patients with Parkinson's disease, bilateral coordination was impaired (Abe et al., 2003; Asai et al., 2003). Crossed inhibition was modulated by transcranial magnetic stimulation over the primary motor cortex (Hanna-Boutros et al., 2014). Based on those previous findings, supraspinal descending motor drive is not ruled out from the mechanism underlying the left-right coordination of the rhythmic bilateral movement. To rule out the possible effect of the supraspinal descending motor drive on bilateral coordination, further studies

on the patients with complete spinal cord injury, as investigated previously for observing the activity of the CPG in humans (Dimitrijevic et al., 1998), are needed.

CONCLUSIONS

In this article, previous studies on the phase-dependent crossed inhibition underlying the anti-phase coordination of the rhythmic movement of the legs were reviewed. V0 commissural interneurons mediating crossed inhibition of the contralateral half center likely contribute to the alternate activity of the left and right CPGs. Crossed inhibition of the contralateral leg motor system has been reported in previous studies in humans. Accordingly, alternate activity between the left and right CPGs may be coordinated by crossed inhibition of the spinal cord in humans. On the one hand, a previous finding suggested that the flexor half center is inhibited during the activity of the contralateral extensor half center. On the other hand, another recent study indicated that the extensor half center is inhibited at the period switching the activity from the extensor to flexor half center while the contralateral limb is at the period switching the activity from the flexor to extensor half center. Future studies are needed for further insight into those findings.

AUTHOR CONTRIBUTIONS

KH wrote this article.

REFERENCES

Abe, K., Asai, Y., Matsuo, Y., Nomura, T., Sato, S., Inoue, S., et al. (2003). Classifying lower limb dynamics in Parkinson's disease. *Brain Res. Bull.* 61, 219–226. doi: 10.1016/s0361-9230(03)00119-9

Asai, Y., Nomura, T., Abe, K., Matsuo, Y., and Sato, S. (2003). Classification of dynamics of a model of motor coordination and comparison with Parkinson's disease data. *Biosystems* 71, 11–21. doi: 10.1016/s0303-2647(03)00105-9

Bellardita, C., and Kiehn, O. (2015). Phenotypic characterization of speed-associated gait changes in mice reveals modular organization of locomotor networks. *Curr. Biol.* 25, 1426–1436. doi: 10.1016/j.cub.2015.04.005

Bloem, B. R., Allum, J. H. J., Carpenter, M. G., and Honegger, F. (2000). Is lower leg proprioception essential for triggering human automatic postural responses? *Exp. Brain Res.* 130, 375–391. doi: 10.1007/s002219900259

Brown, T. G. (1911). The intrinsic factors in the act of progression in the mammal. *Proc. R. Soc. Lond. B* 84, 308–319. doi: 10.1098/rspb.1911.0077

Brown, T. G. (1914). On the nature of the fundamental activity of the nervous centres; together with an analysis of the conditioning of rhythmic activity in progression and a theory of the evolution of function in the nervous system. *J. Physiol.* 48, 18–46. doi: 10.1113/jphysiol.1914.sp001646

Butt, S. J., Lebret, J. M., and Kiehn, O. (2002). Organization of left-right coordination in the mammalian locomotor network. *Brain Res. Rev.* 40, 107–117. doi: 10.1016/s0165-0173(02)00194-7

Carson, R. G. (2005). Neural pathways mediating bilateral interactions between the upper limbs. *Brain Res. Rev.* 49, 641–662. doi: 10.1016/j.brainresrev.2005.03.005

Cheng, J., Brooke, J. D., Misiaszek, J. E., and Staines, W. R. (1998). Crossed inhibition of the soleus H reflex during passive pedalling movement. *Brain Res.* 779, 280–284. doi: 10.1016/s0006-8993(97)01168-2

Choi, J. T., and Bastian, A. J. (2007). Adaptation reveals independent control networks for human walking. *Nat. Neurosci.* 10, 1055–1062. doi: 10.1038/nn1930

Collins, D. F., McIlroy, W. E., and Brooke, J. D. (1993). Contralateral inhibition of soleus H reflexes with different velocities of passive movement of the opposite leg. *Brain Res.* 603, 96–101. doi: 10.1016/0006-8993(93)91303-a

Crone, S. A., Zhong, G., Harris-Warrick, R., and Sharma, K. (2009). In mice lacking V2a interneurons, gait depends on speed of locomotion. *J. Neurosci.* 29, 7098–7109. doi: 10.1523/JNEUROSCI.1206-09.2009

Danner, S. M., Shevtsova, N. A., Frigon, A., and Rybak, I. A. (2017). Computational modeling of spinal circuits controlling limb coordination and gaits in quadrupeds. *Elife* 6:e31050. doi: 10.7554/eLife.31050

Dietz, V. (2002). Do human bipeds use quadrupedal coordination? *Trends Neurosci.* 25, 462–467. doi: 10.1016/s0166-2236(02)02229-4

Dietz, V., Zijlstra, W., and Duysens, J. (1994). Human neuronal interlimb coordination during split-belt locomotion. *Exp. Brain Res.* 101, 513–520. doi: 10.1007/BF00227344

Dimitrijevic, M. R., Gerasimenko, Y., and Pinter, M. M. (1998). Evidence for a spinal central pattern generator in humans. *Ann. N Y Acad. Sci.* 860, 360–376. doi: 10.1111/j.1749-6632.1998.tb09062.x

Dunstheimer, D., Hebestreit, H., Staschen, B., Straßburg, H., and Jeschke, R. (2001). Bilateral deficit during short-term, high-intensity cycle ergometry in girls and boys. *Eur. J. Appl. Physiol.* 84, 557–561. doi: 10.1007/s004210100406

Frigon, A. (2012). Central pattern generators of the mammalian spinal cord. *Neuroscientist* 18, 56–69. doi: 10.1177/1073858410396101

Frigon, A., and Rossignol, S. (2008). Short-latency crossed inhibitory responses in extensor muscles during locomotion in the cat. *J. Neurophysiol.* 99, 989–998. doi: 10.1152/jn.01274.2007

Giuliani, C. A., and Smith, J. L. (1985). Development and characteristics of airstepping in chronic spinal cats. *J. Neurosci.* 5, 1276–1282. doi: 10.1523/JNEUROSCI.05-05-01276.1985

Goulding, M. (2009). Circuits controlling vertebrate locomotion: moving in a new direction. *Nat. Rev. Neurosci.* 10, 507–518. doi: 10.1038/nrn2608

Guertin, P. A. (2009). The mammalian central pattern generator for locomotion. *Brain Res. Rev.* 62, 45–56. doi: 10.1016/j.brainresrev.2009.08.002

Hanna-Boutros, B., Sangari, S., Karasu, A., Giboin, L.-S., and Marchand-Pauvert, V. (2014). Task-related modulation of crossed spinal inhibition between human lower limbs. *J. Neurophysiol.* 111, 1865–1876. doi: 10.1152/jn.00838.2013

Hayashi, R., Ogata, K., Nakazono, H., and Tobimatsu, S. (2019). Modified ischaemic nerve block of the forearm: use for the induction of cortical plasticity in distal hand muscles. *J. Physiol.* 597, 3457–3471. doi: 10.1113/JP277639

Hayes, H. B., Chang, Y.-H., and Hochman, S. (2012). Stance-phase force on the opposite limb dictates swing-phase afferent presynaptic inhibition during locomotion. *J. Neurophysiol.* 107, 3168–3180. doi: 10.1152/jn.01134.2011

Hiraoka, K., Chujyo, Y., Hatano, S., Fukuhara, K., and Yamanaka, Y. (2014). Effects of contralateral movement on the soleus H-reflex during in-phase and antiphase movements of the ankles. *Motor Control* 18, 88–100. doi: 10.1123/mc.2013-0029

Jordan, L. M., Liu, J., Hedlund, P. B., Akay, T., and Pearson, K. G. (2008). Descending command systems for the initiation of locomotion in mammals. *Brain Res. Rev.* 57, 183–191. doi: 10.1016/j.brainresrev.2007.07.019

Kautz, S. A., Brown, D. A., Van der Loos, H. F. M., and Zajac, F. E. (2002). Mutability of bifunctional thigh muscle activity in pedaling due to contralateral leg force generation. *J. Neurophysiol.* 88, 1308–1317. doi: 10.1152/jn.2002.88.3.1308

Kelso, J. S., and Schöner, G. (1988). Self-organization of coordinative movement patterns. *Hum. Mov. Sci.* 7, 27–46. doi: 10.1016/0167-9457(88)90003-6

Kiehn, O. (2006). Locomotor circuits in the mammalian spinal cord. *Ann. Rev. Neurosci.* 29, 279–306. doi: 10.1146/annurev.neuro.29.051605.112910

Kiehn, O., Dougherty, K. J., Hägglund, M., Borgius, L., Talpalar, A., and Restrepo, C. E. (2010). Probing spinal circuits controlling walking in mammals. *Biochem. Biophys. Res. Commun.* 396, 11–18. doi: 10.1016/j.bbrc.2010.02.107

Kjaerulff, O., and Kiehn, O. (1996). Distribution of networks generating and coordinating locomotor activity in the neonatal rat spinal cord *in vitro*: a lesion study. *J. Neurosci.* 16, 5777–5794. doi: 10.1523/JNEUROSCI.16-18-05777.1996

Kjaerulff, O., and Kiehn, O. (1997). Crossed rhythmic synaptic input to motoneurons during selective activation of the contralateral spinal locomotor network. *J. Neurosci.* 17, 9433–9447. doi: 10.1523/JNEUROSCI.17-24-09433.1997

Kudo, N., and Yamada, T. (1987). N-Methyl-d, l-aspartate-induced locomotor activity in a spinal cord-indlimb muscles preparation of the newborn rat studied *in vitro*. *Neurosci. Lett.* 75, 43–48. doi: 10.1016/0304-3940(87)90072-3

McCrea, D. A., and Rybak, I. A. (2008). Organization of mammalian locomotor rhythm and pattern generation. *Brain Res. Rev.* 57, 134–146. doi: 10.1016/j.brainresrev.2007.08.006

McIllroy, W. E., Collins, D. F., and Brooke, J. D. (1992). Movement features and H-reflex modulation. II. Passive rotation, movement velocity and single leg movement. *Brain Res.* 582, 85–93. doi: 10.1016/0006-8993(92)90320-9

Misiaszek, J. E., Cheng, J., Brooke, J. D., and Staines, W. R. (1998). Movement-induced modulation of soleus H reflexes with altered length of biarticular muscles. *Brain Res.* 795, 25–36. doi: 10.1016/s0006-8993(98)00246-7

Mori, N., Horino, H., Matsugi, A., Kamata, N., and Hiraoka, K. (2015). Tonic suppression of the soleus H-reflex during rhythmic movement of the contralateral ankle. *J. Phys. Ther. Sci.* 27, 1287–1290. doi: 10.1589/jpts.27.1287

Nomura, Y., Jono, Y., Tani, K., Chujo, Y., and Hiraoka, K. (2016). Corticospinal modulations during bimanual movement with different relative phases. *Front. Hum. Neurosci.* 10:95. doi: 10.3389/fnhum.2016.00095

Perry, J. (1992). *Gait Analysis: Normal and Pathological Function.* Thorofare, NJ: Slack, Inc.

Prokop, T., Berger, W., Zijlstra, W., and Dietz, V. (1995). Adaptational and learning processes during human split-belt locomotion: interaction between central mechanisms and afferent input. *Exp. Brain Res.* 106, 449–456. doi: 10.1007/BF00231067

Ruder, L., Takeoka, A., and Arber, S. (2016). Long-distance descending spinal neurons ensure quadrupedal locomotor stability. *Neuron* 92, 1063–1078. doi: 10.1016/j.neuron.2016.10.032

Rybak, I. A., Dougherty, K. J., and Shevtsova, N. A. (2015). Organization of the mammalian locomotor CPG: review of computational model and circuit architectures based on genetically identified spinal interneurons. *eNeuro* 2:ENEURO.0069-15.2015. doi: 10.1523/ENEURO.0069-15.2015

Shih, P. C., Steele, C. J., Nikulin, V., Villringer, A., and Sehm, B. (2019). Kinematic profiles suggest differential control processes involved in bilateral in-phase and anti-phase movements. *Sci. Rep.* 9:3273. doi: 10.1038/s41598-019-40295-1

Stanislaus, V., Mummidisetty, C. K., and Knikou, M. (2010). Soleus H-reflex graded depression by contralateral hip afferent feedback in humans. *Brain Res.* 1310, 77–86. doi: 10.1016/j.brainres.2009.11.013

Stein, R. B. (1995). Presynaptic inhibition in humans. *Prog. Neurobiol.* 47, 533–544. doi: 10.1016/0301-0082(95)00036-4

Stein, R. B., and Capaday, C. (1988). The modulation of human reflexes during functional motor tasks. *Trends Neurosci.* 11, 328–332. doi: 10.1016/0166-2236(88)90097-5

Stubbs, P. W., and Mrachacz-Kersting, N. (2009). Short-latency crossed inhibitory responses in the human soleus muscle. *J. Neurophysiol.* 102, 3596–3605. doi: 10.1152/jn.00667.2009

Stubbs, P. W., Nielsen, J. F., Sinkjær, T., and Mrachacz-Kersting, N. (2011a). Crossed spinal soleus muscle communication demonstrated by H-reflex conditioning. *Muscle Nerve* 43, 845–850. doi: 10.1002/mus.21964

Stubbs, P. W., Nielsen, J. F., Sinkjær, T., and Mrachacz-Kersting, N. (2011b). Phase modulation of the short-latency crossed spinal response in the human soleus muscle. *J. Neurophysiol.* 105, 503–511. doi: 10.1152/jn.00786.2010

Suzuki, S., Nakajima, T., Mezzarane, R. A., Ohtsuka, H., Futatsubashi, G., and Komiyama, T. (2014). Differential regulation of crossed cutaneous effects on the soleus H-reflex during standing and walking in humans. *Exp. Brain Res.* 232, 3069–3078. doi: 10.1007/s00221-014-3953-6

Talpalar, A. E., Bouvier, J., Borgius, L., Fortin, G., Pierani, A., and Kiehn, O. (2013). Dual-mode operation of neuronal networks involved in left-right alternation. *Nature* 500, 85–88. doi: 10.1038/nature12286

Ting, L. H., Raasch, C. C., Brown, D. A., Kautz, S. A., and Zajac, F. E. (1998). Sensorimotor state of the contralateral leg affects ipsilateral muscle coordination of pedaling. *J. Neurophysiol.* 80, 1341–1351. doi: 10.1152/jn.1998.80.3.1341

Vercauteren, K., Pleysier, T., Van Belle, L., Swinnen, S. P., and Wenderoth, N. (2008). Unimanual muscle activation increases interhemispheric inhibition from the active to the resting hemisphere. *Neurosci. Lett.* 445, 209–213. doi: 10.1016/j.neulet.2008.09.013

Yang, J. F., Lamont, E. V., and Pang, M. Y. (2005). Split-belt treadmill stepping in infants suggests autonomous pattern generators for the left and right leg in humans. *J. Neurosci.* 25, 6869–6876. doi: 10.1523/JNEUROSCI.1765-05.2005

Conflict of Interest: The author declares that the research was conducted in the absence of any commercial or financial relationships that could be construed as a potential conflict of interest.

frontiers in Human Neuroscience

CASE REPORT
published: 03 June 2021
doi: 10.3389/fnhum.2021.659415

Early Development of Locomotor Patterns and Motor Control in Very Young Children at High Risk of Cerebral Palsy, a Longitudinal Case Series

Annike Bekius[1,2], Margit M. Bach[1], Laura A. van de Pol[3], Jaap Harlaar[2,4], Andreas Daffertshofer[1], Nadia Dominici[1†] and Annemieke I. Buizer[2,5†]*

[1] Department of Human Movement Sciences, Faculty of Behavioural and Movement Sciences, Amsterdam Movement Sciences & Institute for Brain and Behavior Amsterdam, Vrije Universiteit Amsterdam, Amsterdam, Netherlands, [2] Department of Rehabilitation Medicine, Amsterdam Movement Sciences, Amsterdam Universitair Medisch Centrum, Vrije Universiteit Amsterdam, Amsterdam, Netherlands, [3] Department of Pediatric Neurology, Amsterdam Universitair Medisch Centrum, Vrije Universiteit Amsterdam, Amsterdam, Netherlands, [4] Department of Biomechanical Engineering, Delft University of Technology, Delft, Netherlands, [5] Emma Children's Hospital, Amsterdam Universitair Medisch Centrum, Vrije Universiteit Amsterdam, Amsterdam, Netherlands

OPEN ACCESS

Edited by:
William C. Gaetz, Children's Hospital of Philadelphia, United States

Reviewed by:
Laura Prosser, Children's Hospital of Philadelphia, United States
Christos Papadelis, Cook Children's Medical Center, United States

***Correspondence:**
Nadia Dominici
n.dominici@vu.nl

† These authors have contributed equally to this work

Specialty section:
This article was submitted to Motor Neuroscience, a section of the journal Frontiers in Human Neuroscience

Received: *27 January 2021*
Accepted: *16 April 2021*
Published: *03 June 2021*

Citation:
Bekius A, Bach MM, van de Pol LA, Harlaar J, Daffertshofer A, Dominici N and Buizer AI (2021) Early Development of Locomotor Patterns and Motor Control in Very Young Children at High Risk of Cerebral Palsy, a Longitudinal Case Series. Front. Hum. Neurosci. 15:659415. doi: 10.3389/fnhum.2021.659415

The first years of life might be critical for encouraging independent walking in children with cerebral palsy (CP). We sought to identify mechanisms that may underlie the impaired development of walking in three young children with early brain lesions, at high risk of CP, via comprehensive instrumented longitudinal assessments of locomotor patterns and muscle activation during walking. We followed three children (P1–P3) with early brain lesions, at high risk of CP, during five consecutive gait analysis sessions covering a period of 1 to 2 years, starting before the onset of independent walking, and including the session during the first independent steps. In the course of the study, P1 did not develop CP, P2 was diagnosed with unilateral and P3 with bilateral CP. We monitored the early development of locomotor patterns over time via spatiotemporal gait parameters, intersegmental coordination (estimated via principal component analysis), electromyography activity, and muscle synergies (determined from 11 bilateral muscles via nonnegative matrix factorization). P1 and P2 started to walk independently at the corrected age of 14 and 22 months, respectively. In both of them, spatiotemporal gait parameters, intersegmental coordination, muscle activation patterns, and muscle synergy structure changed from supported to independent walking, although to a lesser extent when unilateral CP was diagnosed (P2), especially for the most affected leg. The child with bilateral CP (P3) did not develop independent walking, and all the parameters did not change over time. Our exploratory longitudinal study revealed differences in maturation of locomotor patterns between children with divergent developmental trajectories. We succeeded in identifying mechanisms that may underlie impaired walking development in very young children at high risk of CP. When verified in larger sample sizes, our approach may be considered a means to improve prognosis and to pinpoint possible targets for early intervention.

Keywords: development of walking, early brain lesions, electromyography, muscle synergies, intersegmental coordination

INTRODUCTION

Cerebral palsy (CP) is a neurodevelopmental disorder caused by non-progressive brain lesions before birth or in the first year of life (Himmelmann and Uvebrant, 2018). The distribution of CP can be unilateral or bilateral, depending on the site of the brain lesion. CP covers a wide clinical spectrum of mobility levels, varying from walking independently to being completely wheelchair dependent. Functional mobility in CP is classified using the Gross Motor Function Classification System (GMFCS) (Palisano et al., 1997). The levels of the GMFCS range from I to V, with children at level I and II ultimately walking without aids and children at level III needing a walking aid. Children at levels IV and V (primarily) use a wheelchair for their mobility.

Walking is the most important mode of locomotion in everyday life. Typically developing (TD) children take their first independent steps (FS) between the age of 9 and 18 months, but this milestone is often delayed or not achieved in children with CP. Developmental stages of locomotion usually occur at a later age in children with CP compared to TD children (Largo et al., 1985; Meyns et al., 2012). The maturation of walking patterns is reflected in both kinematic and neuromuscular measures (Dewolf et al., 2020). Understanding the mechanisms that underlie abnormal development of independent walking (IW) is important for the design of early interventions that aim at improving function mobility in children with CP.

Older children with CP appear to retain some of the characteristics of the younger TD children during the early phases of the development of walking (Berger et al., 1984; Leonard et al., 1991). In TD children, the foot trajectory during swing (the time course of the vertical foot displacements) develops starting from a prominent centered single-peak foot lift in toddlers to the stereotyped double-peaked trajectory with a minimum foot clearance during midswing in older children and healthy adults (Dominici et al., 2007). Indeed, the mature two-peaked foot trajectory reflects the accurate endpoint control strategy that is the result of the intersegmental coordination in both limbs (Winter, 1992; Ivanenko et al., 2002). By contrast, in children with CP, a single-peak foot lift similar to TD toddlers may persist, often specific to the most affected side in unilateral CP (Cappellini et al., 2016). While in TD children the intersegmental coordination of the lower limb segments quickly develops (Cheron et al., 2001; Ivanenko et al., 2004a, 2007; Dominici et al., 2011)—typically, intersegmental coordination develops rapidly in the first few months after the onset of IW (Cheron et al., 2001)—in children with CP, this may be less pronounced (Leonard et al., 1991; Berger, 1998). Apparently, intersegmental coordination matures less or much slower in children with CP. In unilateral CP, this has been shown to be specific to the most affected body side (Cappellini et al., 2016).

One way to assess neuromuscular control during walking in healthy individuals and patient populations is through muscle synergy analysis. Walking requires refined neuromuscular coordination, and the central nervous system arguably simplifies neuromuscular control during walking by the recruitment of groups of muscles, called muscle synergies or locomotor modules (Ivanenko et al., 2005; Hart and Giszter, 2010; Dominici et al., 2011; Bizzi and Cheung, 2013). During typical development, the number of basic activation patterns increases from two, during neonate stepping, to four, when children walk independently (Dominici et al., 2011; Sylos-Labini et al., 2020). Muscle activity patterns during walking in older children with CP seem to match the patterns of TD toddlers (Cappellini et al., 2016), suggesting that also the maturation of the activation of individual muscles lags behind in children with CP. School-age children with CP recruit fewer muscle synergies compared to TD children, and it seems that they employ "simpler" neuromuscular control strategies (Steele et al., 2015; Tang et al., 2015; Schwartz et al., 2016; Shuman et al., 2016, 2017, 2018, 2019; Goudriaan et al., 2018; Hashiguchi et al., 2018; Bekius et al., 2020). In children with CP, the temporal structure of muscle synergies, i.e., their activation patterns, largely agrees with that of TD toddlers; i.e., they contain wider activation bursts compared to older TD children.

Combining kinematic and neural measures can provide additional insight into motor development and may help to detect early motor deficits (Dewolf et al., 2020). Yet, previous studies investigating locomotor patterns in young children with CP had a cross-sectional design (Cappellini et al., 2016, 2018), which may limit inferences about how changes in neuromuscular control are related to the altered development of walking. In addition, a limited number of recorded muscles in previous studies (Steele et al., 2013; Tang et al., 2015; Shuman et al., 2016, 2017; Bekius et al., 2020) may limit the conclusions on the spatiotemporal structure of muscle activity patterns. A more detailed and comprehensive assessment of multimuscle coordinated patterns is needed (Damiano, 2015). The aim of the current exploratory longitudinal study was to investigate the development of locomotor patterns and motor control during walking in very young children with early brain lesions, at high risk of CP. The focus was on development starting before the onset of IW, covering a period of 1 to 2 years, with the aim to record the emergence of the FS. We studied locomotor patterns using kinematic analysis and motor control using muscle synergy analysis. We hypothesized (1) intersegmental dependency and muscle synergy structure to change over time after IW onset and (2) the development of gait kinematics and muscle synergies to be delayed in children with a diagnosis of CP. We also expected (3) differential changes of gait kinematics on the most vs. the least affected side when unilateral CP was diagnosed, and (4) the number of synergies to be reduced the more a child was affected by CP.

MATERIALS AND METHODS

Participants

Three children with early brain lesions, at high risk of CP and not yet walking independently, were included in this longitudinal study. The participants were recruited from the Department of Pediatric Rehabilitation and the Department of Pediatric Neurology at the Amsterdam University Medical Centers (Amsterdam UMC, location VUmc). The study was approved by the Medical Ethics Committee of the Amsterdam UMC (location VUmc) (NL59589.029.16). The parents of all

TABLE 1 | Participant characteristics.

Participant	Gender	Session	Walking ability	Age (mo)	CA (mo)	WA (mo)	Distribution	Subtype	GMFCS	Brain damage	BW (kg)	BL (cm)	N strides
P1	F	1	SW	12.7	12.7	−1.8	Bi	Spastic	HR	Infection	7.8	75	37
		2	FS	15.2	15.2	0.8	Bi	Spastic	HR		8.8	74	47
		3	IW	17.5	17.5	3.1	Bi	Spastic	I		9.4	80	62
		4	IW	22.3	22.3	7.9	Bi	Spastic	I		10.6	85	42
		5	IW	27.2	27.2	12.8	Bi	Undef	n/a		11.0	87	33
P2	M	1	SW	14.5	14.6	−6.6	Uni R	Spastic	HR	Media infarction	11.1	84	0
		2	SW	19.2	19.3	−1.4	Uni R	Spastic	HR		12.0	84	52
		3	FS	22.1	22.2	0.3	Uni R	Spastic	I		12.4	91	29
		4	IW	24.6	24.7	2.8	Uni R	Spastic	I		12.0	89	40
		5	IW	26.9	27	5.1	Uni R	Spastic	I		12.4	90	54
P3	F	1	SW	31.7	30.0	—	Bi	Spastic	III	PVL	12.7	85	60
		2	SW	35.4	33.7	—	Bi	Spastic	III		12.8	90	36
		3	SW	42.8	41.1	—	Bi	Spastic	III		14.0	95	59
		4	SW	49.1	47.4	—	Bi	Spastic	III		15.0	105	48
		5	SW	56.1	53.6	—	Bi	Spastic	III		12.6	105	51

F, female; M, male; SW, supported walking; FS, first steps; IW, independent walking; mo, months; CA, corrected age; WA, walking age (expressed as time since onset of independent walking); Bi, bilateral; Uni, unilateral; R, right; undef, undefined; GMFCS, gross motor function classification system; n/a, not applicable; HR, high risk; asym, asymmetric; sym, symmetric; PVL, periventricular leukomalacia; BW, body weight; BL, body length; N, number.

children were informed about the procedure of the study and provided written informed consent prior to participation in accordance with the declaration of Helsinki for medical research involving human participants.

Study Design

Experiments were performed in the clinical gait laboratory of the Department of Rehabilitation Medicine at the Amsterdam UMC, location VUmc. The laboratory setting and experimental procedures were adapted to the children, such that the risks were equal or lower to that of walking at home. The responsible investigators, one or both parents of the child, and a pediatric physiotherapist were present during the experiments.

Every participant underwent five consecutive gait analysis sessions within a period of 1–2 years, to record development from supported walking (SW), to FS, to IW. SW sessions were conducted prior to IW onset. There, the pediatric physiotherapist, experimenter, or parent supported the child during stepping attempts by its trunk or arms. FS sessions were recorded when the children performed their first unsupported steps. They were scheduled within 2 weeks of first unaided walking experience, as reported by the parents. All sessions recorded after the FS session were labeled IW (**Table 1**).

All children walked barefoot on a treadmill during SW sessions and over ground during FS and IW sessions. If children wore ankle-foot orthoses in daily life, these were removed during the experiment. The treadmill speed was adjusted to induce a walking pattern and turned to a comfortable speed for the child. During FS and IW sessions, children were encouraged to walk in a straight line at a comfortable walking speed.

Data Acquisition

During every session, full-body kinematics were recorded bilaterally and sampled at 100 Hz using a VICON system (Oxford, UK) with 12 cameras surrounding the 10-m-long walking area. Reflective markers (diameter 14 mm) were attached to the skin of the participants representative of anatomical reference points overlying the following bony landmarks on both sides of the body (**Figure 1A**): glenohumeral joint (GH), seventh cervical vertebra (C7), ear (EAR), forehead (FHEAD), ulnar styloid (WRI), lateral humeral epicondyle (ELB), iliac spinal crest (IL), greater trochanter (GT), lateral femur epicondyle (LE), lateral malleolus (LM), and head of fifth metatarsophalangeal joint (5MT). In addition, videos were recorded at 50 Hz using the VICON system using two cameras placed in the sagittal plane.

Muscle activity was assessed by means of surface electromyography (EMG) from 11 pairs of bilateral leg and trunk muscles, i.e., tibialis anterior (TA), gastrocnemius medialis (GM), gastrocnemius lateralis (GL), soleus (SOL), rectus femoris (RF), vastus medialis (VM), vastus lateralis (VL), biceps femoris (BF), tensor fascia latae (TFL), gluteus maximus (GLM), and erector spinae at L2 level (ES). Mini-golden reusable surface EMG disc–electrode pairs (15-mm-diameter electrodes, acquisition area of 4 mm^2) were placed at the approximate location of the muscle belly on the cleaned skin, with interelectrode spacing of ∼1.5 cm. EMG electrode placement was performed according to the Surface Electromyography for the Non-Invasive Assessment of Muscles protocol (Hermens et al., 2000) and the recommendations for minimizing cross-talk between adjacent muscles that were described in detail previously (Ivanenko et al., 2004b, 2005; Dominici et al., 2011). Preamplified EMG sensor units were attached to the skin and fixed with elastic gauzes, to minimize movement artifacts (**Figure 1A**). Two Cometa

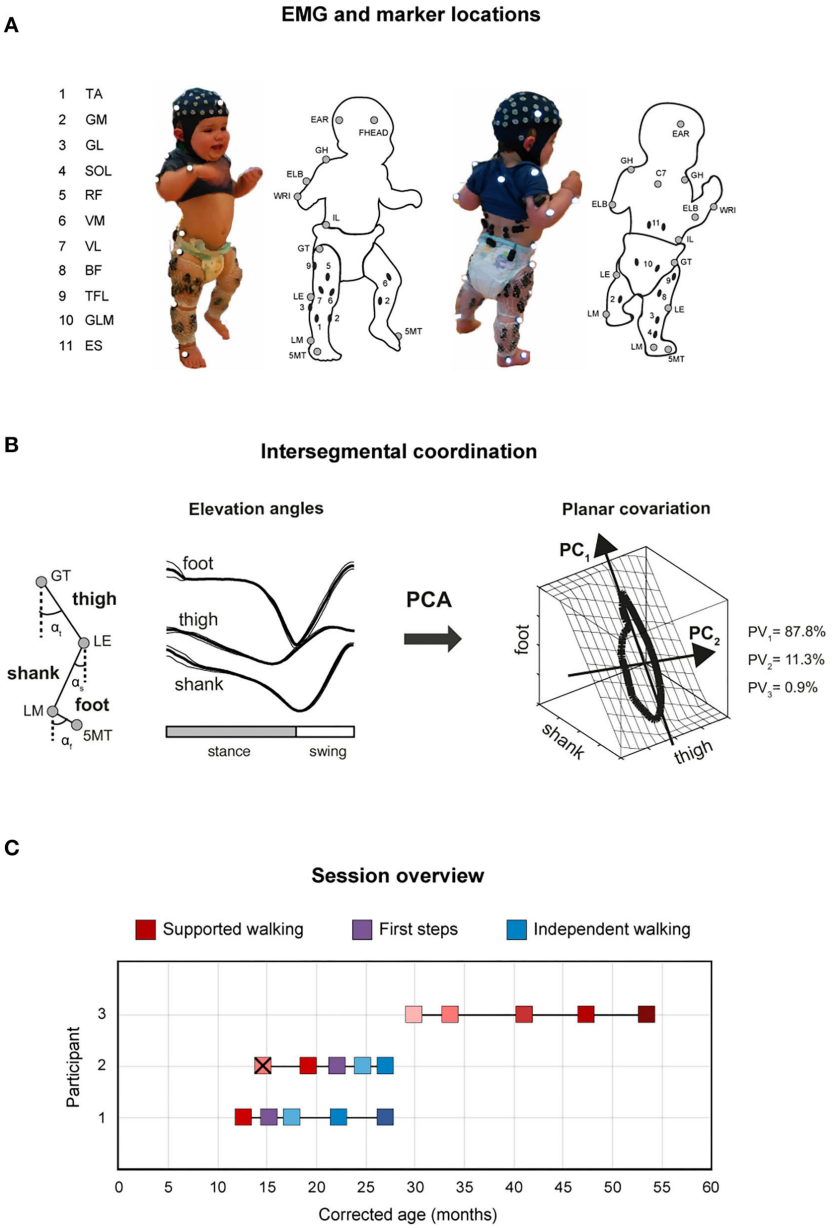

FIGURE 1 | Experimental setup and gait analysis session overview. **(A)** Marker locations are denoted by gray circles, and EMG electrode locations by black ovals. 5MT, head of fifth metatarsophalangeal joint; LM, lateral malleolus; LE, lateral femur epicondyle; GT, greater trochanter; IL, iliac crest; WRI, ulnar styloid; ELB, lateral humeral epicondyle; GH, glenohumeral joint; C7, seventh cervical vertebra; EAR, ear; FHEAD, forehead; TA, tibialis anterior; GM, gastrocnemius medialis; GL, gastrocnemius lateralis; SOL, soleus; RF, rectus femoris; VM, vastus medialis; VL, vastus lateralis; BF, biceps femoris; TFL, tensor fascia latae; GLM, gluteus maximus; ES, erector spinae at L2 level. **(B)** Schematic illustration of principal component (PC) analysis of elevation angles of lower limb segments (thigh: α_t, shank: α_s, foot: α_f), and its corresponding gait loop plotted three-dimensionally in one representative typically developing child (4 years old) during walking. A loop is obtained by plotting the thigh elevation angle vs. shank and foot elevation angles (after mean values subtraction). The shape and orientation of the gait loop reflect the coordination of limb segments as described by PC_1 (reflects the largest variance, which corresponds to the length of the gait loop), and PC_2 (the second largest variance, which corresponds to the width of the loop), here indicated with black arrows. Percentage of total variation explained by the three PCs (PV_1-PV_3) are indicated. Note in adult and older children walking, two principal components typically account for ∼99% of the total variance ($PV_3 = 0.9\%$ in the example). **(C)** Gait analyses over time (corrected age, in months) for P1–P3 showing supported walking (SW: shades of red), first steps (FS: purple), and independent walking (IW: shades of blue). Different color shades from light to dark indicate the change in age and/or independent walking experience. P3 did not start to walk independently. X means the child did not take any steps during that session.

Mini Wave wireless 16-channel EMG systems (Cometa, s.r.l, Italy) were used, and EMG signals were sampled at 1 kHz. Electroencephalography (EEG) recordings were made but not analyzed here. Sampling of kinematic, video, and EMG signals was synchronized.

Data Analysis

The gait patterns were described by (1) kinematics: (a) spatiotemporal gait parameters, including walking velocity, stride duration, and double support duration; (b) intersegmental coordination, estimated via principal component analysis (PCA) of the elevation angles of thigh, shank, and foot segments (Borghese et al., 1996); and (2) neuromuscular control: EMG activity and muscle synergies characteristics, described by the full width at half maximum (FWHM) of the muscle activity, temporal activation patterns of the muscle synergies, and variability accounted for (VAF). Gait initiation and termination, as well as jumps and turns, were discarded from analysis. The lower body was modeled as an interconnected chain of rigid segments: GT-LE for the thigh, LE-LM for the shank, and LM-5MT for the foot. All analyses were conducted in MATLAB (version 2020a, MathWorks Inc., Natick, MA, USA).

Spatiotemporal Gait Parameters

Step events were manually defined based on the video recordings and later confirmed using the kinematic data. We defined a stride from foot strike to foot strike of the ipsilateral foot, stance duration as the percentage of the gait cycle from foot strike to foot off. Stride velocity was computed using the corresponding stride length (three-dimensional displacement of the LM marker) and duration of both legs. Data were time-interpolated over individual gait cycles to fit a normalized 201-point time base.

Intersegmental Coordination

We constructed elevation angles of the thigh, shank, and foot segments (α_t, α_s, and α_f, respectively) to correspond with angles between the segment projected on the sagittal plane and the vertical, i.e., to be positive in the forward direction when distal markers fell anterior to the proximal one. In healthy adults and older children, these elevation angles describe a path (gait loop) that lies close to a plane that is defined by their eigenvectors (**Figure 1B**). To examine the development of intersegmental coordination (the gait loop and the corresponding plane) across sessions within subjects, PCA was applied to lower limb elevation angles of each gait cycle, for each session and participant separately (Borghese et al., 1996; Bianchi et al., 1998; Ivanenko et al., 2007; Dominici et al., 2010). Briefly, we computed the covariance matrix of the thigh–shank–foot elevation angels (after subtraction of the mean value of each angular coordinate) across the gait cycle. The three principal components (PC_1-PC_3) including the explained variance (PV_1-PV_3) and eigenvectors ($\mathbf{u_1}$–$\mathbf{u_3}$), were obtained (**Figure 1B**). In general, the first two eigenvectors lie on the best-fitting plane of angular covariation, with $\mathbf{u_2}$ orthogonal to $\mathbf{u_1}$, whereas the third eigenvector, $\mathbf{u_3}$, is the normal to the covariation plane and defines the plane orientation. For every eigenvector, the parameters u_{it}, u_{is}, and u_{if} correspond to the direction cosines with the positive semiaxis of the thigh, shank, and foot angular coordinates, respectively. The percentages of variance accounted for by the second (PV_2) and third (PV_3) eigenvectors were assessed and compared between sessions, as well as the rotation of the normal to the plane by using the u_{3t} parameter (Bianchi et al., 1998; Dominici et al., 2007, 2010; Cappellini et al., 2018).

Muscle Activity

EMG signals were notch and high-pass filtered (fourth-order Butterworth 50 ± 0.01 Hz, and >30 Hz, respectively), full-wave rectified, and subsequently low-pass filtered (fourth-order Butterworth <10 Hz) to obtain linear envelopes. For some sessions, EMG data from few muscles had to be discarded because of sustained artifacts after filtering. Possible contamination of the EMG recordings could be detected by the electrical cross-talk due to volume conduction of activity across adjacent muscles. This issue is particularly relevant when recording many muscles in young children because of their small body size and the resulting close spacing of nearby muscles. Nevertheless, the small size of the EMG electrodes used in our settings and the chosen interelectrode distance should have minimized the pickup from adjacent muscles. Anyway, we attempt to quantify the potential electrical cross-talk by performing a cross-correlation analysis of selected pairs of adjacent flexor/extensor muscles. Cross-correlation was computed after notch (50 Hz) and high-pass (30 Hz) filtering the EMG data to remove any possible power line noise and movement artifacts. We identified the peak of the normalized cross-correlation >0.3 between flexors and extensors as suspect cross-talk (d'Avella et al., 2011; Dominici et al., 2011) in 0.1% to 9.9% of strides, although the values of the correlation coefficients were generally not very high (**Supplementary Table 3**). We verified that the removal of those strides potentially affected by cross-talk did not change any conclusion drawn from those analyses.

The data were time-normalized for each limb to $t = 201$ data points per gait cycle. The FWHM of the muscle activity was determined based on the minimum-subtracted envelopes of muscle activity patterns (Alves-Pinto et al., 2016; Cappellini et al., 2016, 2018; Bach et al., 2021), separately for every muscle, gait cycle, and session. To ease comparison of our experimental finding with literature, we also reported the FWHM of the mean muscle activity for each muscle and session (**Supplementary Material 1**). In case of muscle activations with more than one peak, the peak with the largest maximum was chosen as the main peak. The FWHM quantifies the duration of the burst of activity as it equals the sum of the durations of the intervals in which the EMG signal exceeded half of their maximum. That is, the larger the FWHM, the longer the muscle contraction is sustained.

Muscle Synergies

Per session, EMG amplitudes of every muscle were normalized to the maximum of their mean value across strides plus its standard deviation (SD). Non-negative matrix factorization (NMF) was applied to the unilateral gait-cycle averaged EMG envelopes to extract muscle synergies. NMF decomposes the EMG into $i = 1, \ldots, n$ temporal activation patterns H_i and corresponding

synergy weights W_i by mean of the linear combination

$$EMG = \sum_{i=1}^{n} H_i W_i + e,$$

where the preprocessed *EMG* data ($m \times t$ matrix, where m is the number of muscles, here 11, and t is the number of time points, here 201) are a linear combination of the temporal activation patterns H ($n \times t$ matrix, where $n < m$ is a predetermined number of synergies, see below) and synergy weights W ($m \times n$ matrix), and e denotes the residual error.

The reconstruction accuracy of the extracted synergies was determined by calculating the percent of VAF, which is the ratio of the sum of squared errors to the total sum of squares computed with respect to the mean (Dominici et al., 2011; Cappellini et al., 2016). In order to compare the synergy patterns between sessions, we aimed to fix the number of synergies per participant across sessions, by varying the number of synergies from 1 to 8 and exploring the VAF slopes and synergy patterns across sessions. In addition, we investigated VAF by one synergy (VAF1, Steele et al., 2015; Shuman et al., 2019) and compared this parameter between sessions.

To quantitatively characterize differences in the duration of synergy activation patterns, we also computed the corresponding FWHM (Cappellini et al., 2016, 2018; Bach et al., 2021), in line with the approach of the muscle activation patterns (see above).

Statistical Analysis

Statistical analyses were performed using SPSS (IBM SPSS Statistics for Mac, version 26.0; IBM Corp., Armonk, NY, USA). All data are reported as mean (±SD). Normality was assessed using Q–Q plots, and homogeneity of variance was tested using a Levene test. Development of spatiotemporal gait parameters, intersegmental coordination values, and FWHM per muscle across sessions within each participant was assessed using a linear mixed-effects model (LMM, Molenberghs and Verbeke, 2000). LMM corrects for interdependency of repeated measures within one participant using random effects, and the number of observations per sessions can vary. We fitted an LMM with PV_2, PV_3, u_{3t}, stance duration, double support, velocity, and FWHM per muscle as outcome variables. *Session* was included as fixed and *trial* as random effect. To test whether development of the outcome variables differed between sides in P2, the interaction between session and side was included for P2. For all analyses, $p < 0.05$ was considered statistically significant.

RESULTS

Medical History

Child P1 (female) was born at term after an uneventful pregnancy. Birth was complicated by umbilical cord entanglement and perinatal asphyxia with Apgar scores of 4 and 5, respectively, after 1 and 5 min, respectively. Clinically, she recovered quickly, and there was no indication for therapeutic hypothermia. Because of a possible infection, she was treated with antibiotics for 7 days, but blood cultures remained negative. Twenty-two hours after birth, she developed severe neonatal convulsions, for which the child was treated with phenobarbitone, midazolam, lidocaine, and levetiracetam. A magnetic resonance imaging (MRI) scan at the age of 4 days revealed extensive bilateral signal changes in the white matter of the frontal, temporal, parietal, and occipital lobes; corticospinal tracts; internal capsule; and thalamus. A probable diagnosis of hypoxic–ischemic encephalopathy due to perinatal asphyxia was made. Neurological examination at the age of 8 months showed a mild developmental delay and a mild paresis of the left arm. At follow-up, until the age of 3.5 years, development appeared normal, and no further abnormalities were found via neurological examination, excluding a diagnosis of CP.

Child P2 (male) was also born at term after an uneventful pregnancy. The child developed normally in the first 3 months of life, although it was noted that the right arm appeared stiffer when parents changed clothes. When 3 months old, asymmetry in upper extremity motor function was established. At the age of 5 months, he developed West syndrome for which he was successfully treated with levetiracetam and vigabatrin. Neurological examination at the age of 8 months showed spastic paresis of the right arm with hyperreflexia of the knee tendon reflex at the right side. An MRI scan of the brain at the age of 8 months showed a congenital infarction of the medial cerebral artery at the left side. A diagnosis of unilateral spastic CP, GMFCS I, was made.

Child P3 (female) was born preterm after 33 weeks and 1 day of pregnancy. At the age of 3 weeks, she suffered a group B streptococcal infection. She showed a developmental delay and rolled over for the first time at the corrected age of 11 months, and the tone of the lower extremities had been high since the first weeks. An MRI scan of the brain at the corrected age of 12 months showed periventricular leukomalacia, related to prematurity. A diagnosis of bilateral spastic CP, GMFCS III, was made.

Gait Analysis Session Overview

For P1 and P2, the sessions covered a period of 14.5 and 12.4 months in between the first and the last session and included one and two SW sessions, respectively, an FS session, and three and two IW sessions, respectively. For P3, the sessions covered a period of 24 months and included five SW sessions (**Figure 1C**). P1 started to walk at a typical age, i.e., 14 months old, whereas P2 took its FS around the corrected age of 22 months old. P3 did not walk independently yet at the corrected age of 53 months. During the first session of P2 (corrected age 14.6 months), the child did not take any steps; thus, for this participant, only four sessions are reported in the following.

Spatiotemporal Gait Parameters

Video analysis revealed that P1 had a flat foot strike in sessions 1 and 2 (SW and FS, respectively), whereas both feet showed a heel strike from session 3 (IW) onward. P2 had a flat foot strike of both feet from sessions 2 to 4 (SW, FS, and IW, respectively), and during session 5 (IW), only the least affected leg showed a heel strike. P3 had a toe landing and was crossing her legs in all sessions.

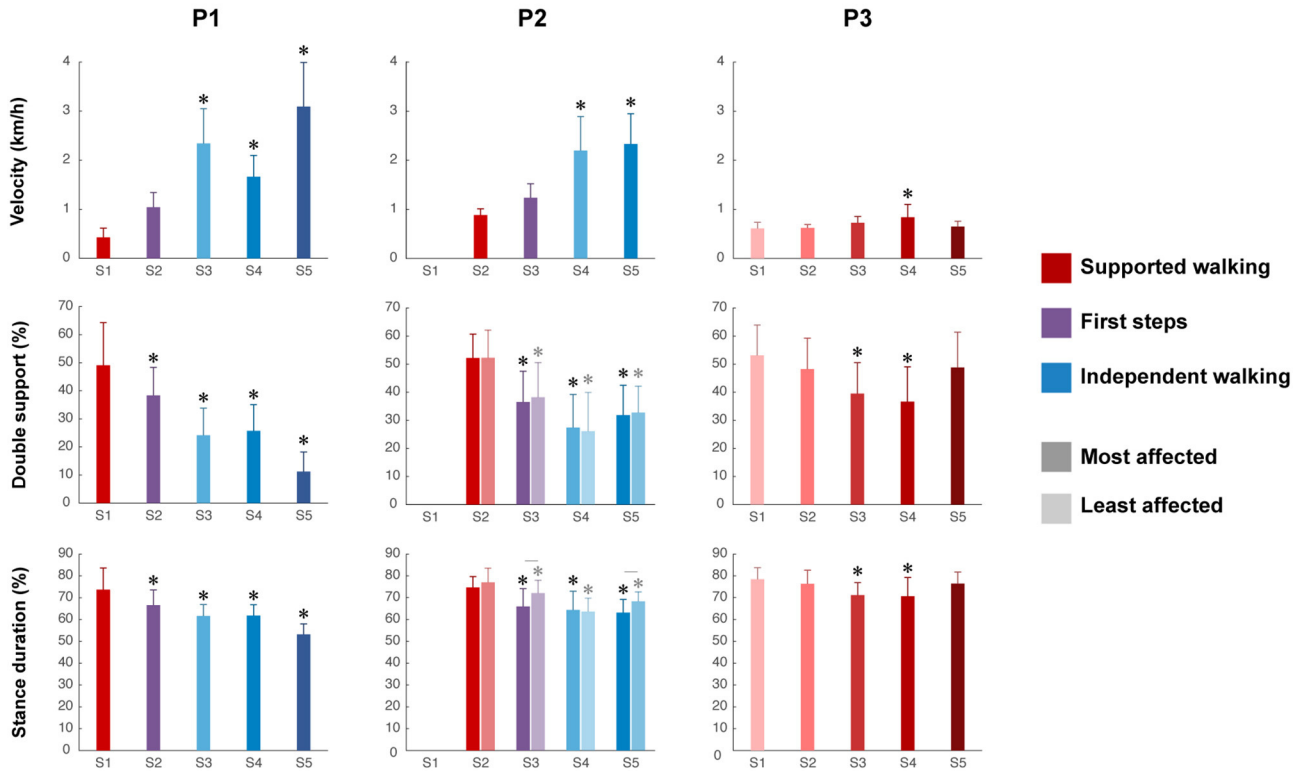

FIGURE 2 | Spatiotemporal gait parameters. Velocity, percentage of double support and stance duration from S1 to S5. Error bars indicate SDs. For the percentage of double support and stance duration of P2, the most affected side (dark color) and least affected side (light color) are shown, whereas for P1 and P3, one side is shown. Significant linear differences across sessions are denoted by asterisks, and significant interactions between session and side are denoted by lines between the most and least affected sides for P2 ($p < 0.05$).

Walking velocity showed a significant main effect of session in all children (P1, $p < 0.001$; P2, $p < 0.001$; P3, $p < 0.01$). For P1, a significant increase was found from SW session 1 to IW sessions 3 to 5 (**Figure 2** and **Supplementary Table 1**). For P2, a significant increase was found from SW session 2 to IW sessions 4 to 5. For P3, a significant increase was found between SW sessions 1 and 4, but walking velocity decreased again in session 5.

The percentage of double support phase showed a significant main effect of session in all children (P1, $p < 0.001$; P2, $p < 0.01$; P3, $p < 0.001$). For P1, a significant decrease was found between SW session 1 and all sessions (**Figure 2** and **Supplementary Table 1**). For P2, a significant decrease was found between SW session 2 and all sessions, in both the most and least affected side. For P3, a significant decrease was found between SW session 1 and SW sessions 3 to 4, but the percentage of double support phase increased again in session 5.

The percentage of relative stance duration showed a significant main effect of session in all children (P1, $p < 0.001$; most affected side P2, $p < 0.05$; least affected side P2, $p < 0.001$; P3, $p < 0.001$). For P1, a significant decrease was found between SW session 1 and all sessions (**Figure 2** and **Supplementary Table 1**). For P2, a significant decrease was found between SW session 2 and all sessions in both the most affected and least affected side, although the developmental slope differed between sides, as shown by a significant interaction effect between session and side ($p < 0.01$). For P3, a significant decrease was between SW session 1 and SW sessions 3–4, but the percentage of relative stance duration increased again in session 5.

Intersegmental Coordination

The intersegmental coordination of the thigh–shank–foot elevation angles was compared across sessions for the three participants and was evaluated using PCA. The planar covariation of the leg elevation angles is directly related to the dimensionality of the original data set, and the method is shown in **Figure 1B**. In summary, **Figure 3** shows the mean gait loops for all sessions of each participant and its corresponding values of planar covariation.

The percentage of variance accounted for by the second eigenvector (PV_2) showed a significant main effect of session in P1 ($p < 0.001$), the least affected side of P2 ($p < 0.01$), and P3 ($p < 0.001$), but not in the most affected side of P2 ($p = 0.110$). For P1, a significant decrease was found between SW

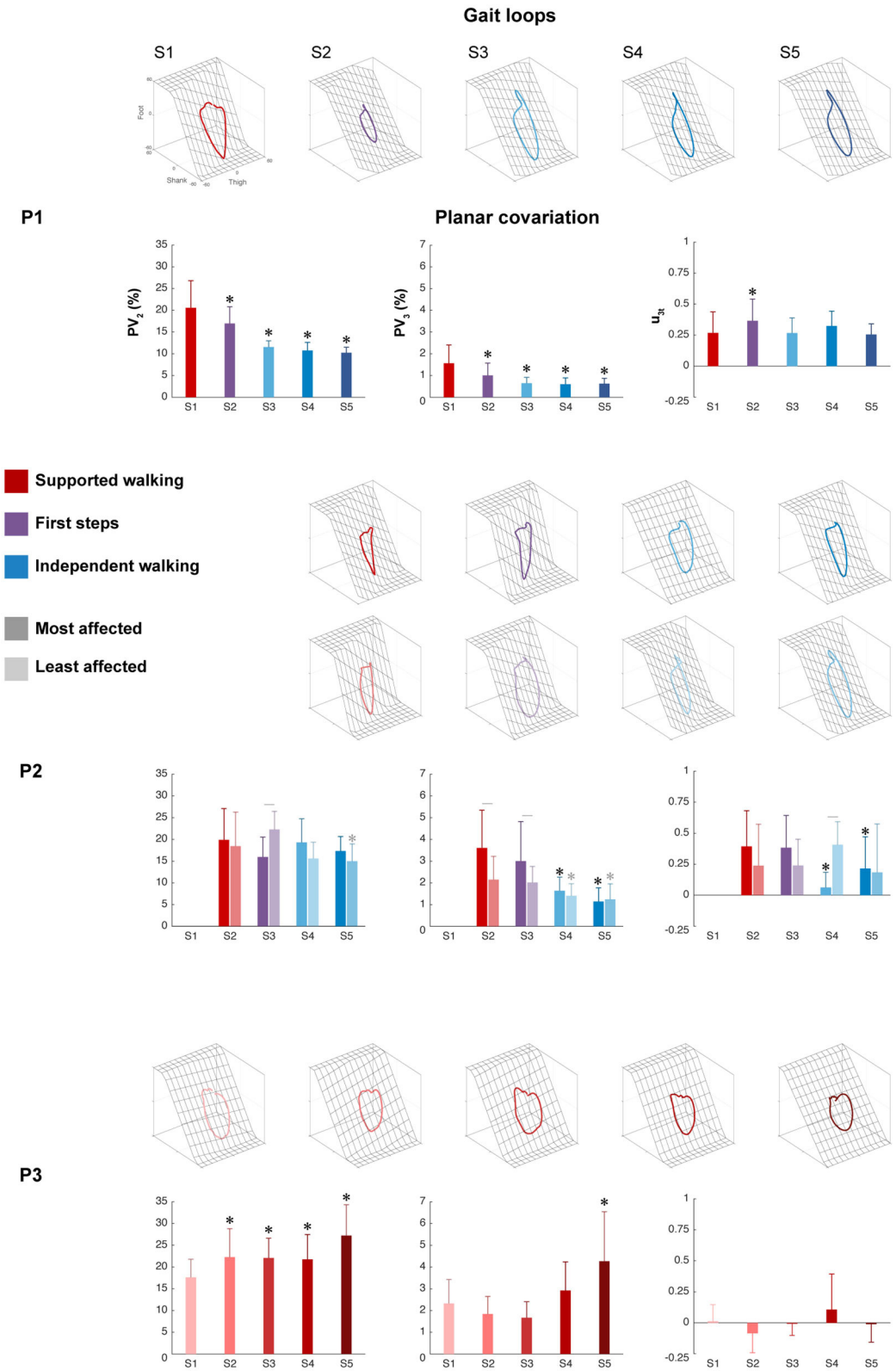

FIGURE 3 | Intersegmental coordination. Gait loops plus the corresponding mean percentage of total variance explained by the second and third eigenvectors (PV_2 and PV_3), and the mean orientations of the normal to the plane (u_{3t}) are shown from S1 to S5 for each participant. Error bars indicate SDs across strides. For P2, the most affected side (dark color) and the least affected sides (light color) are shown, whereas for P1 and P3, one side is shown. Significant differences with session 1 are marked by asterisks, and significant interactions between session and side are denoted by lines between the most and least affected sides for P2 ($p < 0.05$).

session 1 and all sessions, indicating a reduction in the width of the gait loop from SW to IW, which is also visible in the changes of gait loops for the IW sessions compared to the SW session (**Figure 3** and **Supplementary Table 1**). The least affected side of P2 showed a significant decrease between SW session 2 and IW session 5, but an increase during FS session 3. In contrast, P3 showed a significant increase between SW session 1 and all sessions, but the gait loops showed similar shapes in all the sessions.

The percentage of variance accounted for by the third eigenvector (PV_3), which quantified the planarity of the gait loop, showed a significant main effect of session in P1 ($p < 0.001$), the most and least affected sides of P2 ($p < 0.001$ and $p < 0.01$, resp.) and P3 ($p < 0.01$). For P1, a significant decrease was found between SW session 1 and all sessions, indicating a reduction in the deviation from planarity (**Figure 3** and **Supplementary Table 1**). For P2, a significant decrease was found between SW session 2 and IW sessions 4 to 5 in both the most and least affected side. In contrast, P3 showed a significant increase in PV_3 between SW sessions 1 and 5.

The orientation of the covariance plane (u_{3t}) showed a significant main effect of session in P1 ($p < 0.001$), the most and least affected sides of P2 ($p < 0.001$ and $p < 0.01$, resp.) and P3 ($p < 0.01$). For P1, a significant increase was found between SW session 1 and FS session 2, whereas the most affected side of P2 showed a significant decrease between SW session 1 and IW sessions 4 to 5 (**Figure 3** and **Supplementary Table 1**). In both the least affected side of P2 and in P3, there was no significant difference between session 1 and the other sessions. The analysis showed a significant session interaction effect between session and side for PV_2, PV_3, and u_{3t} ($p < 0.001$ for all) in P2, indicating that these parameters developed differently over time for the most and least affected side.

Muscle Activity

Despite the large variability in EMG activity between strides per muscle, we could observe a clear modification between different sessions in P1 and P2. All activation patterns became smoother and displayed increasingly distinct peaks (**Figure 4A**). A short burst of activity was present around foot strike in the TA and calf muscles (GM, GL, and SOL) of P3 during all sessions (see zoom-in view of P3 **Figure 4A**), in the SW and FS sessions of P2, in particular in the most affected leg. In P1, this activity was absent.

For P1, FWHM showed a significant main effect of session for all muscles except GL ($p = 0.072$). FWHM of TA, GM, SOL, RF, VL, BF, and ES significantly increased from SW session 1 to IW sessions 3 to 5, and of GLM from FS session 2 to IW sessions 4 to 5. In contrast, FWHM significantly decreased from FS session 2 to IW session 3 for TFL, and to sessions 3 to 4 for VM (**Figure 4B** and **Supplementary Table 2**).

For P2, FWHM showed a significant main effect of session for all muscles in the most affected side, and for all muscles except TA ($p = 0.061$) and GL ($p = 0.682$) in the least affected side. In the most affected side, FWHM of TA, GM, GL, RF, BF, and TFL was significantly higher during IW sessions 4 to 5 compared to SW session 2, whereas FWHM of SOL, VM, VL, and ES already increased during FS session 3. In the least affected side of P2, FWHM of GM, VM, BF, and GLM significantly increased during IW sessions 4 to 5 compared to SW session 2, whereas FWHM of RF, TFL, and ES already increased during FS session 3. FWHM of SOL was only significantly larger during IW session 5 compared to SW session 1 (**Figure 4B** and **Supplementary Table 2**). An interaction effect between session and side was found for GM, SOL, RF, BF, and GLM ($p < 0.01$), indicating that FWHM of these muscles developed differently in the most compared to the least affected side.

For P3, FWHM showed a significant main effect of session for all muscles ($p < 0.05$), except RF ($p = 0.120$). FWHM of TA, SOL, VM, BF, and TFL was significantly smaller in session 1 compared to all other sessions. FWHM of GM and GLM was significantly larger during sessions 4 to 5 and of GL during sessions 2, 3, and 5, compared to the first recorded session (**Figure 4B** and **Supplementary Table 2**). In all participants, variability in FWHM between strides was large.

The results of the FWHM computed on the average muscle activity can be found in **Supplementary Material 1**. Similar to the results shown in **Figure 4B**, this analysis revealed clear changes between different sessions in P1 and P2. In contrast, P3 showed similar duration of the main bursts of the mean activity of almost all the muscles between sessions, and on average wider EMG bursts with respect to P1 and P2.

Muscle Synergies

P1 showed an increase in VAF_1 after FS. The most affected side of P2 showed an increase in VAF_1 from SW to IW where it stayed constant, whereas the least affected leg showed a decreasing trend in VAF_1 from FS to IW. VAF_1 was higher for the most compared to the least affected leg during the FS and IW sessions, but vice versa for the SW session. For P3, VAF_1 slightly differed between sessions, but there was no clear trend (**Figure 5A**). Based on the VAF slopes and exploration of the synergy patterns, P1 and P2 generally recruited four synergies across sessions, whereas P3 recruited two synergies. To compare activations patterns across sessions, we fixed the number of synergies of P1 and P2 to four, and of P3 to two.

Synergies were ordered based on the highest correlations between the synergy weights per session (**Figures 5B,C**). For P1, FWHM of synergy pattern 1 (Syn1) and 2 (Syn2) decreased, i.e., bursts become narrower. By contrast, FWHM of Syn3 increased toward session 4, but decreased again in session 5. Syn4 did not change in FWHM. Despite the changes of synergy patterns of P2, FWHM appeared quite variable between sessions, and we failed to identify any (qualitative) trend. P3 showed an increase in FWHM of Syn4 over time.

Despite the development in synergy activation patterns in P1 and P2, the synergy weights appeared similar across sessions (**Figure 5D**). In P1 and P2, mainly RF, VM, VL, and BF were active in Syn1, and GM, GL, and SOL in Syn2. ES, and TA to a lesser extent, dominated Syn3, and TA and RF in Syn4. P3 showed simultaneous activations of GM, GL, SOL, RF, VM, VL, TFL, and GLM in Syn2, whereas TA and ES were present in Syn4.

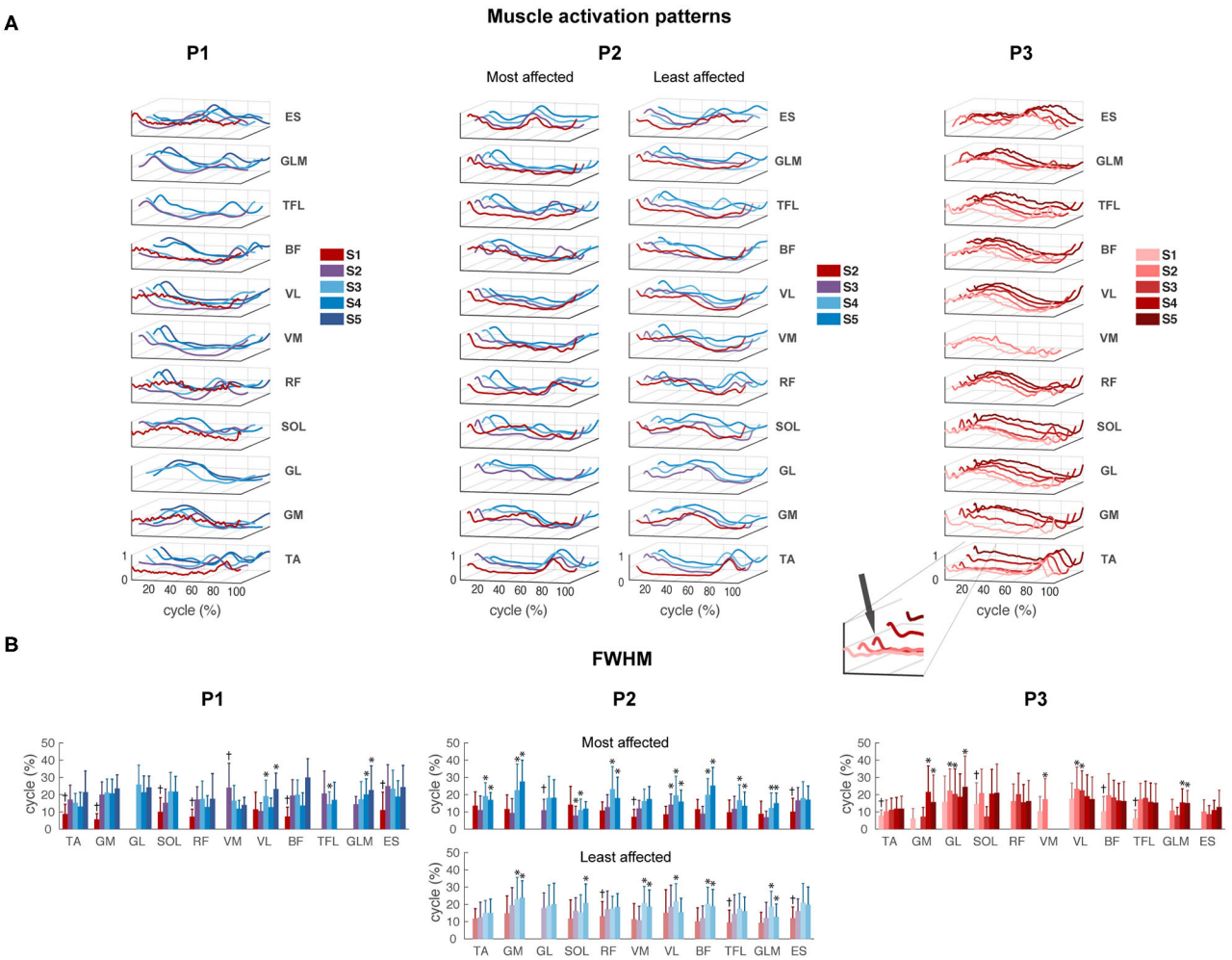

FIGURE 4 | EMG activity. **(A)** Muscle activation patterns averaged across strides per session for P1–P3, for the most and least affected legs in P2. The peak around foot strike is emphasized in the zoom-in view of the TA muscle of P3. **(B)** Full-width of the half maximum (FWHM) per muscle per session in P1–P3. TA, tibialis anterior; GM, gastrocnemius medialis; GL, gastrocnemius lateralis; SOL, soleus; RF, rectus femoris; VM, vastus medialis; VL, vastus lateralis; BF, biceps femoris; TFL, tensor fascia latae; GLM, gluteus maximus; ES, erector spinae at L2 level. *Significant difference compared to the first recorded session of this muscle. †All sessions are significantly different from the first recorded session.

DISCUSSION

Our longitudinal study captured the early development of walking in three young children at high risk of CP via comprehensive instrumented gait assessments. The exploratory findings illustrate how the combination of kinematic and EMG measures can contribute to our understanding of walking maturation in children with early brain lesions.

We followed three children with divergent development trajectories. Two of them made the transition from SW to IW, whereas the third child had not reached IW at 4.5 years of age. Spatiotemporal gait parameters, intersegmental coordination, and neuromuscular control changed from SW to IW in the child who did not develop CP and the child with unilateral CP. Maturation of gait patterns was delayed in the child with unilateral CP and differed between sides. Walking development appeared entirely absent in the more severely affected child with bilateral CP.

Spatiotemporal gait parameters and intersegmental coordination changed over time from SW to IW in the child without CP, and the child with unilateral CP, although to a lesser extent, whereas there was no development in the child with bilateral CP. This was expected in view of previous research reporting developmental trajectories in children with CP that differ from those in TD children (Berger et al., 1984; Leonard et al., 1991; Berger, 1998). The rapid maturation of planar covariation in the first months after the FS was present whenever children developed IW, irrespective of their age at their first steps. The most affected side of the child with unilateral CP deviated more from planarity than the least affected side during SW and FS, although it was comparable between sides during IW. These results suggest that the intersegmental

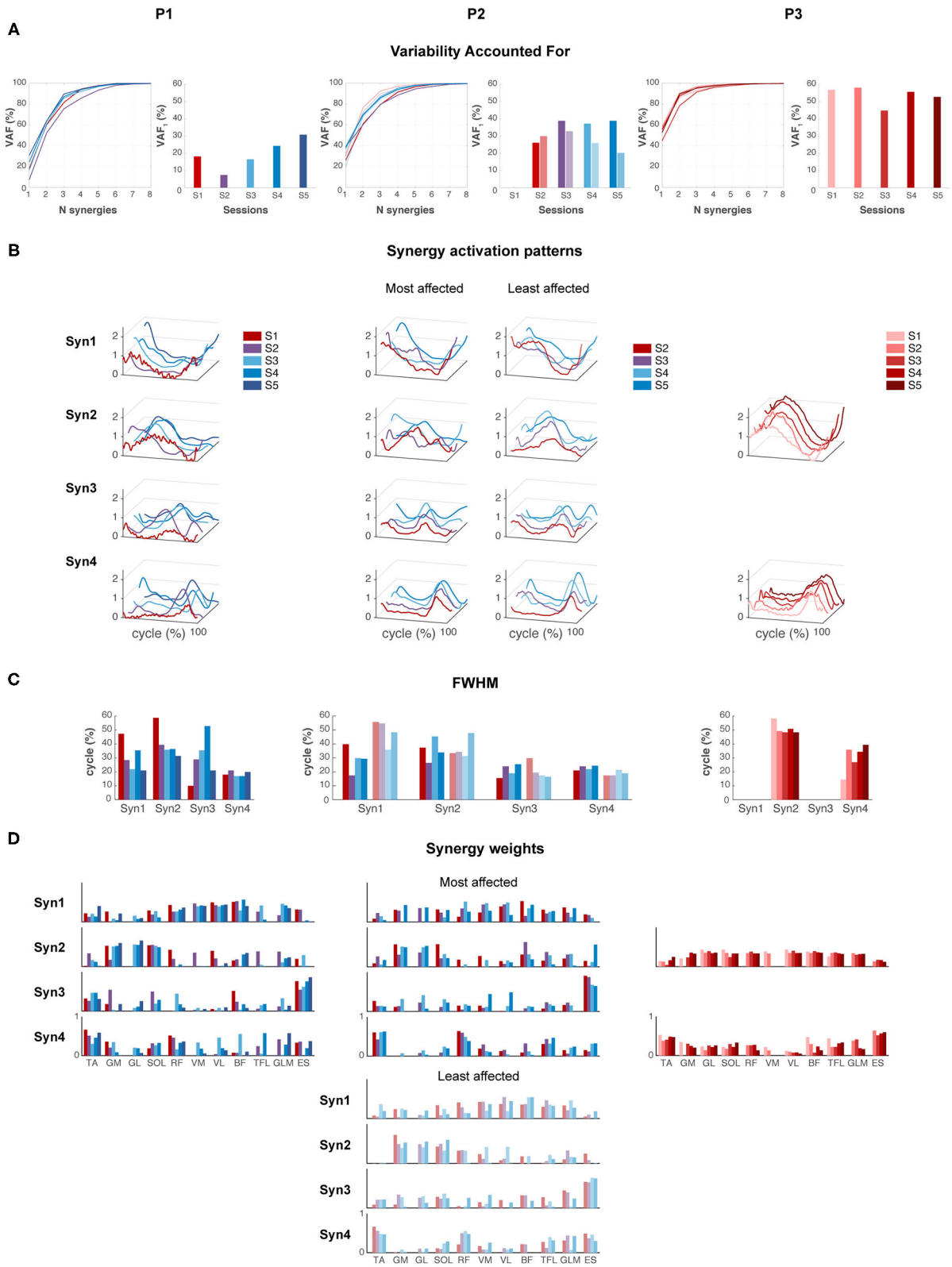

FIGURE 5 | Muscle synergies. **(A)** Variability accounted for (VAF) by one to eight synergies, and for the first synergy (VAF1). **(B)** Synergy activation patterns for a fixed number of synergies: four for P1 and P2, and two for P3. **(C)** Full-width of the half maximum (FWHM) per muscle synergy. **(D)** Synergy weights: contribution of each muscle to each synergy across sessions.

coordination matured side-specific from just before IW onset during the consecutive 6 months. This period might be devoted to postural gait requirements, whereas in the following years, gait coordination is (merely) refined (Bril and Breniere, 1992; Breniere and Bril, 1998).

In contrast to the rapid maturation of intersegmental coordination after the onset of IW, muscle activity and its major burst duration appeared quite variable between strides in the first 6 to 12 months after the FS. This agrees with previous findings from, e.g., Chang et al. (2006). Probably, toddlers slowly discover how to optimize their muscular activity. In our study, the duration of EMG bursts increased from SW to IW. Cappellini et al. (2016) reported a decrease in FWHM from TD toddlers (1–3 years old) to older TD children, whereas this reduction was not visible in the TD toddler group. The latter falls in the (corrected) age range in our study. Moreover, Cappellini et al. (2016) reported wider EMG bursts in children with CP (2–11 years old), arguably similar to muscle activation patterns in TD toddlers. Similar results were reported by Prosser et al. (2010) in children with CP (2–9 years old) when compared with TD children with similar walking experience (average of 28 months of walking experience). Despite the presence of young children, the age range of the children with CP included in these cross-sectional studies is quite large. In our study, we did not have a TD control group, but we did observe wider average EMG bursts in the more severely affected child with bilateral CP with respect to the children who developed IW. Here we would like to note that gait patterns and their corresponding muscle activity are highly variable in toddlers. It is well possible that a reduction in EMG burst duration occurs later on during development, while children refine their motor pattern (see above). We did notice short bursts of EMG activity immediately after foot strike in the shank and calf muscles of the child with bilateral CP and the calf muscles of mainly the most affected leg of the child with unilateral CP, which might have been caused by spasticity, i.e., hyperreflexive reactions upon muscle stretch following foot strike (Forssberg, 1985).

The control modules that account for muscle activity during walking seemed to develop in the children who developed IW, whereas there were no major changes in the more severely affected child with bilateral CP. The two children walking independently recruited four synergies, whereas the child without the ability to walk independently recruited only two synergies. While gait kinematics improved during IW in the child with unilateral CP, the modulation of groups of muscles to efficiently perform this motor action may have lagged behind. This finds support by previous research reporting the absence of a direct relation between gait kinematics and muscle activations (Buurke et al., 2008) or muscle synergies (Booth et al., 2019). In fact—if true—this implies that gait kinematics and neuromuscular control may follow a different developmental path. The muscle synergy patterns of the child with bilateral CP resemble that of the "primitive" neonate stepping, recruiting two wider synergies with a lot of co-contraction in antagonist muscles (Dominici et al., 2011). Neonate stepping reflects the immature walking pattern that lacks a heel strike and with the tendency to walk on the toes (Forssberg, 1985). Put differently, the child with bilateral CP might still depend mainly on spinal input, whereas supraspinal influence is lacking.

The children were small, especially in the early sessions, yielding limited space for EMG electrodes and, as a consequence, a possible contamination of the EMG recordings due to electrical cross-talk between adjacent muscles that could have affected the data quality. However, the small size of the EMG electrodes used in our experiments and the chosen interelectrode distance should have minimized the pickup from nearby muscles. While it is not possible to dissociate coactivation from cross-talk in adjacent muscles, muscle synergy analysis can identify whether a muscle is activated independent from an adjacent muscle even in the presence of crosstalk. It has been recognized that, if cross-talk did exist, it would likely have affected only the synergy weights and not the number of muscle synergies or the temporal activation patterns (Ivanenko et al., 2004b; Chvatal and Ting, 2013).

In addition, the child with bilateral CP was already 2.5 years old at the time of the first session, whereas it would have certainly been interesting to investigate its walking pattern below that age. Presumably, it would have been a very similar pattern given the little change observed between the ages of 2.5 and 4.5 years for this child.

We identified changes in gait kinematics and neuromuscular control underlying the development of walking in three cases at high risk of CP with divergent developmental trajectories. We showed that such analyses are feasible in very young children. Future longitudinal research with a larger sample of children at high risk of CP could and should provide more insight into the underlying mechanisms of the development of walking. Yet, to establish whether muscle synergies are encoded in the cortex (Zandvoort et al., 2019) or whether they originate solely from spinal cord (Ivanenko et al., 2008; Cappellini et al., 2010) or brainstem (Schepens and Drew, 2004) remains a topic of debate (Bizzi and Cheung, 2013). To solve this puzzle, supplementing our approach by, e.g., synchronous EEG recordings, appears a valid option. Following this idea might be an important step toward the design of early interventions targeting the neural pathways. Combined with the use of novel technologies, such as wearable sensors (Redd et al., 2019; Xu et al., 2019; Airaksinen et al., 2020), and treatments such as feedback training (Booth et al., 2019), and electrical stimulation of muscles, tendons (Sommerfelt et al., 2001; Stackhouse et al., 2007; Wright et al., 2012), or spinal cord (Solopova et al., 2017), during the critical period of walking development, we might become able to improve early identification of motor deficits in children with early brain lesions and identify targets for early intervention to effectively improve walking function in CP.

DATA AVAILABILITY STATEMENT

The original contributions presented in the study are included in the article/**Supplementary Material**, further inquiries can be directed to the Corresponding author.

ETHICS STATEMENT

The studies involving human participants were reviewed and approved by Medical Ethics Committee (METc) of the Amsterdam UMC (location VUmc) (NL59589.029.16). Written informed consent to participate in this study was provided by the participants' legal guardian/next of kin.

AUTHOR CONTRIBUTIONS

ABe, ABu, and ND designed the study. ABu and LvdP assisted in the recruitment of CP participants. ABe and ND carried out the measurements. ABe, MB, ABu, and ND performed the data analysis, and carried out drafting the manuscript. All the authors have read and concurred with the content in the final manuscript.

FUNDING

This project has received funding from the European Research Council (ERC) under the European Union's Horizon 2020 research and innovation programme (grant agreement n. 715945 Learn2Walk) and from the Dutch Organization for Scientific Research (NWO) VIDI grant (grant agreement n. 016.156.346 FirSTeps).

ACKNOWLEDGMENTS

We would like to thank the parents and children who participated in this study. We would like to express our appreciation for the support by the pediatric physiotherapists Danny Cornelissen, Eefje Muselaers and Emma Verwaaijen, and the researchers Marije Goudriaan, Marzieh Borhanazad, and Coen Zandvoort for their support during the experiments.

SUPPLEMENTARY MATERIAL

The Supplementary Material for this article can be found online at: https://www.frontiersin.org/articles/10.3389/fnhum.2021.659415/full#supplementary-material

REFERENCES

Airaksinen, M., Rasanen, O., Ilen, E., Hayrinen, T., Kivi, A., Marchi, V., et al. (2020). Automatic posture and movement tracking of infants with wearable movement sensors. *Sci. Rep.* 10:169. doi: 10.1038/s41598-019-56862-5

Alves-Pinto, A., Blumenstein, T., Turova, V., and Lampe, R. (2016). Altered lower leg muscle activation patterns in patients with cerebral palsy during cycling on an ergometer. *Neuropsychiatr. Dis. Treat.* 12, 1445–1456. doi: 10.2147/NDT.S98260

Bach, M. M., Daffertshofer, A., and Dominici, N. (2021). Muscle synergies in children walking and running on a treadmill. *Front. Hum. Neurosci.* 15:637157. doi: 10.3389/fnhum.2021.637157

Bekius, A., Bach, M. M., van der Krogt, M. M., de Vries, R., Buizer, A. I., and Dominici, N. (2020). Muscle synergies during walking in children with cerebral palsy: a systematic review. *Front. Physiol.* 11:632. doi: 10.3389/fphys.2020.00632

Berger, W. (1998). Characteristics of locomotor control in children with cerebral palsy. *Neurosci. Biobehav. Rev.* 22, 579–582. doi: 10.1016/S0149-7634(97)00047-X

Berger, W., Altenmueller, E., and Dietz, V. (1984). Normal and impaired development of children's gait. *Hum. Neurobiol.* 3, 163–170.

Bianchi, L., Angelini, D., Orani, G. P., and Lacquaniti, F. (1998). Kinematic coordination in human gait: relation to mechanical energy cost. *J. Neurophysiol.* 79, 2155–2170. doi: 10.1152/jn.1998.79.4.2155

Bizzi, E., and Cheung, V. C. (2013). The neural origin of muscle synergies. *Front. Comput. Neurosci.* 7:51. doi: 10.3389/fncom.2013.00051

Booth, A. T. C., van der Krogt, M. M., Harlaar, J., Dominici, N., and Buizer, A. I. (2019). Muscle synergies in response to biofeedback-driven gait adaptations in children with cerebral palsy. *Front. Physiol.* 10:1208. doi: 10.3389/fphys.2019.01208

Borghese, N. A., Bianchi, L., and Lacquaniti, F. (1996). Kinematic determinants of human locomotion. *J. Physiol.* 494, 863–879. doi: 10.1113/jphysiol.1996.sp021539

Breniere, Y., and Bril, B. (1998). Development of postural control of gravity forces in children during the first 5 years of walking. *Exp. Brain Res.* 121, 255–262. doi: 10.1007/s002210050458

Bril, B., and Breniere, Y. (1992). Postural requirements and progression velocity in young walkers. *J. Mot. Behav.*, 24, 105–116. doi: 10.1080/00222895.1992.9941606

Buurke, J. H., Nene, A. V., Kwakkel, G., Erren-Wolters, V., Ijzerman, M. J., and Hermens, H. J. (2008). Recovery of gait after stroke: what changes? *Neurorehabil. Neural. Repair.* 22, 676–683. doi: 10.1177/1545968308317972

Cappellini, G., Ivanenko, Y. P., Dominici, N., Poppele, R. E., and Lacquaniti, F. (2010). Migration of motor pool activity in the spinal cord reflects body mechanics in human locomotion. *J. Neurophysiol.* 104, 3064–3073. doi: 10.1152/jn.00318.2010

Cappellini, G., Ivanenko, Y. P., Martino, G., MacLellan, M. J., Sacco, A., Morelli, D., et al. (2016). Immature spinal locomotor output in children with cerebral palsy. *Front. Physiol.* 7:478. doi: 10.3389/fphys.2016.00478

Cappellini, G., Sylos-Labini, F., MacLellan, M. J., Sacco, A., Morelli, D., Lacquaniti, F., et al. (2018). Backward walking highlights gait asymmetries in children with cerebral palsy. *J. Neurophysiol.* 119, 1153–1165. doi: 10.1152/jn.00679.2017

Chang, C. L., Kubo, M., Buzzi, U., and Ulrich, B. (2006). Early changes in muscle activation patterns of toddlers during walking. *Infant Behav. Dev.* 29, 175–188. doi: 10.1016/j.infbeh.2005.10.001

Cheron, G., Bouillot, E., Dan, B., Bengoetxea, A., Draye, J. P., and Lacquaniti, F. (2001). Development of a kinematic coordination pattern in toddler locomotion: planar covariation. *Exp. Brain Res.* 137, 455–466. doi: 10.1007/s002210000663

Chvatal, S. A., and Ting, L. H. (2013). Common muscle synergies for balance and walking. *Front. Comput. Neurosci.* 7:48. doi: 10.3389/fncom.2013.00048

Damiano, D. (2015). Muscle synergies: input or output variables for neural control? *Dev. Med. Child Neurol.* 57, 1091–1092. doi: 10.1111/dmcn.12843

d'Avella, A., Portone, A., and Lacquaniti, F. (2011). Superposition and modulation of muscle synergies for reaching in response to a change in target location. *J. Neurophysiol.* 106, 2796–2812. doi: 10.1152/jn.00675.2010

Dewolf, A. H., Sylos-Labini, F., Cappellini, G., Lacquaniti, F., and Ivanenko, Y. (2020). Emergence of different gaits in infancy: relationship between developing neural circuitries and changing biomechanics. *Front. Bioeng. Biotechnol.* 8:473. doi: 10.3389/fbioe.2020.00473

Dominici, N., Ivanenko, Y. P., Cappellini, G., d'Avella, A., Mondi, V., Cicchese, M., et al. (2011). Locomotor primitives in newborn babies and their development. *Science* 334, 997–999. doi: 10.1126/science.1210617

Dominici, N., Ivanenko, Y. P., Cappellini, G., Zampagni, M. L., and Lacquaniti, F. (2010). Kinematic strategies in newly walking toddlers stepping over different support surfaces. *J. Neurophysiol.* 103, 1673–1684. doi: 10.1152/jn.00945.2009

Dominici, N., Ivanenko, Y. P., and Lacquaniti, F. (2007). Control of foot trajectory in walking toddlers: adaptation to load changes. *J. Neurophysiol.* 97, 2790–2801. doi: 10.1152/jn.00262.2006

Forssberg, H. (1985). Ontogeny of human locomotor control. I. Infant stepping, supported locomotion and transition to independent locomotion. *Exp. Brain Res.* 57, 480–493. doi: 10.1007/BF00237835

Goudriaan, M., Shuman, B. R., Steele, K. M., Van den Hauwe, M., Goemans, N., Molenaers, G., et al. (2018). Non-neural muscle weakness has limited influence on complexity of motor control during gait. *Front. Hum. Neurosci.* 12:5. doi: 10.3389/fnhum.2018.00005

Hart, C. B., and Giszter, S. F. (2010). A neural basis for motor primitives in the spinal cord. *J. Neurosci.* 30, 1322–1336. doi: 10.1523/JNEUROSCI.5894-08.2010

Hashiguchi, Y., Ohata, K., Osako, S., Kitatani, R., Aga, Y., Masaki, M., et al. (2018). Number of synergies is dependent on spasticity and gait kinetics in children with cerebral palsy. *Pediatr. Phys. Ther.* 30, 34–38. doi: 10.1097/PEP.0000000000000460

Hermens, H. J., Freriks, B., Disselhorst-Klug, C., and Rau, G. (2000). Development of recommendations for SEMG sensors and sensor placement procedures. *J. Electromyogr. Kinesiol.* 10, 361–374. doi: 10.1016/S1050-6411(00)00027-4

Himmelmann, K., and Uvebrant, P. (2018). The panorama of cerebral palsy in Sweden part XII shows that patterns changed in the birth years 2007–2010. *Acta Paediatrica* 107, 462–468. doi: 10.1111/apa.14147

Ivanenko, Y. P., Cappellini, G., Dominici, N., Poppele, R. E., and Lacquaniti, F. (2005). Coordination of locomotion with voluntary movements in humans. *J. Neurosci.* 25, 7238–7253. doi: 10.1523/JNEUROSCI.1327-05.2005

Ivanenko, Y. P., Cappellini, G., Poppele, R. E., and Lacquaniti, F. (2008). Spatiotemporal organization of alpha-motoneuron activity in the human spinal cord during different gaits and gait transitions. *Eur. J. Neurosci.* 27, 3351–3368. doi: 10.1111/j.1460-9568.2008.06289.x

Ivanenko, Y. P., Dominici, N., Cappellini, G., Dan, B., Cheron, G., and Lacquaniti, F. (2004a). Development of pendulum mechanism and kinematic coordination from the first unsupported steps in toddlers. *J. Exp. Biol.* 207(Pt 21), 3797–3810. doi: 10.1242/jeb.01214

Ivanenko, Y. P., Dominici, N., and Lacquaniti, F. (2007). Development of independent walking in toddlers. *Exerc. Sport Sci. Rev.* 35, 67–73. doi: 10.1249/JES.0b013e31803eafa8

Ivanenko, Y. P., Grasso, R., Macellari, V., and Lacquaniti, F. (2002). Control of foot trajectory in human locomotion: role of ground contact forces in simulated reduced gravity. *J. Neurophysiol.* 87, 3070–3089. doi: 10.1152/jn.2002.87.6.3070

Ivanenko, Y. P., Poppele, R. E., and Lacquaniti, F. (2004b). Five basic muscle activation patterns account for muscle activity during human locomotion. *J. Physiol.* 556(Pt 1), 267–282. doi: 10.1113/jphysiol.2003.057174

Largo, R. H., Molinari, L., Weber, M., Comenale Pinto, L., and Duc, G. (1985). Early development of locomotion: significance of prematurity, cerebral palsy and sex. *Dev. Med. Child Neurol.* 27, 183–191. doi: 10.1111/j.1469-8749.1985.tb03768.x

Leonard, C. T., Hirschfeld, H., and Forssberg, H. (1991). The development of independent walking in children with cerebral palsy. *Dev. Med. Child Neurol.* 33, 567–577. doi: 10.1111/j.1469-8749.1991.tb14926.x

Meyns, P., Desloovere, K., Van Gestel, L., Massaad, F., Smits-Engelsman, B., and Duysens, J. (2012). Altered arm posture in children with cerebral palsy is related to instability during walking. *Eur. J. Paediatr. Neurol.* 16, 528–535. doi: 10.1016/j.ejpn.2012.01.011

Molenberghs, G., and Verbeke, G. (2000). *Linear Mixed Models for Longitudinal Data*. New York, NY: Springer. doi: 10.1007/978-1-4419-0300-6

Palisano, R., Rosenbaum, P., Walter, S., Russell, D., Wood, E., and Galuppi, B. (1997). Development and reliability of a system to classify gross motor function in children with cerebral palsy. *Dev. Med. Child Neurol.* 39, 214–223. doi: 10.1111/j.1469-8749.1997.tb07414.x

Prosser, L. A., Lee, S. C., VanSant, A. F., Barbe, M. F., and Lauer, R. T. (2010). Trunk and hip muscle activation patterns are different during walking in young children with and without cerebral palsy. *Phys. Ther.* 90, 986–997. doi: 10.2522/ptj.20090161

Redd, C. B., Barber, L. A., Boyd, R. N., Varnfield, M., and Karunanithi, M. K. (2019). "Development of a wearable sensor network for quantification of infant general movements for the diagnosis of cerebral palsy," in *Paper Presented at the 2019 41st Annual International Conference of the IEEE Engineering in Medicine and Biology Society (EMBC)* (Berlin). doi: 10.1109/EMBC.2019.8857377

Schepens, B., and Drew, T. (2004). Independent and convergent signals from the pontomedullary reticular formation contribute to the control of posture and movement during reaching in the cat. *J. Neurophysiol.* 92, 2217–2238. doi: 10.1152/jn.01189.2003

Schwartz, M. H., Rozumalski, A., and Steele, K. M. (2016). Dynamic motor control is associated with treatment outcomes for children with cerebral palsy. *Dev. Med. Child Neurol.* 58, 1139–1145. doi: 10.1111/dmcn.13126

Shuman, B., Goudriaan, M., Bar-On, L., Schwartz, M. H., Desloovere, K., and Steele, K. M. (2016). Repeatability of muscle synergies within and between days for typically developing children and children with cerebral palsy. *Gait Posture* 45, 127–132. doi: 10.1016/j.gaitpost.2016.01.011

Shuman, B. R., Goudriaan, M., Desloovere, K., Schwartz, M. H., and Steele, K. M. (2018). Associations between muscle synergies and treatment outcomes in cerebral palsy are robust across clinical centers. *Arch Phys. Med. Rehabil.* 99, 2175–2182. doi: 10.1016/j.apmr.2018.03.006

Shuman, B. R., Goudriaan, M., Desloovere, K., Schwartz, M. H., and Steele, K. M. (2019). Muscle synergies demonstrate only minimal changes after treatment in cerebral palsy. *J. Neuroeng. Rehabil.* 16:46. doi: 10.1186/s12984-019-0502-3

Shuman, B. R., Schwartz, M. H., and Steele, K. M. (2017). Electromyography data processing impacts muscle synergies during gait for unimpaired children and children with cerebral palsy. *Front. Comput. Neurosci.* 11:50. doi: 10.3389/fncom.2017.00050

Solopova, I. A., Sukhotina, I. A., Zhvansky, D. S., Ikoeva, G. A., Vissarionov, S. V., Baindurashvili, A. G., et al. (2017). Effects of spinal cord stimulation on motor functions in children with cerebral palsy. *Neurosci. Lett.* 639, 192–198. doi: 10.1016/j.neulet.2017.01.003

Sommerfelt, K., Markestad, T., Berg, K., and Saetesdal, I. (2001). Therapeutic electrical stimulation in cerebral palsy: a randomized, controlled, crossover trial. *Dev. Med. Child. Neurol.* 43, 609–613. doi: 10.1017/S0012162201001104

Stackhouse, S. K., Binder-Macleod, S. A., Stackhouse, C. A., McCarthy, J. J., Prosser, L. A., and Lee, S. C. (2007). Neuromuscular electrical stimulation versus volitional isometric strength training in children with spastic diplegic cerebral palsy: a preliminary study. *Neurorehabil. Neural. Repair.* 21, 475–485. doi: 10.1177/1545968306298932

Steele, K. M., Rozumalski, A., and Schwartz, M. H. (2015). Muscle synergies and complexity of neuromuscular control during gait in cerebral palsy. *Dev. Med. Child Neurol.* 57, 1176–1182. doi: 10.1111/dmcn.12826

Steele, K. M., Tresch, M. C., and Perreault, E. J. (2013). The number and choice of muscles impact the results of muscle synergy analyses. *Front. Comput. Neurosci.* 7:105. doi: 10.3389/fncom.2013.00105

Sylos-Labini, F., La Scaleia, V., Cappellini, G., Fabiano, A., Picone, S., Keshishian, E. S., et al. (2020). Distinct locomotor precursors in newborn babies. *Proc. Natl. Acad. Sci. U.S.A.*, 117, 9604–9612. doi: 10.1073/pnas.1920984117

Tang, L., Li, F., Cao, S., Zhang, X., Wu, D., and Chen, X. (2015). Muscle synergy analysis in children with cerebral palsy. *J. Neural. Eng.* 12:046017. doi: 10.1088/1741-2560/12/4/046017

Winter, D. A. (1992). Foot trajectory in human gait: a precise and multifactorial motor control task. *Phys. Ther.* 72, 45–53. doi: 10.1093/ptj/72.1.45

Wright, P. A., Durham, S., Ewins, D. J., and Swain, I. D. (2012). Neuromuscular electrical stimulation for children with cerebral palsy: a review. *Arch. Dis. Child.* 97, 364–371. doi: 10.1136/archdischild-2011-300437

Xu, S., Jayaraman, A., and Rogers, J. A. (2019). Skin sensors are the future of health care. *Nature* 571, 319–321. doi: 10.1038/d41586-019-02143-0

Zandvoort, C. S., van Dieen, J. H., Dominici, N., and Daffertshofer, A. (2019). The human sensorimotor cortex fosters muscle synergies through cortico-synergy coherence. *Neuroimage* 199, 30–37. doi: 10.1016/j.neuroimage.2019.05.041

Conflict of Interest: The authors declare that the research was conducted in the absence of any commercial or financial relationships that could be construed as a potential conflict of interest.

frontiers in Human Neuroscience

ORIGINAL RESEARCH
published: 09 June 2021
doi: 10.3389/fnhum.2021.668918

Neural Entrainment Meets Behavior: The Stability Index as a Neural Outcome Measure of Auditory-Motor Coupling

Mattia Rosso[1]*, *Marc Leman*[1] and *Lousin Moumdjian*[1,2,3]

[1]Institute of Psychoacoustics and Electronic Music (IPEM), Faculty of Arts and Philosophy, Ghent University, Ghent, Belgium, [2]UMSC Hasselt-Pelt, Limburg, Belgium, [3]REVAL Rehabilitation Research Center, Faculty of Rehabilitation Sciences, Limburg, Belgium

OPEN ACCESS

Edited by:
Daniela De Bartolo,
Sapienza University of Rome, Italy

Reviewed by:
Johanna Maria Rimmele,
Max Planck Society (MPG), Germany
Daniel Charles,
University of California, Merced, United States
Andrew L. Bowers,
University of Arkansas, United States

***Correspondence:**
Mattia Rosso
mattia.rosso@ugent.be

Specialty section:
This article was submitted to Motor Neuroscience, a section of the journal Frontiers in Human Neuroscience

Received: 17 February 2021
Accepted: 29 April 2021
Published: 09 June 2021

Citation:
Rosso M, Leman M and Moumdjian L (2021) Neural Entrainment Meets Behavior: The Stability Index as a Neural Outcome Measure of Auditory-Motor Coupling. Front. Hum. Neurosci. 15:668918. doi: 10.3389/fnhum.2021.668918

Understanding rhythmic behavior in the context of coupled auditory and motor systems has been of interest to neurological rehabilitation, in particular, to facilitate walking. Recent work based on behavioral measures revealed an entrainment effect of auditory rhythms on motor rhythms. In this study, we propose a method to compute the neural component of such a process from an electroencephalographic (EEG) signal. A simple auditory-motor synchronization paradigm was used, where 28 healthy participants were instructed to synchronize their finger-tapping with a metronome. The computation of the neural outcome measure was carried out in two blocks. In the first block, we used Generalized Eigendecomposition (GED) to reduce the data dimensionality to the component which maximally entrained to the metronome frequency. The scalp topography pointed at brain activity over contralateral sensorimotor regions. In the second block, we computed instantaneous frequency from the analytic signal of the extracted component. This returned a time-varying measure of frequency fluctuations, whose standard deviation provided our "*stability index*" as a neural outcome measure of auditory-motor coupling. Finally, the proposed neural measure was validated by conducting a correlation analysis with a set of behavioral outcomes from the synchronization task: resultant vector length, relative phase angle, mean asynchrony, and tempo matching. Significant moderate negative correlations were found with the first three measures, suggesting that the stability index provided a quantifiable neural outcome measure of entrainment, with selectivity towards phase-correction mechanisms. We address further adoption of the proposed approach, especially with populations where sensorimotor abilities are compromised by an underlying pathological condition. The impact of using stability index can potentially be used as an outcome measure to assess rehabilitation protocols, and possibly provide further insight into neuropathological models of auditory-motor coupling.

Keywords: auditory-motor coupling, entrainment, synchronization, instantaneous frequency, eigendecomposition, finger-tapping, stability index, EEG

INTRODUCTION

Auditory stimuli such as music or metronomes can entrain human movement, and this phenomenon can be used for neurological rehabilitation purposes. Particularly, evidence has been established that auditory stimuli can facilitate walking in persons with Parkinson's disease (Ghai et al., 2018; De Bartolo et al., 2020), stroke (Yoo and Kim, 2016; Hutchinson et al., 2020), and multiple sclerosis (Moumdjian et al., 2019b). Auditory stimuli convey temporal structures that serve as affordances for the motor system to interact with (Leman, 2016). In our previous work, we showed that auditory rhythms can entrain a person's motor rhythms, thus affecting abilities for walking. The underlying mechanism can be explained in terms of sensorimotor phase-locking, prediction error minimization, and/or dynamical interactions (Phillips-Silver et al., 2010; Leman, 2016). The outcome of an entrainment process is typically a more stable state of synchronization (Phillips-Silver et al., 2010; Moens et al., 2014; Leman, 2016). So far, the entrainment effect has been quantified by means of behavioral outcome measures, in particular temporal outcomes of the rhythmic auditory-motor coupling (Moumdjian et al., 2018), which contributed to a better understanding of underlying mechanisms as a result of the interaction (Moumdjian et al., 2019c, 2020), and to the development of task-oriented training tools for walking in persons with the neurological disease of multiple sclerosis (Moumdjian et al., 2019a,b).

Part of the variability in entrainment can be attributed to individual synchronization abilities. When presented with auditory stimuli and asked to walk to them, there are participants who spontaneously synchronize, and others who do not. This ability is not only limited to neurological populations (Moumdjian et al., 2019c), but also holds true for healthy participants (Van Dyck et al., 2015) where the percentage of spontaneous synchronizers vs. non-synchronizers is about 50% −50%. A number of factors contribute to the tendency to rhythmically entrain and synchronize (Wilson and Cook, 2016). The first factor is temporal perception and prediction. Studies on Parkinson's disease have concluded that those participants with higher perceptual sensorimotor synchronization abilities, quantified by behavioral sensorimotor tapping tasks involving finger tapping (Dalla Bella et al., 2017b), had a better outcome on their walking parameters after being subjected to walk to auditory stimuli (Dalla Bella et al., 2017a). The second factor is motor (e.g., physical capacity) and/or cognitive (e.g., attentive and pre-attentive) functions. For example, studies comparing spontaneous and instructed synchronization of walking (Leow et al., 2018; Moumdjian et al., 2019c) and running (Van Dyck et al., 2020) to music have been conclusive that explicit instructions to synchronize resulted in a higher synchronization tendency, as compared to spontaneous synchronization. The former study also noted this difference across different motor thresholds which was provided as a result of walking to different tempi, starting from the natural comfortable tempo and up to + 10%, in increments of 2% (Moumdjian et al., 2019b,c).

Up to now, most studies on neurological populations, investigating entrainment and synchronization during walking tasks, are based on empirical evidence using behavioral outcomes (Moumdjian et al., 2018). However, we believe that the development of complementary neurological outcomes could offer a further understanding of entrainment and synchronization, potentially leading to the development of more individualized and more fine-tuned rehabilitation approaches.

The present study, therefore, aims at quantifying a neural outcome measure of entrainment and synchronization in combination with behavioral outcomes. We propose the use of electroencephalography (EEG) as a method to measure neural entrainment of the motor system to rhythmic stimuli. The novel outcome measure is based on a finger tapping task (Bavassi et al., 2013; McPherson et al., 2018; Lopez and Laje, 2019). **Figure 1** shows a graphical illustration of this study's rationale and proposed contribution to the current state of the art.

Our approach is based on Steady-State Evoked Potentials (SSEPs) (Vialatte et al., 2010; Norcia et al., 2015). Given a steady periodic stimulation, a series of subsequent evoked responses are elicited in the electrical brain activity, generating a periodic pattern of transients in the EEG signal. By transforming the signal to the frequency domain by means of Fast Fourier Transform (FFT), it can be observed that the EEG spectrum is dominated by a prominent peak at the stimulation frequency and its harmonics. Upon exposure to rhythmic auditory stimuli, patterns emerge in brain activity and match the dominant spectral features of the stimulation. Studies show that neural entrainment can be measured at different hierarchical levels of the stimulus temporal structure, or of its representation (Nozaradan et al., 2011). As the sound envelope of a musical stimulus exhibits a periodic low-frequency amplitude modulation in correspondence with the beat, it is possible to observe a match between the beat-related harmonics of the EEG spectrum and the sound spectrum (Lenc et al., 2018). However, the observed entrained components are not always entirely driven by sensory stimulation. In fact, given the same energy in the stimulus, SSEP amplitude is modulated by attention (Andersen et al., 2011; Kashiwase et al., 2012), internal representation of metric structure (Nozaradan et al., 2012), sensorimotor integration (Nozaradan et al., 2015) and interpersonal coordination (Varlet et al., 2020).

The SSEP technique is relatively straightforward in modeling bottom-up and top-down components of rhythm perception in terms of Fourier coefficients. However, in order to link behavioral entrainment to a neural outcome measure, we believe that the signal phase should not be left out of the picture. Rajendran and Schnupp (2019) showed that shuffling the phase of a signal resulted in drastic differences in its time domain representation, whereas it remained invariant in the frequency domain. Although the analysis of peak amplitudes or z-scoress in a static spectrum might convey information about the outcome of neural entrainment, it is arguably insensitive to its dynamics in the time domain. One should consider that oscillatory processes in the brain are hardly stationary (Cohen, 2017) and the very definition of entrainment implies that an oscillator dynamically changes its frequency in order to achieve stable synchronization. This is precisely the phenomenon we intend to capture. Therefore, in order to quantify neural entrainment of

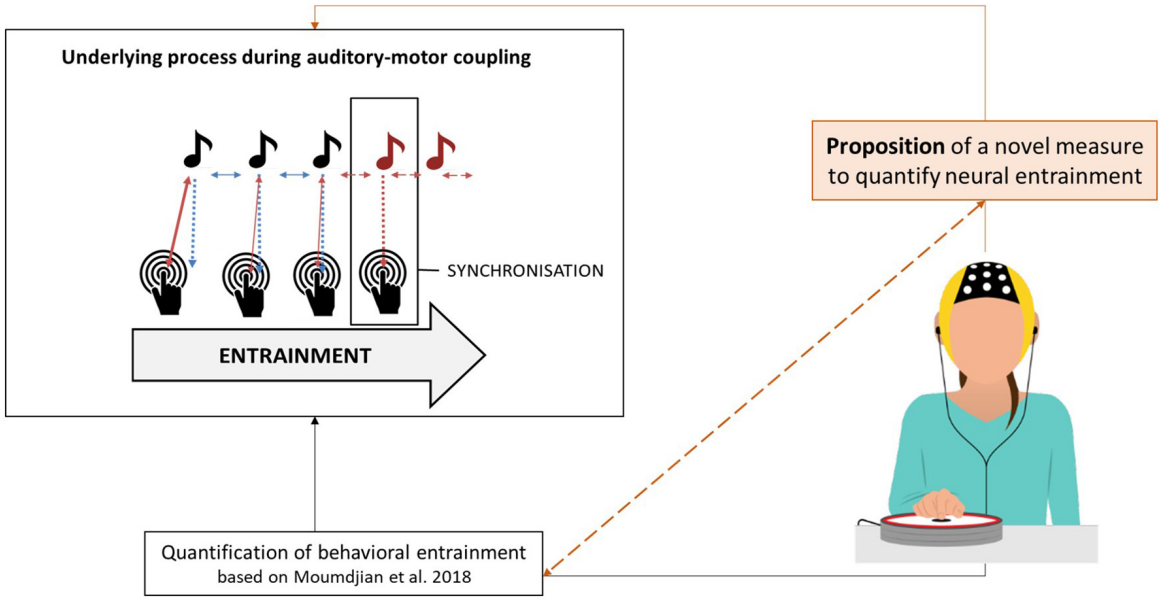

FIGURE 1 | Graphical illustration of the study's rationale and the proposed contribution to the current state of the art.

rhythmic stimuli, we argue in favor of a time-varying measure based on the phase of the neural entrained component.

With this study, we progress beyond the state of the art in the research on neural entrainment by optimizing the calculation of a neural outcome measure of auditory-motor coupling. We argue that such a measure can be used together with its behavioral counterparts. In combination, both the behavioral and neurological measures may unveil a further layer of the underlying mechanisms of the rich dynamical processes during motor and auditory interactions. Our first aim is to extract from the EEG signal the component which is maximally entrained to a periodic stimulus. For that, we compute a *stability index* to quantify frequency fluctuations over time. Our second aim is to validate the proposed index with a set of quantified behavioral outcome measures of auditory-motor coupling and entrainment (Moumdjian et al., 2018). In an auditory-motor coupling task, healthy participants were instructed to tap their index finger synchronizing to an auditory metronome (as illustrated in **Figure 1**). We hypothesized that our stability index would significantly correlate with the behavioral measures of entrainment. Specifically, a stable behavioral performance is expected to correlate with a stable entrained component, whereas a poor performance would result in wider frequency fluctuations over time.

MATERIALS AND METHODS

Participants

Twenty-eight (N = 28) right-handed participants took part in the study (18 females, 10 males; mean age = 29.07 years, standard deviation = 5.73 years). None of them had a history of neurological, major medical, or psychiatric disorders. All of them declared not to be professional musicians upon recruitment, although some of them had musical experience. Handedness was assessed by means of the Edinburgh Handedness Inventory (Oldfield, 1971). The experiment was approved by the Ethics Committee of Ghent University (Faculty of Arts and Philosophy) and informed written consent was obtained from each participant, who received a 15€ coupon as economic compensation for their participation.

Experimental Procedure

The experimental task consisted of a tapping synchronization paradigm, in a sitting position. Participants were provided with a custom-made pad containing piezo sensors to detect tapping onsets, and were instructed to tap their right index finger along with the assigned metronome during 390 seconds. During the task, participants were sitting on a comfortable chair equipped with armrests, so that their elbow could lay in a fixed position. Tapping movements were limited to wrist flexion in order to prevent movement-artifacts contamination of the EEG signal. Participants were monitored online and video-recorded by means of a USB camera to verify their compliance with the instructions. The importance of avoiding head and trunk movements was stressed.

Auditory Stimuli

Participants were presented with the stimuli *via* DefenderShield® air-tube earplugs. Ableton Live 10® was adopted as software for the metronome stimuli presentation. A periodic auditory cue was presented at a rate of 100 BPM to half of the participants, and 98.5 BPM to the other half (1.67 Hz and 1.64 Hz, respectively). The reason for such a minimal gap lies in the rationale of a larger experimental design in which the recordings were performed (Rosso et al., under review).

Behavioral Data Acquisition

Finger tapping onsets were recorded with a Teensy 3.2 microcontroller, operating as serial/MIDI hub in the setting. On the one hand, it received an analog input from piezo sensors inside the pads and printed on the serial port of the stimulation computer a timestamp each time a finger-tap pushed the signal above a resting threshold. The threshold was conservative enough to prevent false positives due to signal bouncing. Every time a metronome beat onset was presented to a participant, a MIDI message was sent to the Teensy to log its timestamp on the serial port. All timestamps were rounded to 1 ms resolution, which corresponds to 1 kHz sampling rate. The same device triggered the start of the EEG recording by sending a TTL trigger *via* a BNC connection.

Outcome Measures

Behavioral data and neurophysiological data were measured. These are outlined below:

Behavioral Data

The timestamps of finger-tapping and metronome beat onsets were imported in Matlab® and used to calculate a set of behavioral outcome measures of auditory-motor coupling and entrainment (Moumdjian et al., 2018). Before doing so, we removed the finger-tapping onsets following the previous one by less than 350 ms, as false positives could occasionally be recorded when a participant pushed the pad for too long or accidentally laid the hand on it. On average, 0.4 false positives were removed for every participant (standard deviation = 0.8). From the finger-tapping and metronome beat onsets time series, we calculated the following measures: relative phase angle, resultant vector length, mean asynchrony, and tempo matching. Below, details of the measures and the formulae used calculate these measures are outlined (Moens et al., 2014; Moumdjian et al., 2018):

Relative Phase Angle

This is an error measure of synchronization based on the phase difference between two oscillators (i.e., the participant tapping and the metronome beat onsets).

$$\varphi \;=\; 360 * \left(\frac{T_n - B_n}{B_{(n+1)} - B_n} \right)$$

Where T_n is the participant's tap onset n and B_n is the onset of the closest metronome beat. A negative angle indicates that the participant is tapping ahead of the metronome beat, while a positive angle indicates that the participant's tap is lagging behind the metronome beat. Alternatively, following recent work on modeling participants and periodic cues of systems of coupled oscillators in finger-tapping studies (Heggli et al., 2019), we processed the phase time series for participants and metronomes by interpolating the onsets as a ramp wave, wrapped from 0 to 2π radians at 1 kHz sampling rate. Provided with an estimate of the oscillators' positions on their cycle with a temporal resolution of 1 ms, we subtracted each participant's phase time series from the respective metronome. Finally, the CircStats toolbox (Berens, 2009) for Matlab® was used to calculate the mean angle from the resulting relative phase time series (in radians).

Resultant Vector Length

This expresses the stability of the relative phase angles over time. A unimodal distribution implies a high resultant vector length, whereas uniform and bipolar distributions result in a low resultant vector length. The measure was processed with the CircStats toolbox (Berens, 2009), using the relative phase time series as input. The measure ranges from 0 to 1, where 1 indicates perfect synchronization over time at a given relative phase angle and is calculated as follows:

$$R \;=\; \left| \frac{1}{N} \sum_{n\,=\,1}^{N} e^{i\phi T_n} \right|$$

Mean Asynchrony

This consists of the mean difference between the participant's tap onsets and the respective closest metronome's beat onset expressed in milliseconds.

$$\textit{Mean asynchrony} \;=\; \frac{1}{N} \sum_{n\,=\,1}^{N} T_n - B_n$$

Tempo Matching Accuracy

This indicates to what extent the overall tempo of the participant's tapping matches with the tempo of the metronome beats, based on inter-onset-intervals (IOIs). Inter-beat deviation (IBD) is calculated as the mean difference of a subject's IOIs with respect to the inter-beat-intervals.

$$IDB \;=\; \frac{1}{N} \sum_{n\,=\,2}^{N} \frac{(B_n - B_{(n-1)}) - (T_n - T_{(n-1)})}{B_n - B_{(n-1)}}$$

Neurophysiological Data

In order to compute our proposed outcome measure of neural entrainment, the following EEG processing pipeline was conducted. It consists of signal pre-processing, extraction of the entrained component *via* generalized eigendecomposition, and the computation of the stability index. The workflow is summarized in **Figure 2**.

Data Acquisition

Participants were equipped with a 64-channel waveguard™ original EEG headset (10-10 system, with Ag/AgCl electrodes). Data were recorded with an ANT-Neuro *eego*™*mylab* system at 1 kHz sampling rate. Impedances were monitored in the *eego*™ software environment and kept below 20 kΩ. In comparison with stricter thresholds (e.g., 5 kΩ or 10 kΩ), the choice made it feasible to maximize the homogeneity of impedance levels across electrodes, and in turn, optimize the covariance matrices used in our source separation. A referential montage was adopted, with "CPz" as the reference electrode.

Pre-processing

Pre-processing was carried out with a pipeline integrating functions from the *Fieldtrip toolbox* (Oostenveld et al., 2011) for

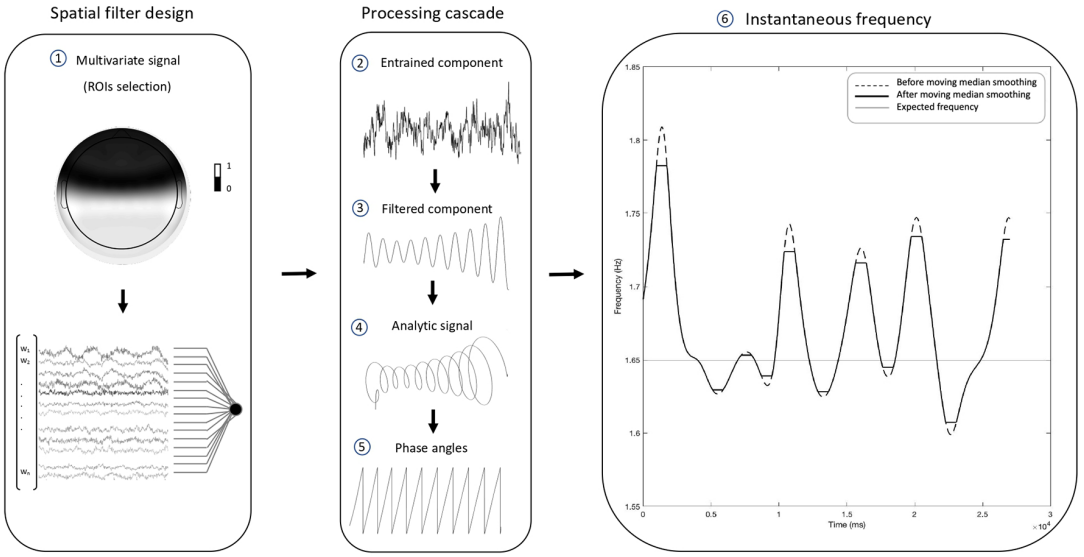

FIGURE 2 | Electroencephalographic (EEG) processing pipeline. The present pipeline illustrates the steps through which the proposed stability index was computed. Following the pre-processing, generalized eigendecomposition (GED) was performed on a broad set of regions of interest (ROIs). The vector of weights w associated with the highest eigenvalue was used as a spatial filter. By multiplying the data from the 37 channels behind the frontocentral line (1), we produced a single time series. The weights of the excluded channels were set to 0. The resulting "entrained component" (2) went through a cascade of computational steps: first, it was narrow-band filtered with a Gaussian filter centered at the stimulus frequency, in order to extract reliable phase time series unaffected by broad-band components (center = 1.65 Hz; width at half-maximum = 0.3 Hz). The "filtered component" (3) was then Hilbert-transformed to produce the "analytic signal" (4), from which we computed the "phase angles" time series (5). Finally, the phase was unwrapped, its first derivative was used to compute the "instantaneous frequency" (6), and a sliding moving median was applied in order to level out eventual artifactual peaks. The plot shows how the pipeline results in a time-varying measure of frequency over time, which fluctuates around the stimulation frequency (i.e., the thin horizontal line intercepting the y-axis at 1.65 Hz). The standard deviation of the instantaneous frequency provides a global measure of the stability of the entrained component for a given time window, which in our case was the whole duration of the task. We named such a global measure "stability index", for it equals 0 in the case of a flat horizontal line. Such a scenario would be observed in the ideal case of a perfectly stable component oscillating like a simple sine wave.

Matlab (MathWorks Inc., USA). Bad channels were identified by means of visual inspection of raw time series and variance distribution across channels. The recordings were re-referenced to the average of all the electrodes after channel rejection, to avoid noise leakage into the average. A high-pass Butterworth filter with 1 Hz cut-off was applied to the raw recordings to remove slow drifts. We preferred to choose this conservative threshold, given that occasional head movements and sweat potentials are more likely to occur over a long continuous recording. A low-pass Butterworth filter with 45 Hz cut-off was applied to remove high-frequency muscular activity. A notch filter centered at 50 Hz was applied to remove power-line noise up to the 3rd harmonic.

Independent component analysis (ICA) was conducted on full rank data to remove blinks and eye-movement artifacts, by means of visual inspection of topographical maps and time series of component activation. For this purpose, we ran the "runica" algorithm as implemented in Fieldtrip, excluding the reference "CPz" and the bad channels time series from the input matrix. Only those components which exhibited the stereotyped frontal distribution generated by blinks and lateral eye movements were removed. Although other artifactual sources could have been identified, we limited the selection to a few unambiguous components for the sake of replicability. A minimum of one and a maximum of three components were removed for every participant. The dataset was inspected prior to ICA decomposition and following ICA back-projection. Special attention was given to the electrodes where the activation of the artifactual component was maximal, namely the F, AF, and Fp clusters. Rejected bad channels were finally reconstructed after artifact removal, by computing a weighted average of all neighbors as implemented in Fieldtrip.

Recordings were treated as a continuous experimental run, without segmentation in epochs. This implies that no "bad trials" were removed. Further in this section, we will present how we dealt with transient bursts of artifactual activity in the continuous recording.

Generalized Eigendecomposition (GED)

In order to avoid channel selection bias while optimizing the signal-to-noise ratio between the entrained component and the broadband neural activity, we applied GED as first described in the context of source separation for rhythmic entrainment (Cohen and Gulbinaite, 2017). The technique consists of a spatial filter to reduce the multivariate dataset to one dimension, guided by some criteria: in this case, it was attunement to the stimulation frequency. This was achieved by computing the weighted average of a set of channels, where the vector of weights W was calculated by solving the following eigenequation:

$$R^{-1}SW = \Lambda W$$

where S is the covariance matrix calculated from the narrow-band filtered signal; R is the reference covariance matrix calculated from the broad-band signal; Λ is a set of eigenvalues. GED identifies eigenvectors W that best separate the signal ("S") covariance from the reference ("R") covariance matrix. The eigenvector associated with the largest eigenvalue is taken as a spatial filter. That eigenvector is then used to multiply the raw channel data to produce the single time series of our target entrained component. In the present work, a subset of 37 channels located behind the frontocentral "FC" line (mastoids excluded) was selected. By doing so, we intended to constrain the source separation and target a sensorimotor component entrained to the auditory stimulus. The excluded channels form the cluster which is typically expected from a purely auditory response at the scalp level (Nozaradan et al., 2011, 2015). The regions of interest (ROIs) selection is visually illustrated in **Figure 2**.

Given we were explicitly looking for frequency fluctuations, our narrow-band filter needed to be large enough in order to leave room for fluctuations around the entrained frequency. We designed our filter as a Gaussian function in the frequency domain, with the center at 1.654 Hz and a width of 0.3 Hz at half of the maximum gain. The center corresponds to the average of the two metronome frequencies. Given that the minimal difference across frequencies (1.667 Hz and 1.641 Hz) was tested to be negligible, we opted to design one single filter centered on their average. Such parameter represents an optimal trade-off in our application since it allows for fluctuations around the center frequency without overlapping with the high-pass band filter (cut-off = 1 Hz). We then filtered the signal on the whole subset of 37 channels by performing element-wise multiplication between the signal spectrum and the filter kernel. The resulting spectrum was eventually transformed with inverse Fast Fourier Transform back in the time domain. The frequency-domain representation of the filter kernel is provided in **Supplementary Figure 1**, along with additional information in the figure's description.

The reference R covariance matrix was here computed from the broadband multivariate signal. Our choice differs from the approach originally proposed by Cohen and Gulbinaite (2017) in that they propose a use-case for higher frequency ranges, which allows us to average the R matrices computed from two narrow-band Gaussian flankers neighboring the central filter on both sides. Their rationale was to minimize the contribution of intrinsic non-task-related rhythms in frequency ranges far from the one of interest, while avoiding bias from upper and lower frequency neighbors. Given that we were dealing with low frequencies (<2 Hz), it was not desirable for us to narrow-band filter the signal in a lower flanker, as we would have reached below the high-pass filter cut-off at 1 Hz (see **Supplementary Figure 1**). Therefore, if we adopted flankers, we would have had a bias to the right side of the spectrum.

In order to compute the respective covariance matrices from the broad-and narrow-band signals, we used the onset timing of the finger-taps performed by the participant to define time windows from −100 ms to 500 ms around the events. The approach provided us with a considerable number of covariance matrices for each recording (645 finger-taps were expected on average), such that we could remove the ones whose Euclidean distance from the grand-average covariance matrix exceeded the 2.23 *z*-scoress (i.e., corresponding to a probability of 0.013). The grand-average S and R covariance matrices were then calculated free from the occasional burst of artifactual activity over the long recording, compensating from the impossibility of performing a procedure of trial-removal during the pre-processing.

The quality of our GED application was assessed by inspecting the eigenspectrum, the topographical activation map, and the power spectrum of the extracted component (see **Figure 3**).

Stability Index

Once the entrained component was computed, we applied on it the same Gaussian filter (center at 1.654 Hz and 0.3 Hz width at half maximum) in order to extract reliable phase time series from the analytic signal. We calculated the analytic signal with the Hilbert transform and computed the instantaneous frequency time series from the first derivative of the unwrapped phase angles time series as indicated in Cohen (2014). The instantaneous frequency of a dynamical oscillating system can be defined as the change in the phase per unit time (Boashash, 1992). The derivative can then be converted to Hz applying the following formula:

$$Hz_t = \frac{s(\phi_t - \phi_{t-1})}{2\pi}$$

where s indicates the data sampling rate and Φ_t indicates the (unwrapped) phase angle at time t. A sliding moving median with a window width of 400 samples was used to smooth the instantaneous frequency time series, to remove occasional extreme bursts due to artifactual activity distorting phase time series. Finally, we calculated the standard deviation of instantaneous frequency over the whole task as a global measure of frequency stability over time, which we named the "stability index". A high standard deviation is thus indicative of wide instantaneous frequency fluctuations, and less overall stability of the entrained component. A standard deviation equal to 0 indicates a perfectly stable component, with the instantaneous frequency being a flat line at the constant value of the stimulus frequency.

Statistical Analysis

In order to validate our neural outcome measure, we calculated the Spearman coefficient for the correlation between the stability index and the four behavioral outcome measures (Moumdjian et al., 2018) reported above. This technique assesses the strength and significance of monotonic relationships between variables, regardless of its linearity. The Spearman correlation coefficient computed on continuous variables is the equivalent of the Pearson correlation coefficient computed on their ranks: it is exempt from the assumption of normal distribution of the pair of variables and robust to outliers and scaling effects. The following classification was used to categorize the correlation (Hinkle et al., 2002): 0.00–0.30 "negligible correlation", 0.30–0.50 "low

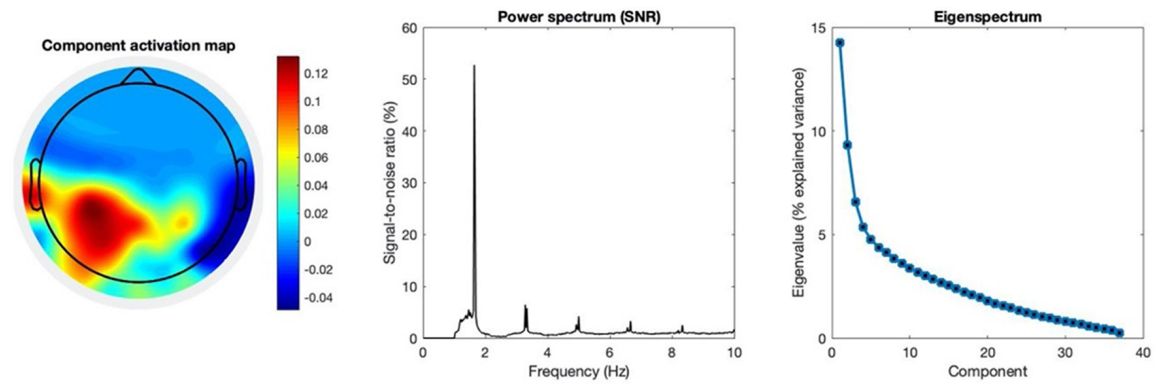

FIGURE 3 | Group-level assessment of the source separation. The following criteria were used to assess the quality of our source separation *via* generalized eigendecomposition (GED). **(A)** Topography. The grand-average coefficients of activation are shown in the topographic plot: maximal activation was recorded at the left centroparietal "CP" cluster and at left temporal electrodes ("T7" and "TP7"). It should be noted that we explicitly excluded from the spatial filter the channels located beyond the frontocentral line, for we intended to maximize an entrained response related to sensorimotor processing in the context of the task. **(B)** SNR spectrum. The grand-average power spectrum is represented here in the percentage signal-to-noise ratio between each data point and the mean power in the neighboring bins (0.5 Hz), in order to remove the physiological 1/f component of the spectrum (Freeman et al., 2003). **(C)** Eigenspectrum. The grand-average eigenvalues sorted in descending order exhibit a steep exponential decay. The vector of weights *w* used for our spatial filter is the one associated with the highest eigenvalue λ. Before averaging, eigenvalues were normalized and expressed as percentage of explained variance. All grand-averages were computed on the whole sample of participants (N = 28).

correlation", 0.50–0.070 "moderate correlation", 0.70–0.90 "high correlation", 0.90–0.100 "very high correlation".

RESULTS

Behavioral Outcome Measures

On a group level, we report that participants anticipated their tapping onsets relative to the beat, with a mean relative phase angle of -1.050 ± 0.681 radians and a mean asynchrony of -77.472 ± 40.603 ms. In addition, on a group level, they obtained a consistent synchronization with a relative vector length of 0.831 ± 0.156, and a consistent period measured by the inter-beat deviation of -0.001 ± 0.01. The individual participant behavioral results of these outcomes are reported in **Table 1**.

Neural Outcome Measures

Generalized Eigendecomposition

The source separation successfully extracted the entrained neural component of interest, as assessed by its spectral features and its topographical map of activation. The component associated with the higher eigenvalue was selected for our analyses. Additionally, we verified that the component associated with the second eigenvalue was not related to the behavioral performance. More details about the second component are provided in the **Supplementary Figures 2**, **3**. A detailed profile of the first component is provided in **Figure 3**, and its functional meaning will be further discussed in the next section.

Stability Index

The stability index was computed as the standard deviation of the component's instantaneous frequency, as described in the "Materials and Methods" section. On a group level, the stability index resulted in 0.062 ± 0.030 Hz. A stability index of 0 indicates a perfectly stable component, without any frequency fluctuation over time. The individual participant results of the stability index are reported in **Table 1**.

Correlation Analysis

As shown in **Figure 4**, Spearman correlation between the behavioral outcome measures of entrainment and the stability index revealed significant moderate negative correlations for relative phase angle, resultant vector length and mean asynchrony ($r = -0.566$, $p < 0.001$; $r = -0.652$, $p < 0.001$; $r = -0.523$, $p = 0.005$, respectively). A non-significant negligible correlation was found for the inter-beat deviation ($r = 0.107$, $p = 0.583$).

DISCUSSION

The main contribution of the present work is methodological, motivated by the need to compute a neural outcome measure of neural entrainment in the context of auditory-motor coupling and prospectively applying auditory-motor coupling paradigms for the purpose of neurological rehabilitation. We proposed a novel processing pipeline to compute the stability index, and validated this neural outcome measure by testing its correlation with a set of behavioral outcome measures in the context of a finger-tapping task.

Behaviorally, participants exhibited the mean negative asynchrony typically reported in finger-tapping synchronization tasks performed by healthy participants (Aschersleben, 2002). The mean negative asynchrony and the negative relative phase angles confirmed that all participants but one tapped on average ahead of the metronome, anticipating the beat. Additionally,

TABLE 1 | The results of neural and behavioral outcome measures of entrainment per participant.

Participant ID	Neural outcome measure of entrainment	Behavioral outcome measures of entrainment			
	Stability Index (frequency fluctuation—std)	Relative phase angle (radians)	Resultant vector length (0-1)	Mean asynchrony (ms)	Inter-beat deviation (ratio)
1	0.033	−0.387	0.958	−37.259	0.000
2	0.088	−2.332	0.647	−76.046	−0.003
3	0.023	−0.436	0.952	−41.668	−0.006
4	0.024	−0.464	0.975	−44.403	0.000
5	0.057	0.078	0.939	7.412	−0.008
6	0.138	−1.503	0.711	−122.858	0.008
7	0.077	−0.867	0.787	−83.514	−0.002
8	0.060	−0.772	0.803	−76.068	−0.003
9	0.056	−2.543	0.298	−26.583	0.042
10	0.061	−1.337	0.629	−114.613	0.001
11	0.037	−0.547	0.898	−53.906	0.000
12	0.086	−1.349	0.817	−120.805	0.000
13	0.070	−2.358	0.500	−41.690	−0.002
14	0.088	−1.273	0.800	−122.573	−0.024
15	0.045	−0.790	0.872	−74.723	0.001
16	0.125	−1.364	0.900	−130.310	0.001
17	0.051	−1.621	0.843	−152.019	0.003
18	0.028	−0.590	0.955	−57.088	−0.001
19	0.030	−0.744	0.943	−72.028	−0.009
20	0.074	−2.285	0.795	−156.864	0.001
21	0.076	−0.301	0.820	−27.093	−0.020
22	0.050	−0.574	0.943	−55.641	0.001
23	0.069	−1.223	0.824	−118.943	−0.004
24	0.032	−0.937	0.871	−90.031	−0.001
25	0.030	−0.674	0.960	−65.188	−0.001
26	0.041	−0.519	0.963	−50.530	−0.002
27	0.117	−1.018	0.931	−99.138	0.001
28	0.062	−0.670	0.942	−65.033	−0.004

Abbreviations: std, standard deviation; ms, milliseconds.

by looking at the resultant vector lengths, we also note that consistent synchronization was maintained throughout the task. Given these results, we can deduce that all subjects were engaged in the process of entraining their finger-taps to the auditory beats of the metronome.

As for the data captured by the EEG, our GED implementation was effective in extracting the target component maximally entrained to the rhythmic stimulus. **Figure 3** provides a quality check for our source separation by combining the following three criteria at the group-level. The first, topography: the grand-average activation map of the selected component shows maximal activity in the left centroparietal cluster and in the left temporal electrodes. Such distribution strongly suggests the involvement of primary sensorimotor areas, given it is contralateral to the effector (i.e., the right hand). The same pattern was previously reported for movement-related SSEPs in the context of overt synchronized behavior (Nozaradan et al., 2015), and clearly differs from the frontocentral topography typical of auditory cortical responses in absence of movement (Nozaradan et al., 2012). Given our focus on sensorimotor dynamics underlying overt behavior, our spatial filter was constrained within the whole set of channels located behind the frontocentral line. Second, the power spectrum: a single major peak stands out at the metronome's frequency, accompanied by harmonics whose power approximately follows a 1/f distribution. The dominance of the target frequency over the spectrum shows that the extracted component is effectively fine-tuned to the rhythmic stimulation. Third, the eigenspectrum: by sorting the eigenvalues in descending order, it is evident how the first one eigenvalue stands out over the rest of the spectrum. Such a condition is particularly desirable when the goal is to reduce the dimensionality of a multivariate dataset to one single component that satisfies a given criterion. The eigenvector associated with the highest eigenvalue could then be reliably used to weight the electrodes average, and reduce the dimensionality of the dataset to one entrained component.

Applying GED in the context of neural entrainment (Cohen and Gulbinaite, 2017) is an established method of optimizing source separation in this context, with avoidance of major drawbacks of electrode selection. To elaborate, we chose this approach instead of selecting a time series based on a single electrode or on a small cluster of electrodes in order to avoid subjective judgment to some degree. Despite this drawback, electrode selection is a rather common practice in the SSEP literature (Keitel et al., 2010; Andersen et al., 2011, 2012; Kashiwase et al., 2012; Rossion et al., 2012). In addition, with our spatial filter, we: (a) decrease the risk of attenuating the response in some subjects due to individual variability and (b) are not confounded by exposure to noise which might selectively affect a single channel. Although it is true that computing a non-weighted average over the whole scalp is sometimes proposed as a practice to avoid selection bias (e.g.,

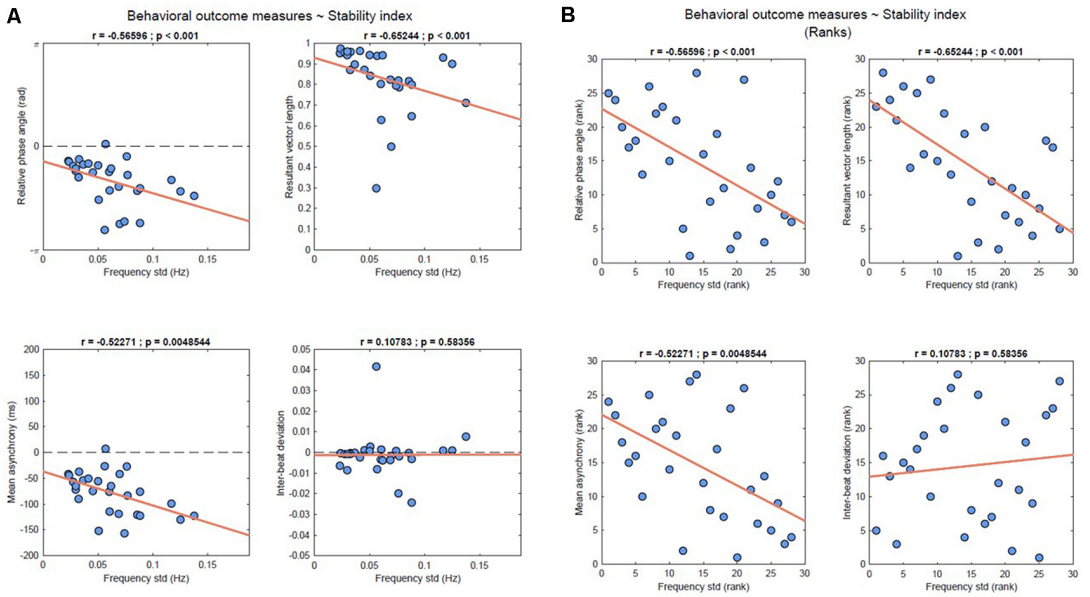

FIGURE 4 | (A) Results of the Spearman's correlation analysis between the behavioral outcome measures and stability index of all study participants. Data are represented on the original scale. **(B)** Correlations between the ranks for the behavioral outcome measures and stability index of all study participants.

see Nozaradan et al., 2016), the entrained response would be heavily attenuated by broadband components unrelated to the task. On the other hand, a weighted average oriented by spectral criteria would clearly overcome such issues. Most importantly, our methodology of GED application was optimal for single-trial analysis and provided us with a single time series whose time-course and dynamics could be further analyzed. Such time series represented the starting point of our pipeline towards the computation of the stability index (see **Figure 2**). It should also be noted that rhythmic motor acts such as finger-tapping (Moelants, 2002; McAuley, 2010) and walking (MacDougall and Moore, 2005) operate within the low delta frequency range (Morillon et al., 2019), which implies that long trials are needed to measure the dynamics of slower oscillatory components.

In order to validate our neural outcome measure of auditory-motor coupling, we ran correlation analyses with a set of behavioral measures of synchronization accuracy and stability (Moumdjian et al., 2018) in the context of a finger-tapping task to a metronome's beats. The stability index exhibited moderate negative correlations with the relative phase angles, the mean asynchrony, and the resultant vector length. To explain our results, we first provide an explanation of the pattern we observed in the context of the stability of the frequency fluctuations, which are used to quantify the stability index. We observed less stability in the frequency fluctuations of the neural entrained component when the finger-taps were further away and with a wider distribution relative to the beats, as reported by the relative phase angles and resultant vector length, respectively. Conversely, when the finger taps were closer to and in anticipation of the beat, with a narrow distribution, we observed that the entrained neural component stabilized its frequency fluctuations. The results confirmed the hypothesis that these frequency fluctuations, as quantified by the stability index, correlated with the behavioral outcome measures of entrainment.

With our results, we also observed that the stability index was selectively correlated with measures of phase error correction mechanisms, and not with those of period error correction. This is consistent with the fact that the stability index was not correlated to the inter-beat deviations—which is a measure for quantifying tempo matching (Moumdjian et al., 2018). In turn, tempo matching is an outcome which describes error correction in a period. With the above explanations, our results are suggestive that the stability index quantifies neural entrainment, yet limited to corrections in phase. However, we do not rule out the possibility that we did not find any significant correlation due to the very low individual variability in inter-beat deviations, which resulted in a small slope of the regression line. The result indicates that participants were very accurate in matching the period of the metronome over the whole duration of the task.

The selectivity of these correlations further supports the relevance of temporal dynamics at the micro-timing scale. By picking up on the notion of "neural entrainment to the beat", which is traditionally inferred from the Fourier coefficients of a "static" spectrum, we developed it towards a phase-based measure to make it sensitive to the temporal structure of the stimulus (Rajendran and Schnupp, 2019) and to behavioral dynamics. From our standpoint, in order to "entrain to the beat" a neural component should not only be tuned to the stimulus frequency, but it should dynamically attune depending on the ongoing entrained behavior. The stability index proposed in this context shows how frequency fluctuates over time as a function of the distance from in-phase synchronization (the phase angles and asynchrony) and consistency of the established relative-

phase during the course of the task (resultant vector length). Previous work provided evidence on the correlation between cortical entrainment and overt sensorimotor synchronization (Nozaradan et al., 2016), recording brain activity by the means of the EEG during a passive listening task and subsequently performing the behavioral task. The authors detected entrained cortical activity on the frontocentral cluster of electrodes where auditory responses are typically detected, hypothesizing that SSEPs amplitudes would predict behavioral measures of overt entrainment. Interestingly enough, a dissociation emerged in the correlations between their measure of neural entrainment and behavioral accuracy, when compared to behavioral consistency. Specifically, the amplitude of SSEPs was related to mean asynchrony (accuracy) rather than to the resultant vector length (consistency), suggesting that the two are supported by distinct neural mechanisms when processing the beat of an auditory rhythm. In the scenario we proposed, with the goal of relating neural entrainment to the dynamics of overt behavior, we identified a lateralized component plausibly related to primary sensorimotor areas. The stability index computed from such component was related to both behavioral accuracy and consistency. Our finding is arguably not in contradiction with previous evidence, but rather complementary.

One may argue that the correlation we found between the stability index and the resultant vector length could be spurious, a sort of epiphenomenon entirely explainable by afferent proprioceptive feedback. Following this argument, stable rhythmic behavior could produce steady responses in primary somatosensory areas (Piitulainen et al., 2013; Bourguignon et al., 2015). Our task cannot exclude the possibility that such afferent components lead to a spurious correlation between the stability index and resultant vector length, which quantifies behavioral consistency. Nevertheless, such interpretation cannot explain our crucial finding that the stability index also correlated with behavioral accuracy. To elaborate, a more stable entrained component was associated with smaller synchronization errors, as quantified by measures of asynchrony and relative phase. In this context, these are behavioral indicators of error correction. Since we showed that a more stable entrained component correlated with smaller error relative to the beat, we propose that the stability index is not merely determined by proprioceptive feedback. We thus argue that our results rather align with evidence that motor cortices play a critical role in supporting auditory perception and prediction (Fujioka et al., 2012; Morillon and Baillet, 2017; Assaneo et al., 2021). In addition, within the limits of our auditory-motor task, we pick up on the notion of active sampling (Morillon et al., 2019), to propose that entrainment dynamics driven by the motor system seem to play an active role in the predictive mechanism of error minimization underpinning auditory-motor coupling (Vuust and Witek, 2014). However, with the current experimental design, we cannot rule out that distinct motor, sensory and cognitive processes were to some extent mixed in the entrained component. This represents an important limitation of the present study. A finer disentanglement of the neural processes underlying entrainment should be addressed by future work, with dedicated experimental designs.

With our work, we thus contributed methodologically to the investigation of neural entrainment. Our method consists of extracting the oscillatory component in the EEG signal which is maximally entrained to a rhythmic auditory stimulus and subsequently quantifying the stability of fluctuations over time. The impact of this contribution has valuable prospects within the domain of neurological rehabilitation. In previous work, we have investigated motor and auditory entrainment in participants with multiple sclerosis and healthy controls. Specifically, behavioral time series were analyzed by means of detrended fluctuation analysis (DFA; Moumdjian et al., 2020). Differences in gait dynamics were attributed to the process of error-correction minimization, which are required to dynamically interact with continuous and discrete auditory structures (Moumdjian et al., 2020) typically present in music and metronomes, respectively. Although clinically relevant, complementing such studies with neural outcome measures such as the stability index would allow to explain the process of error-correction minimization further, at the level of neural dynamics. Such a prospect has a strong indication to optimize the individualized rehabilitation procedure.

In conclusion, our approach can be used for better understanding the dynamics of an entrained system over time. While the stability index provides a global neural outcome measure correlated with the overall synchronization performance, the instantaneous frequency time series can offer a more fine-grained picture of the dynamics of neural entrainment. Neural and behavioral measurements can be complemented within a comparative setting between healthy population and neuropathological models, offering the possibility to dissociate neural mechanisms based on a mapping of selective lesions. Such neuropathological models can be recruited through studies conducted on participants with neurological diseases, where components of cognitive, motor or, perceptual functions can be isolated. For instance, cerebellar lesions cover particular interest given the role of the cerebellum in encoding the timing of events at the micro-timing scale (Ivry et al., 1988; Ivry and Keele, 1989; Ivry and Schlerf, 2008), and given that their neural entrainment to auditory rhythms is selectively compromised at faster tempi (Nozaradan et al., 2017). Respectively, this unfolding of observations would expand the knowledge of the complex dynamic interaction when entraining motor and auditory systems to one another. In turn, it would pave ways towards the development of state-of-the-art approaches within the domain of neurological rehabilitation.

DATA AVAILABILITY STATEMENT

The datasets presented in this article are not readily available because the raw data generated for the current study (from the EEG recordings) are a part of a bigger experimental design. Given software restrictions, we are not able to disintangle the applicable dataset from this study at the level of the raw recordings. However, it is possible for us to provide pre-processed data of the experimental condition used in this study upon request. Requests to access the datasets should be directed to mattia.rosso@ugent.be.

ETHICS STATEMENT

The studies involving human participants were reviewed and approved by Ethics Committee of Ghent University (Faculty of Arts and Philosophy). The patients/participants provided their written informed consent to participate in this study.

AUTHOR CONTRIBUTIONS

MR was responsible for study conceptualization, data collection, processing and analysis, and writing of the manuscript. ML was responsible for data interpretation and manuscript writing. LM was responsible for study conceptualization, data interpretation, and writing of the manuscript. All authors contributed to the article and approved the submitted version.

FUNDING

The present study was funded by Bijzonder Onderzoeksfonds (BOF) from Ghent University (Belgium).

ACKNOWLEDGMENTS

We would like to acknowledge Mr. Ivan Schepers, for his technical support towards developing the tapping pad hardware.

SUPPLEMENTARY MATERIAL

The Supplementary Material for this article can be found online at: https://www.frontiersin.org/articles/10.3389/fnhum.2021.668918/full#supplementary-material.

SUPPLEMENTARY FIGURE 1 | Narrow-band filter kernel for GED. The figure shows the wavelet kernel in the frequency domain, centered on the target frequency of 1.65 Hz. In order to set the width of the Gaussian, we opted for a filter that would allow some extent of fluctuations around the centered frequency, without overlapping with the high-pass band filter (cut-off = 1 Hz). We found an optimal trade-off by setting the Gaussian width at half-maximum at 0.3 Hz. It is important to note that the correlations with the behavioral measures reported in the present work are invariant to such parameters. However, one should be aware that the scale of the stability index is inversely proportional to the width of the narrow-band filter. This is due to the fact that a wider filter allows for wider frequency fluctuations. Finally, the scale of the stability index is also affected by the filter shape. It was previously proposed that symmetric plateau-shaped filters should be preferred over a Gaussian when investigating frequency shifts, since the latter is biased towards the center frequency (Cohen, 2014). However, we found that the correlations are invariant when comparing plateau-shaped FIR and Gaussian-shaped, as long as both are symmetrical. After verifying the invariance of the results, we opted for a Gaussian filter for the sake of parsimony and replicability: given that the center frequency is constrained by the rate of the stimulation, the width is the only parameter to be defined by the data analyst.

SUPPLEMENTARY FIGURE 2 | Component #2. As it can be evicted by the right-most plot, the second eigenvalue detaches to some extent in the eigenspectrum. We present here the activation map and the power spectrum (normalized to signal-to-noise ratio) of the component associated with the second eigenvalue. The spectral profile is clearly characterized by dominant peaks at entrained frequency and harmonics, which is to be expected given the spectral criterion adopted for the GED. It is noteworthy that the signal-to-noise ratio is considerably lower as compared to the first component. Critically, no meaningful pattern emerged from the topographical activation map.

SUPPLEMENTARY FIGURE 3 | Component #2 (correlations with behavioral outcome measures). The stability index was computed from the second component, and its correlations with the behavioral outcome measures were tested. Correlations were considerably weaker than the ones for the component associated with the highest eigenvalue, as quantified by the Spearman correlation coefficients. Results are showed in the original scale and transformed to ranks. This evidence suggests that the first component alone is related to neural entrainment in the context of the experimental task. Acknowledging that we still cannot completely rule out the merging of different neural processes across components, the approach hereby proposed has proved to be valid in extracting one single component related to auditory-motor coupling.

REFERENCES

Andersen, S. K., Fuchs, S., and Muller, M. M. (2011). Effects of feature-selective and spatial attention at different stages of visual processing. *J. Cogn. Neurosci.* 23, 238–246. doi: 10.1162/jocn.2009.21328

Andersen, S. K., Muller, M. M., and Martinovic, J. (2012). Bottom-up biases in feature-selective attention. *J. Neurosci.* 32, 16953–16958. doi: 10.1523/JNEUROSCI.1767-12.2012

Aschersleben, G. (2002). Temporal control of movements in sensorimotor synchronization. *Brain Cogn.* 48, 66–79. doi: 10.1006/brcg.2001.1304

Assaneo, F. M., Rimmele, J. M., Perl, Y. S., and Poeppel, D. (2021). Speaking rhythmically can shape hearing. *Nat. Hum. Behav.* 5, 71–82. doi: 10.1038/s41562-020-00962-0

Bavassi, M. L., Tagliazucchi, E., and Laje, R. (2013). Small perturbations in a finger-tapping task reveal inherent nonlinearities of the underlying error correction mechanism. *Hum. Mov. Sci.* 32, 21–47. doi: 10.1016/j.humov.2012.06.002

Berens, P. (2009). CircStat: A MATLAB toolbox for circular statistics. *J. Stat. Softw.* 31, 1–21. doi: 10.18637/jss.v031.i10

Boashash, B. (1992). Estimating and interpreting the instantaneous frequency of a signal. I. Fundamentals. *IEEE* 80, 520–538.

Bourguignon, M., Piitulainen, H., De Tiege, X., Jousmaki, V., and Hari, R. (2015). Corticokinematic coherence mainly reflects movement-induced proprioceptive feedback. *NeuroImage* 106, 382–390. doi: 10.1016/j.neuroimage.2014.11.026

Cohen, M. X. (2014). Fluctuations in oscillation frequency control spike timing and coordinate neural networks. *J. Neurosci.* 34, 8988–8998. doi: 10.1523/JNEUROSCI.0261-14.2014

Cohen, M. X. (2017). Where does EEG come from and what does it mean. *Trends Neurosci.* 40, 208–218. doi: 10.1016/j.tins.2017.02.004

Cohen, M. X., and Gulbinaite, R. (2017). Rhythmic entrainment source separation, Optimizing analyses of neural responses to rhythmic sensory stimulation. *Neuroimage* 147, 43–56. doi: 10.1016/j.neuroimage.2016.11.036

Dalla Bella, S., Benoit, C. E., Farrugia, N., Keller, P. E., Obrig, H., Mainka, S., et al. (2017a). Gait improvement via rhythmic stimulation in Parkinson's disease is linked to rhythmic skills. *Sci. Rep.* 7:42005. doi: 10.1038/srep42005

Dalla Bella, S., Farrugia, N., Benoit, C. E., Begel, V., Verga, L., Harding, E., et al. (2017b). BAASTA, battery for the assessment of auditory sensorimotor and timing abilities. *Behav. Res. Methods* 49, 1128–1145. doi: 10.3758/s13428-016-0773-6

De Bartolo, D., Morone, G., Giordani, G., Antonucci, G., Russo, V., Fusco, A., et al. (2020). Effect of different music genres on gait patterns in Parkinson's disease. *Neurol. Sci.* 41, 575–582. doi: 10.1007/s10072-019-04127-4

Freeman, W. J., Holmes, M. D., Burke, B. C., and Vanhatalo, S. (2003). Spatial spectra of scalp EEG and EMG from awake humans. *Clin. Neurophysiol.* 114, 1053–1068. doi: 10.1016/s1388-2457(03)00045-2

Fujioka, T., Trainor, L. J., Large, E. W., and Ross, B. (2012). Internalized timing of isochronous sounds is represented in neuromagnetic beta oscillations. *J. Neurosci.* 32, 1791–1802. doi: 10.1523/JNEUROSCI.4107-11.2012

Ghai, S., Ghai, I., Schmitz, G., and Effenberg, A. O. (2018). Effect of rhythmic auditory cueing on parkinsonian gait: A systematic review and meta-analysis. *Sci. Rep.* 8:506. doi: 10.1038/s41598-017-16232-5

Heggli, O. A., Cabral, J., Konvalinka, I., Vuust, P., and Kringelbach, M. L. (2019). A Kuramoto model of self-other integration across interpersonal synchronization strategies. *PLoS Comput. Biol.* 15:e1007422. doi: 10.1371/journal.pcbi.1007422

Hinkle, D. E., Wiersma, W., and Jurs, S. G. (2002). Applied statistics for the behavioral sciences: houghton mifflin. *J. Educ. Stat.* 15, 1–84. doi: 10.2307/1164825

Hutchinson, K., Sloutsky, R., Collimore, A., Adams, B., Harris, B., Ellis, T. D., et al (2020). A music-based digital therapeutic, proof-of-concept automation of a progressive and individualized rhythm-based walking training program after stroke. *Neurorehabil. Neural Repair.* 34, 986–996. doi: 10.1177/1545968320961114

Ivry, R. B., and Keele, S. W. (1989). Timing functions of the cerebellum. *J. Cogn. Neurosci. Spring* 1, 136–152. doi: 10.1162/jocn.1989.1.2.136

Ivry, R. B., Keele, S. W., and Diener, H. C. (1988). Dissociation of the lateral and medial cerebellum in movement timing and movement execution. *Exp. Brain Res.* 73, 167–180. doi: 10.1007/BF00279670

Ivry, R. B., and Schlerf, J. E. (2008). Dedicated and intrinsic models of time perception. *Trends Cogn. Sci.* 12, 273–280. doi: 10.1016/j.tics.2008.04.002

Kashiwase, Y., Matsumiya, K., Kuriki, I., and Shioiri, S. (2012). Time courses of attentional modulation in neural amplification and synchronization measured with steady-state visual-evoked potentials. *J. Cogn. Neurosci.* 24, 1779–1793. doi: 10.1162/jocn_a_00212

Keitel, C., Andersen, S. K., and Muller, M. M. (2010). Competitive effects on steady-state visual evoked potentials with frequencies in- and outside the alpha band. *Exp. Brain. Res.* 205, 489–495. doi: 10.1007/s00221-010-2384-2

Leman, M. (2016). *The Expressive Moment: How Interaction (with Music) Shapes Human Empowerment*. Cambridge, USA: MIT press.

Lenc, T., Keller, P. E., Varlet, M., and Nozaradan, S. (2018). Neural tracking of the musical beat is enhanced by low-frequency sounds. *Proc. Natl. Acad. Sci. U S A* 115, 8221–8226. doi: 10.1073/pnas.1801421115

Leow, L. A., Waclawik, K., and Grahn, J. A. (2018). The role of attention and intention in synchronization to music: effects on gait. *Exp. Brain Res.* 236, 99–115. doi: 10.1007/s00221-017-5110-5

Lopez, S. L., and Laje, R. (2019). Spatiotemporal perturbations in paced finger tapping suggest a common mechanism for the processing of time errors. *Sci. Rep.* 9:17814. doi: 10.1038/s41598-019-54133-x

MacDougall, H. G., and Moore, S. T. (2005). Marching to the beat of the same drummer: the spontaneous tempo of human locomotion. *J. Appl. Physiol.* 99, 1164–1173. doi: 10.1152/japplphysiol.00138.2005

McAuley, J. D. (2010). "Tempo and rhythm," in *Music Perception*, eds M. Riess Jones, Richard R. Fay and Arthur N. Popper (New York, NY: Springer), 165–199.

McPherson, T., Berger, D., Alagapan, S., and Frohlich, F. (2018). Intrinsic rhythmicity predicts synchronization-continuation entrainment performance. *Sci. Rep.* 8:11782. doi: 10.1038/s41598-018-29267-z

Moelants, D. (2002). "Preferred tempo reconsidered," in *Proceedings of the 7th International Conference on Music Perception and Cognition*, (Sydney: Causal Productions), 580–583.

Moens, B., Muller, C., van Noorden, L., Franěk, M., Celie, B., Boone, J., et al. (2014). Encouraging spontaneous synchronisation with D-Jogger, an adaptive music player that aligns movement and music. *PLoS One* 9:e114234. doi: 10.1371/journal.pone.0114234

Morillon, B., Arnal, L. H., Schroeder, C. E., and Keitel, A. (2019). Prominence of delta oscillatory rhythms in the motor cortex and their relevance for auditory and speech perception. *Neurosci. Biobehav. Rev.* 107, 136–142. doi: 10.1016/j.neubiorev.2019.09.012

Morillon, B., and Baillet, S. (2017). Motor origin of temporal predictions in auditory attention. *Proc. Natl. Acad. Sci. U S A* 114, E8913–E8921. doi: 10.1073/pnas.1705373114

Moumdjian, L., Buhmann, J., Willems, I., Feys, P., and Leman, M. (2018). Entrainment and synchronization to auditory stimuli during walking in healthy and neurological populations: a methodological systematic review. *Front. Hum. Neurosci.* 12:263. doi: 10.3389/fnhum.2018.00263

Moumdjian, L., Maes, P. J., Dalla Bella, S., Decker, L. M., Moens, P. F., Feys, P., et al. (2020). Detrended fluctuation analysis of gait dynamics when entraining to music and metronomes at different tempi in persons with multiple sclerosis. *Sci. Rep.* 10:12934. doi: 10.1038/s41598-020-69667-8

Moumdjian, L., Moens, B., Maes, P. J., Geel, F. V., Ilsbroukx, S., Borgers, S., et al. (2019a). Continuous 12 min walking to music, metronomes and in silence: auditory-motor coupling and its effects on perceived fatigue., motivation and gait in persons with multiple sclerosis. *Mult. Scler. Relat. Disord.* 35, 92–99. doi: 10.1016/j.msard.2019.07.014

Moumdjian, L., Moens, B., Maes, P. J., Nieuwenhoven, J. V., Wijmeersch, B. V., Leman, M., et al. (2019b). Walking to music and metronome at various tempi in persons with multiple sclerosis: a basis for rehabilitation. *Neurorehabil. Neural Repair* 33, 464–475. doi: 10.1177/1545968319847962

Moumdjian, L., Moens, B., Vanzeir, E., De Klerck, B., Feys, P., and Leman, M. (2019c). A model of different cognitive processes during spontaneous and intentional coupling to music in multiple sclerosis. *Ann. N Y Acad. Sci.* 1445, 27–38. doi: 10.1111/nyas.14023

Norcia, A. M., Appelbaum, L. G., Ales, J. M., Cottereau, B. R., and Rossion, B. (2015). The steady-state visual evoked potential in vision research: a review. *J. Vis.* 15:4. doi: 10.1167/15.6.4

Nozaradan, S., Peretz, I., Missal, M., and Mouraux, A. (2011). Tagging the neuronal entrainment to beat and meter. *J. Neurosci.* 31, 10234–10240. doi: 10.1523/JNEUROSCI.0411-11.2011

Nozaradan, S., Peretz, I., and Keller, P. E. (2016). Individual differences in rhythmic cortical entrainment correlate with predictive behavior in sensorimotor synchronization. *Sci. Rep.* 6:20612. doi: 10.1038/srep20612

Nozaradan, S., Peretz, I., and Mouraux, A. (2012). Selective neuronal entrainment to the beat and meter embedded in a musical rhythm. *J. Neurosci.* 32, 17572–17581. doi: 10.1523/JNEUROSCI.3203-12.2012

Nozaradan, S., Schwartze, M., Obermeier, C., and Kotz, S. A. (2017). Specific contributions of basal ganglia and cerebellum to the neural tracking of rhythm. *Cortex* 95, 156–168. doi: 10.1016/j.cortex.2017.08.015

Nozaradan, S., Zerouali, Y., Peretz, I., and Mouraux, A. (2015). Capturing with EEG the neural entrainment and coupling underlying sensorimotor synchronization to the beat. *Cereb. Cortex* 25, 736–747. doi: 10.1093/cercor/bht261

Oldfield, R. C. (1971). The assessment and analysis of handedness: the edinburgh inventory. *Neuropsychologia* 9, 97–113. doi: 10.1016/0028-3932(71)90067-4

Oostenveld, R., Fries, P., Maris, E., and Schoffelen, J. M. (2011). FieldTrip: Open source software for advanced analysis of MEG, EEG and invasive electrophysiological data. *Comput. Intell. Neurosci.* 2011:156869. doi: 10.1155/2011/156869

Phillips-Silver, J., Aktipis, C. A., and Bryant, G. A. (2010). The ecology of entrainment: foundations of coordinated rhythmic movement. *Music Percept.* 28, 3–14. doi: 10.1525/mp.2010.28.1.3

Piitulainen, H., Bourguignon, M., De Tiege, X., Hari, R., and Jousmaki, V. (2013). Corticokinematic coherence during active and passive finger movements. *Neuroscience* 238, 361–370. doi: 10.1016/j.neuroscience.2013.02.002

Rajendran, V. G., and Schnupp, J. W. H. (2019). Frequency tagging cannot measure neural tracking of beat or meter. *Proc. Natl. Acad. Sci. U S A* 116, 2779–2780. doi: 10.1073/pnas.1820020116

Rossion, B., Prieto, E. A., Boremanse, A., Kuefner, D., and Van Belle, G. (2012). A steady-state visual evoked potential approach to individual face perception: effect of inversion, contrast-reversal and temporal dynamics. *NeuroImage* 63, 1585–1600. doi: 10.1016/j.neuroimage.2012.08.033

Van Dyck, E., Buhmann, J., and Lorenzoni, V. (2020). Instructed versus spontaneous entrainment of running cadence to music tempo. *Ann. N Y Acad. Sci.* 1489, 91–102. doi: 10.1111/nyas.14528

Van Dyck, E., Moens, B., Buhmann, J., Demey, M., Coorevits, E., Dalla Bella, S., et al. (2015). Spontaneous entrainment of running cadence to music tempo. *Sports Med. Open* 1:15. doi: 10.1186/s40798-015-0025-9

Varlet, M., Nozaradan, S., Nijhuis, P., and Keller, P. E. (2020). Neural tracking and integration of 'self' and 'other' in improvised interpersonal coordination. *Neuroimage* 206:116303. doi: 10.1016/j.neuroimage.2019.116303

Vialatte, F. B., Maurice, M., Dauwels, J., and Cichocki, A. (2010). Steady-state visually evoked potentials, focus on essential paradigms and future perspectives. *Prog. Neurobiol.* 90, 418–438. doi: 10.1016/j.pneurobio.2009.11.005

Vuust, P., and Witek, M. A. (2014). Rhythmic complexity and predictive coding, a novel approach to modeling rhythm and meter perception in music. *Front. Psychol.* 5:1111. doi: 10.3389/fpsyg.2014.01111

Wilson, M., and Cook, P. F. (2016). Rhythmic entrainment: Why humans want to: fireflies can't help it, pet birds try and sea lions have to be bribed. *Psychon. Bull. Rev.* 23, 1647–1659. doi: 10.3758/s13423-016-1013-x

Yoo, G. E., and Kim, S. J. (2016). Rhythmic auditory cueing in motor rehabilitation for stroke patients: systematic review and meta-analysis. *J. Music Therapy* 53, 149–177. doi: 10.1093/jmt/thw003

Conflict of Interest: The authors declare that the research was conducted in the absence of any commercial or financial relationships that could be construed as a potential conflict of interest.

frontiers in Human Neuroscience

ORIGINAL RESEARCH
published: 26 July 2021
doi: 10.3389/fnhum.2021.684950

Electrophysiological and Transcriptomic Features Reveal a Circular Taxonomy of Cortical Neurons

Alejandro Rodríguez-Collado and Cristina Rueda*

Department of Statistics and Operations Research, Universidad de Valladolid, Valladolid, Spain

The complete understanding of the mammalian brain requires exact knowledge of the function of each neuron subpopulation composing its parts. To achieve this goal, an exhaustive, precise, reproducible, and robust neuronal taxonomy should be defined. In this paper, a new circular taxonomy based on transcriptomic features and novel electrophysiological features is proposed. The approach is validated by analysing more than 1850 electrophysiological signals of different mouse visual cortex neurons proceeding from the Allen Cell Types database. The study is conducted on two different levels: neurons and their cell-type aggregation into Cre lines. At the neuronal level, electrophysiological features have been extracted with a promising model that has already proved its worth in neuronal dynamics. At the Cre line level, electrophysiological and transcriptomic features are joined on cell types with available genetic information. A taxonomy with a circular order is revealed by a simple transformation of the first two principal components that allow the characterization of the different Cre lines. Moreover, the proposed methodology locates other Cre lines in the taxonomy that do not have transcriptomic features available. Finally, the taxonomy is validated by Machine Learning methods which are able to discriminate the different neuron types with the proposed electrophysiological features.

Keywords: neuronal taxonomy, statistical model, cell-type classification, allen cell types database, machine learning, frequency modulated Möbius model, FMM

OPEN ACCESS

Edited by:
Daniela De Bartolo,
Sapienza University of Rome, Italy

Reviewed by:
Alexey Kozlenkov,
Icahn School of Medicine at Mount Sinai, United States
Alexander Komendantov,
George Mason University, United States
Parviz Ghaderi,
Shahid Beheshti University of Medical Sciences, Iran

****Correspondence:***
Alejandro Rodríguez-Collado
alejandrorodriguezcollado@gmail.com

Specialty section:
This article was submitted to Motor Neuroscience, a section of the journal Frontiers in Human Neuroscience

Received: *24 March 2021*
Accepted: *28 June 2021*
Published: *26 July 2021*

Citation:
Rodríguez-Collado A and Rueda C (2021) Electrophysiological and Transcriptomic Features Reveal a Circular Taxonomy of Cortical Neurons. Front. Hum. Neurosci. 15:684950. doi: 10.3389/fnhum.2021.684950

1. INTRODUCTION

Understanding the nervous system's mechanisms and capabilities, such as the conscience and cognition, remain one of the most challenging and interesting unresolved problems in biology. It requires a precise description of the structure and function of each brain region, including the study of the neuronal circuits and neurons composing them. Furthermore, one fundamental prerequisite in this subsequent structural division study is the creation of a solid neuronal cell-type classification or taxonomy. As Zeng and Sanes (2017) explain, cells in the nervous system should be hierarchically classified into different levels, mainly into classes, subclasses and types. This property makes the taxonomy define relationships between cell types, as well as making it easier to update in the light of new information. At class level, cells are classified into non-neuronal cells and neurons, which in turn can be classified into excitatory and inhibitory neurons, local and projection (Melzer and Monyer, 2020 and references therein). Excitatory neurons are

habitually morphologically spiny, have a long apical dendrite, and exhibit less variability in their electrophysiological features. Inhibitory neurons are broadly aspiny, have a more compact dendritic structure and tend to spike faster. Also, at class level, neurons can be classified based on their neurotransmitter into GABAergic and glutamatergic. The latter are mostly excitatory and brain-area specific, while the former are broadly inhibitory and not-area specific. Neuron subclasses can be defined with different methods. In particular, Cre recombinase-dependent reporter transgenic mouse lines are used here. Moreover, many authors consider GABAergic neurons to belong to four classes based on the expression of certain principal markers: Pvalb (parvalbumin) positive, Vip (vasoactive intestinal peptide) positive, Sst (somatostatin) positive, and cells that express Htr3a (5-hydroxytryptamine receptor 3A) but are Vip negative. These groups are suitable for classification because they account for nearly the totality of neurons in certain brain regions as well as being largely expressed in a non-overlapping manner revealing neuron types with different properties (Tremblay et al., 2016). On the other hand, glutamatergic neurons can also be grouped based on gene markers, such as Cux2 (Cut like homeobox 2), Rorb (RAR related orphan receptor B), or Ctgf (Connective tissue growth factor), or alternatively based on their laminar locations and the locations to which they project their axons. Aside from these previous statements, the different studies unearth discrepancies in terms of number of neuronal types, their characteristics, and the existing order between them as is reviewed in the next paragraph.

The definition of a solid neuronal taxonomy is a challenging task. Heterogeneity between cells arises due to different electrophysiological, morphological, and/or genetic features, but also due to differences in cell age, environmental conditions, and other sources of noise. Another concerning issue is the reproducibility of the approach. The open challenge of creating a neuronal taxonomy has recently generated many studies, mainly due to the increase in data availability as well as the rise in data computational methods. A recent overview of the matter can be found in Zeng and Sanes (2017). In particular, the taxonomy of the mouse visual cortex cells has been the focus of recent research. In Tasic et al. (2016, 2018), taxonomies based on transcriptomic characteristics obtained from single RNA sequencing are presented. Electrophysiological taxonomies are predominantly based on patch-clamp recordings of neuron membrane potential signals that contain action potential curves (APs), as is done in Ghaderi et al. (2018) and Teeter et al. (2018). Furthermore, Gouwens et al. (2019) presents a taxonomy based on the combination of electrophysiological and morphological features, while part of this taxonomy is expanded with transcriptomic features in Gouwens et al. (2020).

It should be noted that electrophysiological features are easier to measure than other types of features and can be simultaneously recorded on hundreds of cells using scalable techniques such as optical imaging of electrical activity (Zeng and Sanes, 2017). Furthermore, taxonomies based on this type of features are easier to reproduce. However, the features traditionally used in this type of taxonomy lack interpretability as they are not directly related to the observed potential difference signal. Most of these studies extract the features with dimensional reducing techniques (as is the case of Ghaderi et al., 2018 or Gouwens et al., 2019 among others) or the features are model parameters such as the leaky integrate and fire models (as in Teeter et al., 2018). A brief overview of the latter models can be found in Lynch and Houghton (2015).

The aim of this paper is to derive an electrophysiological-transcriptomic circular taxonomy of visual cortex Cre lines, using data from *Mus Musculus* of the Allen Cell Types database (ACTD; http://celltypes.brain-map.org). This database is freely available and has been the reference data for many authors, such as Teeter et al. (2018) and references therein. On the one hand, the electrophysiological features at Cre line level are the median of those generated at the cell level from fitting a frequency modulated Möbius (FMM) model to the observed cell signals. The FMM model is a flexible model defined by 13 parameters that accurately describes the AP shape. The monocomponent FMM model is presented in Rueda et al. (2019) and model extensions to analyse neuronal dynamics are shown in Rueda et al. (2021) and Rodríguez-Collado and Rueda (2021). Some relevant and robust theoretical properties of the model are shown in the former paper while, in the latter, an FMM representation of the famed Hodgkin-Huxley model is proposed.

On the other hand, the number of core cells by genetic cluster and Cre line from Tasic et al. (2016) has been used as transcriptomic features. Finally, the morphological features have not been used as they are sparsely available compared to other kinds of measurements and they seem to be not as discriminant for Cre lines as the other kinds of features, as seen in Gouwens et al. (2020).

The formulation of a circular taxonomy is one of the most original aspects of this work. Many studies devoted to generate taxonomies provide visualizations based on circular tree in which any two nodes in the tree can be connected by lines to combine different quantitative information. The circular tree is just an alternative display of the habitual linear layout. Different computational tools have been developed to provide such a visualizations, in particular to represent genomic data (Moore et al., 2020 is among the most recent ones). Besides, principal component analysis (PCA) combined with hierarchical clustering has been considered in different disciplines and taxonomies are

Abbreviations: ACTD, Allen cell types database; AP, action potential curve; AvNNet, model averaged neural network; CPCA, circular principal components analysis; FMM, frequency modulated Möbius; GBDT, gradient boosting decision trees; L2-6, layers 2 to 6; LDA, linear discriminant analysis; MLE, maximum likelihood estimator; PCA, principal components analysis; RF, random forest; RNA, ribonucleic acid; SDK, software development kit; SVM, support vector machine; Chat, choline o-acetyltransferase; Chrna2, cholinergic receptor nicotinic alpha 2; Ctgf, connective tissue growth factor; Cux2, cut like homeobox 2; Esr2, estrogen receptor 2; Gad2, glutamate decarboxylase 2; Glt25d2, glycosyltransferase 25 domain containing 2; Htr3a, 5-hydroxytryptamine receptor 3A; Ndnf, neuron derived neurotrophic factor; Nkx2.1, NK2 homeobox 1; Nos1, nitric oxide synthase 1; Nr5a1, nuclear receptor subfamily 5 group A member 1; Ntsr1, neurotensin receptor 1; Oxtr, oxytocin receptor; Pvalb, parvalbumin; Rbp4, retinol-binding protein 4; Rorb, RAR related orphan receptor B; Scnn1a, sodium channel epithelial 1 alpha subunit; Sim1, single-minded homolog 1; Slc32a1, solute carrier family 32 member 1; Sst, somatostatin; Tlx3, T-cell leukemia homeobox protein 3; Vip, vasoactive intestinal peptide.

visualized in the plot of the two first principal components (Argüelles et al., 2014; Žurauskienė and Yau, 2016; Gautier et al., 2019 among others).

Our proposal can be seen as a combination of a visualization tool, as it uses a circular tree, and as a combined clustering approach that uses the circular order defined with the two first principal components. The dissimilarity measure is a circular distance instead of a Euclidean distance and the location of clusters in the circle is derived from the location of the clusters in the two dimensional plane of the two first principal components. Thus, this is not just a visualization tool, but a genuine circular taxonomy.

Finally, the proposed taxonomy is validated by showing that signals from different neuronal cell types are accurately discriminated by the FMM model parameters.

2. MATERIALS AND METHODS

2.1. Statistical Methods

Let $X(t_i)$ denote the potential difference in the neuron's membrane at each of the observed time points t_i, $i = 1, ..., n$. The latter are assumed to be in $[0, 2\pi]$. Otherwise, consider $t' \in [t_0, T + t_0]$ with t_0 as the initial time value and T as the period. Transform the time points by $t = \frac{(t'-t_0)2\pi}{T}$.

In this section, the statistical methods used in the manuscript are described. These include the FMM model, circular principal components analysis (CPCA) and, Machine Learning supervised methods.

2.1.1. FMM Model

The proposed model to analyse AP data is a three-component FMM model, as defined in Rueda et al. (2021) which implies that each AP is modeled using three waves, labeled A, B, and C. The physiological meaning of these waves is given below, after the mathematical presentation.

Mathematically, the waves are defined as follows:

$$W_J(t) = W(t, \boldsymbol{\upsilon_J}) = \\ = A_J \cos\left(\beta_J + 2\arctan\left(\omega_J \tan\left(\frac{t-\alpha_J}{2}\right)\right)\right), \\ J \in \{A, B, C\} \quad (1)$$

where $\boldsymbol{\upsilon_J} = (A_J, \alpha_J, \beta_J, \omega_J)'$ is a four-dimensional parameter describing the shape of the wave. The A parameter represents the wave amplitude whereas α is a location parameter. The parameters β and ω determine the skewness and kurtosis of the wave. More details about the interpretation of the parameters can be found in Rueda et al. (2019).

Moreover, the FMM model is defined as a signal plus error model, as follows:

$$X(t_i) = \mu(t_i, \boldsymbol{\theta}) + e(t_i) = \\ M + \sum_{J\in\{A,B,C\}} W(t_i, \boldsymbol{\upsilon_J}) + e(t_i), \quad i = 1, ..., n \quad (2)$$

where,

- $\boldsymbol{\theta} = (M, \boldsymbol{\upsilon_A}, \boldsymbol{\upsilon_B}, \boldsymbol{\upsilon_C})$ verifying:
  1. $M \in \Re$; $\boldsymbol{\upsilon_J} \in \Re^+ \times [0, 2\pi] \times [0, 2\pi] \times [0, 1]$; $J \in \{A, B, C\}$
  2. $\alpha_A \leq \alpha_B \leq \alpha_C$
- $(e(t_1), ..., e(t_n))' \sim N_n(0, \sigma^2 \boldsymbol{I})$.

The restrictions on the αs guarantee identifiability.

Other important parameters of practical use are peak and trough times, denoted by t_J^U and t_J^L, respectively, and the distances between the model waves, denoted by d_{JK}. All of them are defined as follows:

$$t_J^U = \alpha_J + 2\arctan\left(\frac{1}{\omega_J}\tan\left(\frac{-\beta_J}{2}\right)\right); \\ t_J^L = \alpha_J + 2\arctan\left(\frac{1}{\omega_J}\tan\left(\frac{\pi-\beta_J}{2}\right)\right) \; J \in \{A, B, C\} \quad (3)$$

$$d_{JK} = 1 - \cos(\alpha_J - \alpha_K) \qquad J, K \in \{A, B, C\}, J \neq K \quad (4)$$

The papers Rueda et al. (2021) and Rodríguez-Collado and Rueda (2021) provide model properties as well as detail the algorithm used to fit the models. In particular, the second paper presents a restricted FMM model for AP trains, while in the first one data from ACTD is concisely analyzed. Also, the associated phase space of the model is studied and relevant properties are provided.

In **Figure 1**, the fitted FMM model prediction and wave decomposition of postsynaptic APs from a GABAergic neuron (**Figure 1A**) and a glutamatergic neuron (**Figure 1B**) are shown. W_A represents the repolarization and, partly, the depolarization while W_B describes the end of the depolarization, and the hyperpolarization. Glutamatergic cells tend to have wider APs with a bigger amplitude (values of β_A smaller than π and higher values of ω_A and A_A) than GABAergic cells. Furthermore interesting differences can be observed between the two types in terms of the parameters of W_B, particularly in β_B and ω_B. The third wave, W_C, is heteromorphous: in some cases, this wave completes the AP shape (as is typical in GABAergic neurons), while in other cases it accounts for potential differences before and after the spike (as happens in most of the glutamatergic neurons). Also, W_A, W_B, and W_C seem to be related to the potassium, sodium, and calcium conductances that appear in Gouwens et al. (2018).

2.1.2. Circular Principal Components Analysis (CPCA)

The CPCA is a procedure that generates a circular variable which gathers the maximum variability. A basic reference is Scholz (2007). Briefly, given a data base in matrix form, let $\mathbf{e}_1$ and $\mathbf{e}_2$ be the first two eigenvectors extracted with principal component analysis (Hastie et al., 2009). Consider the transformation in which the eigenvectors are projected onto the unit circle as follows:

$$(e_{1,i}, e_{2,i}) = \left(\frac{e_{1,i}}{\sqrt{e_{1,i}^2 + e_{2,i}^2}}, \frac{e_{2,i}}{\sqrt{e_{1,i}^2 + e_{2,i}^2}}\right) \qquad \forall i \in 1, ..., n \quad (5)$$

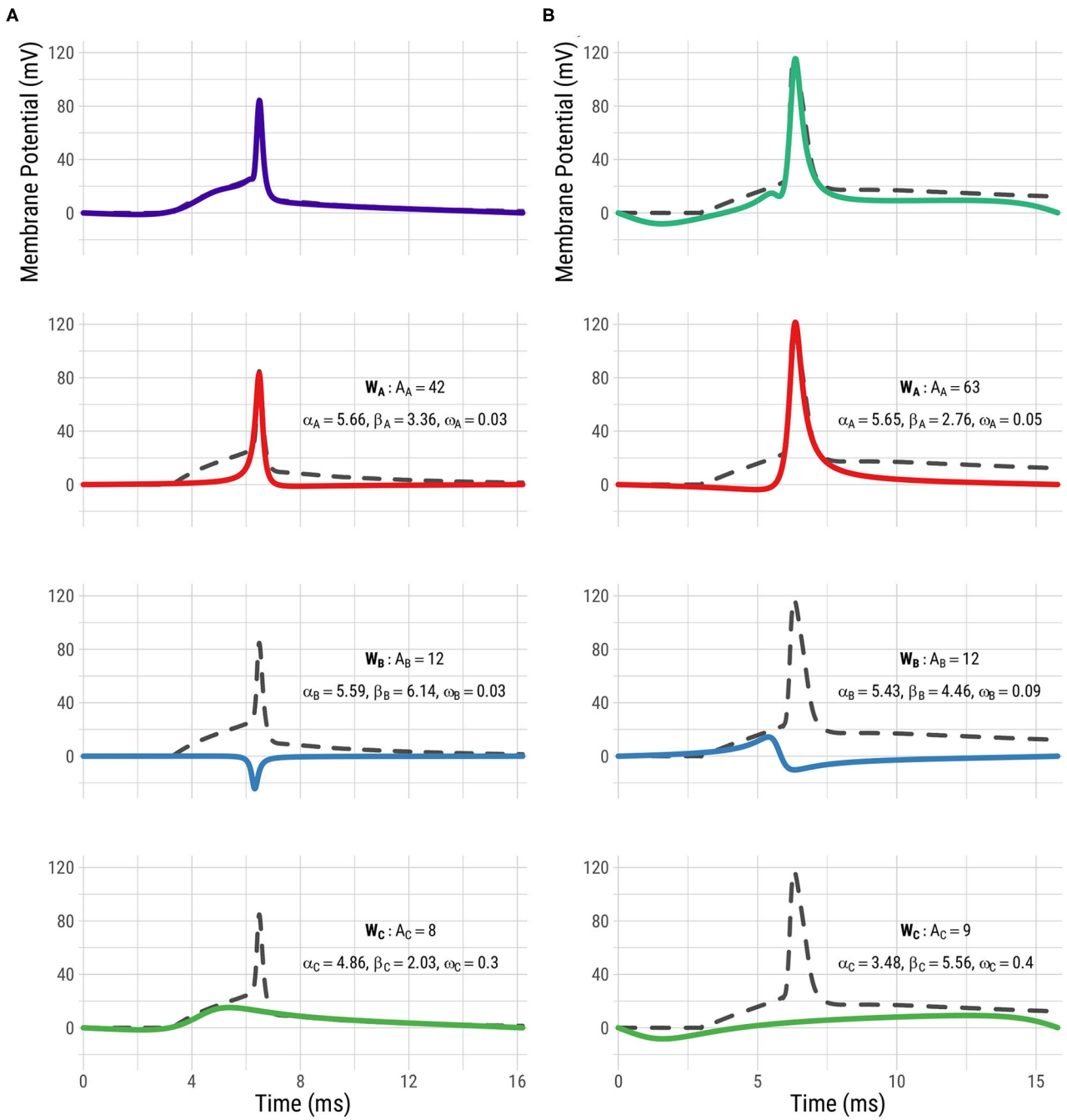

FIGURE 1 | FMM analysis of postsynaptic APs from GABAergic and glutamatergic neurons. First row: FMM prediction (solid line) and observed signal (dashed line) of postsynaptic APs from a GABAergic neuron **(A)** and a glutamatergic neuron **(B)**. Rows 2 – 4: Models' corresponding wave decomposition (W_A in red, W_B in blue and W_C in green) along with their parameters.

A circular order can be defined with $\theta_i = \arctan\left(\frac{e_{1,i}}{e_{2,i}}\right), \forall i \in 1, ..., n$, which is called the first circular principal component.

2.1.3. Machine Learning Supervised Methods

Various Machine Learning supervised methods have been considered in the paper. The simple linear discriminant analysis (LDA) method serves as benchmark for the results while, at the other extreme, the complex and "black box" methods support vector machines of polynomial kernel (SVM) and model averaged neural network (AvNNet) methods have been considered. The former habitually achieves outstanding results in neuronal dynamics, as seen in Teeter et al. (2018) among

others. In between these two extremes, interpretable ensembles of decision tree methods have been used, particularly random forest (RF), which has been proved to attain great results without requiring precise hyperparameter tuning (as explained in Fernandez-Delgado et al., 2014) and gradient boosting decision trees (GBDT), also capable of achieving outstanding results while not being as popular (Zhang et al., 2017). Brief descriptions of these methods are provided in the **Supplementary Material** based on Hastie et al. (2009) and Izenman (2008).

2.2. Dataset

The ACTD includes electrophysiological data of high temporal resolution of membrane potential from individual mouse recordings. A signal from each mouse neuron in the ACTD has been analyzed; particularly the signal generated by the short square stimulus with the lowest stimulus amplitude that elicited a single AP. A small set of neurons that elicited two APs with the selected stimulus were initially discarded for the analysis. See Allen Brain Institute (2015) to learn about the stimulus types applied in the database. Each signal has been preprocessed and analyzed according to the algorithm described shortly after.

A total of 1,892 experiments, from mouse cells of 24 different Cre lines, have been analyzed. Beforehand, experiments from three Cre lines were discarded as they did not have a sufficient sample size (<10 observations). The distribution of signals according to Cre line is given in **Table 1**, whereas their full names are described on the abbreviations section. Illustrated colors correspond to the different Cre lines in all figures. To facilitate the reading, the appearance order of the Cre lines in the table goes in accordance with the order proposed later in the paper. Throughout the manuscript, the characteristics of each Cre line have been illustrated in two different ways: using median values and using representative neurons, selected from among the neurons in the Cre line with the highest goodness of fit that had all the extracted features between the 5th and 95th percentiles.

TABLE 1 | Number of cells of each Cre line by neuronal class.

Cre line	Total	Exc.	Inh.
Pvalb	214	0	214
Slc32a1*	27	0	27
Nkx2.1	48	0	48
Ndnf	92	23	69
Gad2*	19	0	19
Htr3a	159	10	149
Sst	120	2	118
Nos1	67	6	61
Oxtr*	46	19	27
Chrna2	70	25	45
Chat	67	0	67
Vip	122	19	103
Cre line	**Total**	**Exc.**	**Inh.**
Ctgf	59	55	4
Tlx3*	40	40	0
Sim1*	30	30	0
Glt25d2*	10	10	0
Ntsr1	67	62	5
Esr2*	30	29	1
Rbp4	87	86	1
Scnn1a-Tg2	53	48	5
Rorb	173	150	23
Scnn1a-Tg3	89	86	3
Cux2	79	78	1
Nr5a1	84	83	1

*Cre lines without available transcriptomic features are marked with *.*

2.2.1. Transcriptomic Features

In order to incorporate genetic information in the study, the number of core cells by genetic cluster and Cre line have been grouped into eight genetic markers: Ndnf, Vip, Sst, Pvalb, L2-L4 (layers 2-4), L5 (layer 5), L6 (layer 6), and non-neuronal. Some Cre lines present in the current study were not present in the aforementioned paper. These Cre lines without available transcriptomic features have been marked with an asterisk (*) throughout the paper.

2.3. Programming Languages

The experimentation has been developed combining Python and R. Python has been used for data acquisition and transformation using the functions provided by Allen SDK (Allen Institute, 2015), while R fits the FMM models with the corresponding package available at the Comprehensive R Archive Network (https://cran.r-project.org/package=FMM) and analyses the results.

The R packages (Venables and Ripley, 2002; Karatzoglou et al., 2004; Chen and Guestrin, 2016; Breiman et al., 2018; Ripley, 2020) and the auxiliary package for learning procedures caret (Kuhn, 2018) have been used to implement the Machine Learning procedures.

Moreover, the libraries Shiny (Chang et al., 2020), Shinydashboard (Chang and Borges Ribeiro, 2018), and ggplot2 (Wickham, 2016) have been considered to develop a Shiny dashboard app.

2.4. Implemented Algorithm

A flowchart of the preprocessing procedure and the estimation algorithm is depicted in **Figure 2**. First of all, in the preprocessing stage, the APs in the signal are extracted. Each AP segment is defined as $[t_S-2d, t_S+3d]$, with t_S denoting the time of the spike's peak and d the time needed by the neuron to spike following the application of the stimulus. In real cases where the application time of the stimulus is unknown, a similar procedure can be applied preserving the uneven cut proposed, such as $[t_S-2k, t_S+3k]$, being k a particular amount of time normally in milliseconds. It is assumed that the segments to be analyzed represent complete APs, in particular, $X(t_1) \simeq X(t_n)$.

In a second stage, the parameters are estimated with the backfitting algorithm implemented in the package FMM of the programming language R, first presented in Fernández et al.

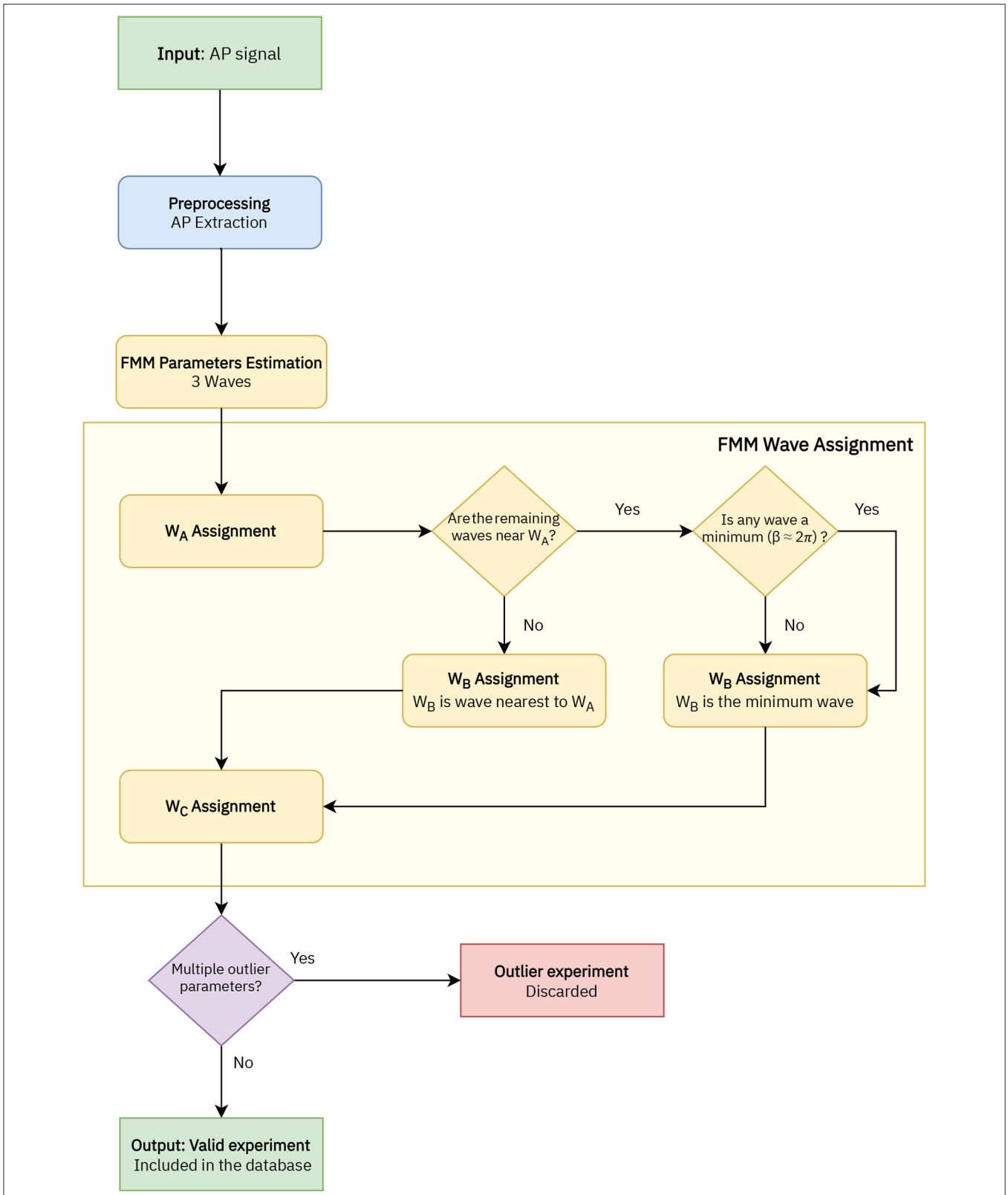

FIGURE 2 | Flowchart of the implemented algorithm to analyse the AP signals with the FMM model, which includes four stages: AP extraction, FMM parameters estimation, wave assignation, and outlier detection.

(2021). Three iterations of the backfitting algorithm are executed to extract the three waves. In each iteration, a single FMM wave is fitted to the residue of the previous iterations. The backfitting algorithm is repeated until the goodness of fit increase between two successive iterations is not significant. From a theoretical point of view, the backfitting algorithm is a standard procedure to find the maximum likelihood estimator (MLE) in additive semiparametric and non-parametric models (to learn more about the algorithm, see Hastie and Tibshirani, 1986). Besides, the experience in simulated and real data shows that the failure in convergence to the MLE does not likely happen (Rueda et al., 2021). From a computational point of view, the backfitting algorithm is efficient.

In the next stage the wave assignation is done. The proposed procedure is firstly presented in this paper and is specific to this study. Let the subscripts $i = \{1, 2, 3\}$ denote the three estimated waves initially given by the backfitting algorithm. The labels A, B, and C are assigned as follows:

1. $W_A = W_j/j = \arg\max_{i=1,2,3} A_i$.
2. Assuming the $W_A = W_1$, $W_B = W_j/j = \arg\min_{i=2,3} d_{Ai}$, except in cases where $|d_{A2} - d_{A3}| < 0.05$ and $\min(d(\beta_2, 2\pi), d(\beta_3, 2\pi)) < 0.3$, with $d(\beta_i, 2\pi)$ being the distance between the β parameter and 2π. In these cases $W_B = W_j/j = \arg\min_{i=2,3} d(\beta_i, 2\pi)$.
3. Finally, W_C is the remaining wave.

The model is validated with the R^2 statistic, which is the proportion of the variance explained by a model out of the total variance, as follows:

$$R^2 = 1 - \frac{\sum_{i=1}^{n}(X(t_i) - \hat{\mu}(t_i, \boldsymbol{\theta}))^2}{\sum_{i=1}^{n}(X(t_i) - \overline{X})^2} \tag{6}$$

where $\overline{X}$ is the neuron's mean potential difference and $\hat{\mu}(t_i)$ represents the fitted value at $t_i, i = 1, ..., n$. Finally, signals with multiple outlier values in significant parameters of the model related to the Cre line distribution have been discarded.

3. RESULTS

3.1. FMM Features for Cell Type Characterization

The FMM model gives an accurate fit of the observed signals, the R^2 global mean $\pm$ standard deviation being equal to 0.9868 ± 0.0066. GABAergic neurons are slightly better fitted as their mean R^2 is 0.9903 ± 0.0054, while for glutamatergic neurons it is 0.9823 ± 0.0053. A Shiny app has been developed to illustrate the differences in the typical APs of the various GABAergic and glutamatergic Cre lines. It can be accessed through https://alexarc26.shinyapps.io/median_ap_profile_by_cre_line/. The interface of the app, which is shown in **Figure 3**, consists basically of two parts: in the top half the median APs, along with their wave decomposition by Cre line, are depicted, while the controls of the main figure are in the bottom half. These include the possibility of selecting the different Cre lines of the database (up to nine different can be selected simultaneously), selecting just inhibitory or excitatory neurons, and selecting whether the wave sum or the parameters of the model should be plotted.

A total of 40 cells have been discarded due to having multiple outlier values.

The boxplots for the main parameters of the model by Cre line are plotted in **Supplementary Figures 1–5**. In these figures, the parameter values of the representative neurons from each Cre line have been highlighted as stars. These plots illustrate the potential of various parameters to discriminate between the different Cre lines such as β_A, ω_B, and $\sin(\beta_C)$. The plots also show that the GABAergic neurons exhibit more variability in their electrophysiological features, as Gouwens et al. (2019) points out.

Furthermore, the differences between Cre lines are apparent not only in the time domain, but in the associated phase space. In **Figure 4**, the fitted FMM models and associated phase space of representative examples of GABAergic Cre lines (**Figure 4A**) and glutamatergic Cre lines (**Figure 4B**) are shown. The APs from GABAergic neurons exhibit mainly spiky patterns with a pronounced depolarization before the spike threshold, whereas the APs of glutamatergic neurons are wider and have a more prolonged hyperpolarization. The phase space representations reveal differences between classes and Cre lines, specifically in terms of the perimeter, area, and shape of the "nose."

3.2. Circular Taxonomy

The taxonomy is defined at Cre line level. For this purpose, the median values of the electrophysiological features by Cre line have been used (note that the stimulus amplitude has not been considered to derive the circular taxonomy), along with the transcriptomic marker features. Due to notable distribution differences between the two feature sets, separate PCAs have been conducted.

Firstly, the electrophysiological features PCA is conducted and two components are extracted (explained variance: 82.40 %). The correlation of the variables with the extracted components and the Cre lines' PCA projections and CPCA transformations are depicted in **Supplementary Figures 6**, **8**. The different Cre lines are distinguished in the circular disposition and it is possible to tell apart most of the glutamatergic from GABAergic. This order is used later to place Cre lines without having any transcriptomic feature available in the taxonomy. The blank space between the Pvalb and Nr5a1 Cre lines observed in **Supplementary Figure 8** corresponds to non-neuronal cells, unavailable in the studied data.

Secondly, six components are extracted from the transcriptomic features as their explained variance was medium to low (93.47%). The correlation of the variables with the extracted components and the Cre lines' PCA projections and CPCA transformations are depicted in **Supplementary Figures 7**, **9**. It is particularly relevant to note that the transcriptomic CPCA only distinguishes three groups of Cre lines.

One final ensemble PCA is conducted with the extracted electrophysiological and transcriptomic components. The corresponding CPCA is shown in **Figure 5**, which is one of the main results of this study. The figure shows the order between

FIGURE 3 | App interface. **(Top)** Cre lines' median APs (dashed lines) along with the wave decomposition (solid lines). **(Bottom)** Interface controls for the selection of the Cre lines and the displayed elements.

Cre lines and the circular distance between two consecutive Cre lines, represented by the arc amplitudes. The main novelty of the defined taxonomy is its circular topology, unlike the previous linear proposals. Moreover, for the first time to our knowledge, some Cre lines have been located in a taxonomy. Nevertheless, a relevant difference with respect to other proposals, such as those of Gouwens et al. (2019) and Tasic et al. (2016), is that the Ndnf and Htr3a Cre lines turn out to be similar to other GABAergic neurons, and not to non-neuronal cells. Further details of the final PCA results can be found in **Supplementary Figure 10**.

The taxonomy is in agreement with others derived recently for mouse visual cortex neurons in several aspects. First, Cre lines that have similar characteristics are kept together (Vip and Chat, Htr3a and Ndnf, Pvalb and Nkx2.1 among others) as in Zeng and Sanes (2017) and Tasic et al. (2016). Second, the non-neuronal cell position between the GABAergic Pvalb Cre line and the glutamatergic Nr5a1 and Cux2 Cre lines -present in the upper layers of the visual cortex- coincides with the taxonomy of Tasic et al. (2018). Within the glutamatergic neurons, the Ctgf and Ntsr1 Cre lines -common in deeper layers- are the most similar in characteristics to the GABAergic neurons. In particular, this disposition is like those in Gouwens et al. (2019) and Tasic et al. (2016), after rearranging the results of the latter study, as can be seen in **Supplementary Figure 11**.

In order to validate the taxonomy, five transcriptomic-electrophysiological subclasses have been defined using **Figure 5**. These include four major GABAergic subclasses and one glutamatergic subclass specified in **Table 2**. In the next subsection, Machine Learning methods are used to discriminate these subclasses at neuronal level.

3.3. Cell-Type Classification

This classification problem, which is conducted at the cell level, has been addressed by other authors in many different ways, varying features and other factors such as the number, composition, and definition of the subclasses or the selection of cells to be classified.

In this study, the FMM derived features have been considered. Specifically, 37 features have been used, including the basic parameters, peak and trough times -and their model values-, the explained variance of each wave and the distance between waves. Also, the cell's reporter status and the origin layer have been considered as predictors. Several Machine Learning methods were tested. Note that some classifiers assume that the predictors are Euclidean, but α and β are circular parameters. The former and β_A can be considered Euclidean as they take values concentrated in a small arc. However, sine and cosine transformations are applied to both β_B and β_C.

All the classifiers except LDA had their hyperparameters tuned in a prior training-validation step. Afterwards, a 10-fold cross validation was performed on the tuned classifier to estimate its discrimination capacity. The dataset was divided into 10 equally sized splits. In 10 iterations, nine of the subsets were used to train the model, while the tenth serves as test. The discrimination capacity was evaluated in terms of the accuracy, percentage of observations correctly classified, and the kappa statistic, which measures the improvement over a random classification. A general overview of these matters can be found on Hastie et al. (2009).

The classification problem was tackled in three different stages. The results can be seen in **Table 3**. In the first stage (A),

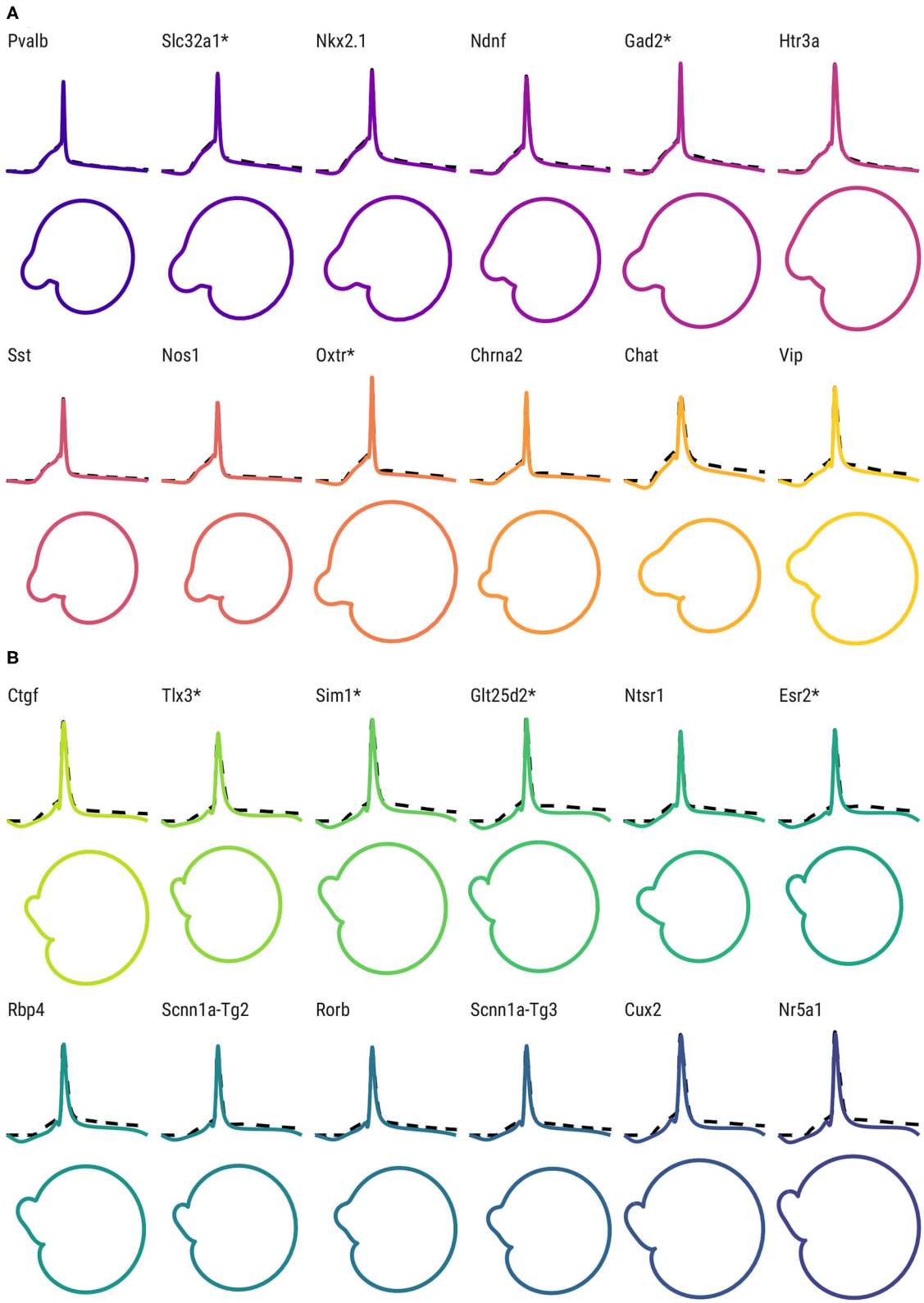

FIGURE 4 | AP shape and phase space for the representative neurons of each Cre line. (Top) FMM predictions (solid lines) and observed AP signals (dashed lines) of representative neurons of GABAergic Cre lines **(A)** and glutamatergic Cre lines **(B)**. Bottom: corresponding trajectories in the phase space. Cre lines without available transcriptomic features are marked with *.

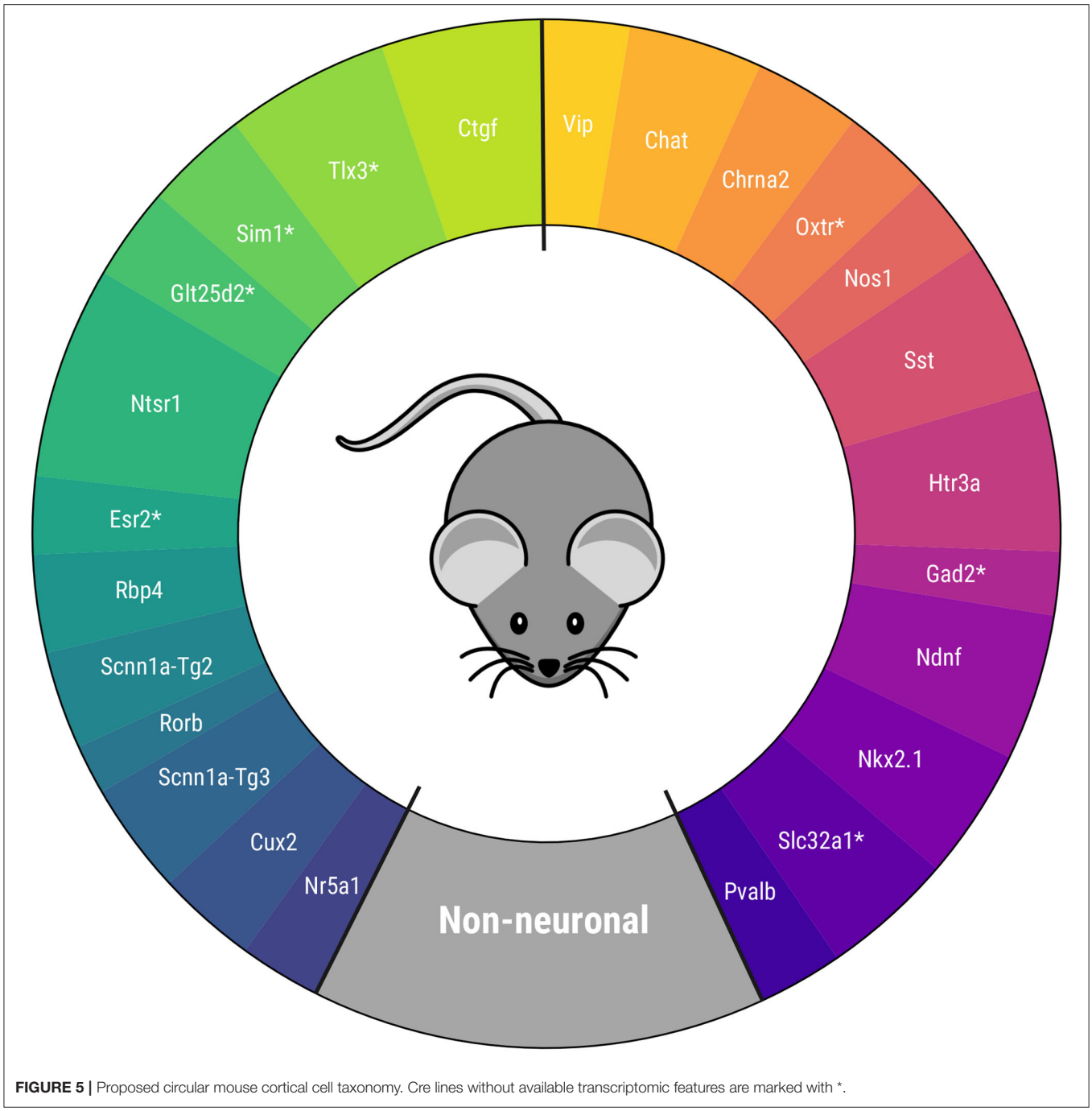

FIGURE 5 | Proposed circular mouse cortical cell taxonomy. Cre lines without available transcriptomic features are marked with *.

TABLE 2 | Defined subclasses and Cre lines composing them.

1. Pvalb+			2. Htr3a+			3. Sst+					4. Vip+	
Pvalb	Slc32a1*	Nkx2.1	Ndnf	Gad2*	Htr3a	Sst	Nos1	Oxtr*	Chrna2		Chat	Vip
5. Glutamatergic												
Ctgf	Tlx3 *	Sim1 *	Glt25d2*	Ntsr1	Esr2 *	Rbp4	Scnn1a-Tg2	Rorb	Scnn1a-Tg3		Cux2	Nr5a1

*Cre lines without available transcriptomic features are marked with *.*

TABLE 3 | Cross-validated accuracy and kappa statistic of the different Machine Learning methods in the discrimination of the subclasses (left, best performer classifiers are marked in bold) and cross-validated confusion matrix of the best performer classifier -AvNNet in all cases- (right) in each of the defined stages.

(A) Raw 5 subclass classification

	Accuracy (%)	Kappa			True class				
					Pvalb+ (%)	Htr3a+ (%)	Sst+ (%)	Vip+ (%)	Glut. (%)
LDA	66.1	0.519	Prediction	Pvalb+	86.9	10.7	12.2	3.7	0.7
RF	73.8	0.628		Htr3a+	7.9	48.2	6.6	10.0	1.1
GBDT	73.4	0.622		Sst+	4.5	18.9	60.7	6.3	1.2
SVM	74.1	0.632		Vip+	0.7	5.9	2.6	35.4	2.0
AvNNet	**75.2**	**0.648**		Glut.	0.0	16.3	17.8	44.4	94.9

(B) Clean 5 subclass classification

	Accuracy	Kappa			True class				
					Pvalb+ (%)	Htr3a+ (%)	Sst+ (%)	Vip+ (%)	Glut. (%)
LDA	72.0	0.608	Prediction	Pvalb+	86.9	12.6	13.1	4.1	0.0
RF	77.9	0.688		Htr3a+	6.6	54.9	8.8	10.0	0.4
GBDT	77.8	0.688		Sst+	5.5	18.6	72.5	4.7	0.8
SVM	79.1	0.703		Vip+	0.7	7.6	2.8	46.5	2.9
AvNNet	**80.3**	**0.723**		Glut.	0.4	6.3	2.8	34.3	95.9

(C) 4 subclass classification

	Accuracy (%)	Kappa			True class			
					Pvalb+ (%)	Sst+ (%)	Vip+ (%)	Glut. (%)
LDA	80.1	0.690	Prediction	Pvalb+	93.1	14.7	4.7	0.2
RF	84.7	0.769		Sst+	6.5	79.9	6.5	0.6
GBDT	85.2	0.773		Vip+	0.4	3.6	58.8	3.9
SVM	86.0	0.786		Glut.	0.0	1.8	30.0	96.9
AvNNet	**87.5**	**0.810**						

(C+) 4 subclass classification, including the stimulus amplitude feature

	Accuracy (%)	Kappa			True class			
					Pvalb+ (%)	Sst+ (%)	Vip+ (%)	Glut. (%)
LDA	80.9	0.706	Prediction	Pvalb+	93.1	14.3	5.3	0.2
RF	89.4	0.841		Sst+	6.5	79.5	4.1	1.2
GBDT	89.1	0.837		Vip+	0.0	3.1	82.4	1.7
SVM	91.2	0.867		Glut.	0.3	3.1	8.2	96.9
AvNNet	**91.3**	**0.868**						

the proposed classifiers were studied in the raw dataset, without discarding any observation or Cre lines. More than 75% of the cells could be correctly classified in their corresponding subclass by the AvNNet method; similar results were attained by SVM and RF. Observing the corresponding confusion matrix, it can be seen how the glutamatergic and Pvalb+ subclasses are most clearly discriminated, while more than half of the observations of the Htr3a+ and Vip+ subclasses are misclassified.

In the second stage (B), the GABAergic neurons that were not inhibitory and glutamatergic neurons that were not excitatory were discarded, leaving a total of 1,704 observations. The accuracy is excellent for a five-class problem, with more than 80% of the neurons being correctly discriminated by the AvNNet classifier. The second best result corresponds to SVM, followed closely by RF and GBDT, while LDA may be too simple for the task at hand. It is relevant to note that, in most of the cases, the misclassifications occurred between consecutive subclasses in the proposed circular taxonomy (i.e., Htr3a+ cells are mostly confused with Pvalb+ and Sst+, while Glutamatergic cells are misclassified with Vip+ cells). It seems that, at this stage, Sst+ cells are guessed correctly much better than in (A); the prediction of Htr3a+ and Vip+ subclasses have improved, but still, only 50% of the instances are correctly classified.

In the third stage (C), the classification problem has been solved with 1,304 observations, after discarding the observations from the Htr3a+ subclass as well as the observations from Cre lines without transcriptomic features (marked with *). The results are outstanding, as more than 87% of the observations are correctly discriminated in the proposed four classes. The best results are attained by the AvNNet and SVM classifiers. The Pvalb+ and Glutamatergic subclasses are well-identified in more than 93% of the cases, while Sst+ and Vip+ approximately in 80 and 60% of the cases, respectively. Finally, if the stimulus amplitude is added to the predictors feature set (stage C+), the

AvNNet classifier discriminates correctly more than 91% of the instances, being the accuracy increase particularly notable in the Vip+ subclass.

The results of LDA clearly show evidence that the subclasses cannot be linearly discriminated. The RF and GBDT classifiers may have attained worse results than the "black box" methods in all the stages, but they offer interpretability in exchange, as feature relevance in the classification can be measured. In all the stages, the same features are highlighted as relevant. Particularly, β_A seems to be the most relevant feature, being at least 1.5 the relevance of the second most important feature in all cases. Other discriminant features are ω_A, d_{AB}, d_{AC}, t_C^L, t_A^U, and α_C. The shape of the APs' repolarization and depolarization phases captured by W_A seem to characterize the different subclasses.

4. DISCUSSION

In this paper, the FMM approach for electrophysiological feature extraction has been presented and used to describe a circular taxonomy in mouse cortical cells.

Relevant AP characteristics such as its width, amplitude, kurtosis, and skewness, among others, are represented by the FMM parameters. Furthermore, additional features standardly used in other studies can easily be defined in terms of the basic parameters, as has been done with the peak time and other features. Even more, the same set of parameters characterizes the phase space. As such, it is not necessary to resort to additional feature sets, as is the case in Gouwens et al. (2020).

A novel property to highlight of the proposed taxonomy is that it is circular. The latter addresses the need for neuronal types to be considered a continuum, discussed by many authors such as Gouwens et al. (2020) and Tasic et al. (2018). Previous proposals, being linear, consider cell types situated at the extremes to be opposite in terms of their characteristics. However, this does not reflect reality: cell types situated at the extremes habitually have a higher degree of similarity than the existing similarity between them and other types situated in the taxonomy's center. The taxonomy also follows the levels proposed by Zeng and Sanes (2017): at class levels, cells are either glutamatergic, GABAergic, or non-neuron while, at subclass level, GABAergic neurons can be either Pvalb positive, Vip positive, Sst positive, or Htr3a positive-Vip negative. Furthermore, at type level, the cells are classified according to the expressed Cre line. In fact, some Cre lines have been included in a taxonomy for the first time to our knowledge.

Despite some minor differences, the taxonomy's Cre line disposition proposal is in agreement with the literature about mouse visual cortex neuron types. Furthermore, the Cre lines can be characterized using different FMM elements, such as its waves or parameters, that represent AP differences. In fact, the potential of the FMM parameters to discriminate glutamatergic neurons and the four major types of GABAergic neurons has been proved. Among GABAergic neurons, Pvalb+ have the APs with the highest skewness and the lowest kurtosis, while in APs of Vip+ occurs the opposite. The APs from both Sst+ and Htr3a+ exhibit intermediate characteristics, being the latter subclass particularly heterogeneous.

In short, the proposed taxonomy is hierarchical, continuous, easily reproducible, and based on robust, interpretable, and discriminant features, essential feature properties to successfully solve a classification problem, as many experts on *Feature Engineering* state (Duboue, 2020; Heaton, 2020 among recent works on the matter). It is relevant to note that many alternative electrophysiological feature proposals lack at least one of these properties. To the best of our knowledge, this is the first study in which the circular order from the principal components is considered. A very simple idea that we hypothesize that can help in the challenges of inferring cellular relationships. However, the aim of this study is not to develop new theories but to present the new approach and the resulting circular taxonomy for mouse Cre lines. Further studies are necessary to contrast the circular taxonomy and the biological evidences.

A limitation of the presented study is that features have only been extracted from a single signal with a single AP generated from a short square stimulus. On the one hand, it remains to be seen if the application of the FMM approach on multiple signals of the same neuron could generate useful features. However, this question is up in the air as the independence of the AP shape from the applied stimulus is assumed by some authors, such as Raghavan et al. (2019), whereas others like de Polavieja et al. (2005) state that the AP shape is affected by the recent history of applied stimuli. On the other hand, the use of the proposed method in multi-AP signals could be profitable, extracting other interesting features such as the interspike distance or the neuron's firing rate.

As future work, the proposed taxonomy could be refined by using transcriptomic features at cell level, not only at Cre line level. Also, the taxonomy should be validated further in other databases. The classifier methods presented in this work would profit from an increased sample size of each neuronal type and could probably discriminate better the different classes. In particular, the Htr3a+ subclass has turned out to particularly problematic to distinguish. However, other authors such as Gouwens et al. (2018) have already remarked that electrophysiological features do not discriminate this neuron type particularly well.

DATA AVAILABILITY STATEMENT

Publicly available datasets were analyzed in this study. This data can be found at: http://celltypes.brain-map.org.

AUTHOR CONTRIBUTIONS

AR-C developed the computational code for data acquisition and analysis, processed and analyzed data, and wrote and revised the

manuscript. CR conceived the aims, methodological proposal, conceptual design, and wrote and revised the manuscript. Both authors contributed to the article and approved the submitted version.

FUNDING

The authors gratefully acknowledge the financial support received by the Spanish Ministerio de Ciencia e Innovación, Universidad de Valladolid and Banco Santander [PID2019-106363RB-I00 to CR and Call for predoctoral contracts of the UVa 2020 to AR-C].

SUPPLEMENTARY MATERIAL

The Supplementary Material for this article can be found online at: https://www.frontiersin.org/articles/10.3389/fnhum.2021.684950/full#supplementary-material

REFERENCES

Allen Brain Institute (2015). *Allen Cell Types Database - Electrophysiology*. Technical report. Available online at: http://help.brain-map.org/download/attachments/8323525/CellTypes_Ephys_Overview.pdf?version=2&modificationDate=1508180425883&api=v2

Allen Institute (2015). *Allen SDK. Python Package Version 0.3.4*.

Argüelles, M., Benavides, C., and Fernández, I. (2014). A new approach to the identification of regional clusters: hierarchical clustering on principal components. *Appl. Econ*. 46, 2511–2519. doi: 10.1080/00036846.2014.904491

Breiman, L., Cutler, A., Liaw, A., and Wiener, M. (2018). *Package 'randomForest' Manual. CRAN. R Package Version 4.6-14*. Whitehouse Station.

Chang, W., and Borges Ribeiro, B. (2018). *Shinydashboard: Create Dashboards With 'Shiny'. R Package Version 0.7.1*. Minneapolis.

Chang, W., Cheng, J., Allaire, J., Xie, Y., and McPherson, J. (2020). *Shiny: Web Application Framework for R. R Package Version 1.5.0*. Minneapolis.

Chen, T., and Guestrin, C. (2016). "XGBoost: a scalable tree boosting system," in *Proceedings of the 22nd ACM SIGKDD International Conference on Knowledge Discovery and Data Mining, KDD '16* (New York, NY: ACM), 785–794. doi: 10.1145/2939672.2939785

de Polavieja, G. G., Harsch, A., Kleppe, I., Robinson, H. P. C., and Juusola, M. (2005). Stimulus history reliably shapes action potential waveforms of cortical neurons. *J. Neurosci*. 25, 5657–5665. doi: 10.1523/JNEUROSCI.0242-05.2005

Duboue, P. (2020). *The art of Feature Engineering: Essentials for Machine Learning, 1st Edn*. Vancouver, BC: Cambridge University Press. doi: 10.1017/9781108671682

Fernández, I., Rodríguez-Collado, A., Larriba, Y., Lamela, A., Canedo, C., and Rueda, C. (2021). FMM: An R package for modeling rhythmic patterns in oscillatory systems. *arxiv.org/abs/2105.10168*.

Fernandez-Delgado, M., Cernadas, E., Barro, S., and Amorim, D. (2014). Do we need hundreds of classifiers to solve real world classification problems? *J. Mach. Learn. Res*. 15, 3133–3181.

Gautier, Y., Meurice, P., Coquery, N., Constant, A., Bannier, E., Serrand, Y., et al. (2019). Implementation of a new food picture database in the context of fMRI and visual cognitive food-choice task in healthy volunteers. *Front. Psychol*. 10:2620. doi: 10.3389/fpsyg.2019.02620

Ghaderi, P., Marateb, H., and Safari, M.-S. (2018). Electrophysiological profiling of neocortical neural subtypes: a semi-supervised method applied to *in vivo* whole-cell patch-clamp data. *Front. Neurosci*. 12:823. doi: 10.3389/fnins.2018.00823

Gouwens, N., Berg, J., Feng, D., Sorensen, S., Zeng, H., Hawrylycz, M., et al. (2018). Systematic generation of biophysically detailed models for diverse cortical neuron types. *Nat. Commun*. 9:710. doi: 10.1038/s41467-017-02718-3

Gouwens, N., Sorensen, S., Berg, J., Lee, C., Jarsky, T., Ting, J., et al. (2019). Classification of electrophysiological and morphological neuron types in the mouse visual cortex. *Nat. Neurosci*. 22, 1182–1195. doi: 10.1038/s41593-019-0417-0

Gouwens, N. W., Sorensen, S. A., Baftizadeh, F., Budzillo, A., Lee, B. R., Jarsky, T., et al. (2020). Integrated morphoelectric and transcriptomic classification of cortical gabaergic cells. *Cell* 183, 935–953. doi: 10.1016/j.cell.2020.09.057

Hastie, T., and Tibshirani, R. (1986). Generalized additive models. *Stat. Sci*. 1, 297–310. doi: 10.1214/ss/1177013604

Hastie, T., Tibshirani, R., and Jerome, F. (2009). *The Elements of Statistical Learning: Data Mining, Inference, and Prediction, 2nd Edn*. New York, NY: Springer.

Heaton, J. (2020). An empirical analysis of feature engineering for predictive modeling. *arxiv.org/abs/1701.07852*.

Izenman, A. J. (2008). *Modern Multivariate Statistical Techniques: Regression, Classification, and Manifold Learning, 1st Edn*. New York, NY: Springer. doi: 10.1007/978-0-387-78189-1

Karatzoglou, A., Smola, A., Hornik, K., and Zeileis, A. (2004). kernlab-an S4 package for kernel methods in R. *J. Stat. Softw*. 11, 1–20. doi: 10.18637/jss.v011.i09

Kuhn, M. (2018). *Package 'caret' Manual. CRAN. R Package Version 6.0-86*. New London County.

Lynch, E. P., and Houghton, C. J. (2015). Parameter estimation of neuron models using *in-vitro* and *in-vivo* electrophysiological data. *Front. Neuroinform*. 9:10. doi: 10.3389/fninf.2015.00010

Melzer, S., and Monyer, H. (2020). Diversity and function of corticopetal and corticofugal gabaergic projection neurons. *Nat. Rev. Neurosci*. 21, 1–17. doi: 10.1038/s41583-020-0344-9

Moore, R., Harrison, A., Mcallister, S., Polson, S., and Wommack, K. E. (2020). Iroki: automatic customization and visualization of phylogenetic trees. *PeerJ* 8:e8584. doi: 10.7717/peerj.8584

Raghavan, M., Fee, D., and Barkhaus, P. (2019). "Generation and propagation of the action potential," in *Handbook of Clinical Neurology, Vol. 160* (Milwaukee: Elsevier), 3–22. doi: 10.1016/B978-0-444-64032-1.00001-1

Ripley, B. (2020). *nnet: Feed-Forward Neural Networks and Multinomial Log-Linear Models. R Package Version 7.3-14*. New York, NY.

Rodríguez-Collado, A., and Rueda, C. (2021). A Simple Parametric Representation of the Hodgkin-Huxley Model. *PLOS One*. Available online at: https://www.biorxiv.org/content/early/2021/01/11/2021.01.11.426189 (accessed July 9, 2021).

Rueda, C., Larriba, Y., and Peddada, S. (2019). Frequency modulated Möbius model accurately predicts rhythmic signals in biological and physical sciences. *Sci. Rep*. 9, 1–10. doi: 10.1038/s41598-019-54569-1

Rueda, C., Rodríguez-Collado, A., and Larriba, Y. (2021). A novel wave decomposition for oscillatory signals. *IEEE Trans. Signal Process*. 69, 960–972. doi: 10.1109/TSP.2021.3051428

Scholz, M. (2007). "Analysing periodic phenomena by circular PCA," in *Bioinformatics Research and Development*, eds S. Hochreiter and R. Wagner (Berlin; Heidelberg: Springer), 38–47. doi: 10.1007/978-3-540-71233-6_4

Tasic, B., Menon, V., Nguyen, T. N., Kim, S., Jarsky, T., Yao, Z., et al. (2016). Adult mouse cortical cell taxonomy revealed by single cell transcriptomics. *Nat. Neurosci*. 19, 335–346. doi: 10.1038/nn.4216

Tasic, B., Yao, Z., Graybuck, L., Smith, K., Nguyen, T. N., Bertagnolli, D., et al. (2018). Shared and distinct transcriptomic cell types across neocortical areas. *Nature* 563, 72–78. doi: 10.1038/s41586-018-0654-5

Teeter, C., Iyer, R., Menon, V., Gouwens, N., Feng, D., Berg, J., et al. (2018). Generalized leaky integrate-and-fire models classify multiple neuron types. *Nat. Commun*. 9, 1–15. doi: 10.1038/s41467-017-02717-4

Tremblay, R., Lee, S., and Rudy, B. (2016). GABAergic interneurons in the neocortex: from cellular properties to circuits. *Neuron* 91, 260–292. doi: 10.1016/j.neuron.2016.06.033

Venables, W. N., and Ripley, B. D. (2002). *Modern Applied Statistics With S, 4th Edn*. New York, NY: Springer. doi: 10.1007/978-0-387-21706-2

Wickham, H. (2016). *ggplot2: Elegant Graphics for Data Analysis, 2nd Edn*. New York, NY: Springer - Verlag.

Zeng, H., and Sanes, J. (2017). Neuronal cell-type classification: challenges, opportunities and the path forward. *Nat. Reviews Neurosci.* 18, 530–546. doi: 10.1038/nrn.2017.85

Zhang, C., Liu, C., Zhang, X., and Almpanidis, G. (2017). An up-to-date comparison of state-of-the-art classification algorithms. *Expert Syst. Appl.* 82, 128–150. doi: 10.1016/j.eswa.2017.04.003

Žurauskienė, J., and Yau, C. (2016). pcareduce: Hierarchical clustering of single cell transcriptional profiles. *BMC Bioinformatics* 17:140. doi: 10.1186/s12859-016-0984-y

Conflict of Interest: The authors declare that the research was conducted in the absence of any commercial or financial relationships that could be construed as a potential conflict of interest.

frontiers in Human Neuroscience

ORIGINAL RESEARCH
published: 09 August 2021
doi: 10.3389/fnhum.2021.649533

Generalized Finite-Length Fibonacci Sequences in Healthy and Pathological Human Walking: Comprehensively Assessing Recursivity, Asymmetry, Consistency, Self-Similarity, and Variability of Gaits

Cristiano Maria Verrelli[1]*, *Marco Iosa*[2,3], *Paolo Roselli*[4,5], *Antonio Pisani*[6,7], *Franco Giannini*[1] and *Giovanni Saggio*[1]

[1] Department of Electronic Engineering, University of Rome Tor Vergata, Rome, Italy, [2] Department of Psychology, Sapienza University of Rome, Rome, Italy, [3] Laboratory for the Study of Mind and Action in Rehabilitation Technologies, Istituto di Ricovero e Cura a Carattere Scientifico Santa Lucia Foundation, Rome, Italy, [4] Department of Mathematics of University of Rome Tor Vergata, Rome, Italy, [5] Institut de Recherche en Mathématique et Physique, Universite' Catholique de Louvain, Ottignies-Louvain-la-Neuve, Belgium, [6] Department of Brain and Behavioral Sciences, University of Pavia, Pavia, Italy, [7] Istituto di Ricovero e Cura a Carattere Scientific Mondino Foundation, Pavia, Italy

OPEN ACCESS

Edited by:
Mariagiovanna Cantone, Sant'Elia Hospital, Italy

Reviewed by:
Marco Tramontano, Santa Lucia Foundation (IRCCS), Italy
Alberto Ranavolo, National Institute for Insurance Against Accidents at Work (INAIL), Italy
Concetto Spampinato, University of Catania, Italy

***Correspondence:**
Cristiano Maria Verrelli
verrelli@ing.uniroma2.it

Specialty section:
This article was submitted to Motor Neuroscience, a section of the journal Frontiers in Human Neuroscience

Received: 05 January 2021
Accepted: 05 July 2021
Published: 09 August 2021

Citation:
Verrelli CM, Iosa M, Roselli P, Pisani A, Giannini F and Saggio G (2021) Generalized Finite-Length Fibonacci Sequences in Healthy and Pathological Human Walking: Comprehensively Assessing Recursivity, Asymmetry, Consistency, Self-Similarity, and Variability of Gaits. Front. Hum. Neurosci. 15:649533. doi: 10.3389/fnhum.2021.649533

Healthy and pathological human walking are here interpreted, from a temporal point of view, by means of dynamics-on-graph concepts and generalized finite-length Fibonacci sequences. Such sequences, in their most general definition, concern two sets of eight specific time intervals for the newly defined *composite gait cycle*, which involves two specific couples of overlapping (left and right) gait cycles. The role of the golden ratio, whose occurrence has been experimentally found in the recent literature, is accordingly characterized, without resorting to complex tools from linear algebra. Gait recursivity, self-similarity, and asymmetry (including double support sub-phase consistency) are comprehensively captured. A new gait index, named Φ-*bonacci gait number*, and a new related experimental conjecture—concerning the position of the foot relative to the tibia—are concurrently proposed. Experimental results on healthy or pathological gaits support the theoretical derivations.

Keywords: gait analysis, walking gait, asymmetry, self-similarity, golden ratio, fibonacci sequence, locomotion, neuroscience

1. INTRODUCTION

Four time intervals—associated with the durations of gait cycle, swing, stance and double support phases—characterize, from a temporal point of view, symmetric and recursive human walking (Dugan and Bat, 2005). Recently, the ratio between swing and double support phases durations has been experimentally recognized in Iosa et al. (2013)[1] to be close, in healthy subjects symmetrically and recursively walking at comfortable speed of about 4 km/h (Cavagna and Margaria, 1966), to the golden ratio $\phi = (1+\sqrt{5})/2 \approx 1.618$. Such an irrational number ϕ is the positive solution to the equation $x^2 = 1 + x$. It is related to the Euclid's problem of cutting in a self-proportional way a

[1] Spatio-temporal gait parameters are analyzed in Iosa et al. (2013) by using a stereo-photogrammetric system with 6 cameras.

given straight segment (Iosa et al., 2017, 2019). In this light, ϕ turns out to describe self-similarity in symmetric walking (Iosa et al., 2019). Indeed, most of the literature agrees that the foot off reliably occurs at 60–62% of a physiological gait when the subject is (symmetrically and recursively) walking at comfortable speed[2]. On the other hand, it has been also experimentally shown that patients with Parkinson's Disease—known to be characterized by tremor at rest, rigidity, akinesia, or bradykinesia, and postural instability—have such a smooth, graceful and melodic flow of movement being reduced, with their gait self-similarity being altered (Iosa et al., 2016b). Notice how all the experimental evidences above move along the direction of using temporal gait analyses to complement, in clinical or general performance evaluations (Salarian et al., 2004; Wang et al., 2012; do Carmo Vilas-Boas and Cunha, 2016; Ren et al., 2016; Serrao et al., 2017; Ricci et al., 2019b), the classical gait analyses including motion analysis, dynamic electromyography, force plate recordings, energy cost measurements or energetics, measurement of stride characteristics (Dugan and Bat, 2005; Greene et al., 2010; Saggio and Sbernini, 2011). However, human walking naturally includes asymmetric and non-recursive components, especially in pathological cases, so that at least eight (in place of four) time intervals have to be considered. These time intervals include the gait cycle, swing, stance, double support durations for both the left and right lower limbs (Marino et al., 2020).

This work definitely exploits the ideas underlying a fractal approach to the question[3], in which the larger scale structure resembles the subunit structure. It moves along the direction of providing special interest to the simplest and most general way of transformation when a new domain is composed of two previous ones, with a consequent internal evolutionary process including the generation of a self-referential loop[4]. In particular, this paper provides original mathematically-founded arguments addressing the ¬-{symmetry and recursivity} question above. As in Marino et al. (2020), the crucial role of ϕ is found to be intrinsically related to the mathematical description of the human walking, rather than to be associated with the special solution constituted by a temporally self-similar gait[5]. However, differently from Marino et al. (2020), no complex tools from linear algebra, associating special ϕ-dependent subspaces with a common temporal model for human walking and running gaits, are here employed. Instead, human walking is here described in terms of generalized finite-length Fibonacci sequences (Horadam, 1961)[6] and dynamics-on-graph concepts (an interpretation in terms of Shannon entropy is also presented in **Appendix A**). Furthermore, in contrast to Marino et al. (2020), the new mathematical concept of *composite gait cycle* is here innovatively analyzed: it involves (see **Figure 1**) two specific couples of overlapping gait cycles, namely the left and right gait cycles and the *adjoint* right and left gait cycles, while extending the idea of stride-to-stride interval (Kavanagh et al., 2006) and step-by-step interval (Potdevin et al., 2007). The analysis presented in this paper generalizes the one in Iosa et al. (2013), as much as the new index of section 2, named Φ-*bonacci gait number*, constitutes the most straightforward generalization of the gait ratio in Iosa et al. (2013) to the case in which non-{symmetric and recursive} components of walking (including the concept of double support consistency) occur. Furthermore, differently from the area of the *Synchronicity Rectangle* in Marino et al. (2020), such a new index takes its minimum zero-value just when the *enforced adjoint symmetric self-similarity* occurs. The above index, which can be naturally extended to even assess *gait index variability* along past walking gaits (**Appendix B**), also innovatively involves a term relying on a new experimental conjecture (section 2) that opens new analysis and diagnosis perspectives on the internal analysis of the double support phase. An experimental support to the results of this paper is finally provided in section 3, with a detailed discussion being reported in section 4.

2. MATERIALS AND METHODS

2.1. Walking Phase Partition

Walking is defined as the bipedal locomotion gait (Kirtley, 2006; Iosa et al., 2013) such that: (1) at least one limb is in contact with the ground; (2) the contact phases are alternated by the two limbs. In particular, condition 1. excludes, in walking, the following possible state of the limbs: {no limbs in contact with the ground}. Even though each gait cycle conventionally starts and finish with consecutive foot strikes of the same foot (being formed by the stance and the swing of the same limb), we here adopt, as in Marino et al. (2020), the compactly comprehensive modeling of **Figure 2**, which defines the right and left gait cycles, with duration GC_r, GC_l, as the time intervals (or phases) between two consecutive strikes of the right foot, namely $FS_{r,a}$ and $FS_{r,b}$, and two consecutive lift off of the left foot, namely $FO_{l,a}$ and $FO_{l,b}$, respectively. This way, as we shall see, the same right swing phase appearing in the left stance phase is the one that is involved in the definition of the right gait cycle (see **Figure 2**). Analogously define the *adjoint* right and left gait cycles, with duration GC_r^{adj}, GC_l^{adj}, as the time intervals (or phases) between two consecutive lift off of the right foot, namely $FO_{r,x}$ and $FO_{r,y}$, and two consecutive strikes of the left foot, namely $FS_{l,x}$ and $FS_{l,y}$, respectively, with $FO_{r,x}$ and $FS_{l,x}$ immediately preceding

[2]It is worth noting that a similar percentage $61.06\% \equiv 1 - \phi = 1/\phi$ is the same that appears, in a normal subject performing a head-up tilt, as the ratio between the LF (low frequency) component and the total power in the Heart Rate Variability context (The European Society of Cardiology & the North American Society of Pacing & Electrophysiology, 1996, pag. 361, Figure 5.f), whereas $38.94\% \equiv 1/\phi^2$ equals the ratio between the LF total-power-complement and the total power.

[3]The generic idea that walking can have a fractal structure can be found in Hausdorff et al. (1995), while the existence of significant alterations from such a structure in patients with Parkinson's Disease has been suggested in Hausdorff et al. (2003).

[4]As reported in Igamberdiev (2004), certain recursive limits become fundamental canons of perfection formed as memorization within reflective loops.

[5]With respect to this, notice that, even in the symmetric and recursive case, the ratio between swing and double support phases durations in healthy subjects walking at comfortable speed slightly differs from ϕ, so that a perfectly self-similar gait does not occur in practice, with a consequent mismatch arising between occurred temporal events and currently available related analysis.

[6]A completely different use of Fibonacci numbers is, instead, suggested in Iosa et al. (2017), which is related to the interpretation of ϕ as the convergent equilibrium of the Ultimatum Game.

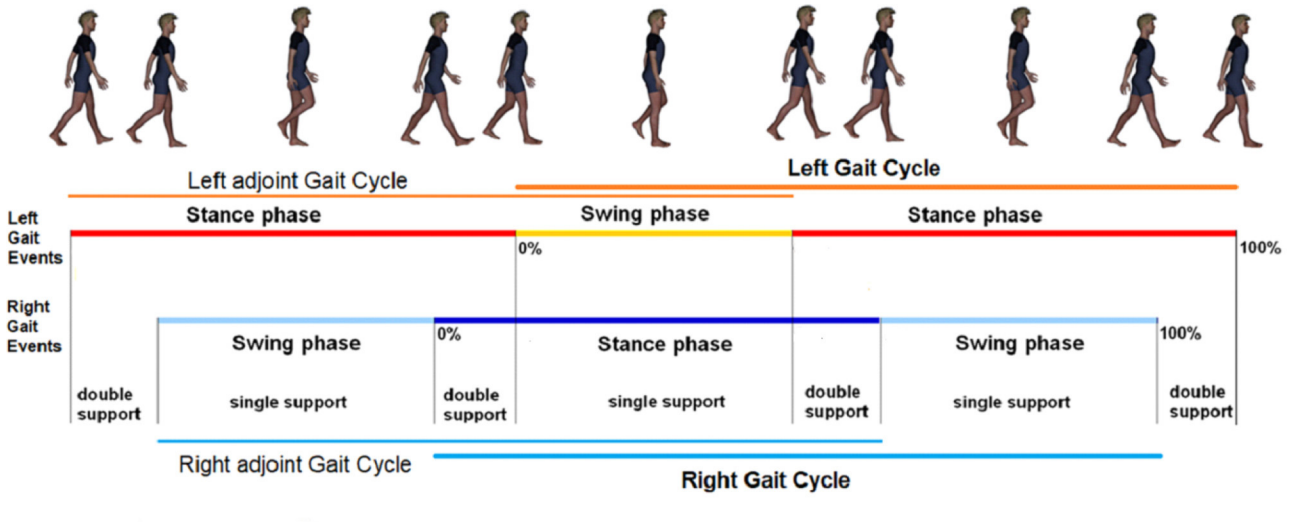

FIGURE 1 | Partitions of the walking gaits.

$FS_{r,a}$ and $FO_{r,x}$, respectively (see **Figure 2**). Here: GC stands for Gait Cycle; FS stands for Foot Strike; FO stands for Foot Off; r and l stand for right and left, respectively; adj stands for adjoint. Thereafter: ST stands for STance; SW stands for SWing; DS stands for Double Support.

Remark: As shown in **Figure 2**, each stance contains the contralateral swing besides the double support sub-phase with the left foot behind and the right foot ahead and the double support sub-phase with the right foot behind and left foot ahead. This will be crucial in defining the double support consistency concept of the reminder of this paper. On the other hand, the need of considering the adjoint gait relies on the fact that the assumption of gait symmetry and recursivity often decays in pathological walking.

First refer to the right and left gait cycles, with duration GC_r, GC_l. The phase in the right (resp., left) gait cycle in which the right (resp., left) limb is in-contact with the ground is named right (resp., left) stance and has time duration ST_r (resp., ST_l). The right swing and left swing phases are defined as the time intervals in which the right (resp., left) limb is not in contact with the ground during the right (resp., left) gait cycle (Iosa et al., 2013). Their durations are given by[7]:

$$SW_r = GC_r - ST_r, \quad SW_l = GC_l - ST_l. \tag{1}$$

As aforementioned, during walking, there cannot be a double float phase in which both feet are off the ground (condition 1.), so that the left swing phase (resp., right swing phase) must be entirely contained in the right stance phase (resp., left stance phase). The non-negative difference between their durations leads to the definition of the right (resp., left) double support phase that is entirely contained in the right gait cycle (resp., left gait cycle). Its duration DS_r (resp., DS_l) is given by:

$$DS_r = ST_r - SW_l \quad (DS_l = ST_l - SW_r). \tag{2}$$

The durations DS_r and DS_l in turn satisfy $DS_r = DS_x + DS_y$, $DS_l = DS_y + DS_z$, where DS_x, DS_y, DS_z denote the durations of the double support sub-phases highlighted in **Figure 2**. On the other hand, the same quantities can be introduced for the *adjoint* right and left gait cycles, with duration GC_r^{adj}, GC_l^{adj}. They are denoted by ST_r^{adj}, ST_l^{adj}, SW_r^{adj}, SW_l^{adj}, DS_r^{adj}, DS_l^{adj} and satisfy by definition (see **Figure 2**): $DS_r^{adj} = DS_r$, $SW_l^{adj} = SW_l$, $ST_r^{adj} = ST_r$. Again, the durations DS_r^{adj} and DS_l^{adj} in turn satisfy $DS_r^{adj} = DS_x + DS_y$, $DS_l^{adj} = DS_w + DS_x$, where DS_x denotes the duration of the double support sub-phase highlighted in **Figure 2**.

The following proposition holds. It generalizes the corresponding one in Marino et al. (2020), while it allows to extend the analysis of Iosa et al. (2013) to pathological gaits in which the inequalities: $GC_r \neq GC_l$ (resp., $GC_r^{adj} \neq GC_l^{adj}$), $ST_r \neq ST_l$ (resp., $ST_r^{adj} \neq ST_l^{adj}$), $SW_r \neq SW_l$ (resp., $SW_r^{adj} \neq SW_l^{adj}$), $DS_r \neq DS_l$ (resp., $DS_r^{adj} \neq DS_l^{adj}$) possibly occur.

Proposition 1: *Given the 16 time intervals durations* GC_r, GC_l, ST_r, ST_l, SW_r, SW_l, DS_r, DS_l, GC_r^{adj}, GC_l^{adj}, ST_r^{adj}, ST_l^{adj}, SW_r^{adj}, SW_l^{adj}, DS_r^{adj}, DS_l^{adj} *(under* $DS_r^{adj} = DS_r$, $SW_l^{adj} = SW_l$, $ST_r^{adj} = ST_r$*), they define a composite walking cycle if the following*

[7]The swing duration is sometimes denoted by SS, with SS standing for Single Support.

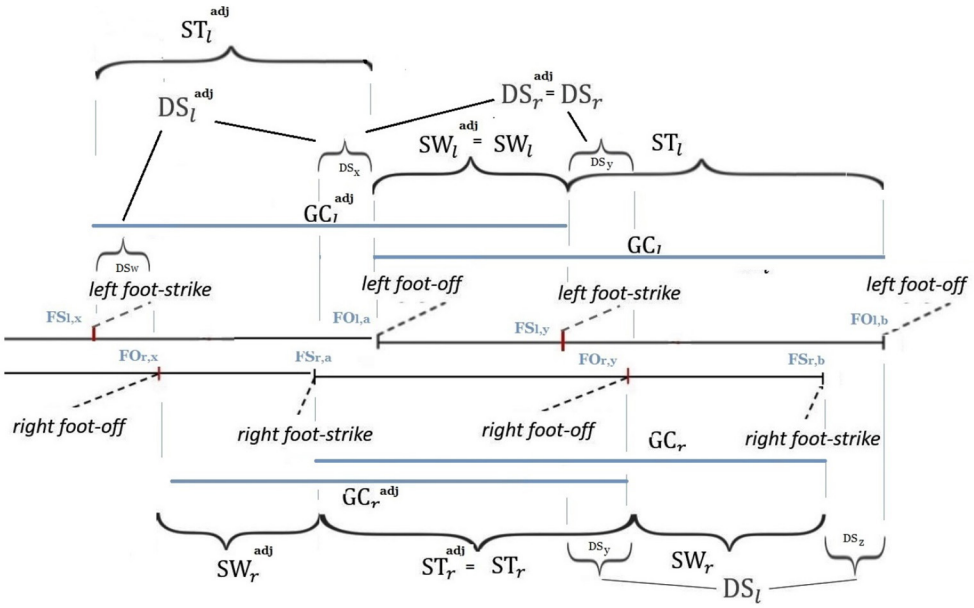

FIGURE 2 | *Composite gait cycle*: right and left gait cycles and *adjoint* right and left gait cycles.

eight equality constraints are satisfied:

$$\begin{aligned} \mathrm{ST}_r &= \mathrm{DS}_r + \mathrm{SW}_l, \quad \mathrm{GC}_r = \mathrm{DS}_r + \mathrm{SW}_l + \mathrm{SW}_r \\ \mathrm{ST}_l &= \mathrm{DS}_l + \mathrm{SW}_r, \quad \mathrm{GC}_l = \mathrm{DS}_l + \mathrm{SW}_r + \mathrm{SW}_l. \\ \mathrm{ST}_r^{\mathrm{adj}} &= \mathrm{DS}_r^{\mathrm{adj}} + \mathrm{SW}_l^{\mathrm{adj}}, \quad \mathrm{GC}_r^{\mathrm{adj}} = \mathrm{DS}_r^{\mathrm{adj}} + \mathrm{SW}_l^{\mathrm{adj}} + \mathrm{SW}_r^{\mathrm{adj}} \\ \mathrm{ST}_l^{\mathrm{adj}} &= \mathrm{DS}_l^{\mathrm{adj}} + \mathrm{SW}_r^{\mathrm{adj}}, \quad \mathrm{GC}_l^{\mathrm{adj}} = \mathrm{DS}_l^{\mathrm{adj}} + \mathrm{SW}_r^{\mathrm{adj}} + \mathrm{SW}_l^{\mathrm{adj}}. \end{aligned} \tag{3}$$

2.2. Generalized Finite-Length Fibonacci Sequences and Classification

Define the two (right and left) chains that are represented by the sequences:

$$\begin{aligned} \mathrm{DS}_r \;&\rightarrow\; \mathrm{SW}_l \;\rightarrow\; \mathrm{ST}_r \;\rightarrow\; \mathrm{GC}_r \\ \mathrm{DS}_l \;&\rightarrow\; \mathrm{SW}_r \;\rightarrow\; \mathrm{ST}_l \;\rightarrow\; \mathrm{GC}_l, \end{aligned}$$

along with their *adjoint* versions[8]:

$$\begin{aligned} \mathrm{DS}_r^{\mathrm{adj}} \;&\rightarrow\; \mathrm{SW}_l^{\mathrm{adj}} \;\rightarrow\; \mathrm{ST}_r^{\mathrm{adj}} \;\rightarrow\; \mathrm{GC}_r^{\mathrm{adj}} \\ \mathrm{DS}_l^{\mathrm{adj}} \;&\rightarrow\; \mathrm{SW}_r^{\mathrm{adj}} \;\rightarrow\; \mathrm{ST}_l^{\mathrm{adj}} \;\rightarrow\; \mathrm{GC}_l^{\mathrm{adj}}. \end{aligned}$$

The symmetric and recursive case and the (more general) non-{symmetric and recursive} one will be distinguished, in order to make the asymmetric walking be viewed as a natural extension of the symmetric and recursive one.

Symmetric and recursive walking. The following equalities: $\mathrm{GC}_r = \mathrm{GC}_l = \mathrm{GC}_r^{\mathrm{adj}} = \mathrm{GC}_l^{\mathrm{adj}} = \mathrm{GC}$, $\mathrm{ST}_r = \mathrm{ST}_l = \mathrm{ST}_l^{\mathrm{adj}} = \mathrm{ST}_r^{\mathrm{adj}} = \mathrm{ST}$, $\mathrm{SW}_r = \mathrm{SW}_l = \mathrm{SW}_r^{\mathrm{adj}} = \mathrm{SW}_l^{\mathrm{adj}} = \mathrm{SW}$, $\mathrm{DS}_r = \mathrm{DS}_l = \mathrm{DS}_l^{\mathrm{adj}} = \mathrm{DS}_r^{\mathrm{adj}} = \mathrm{DS}$ hold in symmetric and recursive walking, so that the two above chains and their *adjoint* versions collaps into one, namely into $\mathrm{DS} \rightarrow \mathrm{SW} \rightarrow \mathrm{ST} \rightarrow \mathrm{GC}$.

The following proposition holds, whose proof directly comes from (3), once it is specialized to the symmetric and recursive case.

Proposition 2: *The chain DS → SW → ST → GC represents a (generalized)* (a, b)*-generated 4-length Fibonacci sequence*[9] *of the form:*

$$a, \quad b, \quad c, \quad d \tag{4}$$

with a, b, c, d being non-negative numbers such that $c = a + b$ *and* $d = b + c$.

According to Horadam (1961), the golden ratio ϕ is a natural, feasible fixed point[10] for the consecutive ratios b/a, c/b and d/c that are related to the generalized 4-length Fibonacci sequence (4). In fact, when $b/a = \phi$, then $c/b = (a+b)/b = 1/\phi + 1 = \phi$ and $d/c = (b+c)/c = 1/\phi + 1 = \phi$ result. In this case, the sequence is described by the model: $y(k+1) = \phi y(k)$, $k = 0, 1, 2$, where $y(0) = a$, $y(1) = b$, $y(2) = c$, $y(3) = d$. One value thus *determines* the whole sequence[11], in the sense that *the value of*

[8]For the sake of clarity, we do not explicitly use, in this subsection, the fact that $\mathrm{DS}_r^{\mathrm{adj}} = \mathrm{DS}_r$, $\mathrm{SW}_l^{\mathrm{adj}} = \mathrm{SW}_l$, $\mathrm{ST}_r^{\mathrm{adj}} = \mathrm{ST}_r$.

[9]Note that, in the case of DS = 0 (namely, in the limit case at which walking switches into running), sequence (4)—normalized with respect to SW—, reduces to the classical Fibonacci sequence generated by 0, 1.

[10]The other fixed point $(1 - \phi)$ for the consecutive ratios b/a, c/b and d/c is not feasible when, as in this case, a and b are non-negative.

[11]Notice the meaningful similarity between the 4-length sequence a = DS, b = SW, c = ST, d = GC (in the walking cycle) and the 4-length sequence a = D-S-2IV$_r$, b = S+IV$_r$, c = I$_f$, d = R-R (in the cardiac cycle measured after 15 min of rest

just one ratio identically characterizes the whole sequence of ratios (see the Shannon entropy- based interpretation of **Appendix A**).

Non-{symmetric and recursive} walking. Define the quantities $\Delta SW = SW_l - SW_r$, $\Delta SW^{adj} = SW_l^{adj} - SW_r^{adj}$. The following proposition, whose proof again comes from (3), provides the main result of this subsection.

Proposition 3: *Let* $c_I = ST_r$, $c_{II} = ST_l$, $d_I = GC_r + \Delta SW$, $d_{II} = GC_l - \Delta SW$. *The two sequences*

$$\begin{aligned} I: &\quad a_I, \quad b_I, \quad c_I, \quad d_I \\ II: &\quad a_{II}, \quad b_{II}, \quad c_{II}, \quad d_{II} \end{aligned} \tag{5}$$

are (generalized) 4-length Fibonacci sequences, generated by $a_I = DS_r$, $b_I = SW_l$, *and* $a_{II} = DS_l$, $b_{II} = SW_r$, *respectively. The same holds for the corresponding* adjoint *sequences*[12]

$$\begin{aligned} I^{adj}: &\quad a_I^{adj}, \quad b_I^{adj}, \quad c_I^{adj}, \quad d_I^{adj} \\ II^{adj}: &\quad a_{II}^{adj}, \quad b_{II}^{adj}, \quad c_{II}^{adj}, \quad d_{II}^{adj} \end{aligned}$$

that involve the quantities: $a_I^{adj} = DS_r^{adj}$, $b_I^{adj} = SW_l^{adj}$, $a_{II}^{adj} = DS_l^{adj}$, $b_{II}^{adj} = SW_r^{adj}$, $c_I^{adj} = ST_r^{adj}$, $c_{II}^{adj} = ST_l^{adj}$, $d_I^{adj} = GC_r^{adj} + \Delta SW^{adj}$, $d_{II}^{adj} = GC_l^{adj} - \Delta SW^{adj}$.

Sequences (5) thus constitute multiple—namely, two—copies of (4), with the same happening for the *adjoint* sequences. The golden ratio ϕ here thus possibly occurs as a natural, feasible fixed point for the consecutive ratios b_I/a_I, c_I/b_I, d_I/c_I and b_{II}/a_{II}, c_{II}/b_{II}, d_{II}/c_{II}, with the same again happening for the *adjoint* sequences.

It is straightforward to note that the mean [element by element] of the two sequences I and II in (5) is again a (generalized) 4-length Fibonacci sequence of the form (4). Its elements are constituted by the mean double support, mean swing, mean stance, mean gait cycle, respectively [X-mean $\bar{X}$ denotes the quantity: $(X_l + X_r)/2$]. The resulting mean sequence again exhibits ϕ as a fixed point for consecutive ratios (apply Proposition 2), so that the same structure of (4) is actually preserved in the non-{symmetric and recursive} case, at the price, however, of just considering the corresponding mean values. All the same happens for the *adjoint* sequences.

A dynamics-on-graph interpretation is provided hereafter. It will lead to a classification of gaits in terms of self-similarity at different magnitudes. The related Shannon-index-based interpretation (Friedkin et al., 2016; Parsegov et al., 2017) can be found in **Appendix A**.

Let us distinguish again between the symmetric and recursive case and the non-{symmetric and recursive} one.

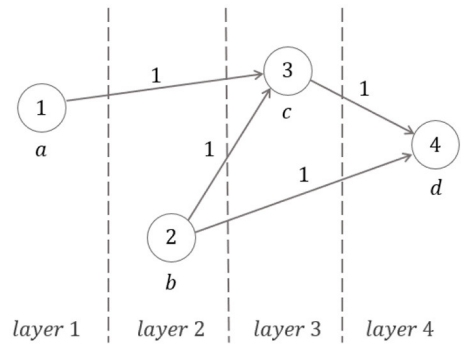

FIGURE 3 | Symmetric and recursive walking: dynamics-on-graph interpretation.

Symmetric and recursive case. Consider sequence (4). Let x_j denote the node (or vertex) j (belonging to layer j) represented in **Figure 3** ($j = 1, 2, 3, 4$), with $x_1 = a, x_2 = b, x_3 = c, x_4 = d$.

Write

$$x_j = \sum_{i=1}^{4} a_{ij} x_i + x_j(0),$$

where: $x_j(0)$ is different from zero only when the input degree of the vertex j is equal to zero; a_{ij} is the $(i, j)-$element of the adjacency-like matrix:

$$A_d = \begin{bmatrix} 0 & 0 & 1 & 0 \\ 0 & 0 & 1 & 1 \\ 0 & 0 & 0 & 1 \\ 0 & 0 & 0 & 0 \end{bmatrix}, \tag{6}$$

showing that the input-degree is either zero or two for any vertex. When the fixed point ϕ occurs for the ratios $b/a, c/b, d/c$, the graph of **Figure 3** becomes the strongly connected graph, with all input-degrees being equal to 1 (see **Figure 4**) and with the corresponding ϕ-dependent adjacency-like matrix reading:

$$A_{d\phi} = \begin{bmatrix} 0 & \phi & 0 & 0 \\ 0 & 0 & \phi & 0 \\ 0 & 0 & 0 & \phi \\ \phi^{-3} & 0 & 0 & 0 \end{bmatrix}.$$

While in the first general case two generating values *determine* the components of the whole graph (in the aforementioned sense), in the second self-similar case just one generating value does it. This is actually the ideal physiological gait of a healthy subject symmetrically and recursively walking at comfortable speed, as described in Iosa et al. (2013).

Non-{symmetric and recursive} case. Consider sequences (5) and their *adjoint* versions (in their redundant number of four, though the equalities $DS_r^{adj} = DS_r$, $SW_l^{adj} = SW_l$, $ST_r^{adj} = ST_r$ make the two sequences I and I^{adj} coincident in Proposition 3, according to footnote 12). Let $x_j = [v_j, v_{j+4}]^T$ (resp., $x_j^{adj} = [v_j^{adj}, v_{j+4}^{adj}]^T$) denote the vector with its components, in order,

at supine position), both of them with ϕ as fixed point for the three consecutive ratios d/c, c/b, b/a (Ozturk et al., 2016), where IV_r is the duration of the iso-volumic relaxation phase, D is the diastole duration, S is the systole duration, I_f is the inflow duration, R-R is the interval between two consecutive heart beats. Even notice correspondences with the latest analysis of the ratios of phase durations in the front crawl swimming stroke in Verrelli et al. (2021).

[12]Notice that the two sequences I and I^{adj} coincide, owing to the equalities: $DS_r^{adj} = DS_r$, $SW_l^{adj} = SW_l$, $ST_r^{adj} = ST_r$.

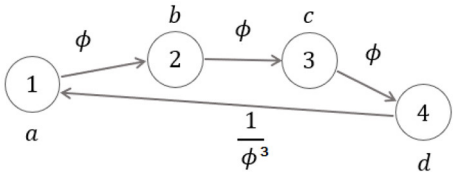

FIGURE 4 | Symmetric and recursive walking with fixed point occurring in the sequence: dynamics-on-graph interpretation.

being constituted by the vertices v_j, v_{j+4} (resp., v_j^{adj}, v_{j+4}^{adj}) belonging to layer j in **Figure 5** ($j = 1, 2, 3, 4$). Write for layers 3 and 4:

$$x_{j+2} = x_{j+1} + \begin{bmatrix} 2-j & j-1 \\ j-1 & 2-j \end{bmatrix} x_j, \quad j = 1, 2$$
$$x_{j+2}^{\text{adj}} = x_{j+1}^{\text{adj}} + \begin{bmatrix} 2-j & j-1 \\ j-1 & 2-j \end{bmatrix} x_j^{\text{adj}}, \quad j = 1, 2.$$

The adjacency-like matrix [characterizing the representation $v_j = \sum_{i=1}^{8} a_{ij} v_i + v_j(0)$ (resp., $v_j^{\text{adj}} = \sum_{i=1}^{8} a_{ij} v_i^{\text{adj}} + v_j^{\text{adj}}(0)$), with $v_j(0)$ (resp. $v_j^{\text{adj}}(0)$) being different from zero only when the input degree of the node j is equal to zero] for the graph represented in **Figure 5**, namely:

$$A_{a,d} = \begin{bmatrix} 0&0&1&0&0&0&0&0 \\ 0&0&1&0&0&0&0&1 \\ 0&0&0&1&0&0&0&0 \\ 0&0&0&0&0&0&0&0 \\ 0&0&0&0&0&0&1&0 \\ 0&0&0&1&0&0&1&0 \\ 0&0&0&0&0&0&0&1 \\ 0&0&0&0&0&0&0&0 \end{bmatrix},$$

can be immediately obtained, again showing that the input-degree is either zero or two for any vertex.

We are now thus able to identify four relevant cases besides the general case in which 6 generating values *determine* the x_j-components (resp., x_j^{adj}-components) for the whole graph. They are in order (take also into account the interpretation in terms of Shannon entropy of **Appendix A**):

- 1-*chain adjoint self-similarity* (or *adjoint minimum-entropy in one chain*): just one ratio among v_2/v_1, v_6/v_5, ${v_6}^{\text{adj}}/v_5^{\text{adj}}$ equals ϕ, with, consequently, just 5 values to *determine* the x_j-components for the whole graph.
- 2-*chains adjoint self-similarity* (or *adjoint minimum-entropy in two chains*): two ratios among v_2/v_1, v_6/v_5, ${v_6}^{\text{adj}}/v_5^{\text{adj}}$ equal ϕ, with, consequently, just 4 values to *determine* the x_j-components for the whole graph.
- *Weak adjoint self-similarity* (or *adjoint asymmetric minimum-entropy*): all the three ratios v_2/v_1, v_6/v_5, and ${v_6}^{\text{adj}}/v_5^{\text{adj}}$ equal ϕ but at least one inequality among $v_2 \neq v_6$, $v_6 \neq v_6^{\text{adj}}$, $v_2 \neq v_6^{\text{adj}}$ holds, with, consequently, just 3 or 2 values to *determine* the x_j-components for the whole graph.
- *Adjoint symmetric self-similarity* (or *adjoint symmetric minimum-entropy*): all the three ratios v_2/v_1, v_6/v_5, ${v_6}^{\text{adj}}/v_5^{\text{adj}}$ equal ϕ under the multiple equality $v_2 = v_6 = v_6^{\text{adj}}$, with, consequently, just 1 value to *determine* the x_j-components for the whole graph.
- *Enforced adjoint symmetric self-similarity* (or *enforced adjoint symmetric minimum-entropy*): adjoint symmetric self-similarity in which the double support sub-phases are equally partitioned (*consistency*), that is $\text{DS}_x = \text{DS}_y$ (and $\text{DS}_w = \text{Dx}_y$, $\text{DS}_y = \text{DS}_z$).

In the last case, ϕ occurs as a fixed point for the consecutive ratios of the sequences in (4) in a symmetric and recursive setting, so that the graphs of **Figure 5** become the (non-minimal-dimension) strongly connected graphs in **Figure 6** (in which each graph reproduces the same **Figure 4** on its top) with all in degrees being equal to 1 and with the corresponding ϕ-dependent adjacency-like matrix reading:

$$A_{a,d\phi} = \begin{bmatrix} 0&\phi&0&0&0&0&0&0 \\ 0&0&\phi&0&0&0&0&0 \\ 0&0&0&\phi&0&0&0&0 \\ 0&0&0&0&0&0&0&1 \\ 1&0&0&0&0&0&0&0 \\ 0&0&0&0&1/\phi&0&0&0 \\ 0&0&0&0&0&1/\phi&0&0 \\ 0&0&0&0&0&0&1/\phi&0 \end{bmatrix}.$$

2.3. A New Experimental Conjecture

The new experimental conjecture of this subsection extends the ideas underlying a fractal approach to the double support sub-phases within the gait[13]. It is inspired from experimental results reported in Novacheck (1998) showing that physiological symmetric walking is not only characterized by a stance duration being close to 62% of gait cycle duration, a swing duration being close to 38% of gait cycle duration, a double support duration being consequently close to 24% of gait cycle duration, but also by an instant of minimum angular position (with negative sign) of the foot relative to the tibia (with a 90 degrees-angle between foot and tibia being plotted at 0°) occurring at about 7% of gait cycle duration in each double support sub-phase (with 5% as percentage for the complementary interval duration). It may thus be interestingly recognized that the structure of a Fibonacci sequence (with fixed point ϕ) appears in the sequence: $5 \times 2 = 10$ ($1/\phi^5 \approx 9.018$); $7 \times 2 = 14$ ($1/\phi^4 \approx 14.591$); 24 ($1/\phi^3 \approx 23.608$); 38 ($1/\phi^2 \approx 38.198$); 62($1/\phi \approx 61.804$); 100.

For the sake of clarity, denote by $\{\text{RHS}^{[1]}, \text{LTO}^{[1]}, \text{LHS}^{[1]}, \text{RTO}^{[1]}, \text{RHS}^{[2]}, \text{LTO}^{[2]}\}$ the sequence of time instants corresponding to the right-heel-strike ($\text{FS}_{r,a}$, $\text{FS}_{r,b}$), left-toe-off ($\text{FO}_{l,a}$, $\text{FO}_{l,b}$), left-heel-strike ($\text{FS}_{l,y}$), right-toe-off ($\text{FO}_{r,y}$) for two subsequent gaits $i = 1, 2$ of **Figure 2**. The

[13]The *adjoint gait* is not considered in this subsection, since recursivity has been already addressed in the preceding subsection.

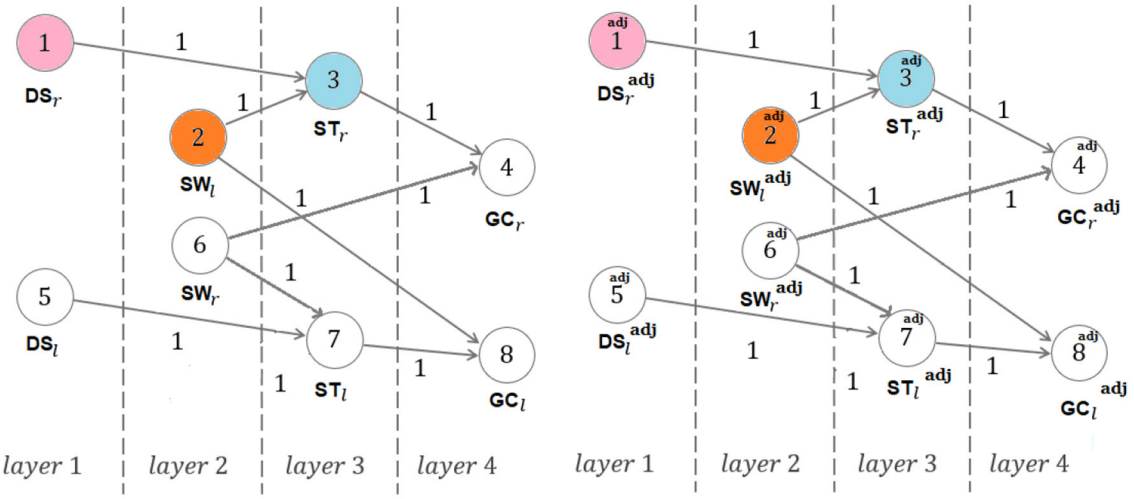

FIGURE 5 | Generic walking: dynamics-on-graph interpretation (same colors denote equal quantities) [$DS_r^{adj} = DS_r$, $SW_l^{adj} = SW_l$, $ST_r^{adj} = ST_r$].

following equalities:

$$\begin{aligned} DS_r &= LTO^{[1]} - RHS^{[1]} + RTO^{[1]} - LHS^{[1]} \\ DS_l &= RTO^{[1]} - LHS^{[1]} + LTO^{[2]} - RHS^{[2]} \\ SW_r &= RHS^{[2]} - RTO^{[1]} \\ SW_l &= LHS^{[1]} - LTO^{[1]} \end{aligned}$$

hold, with ST_r, ST_l, GC_r, GC_l satisfying (3). We are able to present the following conjecture.

Conjecture $\mathcal{C}$**:** *Consider the positive real numbers* z_1, z_2, z_3 *denoting the time distances from* $RHS^{[1]}$, $LHS^{[1]}$, $RHS^{[2]}$ *of the three time instants—belonging to the open sets* $(RHS^{[1]}, LTO^{[1]})$, $(LHS^{[1]}, RTO^{[1]})$, $(RHS^{[2]}, LTO^{[2]})$*—representing the three instants of minimum angular positions (with negative signs) of the (left and right) feet relative to the tibias (with a 90 degrees-angle between foot and tibia being plotted at 0-degrees). The numbers* z_1, z_2, z_3 *are conjectured to characterize the expansion to the left of the (generalized) 4-length Fibonacci sequences (5) into the 6-length (functional) ones* [namely, $b_I = a_I + (z_1 + z_2) + \Delta_I$, $b_{II} = a_{II} + (z_2 + z_3) + \Delta_{II}$ hold]:

$$\begin{aligned} \text{I}: \;& a_I - (z_1 + z_2 + \Delta_I(a_I, b_I, a_{II}, b_{II})),\ z_1 + z_2 \\ & + \Delta_I(a_I, b_I, a_{II}, b_{II}),\ a_I,\ b_I,\ c_I,\ d_I \\ \text{II}: \;& a_{II} - (z_2 + z_3 + \Delta_{II}(a_I, b_I, a_{II}, b_{II})),\ z_2 + z_3 \\ & + \Delta_{II}(a_I, b_I, a_{II}, b_{II}),\ a_{II},\ b_{II},\ c_{II},\ d_{II}, \end{aligned} \tag{7}$$

with the reals $\Delta_I(\cdot)$ *and* $\Delta_{II}(\cdot)$ *being zero (z-*specific expansion*) when symmetric and self-similar gait occurs (i.e., for* $a_I = a_{II}$ *&* $b_I = \phi a_I = b_{II} = \phi a_{II}$*).*

The contribution of Δ_I and Δ_{II} may be related to energy expenditure, with their zero-nature (*z-specific expansion*) in symmetric and self-similar walking being reminiscent of the physical fact that, at the speed at which symmetric and self-similar walking occurs, locomotor system saves energy and its activity is only required to oppose gravity, to maintain postural configurations and to reintegrate energy loss during each cycle (Mochon and McMahon, 1980; Iosa et al., 2016a). When the conjecture above is verified in symmetric and self-similar

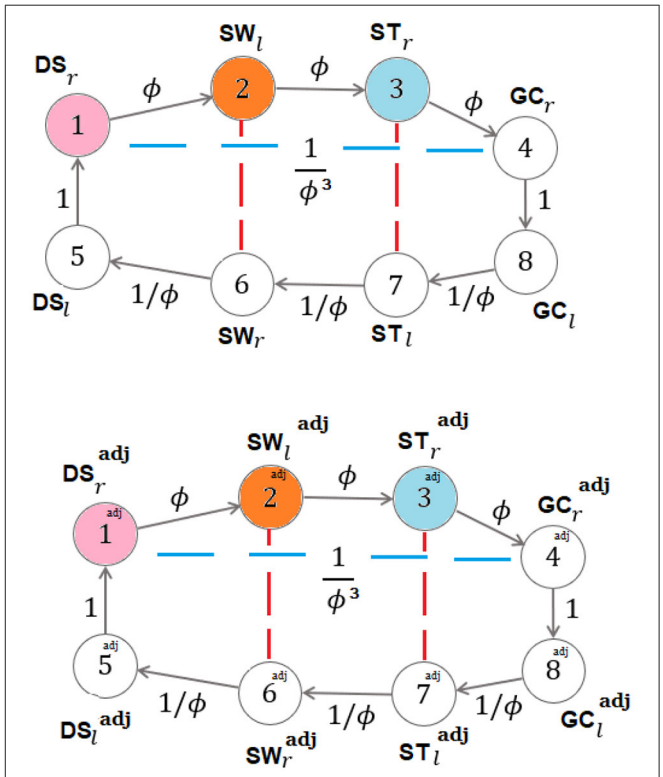

FIGURE 6 | Symmetric and recursive self-similarity for walking with fixed points occurring in all the sequences: dynamics-on-graph interpretation (same colors denote equal quantities) [$DS_r^{adj} = DS_r$, $SW_l^{adj} = SW_l$, $ST_r^{adj} = ST_r$].

walking, the (generalized) 4-length Fibonacci sequences in (5) collapse into one sequence that is being expanded to the left[14], through z_1, z_2, z_3 only, into the 6-length one:

$$a-(z_1+z_2),\ z_1+z_2,\ a,\ b,\ c,\ d, \tag{8}$$

with each element of the above sequence possessing a clear physical meaning and with ϕ occurring as a fixed point for all the consecutive five ratios: $(z_1+z_2)/(a-(z_1+z_2))$, $a/(z_1+z_2)$, b/a, c/b, d/c.

2.4. A New Index: The Φ-bonacci Gait Number

Let λ, δ, μ^{adj}, λ^{adj}, ν^{conj} be positive weights. Given positive reals ξ_n, ξ_d, ξ_v (where n generically stands for numerator, d stands for denominator, v stands for value), define the normalized quantity[15]:

$$\left(\frac{\xi_n}{\xi_d}-\xi_v\right)_{\text{n}}^2=\left(\frac{\xi_n}{\xi_d}\right)^{-1}\left(\frac{\xi_n}{\xi_d}-\xi_v\right)^2. \tag{9}$$

In accordance with the previously presented classification of gaits, the following index, named Φ-*bonacci gait number*:

$$\begin{aligned}\mathcal{Y}_\Phi=&\sqrt{\left(\frac{v_2}{v_1}-\phi\right)_{\text{n}}^2+\left(\frac{v_6}{v_5}-\phi\right)_{\text{n}}^2+\mu^{\text{adj}}\left(\frac{v_6^{\text{adj}}}{v_5^{\text{adj}}}-\phi\right)_{\text{n}}^2}\\&+\lambda\sqrt{\left(\frac{v_6}{v_2}-1\right)_{\text{n}}^2+\lambda^{\text{adj}}\left(\frac{v_6^{\text{adj}}}{v_6}-1\right)_{\text{n}}^2}\\&+\nu^{\text{conj}}\sqrt{\left(\frac{a_I}{z_1+z_2}-\phi\right)_{\text{n}}^2+\left(\frac{a_{II}}{z_2+z_3}-\phi\right)_{\text{n}}^2}\\&+\delta\sqrt{\left(\frac{\text{DS}_x}{\text{DS}_y}-1\right)_{\text{n}}^2}\end{aligned} \tag{10}$$

is introduced in order to characterize the special case of *enforced adjoint symmetric self-similarity* in walking (recall conjecture $\mathcal{C}$). The expression of such an index in (10), once it is explicitly rewritten as

$$\begin{aligned}\mathcal{Y}_\Phi=&\sqrt{\left(\frac{\text{SW}_l}{\text{DS}_r}-\phi\right)_{\text{n}}^2+\left(\frac{\text{SW}_r}{\text{DS}_l}-\phi\right)_{\text{n}}^2+\mu^{\text{adj}}\left(\frac{\text{SW}_r^{\text{adj}}}{\text{DS}_l^{\text{adj}}}-\phi\right)_{\text{n}}^2}\\&+\lambda\sqrt{\left(\frac{\text{SW}_r}{\text{SW}_l}-1\right)_{\text{n}}^2+\lambda^{\text{adj}}\left(\frac{\text{SW}_r^{\text{adj}}}{\text{SW}_r}-1\right)_{\text{n}}^2}\\&+\nu^{\text{conj}}\sqrt{\left(\frac{\text{DS}_r}{z_1+z_2}-\phi\right)_{\text{n}}^2+\left(\frac{\text{DS}_l}{z_2+z_3}-\phi\right)_{\text{n}}^2}\\&+\delta\sqrt{\left(\frac{\text{DS}_x}{\text{DS}_y}-1\right)_{\text{n}}^2},\end{aligned}$$

shows that, differently from the area of the *Synchronicity Rectangle* in Marino et al. (2020), (10) takes its minimum zero-value just when *enforced adjoint symmetric self-similarity* under $\mathcal{C}$ occurs. It turns out to constitute the most natural generalization, to the non-{symmetric and recursive} walking case, of the corresponding gait ratio $|\text{SW}/\text{DS}-\phi|$ defined in Iosa et al. (2013) and Iosa et al. (2016b) for symmetric walking, while it simply incorporates a weighted modification of the index $=|\Delta\text{SW}|/\overline{\text{SW}}$ in Błażkiewicz et al. (2014), evaluated at both the gait and the adjoint gait. A conceptual extension of the use of the Φ-*bonacci gait number* to assess the *gait index variability* along past walking gaits can be naturally introduced, which is briefly reported in **Appendix B**. A simplified version of the above Φ-*bonacci gait number*, named *s*-Φ-*bonacci gait number* (*s* stands for simplified) can be also derived from the previous expression by setting $\mu^{\text{adj}}=\lambda^{\text{adj}}=\nu^{\text{conj}}=0$. This leads to

$$\begin{aligned}\mathcal{Y}_{\Phi[s]}=&\sqrt{\left(\frac{\text{SW}_l}{\text{DS}_r}-\phi\right)_{\text{n}}^2+\left(\frac{\text{SW}_r}{\text{DS}_l}-\phi\right)_{\text{n}}^2}\\&+\lambda\sqrt{\left(\frac{\text{SW}_r}{\text{SW}_l}-1\right)_{\text{n}}^2}+\delta\sqrt{\left(\frac{\text{DS}_x}{\text{DS}_y}-1\right)_{\text{n}}^2}\end{aligned} \tag{11}$$

that is the weighted sum[16] of three terms: (i) the first one to account for the self-similarity contribution to the gait generation; (ii) the second one to account for the swing symmetry contribution to the gait generation; (iii) the third one to account for the *double support consistency*, that is the symmetry, within the gait, between the double support sub-phase with the left foot behind and the right foot ahead and the double support sub-phase with the right foot behind and left foot ahead. A zero value for the *s*-Φ-*bonacci gait number* (11) thus describes the case in which self-similarity, swing symmetry, *double support consistency* occur. Such a simplified index turns out to be useful when data concerning the adjoint gaits and the position of the foot relative to the tibia are not available, as in the case of gait analysis reports (like the ones used in section 3.2), just providing mean values of left and right percentages of stance, swing and double support.

[14]Note that extending such an argument up to the case of infinite-length Fibonacci sequences would lead to asymptotic self-similarity generation. In fact, the limit behavior:

$$\lim_{k\to+\infty}\frac{y_i(k+1)}{y_i(k)}=\lim_{k\to+\infty}\frac{\phi^{k+1}\beta_i-(1-\phi)^k\alpha_i}{\phi^k\beta_i+(1-\phi)^k\phi\alpha_i}=\phi$$

holds.

[15]Different normalizations can be apparently used.

[16]The gains within can be freely chosen by the user, in accordance with the specific analysis requirements.

2.5. Experiments

2.5.1. Experimental Set 1

Experimental results (referred to as results for the *Experimental set 1*) are reported in section 3.1 to test the validity of the conjecture $\mathcal{C}$. *Experimental set 1* is here conceived as a proof of concept. A single healthy subject was tested in two different days—in order to assess phase duration reliability through acquisition *via* different sensor systems (insole, Movit, as described underneath)—and at different speeds—in order to take into account how speed changes are crucial to the presented analysis—. Testing just one healthy subject was considered sufficient at this stage[17]. The main part of the first measurement system is an insole composed of two parts to adapt to different feet and shoes. Four PTF (Polymer Thick Film) force sensors FSR402 (Interlink Electronics Inc, Los Angeles, USA) were placed on the four points characterized by the greatest pressure of the foot (first and second metatarsal head, medial and central heel). The related positions were chosen through the analysis of real walking measurements, acquired by a baropodometric platform and with Pedar® insole (Novel gmch, Germany). They are able to detect the time instants for the first and the last contacts. Secondly, we performed the motion capture and the motion analysis through the Movit System G1 (Captiks, Rome, Italy), which provides accelerometer, gyroscope, magnetometer, quaternion, barometer synced data and is composed of 10-DOF wireless wearable small inertial devices and an USB wireless receiver (Costantini et al., 2018; Ricci et al., 2019a,b; Saggio, 2020).

2.5.2. Experimental Set 2

Experimental results (referred to as results for the *Experimental set 2*) are reported in section 3.2 to illustrate the effectiveness of the *s-Φ-bonacci gait number* (11) in explicitly identifying pathological gaits. A secondary analysis was conducted on data collected and published in previous studies (Iosa et al., 2013, 2016a,b). Three groups were selected: (i) group of healthy control subjects (HCS); (ii) group of patients who are characterized by highly asymmetric deficits [such as patients with hemiparetic stroke, (HSP)]; (iii) group of patients who are characterized by an alteration in gait ratio not always being accompanied by motor asymmetries [such as patients with quite symmetric symptoms due to Parkinson's Disease, (PDP)]. The data were extracted from the database according to the following procedure, which was established to accomplish the purposes of the study: (i) extraction of data of subjects in the three groups who are matched per age and per walking speed (this last condition implied the extraction of healthy subjects walking slowly and patients with deficits slightly affecting gait speed); (ii) extraction of data of patients with stroke who are characterized by an evident gait asymmetry and patients with PD who are characterized by deficits slightly impairing their gait asymmetry. These strict criteria allowed us to extract data concerning just 5 subjects within each group.

[17] As we shall see, a larger number of subjects will be enrolled for the *Experimental set 2*.

3. RESULTS

3.1. Experimental Set 1

Two sets of experiments (3 experiments per set) have been carried out in two different days. The same subject (female, 160 cm, 25 years old, 54 kg) has been involved; 10 meters walking tests in a hallway have been performed at three different speeds for each set of experiments. The temporal analysis concerns two adjacent left and right gaits at steady-state. The sequence of time instants $\{RHS^{[1]}, LTO^{[1]}, LHS^{[1]}, RTO^{[1]}, RHS^{[2]}, LTO^{[2]}\}$ corresponding to the right-heel-strike, left-toe-off, left-heel-strike, right-toe-off for the two considered subsequent gaits $i = 1,2$ has been derived from the measurements acquisitions provided by the two (aforementioned) sensor systems. The Movit system has been able even to provide the three time instants z_1, z_2, z_3. All of the results for the *Experimental set 1* are summarized in **Tables 1**–**4**. Each of **Tables 1**–**3**, concerning experiments at different speeds, report in order (in seconds): (i) the elements of sequence I in (7); (ii) the elements of sequence II in (7); (iii) the consecutive ratios between the elements of sequence I in (7); (iv) the consecutive ratios between the elements of sequence II in (7).

Showing data consistency from different sensor systems. The Bland-Altman analysis, which corresponds to the 24 couples of independently measured values a_i, b_i (i = I,II) in **Tables 1**–**3** coming from Movit and insole, respectively, shows: bias = 0.005046; standard deviation of bias = 0.01083; 95% limits of agreement = {−0.01619, 0.02628}, whereas the related two sequences (Movit and insole, respectively) exhibit: mean = {0.3181, 0.3131}; standard deviation = {0.10996, 0.10674}; lower 95% CI of mean = {0.2717, 0.2680}; upper 95% CI of mean = {0.3646, 0.3582}.

Showing data consistency from repeated experiments. The Bland-Altman analysis, which corresponds to the 12 couples of measured values $(z_1 + z_2)$, $(z_2 + z_3)$, a_i, b_i (i = I,II) in **Tables 1**, **2** for the first and the second experiment (mean = 0.2460, 0.2463), respectively, shows: bias = −0.002325; standard deviation of bias = 0.02134; 95% limits of agreement = {−0.04415, 0.0395}.

Showing occurrence of Fibonacci sequences. The sequences in (5): a_i, b_i, c_i, d_i (i = I,II) of Proposition 3 are confirmed to exactly constitute generalized 4-length Fibonacci sequences for each set of the specific sensor system acquisitions (see again **Tables 1**–**3**), with all the ratios between consecutive elements of such sequences being pretty close to the golden ratio ϕ (especially look at the last ratio) just when the walking speed is 0.97 m/s (approximately constituting the comfortable walking speed for the 160 cm/54 kg- subject under investigation) and relatively different from ϕ as the walking speed differs from 0.97 m/s (see the bottom-halves of **Tables 1**–**3**).

Showing consistency of Conjecture $\mathcal{C}$. The smaller the difference between the walking speed and 0.97 m/s is, the more the sequences (7) are close to constitute the (generalized) 6-length Fibonacci sequence (8), with all the ratios between consecutive elements of such sequences being close to the golden ratio ϕ. This can be seen by considering the following consistency indices reported in **Table 4**: mean values $\Delta(v)$ of all $|\Delta_I|$ and $|\Delta_{II}|$ [from the two experiments when available] at different speeds v (**Tables 1**–**3**); maximum modulus of the mean distance

TABLE 1 | Experimental data (*Experimental set 1*) concerning the elements of the sequences I and II in (7) for a walking speed equal to 0.97 m/s: first experiment (second experiment).

	$a_{\mathrm{I}} - (z_1 + z_2)$	$z_1 + z_2$	$a_{\mathrm{I}} = \mathrm{DS}_r$	$b_{\mathrm{I}} = \mathrm{SW}_l$	$c_{\mathrm{I}} = \mathrm{ST}_r$	$d_{\mathrm{I}} = \mathrm{GC}_r + \Delta\mathrm{SW}$
Movit	0.1018 (0.101)	0.168 (0.169)	0.2698 (0.27)	0.4422 (0.442)	0.712 (0.712)	1.1542 (1.154)
insole			0.269 (0.271)	0.423 (0.44)	0.692 (0.711)	1.115 (1.151)
	$a_{\mathrm{II}} - (z_2 + z_3)$	$z_2 + z_3$	$a_{\mathrm{II}} = \mathrm{DS}_l$	$b_{\mathrm{II}} = \mathrm{SW}_r$	$c_{\mathrm{II}} = \mathrm{ST}_l$	$d_{\mathrm{II}} = \mathrm{GC}_l - \Delta\mathrm{SW}$
Movit	0.101 (0.104)	0.169 (0.165)	0.27 (0.269)	0.48 (0.423)	0.75 (0.692)	1.2108 (1.116)
insole			0.265 (0.274)	0.445 (0.426)	0.71 (0.7)	1.152 (1.139)
		$\frac{z_1+z_2}{\mathrm{DS}_r-(z_1+z_2)}$	$\mathrm{DS}_r/(z_1 + z_2)$	$\mathrm{SW}_l/\mathrm{DS}_r$	$\mathrm{ST}_r/\mathrm{SW}_l$	$(\mathrm{GC}_r + \Delta\mathrm{SW})/\mathrm{ST}_r$
Movit		1.6502 (1.6732)	1.6059 (1.5976)	1.6389 (1.637)	1.6101 (1.6108)	1.6210 (1.6207)
insole				1.5724 (1.6236)	1.6359 (1.6159)	1.6112 (1.6188)
		$\frac{z_2+z_3}{\mathrm{DS}_l-(z_2+z_3)}$	$\mathrm{DS}_l/(z_2 + z_3)$	$\mathrm{SW}_r/\mathrm{DS}_l$	$\mathrm{ST}_l/\mathrm{SW}_r$	$(\mathrm{GC}_r - \Delta\mathrm{SW})/\mathrm{ST}_l$
Movit		1.6732 (1.5865)	1.5976 (1.6303)	1.777 (1.5724)	1.5625 (1.6359)	1.6144 (1.6127)
insole				1.6792 (1.5547)	1.5955 (1.6431)	1.6225 (1.6271)

TABLE 2 | Experimental data (*Experimental set 1*) concerning the elements of the sequences I and II in (7) for a walking speed equal to 1.51 m/s: first experiment (second experiment).

	$a_{\mathrm{I}} - (z_1 + z_2)$	$z_1 + z_2$	$a_{\mathrm{I}} = \mathrm{DS}_r$	$b_{\mathrm{I}} = \mathrm{SW}_l$	$c_{\mathrm{I}} = \mathrm{ST}_r$	$d_{\mathrm{I}} = \mathrm{GC}_r + \Delta\mathrm{SW}$
Movit	0.0487 (0.055)	0.0866 (0.099)	0.1353 (0.154)	0.3457 (0.346)	0.481 (0.5)	0.8267 (0.846)
insole			0.147 (0.145)	0.337 (0.349)	0.484 (0.494)	0.821 (0.843)
	$a_{\mathrm{II}} - (z_2 + z_3)$	$z_2 + z_3$	$a_{\mathrm{II}} = \mathrm{DS}_l$	$b_{\mathrm{II}} = \mathrm{SW}_r$	$c_{\mathrm{II}} = \mathrm{ST}_l$	$d_{\mathrm{II}} = \mathrm{GC}_l - \Delta\mathrm{SW}$
Movit	0.059 (0.07)	0.0855 (0.104)	0.1445 (0.174)	0.3555 (0.365)	0.5 (0.539)	0.8368 (0.885)
insole			0.149 (0.181)	0.36 (0.36)	0.519 (0.541)	0.873 (0.872)
		$\frac{z_1+z_2}{\mathrm{DS}_r-(z_1+z_2)}$	$\mathrm{DS}_r/(z_1 + z_2)$	$\mathrm{SW}_l/\mathrm{DS}_r$	$\mathrm{ST}_r/\mathrm{SW}_l$	$(\mathrm{GC}_r + \Delta\mathrm{SW})/\mathrm{ST}_r$
Movit		1.7782 (1.8)	1.5623 (1.5555)	2.555 (2.2467)	1.3913 (1.445)	1.7187 (1.692)
insole				2.2925 (2.4068)	1.4362 (1.4154)	1.6962 (1.7064)
		$\frac{z_2+z_3}{\mathrm{DS}_l-(z_2+z_3)}$	$\mathrm{DS}_l/(z_2 + z_3)$	$\mathrm{SW}_r/\mathrm{DS}_l$	$\mathrm{ST}_l/\mathrm{SW}_r$	$(\mathrm{GC}_r - \Delta\mathrm{SW})/\mathrm{ST}_l$
Movit		1.4491 (1.4857)	1.69 (1.673)	2.4602 (2.0977)	1.4064 (1.4767)	1.6736 (1.6419)
insole				2.4161 (1.9889)	1.4416 (1.5027)	1.6820 (1.6118)

$M_\phi(v)$ from ϕ [mean from first and second experiment] of all the ratios [Movit] between consecutive elements in sequences (5) at different speeds v (**Tables 1–3**); maximum modulus of the mean distance $M_{\phi,e}(v)$ from ϕ [mean from first and second experiment] of all the ratios [Movit] between consecutive elements in sequences (7) at different speeds v (**Tables 1–3**).

3.2. Experimental Set 2

Even though severe gait deficits may lead to significant differences in most of the spatio-temporal gait parameters (w.r.t. HCS), 15 subjects (5 HCS, 5 HSP, 5 PDP) were selected, who are not only age-matched but also walking-speed-matched. Starting from the values of the gait phases, the (left, right) Gait Ratio GR was computed as the percentage ratio between the (left, right) gait cycle duration and (left, right) stance duration, while the Mean Gait Ratio MGR was given by the average between the left and right GRs. Then, the Symmetry Index SI was computed as the highest GR divided by the smallest GR (among the two feet). The *s-*Φ*-bonacci gait number* $\mathcal{Y}_{\Phi[s]}$ (11) was finally computed ($\lambda = \delta = 1$) and used for comparison. All of the results for the *Experimental set 2* are summarized in **Table 5**. In particular, **Table 5** shows that, despite the similar speeds, the MGR resulted significantly different among the three groups: differences were observed in PDP ($p = 0.008$ vs. HCS, *post-hoc* analysis), whereas no relevant differences were observed in HSP ($p = 0.754$ vs. HCS). However, as expected, the symmetry between the gait ratio evaluated between the left and the right feet resulted lost in HSP ($p = 0.009$ vs. HCS), more than in PDP ($p = 0.222$ vs. HCS). These results confirm that our extraction was effective in finding two groups of slightly severely affected patients, one most in gait harmony (PDP, as also reported in Iosa et al., 2016b), and the other one in gait symmetry (HSP, as also reported in Iosa et al., 2016a).

4. DISCUSSION

Previous results showed that the MGR is close to golden ratio for healthy subjects (Iosa et al., 2013), and far from it for PDP (Iosa et al., 2016b). For patients with stroke, it has been shown that the MGR is strictly related to speed (Iosa et al., 2016a), and hence the MGR of a group walking at a speed that is not significantly lower than the healthy subjects' one, was not expected to be significantly different from the MGR of a healthy subject, as our data here explicitly illustrate. On the other hand, patients with stroke, owing to their hemiparesis, exhibited a more

TABLE 3 | Experimental data (*Experimental set 1*) concerning the elements of the sequences I and II in (7) for a walking speed equal to 0.85 m/s (walking speed equal to 1.1 m/s).

	$a_{\mathrm{I}} - (z_1 + z_2)$	$z_1 + z_2$	$a_{\mathrm{I}} = \mathrm{DS}_r$	$b_{\mathrm{I}} = \mathrm{SW}_l$	$c_{\mathrm{I}} = \mathrm{ST}_r$	$d_{\mathrm{I}} = \mathrm{GC}_r + \Delta\mathrm{SW}$
Movit	0.104 (0.0932)	0.145 (0.156)	0.249 (0.2492)	0.462 (0.4428)	0.7115 (0.692)	1.173 (1.1348)
Insole			0.243 (0.23)	0.467 (0.43)	0.71 (0.66)	1.177 (1.09)
	$a_{\mathrm{II}} - (z_2 + z_3)$	$z_2 + z_3$	$a_{\mathrm{II}} = \mathrm{DS}_l$	$b_{\mathrm{II}} = \mathrm{SW}_r$	$c_{\mathrm{II}} = \mathrm{ST}_l$	$d_{\mathrm{II}} = \mathrm{GC}_l - \Delta\mathrm{SW}$
Movit	0.09 (0.0939)	0.141 (0.1562)	0.231 (0.2501)	0.442 (0.423)	0.673 (0.6731)	1.114 (1.0954)
Insole			0.223 (0.23)	0.44 (0.41)	0.663 (0.64)	1.06 (1.05)
	$\frac{z_1+z_2}{\mathrm{DS}_r-(z_1+z_2)}$		$\mathrm{DS}_r/(z_1 + z_2)$	$\mathrm{SW}_l/\mathrm{DS}_r$	$\mathrm{ST}_r/\mathrm{SW}_l$	$(\mathrm{GC}_r + \Delta\mathrm{SW})/\mathrm{ST}_r$
Movit		1.3942 (1.6738)	1.7172 (1.5974)	1.8554 (1.7768)	1.54 (1.5627)	1.6486 (1.6398)
Insole				1.9218 (1.8695)	1.5203 (1.5348)	1.6577 (1.6515)
	$\frac{z_2+z_3}{\mathrm{DS}_l-(z_2+z_3)}$		$\mathrm{DS}_l/(z_2 + z_3)$	$\mathrm{SW}_r/\mathrm{DS}_l$	$\mathrm{ST}_l/\mathrm{SW}_r$	$(\mathrm{GC}_r - \Delta\mathrm{SW})/\mathrm{ST}_l$
Movit		1.5666 (1.6634)	1.6382 (1.6011)	1.9134 (1.6913)	1.5226 (1.5912)	1.6552 (1.6273)
Insole				1.9730 (1.7826)	1.5068 (1.5609)	1.5987 (1.6406)

asymmetric gait than HCS and PDP. According to **Table 5**, the *s*-Φ-*bonacci gait number* $\mathcal{Y}_{\Phi[s]}$ (11) was simultaneously able to find statistically significant differences between PDP and HCS ($p = 0.008$), and also between HSP and HCS ($p = 0.016$). Furthermore, the compensation strategies adopted by the non-paretic limb made the MGR in HSP similar to the healthy subjects' one, but achieved through an asymmetric and less reliable walking. In other words, the *s*-Φ-*bonacci gait number* $\mathcal{Y}_{\Phi[s]}$ effectively merged the asymmetry with the role of the proportions among gait phases, resulting statistically significant for both the disharmonic gait of PDP and the asymmetric gait of HSP.

Indeed, the main advantage of the Φ-*bonacci gait number* (10) [even in its simplified version (11)] is to consider, in a comprehensive manner, symmetry and harmony of walking in terms of gait phases. Such gait phases have been analyzed since the birth of gait analysis, thought as a science to analyse human movement in a quantitative manner (Perry, 1992). Changes in stance, swing and double support phases are strictly related and intertwined between the two feet (Perry, 1992), so that it turns out to be important assessing such changes in an unique meaningful index. Indeed, when compared to the three gait ratios already proposed in previous studies (Iosa et al., 2016b; Serrao et al., 2017), (10) and (11) have the advantage to consider also asymmetry between right and left lower limb kinematics. These indices are theoretically close to 0 for a perfectly harmonic and symmetric gait and far from 0 for a pathological gait. On the other hand, the analysis performed in the *Experimental set 1* has preliminarily shown consistency of data at the root of such an index computation and phase duration reliability through acquisition *via* different sensor systems. The concurrent validity of the new index [in its version (11)] has been illustrated through the *Experimental set 2*, highlighting the differences between healthy subjects, subjects with hemiparetic stroke characterized by an asymmetric walking, and patients with Parkinson's Disease characterized by a non-harmonic walking.

Anyway, the results of the present study should be interpreted with caution, owing to its specific limits, such as the small size of the samples enrolled in the two experimental sets. Many aspects should be further investigated in future studies. One of them relies on the fact that the Φ-*bonacci gait number* is focused on the proportions among the gait phases, limiting this type of gait analysis to temporal features. It could be certainly interesting to put it in relationship with [and test the correlation between (10)–(11) and quantitative indices related to] the role played by different sensory information in maintaining the gait harmony[18]. On the other hand, an additional potential limit of the present study is that we compared the *s*-Φ-*bonacci gait number* in healthy subjects and patients with stroke or Parkinson's Disease, but if it has to be useful in clinical settings, then this index should exhibit responsiveness to small changes obtained with rehabilitation.

In spite of such aforementioned limits, the present study also possesses points of strength, since it is based on a wide literature illustrating how gait phases are a reliable and valid measure of subject's walking. Even though the capability of the Φ-*bonacci gait number* in highlighting within-subject changes in walking has not been explicitly tested, previous studies have already shown that rehabilitative interventions were able to modify the phases of gait cycle in patients with Parkinson's Disease. In light of the reported changes in terms of stance, swing and double support phases, we might reasonably suppose that also the Φ-*bonacci gait number* can detect patients improvements due to rehabilitation, especially in terms of self-similarity, symmetry,

TABLE 4 | Consistency indices (*Experimental set 1*).

Walking speed v (m/s)	Mean value $\Delta(v)$	$M_{\phi}(v)$	$M_{\phi,e}(v)$
0.97	0.01485	0.0567	0.0567
1.1	0.02715	0.1588	0.1588
0.85	0.069	0.2954	0.2954
1.51	0.107325	0.78285	0.78285

[18]For instance, further studies should clarify the role played by vision (owing to the fact that a reduction of upper body stability and harmony has been exhibited by subjects walking blindfolded Iosa et al., 2012) or by the vestibular system that could be involved in maintaining balance during locomotion (Bent et al., 2005).

TABLE 5 | (*Experimental set 2*): Mean ± standard deviations for age and spatio-temporal gait parameters, computed for patients with Parkinson's Disease (PDP), patients with hemiparetic stroke (HSP) and healthy control subjects (HCS) and compared by Kruskal-Wallis analysis, whose *p*-values are reported in the last column [in bold if statistically significant, whereas the symbol * (besides bold characters) highlights statistical significant differences with respect to HCS at *post-hoc* analyses].

	PDP	HSP	HCS	Kruskal-Wallis analysis
Age (years)	67.6 ± 6.7	64.2 ± 2.0	63.2 ± 2.2	0.288
Walking speed (m/s)	0.99 ±0.28	0.88 ± 0.19	1.02 ± 0.11	0.980
MGR	**1.51 ± 0.07***	1.62 ± 0.06	1.62 ± 0.02	**0.018**
SI	1.02 ± 0.02	**1.11 ± 0.07***	1.01 ± 0.01	**0.008**
$\mathcal{Y}_{\Phi[s]}$	**1.09 ± 0.38***	**0.95 ± 0.51***	0.21 ± 0.10	**0.011**

consistency of the gaits as a valid and repetitive measure for the assessment of walking ability (Teufl et al., 2018).

5. CONCLUSIONS

Healthy and pathological human walking have been characterized from a temporal point of view in terms of two sets of eight specific time intervals concerning the *composite gait cycle*. The corresponding mathematical description in terms of generalized finite-length Fibonacci sequences and dynamics-on-graph concepts has naturally explained the crucial role of the golden ratio ϕ, while extending the related analyses in Iosa et al. (2013) and Marino et al. (2020). An interpretation in terms of Shannon entropy is also included in **Appendix A**. The new gait index (10), named Φ-*bonacci gait number* has been defined to assess recursivity, asymmetry, consistency, and self-similarity of the gait. It relies on a new experimental conjecture that concerns an extended fractal walking decomposition paying attention on the position of the foot relative to the tibia. Experimental results concerning the simplified version (11) of the index (10) have supported the theoretical derivations. Besides the aforementioned contributions, this paper may even provide new perspectives for developing quantitative assessment of human walking, efficient humanoid robotic walkers, and effective neuro-robots for rehabilitation, in line with the related discussion in the recent (Iosa et al., 2017). Finally, by repeatedly extending the application of the adjoint gait (i.e., adjoint gait of the adjoint gait and so on), a collection of indices representing overlapping gaits can be constructed and gait index variability along past walking gaits can be accordingly assessed in a natural way, as described in **Appendix B**.

DATA AVAILABILITY STATEMENT

The raw data supporting the conclusions of this article will be made available by the authors, without undue reservation.

ETHICS STATEMENT

Ethical review and approval was not required for the study on human participants in accordance with the local legislation and institutional requirements. Written informed consent for participation was not required for this study in accordance with the national legislation and the institutional requirements.

AUTHOR CONTRIBUTIONS

CV and MI: conceptualization, writing the review, and editing. CV, MI, PR, and GS: methodology. MI and GS: software and resources. CV, MI, AP, FG, and GS: validation and investigation. CV, MI, and FG: formal analysis. CV: writing the original draft. All authors contributed to the article and approved the submitted version.

FUNDING

This work was partially supported by the Italian National Institute for Insurance against Accidents at Work (INAIL), in the framework of BRIC project: Project STAR - Innovative STrategies, and Approaches for the motor and functional Rehabilitation of subjects with neurovascular adverse event outcomes for reintegration into work.

ACKNOWLEDGMENTS

We are indebted to V. Errico, S. Prioriello, M. Gnucci, M. Tiberti for the experiments execution and related discussions. We are also indebted to L. Antenucci, M. Flemma, F. Violi and E. Oneto for their technical contributions. The first author is indebted with M. Paradiso for having provided a precious link with the Heart Rate Variability and with Prof. R. Marino for having brought to the attention analogies with the Shannon index and the cardiac cycle partition.

REFERENCES

Bent, L., McFadyen, B., and Inglis, J. (2005). Vestibular contributions during human locomotor tasks. *Exerc. Sport Sci. Rev.* 33, 107–113. doi: 10.1097/00003677-200507000-00002

Błażkiewicz, M., Wiszomirska, I., and Wit, A. (2014). Comparison of four methods of calculating the symmetry of spatial-temporal parameters of gait. *Acta Bioeng. Biomech.* 16, 29–35. doi: 10.5277/abb140104

Cavagna, G., and Margaria, R. (1966). Mechanics of walking. *J. Appl. Physiol.* 21, 271–278. doi: 10.1152/jappl.1966.21.1.271

Costantini, G., Casali, D., Paolizzo, F., Alessandrini, M., Micarelli, A., Viziano, A., et al. (2018). Towards the enhancement of body standing balance recovery by means of a wireless audio-biofeedback system. *Med. Eng. Phys.* 54, 74–81. doi: 10.1016/j.medengphy.2018.01.008

do Carmo Vilas-Boas, M., and Cunha, J. (2016). Movement quantification in neurological diseases: methods and applications. *IEEE Rev. Biomed. Eng.* 9, 15–31. doi: 10.1109/RBME.2016.2543683

Dugan, S., and Bat, K. (2005). Biomechanics and analysis of running gait. *Phys. Med. Rehabil. Clin. North Am*. 16, 603–621. doi: 10.1016/j.pmr.2005.02.007

Friedkin, N., Proskurnikov, A., Tempo, R., and Parsegov, S. (2016). Network science on belief system dynamics under logic constraints. *Science* 354, 321–326. doi: 10.1126/science.aag2624

Greene, B., McGrath, D., O'Neill, R., O'Donovan, K., Burns, A., and Caulfield, B. (2010). An adaptive gyroscope-based algorithm for temporal gait analysis. *Med. Biol. Eng. Comput*. 48, 1251–1260. doi: 10.1007/s11517-010-0692-0

Hausdorff, J. (2005). Gait variability: methods, modeling and meaning. *J. Neuroeng. Rehabil*. 2:19. doi: 10.1186/1743-0003-2-19

Hausdorff, J., Peng, C.-K., Ladin, Z., Wei, J., and Goldberger, A. (1995). Is walking a random walk? evidence for long-range correlations in the stride interval of human gait. *J. Appl. Physiol*. 78, 349–358. doi: 10.1152/jappl.1995.78.1.349

Hausdorff, J., Schaafsma, J., Balash, Y., Bartels, A., Gurevich, T., and Giladi, N. (2003). Impaired regulation of stride variability in parkinson's disease subjects with freezing of gait. *Exp. Brain Res*. 149, 187–194. doi: 10.1007/s00221-002-1354-8

Horadam, A. (1961). A generalized fibonacci sequence. *Am. Math. Mon*. 68, 455–459. doi: 10.1080/00029890.1961.11989696

Igamberdiev, A. (2004). Quantum computation, non-demolition-measurements, and reflective control in living systems. *Biosystems* 77, 47–56. doi: 10.1016/j.biosystems.2004.04.001

Iosa, M., Bartolo, D. D., Morone, G., Boffi, T., Mammucari, E., Vannozzi, G., et al. (2019). Gait phase proportions in different locomotion tasks: the pivot role of golden ratio. *Neurosci. Lett*. 699, 127–133. doi: 10.1016/j.neulet.2019.01.052

Iosa, M., Fusco, A., Marchetti, F., Morone, G., Caltagirone, C., Paolucci, S., et al. (2013). The golden ratio of gait harmony: repetitive proportions of repetitive gait phases. *Biomed. Res. Int*. 2013:918642. doi: 10.1155/2013/918642

Iosa, M., Fusco, A., Morone, G., and Paolucci, S. (2012). Effects of visual deprivation on gait dynamic stability. *Sci. World J*. 2012:974560. doi: 10.1100/2012/974560

Iosa, M., Morone, G., Bini, F., Fusco, A., Paolucci, S., and Marinozzi, F. (2016a). The connection between anthropometry and gait harmony unveiled through the lens of the golden ratio. *Neurosci. Lett*. 612, 138–144. doi: 10.1016/j.neulet.2015.12.023

Iosa, M., Morone, G., Fusco, A., Marchetti, F., Caltagirone, C., Paolucci, S., et al. (2016b). Loss of fractal gait harmony in parkinson's disease. *Clin. Neurophysiol*. 127, 1540–1546. doi: 10.1016/j.clinph.2015.11.016

Iosa, M., Morone, G., and Paolucci, S. (2017). Golden gait: an optimization theory perspective on human and humanoid walking. *Front. Neurorob*. 11:69. doi: 10.3389/fnbot.2017.00069

Kavanagh, J., Morrison, S., James, D., and Barrett, R. (2006). Reliability of segmental accelerations measured using a new wireless gait analysis system. *J. Biomech*. 39, 2863–2872. doi: 10.1016/j.jbiomech.2005.09.012

Kirtley, C. (2006). *Clinical Gait Analysis-Theory and Practice*. London: Elsevier Health Sciences; Churchill Livingstone.

Marino, R., Verrelli, C. M., and Gnucci, M. (2020). Synchronicity rectangle for temporal gait analysis: application to parkinson's disease. *Biomed. Signal Proc. Control* 62:102156. doi: 10.1016/j.bspc.2020.102156

Mochon, S., and McMahon, T. (1980). Ballistic walking. *J. Biomech*. 13, 49–57. doi: 10.1016/0021-9290(80)90007-X

Novacheck, T. (1998). The biomechanics of running. *Gait Posture* 7, 77–95. doi: 10.1016/S0966-6362(97)00038-6

Ozturk, E., Yalta, K., and Yetkin, E. (2016). Golden ratio: a subtle regulator in our body and cardiovascular system? *Int. J. Cardiol*. 223, 143–145. doi: 10.1016/j.ijcard.2016.08.147

Parsegov, S., Proskurnikov, A., Tempo, R., and Friedkin, N. (2017). Novel multidimensional models of opinion dynamics in social networks. *IEEE Trans. Autom. Control* 62, 2270–2285. doi: 10.1109/TAC.2016.2613905

Perry, J. (1992). *Gait Analysis: Normal and Pathological Function*. West Deptford, NJ: Slack Incorporated.

Potdevin, F., Femery, V., Decatoire, A., Bosquet, L., Coello, Y., and Moretto, P. (2007). Using effect size to quantify plantar pressure asymmetry of gait of nondisabled adults and patients with hemiparesis. *J. Rehabil. Res. Dev*. 44, 347–354. doi: 10.1682/JRRD.2006.07.0077

Ren, P., Zhao, W., Zhao, Z., Bringas-Vega, M., Valdes-Sosa, P., and Kendrick, K. (2016). Analysis of gait rhythm fluctuations for neurodegenerative diseases by phase synchronization and conditional entropy. *IEEE Trans. Neural Syst. Rehabil. Eng*. 24, 291–299. doi: 10.1109/TNSRE.2015.2477325

Ricci, M., Lazzaro, G. D., Pisani, A., Mercuri, N., Giannini, F., and Saggio, G. (2019a). Assessment of motor impairments in early untreated parkinson's disease patients: the wearable electronics impact. *IEEE J. Biomed. Health Inform.* 24, 120–130. doi: 10.1109/JBHI.2019.2903627

Ricci, M., Terribili, M., Giannini, F., Errico, V., Pallotti, A., Galasso, C., et al. (2019b). Wearable-based electronics to objectively support diagnosis of motor impairments in school-aged children. *J. Biomech*. 83, 243–252. doi: 10.1016/j.jbiomech.2018.12.005

Saggio, G. (2020). "Are sensors and data processing paving the way to completely non-invasive and not-painful medical tests for widespread screening and diagnosis purposes?," in *Proceedings of the 13th International Joint Conference on Biomedical Engineering Systems and Technologies - BIODEVICES*, 207–214. doi: 10.5220/0009098002070214

Saggio, G., and Sbernini, L. (2011). "New scenarios in human trunk posture measurements for clinical applications," in *2011 IEEE International Symposium on Medical Measurements and Applications* (Bari: IEEE), 13–17.

Salarian, A., Russmann, H., Vingerhoets, F., Dehollain, C., Blanc, Y., Burkhard, P., et al. (2004). Gait assessment in parkinson's disease: toward an ambulatory system for long term monitoring. *IEEE Trans. Biomed. Eng*. 51, 1434–1443. doi: 10.1109/TBME.2004.827933

Serrao, M., Chini, G., Iosa, M., Casali, C., Morone, G., Conte, C., et al. (2017). Harmony as a convergence attractor that minimizes the energy expenditure and variability in physiological gait and the loss of harmony in cerebellar ataxia. *Clin. Biomech*. 48, 15–23. doi: 10.1016/j.clinbiomech.2017.07.001

Spellerberg, I., and Fedor, P. (2003). A tribute to claude shannon (1916–2001) and a plea for more rigorous use of species richness, species diversity and the 'shannon-wiener index. *Glob. Ecol. Biogeogr*. 12, 177–179. doi: 10.1046/j.1466-822X.2003.00015.x

Teufl, W., Lorenz, M., Miezal, M., Taetz, B., Frõhlich, M., and Bleser, G. (2018). Towards inertial sensor based mobile gait analysis: event-detection and spatio-temporal parameters. *Sensors* 19, 38. doi: 10.3390/s19010038

The European Society of Cardiology & the North American Society of Pacing & Electrophysiology T. F. (1996). Standard of measurement, physiological interpretation, and clinical use. *Eur. Heart J*. 17, 354–381. doi: 10.1093/oxfordjournals.eurheartj.a014868

Verrelli, C. M., Romagnoli, C., Jackson, R., Ferretti, I., Annino, G., and Bonaiuto, V. (2021). Front crawl stroke in swimming: Ratios of phase durations and self-similarity. *J. Biomech*. 118. doi: 10.1016/j.jbiomech.2021.110267

Wang, J.-S., C.-W.-,Lin, Yang, Y.-T., and Ho, Y.-J. (2012). Walking pattern classification and walking distance estimation algorithms using gait phase information. *IEEE Trans. Biomed. Eng*. 59, 2884–2892. doi: 10.1109/TBME.2012.2212245

Conflict of Interest: The reviewer AR declared an affiliation with INAIL, which provided partial support for this work within the framework of the BRIC project: Project STAR - Innovative STrategies, and Approaches for the motor and functional Rehabilitation of subjects with neurovascular adverse event outcomes for reintegration into work.

The reviewer MT declared a past co-authorship with one of the authors MI to the handling Editor.

APPENDIX A

Shannon-Index-Based Interpretation

Consider the generalized Fibonacci sequence: a, b, c, d (generally arising from the symmetric & recursive or the non-{symmetric & recursive} cases of Propositions 2 and 3, respectively), along with the three ratios: $b/a, c/b, d/c$. Look for a suitably defined string of characters and a corresponding Shannon-index characterization of the case in which the golden ratio ϕ is a fixed point for the consecutive ratios b/a, c/b and d/c and one value determines the whole sequence. With respect, recall that the Shannon index (or diversity index) may be used to quantify the entropy in a string of text (Spellerberg and Fedor, 2003). The more different letters there are, the more difficult it is to correctly predict which letter will be the next one in the string. To this purpose, take the three differences $d_1 = b/a - c/b$, $d_2 = d/c - c/b$, $d_3 = b/a - d/c$ and let M_R be a sufficiently large positive odd integer. Let $\mathcal{P}$ be a finite partition of the compact set $[-M_R, M_R]$, with disjoint blocks (or cells) $\mathcal{A}_j$ of the form:

$$\begin{aligned} \mathcal{A}_j &= [x_j, x_{j+1}], \quad j = 1, 2, \ldots, M_R - 1, \\ \mathcal{A}_j &= [x_j, x_{j+1}], \quad j = M_R, \end{aligned}$$

where $x_{j+1} = x_j + 2$, $j = 1, 2, \ldots, M_R$, and $x_1 = -M_R$. Let $\mathcal{P}_l$ a finite refinement of $\mathcal{P}$ ($l = 0, 1, \ldots, R_l$, R_l is a sufficiently large natural number), with finer blocks $\mathcal{A}^{[l]}_{k[j]} \subset \mathcal{A}_j$ of the form:

$$\mathcal{A}^{[l]}_{k[j]} = [x^{[l]}_{k[j]}, x^{[l]}_{k+1[j]}),$$

where $x^{[l]}_{k+1[j]} = x^{[l]}_{k[j]} + 1/2^l$, $k = 1, \ldots, 2^{(l+1)}$, and $x^{[l]}_{1[j]} = x_j$. For each $l = 0, 1, \ldots, R_l$, define the set of characters (or letters)

$$\Sigma^{[l]} = \{x_1 = x^{[l]}_{1[1]}, \ldots, x^{[l]}_{2^{(l+1)}+1[1]} = x_2 = x^{[l]}_{1[2]}, \ldots, \ldots\}.$$

Consider the string of characters: $(s^{[l]}_1, s^{[l]}_2, s^{[l]}_3)$, where $s^{[l]}_1, s^{[l]}_2, s^{[l]}_3$ belong to the above set $\Sigma^{[l]}$ and $s^{[l]}_m$ ($m = 1, 2, 3$) equals the smallest element of $\mathcal{A}^{[l]}_{k[j]}$ when the difference d_m belongs to the block $\mathcal{A}^{[l]}_{k[j]}$. Let $p^{[l]}_{*r}$ be the number of characters belonging to the r-th character type in the three-elements-string $(s^{[l]}_1, s^{[l]}_2, s^{[l]}_3)$ divided by 3 ($r = 1, \ldots, N^{[l]}$, $N^{[l]} \leq 3$). Finally take the Shannon index for such a string $(s^{[l]}_1, s^{[l]}_2, s^{[l]}_3)$ as

$$\mathcal{H}^{[l]}_s = -\sum_{r=1}^{N^{[l]}} p^{[l]}_{*r} \ln\left(p^{[l]}_{*r}\right),$$

where $\sum_{r=1}^{N^{[l]}} p^{[l]}_{*r} = 1$. The more unequal the abundances of types in the string is, the smaller the corresponding Shannon entropy is made, with $\mathcal{H}^{[l]}_s$ satisfying[19]

$$\mathcal{H}^{[l]}_s \in \left[0, \ln\left(N^{[l]}\right)\right].$$

In particular, if all abundance is concentrated to one type, Shannon entropy is zero and there is no uncertainty in predicting the type of the next entity. The case in which the golden ratio ϕ is a fixed point for the consecutive ratios b/a, c/b and d/c is thus characterized by the condition $\sum_{l=1}^{R_l} \mathcal{H}^{[l]}_s = 0$, for any $R_l \in \mathbb{N} \cup \{0\}$.

APPENDIX B

Introduce the definition of *adjoint* application, i.e.: *given any left or right gait cycle defined as the time interval between two consecutive lift off or two consecutive strikes of the corresponding foot, its* adjoint *is defined as the time interval between two consecutive strikes or two consecutive foot off of the corresponding foot, respectively, starting from the strike or the lift off immediately preceding the lift off or the strike of the considered gait, respectively*. Denote the adjoint of the adjoint gait by the symbol adj2, whereas denote the adjoint of the adjoint of the adjoint gait by the symbol adj3 (see **Figure 7**). The phases within such gaits inherit the same notation. **Figure 7** shows that, by definition, $\mathrm{SW}^{\mathrm{adj2}}_r = \mathrm{SW}^{\mathrm{adj}}_r$, $\mathrm{ST}^{\mathrm{adj2}}_l = \mathrm{ST}^{\mathrm{adj}}_l$, $\mathrm{DS}^{\mathrm{adj2}}_l = \mathrm{DS}^{\mathrm{adj}}_l$, whereas DS_{y2} and DS_{z2} [that characterize the double support $\mathrm{DS}^{\mathrm{adj2}}_l$] satisfy the seam-constraints: $\mathrm{DS}_{y2} = \mathrm{DS}_w$, $\mathrm{DS}_{z2} = \mathrm{DS}_x$. The Φ-*bonacci gait number* at stage -1 can be thus defined as[20]

$$\begin{aligned} \mathcal{Y}_{\Phi,-1} = \Bigg[& \left(\frac{\mathrm{SW}^{\mathrm{adj2}}_l}{\mathrm{DS}^{\mathrm{adj2}}_r} - \phi\right)^2_{\mathrm{n}} + \left(\frac{\mathrm{SW}^{\mathrm{adj2}}_r}{\mathrm{DS}^{\mathrm{adj2}}_l} - \phi\right)^2_{\mathrm{n}} \\ & + \mu^{\mathrm{adj}}_{-1} \left(\frac{\mathrm{SW}^{\mathrm{adj3}}_r}{\mathrm{DS}^{\mathrm{adj3}}_l} - \phi\right)^2_{\mathrm{n}} \Bigg]^{1/2} + \lambda_{-1} \Bigg[\left(\frac{\mathrm{SW}^{\mathrm{adj2}}_r}{\mathrm{SW}^{\mathrm{adj2}}_l} - 1\right)^2_{\mathrm{n}} \\ & + \lambda^{\mathrm{adj}}_{-1} \left(\frac{\mathrm{SW}^{\mathrm{adj3}}_r}{\mathrm{SW}^{\mathrm{adj2}}_r} - 1\right)^2_{\mathrm{n}} \Bigg]^{1/2} + \nu^{\mathrm{conj}}_{-1} \Bigg[\left(\frac{\mathrm{DS}^{\mathrm{adj2}}_r}{z^{\mathrm{adj2}}_1 + z^{\mathrm{adj2}}_2} - \phi\right)^2_{\mathrm{n}} \\ & + \left(\frac{\mathrm{DS}^{\mathrm{adj2}}_l}{z^{\mathrm{adj2}}_2 + z^{\mathrm{adj2}}_3} - \phi\right)^2_{\mathrm{n}} \Bigg]^{1/2} + \delta_{-1} \Bigg[\left(\frac{\mathrm{DS}_{x2}}{\mathrm{DS}_{y2}} - 1\right)^2_{\mathrm{n}} \Bigg]^{1/2}, \end{aligned} \tag{12}$$

where μ^{adj}_{-1}, λ_{-1}, $\lambda^{\mathrm{adj}}_{-1}$, ν^{conj}_{-1}, δ_{-1} are positive gains that play the same role of μ^{adj}, λ, λ^{adj}, ν^{conj}, δ, while $\mathrm{DS}_{x2} + \mathrm{DS}_{y2} = \mathrm{DS}^{\mathrm{adj2}}_r$. Gait index variability can be naturally assessed by comparing the Φ-*bonacci gait numbers* at different stages, through the diversity index computed on the basis of their approximated

[19] Let $[l]$ be omitted for the sake of brevity. Owing to the fact that 0

$$\mathcal{H}_s \leq \sum_{r=1}^{N} p_{*r} \left(\frac{1}{p_{*r} N} - 1\right) + \ln(N) = \ln(N),$$

with $\mathcal{H}_s = \ln(N)$ when $p_{*r} = 1/N$ for all $r = 1, 2, \ldots, N$.

[20] Further extensions to the past gaits can be apparently performed, in order to characterize the *m-cycle gait index variability* along the walking gaits, for any natural m.

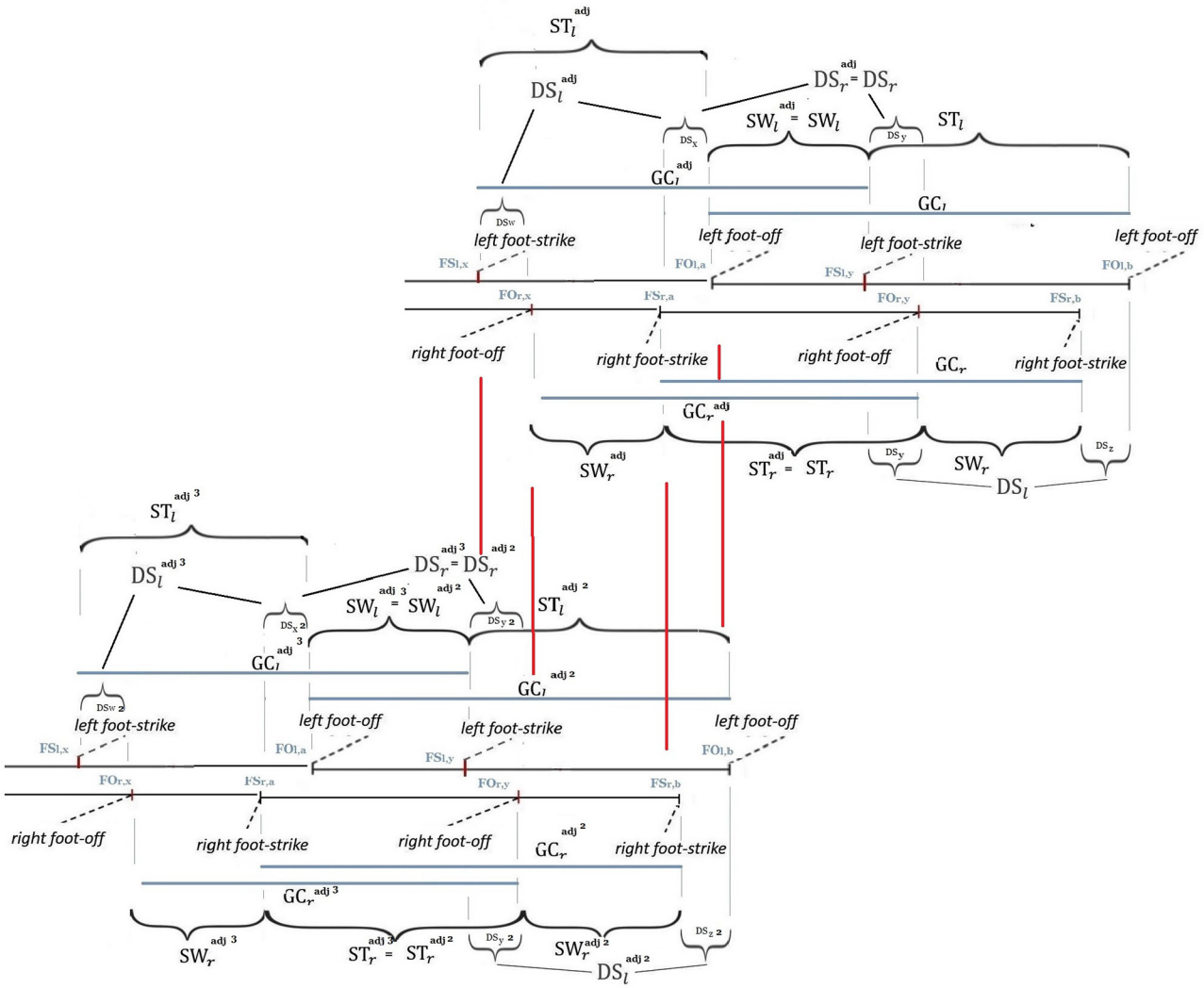

FIGURE 7 | Walking gaits and their repetitive adjoints.

values (in accordance with certain required tolerances). Notice that if the ordered-in-time sequence of left and right foot strike and off is translated into a sequence of beats, then the same tools used to quantify the Heart Rate Variability can be adopted (Hausdorff, 2005). In this respect, a perfectly self-similar, symmetric, consistent, recursive, gait-index-stable walking exhibits a power spectral density with exclusive content at the frequency 2/GC (in Hz if GC measured in seconds). Evaluating gait fluctuations can be used as a complementary way of quantifying gait reliability with respect to age and disease, as well as a means of monitoring the effects of therapeutic interventions and rehabilitation (Hausdorff, 2005), provided that this approach is actually based on all the foot strike and the foot off events.

frontiers in Human Neuroscience

ORIGINAL RESEARCH
published: 12 August 2021
doi: 10.3389/fnhum.2021.715375

The Relation Between Complexity and Resilient Motor Performance and the Effects of Differential Learning

Ruud J. R. Den Hartigh[1], Sem Otten[1], Zuzanna M. Gruszczynska[1,2] and Yannick Hill[1,2,3]*

[1] Department of Psychology, Faculty of Behavioral and Social Sciences, University of Groningen, Groningen, Netherlands, [2] Faculty of Medical Sciences, Center for Human Movement Sciences, University Medical Center Groningen/University of Groningen, Groningen, Netherlands, [3] Institute of Sport and Sport Science, Heidelberg University, Heidelberg, Germany

Complex systems typically demonstrate a mixture of regularity and flexibility in their behavior, which would make them adaptive. At the same time, adapting to perturbations is a core characteristic of resilience. The first aim of the current research was therefore to test the possible relation between complexity and resilient motor performance (i.e., performance while being perturbed). The second aim was to test whether complexity and resilient performance improve through differential learning. To address our aims, we designed two parallel experiments involving a motor task, in which participants moved a stick with their non-dominant hand along a slider. Participants could score points by moving a cursor as fast and accurately as possible between two boxes, positioned on the right- and left side of the screen in front of them. In a first session, we determined the complexity by analyzing the temporal structure of variation in the box-to-box movement intervals with a Detrended Fluctuation Analysis. Then, we introduced perturbations to the task: We altered the tracking speed of the cursor relative to the stick-movements briefly (i.e., 4 s) at intervals of 1 min (Experiment 1), or we induced a prolonged change of the tracking speed each minute (Experiment 2). Subsequently, participants had three sessions of either classical learning or differential learning. Participants in the classical learning condition were trained to perform the ideal movement pattern, whereas those in the differential learning condition had to perform additional and irrelevant movements. Finally, we conducted a posttest that was the same as the first session. In both experiments, results showed moderate positive correlations between complexity and points scored (i.e., box touches) in the perturbation-period of the first session. Across the two experiments, only differential learning led to a higher complexity index (i.e., more prominent patterns of pink noise) from baseline to post-test. Unexpectedly, the classical learning group improved more in their resilient performance than the differential learning group. Together, this research provides empirical support for the relation between complexity and resilience, and between complexity and differential learning in human motor performance, which should be examined further.

Keywords: adaptability, complex systems, detrended fluctuation analysis, non-linear dynamics, pink noise

OPEN ACCESS

Edited by:
Nadia Dominici, VU University Amsterdam, Netherlands

Reviewed by:
Olivier White, INSERM U1093 Cognition, Action et Plasticité Sensomotrice, France
Vanessa R. Simmering, University of Kansas, United States

****Correspondence:***
Ruud J. R. Den Hartigh
j.r.den.hartigh@rug.nl

Specialty section:
This article was submitted to Motor Neuroscience, a section of the journal Frontiers in Human Neuroscience

Received: *26 May 2021*
Accepted: *20 July 2021*
Published: *12 August 2021*

Citation:
Den Hartigh RJR, Otten S, Gruszczynska ZM and Hill Y (2021) The Relation Between Complexity and Resilient Motor Performance and the Effects of Differential Learning. Front. Hum. Neurosci. 15:715375. doi: 10.3389/fnhum.2021.715375

INTRODUCTION

Human motor performance can be considered as inherently complex and dynamic. Whether it is about rhythmical finger tapping, leg movements, or more complicated movements on the sports field, an individual's motor performance emerges out of simultaneous processes at different levels of the motor system, including cells, muscles, limbs, and the brain (e.g., Thelen et al., 1987; Beek et al., 1995; Kelso, 1995; Davids et al., 2014; Den Hartigh et al., 2015). Through these complex dynamics, the human motor system typically organizes itself around metastable states, meaning that its behavior demonstrates a mixture of order (regularity) and disorder (flexibility) (e.g., Kello et al., 2007). This optimal mixture is a hallmark of complexity and expresses itself in the fluctuations of individuals' repeated movements, such as intervals between strides, arm movements or rowing strokes (e.g., Goldberger et al., 2002; Wijnants et al., 2009; Diniz et al., 2011; Marmelat and Delignières, 2012; Den Hartigh et al., 2015).

The characteristic pattern of variation in complex systems behavior is called fractal scaling, 1/f noise, or pink noise, showing high-frequency and low-amplitude fluctuations that are nested within low-frequency and high-amplitude fluctuations (e.g., Wijnants et al., 2012). This nested structure reflects the idea that a system consists of components across different structural levels and timescales that constantly interact. Accordingly, the current state of the system contains the "memory" of its previous states (i.e., long-range (fractal) correlations, see Diniz et al., 2011). In the past decades, accumulating research has demonstrated that diseased or lower-performing systems show deviations from a pink noise pattern, reflecting a loss of complexity. Early studies in this direction, for instance, focused on the temporal structure of heart beat intervals, in order to study the complexity of the cardiovascular system (e.g., Stanley et al., 1992; Peng et al., 1993). These studies typically showed prominent patterns of pink noise in the time series of heart beat intervals of healthy adults. On the other hand, a clear deviation from pink noise (e.g., random variation in intervals) appeared to be a signature of heart failure (see Goldberger et al., 2002). The methods to detect and quantify the temporal structure of heartbeat intervals could also be applied in research on motor performance. For example, a series of studies on human walking has demonstrated that stride interval time series of healthy young adults reveal patterns of pink noise, whereas the stride intervals of people with Huntington or Parkinson disease demonstrate patterns close to so-called white noise (e.g., Hausdorff et al., 1997b; Hausdorff, 2009). This white noise pattern means that more random variation in stride intervals is present, which suggests a worse dynamic organization of the motor system. Accordingly, researchers examining cyclic movements in sports found that skilled athletes demonstrate more prominent patterns of pink noise in their movements than their less-skilled counterparts (e.g., Den Hartigh et al., 2015 in rowing ergometer performance; Nourrit-Lucas et al., 2015 in ski simulator performance).

In line with the findings mentioned above, researchers have suggested that a loss of complexity likely accompanies an impaired ability to adapt to stress or perturbations (e.g., Lipsitz and Goldberger, 1992; Stergiou and Decker, 2011). This fits with the findings by Hausdorff et al. (1997a) that elderly people with higher propensities to fall show more prominent patterns of white noise in their stride intervals compared to elderly "non-fallers" and healthy young adults. It thereby appears that complexity provides the system with both robustness (maintaining proper functioning despite perturbations) and adaptability (adapting to changes or stressors in the environment) (Delignières and Marmelat, 2013; Almurad et al., 2018).

In the behavioral sciences, an individual's ability to maintain robust functioning despite perturbations and to adapt to stressors is called *resilience* (e.g., Carver, 1998; Luthar et al., 2000; Masten, 2001; Smith et al., 2008; Pincus and Metten, 2010; Hill et al., 2018a). Although specific definitions of resilience show some variations, "each of these definitions encompasses complex adaptive change over time" (Pincus and Metten, 2010, p. 357). This complex adaptive change entails that a person is not governed by one fixed state, but can quickly transition between equally functional states if the environment demands adaptations (Kiefer et al., 2018). Proceeding from the idea that the concepts of complexity and resilience are probably related, our first aim was to test this relation in a motor task.

Another topic that has gained significant interest in the past two decades is how complexity, adaptation, and resilience may be improved in human behavior (e.g., Schöllhorn et al., 2012; Kiefer and Myer, 2015; Almurad et al., 2018; Hill et al., 2020b). According to various researchers, system complexity can be improved by exploiting variability (e.g., Van Emmerik and Van Wegen, 2000; Riley and Turvey, 2002; Davids et al., 2003; Stergiou and Decker, 2011; Schöllhorn et al., 2012; Seifert et al., 2013; Liu et al., 2015). Hence, a promising avenue is to apply interventions that take advantage of the important role of variability in finding functionally adaptive movement patterns. A particularly interesting application of this idea is differential learning, which is developed from the perspective of complex dynamical systems (e.g., Schöllhorn et al., 2006, 2009, 2010, 2012; Savelsbergh et al., 2010; Santos et al., 2018). In brief, a differential learning program introduces random noise to destabilize the system, and possibly strengthen the development of metastable states (e.g., Schöllhorn et al., 2009; Gray, 2020). This is in stark contrast with classical learning, which focuses on the development of an ideal movement pattern, deviations from which are considered detrimental to performance. Repetition and corrective feedback are therefore core ingredients of the latter approach. In a differential learning approach, on the other hand, performing various movements for the same task is stimulated without any corrective feedback while performing (Schöllhorn et al., 2006, 2009, 2012; Savelsbergh et al., 2010). Thereby, the learner actively explores a large range of possible motor solutions to a given task, which fosters behavioral adaptations (cf. Latash, 2012). Consequently, differential learning may lead to improved resilient motor performance (i.e., performance while being perturbed by stressors).

The benefits of differential learning have already been demonstrated in the domain of sports, such as soccer (Schöllhorn et al., 2006, 2012; Santos et al., 2018; Gaspar et al., 2019), speed skating (Savelsbergh et al., 2010), and baseball (Gray, 2020). For instance, Savelsbergh et al. (2010) trained novice speed skaters

in their starting posture. The differential learning group began every start with a different posture and received no feedback on their performance. On the other hand, a classical learning group learned the starting posture as described in a skating handbook. A control group just engaged in regular speed skating lessons. The speed skating performance improved most for the participants in the differential learning group, suggesting that their system was better able to adapt to changing environmental constraints, resulting in better performance (Schöllhorn et al., 2006). In line with the possible benefits of differential learning, the second aim of the current study was to examine the effects of this type of learning on complexity and resilient motor performance.

In summary, complex systems tend to organize themselves around metastable states that would allow for adaptation when perturbations are imposed on their behavior. At the same time, the adaptation of a system to perturbations is a core characteristic of resilience (e.g., Pincus and Metten, 2010; Hosseini et al., 2016; Hill et al., 2018a,b). Hence, it is plausible that there is a link between the complexity of a system and its resilient performance. In order to improve complexity, and possibly resilience, differential learning may provide an interesting intervention that exploits the functional role of variability in system behavior. Following this rationale, our research question was: What is the relation between complexity and resilient motor performance, and can they be improved through differential learning? In order to answer this question, we developed a motor task that allowed us to (1) let participants perform repetitive (cyclical) movements, which are particularly useful for the analysis of complexity in time series (e.g., Wijnants et al., 2009, 2012), and (2) introduce perturbations while participants are performing the task. The specific task we used was a lateral movement task in which participants had to move a stick from left to right in order to move a cursor between two boxes on a screen in front of them. We conducted two parallel experiments with this task: one that included maintaining performance while being briefly perturbed at regular intervals, thereby emphasizing the robustness side of resilience, and one including prolonged perturbations that required changes to other performance states, thereby emphasizing the adaptability side. Across the two experiments, we expected a positive relation between complexity and resilient performance (*hypothesis 1*). Furthermore, in contrast to classical learning, we expected that differential learning leads to an improvement of complexity (i.e., more prominent patterns of pink noise in temporal performance fluctuations — *hypothesis 2*). Relatedly, we expected that, in contrast to classical learning, differential learning leads to better resilient motor performance (*hypothesis 3*). Finally, we explored whether the hypothesized effects differ depending on the type of stressors (brief vs. prolonged) introduced.

MATERIALS AND METHODS

Participants

We recruited 82 participants who were living in The Netherlands. Most of these participants were first year psychology students recruited through a participant pool of the university. Thirty-nine participants started, and completed Experiment 1 (M_{age} = 20.54, SD = 2.06; 59% female), and 43 participants started the parallel Experiment 2, of which 40 actually completed it (M_{age} = 21.60, SD = 3.76; 58% female). In both experiments, participants were randomly allocated to either a classical learning condition or a differential learning condition. None of the participants had motor impairments, and all of them had normal or corrected-to-normal vision.

Materials

The device used was designed for the purpose of the current research (see **Figure 1**). This device consisted of a meter-long rail, on which a stick was attached that could move along the entire length of the rail. The position of the stick was recorded with a frequency of 20Hz, and the movements were projected on a screen (Iiyama, 27 inch) in front of the participants. The screen was placed behind the device on a table with adjustable height. Participants could sit down on a non-adjustable chair without armrests.

The task consisted of a game in which participants had to move the cursor from left-to-right between two boxes on the screen. Each time they touched the box, the box turned green and participants won a point, but when overshooting the box turned red and a point was subtracted. The software we made for this research allowed us to manage different settings of the game, such as playing time, tracking speed of the cursor, size and placement of the squares, and graphic cues for the player (e.g., seeing elapsed time, points, or squares changing color when touched).

Procedure

The protocol of the study was approved by the Ethics Committee Psychology of the University of Groningen. The parallel experiments consisted of three meetings, each lasting about 1 h, with a maximum of 5 days in between meetings to retain the influence of the preceding session. The first meeting included a baseline session and a first training session; the second

FIGURE 1 | Illustration of the research setup.

meeting consisted of two training sessions; and the third meeting consisted of the last training session and a posttest. Participants had a 10 min break in between two sessions on the same day. Before the first meeting, we randomly allocated participants to either a classical learning condition or a differential learning condition. At the start of the first meeting, we explained the nature of the experiment and the task participants would have to carry out. We explained how the game had to be played (how to win points), and we told them that there were four sessions in which we aimed to train participants to improve in the game. Subsequently, we asked participants to fill out an informed consent form and a brief questionnaire including questions about age, gender, dominant hand, and possible visual impairments.

Baseline Session

In the baseline session, we asked participants to play the game for 15 min. We specifically instructed them to move the cursor with the stick as fast and accurately as possible between two boxes. Each time they touched a box, it turned green and participants earned a point (which would be lost again when overshooting the target). To avoid interruptions in the task performance, we instructed participants to always maintain the box-to-box movement rhythm, regardless of whether they hit or missed the box. We also emphasized that the goal of the game was to gain as many points as possible and that this could be reached with speed and accuracy.

While playing the game, participants used their non-dominant hand to move the stick, to make the game more challenging (cf. Wijnants et al., 2009, 2012). The first 30 s of the game were not measured so that participants could get used to the task, after which they performed this task for 10 min, uninterrupted. This period was chosen, because it allowed us to collect (at least) 512 data points, which is required for a reliable analysis of the complexity index (Delignières et al., 2006; see section "Complexity" for more information). When the 10 min had passed, we introduced perturbations during the last 5 min of the task. In Experiment 1, these perturbations were brief: every minute we increased the tracking speed of the cursor relative to the stick movement for 4 s, thereby interrupting the cyclic performance that participants needed to maintain. More specifically, when the tracking speed changed, identical movements of the stick temporarily resulted in faster movements of the cursor on the screen. In Experiment 2, these perturbations were prolonged: every minute we changed the tracking speed of the cursor for an entire minute, thereby forcing the participants to adapt and find another performance rhythm. In both experiments, the intensity of the change in tracking speed was different for each perturbation to make sure the participants could not get used to the changes (see **Table 1**).

TABLE 1 | Schedule of tracking speed changes during the last 5 min of the task in Experiment 1 (Brief perturbation) and Experiment 2 (Prolonged perturbation).

Brief perturbation		Prolonged perturbation	
Time (in seconds)	**Sensitivity**	**Time (in seconds)**	**Sensitivity**
630	2	630–690	2
634	1		
690	1.5	691–750	1
694	1		
750	2.5	751–810	1.5
754	1		
810	1.25	811–870	2.5
814	1		
870	1.75	870–930	1.25
874	1		

When the tracking speed changes from 1 to a higher number, identical movements of the stick result in faster movements of the cursor on the screen.

Training Sessions

Following the baseline session, participants of Experiments 1 and 2 were involved in four training sessions, each lasting 20 min. The type of training depended on the condition—classical or differential learning—to which participants were allocated. In accordance with previous literature, at the start of each classical learning session, we provided participants with instructions on how to best execute their movements while performing the task (e.g., Schöllhorn et al., 2006, 2009, 2012). Hence, in our study we instructed participants to, amongst others, maintain a stable position; keep a delicate grip; and position the playing shoulder to the middle of the device to make sure the distance to the left and right box is equal. The remainder of each training session consisted of 10 blocks of 1.5 min each, in which the participants practiced the ideal movement, with breaks of 30 s in between the blocks. During the breaks, we gave participants corrective feedback if necessary.

In the differential learning condition, the training sessions were based on the differential learning principles outlined in previous literature (e.g., Schöllhorn et al., 2006; Savelsbergh et al., 2010; Gray, 2020). As in the classical learning condition, participants also performed 10 blocks of 1.5 min each, with breaks of 30 s in between. However, contrary to the idea of classical learning, they were not trained to perform the movement in the "right way." Rather, in the differential learning condition we used the breaks to give participants instructions to perform additional and irrelevant movements while practicing, thereby adding noise to their movement patterns. These could, for instance, be instructions about which hand to use; sitting down or standing up; making a turn after each movement; playing with closed eyes; and standing on one leg. Additionally, we did not provide participants with any feedback on their performance or movements. This included the absence of verbal feedback, as well as feedback by the software such as earned points, elapsed time, or changing colors of the boxes when hitting or overshooting them. In the differential learning condition, each training session was different and included various instructions for the additional and irrelevant movements. Elaborate descriptions of both the classical and differential training programs are provided in **Supplementary Materials**.

Posttest

The posttest was identical to the baseline session. Hence, the participants performed the task and the first 30 s were not measured. In the next 10 min the participants played the game

without being perturbed. Then, in the last 5 min the participants were exposed to either brief perturbations (Experiment 1) or prolonged perturbations (Experiment 2) with the exact same configurations as in the baseline session. At the end of the posttest, they were debriefed about the true purpose of the study.

Measures

Complexity

In line with previous research on cyclic movements (e.g., walking, lateral arm movements, rowing), we used the time intervals of the left-to-right movements (between the boxes) as a unit of analysis to determine complexity. On these intervals we conducted the detrended fluctuation analysis (DFA) for the first 10 min of each participant's baseline session (i.e., while performing the task without any perturbations). DFA is a technique to determine complexity based on temporal structures in time-series data (Peng et al., 1993). The procedure to perform the DFA was as follows. First, we turned the raw data into a time series of 512 movement intervals (from box-to-box) for each participant. These time series were then divided into bins (time scales) of equal size, in which a least-squares line was fitted to determine the trend in each bin. This trend was subsequently subtracted in the bin to detrend the time series. From the detrended time series, the root-mean-square fluctuation was calculated. This procedure was repeated using different bin sizes (i.e., 4, 8, 16, 32, 64, and 128 intervals) to identify the average fluctuation at each bin size.

The relation between bin size and fluctuation reflects the DFA index (α), which corresponds to the value of the slope of a log-log plot in which fluctuation is plotted against bin size (see **Figure 2**). The closer the DFA index is to 1, the more it reflects a pattern of fractal scaling or pink noise in the time series. A DFA index of 0.5 reflects a white noise pattern, whereas a DFA index of 1.5 is an indication of Brownian noise (i.e., an overly regular pattern, which was not a focus in the current study).

Resilient Performance

In order to determine resilient motor performance of participants, we scored the number of times participants touched the boxes (without overshooting) during the periods in which they were perturbed. In Experiment 1 this score reflected the participants' ability to maintain performance despite being briefly perturbed at regular intervals. In Experiment 2 it reflected the participants' performance while regularly adapting to a new pattern. Indeed, each time the tracking speed of the cursor relative to the stick movements changed, the participants had to adapt to another rhythmic pattern to score points.

Analysis

To test whether there is a positive relation between complexity and resilient motor performance (*hypothesis 1*), we determined the correlation between the DFA index and the box touches during the perturbation period in the baseline sessions of Experiments 1 and 2. To determine the effects of training on complexity (*hypothesis 2*), we conducted a repeated-measures ANOVA with DFA index (α) as the dependent variable. Session (Baseline vs. Posttest) was the within-subjects independent variable, and Training (i.e., Differential vs. Classical) and Perturbation (Brief vs. Prolonged) were the between-subjects independent variables. The latter variable allowed us to explore whether the hypothesized effect is moderated by the type of perturbation. Finally, to test the effects of training on resilient performance (*hypothesis 3*), we also performed a repeated-measures ANOVA with Box touches as the dependent variable, Session (Baseline vs. Posttest) as the within-subjects variable, and Training (i.e., Differential vs. Classical) and Perturbation (Brief vs. Prolonged) as the between-subjects variables.

RESULTS

Complexity and Resilient Performance

In the first 10 min of the baseline session, we determined the DFA index and the number of box touches per minute. Taking the two experiments together, the average value of the DFA index was 0.70 (SD = 0.14), and the average number of box touches per minute was 69.14 (SD = 19.84). A Pearson correlation analysis revealed a positive correlation between the DFA index and the number of box touches in the perturbation period of the first session (r (78) = 0.36, p = 0.001, 95% CI [0.15, 0.54]). This relation was comparable between the two experiments separately (r (38) = 0.42, p = 0.008, 95% CI [0.12, 0.65] for Experiment 1, and r (39) = 0.32, p = 0.043, 95% CI [0.005, 0.58] for Experiment 2). In accordance with *hypothesis 1*, these results suggest that higher levels of complexity (i.e., α closer to 1)[1] are related to better resilient motor performance.

Training and Complexity

In the baseline- and posttest we determined the complexity, and we analyzed whether changes in complexity were influenced by the type of training. The repeated measures ANOVA did not show a main effect for Session [F(1, 75) = 0.93, p = 0.34, η_p^2 = 0.012], nor an interaction effect of Session × Perturbation [F(1, 75) = 0.002, p = 0.96, $\eta_p^2 < 0.001$], or of Session × Training × Perturbation [F(1, 75) = 0.10, p = 0.75, η_p^2 = 0.001]. However, as expected we found an interaction effect of Session × Training with a medium effect size [F(1, 75) = 5.17, p = 0.026, η_p^2 = 0.065]. This effect was qualified by the finding that complexity increased in the Differential learning condition, whereas it slightly decreased in the Classical learning condition (see **Figure 3**). In accordance with *hypothesis 2*, the planned contrast (paired samples t-test) also showed a significant improvement in complexity from the Baseline session (α = 0.69, SD = 0.13) to the Posttest (α = 0.75, SD = 0.13) in the Differential learning condition: t(39) = −2.56, p = 0.014, d = 0.39.

Training and Resilient Performance

In the baseline- and posttest we also determined the number of box touches per minute, and we analyzed whether changes in this number were influenced by the type of training. The

[1]Values of α above 1 are also possible, and would correspond to more prominent patterns of Brownian noise. However, all of our participants demonstrated values within the range from white noise and pink noise, that is, no participant had a value of α larger than 1.

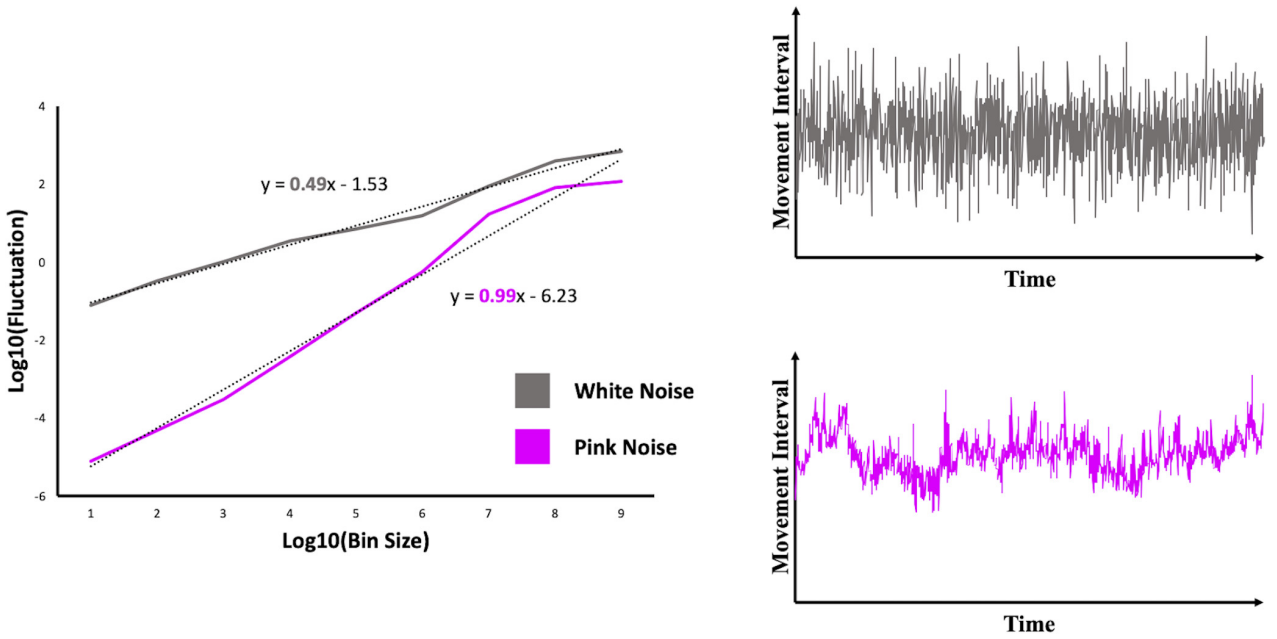

FIGURE 2 | Log-log plots including a scaling relation reflecting simulated time series of white noise (gray line) and pink noise (pink line). The corresponding time series on which the scaling relations are determined, are displayed in the graphs on the right.

repeated measures ANOVA revealed a main effect for Session with a strong effect size [$F(1, 75) = 292.18$, $p < 0.001$, $\eta_p^2 = 0.80$], reflecting a clear improvement in the number of box touches per minute from the Baseline session ($M = 63.09$, $SD = 16.56$) to the Posttest ($M = 95.04$, $SD = 27.07$). We also found an interaction effect of Session × Training with a strong effect size [$F(1, 75) = 19.94$, $p < 0.001$, $\eta_p^2 = 0.21$]. Although we detected the expected improvement in box touches from the Baseline session ($M = 62.39$, $SD = 17.73$) to the Posttest ($M = 86.14$, $SD = 27.44$) in the Differential learning condition [$t(39) = -8.60$, $p < 0.001$, $d = 1.35$], the improvement was stronger in the Classical learning condition. In the latter condition, the number of box touches per minute increased from 63.81 ($SD = 15.47$) in the Baseline session to 104.16 ($SD = 23.70$) in the posttest. In line with this interaction effect, and contrary to *hypothesis 3*, a *post hoc* independent samples *t*-test showed that the box touches were higher in the Posttest for the Classical learning condition [$t(77) = -3.12$, $p = 0.003$, $d = 0.70$].

Finally, we detected a significant Session × Training × Perturbation interaction with a medium effect size [$F(1, 75) = 4.29$, $p = 0.042$, $\eta_p^2 = 0.054$]. This result appears to be qualified by the observation that the beneficial effect of classical learning, in contrast to differential learning, is primarily apparent when participants are exposed to brief perturbations (**Figure 4A**) compared to prolonged perturbations (**Figure 4B**).

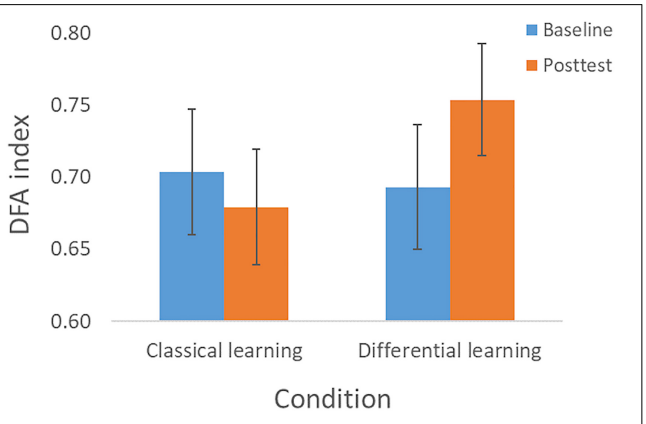

FIGURE 3 | Complexity—as expressed in the DFA index—according to Session (Baseline and Posttest) and Training condition (Classical learning and Differential learning). The error bars correspond to the 95% confidence intervals.

DISCUSSION

In the current research, we aimed to answer the question: What is the relation between complexity and resilient motor performance, and can they be improved through differential learning? In order to answer this question, we developed a task in which participants moved a stick from left-to-right to touch two boxes on a screen in an alternate fashion with a cursor. This task allowed us to determine the complexity of the motor performance, and to determine resilient performance by introducing perturbations while performing the task. In one of the two experiments, the emphasis was on maintaining performance while being briefly perturbed at regular intervals. In

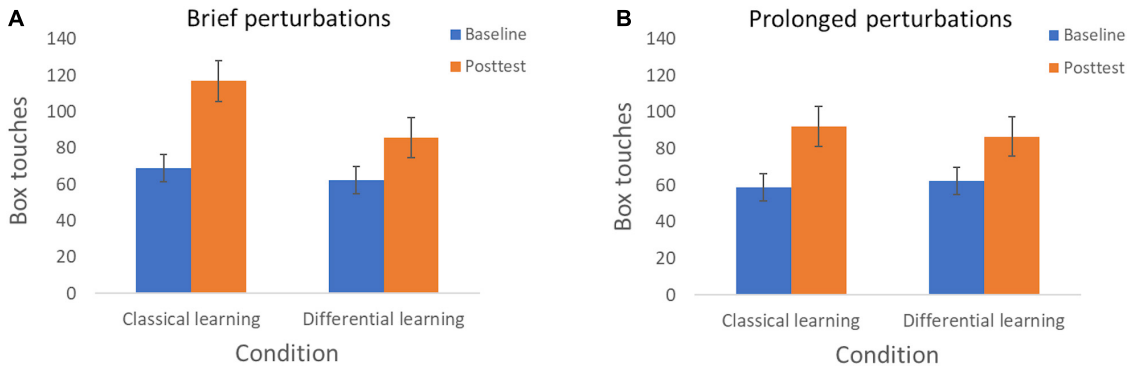

FIGURE 4 | Resilient motor performance—as expressed in box touches—according to Session (Baseline and Posttest) and Training condition (Classical learning and Differential learning). **(A)** Displays the results when being exposed to brief perturbations (Experiment 1), and **(B)** displays the results when being exposed to prolonged perturbations (Experiment 2). The error bars correspond to the 95% confidence intervals.

the other experiment, the focus was on prolonged perturbations that required changes to new performance states.

As expected, in both experiments we found a positive relation between complexity and resilient motor performance. Hence, whether participants needed to maintain performance while being exposed to brief perturbations (Experiment 1), or change to new performance modes (Experiment 2), higher levels of complexity were related to better performance. These results can be considered in line with Pincus and Metten (2010), who conceptualized resilience as the "metaflexibility" of a system. Their conceptualization suggests that resilience is the ability to respond to a perturbation by either becoming rigid and robust (i.e., being able to maintain a previously displayed behavioral state), or flexible and fluid (i.e., being able to easily switch to new behavioral states). Accordingly, our findings support the idea that complexity provides the system with both robustness (maintaining proper functioning despite perturbations) and adaptability (adapting to changes in the environment, see Delignières and Marmelat, 2013; Almurad et al., 2018). More generally, our results are in accordance with the consistent finding that complexity, as expressed in more prominent patterns of pink noise, is related to performance level (e.g., Wijnants et al., 2009; Den Hartigh et al., 2015; Nourrit-Lucas et al., 2015). For instance, Den Hartigh et al. (2015) found that high-skilled rowers demonstrate more prominent patterns of pink noise in their ergometer strokes than lower-skilled rowers. Furthermore, Wijnants et al. (2009) showed increased pink noise scaling when participants became trained in a simple back-and-forth movement task on a tablet. In terms of metastability, this relates to the idea that experts can adapt their movements efficiently to environmental changes (Seifert et al., 2013). More specifically, due to the abundance of motor solutions, and thereby the variability of the movements (Latash, 2012), expert motor systems may smoothly switch between different movement patterns (Kiefer et al., 2018).

In line with the interest in improving complexity (e.g., Schöllhorn et al., 2012; Almurad et al., 2018; Hill et al., 2020a), we tested whether a training program based on differential learning has, in contrast to classical learning, beneficial effects on the complexity of motor performance. Congruent with our hypothesis, we found that only differential training led to more prominent patterns of pink noise from baseline to posttest. Thus, contrary to classical learning, a differential learning program appears to increase complexity in cyclic motor performance. These results support our idea that differential learning aids in the self-organization of metastable states. Relatedly, this type of learning has previously been described as a self-organization training method (Gray, 2020).

Given the positive relation between complexity and resilient motor performance, and the beneficial effects of differential learning on complexity, a positive effect of differential learning on resilient performance was to be expected. It was, however, unanticipated that the effects of classical learning were stronger than the differential learning effects. A possible explanation for this finding is that we used a relatively simple motor task. Differential learning typically allows an individual to gain information about the entire task solution space. Tasks that require, or benefit from, the exploration of a multitude of (creative) solutions may therefore be most appropriate for a differential learning program (e.g., Santos et al., 2018). This resonates with the beneficial effects of differential learning as demonstrated in more ecological and complex tasks, such as playing soccer (Schöllhorn et al., 2006, 2012; Santos et al., 2018; Gaspar et al., 2019) speed skating (Savelsbergh et al., 2010), and playing baseball (Gray, 2020). Hence, classical training may have its benefits when there are fewer degrees of freedom in finding appropriate solutions. This idea was supported by our finding that the beneficial effects of classical training were particularly apparent in Experiment 1 that focused on maintaining the same movement pattern, compared to Experiment 2 that required finding new movement patterns every minute.

Limitations and Future Directions

The task that we used was suitable for determining complexity based on the noise patterns in the between-box movement intervals. Indeed, much research has demonstrated that cyclical movements without external perturbations lend themselves well for the analysis of temporal structures of variation (e.g.,

Goldberger et al., 2002; Wijnants et al., 2009, 2012; Den Hartigh et al., 2015). However, as noted above, it is questionable whether such a task also lends itself well to reveal the possible benefits of differential learning, at least when taking resilient motor performance as an outcome variable. Future research may therefore try to extend the design of the current study to more complex cyclical movement patterns (e.g., rowing, see Den Hartigh et al., 2015, 2018). Extensions to other contexts involving more degrees of freedom are also interesting, provided that they allow the measurement of complexity and the inducement (or determination) of perturbations while performing.

Another avenue for future research is to test different self-organization training methods to improve complexity and resilience (Gray, 2020). An interesting candidate in this light is the constraints-led approach (Davids et al., 2008; Renshaw et al., 2010). In accordance with differential learning, the development of metastable states is a primary aim of this approach. However, instead of adding mere noise like in differential learning, specific task constraints are manipulated to explore the metastable region of the task space. As an illustration, a differential learning approach in boxing would consist of adding noise to the way in which an individual would punch another person, or a bag. A constraint-led approach for boxing was investigated by Hristovski et al. (2006). They manipulated for instance the distance between a boxer and another person or a punching bag. While a very close or far distance primarily affords a specific type of action (e.g., an uppercut or jab), a particular in-between distance would allow boxers to flexibly switch between actions. Training at this "edge of instability" could thereby aid in the development of adaptability of the movement system.

CONCLUSION

In the current study, we aimed to connect some interesting dots on the complexity of human motor performance. Because complexity provides a system with both robustness and adaptability (Delignières and Marmelat, 2013; Almurad et al., 2018), a plausible hypothesis is that a complex system demonstrates resilience. We indeed found that individuals who revealed more prominent patterns of pink noise in their movement patterns, demonstrated better resilient performance, whether they had to adapt to brief (Experiment 1) or prolonged perturbations (Experiment 2). Furthermore, the level of complexity improved through differential learning, which is assumed to foster the development of metastable states that may improve the adaptation to perturbations. However, in our specific task classical training had more beneficial effects on resilient motor performance than differential training. To conclude, although complexity may, in general, be key for a system to adapt to stressors or perturbations while performing, an important question remains how the system can be optimally trained to respond to perturbations in different types of movement tasks.

DATA AVAILABILITY STATEMENT

The datasets and scripts used for this study can be found in the Dataverse repository: doi: 10.34894/1MXM2L.

ETHICS STATEMENT

The protocol of the study was reviewed and approved by the Ethics Committee of Psychology, University of Groningen. The participants provided their written informed consent to participate in this study.

AUTHOR CONTRIBUTIONS

RD and YH developed the theoretical framework. RD, SO, and ZG prepared the experiments. SO and ZG collected the data of the experiments. RD, YH, SO, and ZG performed the data analysis, drafted the article, approved the article to be published, and agreed to be accountable for all aspects of the conducted work. All authors contributed to the article and approved the submitted version.

ACKNOWLEDGMENTS

We thank Remco Willemsen for constructing the device, and Oliver Holder for developing the software for our research.

SUPPLEMENTARY MATERIAL

The Supplementary Material for this article can be found online at: https://www.frontiersin.org/articles/10.3389/fnhum.2021.715375/full#supplementary-material

REFERENCES

Almurad, Z. M., Roume, C., Blain, H., and Delignières, D. (2018). Complexity matching: restoring the complexity of locomotion in older people through arm-in-arm walking. *Front. Physiol.* 9:1766. doi: 10.3389/fphys.2018.01766

Beek, P. J., Peper, C. E., and Stegeman, D. F. (1995). Dynamical models of movement coordination. *Hum. Mov. Sci.* 14, 573–608. doi: 10.1016/0167-9457(95)00028-5

Carver, C. S. (1998). Resilience and thriving: issues, models, and linkages. *J. Soc. Issues* 54, 245–266. doi: 10.1111/j.1540-4560.1998.tb01217.x

Davids, K., Button, C., and Bennett, S. (2008). *Dynamics of Skill Acquisition: A Constraints-Led Approach*. Champaign, IL: Human Kinetics.

Davids, K., Glazier, P., Araújo, D., and Bartlett, R. (2003). Movement systems as dynamical systems: the functional role of variability and its implications for sports medicine. *Sports Med.* 33, 245–260. doi: 10.2165/00007256-200333040-00001

Davids, K., Hristoviski, R., Araújo, D., Balaque-Serre, N., Button, C., and Passos, P. (2014). *Complex Systems in Sport*. London: Routledge.

Delignières, D., and Marmelat, V. (2013). Degeneracy and long-range correlations. *Chaos* 23:043109. doi: 10.1063/1.4825250

Delignières, D., Ramdani, S., Lemoine, L., Torre, K., Fortes, M., and Ninot, G. (2006). Fractal analyses for 'short' time series: a re-assessment of classical methods. *J. Math. Psychol.* 50, 525–544. doi: 10.1016/j.jmp.2006.07.004

Den Hartigh, R. J. R., Cox, R. F. A., Gernigon, C., Van Yperen, N. W., and Van Geert, P. L. C. (2015). Pink noise in rowing ergometer performance and the role of skill level. *Motor Control* 19, 355–369. doi: 10.1123/mc.2014-0071

Den Hartigh, R. J. R., Marmelat, V., and Cox, R. F. A. (2018). Multiscale coordination between athletes: complexity matching in ergometer rowing. *Hum. Mov. Sci.* 57, 434–441. doi: 10.1016/j.humov.2017.10.006

Diniz, A., Wijnants, M. L., Torre, K., Barreiros, J., Crato, N., Bosman, A. M., et al. (2011). Contemporary theories of 1/f noise in motor control. *Hum. Mov. Sci.* 30, 889–905.

Gaspar, A., Santos, S., Coutinho, D., Gonçalves, B., Sampaio, J., and Leite, N. (2019). Acute effects of differential learning on football kicking performance and in countermovement jump. *PLoS One* 14:e0224280. doi: 10.1371/journal.pone.0224280

Goldberger, A. L., Amaral, L. A., Hausdorff, J. M., Ivanov, P. C., Peng, C. K., and Stanley, H. E. (2002). Fractal dynamics in physiology: alterations with disease and aging. *Proc. Natl. Acad. Sci. U.S.A.* 99, 2466–2472. doi: 10.1073/pnas.012579499

Gray, R. (2020). Comparing the constraints led approach, differential learning and prescriptive instruction for training opposite-field hitting in baseball. *Psychol. Sport Exerc.* 51:101797. doi: 10.1016/j.psychsport.2020.101797

Hausdorff, J. M. (2009). Gait dynamics in Parkinson's disease: common and distinct behavior among stride length, gait variability, and fractal-like scaling. *Chaos* 19:026113. doi: 10.1063/1.3147408

Hausdorff, J. M., Edelberg, H. K., Mitchell, S. L., Goldberger, A. L., and Wei, J. Y. (1997a). Increased gait unsteadiness in community-dwelling elderly fallers. *Arch. Phys. Med. Rehabil.* 78, 278–283. doi: 10.1016/s0003-9993(97)90034-4

Hausdorff, J. M., Mitchell, S. L., Firtion, R., Peng, C. K., Cudkowicz, M. E., Wei, J. Y., et al. (1997b). Altered fractal dynamics of gait: reduced stride-interval correlations with aging and Huntington's disease. *J. Appl. Physiol.* 82, 262–269. doi: 10.1152/jappl.1997.82.1.262

Hill, Y., Den Hartigh, R. J. R., Cox, R. F. A., De Jonge, P., and Van Yperen, N. W. (2020a). Predicting resilience losses in dyadic team performance. *Nonlinear Dynamics Psychol. Life Sci.* 24, 327–351.

Hill, Y., Den Hartigh, R. J. R., Meijer, R. R., De Jonge, P., and Van Yperen, N. W. (2018a). Resilience in sports from a dynamical perspective. *Sport Exerc. Perform. Psychol.* 7, 333–341. doi: 10.1037/spy0000118

Hill, Y., Den Hartigh, R. J. R., Meijer, R. R., De Jonge, P., and Van Yperen, N. W. (2018b). The temporal process of resilience. *Sport Exerc. Perform. Psychol.* 7, 363–370.

Hill, Y., Van Yperen, N. W., and Den Hartigh, R. J. R. (2020b). Facing repeated stressors in a motor task: does it enhance or diminish resilience? *J. Mot. Behav.* 24, 1–10. doi: 10.1080/00222895.2020.1852155

Hosseini, S., Barker, K., and Ramirez-Marquez, J. E. (2016). A review of definitions and measures of system resilience. *Reliab. Eng. Syst. Safe* 145, 47–61. doi: 10.1016/j.ress.2015.08.006

Hristovski, R., Davids, K., Araújo, D., and Button, C. (2006). How boxers decide to punch a target: emergent behaviour in nonlinear dynamical movement systems. *J. Sports Sci. Med.* 5, 60–73.

Kello, C. T., Beltz, B. C., Holden, J. G., and Van Orden, G. C. (2007). The emergent coordination of cognitive function. *J. Exp. Psychol. Gen.* 136, 551–568. doi: 10.1037/0096-3445.136.4.551

Kelso, J. A. S. (1995). *Dynamic Patterns: The Self-Organization of Brain and Behavior*. Cambridge, MA: MIT Press.

Kiefer, A. W., and Myer, G. D. (2015). Training the antifragile athlete: a preliminary analysis of neuromuscular training effects on muscle activation dynamics. *Nonlinear Dynamics Psychol. Life Sci.* 19, 489–510.

Kiefer, A. W., Silva, P. L., Harrison, H. S., and Araújo, D. (2018). Antifragility in sport: leveraging adversity to enhance performance. *Sport Exerc. Perform. Psychol.* 7, 342–350. doi: 10.1037/spy0000130

Latash, M. L. (2012). The bliss (not the problem) of motor abundance (not redundancy). *Exp. Brain Res.* 217, 1–5. doi: 10.1007/s00221-012-3000-4

Lipsitz, L. A., and Goldberger, A. L. (1992). Loss of'complexity'and aging: potential applications of fractals and chaos theory to senescence. *J. Am. Med. Assoc.* 267, 1806–1809. doi: 10.1001/jama.1992.03480130122036

Liu, R., Chen, P., Aihara, K., and Chen, L. (2015). Identifying early-warning signals of critical transitions with strong noise by dynamical network markers. *Sci. Rep.* 5:17501.

Luthar, S. S., Cicchetti, D., and Becker, B. (2000). The construct of resilience: a critical evaluation and guidelines for future work. *Child Dev.* 71, 543–562. doi: 10.1111/1467-8624.00164

Marmelat, V., and Delignières, D. (2012). Strong anticipation: complexity matching in interpersonal coordination. *Exp. Brain Res.* 222, 137–148. doi: 10.1007/s00221-012-3202-9

Masten, A. S. (2001). Ordinary magic: resilience processes in development. *Am. Psychol.* 56, 227–238. doi: 10.1037/0003-066x.56.3.227

Nourrit-Lucas, D., Tossa, A. O., Zélic, G., and Delignières, D. (2015). Learning, motor skill, and long-range correlations. *J. Mot. Behave.* 47, 182–189. doi: 10.1080/00222895.2014.967655

Peng, C. K., Mietus, J., Hausdorff, J. M., Havlin, J. M., Stanley, H. E., and Goldberger, A. L. (1993). Long-range anticorrelations and non-gaussian behavior of the heartbeat. *Phys. Rev. Lett.* 70:1343. doi: 10.1103/physrevlett.70.1343

Pincus, D., and Metten, A. (2010). Nonlinear dynamics in biopsychosocial resilience. *Nonlinear Dynamics Psychol. Life Sci.* 14, 353–380.

Renshaw, I., Chow, J. Y., Davids, K., and Hammond, J. (2010). A constraints-led perspective to understanding skill acquisition and game play: a basis for integration of motor learning theory and physical education praxis? *Phys. Educ. Sport Pedagogy* 15, 117–137. doi: 10.1080/17408980902791586

Riley, M. A., and Turvey, M. T. (2002). Variability and determinism in motor behavior. *J. Mot. Behav.* 34, 99–125. doi: 10.1080/00222890209601934

Santos, S., Coutinho, D., Gonçalves, B., Schöllhorn, W., Sampaio, J., and Leite, N. (2018). Differential learning as a key training approach to improve creative and tactical behavior in soccer. *Res. Q. Exerc. Sport* 89, 11–24. doi: 10.1080/02701367.2017.1412063

Savelsbergh, G. J., Kamper, W. J., Rabius, J., De Koning, J. J., and Schöllhorn, W. (2010). A new method to learn to start in speed skating: a differencial learning approach. *Int. J. Sport Psychol.* 41, 415–427.

Schöllhorn, W. I., Beckmann, H., and Davids, K. (2010). Exploiting system fluctuations. differential training in physical prevention and rehabilitation programs for health and exercise. *Medicina* 46, 365–373. doi: 10.3390/medicina46060052

Schöllhorn, W. I., Beckmann, H., Michelbrink, M., Sechelmann, M., Trockel, M., and Davids, K. (2006). Does noise provide a basis for the unification of motor learning theories? *Int. J. Sport Psychol.* 37, 186–206.

Schöllhorn, W. I., Hegen, P., and Davids, K. (2012). The nonlinear nature of learning-a differential learning approach. *Open Sports Sci. J.* 5, 100–112. doi: 10.2174/1875399x01205010100

Schöllhorn, W. I., Mayer-Kress, G., Newell, K. M., and Michelbrink, M. (2009). Time scales of adaptive behavior and motor learning in the presence of stochastic perturbations. *Hum. Mov. Sci.* 28, 319–333. doi: 10.1016/j.humov.2008.10.005

Seifert, L., Button, C., and Davids, K. (2013). Key properties of expert movement systems in sport. *Sports Med.* 43, 167–178. doi: 10.1007/s40279-012-0011-z

Smith, B. W., Dalen, J., Wiggins, K., Tooley, E., Christopher, P., and Bernard, J. (2008). The brief resilience scale: assessing the ability to bounce back. *Int. J. Behav. Med.* 15, 194–200. doi: 10.1080/10705500802222972

Stanley, H. E., Buldyrev, S. V., Goldberger, A. L., Hausdorff, J. M., Havlin, S., Mietus, J., et al. (1992). Fractal landscapes in biological systems: Long-range correlations in DNA and interbeat heart intervals. *Physica A* 191, 1–12. doi: 10.1016/0378-4371(92)90497-e

Stergiou, N., and Decker, L. M. (2011). Human movement variability, nonlinear dynamics, and pathology: is there a connection? *Hum. Mov. Sci.* 30, 869–888. doi: 10.1016/j.humov.2011.06.002

Thelen, E., Kelso, J. A. S., and Fogel, A. (1987). Self-organizing systems and infant motor development. *Dev. Rev.* 7, 39–65. doi: 10.1016/0273-2297(87)90004-9

Van Emmerik, R. E., and Van Wegen, E. E. (2000). On variability and stability in human movement. *J. Appl. Biomech.* 16, 394–406. doi: 10.1123/jab.16.4.394

Wijnants, M. L., Bosman, A. M., Hasselman, F., Cox, R. F. A., and Van Orden, G. (2009). 1/f scaling in movement time changes with practice in precision aiming. *Nonlinear Dynamics Psychol. Life Sci.* 13, 75–94.

Wijnants, M. L., Cox, R. F. A., Hasselman, F., Bosman, A. M. T., and Van Orden, G. (2012). A trade-off study revealing nested timescales of constraint. *Front. Physiol.* 3:116. doi: 10.3389/fphys.2012.00116

Conflict of Interest: The authors declare that the research was conducted in the absence of any commercial or financial relationships that could be construed as a potential conflict of interest.

frontiers in Human Neuroscience

HYPOTHESIS AND THEORY
published: 03 September 2021
doi: 10.3389/fnhum.2021.719388

Why Firing Rate Distributions Are Important for Understanding Spinal Central Pattern Generators

Henrik Lindén† *and Rune W. Berg**†

Department of Neuroscience, Faculty of Health and Medical Sciences, University of Copenhagen, Copenhagen, Denmark

Networks in the spinal cord, which are responsible for the generation of rhythmic movements, commonly known as central pattern generators (CPGs), have remained elusive for decades. Although it is well-known that many spinal neurons are rhythmically active, little attention has been given to the distribution of firing rates across the population. Here, we argue that firing rate distributions can provide an important clue to the organization of the CPGs. The data that can be gleaned from the sparse literature indicate a firing rate distribution, which is skewed toward zero with a long tail, akin to a normal distribution on a log-scale, i.e., a "log-normal" distribution. Importantly, such a shape is difficult to unite with the widespread assumption of modules composed of recurrently connected excitatory neurons. Spinal modules with recurrent excitation has the propensity to quickly escalate their firing rate and reach the maximum, hence equalizing the spiking activity across the population. The population distribution of firing rates hence would consist of a narrow peak near the maximum. This is incompatible with experiments, that show wide distributions and a peak close to zero. A way to resolve this puzzle is to include recurrent inhibition internally in each CPG modules. Hence, we investigate the impact of recurrent inhibition in a model and find that the firing rate distributions are closer to the experimentally observed. We therefore propose that recurrent inhibition is a crucial element in motor circuits, and suggest that future models of motor circuits should include recurrent inhibition as a mandatory element.

Keywords: spinal cord, central pattern generation, firing rate distribution, motor control, balanced network, lognormal

OPEN ACCESS

Edited by:
Marco Iosa,
Sapienza University of Rome, Italy

Reviewed by:
Yury Ivanenko,
Santa Lucia Foundation (IRCCS), Italy
Renato Naville Watanabe,
Federal University of ABC, Brazil

****Correspondence:***
Rune W. Berg
runeb@sund.ku.dk

†These authors have contributed equally to this work

Specialty section:
This article was submitted to Motor Neuroscience, a section of the journal Frontiers in Human Neuroscience

Received: *02 August 2021*
Accepted: *02 June 2021*
Published: *03 September 2021*

Citation:
Lindén H and Berg RW (2021) Why Firing Rate Distributions Are Important for Understanding Spinal Central Pattern Generators. Front. Hum. Neurosci. 15:719388. doi: 10.3389/fnhum.2021.719388

1. INTRODUCTION

Although it is known that the core neural elements of rhythmic movement, the central pattern generators (CPGs), are located in the spinal cord and the medulla, the neuronal architecture of these networks has remained perplexing. Several working hypotheses for the principle behind generation of movements have been proposed, e.g., muscle synergy and traveling wave (Cuellar et al., 2009; Saltiel et al., 2016, 2017; Yokoyama et al., 2017), multiple unit burst generators (Grillner, 1981), and multilayered half-center organization CPG (Ivanenko et al., 2006; McCrea and Rybak, 2008). A common theme in the literature is the half-center organization inspired by Brown (1914), where two rhythm generating modules, which have recurrent excitation, are coupled reciprocally via inhibitory populations to ensure an alternating flexor and extensor activity (McLean and Dougherty, 2015; Kiehn, 2016; Grillner and El Manira, 2020). Using optogenetics and light activation or inhibition of spatially restricted regions in the spinal cord it was possible to

exclusively activate either flexor or extensor rhythms suggesting a modular organization (Hägglund et al., 2013). A modular organization has also been suggested based on analysis of rodent gaits and cellular ablation (Bellardita and Kiehn, 2015) and gaits of human infants (Sylos-Labini et al., 2020). It has been widely suggested that the rhythm generating modules are composed of a recurrently connected excitatory networks, where the rhythm is generated by a subset of neurons with pacemaker properties (Grillner and El Manira, 2020). Nevertheless, modular structures has been difficult to further isolate experimentally (Auyong et al., 2011a,b), and many circuit elements seem to be involved (McLean et al., 2008; Pham et al., 2020) and therefore the details of their architecture, e.g., whether they indeed are composed of recurrent excitation, have been difficult to substantiate. From a stability point of view, however, it is well-known that a population of recurrently connected excitatory neurons without inhibitory interneurons have a propensity to increase their activity in a catastrophic runaway manner (Hennequin et al., 2017; Berg et al., 2019). So, what decides if a network is stable and would a network composed purely of recurrent excitation be sensible for generation of motor activity?

2. RECURRENT NETWORKS: STABLE OR UNSTABLE?

There are many different types of network structures, and the topology of a network determines its stability. This is especially true for recurrent excitatory networks, since activity can create more activity in reverberation and runaway activity. However, recurrent excitatory networks can also become completely silent. So, what decides the stability of an recurrent excitatory network? We may gain some intuition by viewing the recurrent network as a tree-like structure with feed-forward motifs (**Figure 1**). The overall topology can be approximated as a tree-like network, also termed a branch–process, which is simpler to understand. This tree-like assumption has been shown to be a good approximation for many types of real recurrent networks (Melnik et al., 2011).

Branching processes was first studied by Galton and Watson without relation to neuroscience, but in regards to extinction of aristocratic families, passing down family names from one generation to the next (Watson and Galton, 1875). Another example of branching processes is nuclear chain reactions. Fission is utilized in nuclear power plants, and this process also has a tree-like structure. Keeping the reaction going requires careful regulation between activity and curbing the fission process.

The activity that propagates in a tree-like network can either be subcritical (left, **Figure 1**), critical (middle) or supercritical (right). Whether a network is sub-critical or supercritical depends on the so-called the "branching ratio," i.e., the expected number of action potentials in the receiver population that an action potential induces. If the branching ratio is below 1, the neuronal activity will rapidly die out (subcritical). If the branching ratio is above 1, it will rapidly increase with exponential growth until the whole population is active (supercritical). If the network is critical, i.e., between sub- and supercritical, there is a simple power-law relation between the number of activated neurons, n, i.e., the size of an avalanche, and the probability (Beggs and Plenz, 2003; Larremore et al., 2014):

$$p(n) \propto n^{-3/2}$$

For activity to be between silence and runaway activity, i.e., the critical propagation, the branching ratio has to be exactly 1 (Beggs and Plenz, 2003), which makes it unlikely that the network is in a critical state by accident. Rather it likely has some self-organization toward a critical states in order to possess this property (Hesse and Gross, 2014; Rybarsch and Bornholdt, 2014). If there is no such self-organization, the network is expected to be either subcritical (quiescent) or supercritical i.e., activity is rapidly propagating throughout the whole population.

So, are CPG modules subcritical or supercritical? Since the neural activity in subcritical networks rapidly dyes out and remain silent, supercritical networks must constitute the basis for rhythm generation in spinal circuits. Spinal motor circuits may involve multiple modules and layers. To keep things simple, let us imagine a simple half-center model that is composed of two supercritical modules with reciprocal inhibition (**Figure 2A**). When one module becomes active, the network first undergoes a runaway escalation of firing rates where excitation rapidly propagation throughout the network. We consider this "the exponential phase" (**Figures 2B,C**). Once the whole population is reverberating, the neurons reach their maximum firing rates, and the distribution of firing rates become narrow at the highest possible value. In this saturated phase, adaptation starts to be engaged, e.g., via accumulation of intracellular calcium+, and the firing rates drops back down to zero. After some time, the neurons recover and the cycle can start over. Now we have gained an intuition of the basic principle of recurrent excitatory networks, let us examine how the peak firing rates would be distributed in a network-based model of a half-center module.

3. DYNAMICS OF A RECURRENT EXCITATORY NETWORK

In the following we consider a minimal network of recurrently connected excitatory neurons. Let us assume that the excitatory neurons are recurrently connected by synapses which have a wide distribution (and no negative strengths; **Figure 3A**). The synaptic connection strengths are randomly drawn from this distribution resulting in a connectivity matrix (**Figure 3B**). If the overall strength of recurrent connections is strong enough the network becomes super-critical, so that a very small amount of spontaneous activity or external activation will result in a burst of neuronal activity. In such a burst all neurons fire at the maximum firing rate in a synchronized manner when provided by different external drives (**Figures 3C,D**). After a short time intrinsic adaptation in the neurons becomes active to suppress and ultimately terminate the population burst (**Figure 3D**, gray traces). The adaptation is also the reason that the network response is shorter than the input pulse (cf. **Figures 3C,D**). An important aspect with this cyclic activity is that the firing

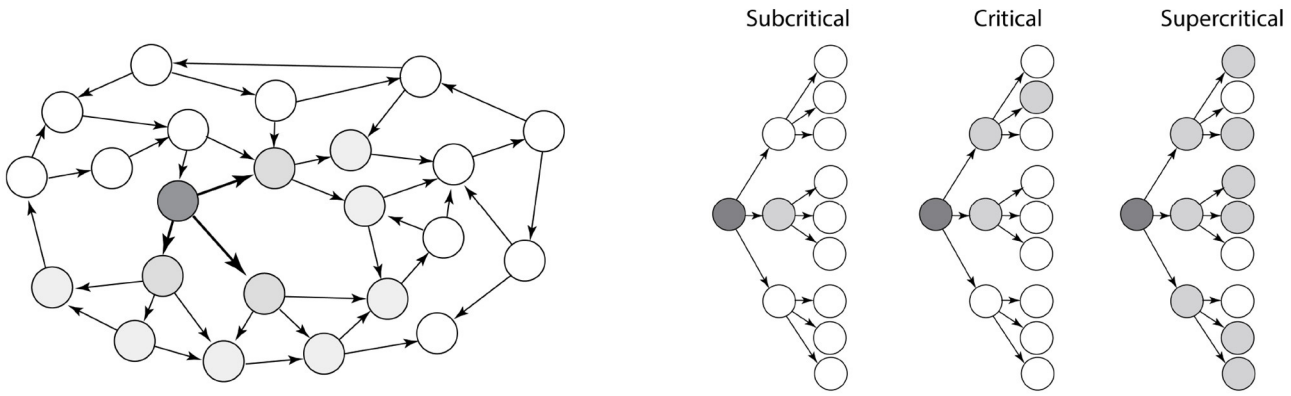

FIGURE 1 | Dynamics of a recurrent excitatory network. **(Left)** A recurrent excitatory network often has embedded tree-like structures, e.g., the dark nodes. **(Right)** The stability of networks with tree-like structure are more simple to characterize. They are either subcritical (left), critical (middle), or supercritical (right). Activity in supercritical networks are unstable and will activate the entire network as exponential growth, whereas the activity in subcritical networks will decay exponentially. Adapted with permission from Larremore et al. (2014).

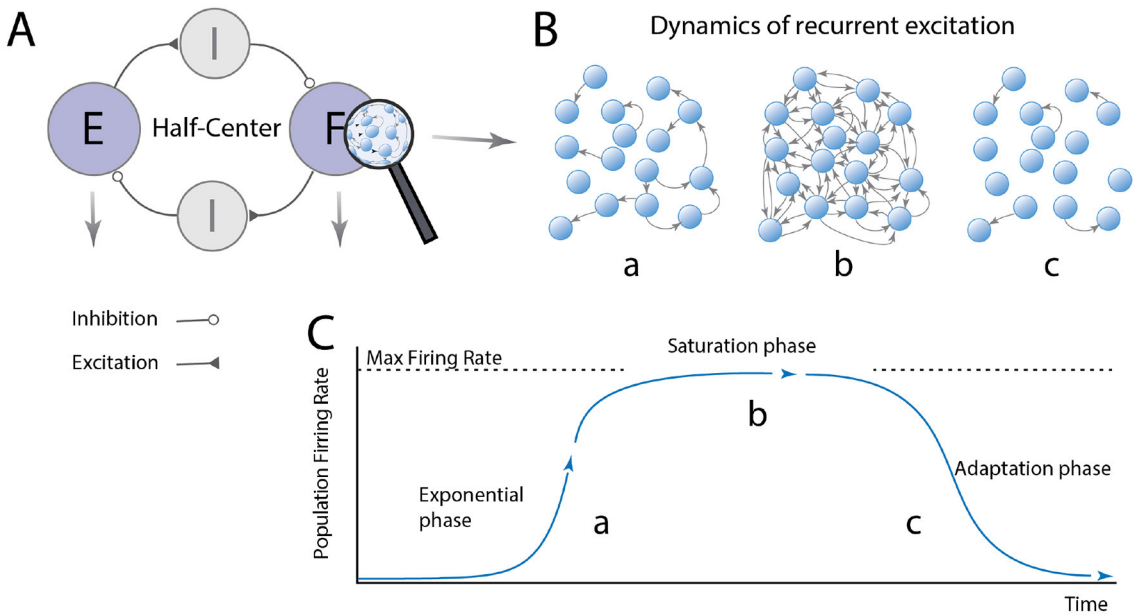

FIGURE 2 | The dynamics of a burst-generator module has 3 phases. **(A)** The half-center organization consists of modules: flexor (F) and extensor (E) modules, which generate rhythmic bursting activity and these are reciprocally connected via inhibitory modules to ensure F/E alternation. **(B,C)** The F/E modules are composed of excitatory neurons with pacemaker properties, which are recurrently connected. The module has three phases: (a) When a neuron fire action potentials (arrows) these quickly activate other neurons, since it is supercritical, resulting in an exponential increase in the network activity. More activity leads to more spikes activating more neurons. Once the activity has propagated to the whole network, the neurons reach their max firing rate the network reach saturation (phase b). Shortly there after the adaptation/pacemaker property turns off the firing in the adaptation phase c, and the activity decay back toward quiescence. During the adaptation phase the quiescence also cease the inhibition to the opposite module, allowing a similar cycle to take place there with a delay. Hence, the population alternates between quiescence and maximal firing rates for all the cells in the module.

rate of the constituent neurons reach their peak firing rates simultaneously, and therefore the distribution of rates across the population is narrow and clustered around the maximum (**Figures 3E,F**). Hence, if this model is meaningful, it should be relatively easy to verify whether a rhythm—generating module is composed of excitatory recurrent connections by observing the distribution of firing rates across the population and identify those neurons who display a high peak firing rate. Surprisingly, however, the distribution of firing rates have rarely been reported neither in experimental studies nor in theoretical investigations of spinal motor circuits. As we will see next, however, the few experimental observations of firing rate distributions do not seem to be in accord with a high and narrow distribution of firing rates.

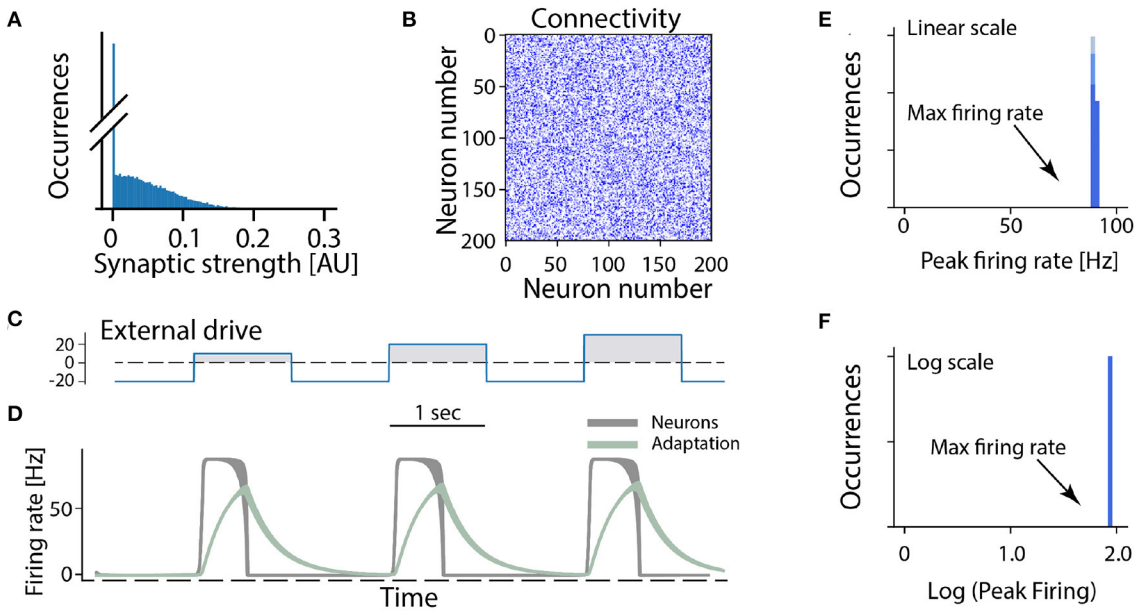

FIGURE 3 | All-or-none behavior of recurrent excitatory networks: model. **(A)** Distribution of synaptic strengths in the model is a truncated Gaussian, with many having zero (no connection). **(B)** Connectivity matrix of the non-zero connections in the network composed of 200 excitatory neurons. **(C)** The external drive to the network has to be kept negative (inhibitory) to keep it silent because the network is unstable (supercritical). Positive pulses was given with increasing amplitude imitating a rhythmic drive. **(D)** The firing rate of the neuronal population (gray overlay) has a prompt increase to maximal firing once the external drive becomes positive. Intrinsic adaptation (green traces) curbs the activity and turns the firing off after some time. Note the population firing is at maximum regardless of input size. **(E,F)** The linear and log distributions of peak firing rates across population have a single mode at maximal firing (arrows) regardless of the input.

4. EXPERIMENTALLY OBSERVED FIRING RATE DISTRIBUTIONS

Our survey of the literature provides two observations: First, a distribution of firing rates across neuronal population has rarely been reported (Petersen and Berg, 2016; Cuellar et al., 2018). Second, those experimental reports that do provide the firing rate distribution, they seem in impressive agreement. The precise firing rates vary from experiment to experiment and region to region, but their distributions all seem to have the same long-tail and skewness toward zero. Spinal interneuronal recordings from cervical CPG of the mudpuppy (**Figure 4A**), show rhythmic (black) and nonrhythmic discharging units during locomotion, both types have distributions lopsided toward the origin. Recordings from the spinal cord in awake macaque monkeys, which were trained to perform visually guided flexion and extension of their wrist in an active ramp provided similar insight (**Figure 4B**). During both flexion (left) and extension (inset) the distribution of firing rates of interneurons in the cervical spine had a strong skewness toward origin qualitatively similar to the mudpuppy data, in spite of their differences in species and motor function. Interneuronal recording from respiratory motor circuitry in the thoracic spinal cord of cats also provided insight to firing rate distributions in motor circuitry (**Figure 4C**). Left column: inspiratory interneurons, right column: expiratory interneurons. Top: identified by antidromic stimulation, bottom both antidromic and by location, white and hatched, respectively. Last, recordings from the lumbar spinal cord of turtle during scratching had skewed firing rate distribution, that closely resembles a log-normal distribution (blue fit, **Figure 4D**), i.e., normally distributed on a log-scale (inset). It is unknown whether the exact shape of the distribution is best described by a log-normal distribution or other skewed distributions, e.g., the gamma-distribution.

Due to the rareness of experimental reports, we include and analyze a data set from zebrafish larvae during active locomotion in response to visual input, that was kindly made available (Severi et al., 2018). It is known that inhibitory interneuron V1 and V2b provide feedback inhibition (Callahan et al., 2019; Sengupta et al., 2021) most notably via Renshaw cells. In this preparation it is possible to record the fluorescent signal from a genetically encoded calcium sensor (GCaMP5G), which is expressed in glycinergic interneurons by the domain for expression of the transcription factor "engrailed1b," which is highly correlated with the onset of locomotion. The fluorescent signal in these inhibitory neurons is an indication of the degree of increase in spiking activity. Hence, using the maximal fluorescent signal across the population, we found the distribution to be skewed, remarkably close to a log-normal (**Figure 5**). The distribution of fluorescent signal could be interpreted in various ways. First, the activity across the cells is uniform, but the distribution of soma size—hence the fluorescent signal—could be log-normal, although the cells have equal firing rates. Second, the cell

size if normally distributed, but their firing rates are log-normally distribution, hence giving a fluorescent signal with a skewed distribution. The increase in fluorescent signal may not ad linearly, as the spiking activity increases. Nevertheless, the observation of a skewed distribution (**Figure 5**) appear in accord with the previous observation and the most parsimonious explanation is that the neurons has a log-normal distribution of firing rates (blue fit, **Figure 4**).

In summary, the meta-analysis indicates a profile of activity across the population, which is skewed toward zero, with a long tail toward higher firing rates. This is at odds with the prediction from a recurrent excitatory network as a driver, where the firing rates should cluster around the maximal firing rate and zero. What could explain this apparent lack of congruence between the conventional model and experimental data?

5. COULD RECIPROCAL INHIBITION HELP?

One of the cornerstones of the half-center organization is reciprocal inhibition. Could reciprocal inhibition help stabilize the firing rates so the population does not switch between silence and maximal firing? The short answer is "no." Reciprocal inhibition exerts its effect on the antagonist module, which is either already silent, or will become silent once the reciprocal inhibition performs its action. When the activity of the antagonistic module is reduced or completely silent, the returning reciprocal inhibition is also reduced or silent. Hence, reciprocal inhibition actually causes mutual dis-inhibition, which is, in effect, positive feedback. Thus, the reciprocal inhibition in a half-center organization actually provides no help in dampening the firing rates, but rather makes the situation worse, by removing inhibition when it is needed.

6. INCLUSION OF RECURRENT INHIBITION

Although there are indications of a sparse connectivity in the CPG structure (Carroll and Ramirez, 2013; Radosevic et al., 2019) the architecture and connectomics of circuits generating motor programs are largely unknown. We know that reciprocal inhibition is indirectly enhancing the instability via dis-inhibition and therefore it does not provide a solution to the problem. So, what is the simplest means to remedy the divergence between these states? As it turns out, recurrent inhibition has an important element in stabilizing the spinal activity. It is known that firing rate distributions are broad for recurrent networks with a balanced between inhibition and excitation (Vogels et al., 2005; Hennequin et al., 2017) and strongly skewed (van Vreeswijk and Sompolinsky, 1996) as seen in experiments. Recurrent inhibition pulls the membrane potential to be less depolarized and in this way the neuron will spike at a lower rate. This also has the effect that more neurons fire action potentials in the fluctuation–driven regime rather than in the mean–driven regime. It is known that at least half of the neurons are active in the fluctuation driven regime during rhythmic scratching (Petersen and Berg, 2016; Berg, 2017). At the same time balanced inhibition and excitation has been observed in at least a subset of neurons in various motor networks (Berg et al., 2007; Petersen et al., 2014; Vestergaard and Berg, 2015; Ramirez and Baertsch, 2018). To illuminate this further, we expanded the model of a recurrent excitatory network presented earlier (**Figure 3**) to include recurrent inhibition, which is also known as "a balanced network." While the pure excitatory network had an all-or-none firing activity, the inclusion of recurrent inhibition to replace the role of intrinsic adaptation enriches the network with the capacity to have a graded response to an external drive (**Figure 6**). Furthermore, the firing rate distribution turns from having a single mode at the maximal firing rate (**Figures 3E,F**) to having a widely distributed peak firing across the population (**Figures 6E,F**). The distributions is also similar to those observed in experiments, i.e., skewed toward zeros with a log-normal appearance. The difference between recurrent excitatory networks and networks where recurrent inhibition is included can be summarized as: (1) the firing rate distributions are very different both in width an location of peaks. (2) the all-or-none vs. graded response to external drive (**Figure 7**).

7. BLOCKING INHIBITION MAKES THE NETWORK UNSTABLE

If recurrent inhibition is indeed a vital element of motor networks, the effect of reducing inhibition should be to increase the overall firing rates and to synchronize the spinal network. Several experiments have been performed where the effects of a systemic block of inhibition by application of either glycinergic antagonists (e.g., strychnine) or GABAergic antagonists (e.g., picrotoxin, bicuculline; Cowley and Schmidt, 1995; Beato and Nistri, 1999; Talpalar et al., 2011, 2013). The general effect is a widespread barrage of intense activity across multiple segments of the spinal cord, which was recorded via the motor nerve output. When reducing inhibition the effective branching ratio grows dramatically, i.e., the expected number of post-synaptic action potential that a presynaptic neuron will increase, and hence the network becomes highly supercritical (**Figure 1**). A seizure-like barrage of activity quickly spread throughout within milliseconds and reverberates the spinal network until some form of adaptation or fatigue turns it off. This is similar to the dynamics of a recurrent excitatory network (**Figure 3**). The activity slowly alternates between intense activity with maximal firing of individual neurons and quiescence, which represents a recovery phase.

8. DISCUSSION

In spite of the striking insight into the CPG architecture that firing rates distributions can provide, they have received remarkably little attention in the motor control literature. Other parts of neuroscience have identified distributions as an important element in theoretical neuroscience (Vegué and Roxin, 2019) and e.g., in the processing of sleep regulation (Levenstein et al., 2017) and decision making (Wohrer et al., 2013). The idea

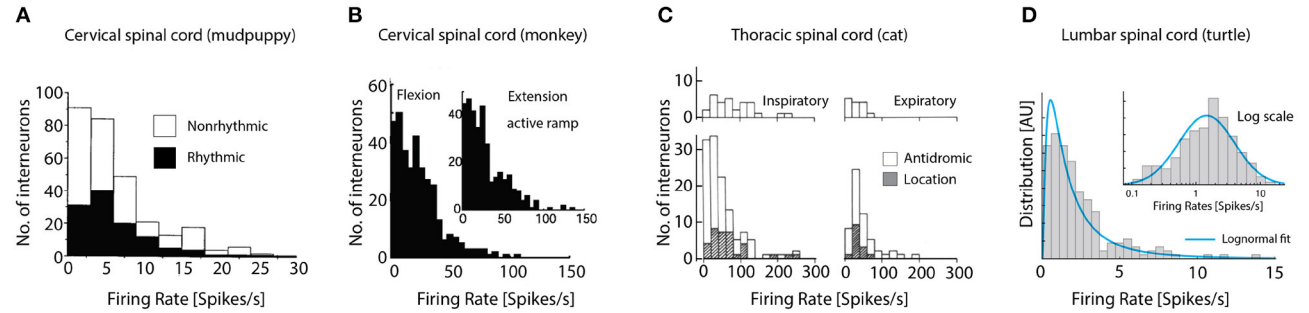

FIGURE 4 | Firing rate distributions across experimental preparations are skewed toward the origin. **(A)** The cervical CPG of the mudpuppy while performing locomotion, show rhythmic (black) and nonrhythmic discharge. **(B)** Cervical interneurons in macaque monkeys performing wrist flexion and extension. **(C)** Interneuronal recording from respiratory motor circuitry in the thoracic cord of cats. Left: inspiratory interneurons, right: expiratory interneurons. Top: identified by antidromic stimulation, bottom inclusion identification by location, white and hatched, respectively. **(D)** Lumbar spinal cord of turtle during scratching has skewed firing rate distribution (left) that is bell-shaped on log scale (blue fit). Reproduced with permission **(A)** Cheng et al. (2002), **(B)** Prut and Perlmutter (2003), **(C)** Kirkwood et al. (1988), and **(D)** Petersen and Berg (2016).

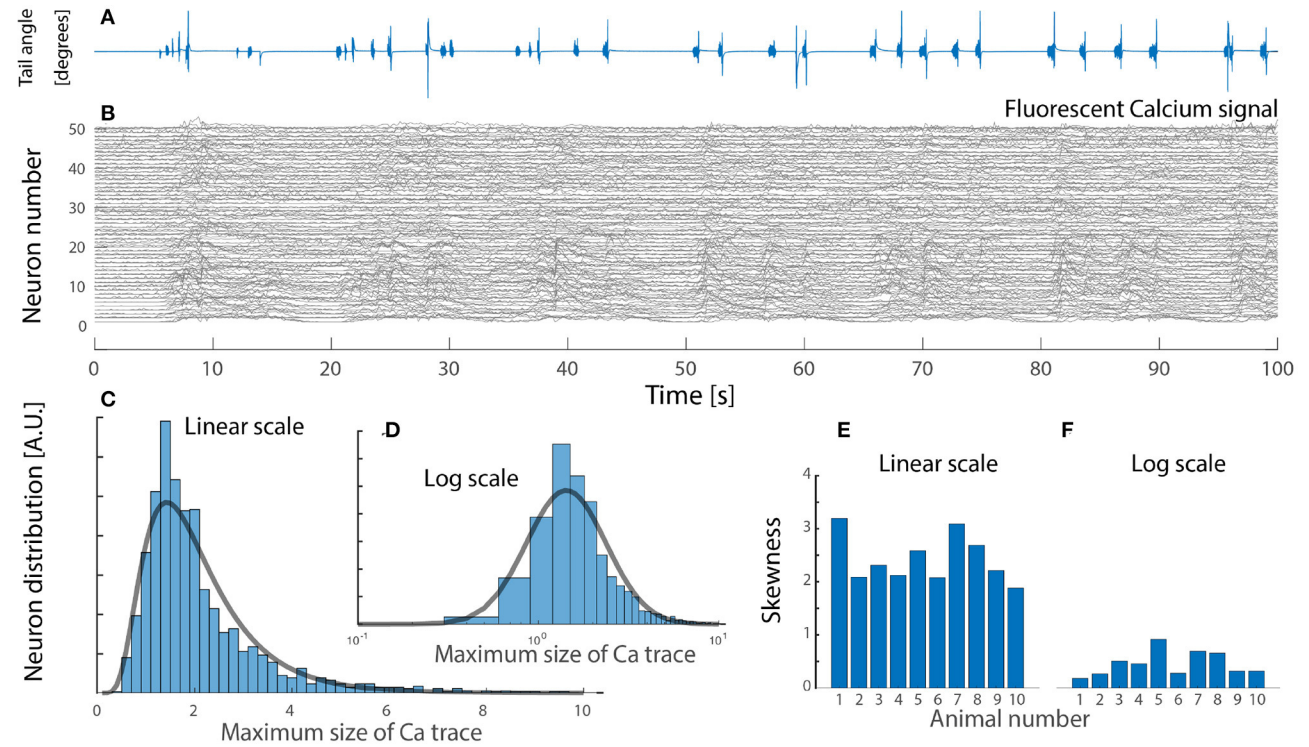

FIGURE 5 | Neuronal imaging of calcium-dependent fluorescent signal in zebrafish larvae hindbrain during visuomotor response has a skewed lognormal-like distribution in peak signal. **(A)** *In-vivo* tail-bending in response to visual input. **(B)** Fluorescent signal ($\Delta F/F$) at neuronal resolution of a glycinergic subpopulation which provide inhibitory feedback during escape response (50 cells shown). **(C)** The maximal calcium response across cells in the population is skewed and lognormal-like (lognormal fit, gray line). **(D)** Same distribution on log scale resembles a normal distribution (gray fit). **(E)** High skewness across the cohort ($n = 10$ animals). **(F)** Skewness on a log scale is closer to zero, i.e., normal distribution. Data kindly provided by Severi et al. (2018) and reanalyzed with permission.

of the "log-normal" brain is inspired by the skewed shape of the firing rate distributions (Mizuseki and Buzsáki, 2013; Buzsáki and Mizuseki, 2014).

Here, we inspect the dynamics of excitatory recurrent networks driven by an external drive. Despite the absence of experimental evidence, this type of network architecture has often been proposed to constitute a module in a half-center model or unit burst generator (McCrea and Rybak, 2008; Grillner and El Manira, 2020). Nevertheless, for a recurrent network to not be silent, it has to be supercritical. In such networks, propagation of activity is rapid due to the tree-like structure (**Figure 1**), which makes it unstable and prone to acceleration

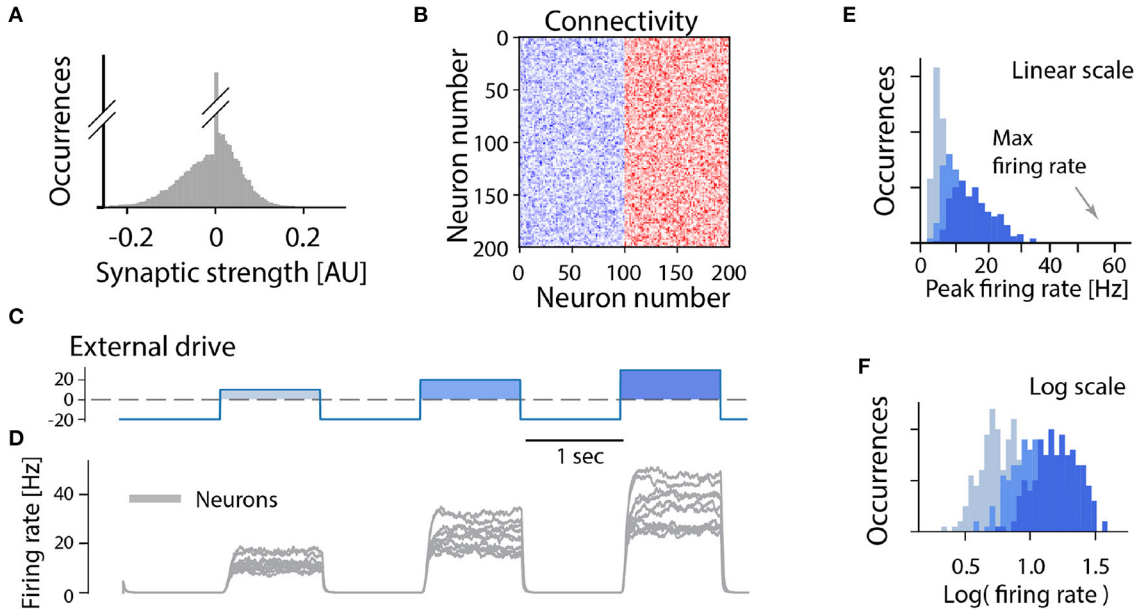

FIGURE 6 | Graded activity in a recurrent excitatory network balanced by inhibition: model. **(A)** Distribution of synaptic strengths in the model is a Gaussian, with a balance around zero. It also have many connections with zero strength (no connection). **(B)** Connectivity matrix of the non-zero connections in the network composed of 100 excitatory (blue) and 100 inhibitory (red) randomly connected neurons. **(C)** The external drive is negative (inhibitory) with positive pulses imitating a rhythmogenic input with increasing amplitude. **(D)** the firing rate of a subset of the neuronal population has diverse peak firing. **(E,F)** The linear- and log-scale distributions of peak firing rates are broad and skewed toward zero far from the maximal firing (arrow). The colors represent increasing external input, light blue: lowest, blue: middle, dark blue: largest input.

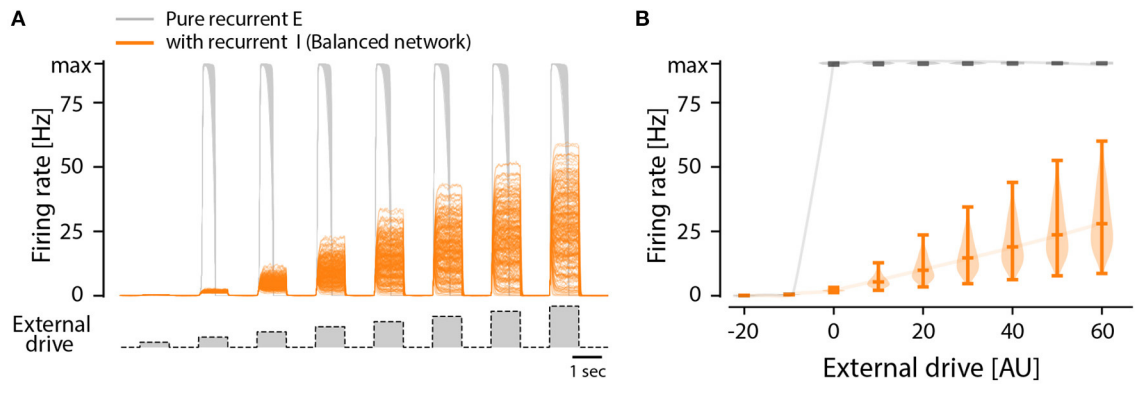

FIGURE 7 | All-or-none vs. graded population response to external drive in two types of model networks: Purely recurrent excitatory network and one including recurrent inhibition, i.e., a balanced network. **(A)** Firing rates of individual neurons in a recurrent excitatory network (gray) and a recurrent network with both excitation and inhibition (orange), i.e., a balanced network, in response to external drive (bottom trace). All neurons in the excitatory network has the same firing rate, i.e., the maximum or minimum, in response to input, whereas the balanced net has a graded mean response with a wide distribution. **(B)** The distribution of firing rates across the population in the balanced net (orange) is wide and has a graded response to input, whereas the excitatory network has an all-or-none response that is narrow.

and reverberation until all cells fire at maximal rates. This also causes recurrent excitatory networks to essentially work by all-or-none activity: Either it is silent or it has maximal activity (**Figure 7**). A consequence of this is that it does not respond in a graded fashion to various external drives and has no ability to modulate the output amplitude. This lack of flexibility seems sub-optimal given the large variety of motor task that the body needs to execute, e.g. fine motor skills vs. heavy lifting, and walking peacefully vs. carrying a large load or walking uphill. Hence there is a strong functional argument against an modular architecture of pure recurrent excitatory connectivity.

Furthermore, comparing the firing rate distributions of recurrent excitatory networks with those from experimental reports, they are incompatible: Experiments show broad distributions skewed toward very low rates, akin to a log-normal (**Figures 4**, **5**), whereas recurrent excitatory networks have a

single mode at maximal firing, or at zero (**Figures 3E,F**). A single mode at maximal firing is the exact opposite of the experimentally observed low firing with a wide skewed distribution. Hence, there are functional arguments against the hypothesis of a recurrent excitatory network as well as experimental evidence against it.

So, if there are both experimental and functional arguments against recurrent excitatory modules, what type of network architecture could constitute modules? As the most parsimonious solution, we suggest including recurrent inhibition to curb the activity. Networks that encompass both recurrent excitation and inhibition has previously been considered "heterodox" and "anarchistic" (Grillner and Jessell, 2009), but so far there are no clear experimental evidence against the presence of recurrent inhibition in motor networks. On the contrary, indications of concurrent inhibition have been observed in various medullary and spinal experiments (Ramirez and Baertsch, 2018; Berg et al., 2019). Such balanced networks are also known to have skewed firing rate distributions with low mean firing (van Vreeswijk and Sompolinsky, 1996; Petersen and Berg, 2016). Further, recurrent inhibition is certainly provided via a type of inhibitory interneuron, the Renshaw cell, which receives collateral excitatory fibers from alpha motor neurons, which it also inhibits. Although, the role of these cells is unknown, they may represent just one example of a general and widespread element of recurrent inhibition in spinal motor circuits. Due to the close proximity of Renshaw cells to motor neurons they have been easy to identify, and therefore well-described. Other types of recurrent inhibition in motor network may be less easily identified and therefore likely to receive less attention. There are many other types of inhibitory interneurons (Bikoff et al., 2016), that have remained uncharacterized, because their circuit motifs are more synaptic layers removed from motoneurons.

To test the impact of recurrent inhibition in our simple model, we substituted half of the excitatory neurons in our model with inhibitory neurons, and this changes the dynamics qualitatively in two ways (**Figure 6**). First, the population response to a different external drive resulted in a graded output (**Figure 7**), hence allowing a more functional dynamics. Second, the firing rate distribution was wide and skewed toward zero in accord with experimental observations (**Figures 6E,F**). It is remarkable that such a simple alteration of recurrent excitatory network can change the population dynamics to something more functional and closer to the experimentally observed. Hence, we propose that recurrent inhibition is an indispensable element in motor networks.

9. METHODS

To understand the effect of recurrent connectivity of the firing rate distribution of spinal networks we consider a population of N=200 neurons that we model in terms of their firing rates. The firing rate r_i of an example neuron i is determined by a static non-linear firing rate function $\phi(x)$ that relates that activity variable x_i (analogous to a membrane potential) to the output firing rate: $r_i(t) = \phi[x_i(t)]$. We used

$$\phi(x_i) = \begin{cases} r_0(1 + \tanh[(x_i - r_0)/r_0]), & \text{for } x_i \leq r_0 \\ r_0 + r_{\max}\tanh[(x_i - r_0)/r_{\max}], & \text{for } x_i > r_0 \end{cases} \quad (1)$$

where r_0 represents the rate at the inflection point and $r_{\max} = 80$ is the maximum deviation of the firing rate from this point. The dynamics of the network is given by

$$\begin{cases} \tau_m \dot{x}_i(t) = -x_i + \sum_j J_{ij}\phi[x_j(t)] - g_w w_i(t) + I_e(t) \\ \tau_a \dot{w}_i(t) = -w_i + \phi[x_i(t)] \end{cases} \quad (2)$$

where J_{ij} represents the recurrent connections in the network (see below) and $I_e(t)$ is a time-varying external drive. The variable w_i represents an intrinsic adaptation that depends on the firing rate and contributes as a negative input to the activity variable x_i with a strength set by the parameter g_w. The time constants τ_m and τ_a determines the time scale of the activity variable x_i and adaptation w_i, respectively. Here we set τ_m = 50 ms and τ_a = 300 ms. Below we outline two different scenarios used in this study, either a network with recurrent excitation and intrinsic adaptation (**Figure 3**) or a network with recurrent excitation and inhibition (but lacking intrinsic adaptation) (**Figure 6**).

Recurrent Excitation and Intrinsic Adaptation

For the case of a network with only recurrent excitation that is counteracted by an intrinsic adaptation, we first generate connection weights J_{ij} from Gaussian distribution with zero mean and a width (standard deviation) set to σ = 0.05. Negative weights are then set to zero, resulting in a truncated distribution with positive only values, where approximately half of the possible connections are zero (**Figure 3A**). We set the strength of adaptation g_w to match the average sum of the incoming connection weights to each neuron: $g_w = 1/N \sum_{ij} J_{ij}$.

Recurrent Excitation and Inhibition

In the model with recurrent excitation and inhibition we first generate the connections as for the case above. Here, however, we consider half of the neurons to be excitatory and half of them to be inhibitory and adjust all connections from the inhibitory connections by a factor g_i =-1.5. This results in a network where recurrent connections are dominated by inhibition (**Figure 6A**). For simplicity we exclude the effect of the intrinsic adaption, i.e., we set g_w = 0.

Software and Code Availability

Numerical simulations of the network model were done using the forward Euler method implemented in custom-written software using Python 3.8. Code for reproducing **Figures 3**, **6**, **7** is available at Berg Lab website (https://berg-lab.net).

DATA AVAILABILITY STATEMENT

The datasets presented in this study can be found in online repositories. The names of the repository/repositories and accession number(s) can be found at: https://www.berg-lab.net.

AUTHOR CONTRIBUTIONS

Both authors listed have made a substantial, direct and intellectual contribution to the work, and approved it for publication.

FUNDING

This work was supported by The Independent Research Fund Denmark (RB), European Research Council (Mobilex, HL), and the Lundbeck Foundation (RB).

ACKNOWLEDGMENTS

Thanks to Claire Wyart and her colleagues for making their zebra fish data set available for further analysis.

REFERENCES

Auyong, N., Ollivier-lanvin, K., and Lemay, M. A. (2011a). Population spatiotemporal dynamics of spinal intermediate zone interneurons during air-stepping in adult spinal cats. *J. Neurophysiol.* 106, 1943–1953. doi: 10.1152/jn.00258.2011

Auyong, N., Ollivier-lanvin, K., and Lemay, M. A. (2011b). Preferred locomotor phase of activity of lumbar interneurons during air-stepping in subchronic spinal cats. *J. Neurophysiol.* 105, 1011–1022. doi: 10.1152/jn.00523.2010

Beato, M., and Nistri, A. (1999). Interaction between disinhibited bursting and fictive locomotor patterns in the rat isolated spinal cord. *J. Neurophysiol.* 82, 2029–2038.

Beggs, J. M., and Plenz, D. (2003). Neuronal avalanches in neocortical circuits. *J. Neurosci.* 23, 11167–11177. doi: 10.1523/JNEUROSCI.23-35-11167.2003

Bellardita, C., and Kiehn, O. (2015). Phenotypic characterization of speed-associated gait changes in mice reveals modular organization of locomotor networks. *Curr. Biol.* 25, 1426–1436. doi: 10.1016/j.cub.2015.04.005

Berg, R. W. (2017). Neuronal population activity in spinal motor circuits: greater than the sum of its parts. *Front. Neural Circuits* 11:103. doi: 10.3389/fncir.2017.00103

Berg, R. W., Alaburda, A., and Hounsgaard, J. (2007). Balanced inhibition and excitation drive spike activity in spinal half-centers. *Science* 315, 390–393. doi: 10.1126/science.1134960

Berg, R. W., Willumsen, A., and Lindén, H. (2019). When networks walk a fine line: balance of excitation and inhibition in spinal motor circuits. *Curr. Opin. Physiol.* 8, 76–83. doi: 10.1016/j.cophys.2019.01.006

Bikoff, J. B., Gabitto, M. I., Rivard, A. F., Drobac, E., Machado, T. A., Miri, A., et al. (2016). Spinal inhibitory interneuron diversity delineates variant motor microcircuits. *Cell* 165, 207–219. doi: 10.1016/j.cell.2016.01.027

Brown, T. G. (1914). On the nature of the fundamental activity of the nervous centres; together with an analysis of the conditioning of rhythmic activity in progression, and a theory of the evolution of function in the nervous system. *J. Physiol.* 48, 18–46. doi: 10.1113/jphysiol.1914.sp001646

Buzsáki, G., and Mizuseki, K. (2014). The log-dynamic brain: how skewed distributions affect network operations. *Nat. Rev. Neurosci.* 15, 264–278. doi: 10.1038/nrn3687

Callahan, R. A., Roberts, R., Sengupta, M., Kimura, Y., Higashijima, S. I., and Bagnall, M. W. (2019). Spinal V2b neurons reveal a role for ipsilateral inhibition in speed control. *eLife* 8, 1–27. doi: 10.7554/eLife.47837

Carroll, M. S., and Ramirez, J.-M. (2013). Cycle-by-cycle assembly of respiratory network activity is dynamic and stochastic. *J. Neurophysiol.* 109, 296–305. doi: 10.1152/jn.00830.2011

Cheng, J., Jovanovic, K., Aoyagi, Y., Bennett, D., Han, Y., and Stein, R. (2002). Differential distribution of interneurons in the neural networks that control walking in the mudpuppy (*Necturus maculatus*) spinal cord. *Exp. Brain Res.* 145, 190–198. doi: 10.1007/s00221-002-1102-0

Cowley, K. C., and Schmidt, B. J. (1995). Effects of inhibitory amino acid antagonists on reciprocal inhibitory interactions during rhythmic motor activity in the *in vitro* neonatal rat spinal cord. *J. Neurophysiol.* 74, 1109–1117.

Cuellar, C. A., De La Torre Valdovinos, B., Huidobro, N., Delgado-Lezama, R., Ornelas-Kobayashi, R., and Manjarrez, E. (2018). The spinal neurons exhibit an ON-OFF and OFF-ON firing activity around the onset of fictive scratching episodes in the cat. *Front. Cell. Neurosci.* 12:68. doi: 10.3389/fncel.2018.00068

Cuellar, C. A., Tapia, J. A., Juarez, V., Quevedo, J., Linares, P., Martinez, L., et al. (2009). Propagation of sinusoidal electrical waves along the spinal cord during a fictive motor task. *J. Neurosci.* 29, 798–810. doi: 10.1523/JNEUROSCI.3408-08.2009

Grillner, S. (1981). "Control of locomotion in bipeds, tetrapods and fish," in *Handbook of Physiology, The Nervous System II. Motor Control*, ed V. B. Brooks (Bethesda, MD: American Physiological Society; Waverly Press), 1179–1236.

Grillner, S., and El Manira, A. (2020). Current principles of motor control, with special reference to vertebrate locomotion. *Physiol. Rev.* 100, 271–320. doi: 10.1152/physrev.00015.2019

Grillner, S., and Jessell, T. M. (2009). Measured motion: searching for simplicity in spinal locomotor networks. *Curr. Opin. Neurobiol.* 19, 572–586. doi: 10.1016/j.conb.2009.10.011

Hägglund, M., Dougherty, K. J., Borgius, L., Itohara, S., Iwasato, T., and Kiehn, O. (2013). Optogenetic dissection reveals multiple rhythmogenic modules underlying locomotion. *Proc. Natl. Acad. Sci. U.S.A.* 110, 11589–11594. doi: 10.1073/pnas.1304365110

Hennequin, G., Agnes, E. J., and Vogels, T. P. (2017). Inhibitory plasticity: balance, control, and codependence. *Annu. Rev. Neurosci.* 40, 557–79. doi: 10.1146/annurev-neuro-072116-031005

Hesse, J., and Gross, T. (2014). Self-organized criticality as a fundamental property of neural systems. *Front. Syst. Neurosci.* 8:166. doi: 10.3389/fnsys.2014.00166

Ivanenko, Y. P., Poppele, R. E., and Lacquaniti, F. (2006). Spinal cord maps of spatiotemporal alpha-motoneuron activation in humans walking at different speeds. *J. Neurophysiol.* 95, 602–618. doi: 10.1152/jn.00767.2005

Kiehn, O. (2016). Decoding the organization of spinal circuits that control locomotion. *Nat. Rev. Neurosci.* 17, 224–238. doi: 10.1038/nrn.2016.9

Kirkwood, P. A., Munson, J. B., Sears, T. A., and Westgaard, R. H. (1988). Respiratory interneurones in the thoracic spinal cord of the cat. *J. Physiol.* 395, 161–192. doi: 10.1113/jphysiol.1988.sp016913

Larremore, D. B., Shew, W. L., and Restrepo, J. G. (2014). "Critical dynamics in complex networks," in *Criticality in Neural Systems*, eds D. Plenz, and E. Niebur (Weinheim: Wiley-VCH Verlag GmbH & Co. KGaA).

Levenstein, D., Watson, B. O., Rinzel, J., and Buzsaki, G. (2017). Sleep regulation of the distribution of cortical firing rates. *Curr. Opin. Neurobiol.* 44, 34–42. doi: 10.1016/j.conb.2017.02.013

McCrea, D. A., and Rybak, I. A. (2008). Organization of mammalian locomotor rhythm and pattern generation. *Brain Res. Rev.* 57, 134–146. doi: 10.1016/j.brainresrev.2007.08.006

McLean, D. L., and Dougherty, K. J. (2015). Peeling back the layers of locomotor control in the spinal cord. *Curr. Opin. Neurobiol.* 33, 63–70. doi: 10.1016/j.conb.2015.03.001

McLean, D. L., Masino, M. A., Koh, I. Y., Lindquist, W. B., and Fetcho, J. R. (2008). Continuous shifts in the active set of spinal interneurons during changes in locomotor speed. *Nat. Neurosci.* 11, 1419–1429. doi: 10.1038/nn.2225

Melnik, S., Hackett, A., Porter, M. A., Mucha, P. J., and Gleeson, J. P. (2011). The unreasonable effectiveness of tree-based theory for networks with clustering. *Phys. Rev. E Stat. Nonlin. Soft Matter Phys.* 83, 1–12. doi: 10.1103/PhysRevE.83.036112

Mizuseki, K., and Buzsáki, G. (2013). PreconfiLgured, skewed distribution of firing rates in the hippocampus and entorhinal cortex. *Cell Rep.* 4, 1010–1021. doi: 10.1016/j.celrep.2013.07.039

Petersen, P. C., and Berg, R. W. (2016). Lognormal firing rate distribution reveals prominent fluctuation-driven regime in spinal motor networks. *eLife* 5:e18805. doi: 10.7554/eLife.18805

Petersen, P. C., Vestergaard, M., Jensen, K. H. R., and Berg, R. W. (2014). Premotor spinal network with balanced excitation and inhibition during motor patterns has high resilience to structural division. *J. Neurosci.* 34, 2774–2784. doi: 10.1523/JNEUROSCI.3349-13.2014

Pham, B. N., Luo, J., Anand, H., Kola, O., Salcedo, P., Nguyen, C., et al. (2020). Redundancy and multifunctionality among spinal locomotor networks. *J. Neurophysiol.* 124, 1469–1479. doi: 10.1152/JN.00338.2020

Prut, Y., and Perlmutter, S. I. (2003). Firing properties of spinal interneurons during voluntary movement. I. State-dependent regularity of firing. *J. Neurosci.* 23, 9600–9610. doi: 10.1523/JNEUROSCI.23-29-09600.2003

Radosevic, M., Willumsen, A., Petersen, P. C., Lindén, H., Vestergaard, M., and Berg, R. W. (2019). Decoupling of timescales reveals sparse convergent CPG network in the adult spinal cord. *Nat. Commun.* 10:2937. doi: 10.1038/s41467-019-10822-9

Ramirez, J.-M., and Baertsch, N. A. (2018). The dynamic basis of respiratory rhythm generation : one breath at a time. *Annu. Rev. Neurosci.* 41, 475–499. doi: 10.1146/annurev-neuro-080317-061756

Rybarsch, M., and Bornholdt, S. (2014). Avalanches in self-organized critical neural networks: a minimal model for the neural SOC universality class. *PLoS ONE* 9:e93090. doi: 10.1371/journal.pone.0093090

Saltiel, P., D'Avella, A., Tresch, M. C., Wyler, K., and Bizzi, E. (2017). Critical points and traveling wave in locomotion: experimental evidence and some theoretical considerations. *Front. Neural Circuits* 11:98. doi: 10.3389/fncir.2017.00098

Saltiel, P., d'Avella, A., Wyler-Duda, K., and Bizzi, E. (2016). Synergy temporal sequences and topography in the spinal cord: evidence for a traveling wave in frog locomotion. *Brain Struct. Funct.* 221, 3869–3890. doi: 10.1007/s00429-015-1133-5

Sengupta, M., Daliparthi, V., Roussel, Y., Bui, T. V., and Bagnall, M. W. (2021). Spinal V1 neurons inhibit motor targets locally and sensory targets distally to coordinate locomotion. *bioRxiv [Preprint].* 016413. doi: 10.1101/2021.01.22.427836

Severi, K. E., Böhm, U. L., and Wyart, C. (2018). Investigation of hindbrain activity during active locomotion reveals inhibitory neurons involved in sensorimotor processing. *Sci. Rep.* 8, 1–11. doi: 10.1038/s41598-018-31968-4

Sylos-Labini, F., Scaleia, V. L., Cappellini, G., Fabiano, A., Picone, S., Keshishian, E. S., et al. (2020). Distinct locomotor precursors in newborn babies. *Proc. Natl. Acad. Sci. U.S.A.* 117, 9604–9612. doi: 10.1073/pnas.1920984117

Talpalar, A. E., Bouvier, J., Borgius, L., Fortin, G., Pierani, A., and Kiehn, O. (2013). Dual-mode operation of neuronal networks involved in left-right alternation. *Nature* 500, 85–88. doi: 10.1038/nature12286

Talpalar, A. E., Endo, T., Low, P., Borgius, L., Hagglund, M., Dougherty, K. J., et al. (2011). Identification of minimal neuronal networks involved in flexor-extensor alternation in the mammalian spinal cord. *Neuron* 71, 1071–1084. doi: 10.1016/j.neuron.2011.07.011

van Vreeswijk, C., and Sompolinsky, H. (1996). Chaos in neuronal networks with balanced excitatory and inhibitory activity. *Science* 274, 1724–1726.

Vegué, M., and Roxin, A. (2019). Firing rate distributions in spiking networks with heterogeneous connectivity. *Phys. Rev. E* 100, 1–15. doi: 10.1103/PhysRevE.100.022208

Vestergaard, M., and Berg, R. W. (2015). Divisive gain modulation of motoneurons by inhibition optimizes muscular control. *J. Neurosci.* 35, 3711–3723. doi: 10.1523/JNEUROSCI.3899-14.2015

Vogels, T. P., Rajan, K., and Abbott, L. F. (2005). Neural network dynamics. *Annu. Rev. Neurosci.* 28, 357–76. doi: 10.1146/annurev.neuro.28.061604.135637

Watson, H. W., and Galton, F. (1875). On the probability of the extinction of families. *J. Anthropol. Inst. Great Britain Ireland* 4, 138–144.

Wohrer, A., Humphries, M. D., and Machens, C. K. (2013). Population-wide distributions of neural activity during perceptual decision-making. *Prog. Neurobiol.* 103, 156–193. doi: 10.1016/j.pneurobio.2012.09.004

Yokoyama, H., Hagio, K., Ogawa, T., and Nakazawa, K. (2017). Motor module activation sequence and topography in the spinal cord during air-stepping in human: insights into the traveling wave in spinal locomotor circuits. *Physiol. Rep.* 5, 1–15. doi: 10.14814/phy2.13504

Conflict of Interest: The authors declare that the research was conducted in the absence of any commercial or financial relationships that could be construed as a potential conflict of interest.

Publisher's Note: All claims expressed in this article are solely those of the authors and do not necessarily represent those of their affiliated organizations, or those of the publisher, the editors and the reviewers. Any product that may be evaluated in this article, or claim that may be made by its manufacturer, is not guaranteed or endorsed by the publisher.

frontiers in Human Neuroscience

ORIGINAL RESEARCH
published: 07 September 2021
doi: 10.3389/fnhum.2021.718829

The Ecological Task Dynamics of Learning and Transfer in Coordinated Rhythmic Movement

*Daniel Leach, Zoe Kolokotroni and Andrew D. Wilson**

Psychology, Leeds School of Social Sciences, Leeds Beckett University, Leeds, United Kingdom

Research spanning 100 years has revealed that learning a novel perception-action task is remarkably task-specific. With only a few exceptions, transfer is typically very small, even with seemingly small changes to the task. This fact has remained surprising given previous attempts to formalise the notion of what a task is, which have been dominated by common-sense divisions of tasks into parts. This article lays out an ecologically grounded alternative, *ecological task dynamics*, which provides us with tools to formally define tasks as experience from the first-person perspective of the learner. We explain this approach using data from a learning and transfer experiment using bimanual coordinated rhythmic movement as the task, and acquiring a novel coordination as the goal of learning. 10 participants were extensively trained to perform 60° mean relative phase; this learning transferred to 30° and 90°, against predictions derived from our previous work. We use recent developments in the formal model of the task to guide interpretation of the learning and transfer results.

Keywords: learning, transfer of learning, bimanual coordination, ecological task dynamics, perceptual information for action

OPEN ACCESS

Edited by:
Giuseppe Vannozzi,
Foro Italico University of Rome, Italy

Reviewed by:
Geoffrey P. Bingham,
Indiana University, United States
Jarrod Blinch,
Texas Tech University, United States

***Correspondence:**
Andrew D. Wilson
a.d.wilson@leedsbeckett.ac.uk;
DrAndrewDWilson@gmail.com

Specialty section:
This article was submitted to Motor Neuroscience, a section of the journal Frontiers in Human Neuroscience

Received: *01 June 2021*
Accepted: *11 August 2021*
Published: *07 September 2021*

Citation:
Leach D, Kolokotroni Z and Wilson AD (2021) The Ecological Task Dynamics of Learning and Transfer in Coordinated Rhythmic Movement. Front. Hum. Neurosci. 15:718829. doi: 10.3389/fnhum.2021.718829

INTRODUCTION

This article is the second part of a series of studies designed to investigate the perception-action mechanisms supporting learning and transfer of learning in coordinated rhythmic movement. Leach et al. (2021) extensively trained 10 participants to produce 90° mean relative phase using coordination feedback (Wilson et al., 2010b). As has been shown before (e.g., Wilson and Bingham, 2008) this training drove participants to stop trying to perceive relative phase with relative direction, and instead to use relative position. We then tested for transfer of this learning, and for the first time found substantial transfer to two other relative phases (60° and 120°). We explained the transfer as being supported by the use of relative position. In this article, we replicated the design of Leach et al. (2021) but now trained participants on 60°. We identified that this also led to them switching information variables to relative position, but contrary to our predictions, this time the learning supported transfer to 30° and 90°.

We will first review the issue of learning and transfer, and the ecological task dynamical analysis we use to understand these results. We will then review Leach et al. (2021) in more detail, to motivate the hypotheses and design of the current study. We will end by considering the implications of our results for ongoing attempts to model learning and performance in this task (Bingham, 2001, 2004a,b; Snapp-Childs et al., 2011; Hearth et al., under review).

Learning and Transfer

One way to study the mechanisms of learning is to examine what else improves after training on some task. If learning one skill improves another, then those two skills must have something important in common that was affected by the learning process. *Transfer of learning* can therefore help us identify the components being brought together to perform these tasks.

Strangely, however, the data from hundreds of studies clearly show that learning rarely transfers in any meaningful way beyond the trained task; any observed transfer is typically small in magnitude. Seemingly small changes in the task requirements can block transfer; for example, training on a pursuit motor task at one speed shows little transfer to the same task at different speeds (Lordahl and Archer, 1958; Namikas and Archer, 1960). Even tasks that seem to have large overlap in the required components can show little transfer; for example, balancing on a slack line does not transfer to balancing on a beam, and vice versa (Serrien et al., 2017). The only way to observe large transfer is to keep the goal the same, but alter the performance requirements (e.g., training a coordinated rhythmic movement with the arms, testing for transfer using the legs, e.g., Kelso and Zanone, 2002).

This pattern is surprising given our typical understanding of what a "task" is and what is required to solve it. The change in speed in the pursuit motor task seems such a small change, but it has such a large effect. Walking on both slacklines and beams seems to require balance, but apparently "balance" is not a single element that can be deployed for different tasks. The data are clear; our current understanding of what makes something "a task" is flawed, and we need a better way. So what is the field currently doing, and what must we do differently?

Learning and transfer as a topic has swung in and out of fashion several times since the earliest experimental work by Thorndike and Woodworth at the turn of the 20th century. The basic logic has remained the same – transfer is expected to occur to the degree that two tasks share common elements. But each time, researchers have conceptualised tasks with intuition grounded in every-day language (e.g., walking on a slack line and a beam both require balance, so balance must be a key component of performance in both tasks) and each time, research has revealed little if any transfer between tasks described this way (for a detailed review, see Schmidt and Young, 1986; Perkins and Salomon, 1992). This intuition-based method is failing to carve nature at the joints. If we are going to break the boom-and-bust research cycle, we need a theory of tasks that is different in kind from the intuition-based theories that have come before. We need an empirically based theory of what tasks look like, from the first person-perspective of the organism.

Ecological Task Dynamics

The ecological approach to perception-action (Gibson, 1979) is a theory of skilled action and learning that proposes a mechanism[1] for how those come about. It characterises the world-to-be-perceived in dynamical terms; objects and events have properties that require units of time, position (and its temporal derivatives) and mass to characterise completely (Bingham, 1988, 1995). Dynamical systems behave when a particular set of these properties are coupled together, and the specifics of the behaviour depend on the composition but also the organisation of the properties; how they are coupled together.

Organism behaviours depend on dynamical properties of the organism, but also of the environment. These properties must be coupled together into a system with a specific composition and organisation for a particular behaviour to emerge from that system. That coupling is, in general, informational, because we are only in mechanical contact with a small fraction of our environment. Gibson proposed, and experimental evidence has confirmed, that perceptual information consists of higher-order invariant information variables in ambient energy media (e.g., the optic array). These variables can specify (map 1:1 to) dynamical properties of the environment (Turvey et al., 1981; Runeson and Frykholm, 1983). Organisms can therefore, in principle, learn to use that information to couple their own bodily dynamics to the behaviourally relevant properties of the environment, and a given behaviour emerges from this particular distributed dynamical system as it plays out over time and space.

There are three implications for learning and transfer in this analysis. First, learning a behaviour entails coupling dynamical properties distributed across the organism and environment via information, and the form of the resulting behaviour emerges from the composition and organisation of the entire organism-environment system, and not just the organism. Learning will therefore only transfer to the extent that the two organism-environment systems share that composition and organisation. Second, changing the organism dynamics but keeping the environmental dynamics the same allows the same information variables to be used in the coupling. This describes the case such as interlimb transfer tasks, where the goal remains the same but the performance requirements change, and as noted above, large transfer of learning is typically observed in these cases. Third, keeping the organism dynamics the same but changing the environmental dynamics means that the information that was previously available is no longer there; it is replaced by information specifying the new environmental dynamics. This describes the case such as the "balancing" experiment (Serrien et al., 2017) and, as noted above, these cases typically produce little or no transfer.

We can therefore put forward a hypothesis. If the dynamical properties within the organism-environment system are changed so that the informational coupling between the organism and environment is changed, this creates a new task dynamic and learning will not transfer. Information defines the boundaries of tasks. This specific application of task dynamics to perception-action systems is called *ecological task dynamics*.

Testing Ecological Task Dynamics

Ecological task dynamics is a new way of characterising tasks that is based on the ecological analysis of behaviour, rather than everyday-language based intuitions about what we do. The proof

[1] Golonka and Wilson (2019) explicitly connect this ecological approach to the neo-mechanist literature in philosophy. The key to being a mechanistic explanation (vs a functional description) is that your model of the task only contains terms that represent the real parts and processes that have been shown to be involved in the task being explained. This is why we emphasise the issue of whether various parts are "real" or not throughout the article.

of the pudding is in the tasting, of course; so can this new notion of task do better than the old in accounting for patterns of learning and transfer?

The ecological task dynamics analysis has so far been developed most completely in the context of coordinated rhythmic movement (e.g., Kelso, 1995). This task asks people to rhythmically move two limbs so as to produce a target mean relative phase (or sometimes to move one limb at some mean relative phase to an oscillator on a monitor). The key phenomena to be explained are that (a) people can readily produce and maintain 0° and 180° at a range of frequencies, although at high frequencies people tend to transition from 180° to 0° without a lot of effort, and (b) other mean relative phases (especially the intermediate 90°) must be learned using some form of feedback.

This task has been formalised in a perception-action task dynamical model (Bingham, 2001, 2004a,b; Snapp-Childs et al., 2011, 2015). This mechanistic model implements the real dynamical properties of the limbs (as phase-driven, nonlinear damped mass springs) and the real informational coupling between them (perceived relative phase, modelled as the relative direction of motion, conditioned on the relative speed). All of the dynamical and information components of the model have been empirically verified to be part of the perception-action system from which coordinated rhythmic movement behaviour emerges (see Golonka and Wilson, 2012 for a review) and the model reproduces all the key phenomena of the task described above. Most relevantly for this paper, these phenomena are caused by the relative direction informational coupling.

Learning experiments have shown that people can improve at 90°, and that they do so by learning to perceive relative phase using relative position instead of relative direction. For example, Wilson et al. (2010a) trained participants to improve their performance at 90° by improving their visual discrimination of 90° movements. Wilson and Bingham (2008) then selectively perturbed candidate information variables and showed that performance at 90° was only fully disrupted by a perturbation of relative position.

There are then two transfer studies relevant to the current paper. The first was Snapp-Childs et al. (2015), who trained participants at 90° on either the unimanual or the bimanual version of the coordination task. Participants moved one or two joysticks so as to produce 90° between two dots on a computer monitor (in the unimanual case, the computer controlled one dot). Participants improved in each training group, and that training then transferred quite significantly between the conditions (proportion transfer was 43–45%). Improvement in performing 90° also transferred to improvements in visual discrimination of 90°. This experiment altered the organism dynamics via training group (i.e., number of limbs) and the informational coupling via the training (switching from relative direction to relative position). But because both versions of the task entailed the same informational coupling at the end of training (relative position) there was transfer between them at the end. Both the unimanual version of the task (Snapp-Childs et al., 2011) and the bimanual version of the task (Bingham, 2001, 2004a,b) have been modelled using the same informational coupling.

Most recently, and directly preceding the current study, Leach et al. (2021) extensively trained 10 participants to produce bimanual 90°. We tested their performance of 0°, 30°, 60°, 90°, 120°, 150°, and 180° and their visual perceptual thresholds for 90° in three Assessment sessions (Baseline, Post-Training, Retention). In the two post training sessions, we also tested their visual perceptual thresholds for 90° under the perturbation of relative position. We found the following main results:

1. All participants learned to produce 90° well, and this was accompanied by a decrease in their visual thresholds for discriminating 90° (replicating Snapp-Childs et al., 2015). Post-training, the improvement in the visual discrimination of 90° was entirely wiped out by the position perturbation, confirming that the participants had improved at 90° by learning to use relative position (replicating Wilson and Bingham, 2008).
2. Learning to produce 90° transferred substantially but asymmetrically to 60° and 120°. We observed a massive 81% transfer to 60°, and a still large 65% transfer to 120°. (We explained the asymmetry as the result of relative speed still acting as a noise term on the perception of relative phase; relative speed increases linearly from 0° to 180°; Snapp-Childs et al., 2011).

Overall, the results of these two transfer studies support the dynamical analysis of what a perception-action task is, from the first-person perspective of the organism. Learning alters the overall task dynamic of the system producing the behaviour, specifically in this case by altering the informational coupling between the limbs. We know that learning transfers to other versions of the task that entail different limb dynamics but can still use the new information coupling (e.g., between the unimanual and bimanual versions of the task); we therefore explained the results of Leach et al by hypothesising only 60° and 120° could be produced using relative position to couple the limbs.

The current experiment is the next step in understanding what happens to the perception-action dynamics responsible for coordinated rhythmic movement after learning. We exactly replicated the design of Leach et al. (2021), but this time we trained participants to produce bimanual 60° and examined the pattern of transfer across six other relative phases. Based on our understanding of the changes in the dynamics so far, we made the following predictions:

1. Participants would be able to learn 60°, and this would entail a switch to using relative position to perceive relative phase. This is tested using the perturbation method, whereby perturbing relative position in a two forced alternative judgement task will completely disrupt trained performance.
2. We know that only 60°, 90°, and 120° have been shown to benefit from using relative position to perceive relative phase. We therefore predicted that learning to perform 60°

would transfer only to 90° and 120°, with the proportion of transfer conditioned by the relative speed[2].

MATERIALS AND METHODS

This experiment's design and analysis plan was preregistered (Leach et al., 2017). Sample size (N = 10) was justified with a power analysis in which the results of Leach et al. (2021) informed the expected transfer effect sizes (see section "**Appendix 1**").

Participants

Eleven adults participated in this study, one of whom chose not to complete the entire procedure leaving a total of 10 participants (19–33 years old, M = 26.1; Male = 3, Female = 7). All participants were free from known neurological defects or motor disabilities, had normal or corrected-to-normal vision and were right-handed (measured with the Edinburgh Handedness Inventory; Oldfield, 1971; Dragovic, 2004). All participants were naïve to the experimental questions. Prior to training, all participant's relative phase production matched the predefined criterion for participation (see section "Criteria"). All participants were recruited using a convenience sample in the surrounding area of Leeds, United Kingdom and paid £15 upon competition of the study. Ethical approval was granted by the Psychology Ethics Committee at Leeds Beckett University, United Kingdom.

Design

The design was identical to that used in Leach et al. (2021) except that the target relative phase being trained was now 60°. All participants performed two types of experimental task; coordinated rhythmic movements (*Action*) and two-alternative forced choice (*Judgements*).

For the Action tasks, there were two within-subject variables. The first is Session (three levels; Baseline, Post Training, and Retention). These sessions were referred to as Assessment sessions, to distinguish them from the Training sessions. The second was Target Phase (seven levels; 0°, 30°, 60°, 90°, 120°, 150°, and 180°). The dependent variable was the Proportion of Time on Target phase ± 20° (PTT20), a valid measure of performance (see Snapp-Childs et al., 2011, 2015 for explicit comparisons of this to other commonly used measures, which motivates us to prefer PTT20).

For Judgement tasks, there was one within-subjects variable, Session (three levels; Baseline, Post Training, and Retention). The dependent variable was the estimated Threshold to identify 60° in the Judgement tasks (the lower the threshold, the greater the ability to discriminate 60°).

[2]Phase cycles that incur movement of opposing directions (oscillators moving toward or away from one another) incur the presence of relative speed. The more the phase cycle incurs movements of opposing direction, the greater the presence of relative speed. This occurs in a linear fashion; at 0° the motion of both oscillators always remains fixed in the same direction, thus the relative speed at 0° is zero. Relative speed is at its highest throughout the movement cycle of 180°, whereby the motion of both oscillators always remains fixed in the opposite direction (Bingham, 2004b; Wilson et al., 2005; Wilson and Bingham, 2008; Snapp-Childs et al., 2011).

Materials

All sessions were performed on a "Windows PC with a 24" Dell monitor located approximately 70 cm from the participants. The computer presented a display of two white dots (∼15 mm), separated vertically (∼35 mm), that moved horizontally across a black background (screen refresh rate 60 Hz, resolution 1,920 × 1,080). The motion of both dots was centred at the screen centre with an amplitude of 300 pixels (∼115 mm). All displays were presented, controlled and recorded by a custom MATLAB toolbox written by ADW incorporating the Pyschtoolbox (Brainard, 1997; Pelli, 1997; Kleiner et al., 2007; http://psychtoolbox.org). Matlab 2014b was used to record and analyse the data.

For Action sessions, participants used two USB Logitech Extreme 3D Pro joysticks. The central spring and the rubber guard were removed to disable force feedback (see **Figure 1**). The vertical position of both dots on the screen was fixed, but the horizontal position of both dots were controlled by the horizontal position of the joysticks, with the left and right joystick corresponding to the top and bottom dots, respectively. The mapping of the joysticks to screen amplitude is set so that required amplitude on the screen does not entail hitting the limits of the joystick range of movement. This forces participants to actively control the joysticks as much as possible, rather than to simply slam into the joystick endpoint to stop.

For Judgement sessions, the participant responded to displays using a USB keyboard. Responding with the "A" and "L" keys for the first and second choice, respectively.

Procedure

Participants performed between nine and thirteen separate sessions on separate days (see **Table 1**). The exact number of sessions performed by each individual participant was dependent on when various criterion were met during training (see section "Criteria"). During the Baseline assessment session, participants performed three different tasks (two Action, one Judgement) in the order described (approximately 45 min to complete). In the Post-Training and Retention assessment sessions, participants repeated the procedure from Baseline with one additional perturbation Judgement session described below (approximately 60 min to complete). Participants completed the Baseline, Training and Post-training sessions within a 3 week time frame, and completed the Retention session 14–24 days after the Post-Training session. Each Training session took approximately 20 min to complete.

Action Task (Assessment Sessions)

All participants were shown an 8 s, 1 Hz demonstration of the first target relative phase (0°) and performed one 20 s practice trial of producing that relative phase at 1 Hz with the joysticks. Participants then performed one block of four 20 s trials in which they controlled the horizontal motion of both dots. The top dot was controlled by the left hand, the bottom dot by the right hand. Participants were instructed to move the joysticks in a smooth, side-to-side, movement to produce the target-phase at

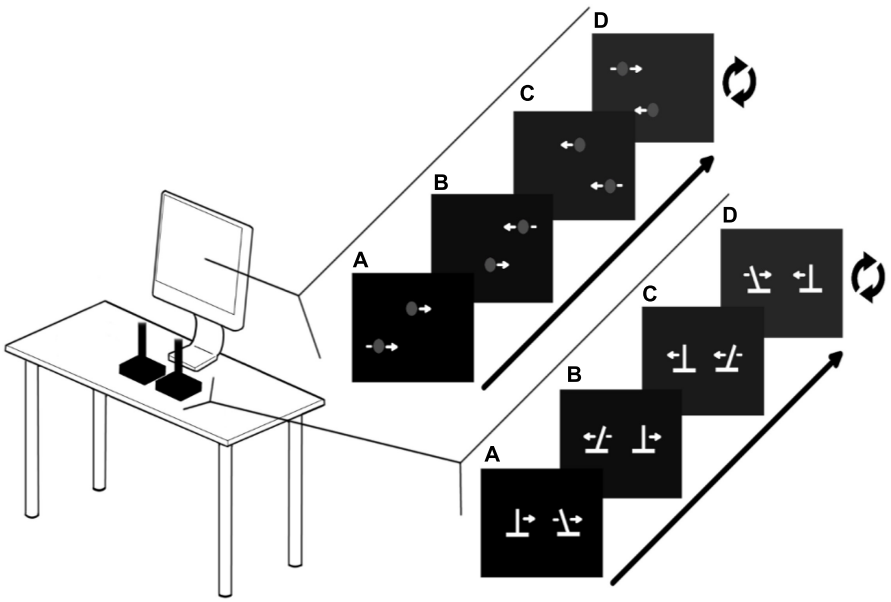

FIGURE 1 | Experimental setup : Action sessions. Participants use both joysticks to control the horizontal movements of the dots on the computer display. The visual display on the computer screen (A) corresponds with the position of the joysticks (A). The figure shows an example of moving at 60°. This is achieved by moving linearly from A to D and repeating. During the training sessions, moving at 60° ± some error triggers the hot-cold signal in which the white dots turn green (grey in figure; see Coordination Feedback).

1 Hz. This block structure was then repeated for 180° and 60° relative phase, in that order.

These data were used to ensure that none of the participants were already able to perform 60° at a level equivalent to 0° and 180° and could take part in the study (see section "Criteria").

TABLE 1 | Experimental design.

Baseline	5× 20 s trials each of bimanual 0°, 180°, *assigned phase* (60°)
1 session	*Criterion for participation: 60° < 0° and 180°; assigned phase (60°) < 0.50*
	5× 20 s trials each of bimanual 30°, 90°, 120°, 150°
	2AFC judgement task (*assigned phase*, 60°)
Training	30× 20 s trials bimanual 60° w/feedback ± 30°
	30× 20 s trials bimanual 60° w/feedback ± 25°
6–10 sessions	30× 20 s trials bimanual 60° w/feedback ± 20°
	30× 20 s trials bimanual 60° w/feedback ± 15°
	30× 20 s trials bimanual 60° w/feedback ± 10°
	30× 20 s trials bimanual 60° w/feedback ± 10°
Post training	5× 20 s trials each of bimanual 0°, 180°, *assigned phase* (60°)
	5× 20 s trials each of bimanual 30°, 90°, 120°, 150°
1 session	2AFC judgement task (*assigned phase*, 60°)
	2AFC judgement task (Perturb Position)
Retention	5× 20 s trials each of bimanual 0°, 180°, 60°
1 session	5× 20 s trials each of bimanual 30°, 90°, 120°, 150°
	2AFC judgement task (*assigned phase*, 60°)
	2AFC judgement task (Perturb Position)

All participants worked through these tasks in the order noted. The feedback bandwidth (e.g., ±30°) indicates over what range from the target-phase the colour feedback is triggered. This is faded over time to drive learning (Wilson et al., 2010a,b). See Criteria regarding the performance-based progression employed.

After this, participants performed a second set of coordinated rhythmic movements to measure baseline performance at 30°, 90°, 120°, and 150°, using the same structure as above.

Judgement Task

Following the action tasks, participants performed a series of two-alternative forced choice (2AFC) judgements for 60°. 2AFC is a standardised psychophysical measure for determining perceptual thresholds (see Wilson and Bingham, 2008; Wilson et al., 2010a; Snapp-Childs et al., 2015 for applications to coordination perception).

Each trial started with a 4 s demonstration trial of 60°, followed by the presentation of a pair of successive displays. Both displays contained two dots moving harmonically on the screen at some mean relative phase, for 4 s at 1 Hz. The dots were centred on the screen, with an amplitude of 300 pixels (∼11.5 cm). Of each pair, one showed two dots moving at 60°, and the other was different from 60°; the order was randomly selected on each trial. The task for the participants is to choose which one of the displays shows 60° (pressing "A" for the first and "L" for the second, with no speed requirement).

How different the two displays were was determined using two independent but interleaved transformed 1-up/2-down staircase procedures. One staircase controlled the different displays less than 60°, one for those greater than 60°. Both used a step size "up" of 10° and a stop rule of 8 reversals. Step size "down" was fixed to 54.88% of the step size "up" according to **Table 5**.1 of Kingdom and Prins (2009); here 5.48°. The initial difference for each staircase was set to 30° and trials only stepped down until the first reversal (first error), after which the staircase procedure

was applied. Participants are given knowledge of results (KR) after each trial ("Correct!" or "Incorrect!"). This procedure is essentially identical to that used in Snapp-Childs et al. (2015) with the addition of the KR.

In the Post Training and Retention sessions, participants repeated the 2AFC task and then completed an additional 2AFC task in which a position perturbation is applied to the display (Wilson and Bingham, 2008). In these displays, the amplitude of the top dot is changed at random on every half cycle, with the constraint that the dot must cross the midline of the screen and cannot exit the screen. The amplitude of the bottom dot is then set to half the top dot's amplitude, so that it varies randomly but in a way that is coupled to the other dot – this preserves the relative phase. Where and when peak amplitude and peak velocity occur therefore change on every half cycle. This preserves mean relative phase (and relative direction information about that relative phase) while making it impossible to use relative position information to perceive relative phase, because there is no stable information about where the dots are within their cycles. This perturbation tests the hypothesis that learning to improve at 60° entails switching to using relative position.

Action Task (Training)

Following Baseline assessment, participants were trained to bimanually produce 60°. The number of training sessions completed by each participant depended on their performance (see section "Criteria"). The number of training sessions across participants varied between 6 and 10.

During each training session, participants performed thirty 20 s trials where their goal was to produce 60°. Participants received *coordination feedback* for all trials except for every fifth trial (Wilson et al., 2010b). This feedback changed the colour of the dots from white to green when performance was within the given error bandwidth of the target relative phase. In the first training session the error bandwidth is set at ±30° and was reduced by ±5° across sessions when the Criterion for Progression was met (to ±25°, ±20°, ±15°, and ±10°). This colour feedback was not present in the Assessment Action tasks; or that reason, coordination feedback is removed every fifth trial to help prevent dependence on it (Kovacs et al., 2009; Snapp-Childs et al., 2015).

After every trial with feedback participants also received KR feedback based on their performance, in which the participant is given a performance percentage (their PTT20 score as a percentage) and a comment (see **Table 2**). Finally, participants received additional KR at the end of each training session in the form of a level-progression statement. This simply stated whether or not the participant would stay at the current level or progress to the next level. We found that this helped participants stay on task and remain motivated through the extensive training.

TABLE 2 | Knowledge of results (performance generated score).

Performance	Comment
<25%	*=This is still a little low – keep trying!*
25–50%	*=Definitely improving – keep it up!*
50–75%	*=Doing great – keep it up!*
>75%	*=This is really great – great job!*

Criteria

Prior to training, all participants' 60° production was substantially worse than 0° and 180° (Mean PTT20: 0.22; 0.77; 0.81, respectively). Participants were then trained in accordance with several pre-defined criteria (see preregistration). In each training session, when PTT20 was greater than 0.5 in at least 20/30 trials, the participant progressed to the next training stage. This was used to confirm that the participant was ready for progression and to avoid occasional poor performance trials from halting progression. Meeting this criterion resulted in the feedback bandwidth of the next training session to be reduced by ±5°; otherwise the feedback was kept the same. Training was stopped if PTT20 was greater than 0.6 in at least 20 trials for the last two training sessions (feedback bandwidth at ±10°), or when participants completed 10 training sessions. Participants completed between 6 and 10 training sessions. All participants progressed to and completed at least one session with the feedback bandwidth set to ±10°.

Data Analysis

Judgements

For the judgement tasks, the computer recorded the responses ("correct" or "incorrect") in relation to the relative phase of the "different" displays that were shown. We separately averaged the difference from 60° of relative phases at which reversals in the staircase procedure occurred for the "different" phases that were greater than 60° and those less than 60°, excluding the first reversal, for each participant. We then averaged those thresholds for each participant.

Movement

The raw movement data is a 60 Hz time series of the position of the joysticks over time. Each time series was centred on 0, filtered with a low-pass Butterworth filter (cut-off frequency 10 Hz), and differentiated to compute the velocity time series. The continuous phase time-series of each joystick was computed as the arctan(V/X) for each data point and the difference between these time series was the relative phase time series. We then computed the proportion of this time series that fell within 20° of the target relative phase (PTT20).

Contrast Analyses

To analyse transfer of learning we used Dependent Measures Contrast Analyses (Rosenthal et al., 2000). This analysis allows us to test for a specific hypothesised pattern of differences across multiple means with a single test (rather than the less powerful and less targeted method of an ANOVA followed by pairwise comparisons). In this experiment, we applied a contrast analysis to performance in the three Assessment sessions at each untrained relative phase in which we tested for the specific pattern of change observed at the trained relative phase of 60°.

The test statistic, t, is computed as

$$t_{\text{contrast}} = \frac{\overline{L}}{\sqrt{\frac{\widehat{\sigma}_L^2}{n}}} \text{ with } L_i = \sum_j^k (x_{ij} \cdot \lambda_j) \quad (1)$$

where x is the data and λ are weights. The λ weights are the way of quantifying the hypothesised pattern, here set by Assessment session performance at 60° (see below). If the data do not differ in the specific way implemented by the Lambda weights (λ), then L_i is near to zero (i.e., H_0 is $L_j = 0$). In terms of transfer, a statistically significant L_i score for data at a particular untrained relative phase indicates that the specific pattern of improvement observed at 60° is also occurring at that particular untrained phase; the learning has transferred.

RESULTS

Performance was examined across Assessment sessions at 60° to identify whether and how participants had improved with the training. The identified pattern of learning was used to set the λ weights for the contrast analyses. These analyses provide the tools to investigate whether the observed pattern of learning at 60° had transferred to any of the other untrained relative phases (0°, 30°, 90°, 120°, 150°, and 180°). This basic analysis plan was then repeated with the Judgement data.

Learning

Refer to **Figure 2**. To examine whether and how training at 60° changed performance at 60°, average PTT20 was analysed using a one-way repeated measures ANOVA with Session (Baseline, Post Training, and Retention) as a within-subject factor.

Participants significantly improved their coordination stability from Baseline to Post Training and that learning was Retained. There was a main effect of Session, $F(2, 18) = 149.95$, $p < 0.001$. Bonferroni-adjusted post-hoc analyses revealed a significant difference between Baseline and Post Training, $t(9) = 15.78$, $p < 0.001$, MD = 0.475, Baseline and Retention, $t(9) = 14.068$, $p < 0.001$, MD = 0.424 but not between Post and Retention $t(9) = 1.712$, $p > 0.05$, and MD = 0.052.

The observed learning pattern mirrored what happened in Leach et al. (2021). Production of 60° was poor at Baseline, it improved significantly with training and this improvement remained stable after the retention period. Using the learning pattern identified at 60°, the λ weights for the Action data were set at -2 for Baseline, 1 for Post Training and 1 for Retention. This was done in accordance with the guidelines set by Rosenthal et al. (2000).

Transfer

Based on the results of Leach et al. (2021), we made explicit predictions regarding where transfer was likely to take place. Learning 90° entails a switch from relative direction to relative position. A consequence of this switch was improvement at 60° and 120°. If relative position affords stability at 60°, 90°, and 120° then learning to produce any of these three relative phases should induce transfer to the other two. Thus, the prediction is that learning 60° will transfer to 90° and 120°. There is no reason that transfer will occur at 0° or 180°, so these phases were not tested. Using the λ weights assigned from the learning data of 60° (-2, 1, and 1), Dependent Measures Contrast Analyses were completed across Assessment sessions for the four criterion tasks (30°, 90°, 120°, and 150°). Any significant results would indicate significant transfer, showing that the same pattern of learning at 60° was present in the criterion task. Any transfer was expected to be very large in effect (*Hedges* $g > 1.5$).

Refer to **Figure 3**. Contrary to our predictions, Dependent Measures Contrast Analyses with *Holm-Bonferroni* corrections revealed significant transfer to 90° $t(9) = 4.476$, $p < 0.001$, $g = 1.415$ and 30° $t(9) = 4.402$, $p < 0.001$, $g = 1.39$ but nowhere else ($p > 0.05$).

Proportion of transfer was calculated across all conditions by taking the difference between Post Training and Baseline performance for the criterion task and dividing that by the difference between the Post Training and Baseline performance for each of the transfer tasks. Performance at 150° (-3%) and 180° (-3%) was negligibly worse as a function of practice at 60°. All other phases increased in performance as a function of practice at 60°. There was some increase of performance at 120° (11%) and 0° (8%), but the only substantial increase was at 90° (45%) and 30° (43%). There was no structural change in the proportional transfer at retention, other than an increase in the transfer to 90° (58%) where all other phases stayed reasonably stable.

Judgement Thresholds

Refer to **Figure 4**. Prior to training, thresholds for identifying which display showed 60° were high ($M = 19.32°$, $SD = 6.53°$). After training, this threshold improved ($M = 14.58°$, $SD = 4.92°$) and remained low after the Retention period ($M = 14.89°$, $SD = 5.77°$).

Contrast Analyses

To test the prediction that the Judgement data mirrors the learning data in the Action task (60°) the λ weights identified in the learning pattern of 60° were used to predict the same pattern in the Judgement data. The lower the threshold, the greater the ability to discriminate between the target relative phase (60°) and other relative phases. Thus, the sign of the λ weights are reversed to comply with the nature of the measure (2 for Baseline, -1 for Post Training, and -1 for Retention). A Dependent Measures Contrast Analysis with the within subjects factor of Session (3 levels; Baseline, Post-Training, and Retention) and the dependent variable of unperturbed judgement thresholds of 60°, revealed a significant effect with a large effect size. Replicating experiment 1, this demonstrates that the Action-driven λ weights are a good fit for the Judgement data, $t(9) = 4.152$, $p < 0.001$, and $g = 1.31$.

Unperturbed and Perturbed Judgement Threshold Comparison

Refer to **Figure 5**. Thresholds for identifying 90° were lower than Baseline in the unperturbed condition in both Post Training ($M = 14.58°$, $SD = 4.92°$) and Retention ($M = 14.89°$, $SD = 5.77°$)

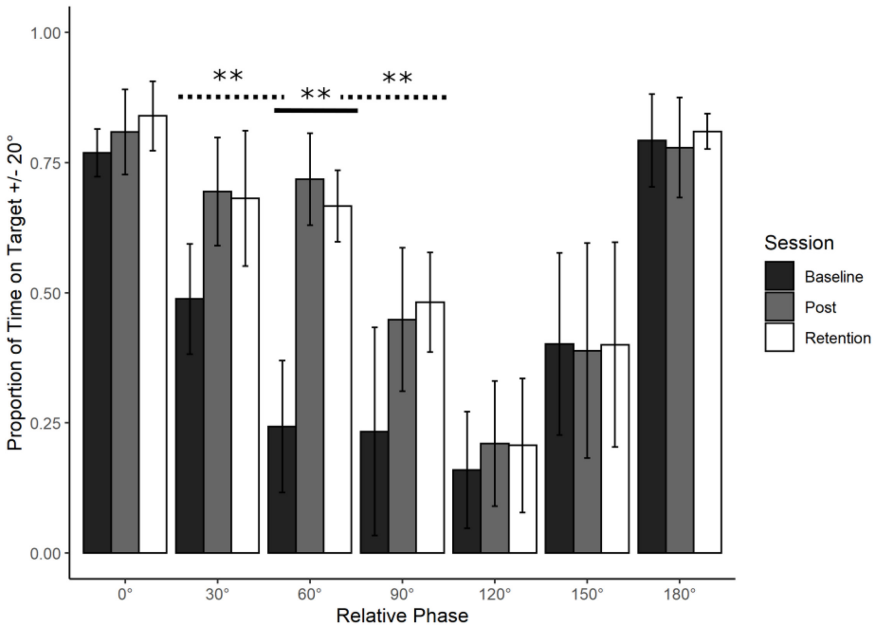

FIGURE 2 | Young adults trained at 60° : Average action data. Average performance data (Proportion of Time on Target ± 20°) with standard error bars for all phases in the three assessment sessions (Baseline, Post Training, and Retention). Significance levels are indicated on the figure (**$p < 0.01$). There was a significant main effect of Session for the trained phase of 60° (solid line). This learning transferred to 30° and 90° (dotted lines, see Transfer section for further detail).

but were extremely high and variable in the perturbed condition for both Post Training (M = 67.12°, SD = 24.63°) and Retention (M = 56.97, SD = 23.12). Participants improved perceiving and moving at 60° by switching to using relative position, and when this was no longer informative about relative phase, they could no longer perform the judgement task.

To compare the Unperturbed judgement thresholds at Post Training and Retention with the Perturbed judgement thresholds we performed an ANOVA on average judgement thresholds with Condition (Unperturbed and Perturbed) and Session (Post Training and Retention) as factors. There was a significant main effect of Condition, $F(1, 18) = 49.71$, $p < 0.001$, with no other significant main or interaction effects. The perturbation resulted in a substantially larger perceptual threshold at Post Training and Retention in comparison to the unperturbed condition (see **Figure 5**). The lower the threshold the better the performance.

Bias Analysis

The dependent variable PTT20 (proportion of time on target within a tolerance range of 20°) is an established measure of assessing performance of the task over time (see Wilson et al., 2010a,b for initial use, and Snapp-Childs et al., 2015, for a detailed comparison with other measures). The standardised bandwidth of ±20° has repeatedly captured changes in performance over the course of learning, so it is reasonable that this experiment uses this bandwidth (for previous studies closely aligned to this one that also use this bandwidth, see Snapp-Childs et al., 2015; Leach et al., 2021).

As per Leach et al. (2021), during the early phases of training, the feedback was triggered over a wide range (±30) and this was then reduced according to performance. In addition, the ±20° bins for each neighbouring relative phase overlap. One potential issue is that what we have reported as transfer (say to 30° ± 20°) could simply be a bias toward one instance of the feedback or time spent moving within the 60° ± 20° bin. For example, when presented with the task of moving at 60° an individual might spend time moving at 45°, which is within our PTT20 threshold for "on target" for both 60° and 30°.

We repeated the transfer analysis with a reduced bandwidth of ±10°[3]. If bias toward a particular instance of the feedback is what is driving the transfer effect, then the results should be characteristically different. That is, the performance landscape should look different. However, if PTT20 is successfully capturing transfer, the results will replicate (likely with a reduced effect, as performing within ±10° requires a higher degree of accuracy).

As per Leach et al. (2021), the learning pattern found with a reduced bandwidth of PTT10 at 90° was identical to the PTT20 result. Participants improved their coordination stability from Baseline to Post Training and that learning was retained. An ANOVA confirmed this with a main effect of Session [F (2, 18) = 117.65, $p < 0.001$]. The difference between Baseline and the other Assessment sessions was driving this effect (both $p < 0.001$), and there was no significant difference between Post Training and Retention ($p > 0.05$).

As the learning pattern was the same at PTT10, the weights for the contrast analysis were set the same (-2, 1, and 1). The pattern of transfer found with the reduced bandwidth mirrors what was found at PTT20, with reduced effect sizes (yet still large

[3]We have kept this as an exploratory analysis because it was not included in our preregistration (Leach et al., 2017).

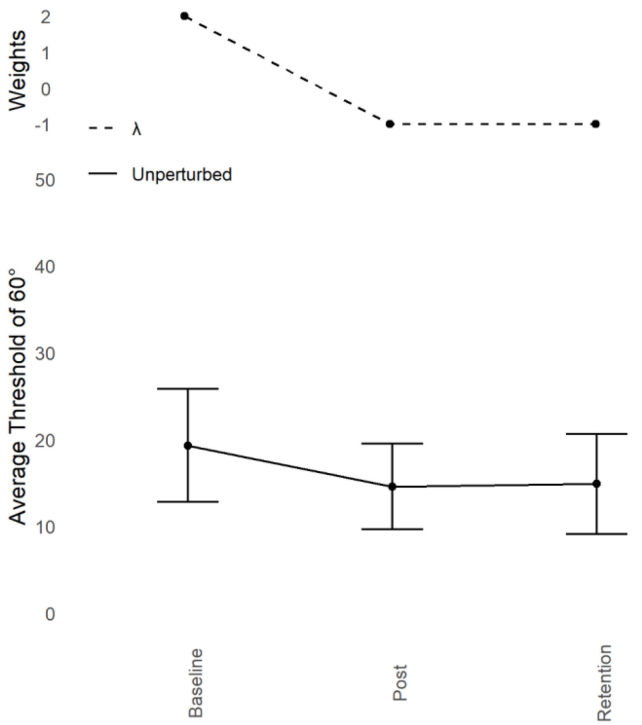

FIGURE 3 | Young adults trained at 60° : Judgement transfer. Average unperturbed Perceptual Judgement Thresholds for 60° (lower) with standard error bars at Baseline, Post Training, and Retention with corresponding Lambda (λ) weights (upper). Average unperturbed thresholds reduced as a function of training over time, indicating an improvement in performance. This improvement remained after the retention period.

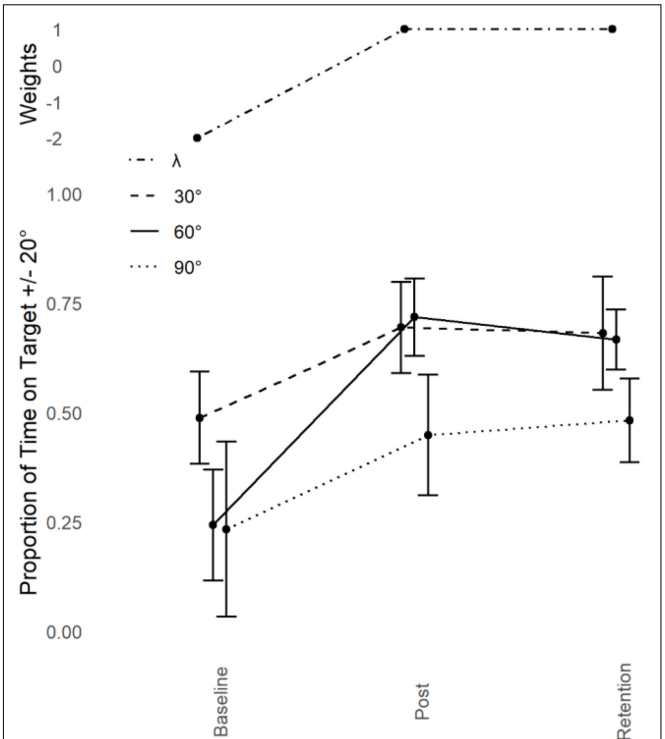

FIGURE 4 | Young adults trained at 60°: Performance transfer. Average performance data (Proportion of Time on Target ± 20°, lower) with standard error bars (lower) for the trained phase of 60° and transfer partners 30° and 90° in the three assessment sessions (Baseline, Post Training, and Retention) with corresponding Lambda (λ) weights (upper).

in magnitude). The learning at 60° transferred to 30° [t (9) = 4.67, $p < 0.001$, and $g = 1.48$] and 90° [t (9) = 4.6, $p < 0.001$, $g = 1.46$], and nowhere else ($p > 0.05$).

This analysis tells us two things. First, the pattern of transfer we observed was not caused by any systematic bias in how participants performed during training. Second, it confirms that the 20° bandwidth for the PTT20 measure is appropriate; the bandwidth doesn't dictate the pattern of results (see also Wilson et al., 2010a who checked bandwidths of 10°, 15°, and 30° and found the same result).

DISCUSSION

This study aimed to further probe the transfer effects found in Leach et al. (2021). There, learning to produce 90° transferred to 60° and 120° and this transfer was supported by the switch to using relative position to perceive relative phase. This study trained participants to produce 60°; we predicted improvement would come with a switch to relative position and a consequent transfer to 90° and 120°.

As predicted, learning to produce 60° improved the visual discrimination of 60°, and this was caused by a switch to relative position (demonstrated by the position perturbation results). We again saw transfer of learning to two different relative phases. However, the location of the transfer went against predictions. Transfer occurred at 30° and 90° and there was no asymmetry; transfer occurred in a proportionally symmetrical manner to both 30° (43%) and 90° (45%). The proportion of transfer was also smaller than in Leach et al. (2021).

We can rule out several possible explanations for the contrasting results. Firstly, we can rule out the idea that participants did not learn relative position at 60°, but some other information variable; the disruptive effect of the perturbation procedure on trained performance is clear. In the position perturbation, relative direction is unaffected and people using it are also unaffected (Wilson and Bingham, 2008). Therefore, participants are not using relative direction as information for learning 60°. Secondly, the smaller magnitude of transfer was not caused by less learning, which was comparable across 90° (0.43 improvement) and 60° (0.48 improvement). Baseline performance of 60° and 90° were also almost identical over both experiments.

Does This Refute Ecological Task Dynamics?

At first glance, these results seem to expose a weakness in the ecological task dynamical approach. We made a prediction, and the results do not accord with that

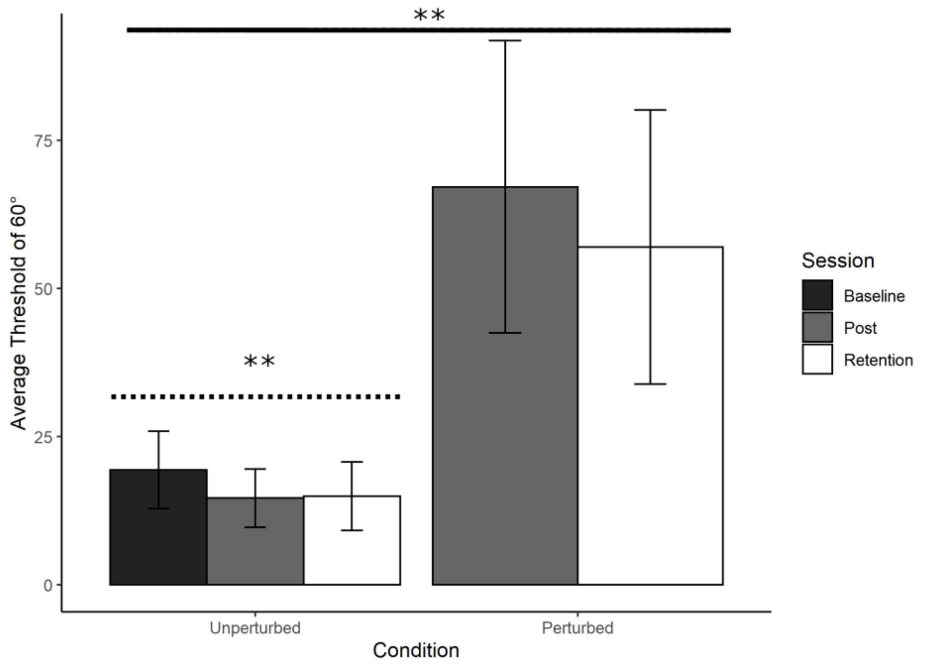

FIGURE 5 | Young adults trained at 60°: Average perceptual judgement thresholds. Average perceptual judgement thresholds for 60° with standard error bars at Baseline, Post training and Retention. Significance levels are indicated on the figure (**$p < 0.01$). There was a significant main effect of Condition, with the perturbation reducing performance (solid line). The contrast analysis demonstrated that the learning data was a good fit for the unperturbed judgement data (dotted line).

prediction. There is another, related literature on coordination dynamics that might accommodate these results; specifically, the dynamical systems account developed primarily by Zanone and Kelso (1994, 1997) and embodied in various versions of the Haken-Kelso-Bunz model (Haken et al., 1985). This account and the ecological task dynamical account are at odds with each other in various ways (Golonka and Wilson, 2019) and perhaps our results favour them over us.

This theoretical framework describes coordination dynamics in terms of attractor layouts, and models learning as a system wide phase transition from a bi-stable (0°, 180°) to a tri-stable arrangement of attractors (0°, 180° plus the trained relative phase). With regards to transfer, experiments tend to find that learning transfers to the symmetry partner of the trained relative phase (where the timing is the same but the lead-lag relations between the limbs is reversed, e.g., 90° and 270°). Less discussed is the fact that experiments often also show improvements in relative phases that neighbour the trained relative phase (e.g., see Figure 1a in Zanone and Kelso, 1997; Hurley and Lee, 2006, also saw transfer from 90° to 135° under one particular feedback condition). This could, in theory, be accounted for by the attractor formed by training being wider than the intrinsic attractors at 0° and 180°, meaning more neighbouring states might be included in the trained attractor.

However, this account has serious issues. There is strong evidence that the attractors are not real parts that are causing behaviours. For example, Zanone and Kelso (1994) predicted that attractor strength would affect learning rates, specifically that learning something close to 0° (e.g., 30°) would be harder than learning something the same distance from 180° (e.g., 150°) because the stronger attractor at 0° would compete with the to-be-learned pattern more fiercely. The opposite is actually true (Fontaine et al., 1997; Wenderoth et al., 2002). Second, a wide attractor is not an especially stable state, nor can it distinguish between the states within it. Our results (especially the bias analysis) show that people were actually moving at the transfer relative phases, and doing so quite well. Finally, with regards to applying these results to the current study, dynamical systems theory experiments use different feedback methods (either visual metronomes or Lissajous figures) and these displays alter the task dynamic by altering the information supporting the coupling, and this changes the overall behaviour of the system quite drastically (e.g., Kovacs et al., 2009, 2011).

So, while attractor dynamics is one legitimate way to describe the system dynamics, it is not an explanation of those system dynamics – there is no mechanism at work in those models (Golonka and Wilson, 2019). This account is effectively just a data-fitting exercise, and it does not help us understand our results. In order to try and develop an actual mechanistic explanation of our results, we will therefore continue to apply the ecological task dynamical approach and its real parts and processes (specifically, information variables and limb dynamics). This approach to defining a task is empirical, and the data are telling us that we do not yet have the right dynamical description of the two trained systems. We are missing a piece of the puzzle,

and so while we do not yet know what that is, we can develop some hypotheses based on the ecological analysis.

Expanding the Task Dynamical Analysis

Right now, the dynamical model of coordinated rhythmic movement (Bingham, 2001, 2004a,b; Snapp-Childs et al., 2011) is a model of the untrained system; the limb dynamics are coupled via relative phase perceived using relative direction. Over training, the limb dynamics remain the same; what changes is the perceptual coupling. Training 90° and 60° both lead to participants being sensitive to the position perturbation, but how they are using that information produces different patterns of transfer. The question is why.

The first option is that the position perturbation judgement task is not as specific as it was designed to be, and participants have in fact learned two different information variables that just happen to both get hit by the position perturbation. This is unlikely. The only other two candidates (relative speed and relative frequency) are both affected by the position perturbation, but Wilson and Bingham (2008) showed that perturbing these individually only added noise to the judgements. In addition, neither is robust information for relative phase.

One slightly more realistic concern is not with the position perturbation method, but with the fact we only implemented it in judgement tasks (Bingham and Pagano, 1998). Task dynamically, the judgement task is modelled by integrating the coupling term over a 2 s window, which is different from using the coupling term to coordinate two limbs. Evidence does show a close relationship between the judgement and production tasks, however; learning to improve on the judgement task transfers to the production task (Wilson et al., 2010a) and vice versa (e.g., Snapp-Childs et al., 2015; Leach et al., 2021, and the current experiment). The tasks overlap informationally, and that remains the important overlap. That said, it will be important to future work to informationally perturb the entire performance dynamic.

We propose at this stage that in both experiments, participants did learn to use relative position, and that the difference emerges over the *process* of learning. Herth et al. (2021) present an expanded version of the Bingham model that accounts for learning 90° and system behaviour post-learning. They add the option of a second coupling term (normed relative position) and a mechanism for switching between the two couplings. This mechanism simply entails using the most detectable variable, and switching if that variable falls below the current perceptual threshold for that variable.

The critical part for us is how they account for the process of learning. At the beginning, participants only have one coupling option; relative direction. They try to use this coupling to produce 90° (or 60°) but only succeed to a certain extent. In the absence of feedback, participants cannot use relative direction to produce sufficiently stable examples of 90° (or 60°) and so relative position is never available to be learned. With coordination feedback, they are supported as they try to produce 90° (or 60°) via relative direction, relative position becomes available, and is learned because it helps (the need for this feedback support was confirmed by Wilson et al., 2010b).

In ecological task dynamic terms, training does not change limb dynamics, and learning both 60° and 90° entails using relative direction and the feedback to bootstrap their way into moving so that relative position is sufficiently invariant to be learned (c.f., Gibson and Gibson, 1955). So both of these trained systems have access to the same resources. By Herth et al's analysis, the only remaining dynamical component that might be different between the two systems is the threshold-based mechanism for switching which variable is currently being used.

That mechanism plays out in the correction of errors. If someone is trying to perform 90° using relative position but accidentally slips into doing 0° or 180° using relative direction, the required correction back to 90° entails switching information variables immediately; the threshold for detecting relative direction at 90° is too high, and relative position is the only detectable option. If, however, someone is trying to perform 60° using relative position but accidentally slips into doing 0° using relative direction, the required correction may not mandate an information switch, at least not immediately. The threshold for detecting relative direction at 60° is high but not catastrophically so, and it may take longer before relative position is a clear winner in the competition embodied in the switching mechanism.

If this is the case, then what is being learning is not just a new information coupling, but a way to shift between couplings, and the way that mechanism plays out at 60° suits 30° and 90° but not 120°, while the way that mechanism plays out at 90° suits 60° and 120° but not 30°. The data and simulations from Herth et al. (2021) support this overall analysis, but there is not yet any specific test of this hypothesis and so it remains completely provisional at this time.

Summary

The current experiment followed on from Leach et al. (2021)'s investigation into learning and transfer of learning. How this works hinges on what constitutes a task; this experiment takes an ecological task dynamical approach to this question in which tasks are defined at the organism-environment scale, with organism and environmental dynamics coupled via perceptual information. While we did not find all of our predicted results, the pattern of data across the two experiments has provided us with a great deal of information about what learning does to the task dynamics of coordinated rhythmic movement. This work continues to be inform and be informed by the mechanistic modelling work by Bingham and colleagues (Bingham, 2001, 2004a,b; Snapp-Childs et al., 2011, 2015; Herth et al., 2021; see Golonka and Wilson, 2012, 2019 for more about the mechanistic aspect) which in turn is informed by and informing the development of the ecological task dynamical approach to perception and action.

DATA AVAILABILITY STATEMENT

The datasets presented in this study can be found in online repositories. The names of the repository/repositories and accession number(s) can be found below: https://osf.io/qtx8f/.

ETHICS STATEMENT

The studies involving human participants were reviewed and approved by Psychology Ethics Committee, Leeds Beckett University. The patients/participants provided their written informed consent to participate in this study.

AUTHOR CONTRIBUTIONS

DL planned and ran the studies, analysed the data, and writing the manuscript. ZK and AW planning the studies and writing the manuscript. All authors contributed to the article and approved the submitted version.

REFERENCES

Bingham, G. P. (1988). Task-specific devices and the perceptual bottleneck. *Hum. Mov. Sci.* 7, 225–264. doi: 10.1016/0167-9457(88)90013-9

Bingham, G. P. (1995). "Dynamics and the problem of visual event recognition," in *Mind as Motion: Dynamics, Behavior and Cognition*, eds R. Port and T. van Gelder (Cambridge, MA: MIT Press), 403–448.

Bingham, G. P. (2001). "A perceptually driven dynamical model of rhythmic limb movement and bimanual coordination," in *Proceedings of the 23rd Annual Conference of the Cognitive Science Society* (Mahwah, NJ: Lawrence Erlbaum Associates, Inc.), 75–79.

Bingham, G. P. (2004a). A perceptually driven dynamical model of bimanual rhythmic movement (and phase perception). *Ecol. Psychol.* 16, 45–53. doi: 10.1207/s15326969eco1601_6

Bingham, G. P. (2004b). "Another timing variable composed of state variables: phase perception and phase driven oscillators," in *Advances in Psychology, Vol 135. Time-to-Contact*, eds H. Hecht and G. J. P. Savelsbergh (Amsterdam: Elsevier), 421–442. doi: 10.1016/S0166-4115(04)80020-7

Bingham, G. P., and Pagano, C. C. (1998). The necessity of a perception–action approach to definite distance perception: monocular distance perception to guide reaching. *J. Exp. Psychol. Hum. Percept. Perform.* 24, 145–168. doi: 10.1037/0096-1523.24.1.145

Brainard, D. H. (1997). The psychophysics toolbox. *Spat. Vis.* 10, 433–436. doi: 10.1163/156856897X00357

Dragovic, M. (2004). Towards an improved measure of the Edinburgh handedness inventory: a one-factor congeneric measurement model using confirmatory factor analysis. *Laterality* 9, 411–419. doi: 10.1080/13576500342000248

Fontaine, R. J., Lee, T. D., and Swinnen, S. P. (1997). Learning a new bimanual coordination pattern: Reciprocal influences of intrinsic and to-be-learned patterns. *Can. J. Exp. Psychol.* 51:1. doi: 10.1037/1196-1961.51.1.1

Gibson, J. J. (1979). *The Ecological Approach to Visual Perception*. New York, NY: Psychology Press.

Gibson, J. J., and Gibson, E. J. (1955). Perceptual learning: differentiation or enrichment? *Psychol. Rev.* 62, 32–41. doi: 10.1037/h0048826

Golonka, S., and Wilson, A. D. (2012). Gibson's ecological approach – a model for the benefits of a theory driven psychology. *Avant* 3, 40–53.

Golonka, S., and Wilson, A. D. (2019). Ecological mechanisms in cognitive science. *Theory Psychol.* 29:095935431987768. doi: 10.1177/0959354319877686

Haken, H., Kelso, J. S., and Bunz, H. (1985). A theoretical model of phase transitions in human hand movements. *Biol. Cybern.* 51, 347–356. doi: 10.1007/BF00336922

Herth, R. A., Zhu, Q., and Bingham, G. P. (2021). The role of intentionality in the performance of a learned 90° bimanual rhythmic coordination during frequency scaling: data and model. *Exp. Brain Res.* doi: 10.1007/s00221-021-06173-x [Epub ahead of print].

Hurley, S. R., and Lee, T. D. (2006). The influence of augmented feedback and prior learning on the acquisition of a new bimanual coordination pattern. *Hum. Mov. Sci.* 25, 339–348. doi: 10.1016/j.humov.2006.03.006

Kelso, J. A. S. (1995). *Dynamic Patterns: The Self-Organization of Human Brain and Behavior*. Cambridge, MA: MIT Press.

Kelso, J. A. S., and Zanone, P. G. (2002). Coordination dynamics of learning and transfer across different effector systems. *J. Exp. Psychol. Hum. Percept. Perform.* 28, 776–797. doi: 10.1037/0096-1523.28.4.776

Kingdom, F. A. A., and Prins, N. (2009). *Psychophysics: A Practical Introduction*. Amsterdam: Elsevier Science.

Kleiner, M., Brainard, D., Pelli, D., Ingling, A., Murray, R., and Broussard, C. (2007). "What's new in Psychtoolbox-3?," in *Proceedings of the Perception 36 European Conference on Visual Perception Abstract Supplement, 14*, Arezzo.

Kovacs, A. J., Buchanan, J. J., and Shea, C. H. (2009). Using scanning trials to assess intrinsic coordination dynamics. *Neurosci. Lett.* 455, 162–167. doi: 10.1016/j.neulet.2009.02.046

Kovacs, A. J., Buchanan, J. J., and Shea, C. H. (2011). Impossible is nothing: 5: 3 and 4: 3 multi-frequency bimanual coordination. *Exp. Brain Res.* 201, 249–259. doi: 10.1007/s00221-009-2031-y

Leach, D., Kolokotroni, Z., and Wilson, A. D. (2017). *Preregistration–Experiment 2: Train 60*. Available online at: https://osf.io/cbthj

Leach, D., Kolokotroni, Z., and Wilson, A. D. (2021). Perceptual information supports transfer of learning in coordinated rhythmic movement. *Psychol. Res.* 85, 1167–1182. doi: 10.1007/s00426-020-01308-1

Lordahl, D. S., and Archer, E. J. (1958). Transfer effects on a rotary pursuit task as a function of first-task difficulty. *J. Exp. Psychol.* 56, 421–426. doi: 10.1037/h0047377

Namikas, G., and Archer, E. J. (1960). Motor skill transfer as a function of intertask interval and pretransfer task difficulty. *J. Exp. Psychol.* 59, 109–112. doi: 10.1037/h0049037

Oldfield, R. C. (1971). The assessment and analysis of handedness: the Edinburgh inventory. *Neuropsychologia* 9, 97–113. doi: 10.1016/0028-3932(71)90067-4

Pelli, D. G. (1997). The VideoToolbox software for visual psychophysics: transforming numbers into movies. *Spat. Vis.* 10, 437–442. doi: 10.1163/156856897X00366

Perkins, D. N., and Salomon, G. (1992). Transfer of learning. *Int. Encycl. Educ.* 2, 6452–6457.

Rosenthal, R., Rosnow, R. L., and Rubin, D. B. (2000). *Contrasts and Effect Sizes in Behavioral Research: A Correlational Approach*. Cambridge: Cambridge University Press. doi: 10.1017/CBO9780511804403

Runeson, S., and Frykholm, G. (1983). Kinematic specification of dynamics as an informational basis for person-and-action perception: expectation, gender recognition, and deceptive intention. *J. Exp. Psychol. Gen.* 112, 585–615. doi: 10.1037/0096-3445.112.4.585

Schmidt, R. A., and Young, D. E. (1986). *Transfer of Movement Control in Motor Skill Learning*. Fort Belvoir, VA: U.S. Army Research Institute for the Behavioural and Social Sciences. doi: 10.1016/B978-0-12-188950-0.50009-6

Serrien, B., Hohenauer, E., Clijsen, R., Taube, W., Baeyens, J. P., and Küng, U. (2017). Changes in balance coordination and transfer to an unlearned balance task after slackline training: a self-organizing map analysis. *Exp. Brain Res.* 235, 3427–3436. doi: 10.1007/s00221-017-5072-7

Snapp-Childs, W., Wilson, A. D., and Bingham, G. P. (2011). The stability of rhythmic movement coordination depends on relative speed: the Bingham model supported. *Exp. Brain Res.* 215, 89–100. doi: 10.1007/s00221-011-2874-x

Snapp-Childs, W., Wilson, A. D., and Bingham, G. P. (2015). Transfer of learning between unimanual and bimanual rhythmic movement coordination: transfer is a function of the task dynamic. *Exp. Brain Res.* 233, 2225–2238. doi: 10.1007/s00221-015-4292-y

Turvey, M. T., Shaw, R. E., Reed, E. S., and Mace, W. M. (1981). Ecological laws of perceiving and acting: in reply to Fodor and Pylyshyn. *Cognition* 9, 237–304. doi: 10.1016/0010-0277(81)90002-0

Wenderoth, N., Bock, O., and Krohn, R. (2002). Learning a new bimanual coordination pattern is influenced by existing attractors. *Motor Control* 6, 166–182. doi: 10.1123/mcj.6.2.166

Wilson, A. D., and Bingham, G. P. (2008). Identifying the information for the visual perception of relative phase. *Percept. Psychophys.* 70, 465–476. doi: 10.3758/PP.70.3.465

Wilson, A. D., Collins, D. R., and Bingham, G. P. (2005). Human movement coordination implicates relative direction as the information for relative phase. *Exp. Brain Res.* 165, 351–361. doi: 10.1007/s00221-005-2301-2

Wilson, A. D., Snapp-Childs, W., and Bingham, G. P. (2010a). Perceptual learning immediately yields new stable motor coordination. *J. Exp. Psychol. Hum. Percept. Perform.* 36, 1508–1514. doi: 10.1037/a0020412

Wilson, A. D., Snapp-Childs, W., Coates, R., and Bingham, G. P. (2010b). Learning a coordinated rhythmic movement with task-appropriate coordination feedback. *Exp. Brain Res.* 205, 513–520. doi: 10.1007/s00221-010-2388-y

Zanone, P. G., and Kelso, J. A. S. (1994). "The coordination dynamics of learning: Theoretical structure and experimental agenda," in *Interlimb Coordination*, eds S. P. Swinnen, H. Heuer, J. Massion, and P. Casaer (San Diego, CA: Academic Press), 461–490. doi: 10.1016/B978-0-12-679270-6.50027-9

Zanone, P. G., and Kelso, J. S. (1997). Coordination dynamics of learning and transfer: collective and component levels. *J. Exp. Psychol. Hum. Percept. Perform.* 23, 1454–1480. doi: 10.1037/0096-1523.23.5.1454

Conflict of Interest: The authors declare that the research was conducted in the absence of any commercial or financial relationships that could be construed as a potential conflict of interest.

APPENDIX 1 – POWER ANALYSIS

Two power analyses were performed using G*Power using the results of Leach et al. (2021) as input.

Detecting Very Large Transfer (Input From 60°)

The following is a power analysis performed on the performance data for detecting transfer from 90° to 60°. The analysis is in the form of a one-sided *t*-test, as is the generation of the *t*-value from the contrast analysis.

Input: Tail(s) = One
Effect size *d* = 2.322
α err prob = 0.05
Total sample size = 10
Output: Noncentrality parameter δ = 7.3428087
Critical *t* = 1.8331129
Df = 9
Power (1-β err prob) = 0.9999998
Power to observe very large effects of transfer (*d* = 2.322) with *N* = 10 is 1-β of >0.99. This level of power is achieved at *N* > = 6.

Detecting Large Transfer (Input From 120°)

The following is a power analysis performed on the performance data for detecting transfer from 90° to 120°.

Input: Tail(s) = One
Effect size *d* = 1.705
α err prob = 0.05
Total sample size = 10
Output: Noncentrality parameter δ = 5.3916834
Critical *t* = 1.8331129
Df = 9
Power (1-β err prob) = 0.9995092
Power to observe an effect size of *d* = 1.705 with the above input is 1-β > 0.99. This level of power is achieved at *N* > = 8.

frontiers in Human Neuroscience

ORIGINAL RESEARCH
published: 13 September 2021
doi: 10.3389/fnhum.2021.717810

Behavioral and Neural Dynamics of Interpersonal Synchrony Between Performing Musicians: A Wireless EEG Hyperscanning Study

Anna Zamm[1†], Caroline Palmer[1], Anna-Katharina R. Bauer[2†], Martin G. Bleichner[2], Alexander P. Demos[1†] and Stefan Debener[2,3]*

[1] Sequence Production Laboratory, Department of Psychology, McGill University, Montreal, QC, Canada, [2] Neuropsychology Laboratory, Institute for Psychology, European Medical School, University of Oldenburg, Oldenburg, Germany, [3] Cluster of Excellence Hearing4All Oldenburg, University of Oldenburg, Oldenburg, Germany

Interpersonal synchrony refers to the temporal coordination of actions between individuals and is a common feature of social behaviors, from team sport to ensemble music performance. Interpersonal synchrony of many rhythmic (periodic) behaviors displays dynamics of coupled biological oscillators. The current study addresses oscillatory dynamics on the levels of brain and behavior between music duet partners performing at spontaneous (uncued) rates. Wireless EEG was measured from $N = 20$ pairs of pianists as they performed a melody first in Solo performance (at their spontaneous rate of performance), and then in Duet performances at each partner's spontaneous rate. Influences of partners' spontaneous rates on interpersonal synchrony were assessed by correlating differences in partners' spontaneous rates of Solo performance with Duet tone onset asynchronies. Coupling between partners' neural oscillations was assessed by correlating amplitude envelope fluctuations of cortical oscillations at the Duet performance frequency between observed partners and between surrogate (re-paired) partners, who performed the same melody but at different times. Duet synchronization was influenced by partners' spontaneous rates in Solo performance. The size and direction of the difference in partners' spontaneous rates were mirrored in the size and direction of the Duet asynchronies. Moreover, observed Duet partners showed greater inter-brain correlations of oscillatory amplitude fluctuations than did surrogate partners, suggesting that performing in synchrony with a musical partner is reflected in coupled cortical dynamics at the performance frequency. The current study provides evidence that dynamics of oscillator coupling are reflected in both behavioral and neural measures of temporal coordination during musical joint action.

Keywords: interpersonal synchrony, temporal coordination, neural entrainment, wireless electroencephalography, hyperscanning

OPEN ACCESS

Edited by:
Daniela De Bartolo, Sapienza University of Rome, Italy

Reviewed by:
Laura Bishop, University of Oslo, Norway
Shannon Proksch, University of California, Merced, United States

****Correspondence:***
Anna Zamm
anna.zamm@mail.mcgill.ca

†Present address:
Anna Zamm, Department of Cognitive Science, Central European University, Budapest, Hungary
Anna-Katharina R. Bauer, Department of Experimental Psychology, Oxford University, Oxford, United Kingdom
Alexander P. Demos, Department of Psychology, University of Illinois at Chicago, Chicago, IL, United States

Specialty section:
This article was submitted to Motor Neuroscience, a section of the journal Frontiers in Human Neuroscience

Received: *31 May 2021*
Accepted: *27 July 2021*
Published: *13 September 2021*

Citation:
Zamm A, Palmer C, Bauer A-KR, Bleichner MG, Demos AP and Debener S (2021) Behavioral and Neural Dynamics of Interpersonal Synchrony Between Performing Musicians: A Wireless EEG Hyperscanning Study. Front. Hum. Neurosci. 15:717810. doi: 10.3389/fnhum.2021.717810

INTRODUCTION

Many joint actions, from ensemble music performance to team rowing, require that partners synchronize the timing of rhythmic (oscillatory) movements. There is growing evidence that interpersonal synchrony of rhythmic movements is influenced by dynamics of entrainment between biological oscillators (Kelso, 1984). An external rhythmic signal such as music may

evoke intrinsic neural oscillations that entrain to the periodicities in the rhythmic sequence. Entrainment occurs when two oscillating systems, which have different periods when they function independently, assume the same period (or integer-ratio related periods) when they interact (Pikovsky et al., 2003). Mathematical entrainment between oscillators is constrained by differences in the intrinsic frequencies of the oscillators, combined with their period coupling (Haken et al., 1985; Strogatz, 2003; Kuramoto, 2012). Coupled oscillators with similar natural frequencies will show greater entrainment than will coupled oscillators with different frequencies (Haken et al., 1985).

Evidence for principles of oscillator entrainment in interpersonal coordination comes from a growing body of behavioral research. Much of this work is based on 'frequency detuning' paradigms from studies of intra-limb coordination (Turvey, 1990) in which partners coordinate the swinging of hand-held pendulums or swaying of rocking chairs that are weighted to have either the same or different frequencies of motion. The synchronization of partners' movements is a function of the difference in their rocking chair or pendulum frequencies (Schmidt and O'Brien, 1997; Richardson et al., 2005, 2007; Lopresti-Goodman et al., 2008).

Music performance studies have directly tested the hypothesis that partners' *spontaneous frequencies*—unconstrained frequencies of self-paced spontaneous rhythmic motion during music performance—influence interpersonal entrainment (Loehr and Palmer, 2011; Zamm et al., 2015, 2016; Palmer et al., 2019). These studies showed that differences in partners' spontaneous rates of solo music performance predicted synchronization accuracy and precision during duet performance paced by a metronome cue. Moreover, smaller differences in partners' spontaneous frequencies were associated with greater duet synchronization accuracy and precision relative to larger differences in spontaneous frequencies.

Evidence to suggest that spontaneous rates of music performance reflect stable intrinsic frequencies comes from several findings. First, individuals who differ in skill, musical preferences, and experience on different instruments have been documented to have consistent spontaneous performance tempi. These consistent individual differences are shown not only in the mean rate but also in the variance (Zamm et al., 2019), with lowest temporal variance at the spontaneous rate and higher variance at both slower and faster rates than the individuals' spontaneous rate. Second, the size and direction of differences in duet partners' spontaneous rates are predictive of how well they synchronize, consistent with the mathematical prediction of similar oscillator frequencies generating greater synchronization (Zamm et al., 2016; Palmer et al., 2019). This finding has been replicated in both music performance and tapping tasks, with musicians and non-musicians (Scheurich et al., 2018). Third, the spontaneous rates are consistent within individuals, across their limb movements and melodies (Zamm et al., 2016), across time of day (Zamm et al., 2019; Wright and Palmer, 2020). Moreover, recent computational work (Roman et al., 2020) indicates that the relationship between musical partners' spontaneous frequencies and interpersonal synchrony can be accurately predicted from a model of biological oscillator entrainment, providing further credence to an oscillator framework of musical synchrony.

Oscillator dynamics are also reflected in electrophysiological brain measures. Electroencephalography (EEG) research has shown that neural oscillations entrain to the frequency of external rhythms (Galambos et al., 1981; Tobimatsu et al., 1999; Ross et al., 2003; Feurra et al., 2011; Bauer et al., 2020). Neural entrainment has been characterized by enhanced spectral energy of EEG oscillations at the stimulus frequency relative to other frequencies, and by phase alignment of EEG oscillations with the stimulus phase (see Lakatos et al., 2019 for a review). Neural entrainment to external rhythms not only supports the ability to accurately perceive rhythms (Henry et al., 2015; Bauer et al., 2018), but also to coordinate the timing of movements with those auditory rhythms (Nozaradan et al., 2013, 2016). Specifically, greater spectral energy of EEG oscillations at the frequency of an external stimulus has been associated with smaller asynchronies between movement and stimulus (Nozaradan et al., 2016).

It has been suggested that partners' neural activity becomes coupled during temporal coordination in joint action (Tomlin et al., 2006; Tognoli et al., 2007; Dumas et al., 2010; Astolfi et al., 2011; Funane et al., 2011; Cui et al., 2012; Müller and Lindenberger, 2014; Lee, 2015). Lindenberger and colleagues showed that guitarists' duet synchronization is accompanied by inter-brain phase coupling of oscillations in the delta frequency range (Lindenberger et al., 2009; Sänger et al., 2012). Novembre et al. (2017) demonstrated that inducing inter-brain coupling through in-phase transcranial alternating current stimulation leads to enhanced interpersonal coordination of dyadic finger tapping relative to anti-phase stimulation. It is unknown how period coupling is reflected in inter-brain correspondences. However, prior work does suggest that period coupling of one's behaviors with external auditory rhythms is associated with enhanced amplitude of cortical oscillations at the coupling frequency relative to other frequencies (Nozaradan et al., 2013, 2016). Thus, we hypothesize that production of a common frequency during duet performance is accompanied by enhanced spectral energy of partners' neural oscillations at the common frequency of partners' performances relative to other frequencies; moreover, we predict that the amplitude envelopes of oscillations at the common frequency are coupled between partners, reflecting co-production of a shared rhythmic structure.

Amplitude envelopes, defined as the absolute value of the Hilbert transform of a neural oscillation, reflect energy fluctuations over time (Bruns et al., 2000). Correlations between the amplitude envelopes of two brain signals measure the degree to which the amplitude fluctuations are temporally correlated. Amplitude envelope correlations (AECs) have been used to detect functional connectivity, that is, synchrony between functional brain networks, both within and across frequency bands (Bruns et al., 2000; Hipp et al., 2012; Zamm et al., 2018). AECs are sensitive to long-range dependencies (Bruns et al., 2000), and MEG studies found that they show superior test-retest reliability relative to other standard functional connectivity metrics (e.g., phase- or coherence-based metrics; Colclough et al., 2016). Moreover, amplitude envelope metrics are less susceptible to measurement jitter than alternative phase-based

metrics, an important consideration for naturalistic music performance conditions. The sensitivity of AECs for detecting inter-brain correspondences between performing musicians has been demonstrated with wireless EEG (Zamm et al., 2018). We apply AECs here to assess inter-brain correspondences at the performance rate of duet performances.

The current study investigated oscillator dynamics of interpersonal synchrony in duet music performance by investigating the extent to which partners' spontaneous performance rates influence interpersonal synchrony during temporally unconstrained performance. We also investigated whether partners display inter-brain coupling of cortical oscillations at the duet performance rate. Duet music performance was used as a model of oscillatory joint action, since music is highly rhythmic and musicians must be able to coordinate production of these rhythms with millisecond precision. We randomly paired pianists and recorded wireless EEG while pianists performed a simple melody in the Solo condition at their spontaneous rate and in Duet performance with their partner. In Duets, partners took turns as Leader to set the pace of performance at their spontaneous rate, in contrast with much of the previous literature on coordinate dynamics of music performance, where musicians produce actions at a cued rate. The use of wireless EEG enabled us to investigate inter-brain synchrony during music performance with minimal artifact (Debener et al., 2012; De Vos et al., 2014a,b). Moreover, use of wireless EEG allowed musicians to move freely and naturally as wireless EEG has been shown to be feasible in mobile conditions (e.g., Scanlon et al., 2020).

We hypothesized that interpersonal coordination in duet music performance is constrained by the amount of coupling needed to overcome differences in partners' natural frequencies. Based on previous findings, Duet tone onset synchronization was predicted to decrease as a function of the difference in partners' spontaneous rates (Loehr and Palmer, 2011; Zamm et al., 2015; Palmer et al., 2019). Larger tone onset asynchronies (Leader − Follower tone onsets) were expected between duet partners with larger differences in spontaneous frequency relative to partners with smaller differences. Furthermore, we hypothesized that frequency coupling is reflected on a neural level during Duet performance. Specifically, we predicted that partners' neural oscillations show increased power at the performance rate of tone production during Duets, reflected as higher spectral amplitude of EEG signals at the Duet frequency relative to other frequencies. Furthermore, higher spectral amplitudes at the performance rate should be positively associated with Duet tone onset synchronization. Finally, partners' amplitude envelopes of neural oscillations should be correlated at the common frequency of Duet music performance, yielding inter-brain correspondences.

MATERIALS AND METHODS

Participants

40 pianists were randomly assigned to 20 pairs (25 female, mean age = 23.96 years, range = 18–40) with six or more years of private piano lessons (mean = 11.16 years, range = 6–18) were recruited from the Oldenburg community. Pianists were included if they had self-reported normal or corrected to normal vision, no current psychiatric or neurological conditions or use of neuropsychiatric medication, self-reported normal hearing confirmed through a pure-tone audiometric screening test (< 20 dB binaurally for the range of tones in the stimulus melody) and right-hand dominance. Handedness was confirmed using the Edinburgh Handedness Inventory (Oldfield, 1971). All participants scored as right-hand dominant (M = 85.9, SD = 17.2), except one individual who showed a tendency toward left-hand dominance (score = 36.8). The study protocol was reviewed by the local ethics committees at the University of Oldenburg and McGill University, and all participants provided informed consent prior to recording, in accordance with the Declaration of Helsinki. EEG data associated with Solo performances from the current sample have been reported in Zamm et al. (2019) to demonstrate the validity of wireless EEG for measuring the neural correlates of music performance; these EEG data are not reported here. EEG data associated with Duet performances from 2 pairs from the current sample have been reported in Zamm et al. (2018) to demonstrate the validity of amplitude envelope correlations for measuring inter-brain correspondences in oscillatory activity.

Materials

Participants performed the popular melody *Bruder Jakob* (Frère Jacques, Brother John) on the piano with their right hand. Participants were familiar with the melody and rehearsed the melody from stimulus notation sent in advance of their arrival at the laboratory; the melody was notated in C major (treble clef) and the rhythm was in binary (4/4) meter and was 32 tones in duration (20 quarter notes, 4 half notes, 8 eighth notes; note range = G3–A4). To control for possible differences in finger movements across pianists, suggested fingerings were indicated on the melody notation (provided by three skilled pianists not in the study).

Equipment

Keystroke Recording

Figure 1 shows the Duet experiment set-up. Two identical Yamaha P35B Musical Instrument Digital Interface (MIDI) DC-powered keyboards (Yamaha Corporation, Japan) were used to record duet piano performances. The keyboards were positioned to face one another in the testing room. A shoulder-level occluder was placed between the keyboards to minimize possible influences of visual cues from a partner's finger movements on duet partners' temporal coordination. Auditory feedback associated with pianists' keystrokes was presented through speakers on each keyboard, and volume was calibrated to equal loudness across keyboards using a sound meter. MIDI information (timestamps, pitch, velocity) from pianists' keystrokes was sent on two separate channels, merged *via* a MIDI-USB merger (Prodipe Corporation, France), and sent to a Linux (Fedora) operating system computer running FTAP MIDI recording software (Finney, 2001). The Linux computer was connected to the local area network (LAN) *via* an ethernet

switch (TP-Lin GmbH). FTAP was adapted to include the Lab Streaming Layer library (LSL; Kothe, 2014[1]), which allowed for sending MIDI keystroke triggers to LabRecorder software (v1.1)[2]) over the LAN.

EEG Recording

Two 24-channel mobile EEG systems (SMARTING mBrain Train LLC[3]), attached to separate elastic electrode caps[4], were used to record EEG data from participants. Electrode positioning followed the international 10–20 system. FCz served as the reference electrode and AFz served as the ground electrode. Electrode impedances were below 20 kOhms before the recording started. Wireless EEG amplifiers (weight = 60 g; size = 82 mm × 51 mm × 12 mm; resolution = 24 bits; sampling rate = 500 Hz) were strapped to the back of each participant's electrode cap between O1 and O2 electrode sites. Digitized EEG data from each participant were sent wirelessly from the amplifier to a Bluetooth receiver placed on the wall directly behind their keyboard. Bluetooth receivers sent this information *via* USB to Windows 7 computers running SmartingLSL, which collected the data using the LSL library and sent the data to LabRecorder over the LAN. LabRecorder synchronized EEG data from both amplifiers with MIDI data by correcting for clock offsets between acquisition computers. For details on synchronizing MIDI and EEG data from a single mobile amplifier, it was confirmed that MIDI and EEG recordings were synchronized with millisecond precision (Zamm et al., 2019). Synchronization between two EEG amplifiers and two MIDI keyboards was confirmed through timing tests which are available upon request.

Experimental Design

Each pianist performed two tasks with the same stimulus melody: a Solo task and a Duet task. The Solo task always preceded the Duet task to ensure that each partner's spontaneous rate (acquired during Solo performance) was not influenced by their partner's performances. The Solo Task measured each pianist's spontaneous rate on 3 trials, where 1 trial included 4 continuous performances of the melody (yielding 12 repetitions per pianist). Each pianist completed 1 practice trial and 3 test trials of Solo performance, yielding a total of 12 Solo test performances of the melody.

The Duet task measured the pianists' tone onset asynchrony while one partner played the role of Leader (partner responsible for cueing the pace of the Duet performance) and the other partner played the role of Follower (partner responsible for performing at the Leader's pace) as they tried to synchronize their performances. Two independent variables were manipulated in a within-subject design. The first independent variable, Musical Role (Leader, Follower) was coded for analyses that examined each pianist as the random variable. The second independent variable, Leader-Order condition, included 2 levels (First-Leader, Second-Leader) and was coded for analyses that examined each pair as the random variable. In the First-Leader condition, the duet partners chose which partner would play the role of Leader. In the Second-Leader condition, the experimenter assigned the role of Leader to the partner who played the role of Follower in the First-Leader condition. Each Leader-Order condition comprised 1 practice trial and 6 test trials of duet performance (1 trial = 4 continuous melody repetitions), yielding a total of 24 Duet test performances of the melody for each of the two conditions (First-Leader, Second-Leader).

Task and Procedure

Pianists were sent the melody's stimulus notation in advance of the study, with the instruction to practice with the notated fingering until memorized. When Duet partners arrived at the lab, they were each given a short practice session and then separately completed a melody memory test, as shown in **Figure 1B**. In the memory test, each partner was instructed to perform the melody without pitch or rhythm errors. While one partner completed the memory test, the other partner waited outside of the testing room. Each partner was given up to two attempts at passing the memory test or else were excluded from the study. All participants passed the memory test after two attempts. After passing the melody memory test, the pianists completed two performance tasks, a Solo task and a Duet task. In the Solo performance task, each partner performed the melody alone with the instruction to produce tone onsets at a regular rate that felt natural and comfortable for them. While one partner completed the Solo performance task, the other partner waited outside of the testing room where they could not hear their partner's performance.

Partners subsequently completed the Duet performance task, in which partners performed the melody together simultaneously. One partner (the Leader) was instructed to set the pace of each performance at a rate that was natural and comfortable for them just as they did during Solo performance, while their partner (the Follower) was instructed to follow the Leader's rate and to synchronize their production of tone onsets with the Leader's. In the First-Leader condition, Duet partners decided amongst themselves who would be the Leader and who would be the Follower. Partners performed 6 test trials of the First-Leader condition. Then, in the Second-Leader condition, partners switched roles and the First Leader became the Follower while their partner became the Leader, and 6 test trials were subsequently performed in this condition. On each trial of the Duet performance, the partner assigned as Leader cued the performance rate by performing the first 8 melody tones alone, allowing the Leader to clearly signal the performance tempo to their partner at the beat level (defined by the first 8 tones which were all quarter notes, by comparison to the rest of the melody which featured a combination of quarter-, eighth-, and half-notes). The Follower joined the Leader on the 9th melody tone, and the rest of the trial was played entirely in unison (the two pianists intended to produce the same pitches at the same time). EEG was recorded during Solo and Duet piano performance tasks. Resting state EEG data was collected from both partners, as was EEG data associated with a second Duet task (after the Second-Leader condition) in which partners performed

[1]https://github.com/sccn/labstreaminglayer/tree/master/LSL/liblsl/

[2]https://github.com/sccn/labstreaminglayer/wiki/LabRecorder.wiki

[3]http://www.mbraintrain.com/smarting/

[4]www.easycap.de

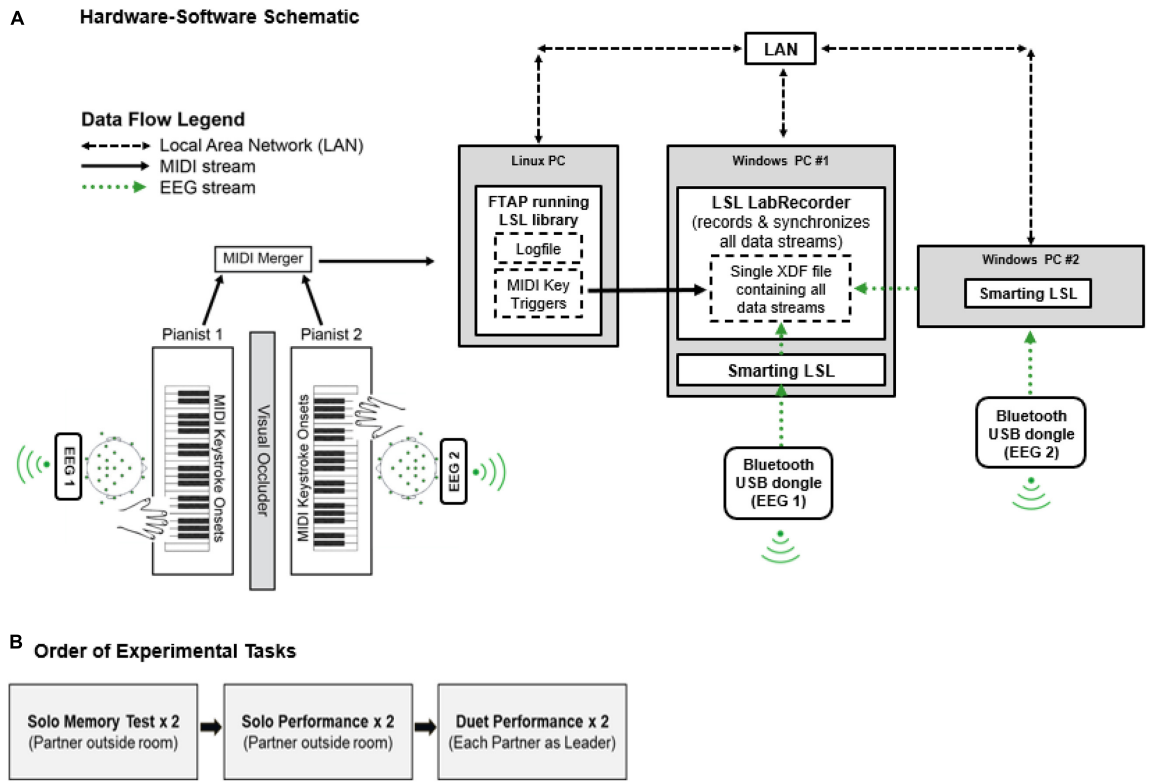

FIGURE 1 | (A) Hardware-software schematic. MIDI keystroke data (solid black arrows) from duet pianists are merged and sent to FTAP software running the LSL library in a Linux OS. LSL sends MIDI time-stamps over the Local Area Network (LAN, dashed black arrows) to LabRecorder software, where timestamps are recorded as keystroke event triggers. EEG data streams (dotted green arrows) from duet pianists are sent *via* Bluetooth to SmartingLSL software running the LSL Library in a Windows OS. LSL sends EEG data streams to LabRecorder software. LabRecorder software synchronizes MIDI and EEG data streams by correcting for clock offsets between respective data acquisition computers (Linux/Windows). Synchronized data streams are stored in a single XDF file for storage. **(B)** Order of Experimental Tasks.

the melody cued by a metronome and there was no Leader; these data are not reported in the current paper.

ANALYSES

Data Cleaning

Identification and Removal of MIDI Keystroke Errors

Since pitch errors in music performance often coincide with timing errors (Drake and Palmer, 2000), melody repetitions containing pitch errors (defined as added or deleted tones) were identified using the MIDI Matcher program in MATLAB (v1.1; Large, 1993) and were excluded from both behavioral and neural analyses (rarely occurring substituted pitches were retained as these do not disrupt the timing of pitch sequencing). For Solo performances, this procedure resulted in exclusion of 3.3% of the total melody repetitions (16/480 melody repetitions; see Zamm et al., 2019). For Duet performances, 3.96% of the total melody repetitions (38/960 melody repetitions) were excluded.

EEG Artifact Correction

EEG data were corrected for artifacts using EEGLAB (Delorme and Makeig, 2004). First, data were concatenated across all trials and conditions in the entire study, filtered between 1 and 40 Hz with a Hanning windowed sinc FIR filter (low pass order = 100; high pass order = 500; Widmann and Schröger, 2012), segmented into consecutive 1 s epochs, and pruned for non-stereotypical artifacts (kurtosis limit = 2). Data were then submitted to extended infomax Independent Component Analysis (ICA; Bell and Sejnowski, 1995; Jung et al., 2000a,b). ICA components that reflected eye blinks, lateral eye movements and other sources of non-cerebral activity were identified and removed from the data. This procedure resulted in the removal of 1–5 components per subject ($M = 2.6$, $SD = 0.98$). Artifact-corrected data were referenced to the common average across electrode sites. A single bad channel was identified in a single participant, and replaced by means of spherical interpolation as implemented in EEGLAB.

Definition of Analysis Window

All behavioral and EEG spectral density measures were computed over a fixed-duration analysis window. The use of a fixed duration window was necessary for spectral density analyses to ensure identical frequency resolution across participants' spectra; behavioral data were analyzed over the same window to ensure that neural and behavioral comparisons were made across the same data segments.

The window duration of 9 s was selected, corresponding to the fastest pair's mean duration of melody performances across Duet conditions (2.4% of total melody performances in the sample were faster than this duration). This window was defined relative to the fastest pair (and not the slowest pair) so that padding was not necessary to achieve equivalent window duration across performances. Neural oscillations at the duet frequency were assumed to show slow (low-frequency) changes over time; therefore for this analysis only we assessed amplitude envelope measures over the full melody performance instead of the shorter 9-second window to allow sufficient time for capturing their temporal dynamics.

Behavioral Measures of Temporal Coordination

Performance Rates

Mean Solo and Duet Performance rates were defined as the mean inter-tone onset interval (IOI, milliseconds) at the quarter-note level across each participant's melody performances (half notes were linearly interpolated prior to IOI computation and off-beat eighth notes were excluded, consistent with rate calculations in previous studies of piano duet performance; Loehr and Palmer, 2011; Zamm et al., 2015, 2016). Mean IOIs for Duet performances were first computed separately for the Leader and Follower. Leaders' and Followers' mean IOIs did not differ significantly in either Leader-order condition, First-Leader: $t(38) = 0.015$, $p = 0.99$; Second-Leader: $t(38) = 0.016$, $p = 0.99$. Therefore, Leaders' and Followers' mean Duet performance IOIs were averaged to yield a single mean Duet IOI for each pair in each Duet condition. To facilitate comparison with EEG frequency spectra, mean Solo and Duet IOIs were converted to Hertz (Hz = 1,000/mean Duet IOI in ms, or # tones/s). Whereas Zamm et al. (2019) converted Solo IOIs to Hz prior to averaging the means (for comparison with EEG measures), the current manuscript changed the method slightly to allow for comparisons between behavioral measures of Solo performance rates with Duet asynchronies, which are computed in milliseconds.

Duet Synchronization

Two well-established measures of tone onset asynchrony were computed for each Duet pair on their Duet performances (Repp and Su, 2013): signed asynchrony and absolute asynchrony. Signed asynchrony was defined as the mean signed difference in piano keystroke onset times that partners intended to perform simultaneously (Leader's onsets − Follower's onsets). Signed asynchrony provides a measure of Leading-Following behavior, where negative values indicate that the Leader's tone onsets preceded the Follower's. Signed duet asynchronies permit tests of the hypothesis that Leading-Following behavior in Duet performance is a function of how much faster the Leader's spontaneous (Solo) rate is relative to the Follower's. Absolute asynchrony was defined as the absolute difference between tone onsets that partners intended to perform simultaneously [abs (Leader's onsets − Follower's onsets)]. Absolute asynchrony provides a measure of a given pair's overall synchronization accuracy, where small asynchrony values indicate high synchronization accuracy. Absolute asynchronies permit tests of the hypothesis that overall synchronization accuracy between performing musicians is associated with the degree to which they showed neural entrainment at the Duet Performance Rate. Both signed and absolute synchronies for each performance were computed as a proportion of the mean Duet IOI for that performance, to adjust for differences in performance rate across pairs.

EEG Measures of Neural Entrainment

Power Spectral Density of Oscillations at Duet Performance Rate

Neural entrainment during Duet performance was defined within each duet condition by the EEG Power Spectral Density (PSD) of each partner, computed at the pair's mean Duet Performance Rate (section "Performance Rates"). This definition is consistent with previous work defining stimulus entrainment by enhanced spectral amplitude of oscillations at the stimulus frequency (Nozaradan et al., 2011, 2012, 2013). The mean Duet Performance Rate was computed as the mean IOI across partners and across melody performances within each Leader-Order condition ($n = 24$ in cases for which no performances were discarded due to errors). PSD was computed separately for each melody repetition and then averaged to obtain a single value per partner, per Leader-Order condition.

To compute PSD, artifact-corrected EEG data were low-pass filtered (Hanning windowed sinc FIR filter, 20 Hz, order 1,000), high-pass filtered (0.1 Hz, order 1,000), and epoched into 9 s segments (for the 2.4% of melody repetitions shorter than 9 s, epochs extended into the beginning of the subsequent melody repetition). To reduce edge effects, epochs were multiplied with a 4,500-point (9 s) Hanning window, and the PSD was computed for each epoch and channel using Welch's method (*pwelch* function in MATLAB; frequency resolution = 0.061 Hz). Resulting power spectra were log-transformed to compensate for $1/f$ power distribution characteristic of EEG data, and then separately averaged across epochs on each channel for each participant.

A noise normalization procedure was subsequently applied by subtracting from each frequency bin the mean power at ± 3 neighboring frequency (± 0.183 Hz) bins (Nozaradan et al., 2011, 2012; Tierney and Kraus, 2013, 2014; Zamm et al., 2019). This procedure should result in cancellation of noise-related spectral peaks and preserve spectral peaks associated with non-noise components. Noise-subtracted mean spectra were subsequently computed for each participant by averaging noise-subtracted spectra across all electrode sites. Mean spectra at a fronto-central Region of Interest (ROI = FC1, FC2, Cz, and Fz) were also computed for each participant, based on previous findings (Zamm et al., 2019) that identified this ROI as showing maximal power at the frequency of the self-paced Solo piano performances. To allow for comparison of spectral power at each pair's unique mean Duet Performance Rate for each condition, power spectra were aligned across participants using a 2.99 Hz window centered on their mean Duet Performance Rate in Hertz (corresponding to ± 24 frequency bins on either side of the Duet Performance Rate, the number of bins between the slowest mean Duet

Performance Rate and the lower edge of the frequency spectrum after noise subtraction).

Amplitude Envelopes of EEG Oscillations at the Duet Performance Rate

Calculation of Amplitude Envelopes

Amplitude envelopes of EEG oscillations at the Duet performance rate were computed to assess the dynamics of the Duet partners' neural responses over time using methods described in detail in Zamm et al. (2018). First, pianists' EEG data in each Duet condition were spatially filtered to extract a single time-course of oscillations at their unique Duet performance rate. Spatial filters were implemented to improve the signal-to-noise ratio associated with neural oscillations at the Duet performance rate while also reducing multiple comparison issues associated with multi-dimensional EEG data. Spatial filters were obtained by submitting each pianist's Solo EEG data—representing an independent data set for the same pianists from a comparable task—to spatio-spectral decomposition (SSD), a linear decomposition algorithm tailored for extracting oscillations in a target frequency band while attenuating neighboring frequencies (Nikulin et al., 2011; Dähne et al., 2014). SSD was computed to extract oscillations in the range of observed Solo performance rates (1.5–3.5 Hz), corresponding closely to the range of observed Duet rates. For each participant, the first and final authors visually selected the SSD spatial filter most clearly representing a stereotypical fronto-central auditory-motor delta topography. After selecting spatial filters for each pianist, each pianist's artifact-corrected Duet EEG data in each condition were filtered around their Duet performance rate (mean Duet rate $\pm$ 0.183 Hz, signal bandwidth = 0.366 Hz, 2nd order butterworth filter), and multiplied with their selected spatial filter, yielding a single time course of neural oscillations at the Duet performance rate. This time course was epoched into segments corresponding to the duration of each melody repetition $\pm$ 2.5 seconds (s) and down-sampled to 100 Hz using an antialiasing FIR filter (pop_resample.m in EEGLAB), which improved the efficiency of subsequent calculations while remaining significantly above the Nyquist criterion. Amplitude envelopes were subsequently defined as the absolute value of the Hilbert transform of each melody epoch. To minimize edge artifacts of the Hilbert transform, 2.5 s tails were trimmed. Zamm et al. (2018) reports further detail on the SSD decomposition, including topographic maps.

Because musicians do not perform the same melody with identical timing across the tone sequence (Palmer, 2013), the number of EEG samples between corresponding melody tones differed across performances. To allow for comparison across performances within each pair and Duet condition, partner's amplitude envelopes were resampled such that the number of samples between corresponding tone events was constant across different performances of the stimulus melody for each pair and condition. First, the minimum number of samples between tone onsets was determined across melody repetitions within the pair and condition. This minimum value was used to resample all IOIs. The number of samples for each eighth-note interval (the shortest notated IOI) was set equal to this number. Quarter notes contained twice this number, whereas half notes contained 4 times this number. Shape-preserving piece-wise cubic interpolation (interp1.m in MATLAB, using "pchip" and "extrap" arguments), which fits a cubic polynomial between each set of interpolation points, was applied to preserve the original shape of the resampled signal. Thus, amplitude envelopes could be averaged across melody repetitions while the data segments being averaged corresponded to the same tone onsets.

Inter-Brain Correlations of Duet Partners' Amplitude Envelopes

To quantify correspondences in the amplitude dynamics of partners' neural oscillations at the Duet performance rate, inter-brain correlations of EEG amplitude envelopes (Amplitude Envelope Correlations, AECs) were assessed for each pair, using the method described in Zamm et al. (2018). Specifically, AECs were computed for each melody repetition within each pair and Leader-order condition. For the first melody repetition in each trial, AECs were computed over data occurring after the 8th tone (during which both partners were performing). Inter-brain AECs for each melody repetition were subsequently converted using the Fisher-*z* transform to ensure normality, and averaged across melody repetitions, within-pair and within-condition.

To test whether observed inter-brain AECs reflected amplitude correspondences specific to each Duet pair, AECs from observed Duet pairs were compared with AECs of surrogate pairs. Surrogate pairs were created within each condition by pairing each Leader with all Followers except their true partner: This procedure yielded 19 surrogate Duet pairs per Leader and per condition. For each surrogate pairing, amplitude envelopes were resampled within Duet condition such that the number of samples between corresponding tone events was constant across melody repetitions, using the same procedure described above. Resampling was necessary because surrogate partners' performances occurred at different rates, and their data could not be compared without resampling relative to the musical event structure. After resampling, amplitude envelopes of corresponding melody repetitions in the trial structure were correlated (24 repetitions per condition), and averaged using the same procedure as for observed pairs. Amplitude envelope correlations were averaged within each surrogate pair across conditions.

RESULTS

Behavioral Measures

Solo Performance Rates

The distribution of individual pianists' Solo performance rates (mean IOI in ms) is shown in **Figure 2A**. The data are displayed by Duet pair, to show the range of differences among randomly assigned partners. Solo rates for each pair are ordered from smallest difference between partners to largest difference. A range of Solo performance rates was observed across participants, with nearly doubled rate increase from the fastest pair average (302 ms) to the slowest pair average (597 ms).

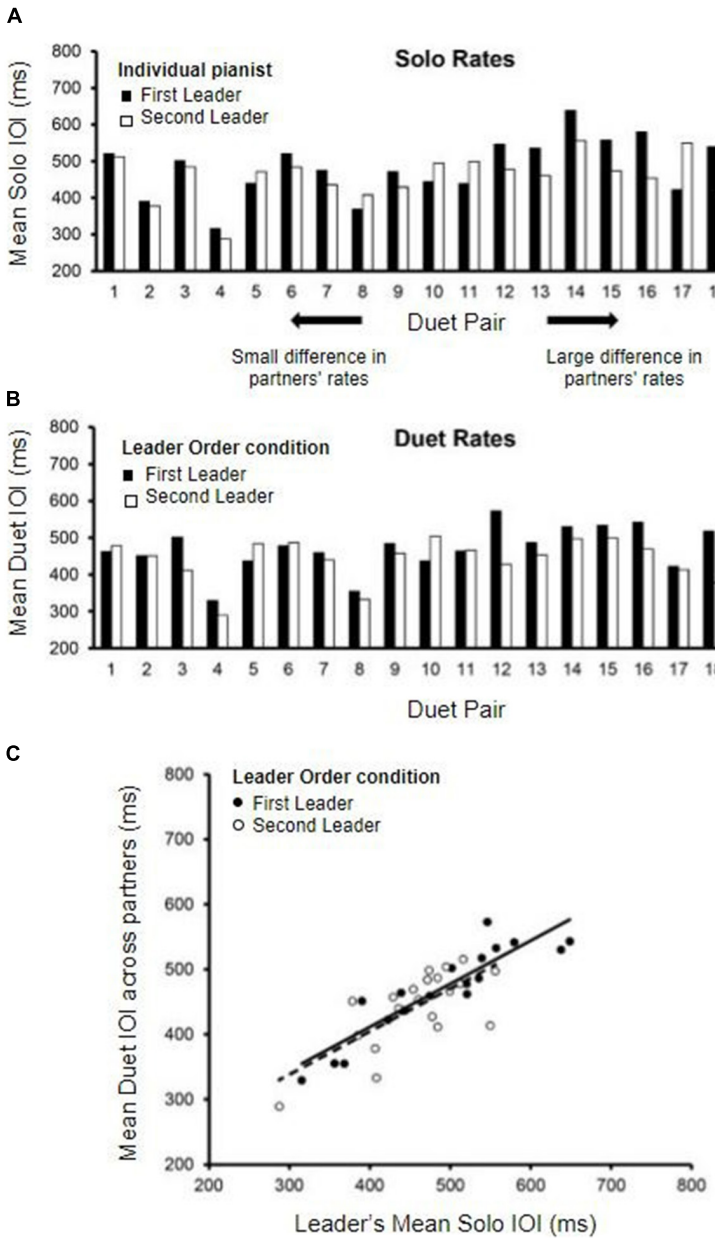

FIGURE 2 | Solo and Duet performance rates. **(A)** Mean Solo performance rates for individual partners; partners are labeled by who served as Leader in the First-Leader (black bars) and Second-Leader (white bars) Duet conditions. Pairs are ordered by the magnitude of difference in partners' Solo rates (smallest difference on the left, largest on the right). **(B)** Mean Duet performance rates for each pair (averaged across partners) in the First-Leader (black bars) and Second-Leader (white bars) conditions. Pairs are ordered the same as in panel **(A)**, by the magnitude of difference in partners' Solo rates. **(C)** Leaders' mean Solo performance rates (x-axis) correlated with Mean Duet performance rates (y-axis) in the First-Leader (black dots) and Second-Leader (white dots) conditions, with trend lines (solid = First-Leader condition; dashed = Second-Leader condition). Each dot represents data from one pair.

The differences between Duet partners' Solo performance rates were examined in terms of the Leader-Order Duet conditions, to determine whether one Leader-Order condition differed from the other for the randomly paired partners. The mean difference in partners' Solo performance rates was 74.26 ms (range = 8.6 to 263.76 ms, SD = 62.07 ms). The First and Second Leaders' Solo rates did not differ significantly, $t(19) = -1.29$, $p = 0.21$ (First-Leader mean = 485.46 ms; Second-Leader mean = 458.23 ms), ensuring that any subsequently observed differences between First-Leader and Second-Leader conditions were not simply a function of their random assignment to Duet pairs.

Duet Performance Rates

We compared the mean Duet performance rates of Leaders and Followers within Leader-Order conditions. Those mean

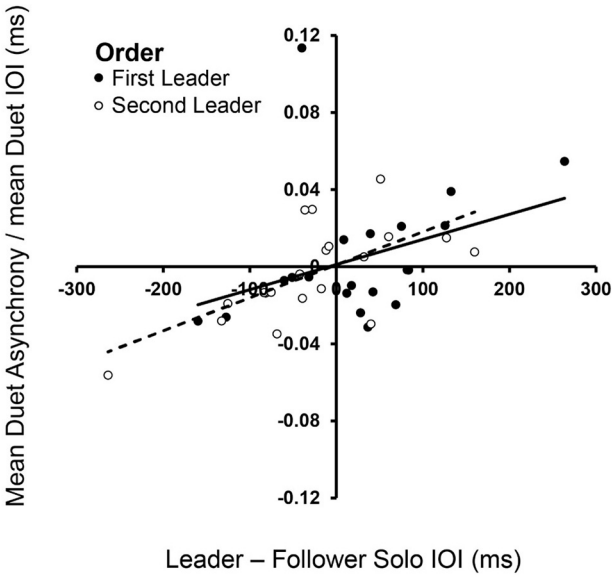

FIGURE 3 | Spontaneous frequencies in Solo performance influence Duet synchronization. Signed differences in partners' mean Solo rates (Leader Solo mean IOI—Follower Solo mean IOI, x-axis) correlated with signed Duet tone onset asynchronies (Leader tone onset—Follower tone onset, divided by mean Duet performance rate) in First-Leader (black dots) and Second-Leader (white dots) conditions. Each dot represents data from one pair.

values indicated that the duet partners were performing at the same rate within condition, as expected [First-Leader means: $t(38) = 0.015$, $p = 0.99$; Second-Leader means: $t(38) = 0.016$, $p = 0.99$]. Therefore, the mean Duet performance rates within condition were defined for each Duet pair as the mean IOI averaged across the two duet partners. The distribution of mean Duet performance rates by Leader-Order condition is shown in **Figure 2B**, which orders pairs the same way as in 2A (by difference in Solo rates). As shown, the difference between First-Leader and Second-Leader mean Duet IOIs tended to be smaller for pairs with smaller differences in Solo rates (left end of **Figures 2A,B**) and larger for pairs with larger differences in Solo rates (right end of **Figures 2A,B**). Duet performance rates in each Leader-Order condition were then correlated with each partner's Solo performance rate to determine whether the Leader set the rate of Duet performance to a value similar to their Solo rate. As shown in **Figure 2C**, the correlations of the Leader's mean Duet performance rates with Leader's Solo rate were significant, [$r\ (18)_{First-Leader} = 0.90$, $r(18)_{Second-Leader} = 0.71$, both p's < 0.001], whereas the correlations with Follower's Solo performance rate were not [$r(18)_{First-Leader} = 0.24$, $p = 0.30$, $r(18)_{Second-Leader} = 0.31$, $p = 0.19$].

To confirm that the Leader's Solo rate had a greater influence on the Duet performance rates than did the Follower's Solo rate, a multiple regression model predicting Duet performance rate from Leader' Solo rate and Follower's Solo rate was implemented separately for each Duet condition. For the First-Leader condition, this regression model yielded a significant fit, $R^2 = 0.81$, $F(2, 17) = 37.70$, $p < 0.001$: The Leader's Solo performance rate contributed significantly, standardized $\beta = 0.908$, $t(17) = 8.36$, $p < 0.001$, whereas the Follower's Solo performance rate did not, standardized $\beta = -0.02$, $t(17) = 0.15$, $p = 0.881$. For the Second-Leader condition, this regression model also yielded a significant fit, $R^2 = 0.52$, $F(2, 17) = 9.22$, $p = 0.002$: Again, the Leader's Solo rate contributed significantly, standardized $\beta = 0.68$, $t(17) = 3.88$, $p = 0.001$, whereas the Follower's rate did not, standardized $\beta = 0.11$, $t(17) = 0.64$, $p = 0.53$. These results confirm that Leaders in both conditions set the tempo of Duet performance close to their Solo performance rate, and Followers performed at the Leaders' rate.

Duet Synchronization and Correlations With Solo Rates

Duet pairs' mean signed asynchronies (Leader − Follower tone onsets, divided by mean Duet IOI) across Leader conditions ranged from negative to positive values (range = −0.056 to 0.113). Tests of Leader Order effects on signed asynchronies yielded no significant differences [$M_{First-Leader} = 0.0047$; $M_{Second-Leader} = -0.0036$, $t(19) = -0.70$, $p = 0.49$]. Duet pairs' mean absolute asynchronies were also computed [abs (Leader − Follower tone onsets) divided by mean Duet IOI], and ranged from 0.033 to 0.124 across Leader conditions. Tests of Leader Order effects on absolute asynchrony indicated no significant differences [$M_{First-Leader} = 0.050$, $M_{Second-Leader} = 0.054$, $t(19) = 1.12$, $p = 0.28$], suggesting that overall synchronization accuracy was not significantly influenced by whether the partner served as Leader in First or Second Leader conditions.

Dynamical systems hypotheses predict that the signed asynchrony, which is the degree to which Leaders' tone onsets preceded Follower's tone onsets, is related to how much faster the Leader's Solo rate is relative to the Follower's (Zamm et al., 2015). We tested this hypothesis by determining whether the signed asynchrony was related to the difference in partners' Solo performance rates, which ranged widely across Duet pairs. **Figure 3** shows that the signed difference in partners' Solo performance rates was significantly correlated with their signed Duet asynchronies in both Leader-Order conditions [First-Leader: $r_s(18) = 0.49$, $p = 0.028$; Second-Leader: $r_s(18) = 0.65$, $p = 0.002$], consistent with dynamical systems predictions that coupling between oscillators is a function of the difference in their natural frequencies.

EEG Power Spectral Density

Channel-Mean PSD Peaks at Duet Performance Rate

EEG spectral power at the Duet Performance Rate was defined for each pianist as mean PSD at the frequency bin closest to the mean Duet Performance Rate, averaged across electrode sites (channel mean PSD). **Figure 4**, top panel, shows mean noise-normalized spectra from members of a sample pair in each Duet condition (First-Leader condition in solid lines, Second-Leader in dashed lines), where black lines depict the Leader in each condition and green lines depict the Follower. Vertical lines indicate the frequency closest to this pair's mean Duet Performance Rate for each condition. This figure illustrates that each partner showed a

peak in spectral power at the frequency closest to the pair's mean Duet Performance Rate in each condition, both when they were Leader and Follower (as expected, since Leaders and Followers had similar rates within performance).

To assess whether each individual pianist's spectral power at the Duet performance rate changed as a function of their musical role (Leader/Follower), a one-way repeated-measures ANOVA on mean noise-normalized PSD at their Duet performance rate was conducted with Role (Leader/Follower) as a fixed factor and Subject as the random variable. Individual pianists' spectral power did not change as a function of musical Role, both across channels, $F(1,39) = 1.256$, $p = 0.269$, and at the auditory-motor ROI, $F(1,39) = 0.287$, $p = 0.595$, indicating stability of spectral power within individual pianists across musical Roles.

Figure 4, bottom left, shows the mean noise-normalized spectra across channels for each pair (light gray lines). The blue line represents the grand average across channels and the red line represents the grand average at the auditory-motor ROI. The significance of this spectral peak for all duet pairs was evaluated separately for each Duet condition. Wilcoxon signed-rank tests were computed on the difference in medians between noise-normalized PSD at the frequency bin closest to the Duet Performance Rate (in Hertz) and mean PSD at the surrounding ± 8 frequency bins (John and Picton, 2000). Both Duet conditions showed statistically significant peaks in spectral power at the Duet Performance Rate relative to the mean of the neighboring frequencies ($z_{\text{First}-\text{Leader}} = 4.50$, $p < 0.001$; $z_{Second-Leader} = 4.31$, $p < 0.001$), confirming the prediction of increased power of neural oscillations at the Duet performance frequency in both Duet conditions.

PSD Peaks at Auditory-Motor ROI

Figure 4, bottom right, shows the mean topography of noise-normalized PSD at the Duet performance rate. It can be observed that power was maximal at fronto-central sites characteristically associated with auditory-motor perception and production (Nozaradan et al., 2011, 2015, 2016; Zamm et al., 2019). We evaluated whether participants showed greater neural entrainment to the Duet performance rate at these electrode sites, specifically at the ROI (section "Power Spectral Density of Oscillations at Duet Performance Rate"). To evaluate whether enhanced spectral power indicated the presence of a peak at the Duet performance rate in both conditions, ROI power at the Duet performance rate was compared with mean ROI power at the surrounding 8 frequency bins (Duet performance rate ± 8 bins). A Wilcoxon signed-rank test indicated that spectral power at the Duet performance rate was indeed higher than power at surrounding frequencies ($z_{\text{First}-\text{Leader}} = 4.31$, $p < 0.001$; $z_{Second-Leader} = 5.15$, $p < 0.001$), confirming the presence of a spectral peak at the Duet rate. A Wilcoxon signed-rank test indicated that ROI spectral power at the Duet rate did not differ between conditions ($z = -0.07$, $p = 0.95$). **Figure 4**, bottom (left, red line), shows the grand average noise-normalized spectrum at the ROI. A clear peak can be observed at the Duet performance rate.

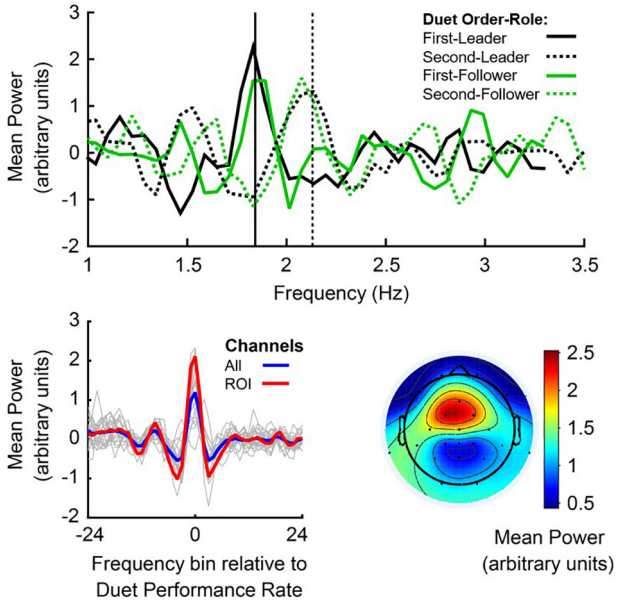

FIGURE 4 | Power Spectral Density, centered at the Duet performance rate. Top panel: Noise-normalized power spectra from a sample pair of duet pianists for First-Leader (solid lines) and Second-Leader conditions (dashed lines), where the Leader's mean Power in each condition is shown in black and the Follower's mean Power in each condition is shown in green. Frequency (Hz) is shown on the x-axis and mean noise-normalized power is shown on the y-axis. Vertical lines indicate the mean Duet performance rate (averaged across partners) in Hertz (# tones per second) in First-Leader (solid vertical) and Second-Leader (dashed vertical) conditions. Bottom panel (left): Mean power spectra centered at the frequency of each Duet performance, shown for each pair in thin gray lines and grand average across pairs in blue; *a priori* defined auditory-motor ROI (FC1, FC2, Fz, and Cz) in red. The zero-frequency bin on the x-axis represents each pair's Duet performance rate (center of each spectrum). Bottom panel (right): Grand average topography of spectral power at the mean Duet performance rate (zero-frequency bin of left panel), averaged within pair across conditions and then across pairs.

PSD at Duet Performance Rate Correlates With Duet Synchronization Accuracy

Next, the Duet pairs' synchronization accuracy (mean absolute asynchrony divided by the mean performance beat IOI) in each condition was compared directly with mean PSD at the Duet performance rate. Synchronization accuracy and mean PSD were negatively correlated for Leaders [$r_{\text{First}-\text{Leader}}$ (18) = −0.569, $p = 0.009$; $r_{\text{Second}-\text{Leader}}$ (18) = −0.571, $p = 0.009$], and less strongly correlated for Followers [$r_{\text{First}-\text{Leader}}$ (18) = −0.285, $p = 0.224$; $r_{\text{Second}-\text{Leader}}$ (18) = −0.448, $p = 0.048$]. As shown in **Figure 5**, the larger the PSD values for Leaders, the smaller the Duet asynchrony. One duet pair in the First Leader condition showed a mean asynchrony value of 0.1236 (12.36% of their mean IOI), slightly greater than 3SD from the mean value for this condition (= 0.1124). The correlation between synchronization accuracy and mean PSD in the First Leader condition recomputed without this pair was marginally significant, $r(17) = -0.4601$, $p = 0.0845$. Due to the small sample

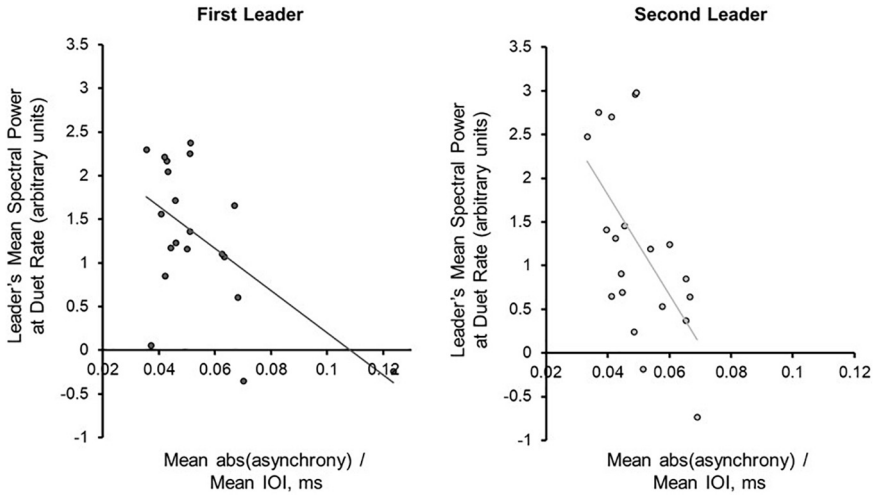

FIGURE 5 | Power Spectral Density at the Duet performance rate is associated with synchronization accuracy. Correlations (with trend lines) of mean duet synchronization accuracy (absolute tone onset asynchrony divided by mean duet IOI) with mean spectral power at the Duet performance rate in the First-Leader (left) and Second-Leader (right) Duet conditions. Each dot represents one pair.

size and the fact this pair's overall synchronization accuracy was still quite high, this pair was retained in subsequent analyses.

For each Duet condition, a multiple regression model was implemented to predict mean absolute Duet asynchrony, adjusted for Duet performance rate, from Leader and Follower PSD at the Duet performance rate. For the First-Leader condition, this model was significant, $R^2 = 0.33$, $p = 0.036$: The Leader's PSD was a significant predictor of Duet asynchrony, standardized $\beta = -0.578$, $t(17) = 2.47$, $p = 0.025$, whereas the Follower's PSD was not, standardized $\beta = 0.02$, $t\ (17) = 0.08$, $p = 0.94$. For the Second-Leader condition, this model was also significant, $R^2 = 0.34$, $p = 0.03$: The Leader' PSD was a marginally significant predictor of Duet PSD, standardized $\beta = -0.480$, $t(17) = 1.88$, $p = 0.08$, whereas the Follower's was not, standardized $\beta = -0.14$, $t(17) = 0.56$, $p = 0.58$. Thus, Leaders' PSD values increased as the Duet partners' asynchrony decreased, regardless of which partner served as Leader (First- or Second-Leader).

EEG Amplitude Envelope Correlations

Figure 6 shows the mean amplitude envelopes computed at the Duet performance rate for a sample pair (Leader/Follower) in First-Leader (Panel A) and Second-Leader (Panel B) Duet conditions. It can be observed from this figure that partners show similar amplitude fluctuations across the time series within each condition. Correspondences in partners' amplitude envelopes were quantified by computing inter-brain Amplitude Envelope Correlations (AECs). As described in section "Inter-Brain Correlations of Duet Partners' Amplitude Envelopes", AECs within each condition were computed as Fisher *r*-to-*z* scores. Because Fisher *r*-to-*z* scores did not differ significantly between First-Leader and Second-Leader conditions, $F(1, 19) = 1.83$, $p = 0.19$, each Duet pair's condition-mean Fisher *r*-to-*z* scores were averaged across conditions. This procedure yielded a single mean Fisher *r*-to-*z* score per Duet pair ($N = 20$), which was then converted to a Pearson's *r*-value. The mean observed AEC across pairs and conditions was $r = 0.26$ (range of *r*-values across pairs $= -0.04$ to 0.57).

Amplitude envelopes may be correlated across Duet partners because they exhibited inter-brain correspondences, or, alternatively, because they performed the same task (each Duet pair performed the same melody). To test whether the AEC values were pair-specific, the observed values were compared with the chance estimate based on mean AECs of each pair's surrogate distribution generated from the re-pairing of data from different duet partners (described in section "Inter-Brain Correlations of Duet Partners' Amplitude Envelopes"). **Figure 7** shows the observed mean amplitude envelope correlation for each pair, and the mean correlation of each pair's surrogate distribution, which represents the expected correlation between amplitude envelopes of pianists performing the same melody at different times. Binomial tests comparing the observed inter-individual envelope correlations with surrogate distributions indicated that the observed correlations were significantly higher than the surrogate correlations. The mean observed inter-pair correlation was higher than the mean chance (across-pair) Pearson correlation values in 15/20 pairs ($p = 0.02$; median observed $r = 0.29$, median surrogate $r = 0.13$).

DISCUSSION

The current study demonstrated that two pianists' spontaneous performance rates were associated with their ability to synchronize actions when performing duets. Specifically, differences in partners' spontaneous rates were positively correlated with Duet asynchronies: Partners with larger differences in spontaneous rates showed larger signed tone onset asynchronies. This finding is consistent with dynamical systems

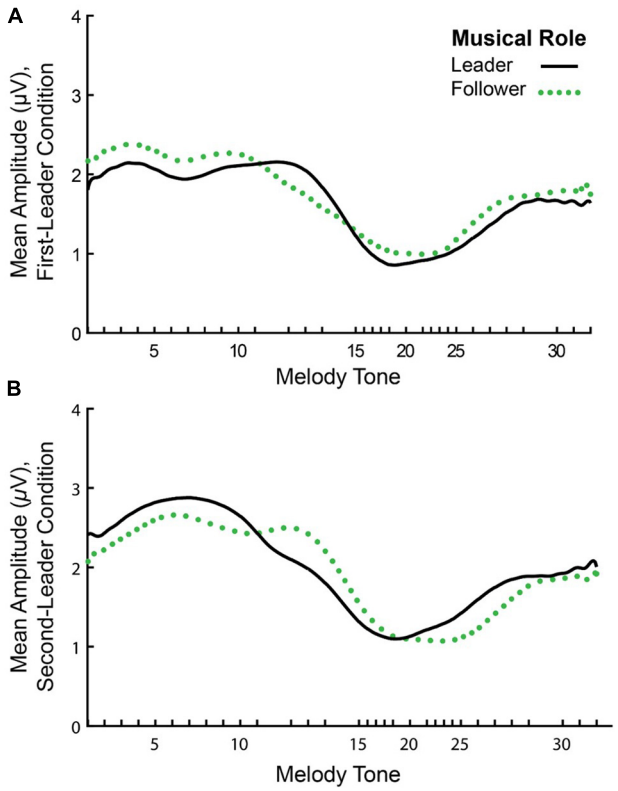

FIGURE 6 | Mean amplitude envelopes of one pair's neural oscillations at the Duet performance rate. Timecourse of amplitude fluctuations in spectral energy at the Duet performance rate for a sample pair in the First-Leader **(A)** and Second-Leader **(B)** conditions. In each condition, the Leader's mean amplitude envelope across 24 melody performances is shown in black (solid line) and the Follower's mean amplitude envelope is shown in green (dotted line).

accounts that predict period coupling between oscillations as a function of the difference in their natural frequencies (Haken et al., 1985; Pikovsky et al., 2003). In contrast to previous studies (Schmidt and O'Brien, 1997; Richardson et al., 2005, 2007; Lopresti-Goodman et al., 2008; Loehr and Palmer, 2011; Zamm et al., 2015, 2016), the pianists' duet performances were not paced by an external cue. Thus, this finding demonstrates non-linear dynamics in human interpersonal coordination in the context of natural, uncued joint action.

The current findings add to a growing body of work indicating that spontaneous music performance rates reflect oscillatory processes that influence auditory-motor entrainment within and between individuals (Zamm et al., 2016, 2018; Scheurich et al., 2018; Palmer et al., 2019; Roman et al., 2020). Whether the spontaneous performance rates reflect intrinsic timekeeping processes or biomechanical constraints is a topic for further research. We also observed period coupling in pianists' neural activity during duet performance. Duet partners' neural oscillations were enhanced at the performance frequency of produced tone onsets (Duet frequency), evidenced by peaks in each partner's power spectral density measures at the Duet frequency. When each partner took turns being the Leader, both partners' spectral peaks were observed at the Duet frequency determined by the Leader. Moreover, enhanced power at the Duet frequency was positively associated with partners' synchronization accuracy, with stronger correlations for Leaders than for Followers. Partners with high synchronization accuracy, measured as smaller tone onset asynchronies, showed higher spectral peaks at the Duet frequency, relative to partners with low synchronization accuracy. Furthermore, synchronization accuracy was better predicted by the Leader's spectral energy associated with the performance rate than by the Follower's spectral energy, suggesting that the spectral peaks at performance frequencies serve as a possible marker of leadership behavior. Furthermore, synchronization accuracy was better predicted by the Leader's spectral energy associated with the performance rate than by the Follower's spectral energy, suggesting that the spectral peaks at performance frequencies serve as a possible marker of leadership behavior. Together, these findings demonstrate a clear link between period coupling seen in interpersonal synchrony measures and in neural oscillations at the frequency of a jointly produced action. One interesting question for future research is what determines inter-subject variability in this overall relationship, and what factors—such as entrainment at higher rhythmic groupings—may allow partners to achieve high synchrony even with low spectral energy at the common frequency of a joint action.

The observed oscillatory cortical activity in the current study may have been influenced by evoked potentials elicited by the perception of rhythmically occurring tone onsets, as suggested by an ongoing debate in the literature over whether rhythmic brain activity reflects purely oscillatory processes or also stimulus-evoked potentials elicited by rhythmic stimuli (see Haegens and Golumbic, 2018 for a review). Although the current design cannot disentangle these potential contributions to the observed cortical activity at the frequency of pianists' performance rates, it should be noted that cortical activity was measured at the mean musical beat frequency, which does not directly necessarily correspond to the frequency at which all tone onsets occur, but rather to the perceived frequency at which tone onsets are grouped (Grahn and Brett, 2007). There is compelling evidence that beat-related brain activity is not purely stimulus-driven, but rather arises from endogenous oscillatory activity; specifically, enhanced spectral power of cortical activity can be observed at the beat frequency that subjects perceive tones to occur at, even when the tones occur at a different frequency (Nozaradan et al., 2011; Fujioka et al., 2015). Thus, enhanced cortical activity at the beat frequency of pianists' performances in the current study likely reflects a combination of endogenous oscillatory processes and stimulus-driven contributions; an important future direction is to design studies that can disentangle these possibilities.

Duet partners also showed temporally correlated fluctuations in amplitude dynamics across the entire performance. Amplitude coupling was observed in the inter-brain correlations of partners' spectral energy at the Duet frequency (rate of performance). Correlations between observed partners' amplitude envelopes were higher on average than correlations between duet pianists who performed the same task but with other partners (surrogate

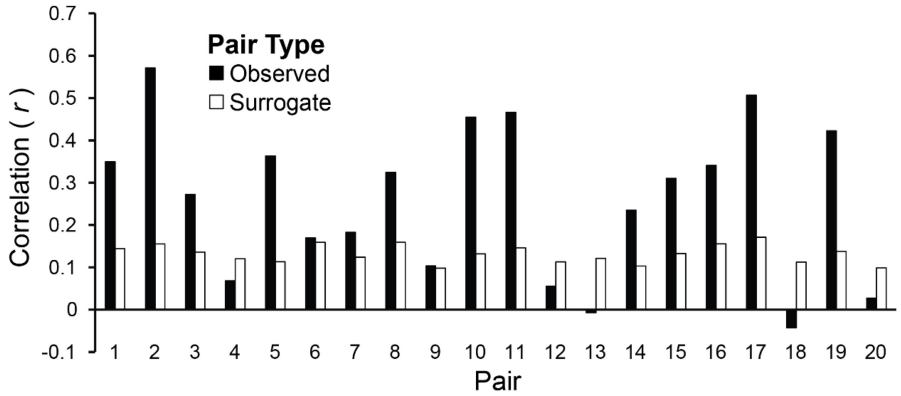

FIGURE 7 | Amplitude envelopes at the Duet performance rate are correlated between duet partners. Mean correlations of duet partners' mean amplitude fluctuations in spectral energy at the Duet performance rate are shown for each pair, averaged across Duet conditions (black bars). Pairs are ordered by difference in Solo performance rates as shown in **Figure 2A** (smallest difference at left, largest at right). Mean correlations of surrogate partners' amplitude envelopes (based on 19 surrogate pairings for each partner with all other partners) are shown for each pair, averaged across Duet conditions (white bars).

pairs), suggesting that inter-brain amplitude coupling is partner-specific and may arise from the temporally distinctive auditory-motor patterns of each performance. It cannot be ruled out that some amount of inter-brain amplitude coupling in the current study arose from partners' perception of musical sequences with identical rhythmic (temporal) properties. Our previous work (Zamm et al., 2018) indeed suggests that amplitude envelopes reflect the unique timing of pianists' performances of the same categorical rhythms, and therefore it is likely that the current inter-brain correlations reflect the specific (unique) way in which each pair produced the notated stimulus rhythm. Moreover, some evidence from functional magnetic resonance imaging suggests that individuals who are independently exposed to temporally identical stimuli show inter-brain similarities in sensory responses (Hasson et al., 2004; Wilson et al., 2007; Hanson et al., 2009). Further work is needed to disentangle the extent to which inter-brain synchrony arises from such purely stimulus-driven mechanisms versus interpersonal joint action. Finally, it should be noted that although the correlations for observed pairs were larger overall than that of surrogate pairs, 5 of 20 pairs showed lower amplitude correlations for observed relative to surrogate pairings; these pairs also showed lower envelope correlations than other pairs, suggesting that possibly these pairs did not display clear amplitude tracking of the musical rhythm. The current envelopes were extracted from spatial filters representing a mix of auditory, motor, and other sources; it is possible that the ability to detect clear amplitude modulations at the beat frequency differs for participants whose entrainment arose from more than one source. An open question for future research is to identify factors that determine individual differences in amplitude envelope coupling.

The current study demonstrates the novel application of amplitude envelope correlations to inter-brain correspondences. Previously used to detect functional connectivity or coupling *within* individuals' brain networks (Bruns et al., 2000; Doron et al., 2012; Hipp et al., 2012), we applied AECs to detect coupling *between* individuals. Although the current findings are agnostic with respect to the relationship between phase-resetting mechanisms of endogenous neural oscillations and transient ERPs in response to rhythmic auditory stimuli (Haegens and Golumbic, 2018; Novembre and Iannetti, 2018), the measures of enhanced power and amplitude envelopes presented here offer insights into the bidirectional (Leader-Follower) period coupling typical of skilled musical ensembles (Demos et al., 2019).

A remaining question is how these amplitude-based metrics of inter-brain correspondences compare with alternative measures of inter-brain synchrony, such as phase-based metrics. Some work suggests that amplitude and phase are related (Canolty et al., 2006; Cohen et al., 2008; Lee and Jeong, 2013; Combrisson et al., 2017); however, amplitude coupling metrics may capture correspondences in cortical oscillations that may not be detected by phase-based metrics (Bruns et al., 2000), and may show greater test-retest reliability (Colclough et al., 2016). Future work should investigate how amplitude- and phase-based metrics of inter-brain correspondences are related, and whether partners with similar natural frequencies of music performance show enhanced inter-brain phase-locking relative to partners with different natural frequencies.

Finally, the current study implements what is to our knowledge the first simultaneous recording of wireless EEG from performing ensemble musicians. Wireless EEG with head-mounted amplifiers enables individual to walk freely, with modest motion artifact (Debener et al., 2012; De Vos et al., 2014a,b). However, movement artifacts due to free walking can confound brain activity (Jacobsen et al., 2020). Although pianists in the current study remained seated and may not have moved as much as during a natural concert performance featuring expressive body movement, or free walking, wireless EEG has been shown to successfully measure brain activity in numerous highly active contexts from motor rehabilitation (Zich et al., 2015) to speech production (Fjaellingsdal et al., 2016) to bike riding (Scanlon et al., 2019) and memory encoding (Piñeyro Salvidegoitia et al., 2019), providing compelling evidence that brain activity can clearly be captured using wireless EEG even

under high activity loads. We thus propose that two wireless EEG amplifiers can capture the coupling dynamics associated with temporal coordination between expressively performing musicians. Future studies may include motion sensors attached to different body parts to explore whether movement artifacts compromise measure of neural interpersonal synchrony. This presents new possibilities for measuring the neural correlates of interpersonal coordination without the motion constraints of traditional EEG. Wireless EEG could be used not only in musical duets but in larger groups such as string quartets and even orchestras, where expressive body gestures may be even more important for communication between performers (Davidson, 2012; Glowinski et al., 2013; Badino et al., 2014). We hope that these findings set a precedent for more ecological measurement of oscillator dynamics between individuals acting together.

DATA AVAILABILITY STATEMENT

The raw data and code supporting the conclusions of this article will be made available by the authors upon reasonable request, without undue reservation.

ETHICS STATEMENT

The studies involving human participants were reviewed and approved by Kommission für Forschungsfolgenabschätzung und Ethik. The participants provided their written informed consent to participate in this study.

AUTHOR CONTRIBUTIONS

AZ designed the experiment in collaboration with co-authors, conducted the experiment, implemented and interpreted analyses, wrote drafts of the manuscript and incorporated the revisions. CP contributed to and provided supervision in experiment design, supervised implementation of data analysis, contributed to interpreting results and assisted in writing and revising the manuscript for publication. A-KRB contributed to experiment design, gave input on implementation of EEG data analyses, and assisted with data interpretation and manuscript revision. MGB contributed to experiment design and technical set-up, gave input on implementation of EEG data analyses, and assisted with data interpretation and manuscript revision. APD gave input on statistical analyses of data, and assisted with manuscript revision. SD supervised and contributed to experiment design and implementation, provided laboratory space and mobile EEG equipment for data collection, supervised implementation of data analysis, and contributed to interpreting results, assisted in writing and revising the manuscript for publication. All authors contributed to the article and approved the submitted version.

FUNDING

This research was supported by a Fellowship from the Erasmus Mundus programme Auditory Cognitive Neuroscience, the McGill Graduate Mobility Award, and the Programme de Bourses d'Excellence pour Étudiants Étrangers (FQRNT) Ph.D. Fellowship to AZ, by NSERC Grant 298173 and a Canada Research Chair to CP, and by Task Group 7 of the Oldenburg University Cluster of Excellence Hearing4All to SD (DFG EXC 1077).

ACKNOWLEDGMENTS

The authors would like to thank Reiner Emkes for technical assistance, Katharina Grote and Felix Feuerhake for assistance with EEG cap preparation, Frances Spidle for assistance with figures, and Manuela Jaeger and Jeremy Thorne for helpful discussion.

REFERENCES

Astolfi, L., Toppi, J., Borghini, G., Vecchiato, G., Isabella, R., De Vico Fallani, F., et al. (2011). "Study of the functional hyperconnectivity between couples of pilots during flight simulation: an EEG hyperscanning study," in *Engineering in Medicine and Biology Society, EMBC, 2011 Annual International Conference of the IEEE* (New Jersey, NJ: IEEE), 2338–2341.

Badino, L., D'ausilio, A., Glowinski, D., Camurri, A., and Fadiga, L. (2014). Sensorimotor communication in professional quartets. *Neuropsychologia* 55, 98–104. doi: 10.1016/j.neuropsychologia.2013.11.012

Bauer, A. K. R., Bleichner, M. G., Jaeger, M., Thorne, J. D., and Debener, S. (2018). Dynamic phase alignment of ongoing auditory cortex oscillations. *Neuroimage* 167, 396–407. doi: 10.1016/j.neuroimage.2017.11.037

Bauer, A. K. R., Debener, S., and Nobre, A. C. (2020). Synchronisation of neural oscillations and cross-modal influences. *Trends Cogn. Sci.* 24, 481–495. doi: 10.1016/j.tics.2020.03.003

Bell, A. J., and Sejnowski, T. J. (1995). An information-maximization approach to blind separation and blind deconvolution. *Neural Comput.* 7, 1129–1159. doi: 10.1162/neco.1995.7.6.1129

Bruns, A., Eckhorn, R., Jokeit, H., and Ebner, A. (2000). Amplitude envelope correlation detects coupling among incoherent brain signals. *Neuroreport* 11, 1509–1514. doi: 10.1097/00001756-200005150-00029

Canolty, R. T., Edwards, E., Dalal, S. S., Soltani, M., Nagarajan, S. S., Kirsch, H. E., et al. (2006). High gamma power is phaselocked to theta oscillations in human neocortex. *Science* 313, 1626–1628. doi: 10.1126/science.1128115

Cohen, M. X., Elger, C. E., and Fell, J. (2008). Oscillatory activity and phase–amplitude coupling in the human medial frontal cortex during decision making. *J. Cogn. Neurosci.* 21, 390–402. doi: 10.1162/jocn.2008.21020

Colclough, G. L., Woolrich, M. W., Tewarie, P. K., Brookes, M. J., Quinn, A. J., and Smith, S. M. (2016). How reliable are MEG resting-state connectivity metrics? *Neuroimage* 138, 284–293. doi: 10.1016/j.neuroimage.2016.05.070

Combrisson, E., Perrone-Bertolotti, M., Soto, J. L., Alamian, G., Kahane, P., Lachaux, J. P., et al. (2017). From intentions to actions: neural oscillations encode motor processes through phase, amplitude and phase-amplitude coupling. *NeuroImage* 147, 473–487. doi: 10.1016/j.neuroimage.2016.11.042

Cui, X., Bryant, D. M., and Reiss, A. L. (2012). NIRS-based hyperscanning reveals increased interpersonal coherence in superior frontal cortex during cooperation. *NeuroImage* 59, 2430–2437. doi: 10.1016/j.neuroimage.2011.09.003

Dähne, S., Nikulin, V. V., Ramirez, D., Schreier, P. J., Müller, K. R., and Haufe, S. (2014). Finding brain oscillations with power dependencies in neuroimaging data. *NeuroImage* 96, 334–348. doi: 10.1016/j.neuroimage.2014.03.075

Davidson, J. W. (2012). Bodily movement and facial actions in expressive musical performance by solo and duo instrumentalists: two distinctive case studies. *Psychol. Music* 40, 595–633. doi: 10.1177/0305735612449896

De Vos, M., Gandras, K., and Debener, S. (2014a). Towards a truly mobile auditory brain–computer interface: exploring the P300 to take away. *Int. J. Psychophysiol.* 91, 46–53. doi: 10.1016/j.ijpsycho.2013.08.010

De Vos, M., Kroesen, M., Emkes, R., and Debener, S. (2014b). P300 speller BCI with a mobile EEG system: comparison to a traditional amplifier. *J. Neural Engin.* 11:036008. doi: 10.1088/1741-2560/11/3/036008

Debener, S., Minow, F., Emkes, R., Gandras, K., and Vos, M. (2012). How about taking a low-cost, small, and wireless EEG for a walk? *Psychophysiology* 49, 1617–1621. doi: 10.1111/j.1469-8986.2012.01471.x

Delorme, A., and Makeig, S. (2004). EEGLAB: an open source toolbox for analysis of single-trial EEG dynamics including independent component analysis. *J. Neurosci. Methods* 134, 9–21. doi: 10.1016/j.jneumeth.2003.10.009

Demos, A. P., Layeghi, H., Wanderley, M. M., and Palmer, C. (2019). Staying together: A bidirectional delay-coupled approach to joint action. *Cogn. Sci.* 43:312766.

Doron, K. W., Bassett, D. S., and Gazzaniga, M. S. (2012). Dynamic network structure of interhemispheric coordination. *Proc. Natl. Acad. Sci. U.S.A* 46, 18661–18668. doi: 10.1073/pnas.1216402109

Drake, C., and Palmer, C. (2000). Skill acquisition in music performance: relations between planning and temporal control. *Cognition* 74, 1–32. doi: 10.1016/s0010-0277(99)00061-x

Dumas, G., Nadel, J., Soussignan, R., Martinerie, J., and Garnero, L. (2010). Inter-brain synchronization during social interaction. *PLoS One* 5:e12166. doi: 10.1371/journal.pone.0012166

Finney, S. A. (2001). FTAP: a linux-based program for tapping and music experiments. *Behav. Res. Meth. Instrum. Comput.* 33, 65–72. doi: 10.3758/bf03195348

Fjaellingsdal, T. G., Ruigendijk, E., Scherbaum, S., and Bleichner, M. G. (2016). The N400 Effect during speaker-switch — towards a conversational approach of measuring neural correlates of language. *Front. Psychol.* 7:854. doi: 10.3389/fpsyg.2016.01854

Feurra, M., Paulus, W., Walsh, V., and Kanai, R. (2011). Frequency specific modulation of human somatosensory cortex. *Front. Psychol.* 2:13. doi: 10.3389/fpsyg.2011.00013

Funane, T., Kiguchi, M., Atsumori, H., Sato, H., Kubota, K., and Koizumi, H. (2011). Synchronous activity of two people's prefrontal cortices during a cooperative task measured by simultaneous near-infrared spectroscopy. *J. Biomed. Optics* 16, 077011–077011. doi: 10.1117/1.3602853

Fujioka, T., Ross, B., and Trainor, L. J. (2015). Beta-Band Oscillations Represent Auditory Beat and Its Metrical Hierarchy in Perception and Imagery. *J. Neurosci.* 35, 15187–15198. doi: 10.1523/jneurosci.2397-15.2015

Galambos, R., Makeig, S., and Talmachoff, P. J. (1981). A 40-Hz auditory potential recorded from the human scalp. *Proc. Natl. Acad. Sci. U.S.A* 78, 2643–2647. doi: 10.1073/pnas.78.4.2643

Glowinski, D., Mancini, M., Cowie, R., Camurri, A., Chiorri, C., and Doherty, C. (2013). The movements made by performers in a skilled quartet: a distinctive pattern, and the function that it serves. *Front. Psychol.* 4:841. doi: 10.3389/fpsyg.2013.00841

Grahn, J. A., and Brett, M. (2007). Rhythm and beat perception in motor areas of the brain. *J. Cogn. Neurosci.* 19, 893–906. doi: 10.1162/jocn.2007.19.5.893

Haegens, S., and Golumbic, E. Z. (2018). Rhythmic facilitation of sensory processing: a critical review. *Neurosci. Biobehav. Rev.* 86, 150–165. doi: 10.1016/j.neubiorev.2017.12.002

Haken, H., Kelso, J. S., and Bunz, H. (1985). A theoretical model of phase transitions in human hand movements. *Biol. Cybern.* 51, 347–356. doi: 10.1007/bf00336922

Hanson, S. J., Gagliardi, A. D., and Hanson, C. (2009). Solving the brain synchrony eigenvalue problem: conservation of temporal dynamics (fMRI) over subjects doing the same task. *J. Comput. Neurosci.* 27, 103–114. doi: 10.1007/s10827-008-0129-z

Hasson, U., Nir, Y., Levy, I., Fuhrmann, G., and Malach, R. (2004). Intersubject synchronization of cortical activity during natural vision. *Science* 303, 1634–1640. doi: 10.1126/science.1089506

Henry, M. J., Herrmann, B., and Obleser, J. (2015). Selective attention to temporal features on nested time scales. *Cerebral Cortex* 25, 450–459. doi: 10.1093/cercor/bht240

Hipp, J. F., Hawellek, D. J., Corbetta, M., Siegel, M., and Engel, A. K. (2012). Large-scale cortical correlation structure of spontaneous oscillatory activity. *Nat. Neurosci.* 15, 884–890. doi: 10.1038/nn.3101

Jacobsen, N. S. J., Blum, S., Witt, K., and Debener, S. (2020). *A Walk in the Park? Characterizing Gait—Related Artifacts in Mobile EEG Recordings*. New Jersey, NJ: Wiley.

John, M. S., and Picton, T. W. (2000). Human auditory steady-state responses to amplitude-modulated tones: phase and latency measurements. *Hear. Res.* 141, 57–79. doi: 10.1016/s0378-5955(99)00209-9

Jung, T. P., Makeig, S., Humphries, C., Lee, T. W., Mckeown, M. J., Iragui, V., et al. (2000a). Removing electroencephalographic artifacts by blind source separation. *Psychophysiology* 37, 163–178. doi: 10.1111/1469-8986.3720163

Jung, T. P., Makeig, S., Westerfield, M., Townsend, J., Courchesne, E., and Sejnowski, T. J. (2000b). Removal of eye activity artifacts from visual event-related potentials in normal and clinical subjects. *Clin. Neurophysiol.* 111, 1745–1758. doi: 10.1016/s1388-2457(00)00386-2

Kelso, J. A. (1984). Phase transitions and critical behavior in human bimanual coordination. *Am. J. Physiol. Regul. Integr. Compa. Physiol.* 246, 1000–1004.

Kothe, C. (2014). *Lab streaming layer (LSL)*. Available online at: https://github.com/sccn/labstreaminglayer$>$.

Kuramoto, Y. (2012). *Chemical Oscillations, Waves, and Turbulence*, Vol. 19. Netherland: Springer Science & Business Media.

Lakatos, P., Gross, J., and Thut, G. (2019). A new unifying account of the roles of neuronal entrainment. *Curr. Biol.* 29, R890–R905.

Large, E. W. (1993). Dynamic programming for the analysis of serial behaviors. *Behav. Res. Meth. Instrum. Comput.* 25, 238–241. doi: 10.3758/BF03204504

Lee, R. F. (2015). Dual logic and cerebral coordinates for reciprocal interaction in eye contact. *PLoS One* 10:e0121791. doi: 10.1371/journal.pone.0121791

Lee, J., and Jeong, J. (2013). Correlation of risk-taking propensity with cross-frequency phase-amplitude coupling in the resting EEG. *Clin. Neurophysiol.* 124, 2172–2180. doi: 10.1016/j.clinph.2013.05.007

Lindenberger, U., Li, S. C., Gruber, W., and Müller, V. (2009). Brains swinging in concert: cortical phase synchronization while playing guitar. *BMC Neurosci.* 10:22. doi: 10.1186/1471-2202-10-22

Loehr, J. D., and Palmer, C. (2011). Temporal coordination between performing musicians. *Q. J. Exp. Psychol.* 64, 2153–2167. doi: 10.1080/17470218.2011.603427

Lopresti-Goodman, S. M., Richardson, M. J., Silva, P. L., and Schmidt, R. C. (2008). Period basin of entrainment for unintentional visual coordination. *J. Motor Behav.* 40, 3–10. doi: 10.3200/jmbr.40.1.3-10

Müller, V., and Lindenberger, U. (2014). Hyper-brain networks support romantic kissing in humans. *PLoS One* 9:e112080. doi: 10.1371/journal.pone.0112080

Nikulin, V. V., Nolte, G., and Curio, G. (2011). A novel method for reliable and fast extraction of neuronal EEG/MEG oscillations on the basis of spatio-spectral decomposition. *NeuroImage* 55, 1528–1535. doi: 10.1016/j.neuroimage.2011.01.057

Novembre, G., and Iannetti, G. D. (2018). Tagging the musical beat: Neural entrainment or event-related potentials? *Proc. Natl. Acad. Sci. U.S.A* 115, E11002–E11003.

Novembre, G., Knoblich, G., Dunne, L., and Keller, P. E. (2017). Interpersonal synchrony enhanced through 20 Hz phase-coupled dual brain stimulation. *Soc. Cogn. Affect. Neurosci.* 12, 662–670. doi: 10.1093/scan/nsw172

Nozaradan, S., Peretz, I., and Keller, P. E. (2016). Individual differences in rhythmic cortical entrainment correlate with predictive behavior in sensorimotor synchronization. *Scientific Rep.* 6:612. doi: 10.1038/srep20612

Nozaradan, S., Peretz, I., Missal, M., and Mouraux, A. (2011). Tagging the neuronal entrainment to beat and meter. *J. Neurosci.* 31, 10234–10240. doi: 10.1523/jneurosci.0411-11.2011

Nozaradan, S., Peretz, I., and Mouraux, A. (2012). Selective neuronal entrainment to the beat and meter embedded in a musical rhythm. *J. Neurosci.* 32, 17572–17581. doi: 10.1523/jneurosci.3203-12.2012

Nozaradan, S., Zerouali, Y., Peretz, I., and Mouraux, A. (2013). Capturing with EEG the neural entrainment and coupling underlying sensorimotor synchronization to the beat. *Cereb. Cortex* 25, 736–747. doi: 10.1093/cercor/bht261

Nozaradan, S., Zerouali, Y., Peretz, I., and Mouraux, A. (2015). Capturing with EEG the neural entrainment and coupling underlying sensorimotor synchronization to the beat. *Cereb. Cortex* 25, 723–747. doi: 10.1093/cercor/bht261

Oldfield, R. C. (1971). The assessment and analysis of handedness: the Edinburgh inventory. *Neuropsychologia* 9, 97–113. doi: 10.1016/0028-3932(71)90067-4

Palmer, C. (2013). "Music performance: Movement and coordination," in *The Psychology of Music, Third Ed*, ed. D. Deutsch (Netherlands: Elsevier Press), 405–422.

Palmer, C., Spidle, F., Koopmans, E., and Schubert, P. (2019). Ears, head and eyes: When singers synchronize. *Q. J. Exp. Psychol.* 72, 2272–2287. doi: 10.1177/1747021819833968

Piñeyro Salvidegoitia, M., Jacobsen, N., Bauer, A. K. R., Griffiths, B., Hanslmayr, S., and Debener, S. (2019). Out and about: Subsequent memory effect captured in a natural outdoor environment with smartphone EEG. *Psychophysiology* 56:e13331. doi: 10.1111/psyp.13331

Pikovsky, A., Kurths, J., Rosenblum, M., and Kurths, J. (2003). *Synchronization: A Universal Concept in Nonlinear Sciences (No. 12)*. Cambridge: Cambridge university press.

Repp, B. H., and Su, Y. H. (2013). Sensorimotor synchronization: a review of recent research (2006–2012). *Psych. Bull. Rev.* 20, 403–452. doi: 10.3758/s13423-012-0371-2

Richardson, M. J., Marsh, K. L., and Schmidt, R. C. (2005). Effects of visual and verbal interaction on unintentional interpersonal coordination. *J. Exp. Psychol.* 31, 62–79. doi: 10.1037/0096-1523.31.1.62

Richardson, M. J., Marsh, K. L., Isenhower, R. W., Goodman, J. R., and Schmidt, R. C. (2007). Rocking together: Dynamics of intentional and unintentional interpersonal coordination. *Hum. Move. Sci.* 26, 867–891. doi: 10.1016/j.humov.2007.07.002

Roman, I. R., Roman, A. S., and Large, E. W. (2020). Hebbian learning with elasticity explains how the spontaneous motor tempo affects music performance synchronization. *bioRxiv* [preprint]. doi: 10.1101/2020.10.15.341610

Ross, B., Draganova, R., Picton, T. W., and Pantev, C. (2003). Frequency specificity of 40-Hz auditory steady-state responses. *Hear. Res.* 186, 57–68. doi: 10.1016/s0378-5955(03)00299-5

Sänger, J., Müller, V., and Lindenberger, U. (2012). Intra-and interbrain synchronization and network properties when playing guitar in duets. *Front. Hum. Neurosci.* 6:312. doi: 10.3389/fnhum.2012.00312

Scanlon, J. E., Jacobsen, N. S. J., Maack, M. C., and Debener, S. (2020). *Does the Electrode Amplification Style Matter? A Comparison of Active and Passive EEG System Configurations During Standing and Walking*. New Jersey, NJ: Wiley.

Scanlon, J. E., Townsend, K. A., Cormier, D. L., Kuziek, J. W., and Mathewson, K. E. (2019). Taking off the training wheels: Measuring auditory P3 during outdoor cycling using an active wet EEG system. *Brain Res.* 1716, 50–61. doi: 10.1016/j.brainres.2017.12.010

Scheurich, R., Zamm, A., and Palmer, C. (2018). Tapping into rate flexibility: musical training facilitates synchronization around spontaneous production rates. *Front. Psychol.* 9:458. doi: 10.3389/fpsyg.2018.00458

Schmidt, R. C., and O'Brien, B. (1997). Evaluating the dynamics of unintended interpersonal coordination. *Ecol. Psychol.* 9, 189–206. doi: 10.1207/s15326969eco0903_2

Strogatz, S. (2003). *Sync: The Emerging Science of Spontaneous Order*. New York: Hyperion.

Tierney, A., and Kraus, N. (2013). The ability to move to a beat is linked to the consistency of neural responses to sound. *J. Neurosci.* 33, 14981–14988. doi: 10.1523/jneurosci.0612-13.2013

Tierney, A., and Kraus, N. (2014). Neural entrainment to the rhythmic structure of music. *J. Cogn. Neurosci.* 27, 400–408. doi: 10.1162/jocn_a_00704

Tobimatsu, S., Zhang, Y. M., and Kato, M. (1999). Steady-state vibration somatosensory evoked potentials: physiological characteristics and tuning function. *Clin. Neurophysiol.* 110, 1953–1958. doi: 10.1016/s1388-2457(99)00146-7

Tognoli, E., Lagarde, J., DeGuzman, G. C., and Kelso, J. S. (2007). The phi complex as a neuromarker of human social coordination. *Proc. Natl. Acad. Sci. U.S.A* 104, 8190–8195. doi: 10.1073/pnas.0611453104

Tomlin, D., Kayali, M. A., King-Casas, B., Anen, C., Camerer, C. F., Quartz, S. R., et al. (2006). Agent-specific responses in the cingulate cortex during economic exchanges. *Science* 312, 1047–1050. doi: 10.1126/science.1125596

Turvey, M. T. (1990). Coordination. *Am. Psychol.* 45:938.

Widmann, A., and Schröger, E. (2012). Filter effects and filter artifacts in the analysis of electrophysiological data. *Front. Psychol.* 3:233. doi: 10.3389/fpsyg.2012.00233

Wilson, S. M., Molnar-Szakacs, I., and Iacoboni, M. (2007). Beyond superior temporal cortex: Intersubject correlations in narrative speech comprehension. *Cerebral Cortex* 18, 230–242. doi: 10.1093/cercor/bhm049

Wright, S. E., and Palmer, C. (2020). Physiological and Behavioural Factors in Musicians' Performance Tempo. *Front. Hum. Neurosci.* 14:311. doi: 10.3389/fnhum.2020.00311

Zamm, A., Palmer, C., Bauer, A. K. R., Bleichner, M. G., Demos, A. P., and Debener, S. (2019). Synchronizing MIDI and wireless EEG measurements during natural piano performance. *Brain Res.* 1716, 27–38. doi: 10/1016/j.brainres.2017.07.001

Zamm, A., Debener, S., Bauer, A. K. R., Bleichner, M. G., Demos, A. P., and Palmer, C. (2018). Amplitude envelope correlations for measuring inter-brain synchrony in performing musicians. *Anna. N. Y. Acad. Sci.* doi: 10.1111/nyas.13738 [Epub Online ahead of print]

Zamm, A., Pfordresher, P. Q., and Palmer, C. (2015). Temporal coordination in joint music performance: effects of endogenous rhythms and auditory feedback. *Exp. Brain Res.* 233, 607–615. doi: 10.1007/s00221-014-4140-5

Zamm, A., Wellman, C., and Palmer, C. (2016). Endogenous rhythms influence interpersonal synchrony. *J. Exp. Psychol.* 42:611. doi: 10.1037/xhp0000201

Zich, C., De Vos, M., Kranczioch, C., and Debener, S. (2015). Wireless EEG with individualized channel layout enables efficient motor imagery training. *Clin. Neurophysiol.* 126, 698–710. doi: 10.1016/j.clinph.2014.07.007

Conflict of Interest: The authors declare that the research was conducted in the absence of any commercial or financial relationships that could be construed as a potential conflict of interest.

frontiers in Human Neuroscience

ORIGINAL RESEARCH
published: 08 October 2021
doi: 10.3389/fnhum.2021.749082

Complexity-Based Analysis of the Variations of Brain and Muscle Reactions in Walking and Standing Balance While Receiving Different Perturbations

Najmeh Pakniyat[1] *and Hamidreza Namazi*[2,3]*

[1] *Independent Researcher, Toronto, ON, Canada,* [2] *Incubator of Kinanthropology Research, Faculty of Sports Studies, Masaryk University, Brno, Czechia,* [3] *College of Engineering and Science, Victoria University, Melbourne, VIC, Australia*

In this article, we evaluated the variations of the brain and muscle activations while subjects are exposed to different perturbations to walking and standing balance. Since EEG and EMG signals have complex structures, we utilized the complexity-based analysis. Specifically, we analyzed the fractal dimension and sample entropy of Electroencephalogram (EEG) and Electromyogram (EMG) signals while subjects walked and stood, and received different perturbations in the form of pulling and rotation (via virtual reality). The results showed that the complexity of EEG signals was higher in walking than standing as the result of different perturbations. However, the complexity of EMG signals was higher in standing than walking as the result of different perturbations. Therefore, the alterations in the complexity of EEG and EMG signals are inversely correlated. This analysis could be extended to investigate simultaneous variations of rhythmic patterns of other physiological signals while subjects perform different activities.

Keywords: muscle, brain, EEG signals, EMG signals, complexity, walking, standing, perturbations

OPEN ACCESS

Edited by:
Daniela De Bartolo, Santa Lucia Foundation, Scientific Institute for Research, Hospitalization and Healthcare (IRCCS), Italy

Reviewed by:
Soheil Gohari, The University of Melbourne, Australia
Reza Khosrowabadi, Shahid Beheshti University, Iran

***Correspondence:**
Hamidreza Namazi
hamidreza.namazi@vu.edu.au

Specialty section:
This article was submitted to Motor Neuroscience, a section of the journal Frontiers in Human Neuroscience

Received: *28 July 2021*
Accepted: *06 September 2021*
Published: *08 October 2021*

Citation:
Pakniyat N and Namazi H (2021) Complexity-Based Analysis of the Variations of Brain and Muscle Reactions in Walking and Standing Balance While Receiving Different Perturbations. Front. Hum. Neurosci. 15:749082. doi: 10.3389/fnhum.2021.749082

INTRODUCTION

Analysis of the alterations in human physiology during different locomotion is very important in sport sciences. Due to the changes in leg muscle activation, while doing different locomotions, many works analyzed EMG signals using various techniques (Oliveira et al., 2014; Subbu et al., 2015; Nazmi et al., 2019; Wang et al., 2019). Besides, since brain activation also changes in different locomotions, many studies worked on the analysis of EEG signals using various techniques (Presacco et al., 2011; Maidan et al., 2019; Bodda et al., 2020; Tortora et al., 2020).

Since the human brain controls muscle activations in different conditions, the variations in muscle and brain activations should be related. Therefore, we hypothesize that the characteristics of EMG and EEG signals should be correlated.

According to the literature, some studies have focused on simultaneous analysis of EEG and EMG signals during walking/running. These studies benefited from different techniques (e.g., frequency and amplitude analyses) to simultaneously analyze the alterations of EEG and EMG signals in case of normal subjects (Petersen et al., 2012; Artoni et al., 2017) and patients with

movements disorders (e.g., Parkinson) (Günther et al., 2019; Roeder et al., 2020), during different types of locomotion (e.g., normal walking, stereotyped walking, and treadmill walking).

Besides all reported works in this area that analyzed brain and leg muscle reactions while performing different movements, no work has been reported that considered the complex structure of these signals for its analysis.

The activation of muscle and brain in the form of EMG and EEG signals have complex structures (Kumarasinghe et al., 2021; Soundirarajan et al., 2021). In fact, complexity is a concept to characterize the behavior of a system that contains many parts which interacting together in a highly variable way (Steven, 2001). Therefore, we can use the fractal theory to quantify their complex structures. Fractal objects have self-similar or self-affine structures that are distributed on every scale inside them. Self-similar fractals have the same scaling in different directions. However, self-affine fractals (e.g., EEG and EMG signals) (Namazi et al., 2021c) are not necessarily identical in different directions. The scaling rules are characterized by "scaling exponents" (dimension). The scaling exponent (ℵ) of fractals is related to their topological dimension (D_T) based on Szpilrajn inequality:

$$\aleph > D_T \tag{1}$$

Many studies have worked on the fractal analysis of biological and physiological time series [e.g., MEG signals (Namazi and Jafari, 2019), R-R time series (Sen and McGill, 2018), GSR signals (Namazi et al., 2021d), RNA random walks (Namazi et al., 2021e)]. However, limited studies have been conducted on the fractal analysis of leg muscle EMG signals while doing various movements. For instance, the reported studies on the fractal analysis on EMG signals which evaluated the coupling among the complexities of leg muscle activations and walking paths (Kamal et al., 2020), analyzed muscle reaction in patients with Parkinson's disease (Ravier et al., 2016), investigated the reaction of vastus lateralis muscle during exercise routine (Garavito et al., 2016), and investigated the fatigue in cycling exercises (Beretta-Piccoli et al., 2018) can be mentioned.

Although the fractal theory has been widely applied in the analysis of the complexity of EEG signals in different conditions [e.g., external stimulation (Babini et al., 2020), detection of brain disorders (Namazi et al., 2020)], however, based on our search, only one reported work analyzed EEG signals during locomotion using fractal theory. In (Mujib Kamal et al., 2020), we showed that the variations of the complexity of EEG signals and walking paths are correlated. In other words, the complexity of EEG signals changes greater if a human walks on a path that is more complex.

The complexity of signals also can be quantified using other methods (e.g., sample entropy and approximate entropy). Sample entropy quantifies the complexity of time series, and it is independent of the data length (Namazi, 2020). Since the recorded signals from various participants were short (0.5–1 s in different conditions) and had various lengths, sample entropy is used in this study to validate the fractal analysis results. Several works quantified the complexity of EMG signals in various locomotions using sample entropy. For instance, the works that investigated the effect of walking speed (Namazi, 2021) and aging (Kang and Dingwell, 2016) on the complexity of leg muscle reaction, and classified Knee osteoarthritis (KOA) in walking at a self-paced speed (Chen et al., 2019), can be mentioned.

Although many reported works analyzed the complex structure of EEG signals in different conditions [e.g., response to different stimuli (Namazi et al., 2021a), classifying brain disorders (Simons et al., 2015)] using sample entropy, however, no reported work evaluated the complexity of EEG signals during walking or running using sample entropy.

Since no work has analyzed the complexity of EEG and EMG signals simultaneously during walking/running, we utilized fractal theory and sample entropy to evaluate the synchronization of the changes in EEG and EMG signals at different standing and walking conditions.

MATERIALS AND METHODS

We investigated the variations of brain and leg muscle reactions in walking and standing while subjects received different perturbations in the form of pulling and visual rotation. Since EEG and EMG signals are complex, we ran fractal analysis and computed their fractal dimension to quantify their complexity.

We used the box-counting algorithm for our analysis (Mat Dawi et al., 2021). It uses a series of same-size (μ) boxes to cover the time series. After that, the number of these boxes (n) is counted. In several steps, the size of these boxes is changed, and finally, and the fractal dimension (FD) is computed as:

$$FD = \lim_{\mu \to 0} \frac{\log n\,(\mu)}{\log 1/\mu} \tag{2}$$

FD in the general form is formulated in eq. 3, in which, e is the order of FD, and p_i indicates the probability (Mat Dawi et al., 2021).

$$FD_e = \lim_{x \to 0} \frac{1}{e-1} \frac{\log \sum_{i=1}^{n} p_i^e}{\log x} \tag{3}$$

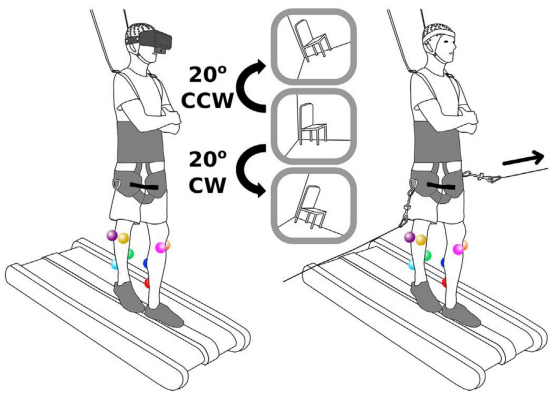

FIGURE 1 | Schematics of the experiment (Peterson and Ferris, 2019).

We also chose sample entropy to quantify the complexity of signals. It is known that the length of data does not affect the value of the sample entropy (Namazi et al., 2021b). Since the recorded EMG and EEG signals from different subjects were short (0.5–1 s) and had various lengths, sample entropy helped us verify the fractal analysis results.

For a time series in the form of $\{y(1), y(2), y(3), ..., y(n)\}$, $Y_z(i) = \{y_i, y_{i+1}, y_{i+2}, ..., y_{i+z-1}\}$ is defined as a template vector and the distance function $d[Y_z(i), Y_z(j)]$ $(i \neq j)$ is to be Chebyshev distance. Then, the sample entropy (*SamEn*) is formulated as (Delgado-Bonal and Marshak, 2019):

$$SamEn = -log\frac{D}{E} \tag{4}$$

Considering ε as the tolerance ($0.2 \times$ *standard deviation of data*), D and E indicate the number of template vector pairs with the condition in (5) and (6):

$$d[Y_{z+1}(i), Y_{z+1}(j)] < \varepsilon \tag{5}$$

$$d[Y_z(i), Y_z(j)] < \varepsilon \tag{6}$$

We computed the fractal exponent and sample entropy of EEG and EMG signals to evaluate the simultaneous alterations of the brain and muscle reactions at different perturbations while subjects stood and walked.

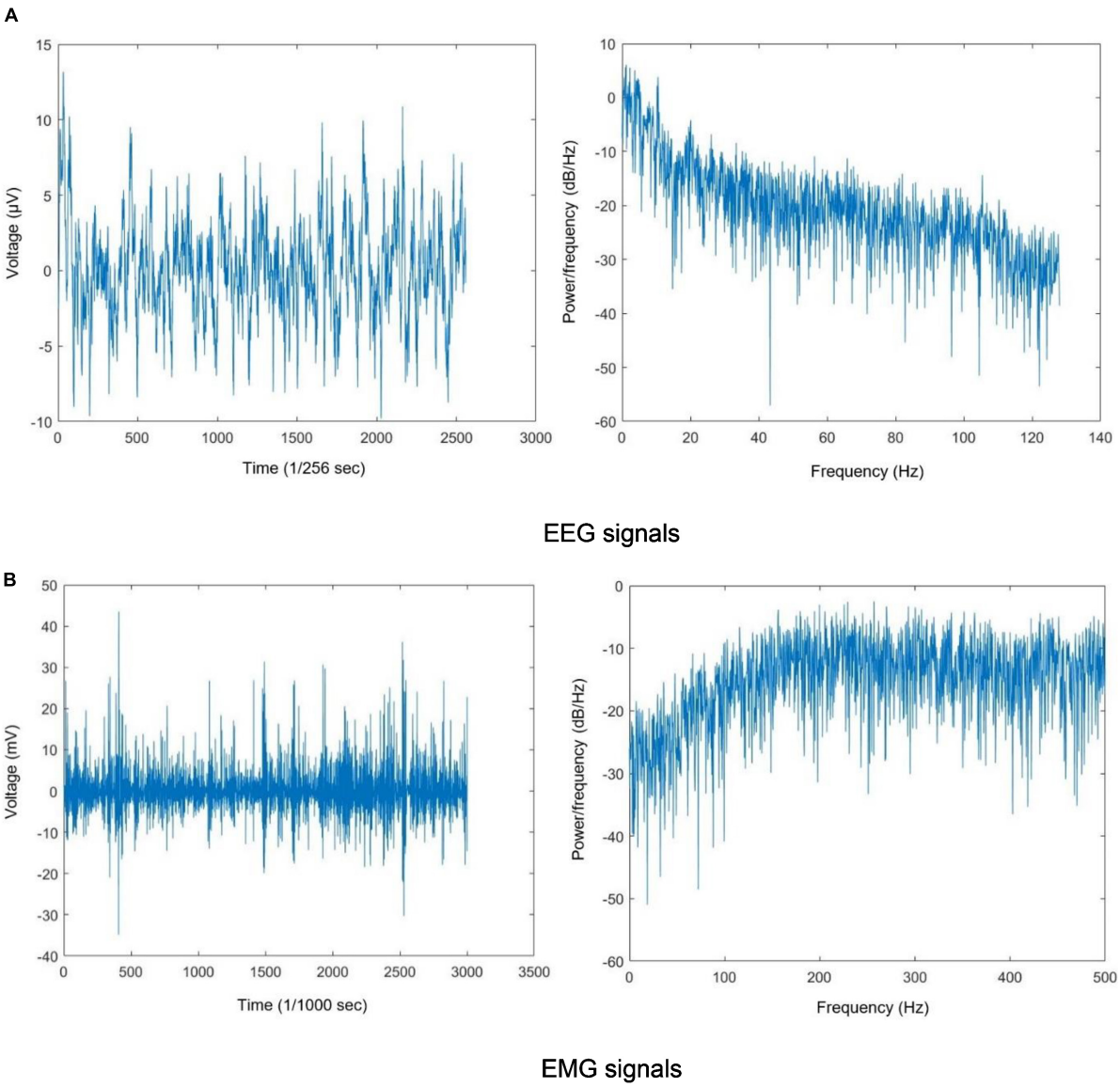

FIGURE 2 | (A) EEG signals and **(B)** EMG signals. The filtered EEG and EMG signals and their periodogram PSD estimate.

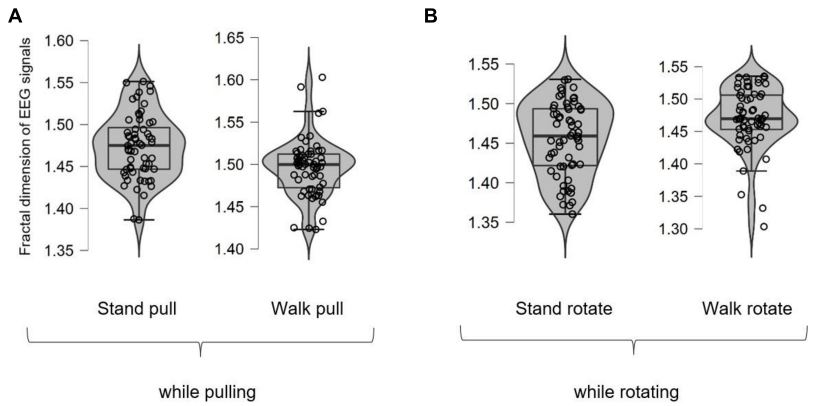

FIGURE 3 | The box plots for the fractal dimension of EEG signals in walking and standing while pulling **(A)** and rotating **(B)**.

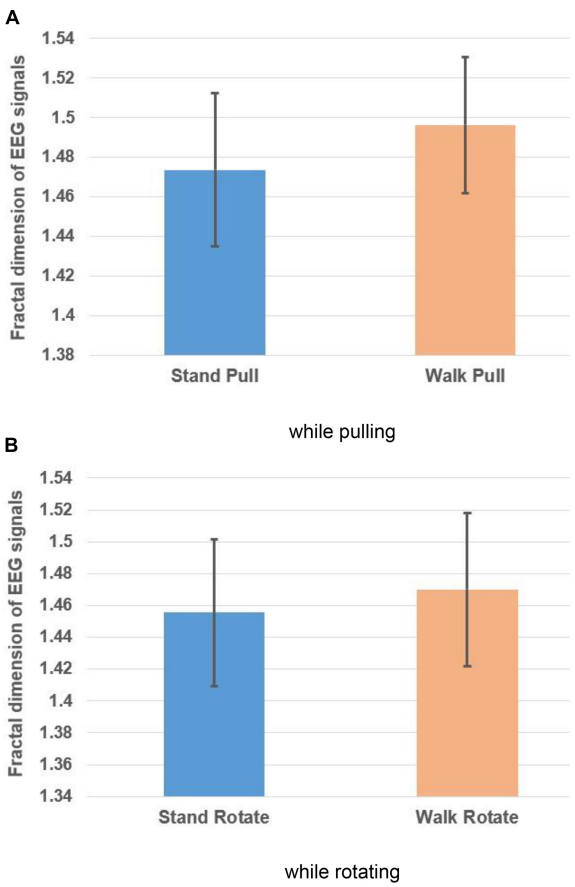

FIGURE 4 | The fractal dimension of EEG signals in walking and standing while pulling **(A)** and rotating **(B)**. Error bars indicate standard deviation.

TABLE 1 | Comparison of the fractal dimension of EEG signals between walking and standing in case of pulling and rotating.

Comparison	*p*-value
Stand pull vs. Walk pull	0.0004
Stand rotate vs. Walk rotate	0.0463

Database and Analysis

In this research, we used the open-access database provided by Peterson & Ferris which is available in Mobile Brain (2021). Their study has been approved by the University of Michigan Health Sciences and Behavioral Sciences Institutional Review Board. All subjects provided written informed consent before commencing the experiment.

This database includes the simultaneously recorded EEG, EMG, EOG, and sacrum/head position data for 30 healthy subjects (15 M, 15 F, 22.5 ± 4.8 years). The lower leg EMG signals (Vicon, Los Angeles, CA) were recorded at 1000 Hz from four electrodes attached to each leg of subjects including LTA (left tibialis anterior), LSOL (left soleus), LMG (left medial gastrocnemius), LPL (left peroneus longus), RTA (right tibialis anterior), RSOL (right soleus), RMG (right medial gastrocnemius), and RPL (right peroneus longus). The approximate locations of EMG electrodes are shown in **Figure 1**. The EEG signals (BioSemi Active II, BioSemi, Amsterdam, NL, United States) were recorded at 512 Hz from 128 channels.

In the experiment, participants walked at 0.22 m/s or stood on a 2.5 cm tall by 12.7 cm wide balance beam mounted to a treadmill. **Figure 1** shows the schematics of the experiment. As can be seen in this figure, subjects wore a body-support harness for safety. Before starting the experiment, subjects were introduced to the experiment. Subjects were avoided from looking around and rotating across their body's longitudinal axis.

Subjects were presented with two types of sensorimotor perturbations including a side-to-side pull at the waist, and a 20-degree field-of-view rotation (**Figure 1**). Two rotational motors on the sides of subjects were used for the side-to-side pull. As shown in **Figure 1**, subjects were pulled using a bar (connected to subjects through a wire) that was connected to one motor. This perturbation lasted for 1 s. At the end of perturbation, the motor rotated back to its starting position. Peterson & Ferris used virtual reality (VR) headset with an attached webcam to rotate the field of

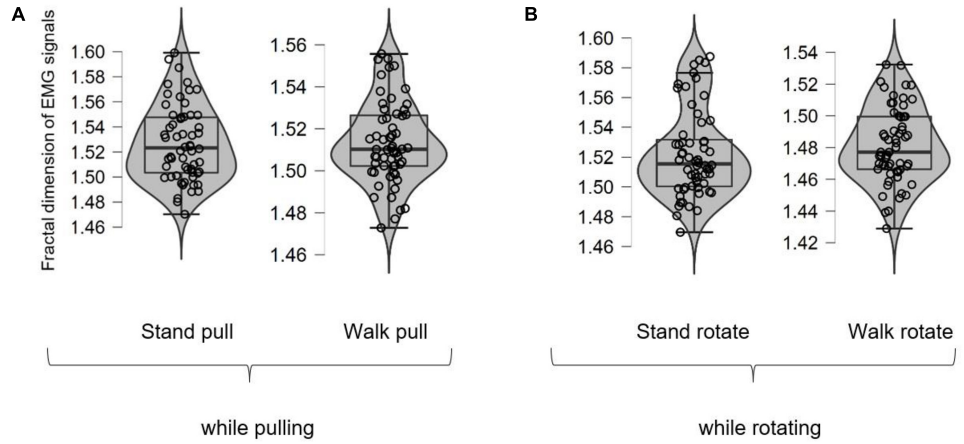

FIGURE 5 | The box plots for the fractal exponent of EMG signals in walking and standing while pulling **(A)** and rotating **(B)**.

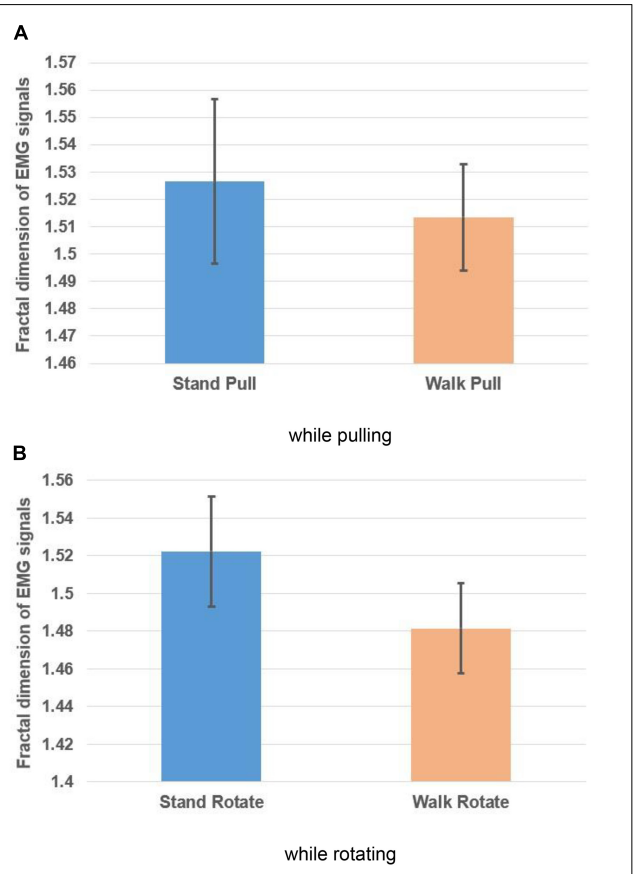

FIGURE 6 | The fractal exponent of EMG signals in walking and standing while pulling **(A)** and rotating **(B)**. Error bars indicate standard deviation.

view of subjects. In fact, the perturbations included rotating the view of subjects 20° clockwise or counterclockwise through VR experience. The rotation of view lasted for 0.5 s before the view returned to its starting position.

Therefore, four conditions were applied on subjects as the combination of the two perturbation types and two physical tasks. It should be noted that each condition lasted 10 min, and subjects experienced 150 perturbations (75 per side, randomized). Please refer to Peterson and Ferris (2019) for more information about the experiment.

Peterson and Ferris (2019) synchronized the EMG and EEG data using a 0.5 Hz square wave. Initially, they downsampled EEG signals to 256 Hz, and then applied a high-pass filter (1 Hz) to the data. They also merged the EEG data across all conditions, referenced to the median channel value for each time point, and removed 60 Hz line noise. They also applied a 1 Hz high pass filter to EMG signals. For understanding the full steps for the pre-processing of signals, please refer to (Peterson and Ferris, 2019).

Figures 2A,B show sample filtered EEG and EMG signals and their frequency information for a participant. These figures show 10 s of EEG data and 3 s of EMG data for better visibility.

We calculated the fractal dimension and sample entropy of filtered signals in the case of both legs in various conditions. The box-counting algorithm was run with the box sizes of $\frac{1}{2}$, $\frac{1}{4}$, $\frac{1}{8}$, $\frac{1}{16}$,. The smallest box size was chosen in the algorithm (Box Counting Algorithm, 2021). The length of the template vector was equal to the embedding dimension (=2). MATLAB R2020b was chosen for our analysis.

The Anderson-Darling test was chosen for checking the normality of results. The test's result indicated the normal distribution of data. We compared the changes in the complexity of signals between standing and walking while pulling and rotating by running the student t-test ($\alpha = 0.05$).

RESULTS

Figure 3 shows different box plots (with whiskers) for the fractal exponent of EEG signals in walking and standing while pulling and rotating. As shown in the case of each plot, the box plot includes a violin element that indicates the probability density of the data at different values. Besides, we also added the jitter

TABLE 2 | Comparison of the fractal exponent of EMG signals between walking and standing in case of pulling and rotating.

Comparison	*p*-value
Stand pull vs. Walk pull	0.0025
Stand rotate vs. Walk rotate	0.0001

TABLE 3 | Comparison of the sample entropy of EEG signals between walking and standing in case of pulling and rotating.

Comparison	*p*-value
Stand pull vs. Walk pull	0.0001
Stand rotate vs. Walk rotate	0.4382

elements to each plot to show the distribution of the data. As it is clear in these plots, only five outliers were identified (in the case of walk pull and walk rotate) which demonstrates the suitability of recorded data for inclusion in the analysis.

Besides, the averaged fractal exponent in walking and standing while pulling and rotating are shown in **Figures 4A,B**, respectively.

As **Figures 4A,B** illustrate, in the case of pulling and rotating, the fractal exponent of EEG signals has bigger values in walking than standing. Therefore, we can state that pulling and rotating of subjects while walking had bigger effects on the changes in the complexity compared to pulling and rotating while subjects stand. Since while walking there are more cognitive loads on subjects, the complexity of their EEG signals increased.

Table 1 lists the results of the student *t*-test which indicates the significant alterations in the fractal exponent among walking and standing conditions in case of pulling and rotating. In other words, walking caused a significant increase in the complexity of EEG signals in pulling and rotating. Besides, pulling of subjects caused a more significant alteration in the complexity of signals among walking and standing than rotating of them.

Figure 5 shows different box plots (with violin and jitter elements) for the fractal exponent of EMG signals in walking and standing while pulling (a) and rotating (b) in the case of different subjects. As it is clear in these plots, only four outliers were identified (in the case of stand rotate) which demonstrates the suitability of recorded data for inclusion in the analysis.

Figures 6A,B, respectively, illustrate the averaged alterations of the fractal exponent of EMG signals in walking and standing while pulling (a) and rotating (b).

As **Figures 6A,B** illustrate, in the case of pulling and rotating, the fractal exponent of EMG signals has bigger values in standing than walking. Therefore, we can state that EMG signals of subjects had lower complexity in walking than standing while pulling and rotating. Comparing these results with the presented results in **Figures 4A,B** indicate reverse trends. In other words, although the complexity of brain reactions increases in walking than standing, the complexity of muscle reaction decreases.

We also compared the alterations in the fractal exponent among walking and standing (in pulling and rotating) using the student *t*-test, and the results are brought in **Table 2**. As shown in **Table 2**, the results indicate significant alterations in the fractal exponent among walking and standing conditions in the case of pulling and rotating. In other words, walking caused a significant decrease in the complexity in pulling and rotating conditions. Comparing the results in **Tables 2**, **3** indicates that brain and leg muscles show significant differences in their reactions between walking and standing.

As was mentioned previously, we also computed the sample entropy of EEG and EMG signals to verify the results of fractal analysis. **Figure 7** shows different box plots (with violin and jitter elements) for the sample entropy of EEG signals in walking and standing while pulling (a) and rotating (b) in the case of different subjects. As it is clear in these plots, only six outliers were identified (in the case of stand pull, walk pull, and walk rotate) which demonstrates the suitability of recorded data for inclusion in the analysis.

Figures 8A,B, respectively, illustrate the variations of the sample entropy of EEG signals in walking and standing while pulling (a) and rotating (b).

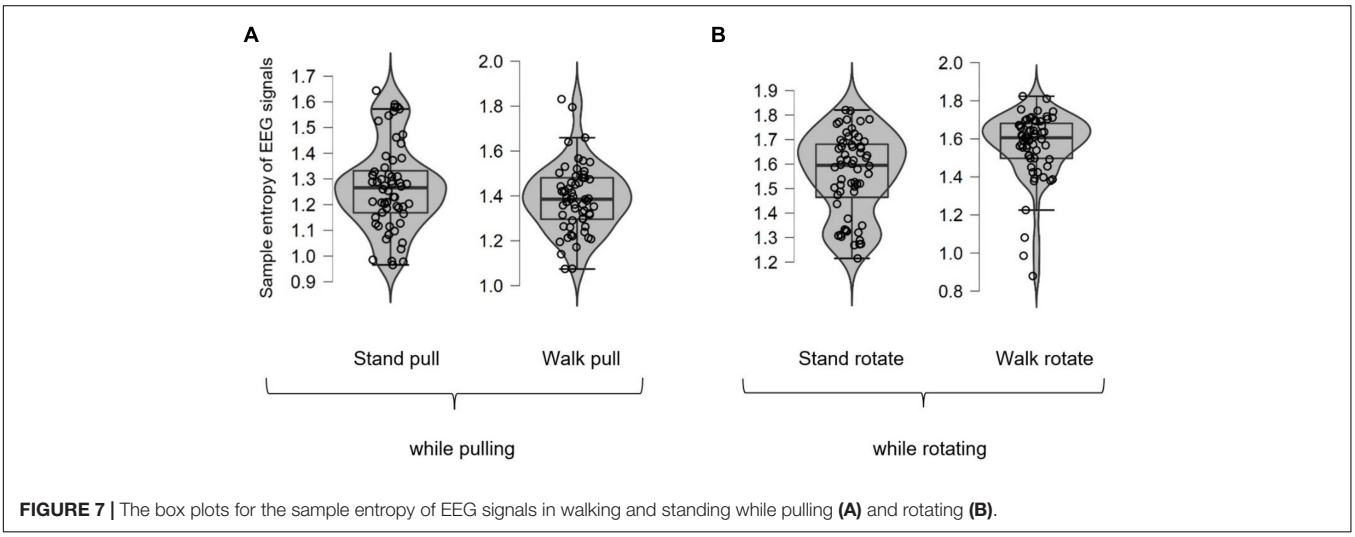

FIGURE 7 | The box plots for the sample entropy of EEG signals in walking and standing while pulling **(A)** and rotating **(B)**.

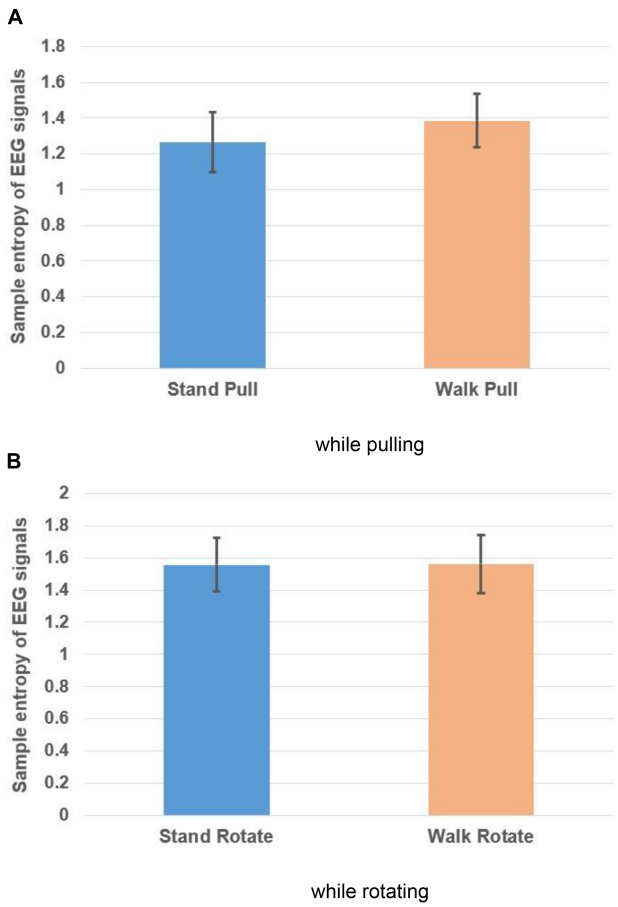

FIGURE 8 | Sample entropy of EEG signals in walking and standing while pulling **(A)** and rotating **(B)**. Error bars indicate standard deviation.

As shown in **Figures 8A,B**, in the case of pulling and rotating, the entropy of EEG signals has bigger values in walking than standing. In other words, pulling, and rotating of subjects while walking caused bigger changes in the complexity compared to pulling and rotating while subjects stand. Comparing these results with the presented results in **Figure 4** indicates that the result of analysis of entropy verified the fractal analysis results.

We also computed the *p*-values using the student *t*-test for comparing the variations in the sample entropy among walking and standing conditions in case of pulling and rotating. As brought in **Table 3**, there is a significant alteration in the sample entropy among walking and standing while pulling of subjects. However, the alterations in the entropy among standing and walking while rotating are not significant. Besides, similar to the results in **Table 1**, pulling of subjects caused a more significant change in the complexity among walking and standing than rotating of them.

Figure 9 shows different box plots (with violin and jitter elements) for the sample entropy of EMG signals in walking and standing while pulling (a) and rotating (b). As it is clear in these plots, only five outliers were identified (in the case of walk pull and stand rotate) which demonstrates the suitability of recorded data for inclusion in the analysis.

Figures 10A,B, respectively, show the variations of the sample entropy of EMG signals in walking and standing while pulling (a) and rotating (b).

As **Figures 10A,B** illustrate, the entropy has bigger values in standing than walking in the case of pulling and rotating. Therefore, we can state that EMG signals of subjects had lower complexity in walking than standing while pulling and rotating. Comparing these results with the presented results in **Figures 6A,B** indicates that the result of entropy verified the fractal analysis results. Besides, comparing these results with the presented results in **Figures 8A,B** indicate reverse trends. In other words, although the complexity of brain reactions increases in walking than standing, the complexity of muscle reaction decreases.

Table 4 compares the entropy of EMG signals among walking and standing (in pulling and rotating) using the student *t*-test. The results demonstrated the significant alterations in the entropy among walking and standing conditions in case of pulling and rotating. In other words, similar to the presented

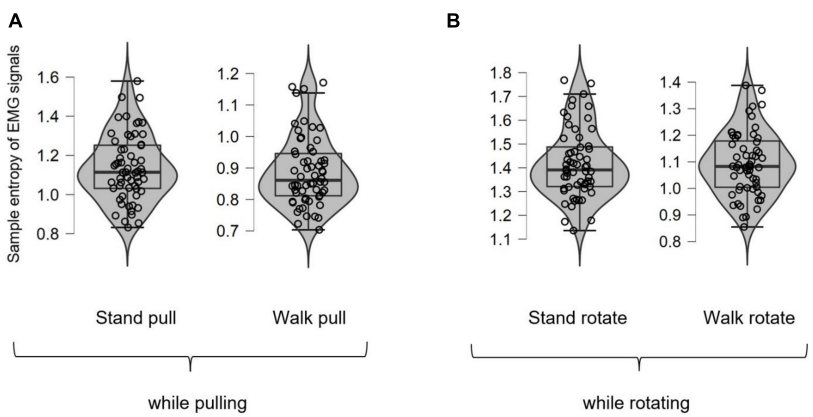

FIGURE 9 | The box plots for the sample entropy of EMG signals in walking and standing while pulling **(A)** and rotating **(B)**.

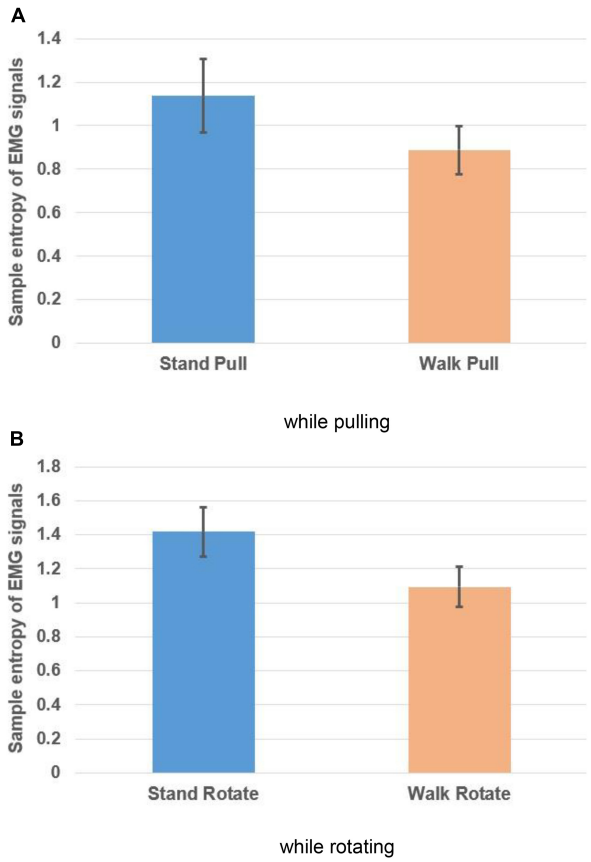

FIGURE 10 | Sample entropy of EMG signals in walking and standing while pulling **(A)** and rotating **(B)**. Error bars indicate standard deviation.

TABLE 4 | Comparison of the sample entropy of EMG signals between walking and standing in case of pulling and rotating.

Comparison	*p*-value
Stand pull vs. Walk pull	0.0001
Stand rotate vs. Walk rotate	0.0001

results in **Table 2**, walking caused a significant decrease in the EMG signals' complexity in both pulling and rotating conditions.

Therefore, EEG signals have greater complexity in walking than rotating, however, EMG signals are less complex in walking than rotating.

CONCLUSION AND DISCUSSION

We analyzed the changes in the brain and leg muscle reactions while subjects walked and stood and received different perturbations (in the form of pulling and rotation) by computing the fractal exponent and sample entropy of EEG and EMG signals.

The results demonstrated that the fractal exponent of EEG signals had greater values in walking than standing while subjects received perturbations. However, the result of the analysis of the fractal exponent of EMG signals showed a reverse trend compared to the obtained results for EEG signals. The analysis of the sample entropy of signals demonstrated similar results with the fractal analysis results. EEG signals have greater sample entropy in walking than standing whereas, the sample entropy of EMG signals has greater values in standing than walking. The result of statistical analysis also supported the obtained results.

Therefore, it can be concluded that the changes in brain and muscle reactions are inversely correlated. These results indicate the importance of complexity-based analysis for finding the connection among brain and muscle activations.

It is known that the brain controls muscle activation through the physiological network of the human body (Bashan et al., 2012). When we are standing or walking, the activity of leg muscles is controlled by the brain through the electrical impulses to the neuromuscular junction. Accordingly, electrical signals are converted into chemical signals allowing for muscle contraction. Therefore, leg muscle and brain activations should be related. The physiological aspect of the observed reverse correlation in this research can be investigated more by simultaneously considering the biological activation of leg muscles and the neural aspect of the brain's control on leg muscles.

Here, we should note that the inverse relationship among the alterations of the complexity of EEG and EMG signals does not affect the importance of the results. Based on the literature, some researchers reported an increment in the EMG signals' complexity in walking than standing (Kamal et al., 2020), whereas some other works found a decrement in the complexity of EMG signals as the walking speed increases (Namazi, 2021). Besides, the observed increment in the EEG signals' complexity in walking is valid according to the provided results in Mujib Kamal et al. (2020). The main important point about these findings is that both fractal theory and sample entropy showed similar results. The findings of this study may challenge the conclusions drawn from other studies (Tao et al., 2015; Flood et al., 2019) that were based on choosing only one technique to quantify the complexity of EEG and EMG signals during walking or other activities.

The obtained results in this study have direct benefits in sport/physiological sciences, when we can link muscle activations to motor control and therefore, understand how the brain controls muscle's activations in various movements in different sports.

We can extend our analyses to other conditions (e.g., walking at various speeds and inclines) to decode the correlation of the EEG-EMG signals in those conditions. Similarly, we can conduct our investigations for patients with various brain [e.g., Parkinson's (Cantello et al., 1995)] and/or movement [e.g., motor stereotypies (Houdayer et al., 2014)] disorders to decode the EEG-EMG signals correlation.

The reported investigation in this study can be extended to evaluate the changes in human physiology while doing standing and walking (or any other movements) and receiving different perturbations. For this purpose, we can apply the complexity-based analysis on the related physiological signals. For instance, since walking affects our respiration rate, we can simultaneously analyze the variations of respiration time series and EEG signals

at different perturbations. Since various organs are working together within the physiological network (Bashan et al., 2012) and are controlled by the brain, a correlation should exist among their related physiological signals. All these analyses are very important in physiological sciences.

DATA AVAILABILITY STATEMENT

Publicly available datasets were analyzed in this study. This data can be found here: https://figshare.com/articles/dataset/Mobile_brain_body_imaging_MoBI_during_sensorimotor_balance_perturbations/14175573.

ETHICS STATEMENT

The studies involving human participants were reviewed and approved by University of Michigan Health Sciences and Behavioral Sciences Institutional Review Board. The patients/participants provided their written informed consent to participate in this study.

AUTHOR CONTRIBUTIONS

HN ran the analysis and drafted the manuscript. Both authors contributed to the article and approved the submitted version.

REFERENCES

Artoni, F., Fanciullacci, C., Bertolucci, F., Panarese, A., Makeig, S., Micera, S., et al. (2017). Unidirectional brain to muscle connectivity reveals motor cortex control of leg muscles during stereotyped walking. *Neuroimage* 159, 403–416. doi: 10.1016/j.neuroimage.2017.07.013

Babini, M. H., Kulish, V. V., and Namazi, H. (2020). Physiological state and learning ability of students in normal and virtual reality conditions: complexity-based analysis. *J. Med. Internet Res.* 22:e17945. doi: 10.2196/17945

Bashan, A., Bartsch, R. P., Kantelhardt, J. W., Havlin, S., and Ivanov, P. C. (2012). Network physiology reveals relations between network topology and physiological function. *Nat. Commun.* 3:702. doi: 10.1038/ncomms1705

Beretta-Piccoli, M., Boccia, G., Ponti, T., Clijsen, R., Barbero, M., and Cescon, C. (2018). Relationship between isometric muscle force and fractal dimension of surface electromyogram. *Biomed. Res. Int.* 2018:5373846. doi: 10.1155/2018/5373846

Bodda, S., Maya, S., Naryanan, M., Potti, E., Sohan, U., Bhuvaneshwari, Y., et al. (2020). Computational analysis of EEG activity during stance and swing gait phases. *Procedia Comput. Sci.* 171, 1591–1597. doi: 10.1016/j.procs.2020.04.170

Box Counting Algorithm (2021). *Box Counting Algorithm*. Available online at: https://www.mathworks.com/matlabcentral/mlc-downloads/downloads/submissions/31951/versions/2/previews/fractalvol.m/index.html (accessed March 1, 2021).

Cantello, R., Gianelli, M., Civardi, C., and Mutani, R. (1995). Parkinson's disease rigidity: EMG in a small hand muscle at "rest". *Electroencephalogr. Clin. Neurophysiol.* 97, 215–222. doi: 10.1016/0924-980X(94)00017-4

Chen, X., Chen, J., Liang, J., Li, Y., Ann Courtney, C., and Yang, Y. (2019). Entropy-based surface electromyogram feature extraction for knee osteoarthritis classification. *IEEE Access* 7:164144–164151. doi: 10.1109/ACCESS.2019.2950665

Delgado-Bonal, A., and Marshak, A. (2019). Approximate entropy and sample entropy: a comprehensive tutorial. *Entropy* 21:541. doi: 10.3390/e21060541

Flood, M. W., Jensen, B. R., Malling, A. S., and Lowery, M. M. (2019). Increased EMG intermuscular coherence and reduced signal complexity in Parkinson's disease. *Clin. Neurophysiol.* 130, 259–269. doi: 10.1016/j.clinph.2018.10.023

Garavito, F., Gonzalez, J., Cabarcas, J., Chaparro, D., Portocarrero, I., and Vargas, A. (2016). "EMG signal analysis based on fractal dimension for muscle activation detection under exercice protocol," in *Proceedings of the 2016 XXI SymposiumSignal Processing, Images and Artificial Vision (STSIVA)*, (Bucaramanga: Institute of Electrical and Electronics Engineers). doi: 10.1109/STSIVA.2016.7743365

Günther, M., Bartsch, R. P., Miron-Shahar, Y., Hassin-Baer, S., Inzelberg, R., Kurths, J., et al. (2019). Coupling between leg muscle activation and EEG during normal walking, intentional stops, and freezing of gait in Parkinson's disease. *Front. Physiol.* 10:870. doi: 10.3389/fphys.2019.00870

Houdayer, E., Walthall, J., Belluscio, B. A., Vorbach, S., Singer, H. S., and Hallett, M. (2014). Absent movement-related cortical potentials in children with primary motor stereotypies. *Mov. Disord.* 29, 1134–1140. doi: 10.1002/mds.25753

Kamal, S. M., Sim, S., Tee, R., Nathan, V., and Namazi, H. (2020). Complexity-based analysis of the relation between human muscle reaction and walking path. *Fluct. Noise Lett.* 19:2050025. doi: 10.1142/S021947752050025X

Kang, H. G., and Dingwell, J. B. (2016). Differential changes with age in multiscale entropy of electromyography signals from leg muscles during treadmill walking. *PLoS One* 11:e0162034. doi: 10.1371/journal.pone.0162034

Kumarasinghe, T., Krejcar, O., Selamat, A., Mat Dawi, N., Herrera-Viedma, E., Frischer, R., et al. (2021). Complexity-based evaluation of the correlation between heart and brain responses to music. *Fractals* 29:150238. doi: 10.1142/S0218348X21502388

Maidan, I., Patashov, D., Shustak, S., Fahoum, F., Gazit, E., Shapiro, B., et al. (2019). A new approach to quantifying the EEG during walking: Initial evidence of gait related potentials and their changes with aging and dual tasking. *Exp. Gerontol.* 126:110709. doi: 10.1016/j.exger.2019.110709

Mat Dawi, N., Kuca, K., Krejcar, O., and Namazi, H. (2021). Complexity and memory-based comparison of the brain activity between ADHD and healthy subjects while playing a serious game. *Fractals* 9:2150202. doi: 10.1142/S0218348X21502029

Mobile Brain (2021). *Mobile Brain/Body Imaging (MoBI) During Sensorimotor Balance Perturbations*. Available online at: https://figshare.com/articles/dataset/Mobile_brain_body_imaging_MoBI_during_sensorimotor_balance_perturbations/14175573 (accessed May 5, 2021).

Mujib Kamal, S., Sim, S., Tee, R., Nathan, V., Aghasian, E., and Namazi, H. (2020). Decoding of the relationship between human brain activity and walking paths. *Technol. Health Care* 28, 381–390. doi: 10.3233/THC-191965

Namazi, H. (2020). Complexity-based classification of the coronavirus genome versus genomes of the human immunodeficiency virus (HIV) and dengue virus. *Fractals* 28:2050129. doi: 10.1142/S0218348X20501297

Namazi, H. (2021). Complexity-based analysis of the correlation between stride interval variability and muscle reaction at different walking speeds. *Biomed. Signal. Process Control.* 69:102956. doi: 10.1016/j.bspc.2021.102956

Namazi, H., Aghasian, E., and Seifi Ala, T. (2020). Complexity-based classification of EEG signal in normal subjects and patients with epilepsy. *Technol. Health Care.* 28, 57–66. doi: 10.3233/THC-181579

Namazi, H., and Jafari, S. (2019). Decoding of wrist movements direction by fractal analysis of magnetoencephalography (MEG) signal. *Fractals* 27:1950001. doi: 10.1142/S0218348X19500014

Namazi, H., Baleanu, D., Omam, S., and Krejcar, O. (2021c). Analysis of the correlation between brain and skin reactions to different types of music. *Fractals* 29:2150124. doi: 10.1142/S0218348X21501243

Namazi, H., Omam, S., Kuca, K., and Krejcar, O. (2021d). Evaluation of the coupling between electroencephalogram (EEG) and galvanic skin response (GSR) signals versus the complex structure of music. *Fractals* 29:2150175. doi: 10.1142/S0218348X21501759

Namazi, H., Selamat, A., and Krejcar, O. (2021e). Complexity-based analysis of the alterations in the structure of coronaviruses. *Fractals* 29:2150123. doi: 10.1142/S0218348X21501231

Namazi, H., Ahamed, M. R. A., Babini, M. H., and Krejcar, O. (2021a). Analysis of the correlation between the human voice and brain activity. *Waves Random Complex Media* 28, 665–674. doi: 10.1080/17455030.2021.1921313

Namazi, H., Baleanu, D., and Krejcar, O. (2021b). Age-based analysis of heart rate variability (HRV) for patients with congestive heart failure. *Fractals* 29:2150135. doi: 10.1142/S0218348X21501358

Nazmi, N., Abdul Rahman, M. A., Yamamoto, S.-I., and Anom Ahmad, S. (2019). Walking gait event detection based on electromyography signals using artificial neural network. *Biomed. Signal Process. Control.* 47, 334–343. doi: 10.1016/j.bspc.2018.08.030

Oliveira, A. S., Gizzi, L., Farina, D., and Kersting, U. G. (2014). Motor modules of human locomotion: influence of EMG averaging, concatenation, and number of step cycles. *Front. Hum. Neurosci.* 8:335. doi: 10.3389/fnhum.2014.00335

Petersen, T. H., Willerslev-Olsen, M., Conway, B. A., and Nielsen, J. B. (2012). The motor cortex drives the muscles during walking in human subjects. *J. Physiol.* 590, 2443–2452. doi: 10.1113/jphysiol.2012.227397

Peterson, S. M., and Ferris, D. P. (2019). Group-level cortical and muscular connectivity during perturbations to walking and standing balance. *Neuroimage* 198, 93–103. doi: 10.1016/j.neuroimage.2019.05.038

Presacco, A., Goodman, R., Forrester, L., and Contreras-Vidal, J. L. (2011). Neural decoding of treadmill walking from noninvasive electroencephalographic signals. *J. Neurophysiol.* 106, 1875–1887. doi: 10.1152/jn.00104.2011

Ravier, P., Jabloun, M., Lamine Talbi, M., Parry, R., Lalo, E., and Buttelli, O. (2016). "Characterizing Parkinson's disease using EMG fractional linear prediction," in *Proceedings of the 2016 24th European Signal Processing Conference (EUSIPCO)*, (Budapest: Institute of Electrical and Electronics Engineers)), 1723–1727. doi: 10.1109/EUSIPCO.2016.7760543

Roeder, L., Boonstra, T. W., and Kerr, G. K. (2020). Corticomuscular control of walking in older people and people with Parkinson's disease. *Sci. Rep.* 10:2980. doi: 10.1038/s41598-020-59810-w

Sen, J., and McGill, D. (2018). Fractal analysis of heart rate variability as a predictor of mortality: a systematic review and meta-analysis. *Chaos* 28:072101. doi: 10.1063/1.5038818

Simons, S., Abasolo, D., and Escudero, J. (2015). Classification of Alzheimer's disease from quadratic sample entropy of electroencephalogram. *Healthc. Technol. Lett.* 2, 70–73. doi: 10.1049/htl.2014.0106

Soundirarajan, M., Aghasian, E., Krejcar, O., and Namazi, H. (2021). Complexity-based analysis of the coupling between facial muscle and brain activities. *Biomed. Signal Process. Control.* 67:102511. doi: 10.1016/j.bspc.2021.102511

Steven, J. (2001). *Emergence: The Connected Lives of Ants, Brains, Cities*. New York, NY: Scribner.

Subbu, R., Weiler, R., and Whyte, G. (2015). The practical use of surface electromyography during running: does the evidence support the hype? A narrative review. *BMJ Open Sport Exerc. Med.* 1:e000026. doi: 10.1136/bmjsem-2015-000026

Tao, W., Zhang, X., Chen, X., Wu, D., and Zhou, P. (2015). Multi-scale complexity analysis of muscle coactivation during gait in children with cerebral palsy. *Front. Hum. Neurosci.* 9:367. doi: 10.3389/fnhum.2015.00367

Tortora, S., Artoni, F., Tonin, L., Chisari, C., Menegatti, E., and Micera, S. (2020). "Discrimination of walking and standing from entropy of EEG signals and common spatial patterns," in *Proceedings of the 2020 IEEE International Conference on Systems, Man, and Cybernetics (SMC)*, (Toronto, ON: Institute of Electrical and Electronics Engineers), 2008–2013. doi: 10.1109/SMC42975.2020.9283212

Wang, M., Wang, X., Peng, C., Zhang, S., Fan, Z., and Liu, Z. (2019). Research on EMG segmentation algorithm and walking analysis based on signal envelope and integral electrical signal. *Photon Netw. Commun.* 37, 195–203. doi: 10.1007/s11107-018-0809-1

Conflict of Interest: The authors declare that the research was conducted in the absence of any commercial or financial relationships that could be construed as a potential conflict of interest.

Publisher's Note: All claims expressed in this article are solely those of the authors and do not necessarily represent those of their affiliated organizations, or those of the publisher, the editors and the reviewers. Any product that may be evaluated in this article, or claim that may be made by its manufacturer, is not guaranteed or endorsed by the publisher.

frontiers in Human Neuroscience

ORIGINAL RESEARCH
published: 21 October 2021
doi: 10.3389/fnhum.2021.749366

Neuromuscular Age-Related Adjustment of Gait When Moving Upwards and Downwards

Arthur H. Dewolf[1], Francesca Sylos-Labini[2], Germana Cappellini[2,3], Dmitry Zhvansky[4], Patrick A. Willems[5], Yury Ivanenko[2] and Francesco Lacquaniti[1,2]*

[1] Department of Systems Medicine and Center of Space Biomedicine, University of Rome Tor Vergata, Rome, Italy, [2] Laboratory of Neuromotor Physiology, IRCCS Santa Lucia Foundation, Rome, Italy, [3] Department of Pediatric Neurorehabilitation, IRCCS Santa Lucia Foundation, Rome, Italy, [4] Laboratory of Neurobiology of Motor Control, Institute for Information Transmission Problems, Moscow, Russia, [5] Laboratoire de Physiologie et Biomecanique de la Locomotion, Université catholique de Louvain, Ottignies-Louvain-la-Neuve, Belgium

OPEN ACCESS

Edited by:
Nadia Dominici, VU University Amsterdam, Netherlands

Reviewed by:
Lars Janshen, Humboldt University of Berlin, Germany
Grzegorz Juras, Jerzy Kukuczka Academy of Physical Education in Katowice, Poland
Alain Frigon, Université de Sherbrooke, Canada

***Correspondence:**
Arthur H. Dewolf
arthur.dewolf@uclouvain.be

Specialty section:
This article was submitted to Motor Neuroscience, a section of the journal Frontiers in Human Neuroscience

Received: *29 July 2021*
Accepted: *28 September 2021*
Published: *21 October 2021*

Citation:
Dewolf AH, Sylos-Labini F, Cappellini G, Zhvansky D, Willems PA, Ivanenko Y and Lacquaniti F (2021) Neuromuscular Age-Related Adjustment of Gait When Moving Upwards and Downwards. Front. Hum. Neurosci. 15:749366. doi: 10.3389/fnhum.2021.749366

Locomotor movements are accommodated to various surface conditions by means of specific locomotor adjustments. This study examined underlying age-related differences in neuromuscular control during level walking and on a positive or negative slope, and during stepping upstairs and downstairs. Ten elderly and eight young adults walked on a treadmill at two different speeds and at three different inclinations (0°, +6°, and −6°). They were also asked to ascend and descend stairs at self-selected speeds. Full body kinematics and surface electromyography of 12 lower-limb muscles were recorded. We compared the intersegmental coordination, muscle activity, and corresponding modifications of spinal motoneuronal output in young and older adults. Despite great similarity between the neuromuscular control of young and older adults, our findings highlight subtle age-related differences in all conditions, potentially reflecting systematic age-related adjustments of the neuromuscular control of locomotion across various support surfaces. The main distinctive feature of walking in older adults is a significantly wider and earlier activation of muscles innervated by the sacral segments. These changes in neuromuscular control are reflected in a reduction or lack of propulsion observed at the end of stance in older adults at different slopes, with the result of a delay in the timing of redirection of the centre-of-mass velocity and of an unanticipated step-to-step transition strategy.

Keywords: aging, neuromechanics of gait, muscle activity analysis, coordination, spinal motoneuronal output, stair and slope

INTRODUCTION

Aging causes various motor (McGibbon, 2003; Perry et al., 2007) and sensory deficits (Skinner et al., 1984; Seidler et al., 2010). Since locomotor activities require a complex interaction of musculoskeletal and neural systems, age-related changes in the gait features can be observed (Winter et al., 1990; Samson et al., 2001; Laufer, 2005; Dewolf et al., 2019b). Indeed, numerous studies have described neuromuscular adjustments of gait to age-related physiological changes (e.g., Monaco et al., 2009; Hortobágyi et al., 2016; Gueugnon et al., 2019). In particular, compared

to young, older adults' gait is characterized by shorter step length, longer relative duration of the stance phase, wider burst of muscle activity (Monaco et al., 2010; Santuz et al., 2020), and a distal to proximal shift of joint moments (DeVita and Hortobagyi, 2000; Silder et al., 2008; Anderson and Madigan, 2014; Franz and Kram, 2014). In turn, this modification of distal joint moment has an impact on gait kinetics and kinematics (Noble and Prentice, 2008; Bleyenheuft and Detrembleur, 2012; Hafer and Boyer, 2018; Dewolf et al., 2019b; Gueugnon et al., 2019).

In healthy young adults, locomotor movements can be accommodated to various situations, such as walking slopes (Hong et al., 2014a,b; Dewolf et al., 2017) or stepping on stairs (McFadyen and Winter, 1988; Silverman et al., 2014), by means of appropriate changes in the intersegmental coordination and muscle activations (Dewolf et al., 2018, 2020b). During walking uphill and upstairs, the height of the center of mass of the body (COM) must be increased each step whereas it must be decreased during walking downhill and downstairs. These adjustments result in changes of positive and negative COM muscular power production/absorption (Dewolf et al., 2019a) and a redistribution of joint moments (Alexander et al., 2017; Montgomery and Grabowski, 2018). In turn, changes in the mechanical demand involve modifications in the neuromuscular control during slope walking (Janshen et al., 2017; Rozumalski et al., 2017; Saito et al., 2018). In particular, because biomechanical mechanisms of locomotion are tightly correlated with specific motor pool activations in the spinal cord (Cappellini et al., 2010), slope walking is associated with a different involvement of the lumbar and sacral motor pools (Dewolf et al., 2019a).

In older adults, altered coordination patterns among the elevation angles of the lower limb segments (Noble and Prentice, 2008; Bleyenheuft and Detrembleur, 2012; Dewolf et al., 2019b; Gueugnon et al., 2019), wider bursts of muscle activity (Santuz et al., 2020; Dewolf et al., 2021) and differential organization of the spinal output (Monaco et al., 2010) have been previously documented for level walking. When stepping on stairs, the strategy adopted by the older adults differs from that of young adults, since older apply knee and ankle moments differently from those of young adults (Reeves et al., 2009). Also, the propulsive moment generated by the trailing leg is reduced in older adults, which impacts the step-to-step transition (Meurisse et al., 2019), especially on positive slopes (Franz and Kram, 2014). On the contrary, the reduced contribution of ankle moment during downhill and downstairs stepping (Lay et al., 2006; Montgomery and Grabowski, 2018) may lessen the age-related modification of gait. The purpose of the present study was therefore to provide quantitative comparison of the output of spinal pattern generators between healthy young and older adults when they modify their power requirements to move up and down. In particular, we investigated the intersegmental coordination, muscle activity and the estimated output of motoneuron (MN) pools located at different spinal level during level and slope walking, as well as during upstairs and downstairs stepping in young and older adults. We expect that some neuromuscular age-related adjustments of gait would be present in all conditions, reflecting specific features of locomotion in older adults. We also tested the hypothesis that greater age-related modifications should be observed during tasks with a greater demand for ankle power generation, and *vice-versa*.

MATERIALS AND METHODS

Participants and Experimental Procedure

Eight young healthy adults (4 males – 4 females; age: 28.4 ± 5.2 years old, mass: 76.4 ± 10.1 kg, height: 1.76 ± 0.05 m, means ± SD) and 10 elderly healthy adults (9 males – 1 female; age: 73.5 ± 4.5 years old, mass: 81.5 ± 5.9 kg, height: 1.76 ± 0.05 m, mean ± SD) participated in the study. Mass and height were not significantly different between young and elderly adults (mass: $t = 0.5$, $p = 0.605$; height: $t = 1.8$, $p = 0.086$). No subject had a recent history of falling; they were able to walk without assistance and did not complain about any musculoskeletal disorders. None of the participants had hearing loss or other pathology that could affect navigation performance and mental spatial representation. All subjects gave their informed written consent. Experiments were performed according to the Declaration of Helsinki and were approved by the local ethics committee of IRCCS Fondazione Santa Lucia (protocol n CE/PROG749).

Subjects were asked to walk wearing their own walking shoes on a treadmill (En-Mill; 1.1 × 0.5 m) at two different imposed speeds [0.56 (2) and 1.11 (4) m s^{-1}(km h−1)] and on three different slopes (0° and ±6°) (**Figure 1**). One elderly adult was unable to walk uphill and downhill at 1.11 m s^{-1} and one young adult was not tested during stair stepping. Between 10 and 15 strides per trial were recorded; a total of 1,540 strides were analyzed. After a short break, the subjects were asked to perform a series of stepping tasks on stairs. The staircase was composed of two wooden steps with a rise height of 13 cm each and depth of 24.5 cm. The subjects performed five repetitions of step ascent followed by step descent, after remaining stationary for a moment at the top of the staircase. Every ascent/descent was performed with the right leg first and ended in double support on top/bottom of the steps. Each subject performed the tasks at a freely chosen speed.

Data Recordings

Bilateral, full-body three-dimensional (3D) kinematics were recorded at 200 Hz by means of a Vicon-612 system (Oxford, United Kingdom) with nine cameras placed around the treadmill or the staircase. Twelve reflective markers were attached to the skin of the subjects overlying the following bilateral landmarks: gleno-humeral joint, lateral epicondyle of the elbow, ulnar process of the wrist, greater trochanter, lateral femoral epicondyle, and lateral malleolus. In addition, four markers were placed on each shoe in approximate correspondence with the heel and fifth metatarso-phalangeal joint. The electromyogram (EMG) data were recorded at 2,000 Hz by means of a Delsys Trigno Wireless System (Boston, MA, United States). The following 12 muscles were recorded on the right side of the body: *gluteus maximus* (Gmax), *tensor fasciae latae* (TFL), *vastus medialis* (VM), *vastus lateralis* (VL), *rectus femoris* (RF), long head of the *biceps femoris,* (BF), *semitendinosus* (ST), *tibialis*

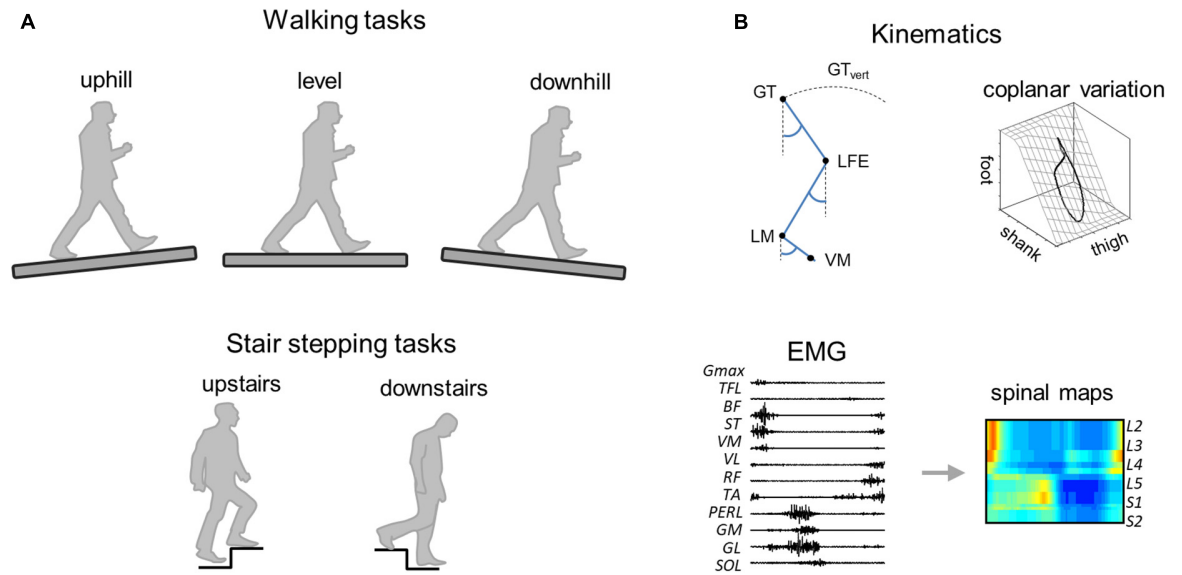

FIGURE 1 | Methodological figure. **(A)** Walking (uphill, level, and downhill) and stair stepping (upstairs and downstairs) tasks. **(B)** Data analysis. GT, greater trochanter; LFE, lateral femoral epicondyle; LM, lateral malleolus; VM, fifth metatarso-phalangeal joint, and GT_{vert}, vertical displacement of GT.

anterior (TA), *medial gastrocnemius* (GM), *lateral gastrocnemius* (LG), *soleus* (SOL), and *peroneus longus* (PERL). EMG electrodes were placed based on recommendation of SENIAM,[1] the European project on surface EMG. To ensure placement of EMG electrodes, muscle bellies were located by means of palpation and the electrodes were oriented along the main direction of the fibers (Kendall et al., 2005). In certain conditions, some electrodes became partially detached and were removed from the analysis on a subject-specific basis. Out of a total of 1,476 EMG recordings, we lost 8% of them. Kinematic and EMG recordings were synchronized on-line.

Kinematic Data Analysis

During walking, the stride was defined as the period between two contacts of the right foot with the ground. During stepping on stairs, the stride was defined as the period between two lift-offs of the right foot (in order to have one complete cycle). Foot-contact/lift-off were estimated according to the local minima of the vertical displacement of the heel/fifth metatarso-phalangeal joint markers, respectively (Ivanenko et al., 2007).

From the marker locations, the orientation of the thigh, shank, foot, and trunk relative to the vertical axis (elevation angle) were computed as described in Borghese et al. (1996). For each subject, the different strides of each trial were normalized by interpolating individual gait cycles over 200 points (i.e., each point corresponding to 0.5% of the stride). To analyze the relative phase of the time-course of the elevation angles during a stride, the phase lags between two adjacent limb-segments were computed by means of cross-correlation function. The trajectory of the COM was estimated by the trajectory of a point located at mid-distance between left and right greater trochanters. The trajectory of this point has been shown to be similar to the trajectory of the COM, estimated from the ground reaction forces (Dewolf et al., 2018). From the coordinates of this point, we estimated the displacement and velocity of the COM.

In order to determine the covariance matrix of the segment elevation angles, a principal component analysis was applied. The eigenvalues and eigenvectors u_i were computed by factoring the covariance matrix from the set of original signals by using a singular value decomposition algorithm. The first two eigenvectors (u_1 and u_2) lie on the best-fitting plane of angular covariation, and the data projected onto the corresponding axes correspond to the first (PC_1) and second (PC_2) principal components. The planarity was evaluated for each condition by calculating the percentage of variance that was explained by u_1 (PV_1), u_2 (PV_2), and u_3 (PV_3). If the data lie perfectly on a plane, PV_3 would be 0%. By definition, the third eigenvector u_3 is orthogonal to the plane defined by u_1 and u_2. The parameter u_{3t} corresponds to the direction cosine with the positive semi-axis of the thigh, and provides a measure of the orientation of the plane (Bianchi et al., 1998).

Electromyogram Data Analysis

The collected raw EMG signals were high-pass filtered (30 Hz), then rectified and low-pass filtered with a zero-lag 4th-order Butterworth filter (10 Hz). A custom-made automatic search for artifacts was also implemented, by comparing the EMG envelope of each gait cycle with the average envelope. The time scale was normalized by interpolating individual gait cycles over 200 points (i.e., every 0.5%). For each condition and for each EMG waveform, the full width at half maximum (FWHM) was calculated as the period during which the EMG activity exceeded half of its maximum (Martino et al., 2014; Dewolf et al., 2020b; Santuz et al., 2020). The center of activity (CoA) of each

[1]https://seniam.org

EMG waveform was also calculated as the angle of the vector that points to the center of mass of the circular distribution (Martino et al., 2014).

The EMG activities were then mapped onto the estimated rostro-caudal location of the MN pools in the human spinal cord from the L2 to S2 segments. This reconstruction is based on the approximate location of MN pools innervating different muscles in the human spinal cord based on published charts of segmental localization (Kendall et al., 2005), as in Ivanenko et al. (2006, 2013). In general, each muscle is innervated by several spinal segments (**Table 1**). To account for size differences in MN pools at each spinal level, this fractional activity value was then multiplied by the estimated segment-specific number of MNs (MN_j), based on Tomlinson and Irving (1977).

To compute the total motor output in each condition, we summed the motor output patterns of each spinal segment over the gait cycle. The minimal activation and the range (maximum-minimum) were then computed. The relative activation of the lumbar and sacral segments in each condition were computed as the average motor output patterns in the upper part of the lumbar segments (sum of the activity from L2 to L4) and the sacral segments (sum of activity from S1 to S2). Note that to reduce overlaps due to maps smoothing, the spinal segment L5 was not taken into account (Dewolf et al., 2019a, 2020a). The FWHM and the timing of the maximal activation were then calculated for both lumbar and sacral segments.

Statistics

For the walking tasks, the statistical analysis was designed to assess the effect of speed of progression, slope, age group (young vs. older adults), and the interaction between these factors. For the stair tasks, the statistical analysis was designed to assess the effect of step direction (ascent vs. descent), age group, and the interaction between these factors. A linear mixed model was applied. The normality of the residuals was tested by means of the Kolmogorov–Smirnov test. Normality was not assumed for five variables (range of motion of the trunk elevation angle and of the thigh elevation angle during walking, shank-foot phase lag, the FWHM of Gmax and the CoA of RF). In those cases, a log transform was applied, and the normality of the residuals was then assumed. The effect size, measure by the eta square (η_p^2), is reported for age group comparisons.

TABLE 1 | Innervation of the lower limb muscles.

	Gmax	TFL	BF	ST	VM	VL	RF	TA	PERL	GM	GL	SOL
L2					X	X	X					
L3					X	X	X					
L4		X		x	X	X	X	X	x			
L5	X	X	x	X				X	X			x
S1	X	X	X	X				X	X	X	X	X
S2	X		X	X						X	X	X

Reference segmental charts for lower limb muscles from Kendall et al. (2005), obtained by combining the anatomical and clinical data from six different sources. A capital X denotes localization agreed on by five or more sources, a small x denotes agreement of three to four sources.

Circular statistics (Berens, 2009) were used to characterize the CoA of each muscle and spinal output. The Rayleigh test (Berens, 2009) was used to check whether the samples were distributed uniformly around the gait cycle or had a common mean direction. In all analyses, the significance level was fixed at $p < 0.05$.

RESULTS

Gait and Kinematic Parameters

We first report the results of walking tasks. The stride period (and thus stride length) decreased with speed ($F_{1,95} = 162.8$; $p < 0.001$; **Figure 2A**) but did not change with the slope ($F_{2,95} = 1.2$; $p = 0.295$) in both age groups. At a given speed, older adults stepped at a higher cadence with shorter strides (shorter stride period) than young adults ($F_{1,95} = 175.1$; $p < 0.001$; $\eta_p^2 = 0.65$). However, the effect of speed on the stride period was greater in young adults (stride period: $F_{1,95} = 4.3$; $p = 0.04$).

The relative duration of the stance phase became smaller when speed increased both in young ($F_{1,95} = 117.4$; $p < 0.001$) and older adults ($F_{1,95} = 6.6.5$; $p = 0.012$; $\eta_p^2 = 0.06$). The relative stance period was also slightly affected by the slope ($F_{1,95} = 3.9$; $p = 0.023$). The down-to-up redirection of the COM velocity at step-to-step transition, defined by the time of occurrence of the minimal vertical velocity of the COM [Vv_{min}] relative to the beginning of the double contact phase (Franz and Kram, 2013; Meurisse et al., 2019), began later in older than in young adults ($F_{1,95} = 6.5$; $p = 0.014$; $\eta_p^2 = 0.13$) and in downhill than uphill walking ($F_{2,95} = 27.3$; $p < 0.001$). As a result, the transition phase began later in older than in young adults.

When speed increased, the range of motion (ROM) of the thigh, shank, and foot elevation angles increased (thigh: $F_{1,95} = 29.3$; $p < 0.001$; shank: $F_{1,95} = 230.3$; $p < 0.001$; foot: $F_{1,95} = 201.2$; $p < 0.001$) in both groups (**Figure 2A**). The inclination of the treadmill affected the ROM of thigh and shank angles (thigh: $F_{1,95} = 28.8.5$; $p < 0.001$; *shank:* $F_{1,95} = 21.4$; $p < 0.001$) but not the ROM of the foot angle ($F_{1,95} = 1.3$; $p = 0.265$). During uphill walking, the thigh ROM increased while the shank ROM decreased as compared to level walking ($p < 0.001$ *Bonferroni post hoc*). The contrary was true for downhill walking ($p < 0.038$ *Bonferroni post hoc*).

Older adults performed smaller amplitude of movement of the different lower-limb segments than young adults (**Figure 2A**; thigh: $F_{1,95} = 6.2$; $p = 0.014$, $\eta_p^2 = 0.1$; shank: $F_{1,95} = 176.2$, $\eta_p^2 = 0.65$; $p < 0.001$; foot: $F_{1,95} = 150.3$; $p < 0.001$, $\eta_p^2 = 0.61$). In addition, older adults walked with a greater mean forward inclination of the trunk relative to the vertical than young adults ($F_{1,95} = 89.6$; $p < 0.001$; $\eta_p^2 = 0.49$).

With regards to stepping on stairs, older adults were slower than young adults (longer stride period) ($F_{1,32} = 5.4$; $p = 0.027$, $\eta_p^2 = 0.16$; **Figure 3B**). In both groups, stepping downstairs was performed faster than moving upstairs ($F_{1,35} = 11.3$; $p = 0.002$). The relative duration of the stance phase was longer when stepping upstairs than downstairs ($F_{1,35} = 6.6$; $p = 0.015$) but it did not differ significantly between young and older adults ($F_{1,35} = 0.1$; $p = 0.739$).

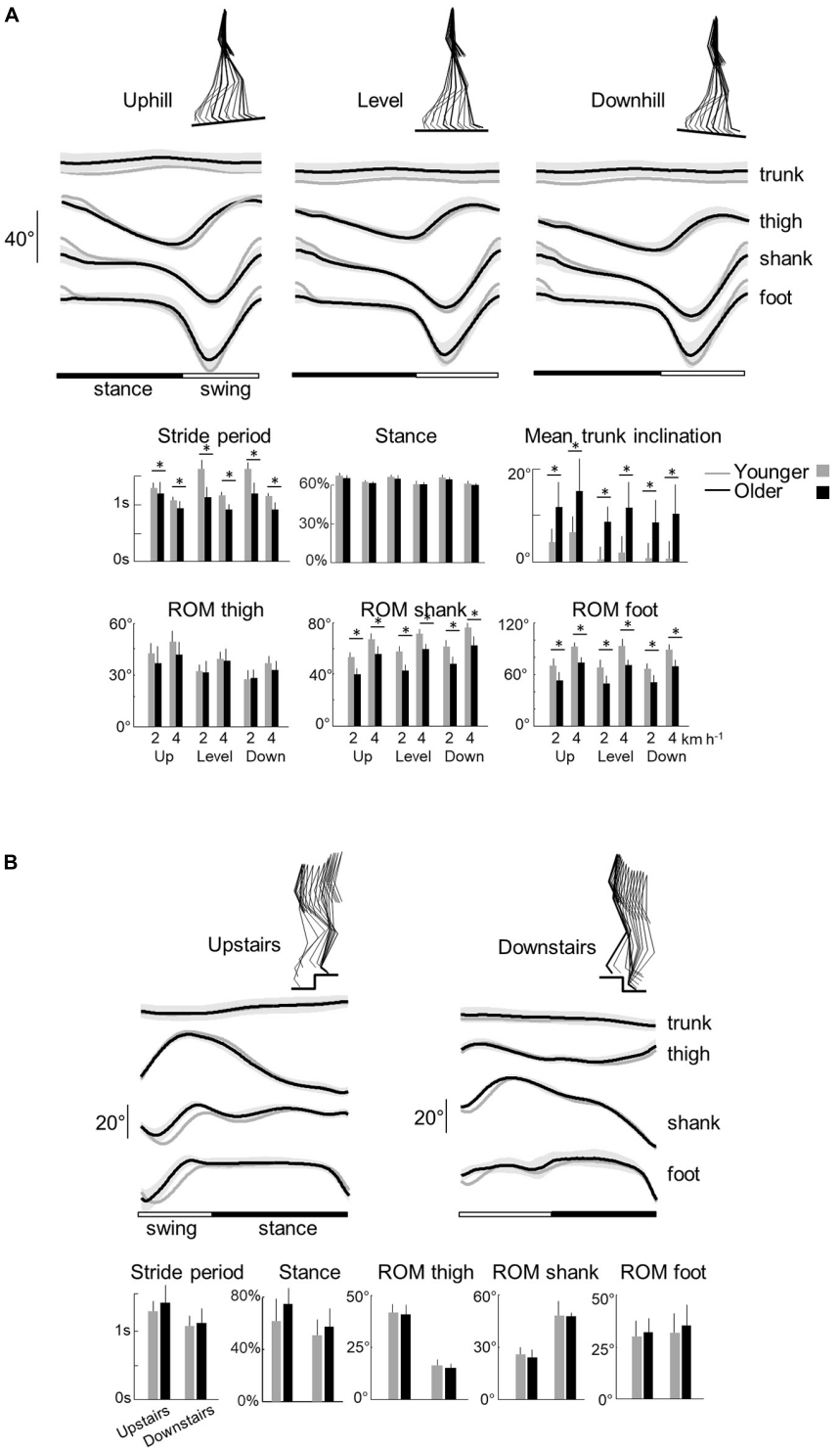

FIGURE 2 | Elevation angles of lower-limb segments and general gait parameters across all conditions in younger and older adults. **(A)** Walking tasks: elevation angles of the trunk, thigh, shank, and foot over a stride. All the curves of each subject walking at a given walking condition were first averaged (mean-curve). The curves presented here are the average of the mean-curves of all the young (gray lines) and older (black lines) adults. The gray zone represents ±1 SD for the older adults. Below, the bar plots present the average stride period, relative stance phase, and mean trunk inclination over one stride, as well as the average range of motion of the thigh, shank, and foot over one stride. Bars are presented for each walking task and at each speed (2 and 4 indicate the speed in km h^{-1}). **(B)** Stair stepping tasks: elevation angles of the trunk, thigh, shank, and foot over a stride. Below, the bar plots present the average stride period, relative stance phase, and the average range of motion of the thigh, shank, and foot over one stride. In all panels, gray bars correspond to young adults, whereas black bars correspond to elderly adults. Thin lines represent one standard deviation. The * indicates a significant effect of age (Student *t*-test, $p < 0.05$).

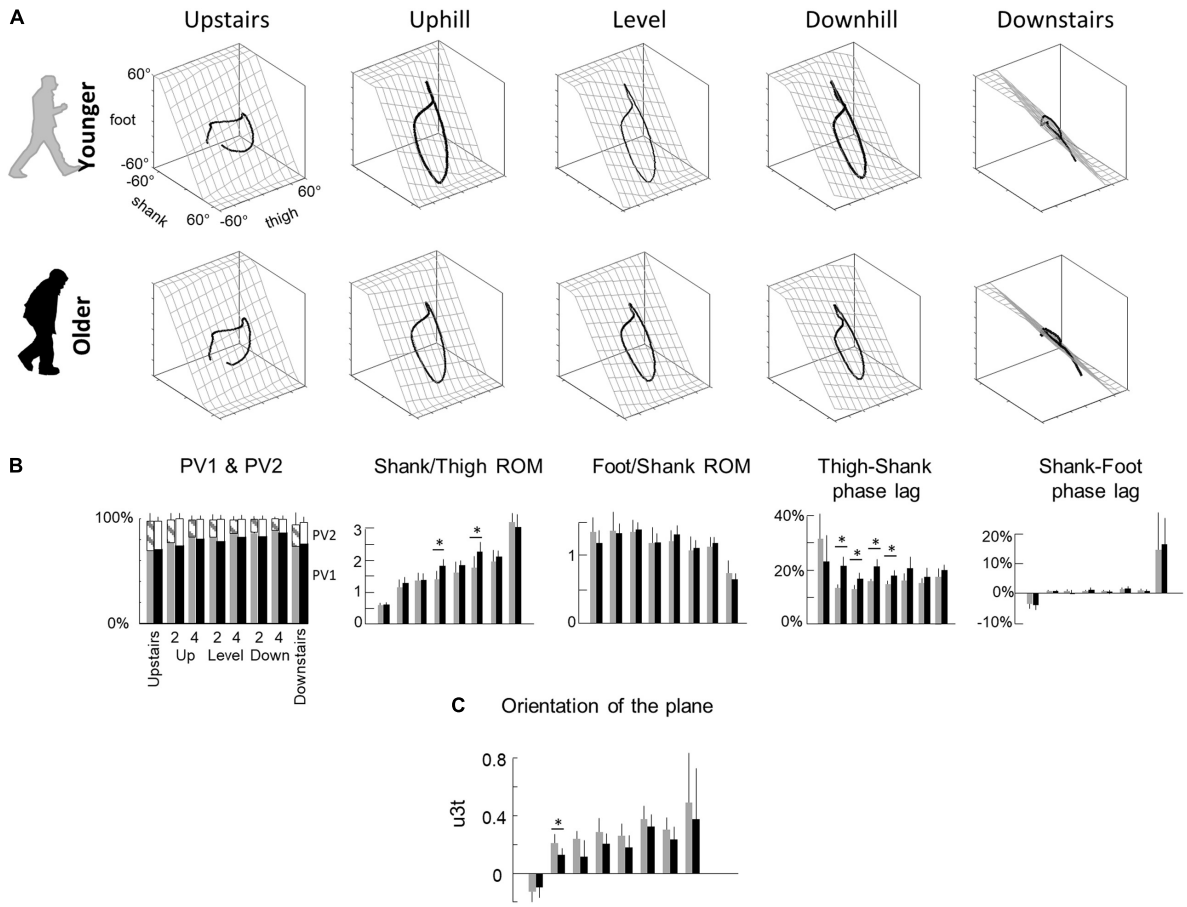

FIGURE 3 | Planar covariation of elevation angles. **(A)** Covariation of the ensemble-average limb-segment elevation angles across young (up) and elderly adults (bottom) in all conditions. Note that when the elevation angles of thigh, shank, and foot are plotted one vs. the other in a x-y-z space, they co-vary along a loop constrained on a plane (x–y). Grids show the best-fitting plane. **(B)** Average percentage of variance accounted for by the first (PV_1) and second (middle – PV_2) eigenvector of the principal component analysis, average amplitude ratios between the range of motion of adjacent segments and phase lags between time curves of elevation angles of adjacent segments. Bars are presented for each condition and at each speed (2 and 4 indicate the speed in km h^{-1}). **(C)** The direction cosines of the normal to the covariation plane with the positive semi-axis of the thigh angular coordinates (u3t). Other indications as in **Figure 2**.

Similar to walking on slopes, upstairs stepping involved an increase of the thigh ROM ($F_{1,35}$ = 374.7; $p < 0.001$) and a decrease of the shank ROM ($F_{1,35}$ = 156.1; $p < 0.001$), as compared to downstairs stepping. No significant difference was found in foot ROM ($F_{1,35}$ = 0.6; p = 0.418). In addition, we found no significant difference on other kinematic parameters between older and young adults (mean trunk inclination, thigh ROM, shank ROM, and foot ROM: all $p > 0.407$).

Intersegmental Coordination When Moving Upwards and Downwards

The coordination between thigh, shank and foot elevation angles was evaluated using principal component analysis (**Figure 3**). **Figure 3A** illustrates the averaged gait loops plotted in 3D during walking on slopes and stepping on stairs in both age groups. Note significantly smaller loops in elderly adults in the walking conditions (related to the smaller ROM reported in the previous section).

In each condition, $PV_1 + PV_2 > 97\%$ indicating an excellent fit of a planar regression on the elevation angles of the three lower limb segments (**Figure 3B**). However, PV_1 was smaller (and PV_2 greater) in older than in young adults during walking (PV_1: $F_{1,95}$ = 19.7; $p < 0.001$; η_p^2 = 0.17; PV2: $F_{1,95}$ = 18.3; $p < 0.001$; η_p^2 = 0.16), but they were similar during stepping on stairs (PV_1: $F_{1,35}$ = 0.2; p = 0.606; PV2: $F_{1,35}$ = 0.1; p = 0.733). Furthermore, PV_1 slightly increased (and PV_2 decreased) with walking speed (PV_1: $F_{1,95}$ = 27.1; $p < 0.001$; PV2: $F_{1,95}$ = 27.6; $p < 0.001$) and was greater in downhill walking and downstairs negotiation (PV_1: $F_{2,95}$ = 29.8; $p < 0.001$; PV2: $F_{2,95}$ = 29.1; $p < 0.001$). The orientation of the plane, shown by the direction cosine u_{3t} (**Figure 3C**), rotated across conditions (with treadmill slope: $F_{1,95}$ = 23.9; $p < 0.001$; with stair conditions: $F_{1,35}$ = 36.1; $p < 0.001$). The u_{3t} was smaller in upstairs stepping and uphill walking, whereas it was greater in downhill walking and downstairs stepping. During walking, u_{3t} was smaller in older than in young adults ($F_{1,95}$ = 25.8; $p < 0.001$; η_p^2 = 0.22), whereas no significant difference was observed during stair negotiation

($F_{1,35}$ = 0.2; p = 0.619). When all conditions were considered together (both stair and slope conditions), the variation of u_{3t} across conditions was more important in young than in older adults (young: $F_{6,62}$ = 11.6; $p < 0.001$; older: $F_{6,76}$ = 9.8; $p = 0.001$).

Both the shape of the loop and the orientation of the plane depend on the amplitude ratio and the time relationship characteristics of the elevation angles of adjacent limb segments (**Figure 3B**). During walking, the ratio between thigh and shank ROM was smaller in elderly adults ($F_{1,95}$ = 21.0; $p < 0.001$; η_p^2 = 0.18) and greater on negative than on positive slopes ($F_{2,95}$ = 62.8; $p < 0.001$). Similarly, the ratio between thigh and shank ROM was smaller when stepping upstairs than downstairs ($F_{1,35}$ = 814.9; $p < 0.001$), but no difference between older and young adults was observed ($F_{1,35}$ = 0.6; p = 0.420). The ratio between shank and foot ROM was affected by conditions in an opposite way: it was greater when stepping upstairs and walking uphill and smaller when stepping downstairs and walking downhill (slope: $F_{2,95}$ = 15.2; $p < 0.001$; stairs: $F_{1,35}$ = 75.8; $p < 0.001$). In all conditions, no effect of age groups was found (walking: $F_{2,95}$ = 0.9; p = 0.336; stepping: $F_{1,35}$ = 3.6; $p < 0.067$). The phase lag between thigh and shank displacement was significantly affected by age during walking ($F_{1,95}$ = 81.4; $p < 0.001$; η_p^2 = 0.47), but not during stepping on stairs ($F_{1,35}$ = 1.3; p = 0.257). The phase lag between shank and foot was not significantly affected by age, whatever the conditions (slope: $F_{1,95}$ = 0.2; p = 0.66; stairs: $F_{1,35}$ = 0.1; p = 0.792).

Muscle Activations

Figure 4A illustrates ensemble averages of rectified EMG envelopes for all walking conditions in young and older adults. EMGs of young adults are visually consistent with those reported in the literature for level and slope walking (Dewolf et al., 2019a, 2020b). The slopes slightly modified the EMG activity: for example, the FWHM of Gmax, BF, and RF were significantly affected by the slope ($F_{1,95}$ = 7.6; p = 0.001; $F_{1,95}$ = 3.4; p = 0.038; $F_{1,95}$ = 5.4; p = 0.006).

In older adults, EMG data remained qualitatively similar to those of young adults. However, many muscles were characterized by a duration and timing of activation different from those of young adults (**Figure 4B**). In particular, the CoA of many muscles occurred significantly earlier in the stride (circular statistics: *Gmax*: $F_{1,95}$ = 23.4; $p < 0.001$; *ST*: $F_{1,95}$ = 7.9; p = 0.006; *VL*: $F_{1,95}$ = 12.6; $p < 0.001$; *RF*: $F_{1,95}$ = 16.1; $p < 0.001$; *TA*: $F_{1,95}$ = 75.5; $p < 0.001$; *PERL*: $F_{1,95}$ = 69.4; $p < 0.001$; *GM*: $F_{1,95}$ = 34.9; $p < 0.001$; *GL*: $F_{1,95}$ = 45.8; $p < 0.001$; *SOL*: $F_{1,95}$ = 69.9; $p < 0.001$). In addition, older adults displayed longer burst of muscle activations than young adults, as assessed by considering the FWHM in the following muscle groups: hamstrings (*BF*: $F_{1,95}$ = 102.2; $p < 0.001$; η_p^2 = 0.53; *ST*: $F_{1,95}$ = 11.5; p = 0.001; η_p^2 = 0.11), knee extensors (VL: $F_{1,95}$ = 5.4; p = 0.02; η_p^2 = 0.06; RF: $F_{1,95}$ = 17.8; $p < 0.001$; η_p^2 = 0.17), and ankle extensors (*GM*: $F_{1,95}$ = 35.4; $p < 0.001$; η_p^2 = 0.17; *GL*: $F_{1,95}$ = 20.4; $p < 0.001$; η_p^2 = 0.19; *SOL*: $F_{1,95}$ = 68.7; $p < 0.001$; η_p^2 = 0.44).

Figure 5A illustrates ensemble averages of rectified EMG envelopes during upstairs and downstairs stepping in young and older adults. Very few differences of EMG duration were observed between upstairs and downstairs: the FWHM of *RF* was significantly greater during downstairs than upstairs stepping ($F_{1,35}$ = 4.6; p = 0.041; **Figure 5B**). An effect of age was also observed, but to a lesser extent than for walking. The FWHM of *BF*, *GM*, and *SOL* (*BF*: $F_{1,35}$ = 13.2; p = 0.001; η_p^2 = 0.34; *GM*: $F_{1,35}$ = 16.8; $p < 0.001$; η_p^2 = 0.39; *SOL*: $F_{1,35}$ = 9.0; p = 0.006; η_p^2 = 0.26) and the CoA of distal muscles occurred earlier in older than younger adults (circular statistics: *TA*: $F_{1,35}$ = 13.4; $p < 0.001$; *PERL*: $F_{1,35}$ = 36.0; $p < 0.001$; *GM*: $F_{1,35}$ = 4.7; p = 0.038; *GL*: $F_{1,35}$ = 5.2; p = 0.03; *SOL*: $F_{1,35}$ = 14.8; $p < 0.001$).

Spinal Motor Output When Moving Upwards and Downwards

Figure 6A presents the spatio-temporal maps derived from the EMG activities of **Figures 4A**, **5A**. In brief, the recorded patterns of EMG activity were mapped onto the spinal cord in approximate rostrocaudal locations of the MN pools. This approach provides information about pattern output during locomotion in terms of lumbosacral segmental control (from L2 to S2) rather than in terms of individual muscle control. In each condition, both the lumbar and sacral segments presented one major spot of activity (Ivanenko et al., 2006; Cappellini et al., 2010; Dewolf et al., 2019a, 2021). The first burst occurs around foot contact and is mainly localized on the lumbar segment whereas the second burst occurs during the second part of stance mainly and is localized on the sacral segment.

Striking age-related differences were observed in the burst timing and duration of those spots of activity. As compared to young adults, older adults had greater FWHM of the lumbar and sacral MN activation during walking (lumbar: $F_{1,95}$ = 46.2; $p < 0.001$; η_p^2 = 0.23; sacral: $F_{1,95}$ = 142.4; $p < 0.001$; η_p^2 = 0.42) and during stepping on stairs (lumbar: $F_{1,35}$ = 33.0; $p < 0.001$; η_p^2 = 0.20; sacral: $F_{1,35}$ = 6.2; p = 0.013; η_p^2 = 0.12). In addition, during walking, the timing of the maximum activation of the sacral segments occurred earlier in old than in young adults ($F_{1,95}$ = 148.6; $p < 0.001$; η_p^2 = 0.46) whereas the timing of maximum activation of the lumbar segments did not change with age ($F_{1,95}$ = 1.1; p = 0.296). The FWHM of the lumbar and sacral bursts changed as a function of the slope, with a longer burst of lumbar segments during downhill walking ($F_{2,95}$ = 16.4; $p < 0.001$) and a longer burst of sacral segment during uphill walking ($F_{2,95}$ = 3.1; p = 0.046). Also, the timing of the maximal activation of the sacral segments occurred earlier during walking downhill ($F_{2,95}$ = 40.2; $p < 0.001$). Note that the effect of age was larger during uphill than during downhill walking (age by slope interaction: $F_{1,95}$ = 30.8; $p < 0.001$). During stepping on stair, the FWHM of lumbar and sacral segments were not significantly affected by the direction of progression. The maximum lumbar activation occurred significantly earlier during downstairs stepping ($F_{1,35}$ = 11.8; p = 0.001) and the maximum sacral activation occurred significantly later during upstairs stepping ($F_{1,35}$ = 54.2; $p < 0.001$). No significant effect of age was observed on these two timings (lumbar: $F_{1,35}$ = 1.8; p = 0.180; sacral: $F_{1,35}$ = 2.7; p = 0.096).

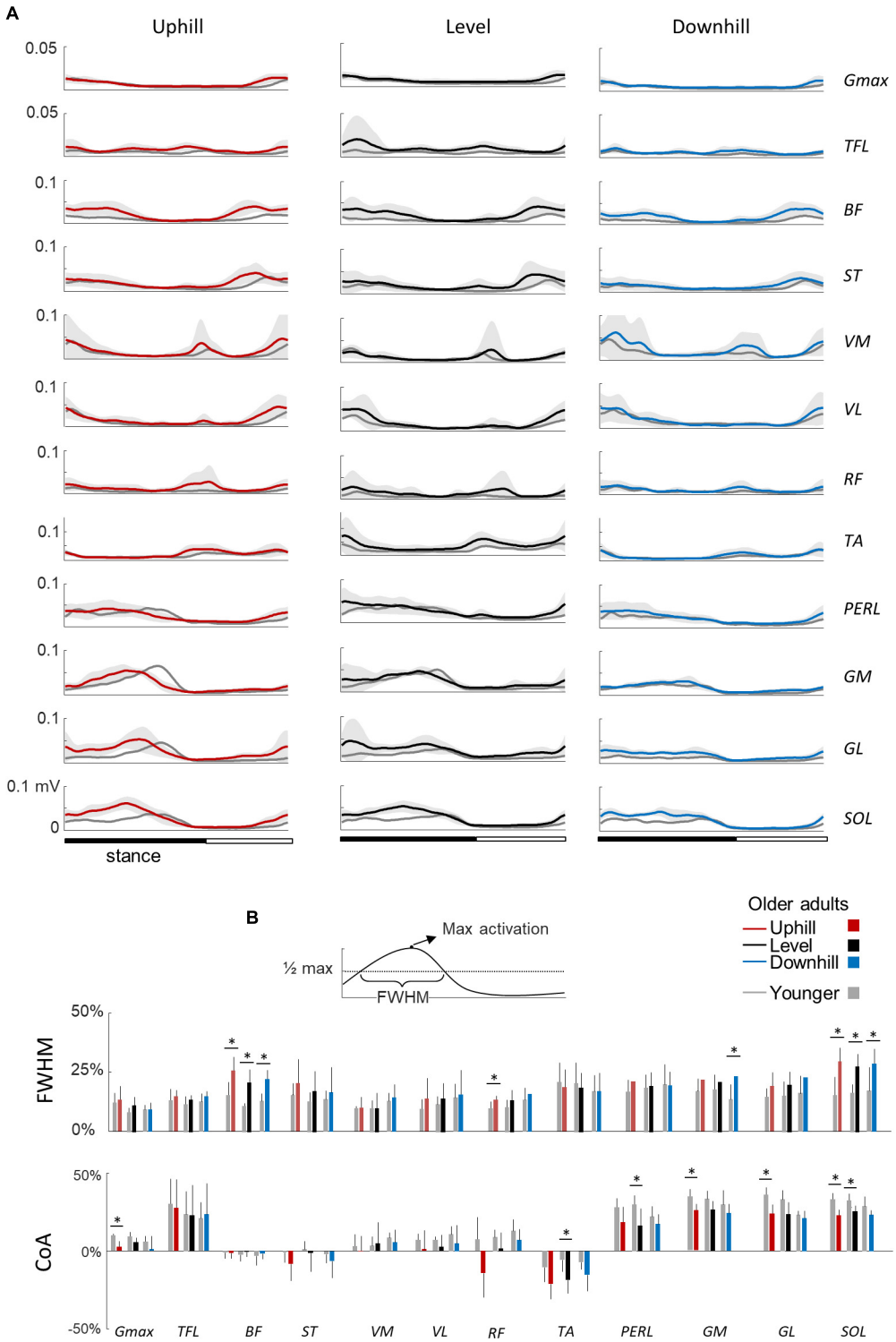

FIGURE 4 | Ensemble-averaged electromyogram (EMG) patterns during uphill, level, and downhill walking in young and older adults. **(A)** Ensemble-averaged EMG patterns over one stride in uphill (red), level (black), and downhill (blue) walking. *Gmax*, gluteus maximus; *TFL*, tensor fascia latae; *VM*, vastus medialis; *VL*, vastus lateralis; *RF*, rectus femoris; *BF*, biceps femoris; *ST*, semitendinous; *TA*, tibialis anterior; *MG*, gastrocnemius medialis; *LG*, lateral gastrocnemius; *SOL*, soleus; *PERL*, peroneus longus. The curves presented here are the average of the mean-curves of all the young (gray lines) and elderly (colored lines) adults. The gray zone represents ±1 SD for the older adults. **(B)** Full Width Half Maximum (FWHM) and center of activity (CoA) of the 12 lower-limb muscles at each walking condition. The bars represent the grand mean of all the young (gray) and the elderly (colored) adults. Thin lines represent one standard deviation. The * indicates a significant effect of age (Student *t*-test, $p < 0.05$).

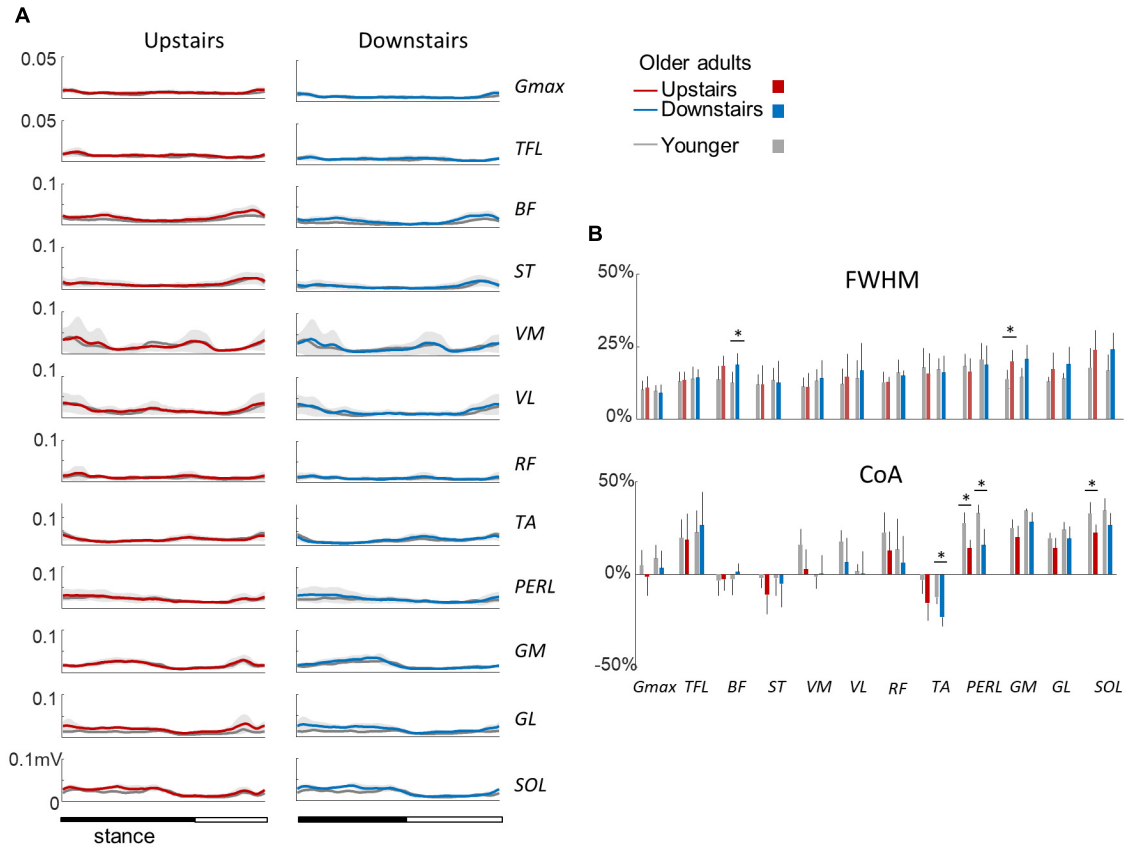

FIGURE 5 | Ensemble-averaged EMG patterns during upstairs and downstairs stepping in young and older adults. **(A)** Ensemble-averaged EMG patterns over one stride in upstairs (red) and downstairs (blue) stepping. **(B)** FWHM and CoA of the 12 lower-limb muscles during stair stepping. Other indications as in **Figure 2**.

The minimal level of activity of the lumbar and sacral segments pooled together (total spinal motor output) and the range of activity (maximum-minimum) remained similar across slopes during walking (minimum: $F_{2,95} = 2.5$; $p = 0.086$; range: $F_{2,95} = 0.2$; $p = 0.821$) and during downstairs or upstairs stepping (minimum: $F_{1,35} = 0.3$; $p = 0.591$; range: $F_{1,35} = 0.4$; $p = 0.528$). In each condition, older adults had always a significantly higher minimal level of activity than younger adults (walking: $F_{1,95} = 82.7$; $p < 0.001$; $\eta_p^2 = 0.48$; stepping: $F_{1,35} = 17.3$; $p < 0.001$; $\eta_p^2 = 0.40$). However, a significant age-effect on the range of activation was only observed during walking ($F_{1,95} = 12.5$; $p < 0.001$; $\eta_p^2 = 0.13$) but not during when stepping on stairs ($F_{1,35} = 0.13$; $p < 0.717$). In addition, the co-activation of lumbar and sacral segments was significantly greater in older than in young adults during slope walking ($F_{2,95} = 3.9$; $p = 0.05$; $\eta_p^2 = 0.06$), but it was not significantly different during stepping on stairs ($F_{1,35} = 0.16$; $p = 0.694$).

DISCUSSION

The purpose of this study was to quantify the effect of aging on the neuromuscular control of gait when moving upwards and downwards. Specifically, we analyzed walking up and down a slope and stepping up and down a stair. As expected, we found common age-related modifications of gait, suggesting specific adjustments of the motor control (Franz, 2016). In all conditions, the activation profiles of ankle extensor and knee flexor muscles were wider and the minimal level of activation of the total spinal output was higher in older than in younger adults. We also found that other age-related differences were present during walking tasks but not when stepping on stairs. As discussed below, the changes may be larger during tasks requiring greater propulsive function of the trailing leg, impacting the step-to-step transitions.

Widening of Muscle Activation in Older Adults

Our results are consistent with prior results showing specific spatiotemporal feature of gait in older adults during both walking (e.g., Herssens et al., 2018) and stair stepping (Williams and Bird, 1992; Startzell et al., 2000). Thus, older tend to take shorter steps during walking (**Figure 2A**) and slower steps when stepping on stairs (**Figure 2B**) than younger adults. In addition, despite the various biomechanical constraints induced by the different situations studied, we observed similar age-related differences on muscle activations, suggesting that gait impairments in older adults cannot depend only on a reduction of force generated by

plantar flexor muscles (Franz, 2016). In particular, the activity profiles of the knee flexor and ankle extensor muscles, innervated from the sacral segments, are significantly wider in older adults in all conditions (**Figures 4A**, **5A**), that could be related to a more robust neuromuscular control (i.e., more able to cope with errors) to deal with poorer balance control (Martino et al., 2015; Santuz et al., 2018). The spinal maps of motoneuron activity also clearly illustrates this finding (**Figure 6A**). Similar widening has already been documented during level walking (Monaco et al., 2010; Santuz et al., 2020; Dewolf et al., 2021).

Higher Activation of Spinal Motor Pools

Another modification of gait in the elderly, shared across the conditions, is the higher minimal level of the spinal motor output (**Figure 6B**), which may contribute to the age-related increase in the metabolic cost of locomotion (Mian et al., 2006). There might be other group or individual differences such as level of physical activity, gender, experience with inclined (mountaineering) walking, which could potentially also contribute to the observed differences. However, it is unlikely that these factors alone can account for the present age-related differences since EMG widening and higher activation of motor pools have been previously reported in other population of patients both for males and females and with different level of physical activity (Monaco et al., 2010; Martino et al., 2018; Santuz et al., 2020). Nevertheless, future research investigating the contribution and interaction of different factors would be beneficial to assess gait of older adults. On the one hand, the higher tonic activation could be related to wider muscle activations, also resulting in increased co-activations (Hortobágyi and DeVita, 2000). The most commonly ascribed role to co-activation is to provide mechanical stability by stiffening joints (Hogan, 1984;

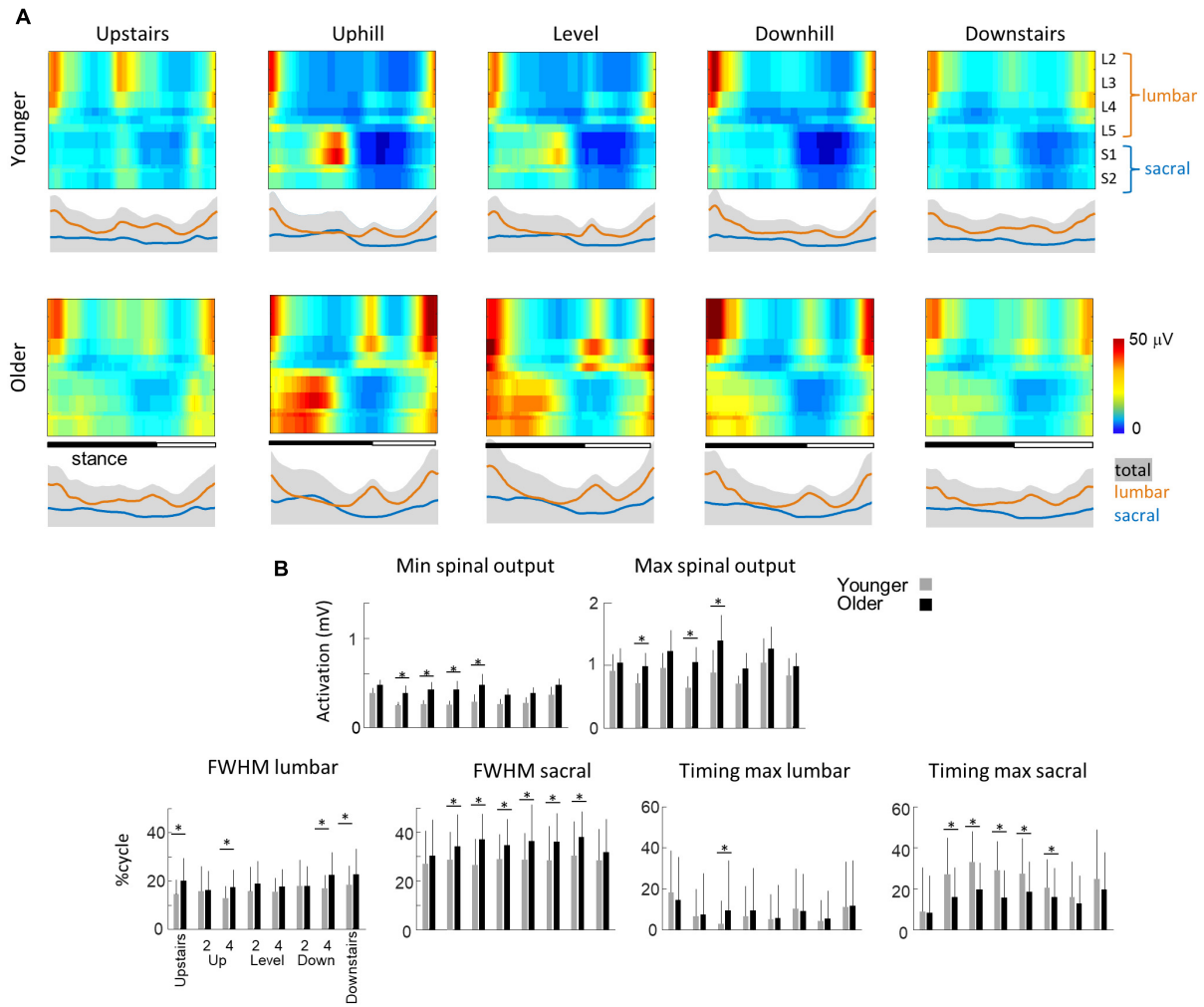

FIGURE 6 | Unilateral spatiotemporal spinal motor outputs computed from ensemble-averaged EMGs across all subjects in all conditions (**Table 1**). **(A)** Motor output (reported in µV) is plotted as a function of gait cycle in young (top) and older (bottom) adults. The thin green and red lines correspond to the activation of the lumbar and sacral segments, respectively. The gray area is the sum of all segments and reflects the level of activation **(B)** average minimal and maximal level of activation of the spinal motor output, average FWHM, and timing of the maximal activation of the lumbar and sacral segments. Bars are presented for each condition and at each speed (2 and 4 indicate the speed in km h^{-1}). Other indications as in **Figure 2**.

Martino et al., 2014). On the other hand, the increased minimal level of the spinal motor output may be related to alterations in the peripheral neuromuscular system, including changes in muscle contractile mechanics (Brooks and Faulkner, 1988), reduction in the number and/or size of type II fibers (Lexell, 1995; Aagaard et al., 2007), partial denervation at the neuromuscular junction (Arizono et al., 1984), or muscle atrophy (Rosenberg, 2011). Consequently, the size of motor units and firing rates used to achieve a given force increase with age (Ling et al., 2009).

Unanticipated Step-to-Step Transition Strategy

During walking, additional age-related differences were present that were not during stepping on stairs. As already documented, older adults adapt their intersegmental coordination and display a different orientation of the covariation plane in all walking conditions (Noble and Prentice, 2008; Bleyenheuft and Detrembleur, 2012; Dewolf et al., 2019b; Gueugnon et al., 2019; **Figure 3A**), shedding light on age-related modifications of the coordination strategies during walking. In particular, the age-related rotation of the plane occurs mainly along the long axis of the gait loop (**Figure 3A**), leading to a smaller u_{3t} (**Figure 3C**). The change in plane orientation is mainly related to a change of the phase shift and range of motion ratio between adjacent lower-limb segments (Borghese et al., 1996; Dewolf et al., 2019b). Most previous studies interpreted the modification of plane orientation in terms of a reduction of ankle plantar-flexion at the end of stance and redistribution of joint moments (Alexander et al., 2017; Montgomery and Grabowski, 2018). Here, we found that the activation of the sacral segments occurred earlier in older as compared to young adults, mainly related to an early activation of ankle plantar-flexor muscles and lack of later activation (**Figure 4A**).

A comparison of different human gaits and developmental considerations highlight the link existing between COM trajectory and functional spinal cord topography (Cappellini et al., 2010; Dewolf et al., 2020c). The reduction of ankle power generation at the end of stance in turn modifies the step-to-step transition in older (Meurisse et al., 2019). Indeed, due to the lack of late push-off from the trailing leg, the down-to-up redirection of the COM velocity starts later in older than in young adults (**Figure 7**). This re-direction can be estimated from the time of occurrence of the minimal vertical velocity of the COM relative to the beginning of the double contact phase (Franz and Kram, 2013; Meurisse et al., 2019). This modification of the timing of sacral activation, related to the earlier activation of plantar-flexor muscles, may be adopted by the older adults to use their plantar-flexor muscles over a more favorable portion of

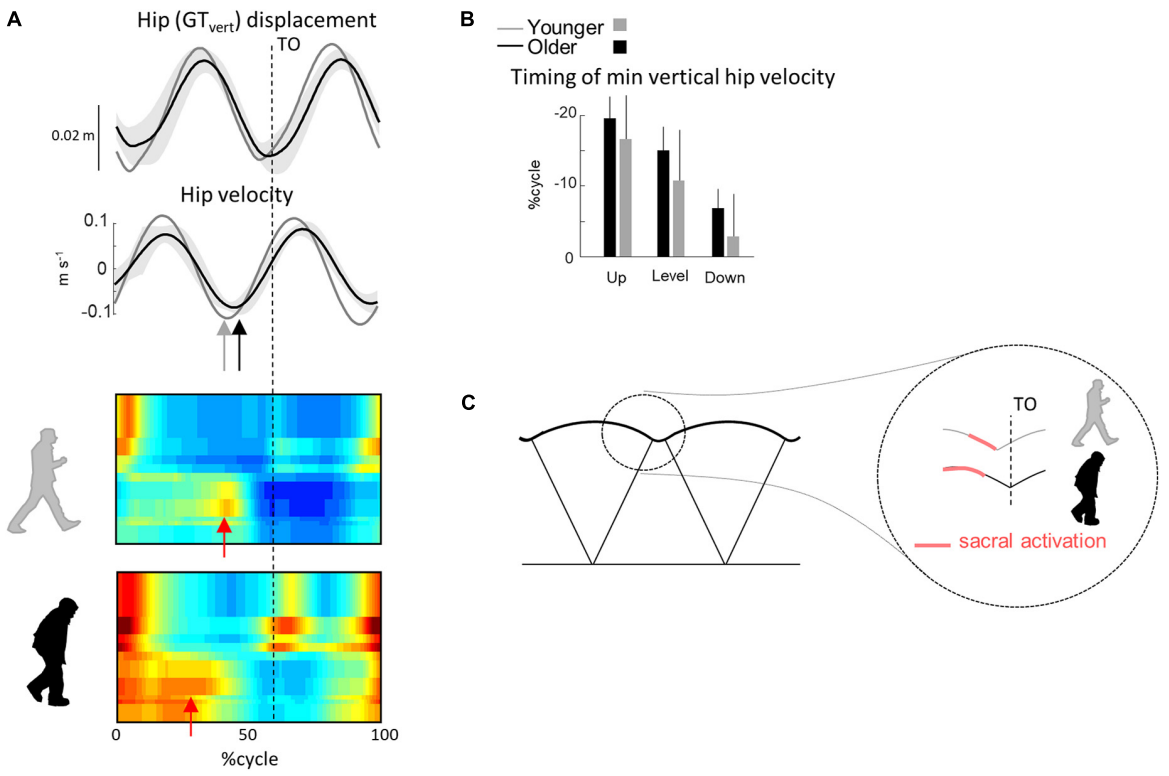

FIGURE 7 | Unilateral spatiotemporal spinal motor outputs computed from ensemble-averaged EMGs across all conditions. **(A)** Motor output (reported in μV) is plotted as a function of gait cycle in young (top) and older (bottom) adults. The thin green and red lines correspond to the activation of the lumbar and sacral segments, respectively. The gray area is the sum of all segments and reflects the level of activation. **(B)** Average minimal and maximal level of activation of the spinal motor output, average FWHM, and timing of the maximal activation of the lumbar and sacral segments. **(C)** Illustration of step-to-step transition. Other indications as in **Figure 2**.

the moment–angle relation (Reeves et al., 2009). In addition, we observed here that the age-related difference in sacral activation timing was greater in uphill than in downhill walking. Similarly, it has been observed that the reduced ankle moment in older adults observed during level walking (Monaco et al., 2009; Hortobágyi et al., 2016; Gueugnon et al., 2019) was even more pronounced during uphill walking (Waanders et al., 2020; Krupenevich et al., 2021), indirectly supporting the idea that the change in activity of sacral motor pools is reflected in changes in muscular power production (Dewolf et al., 2019a).

The findings of this study extend the available information on age-related differences in the neuromuscular control of gait occurring when moving upwards or downwards. Our results further corroborate the idea that aging affects principally the distal (sacral) segments. In addition, we observed that other age-related changes occurred in tasks requiring greater ankle push-off, such as walking uphill. The knowledge gained in the present study may be relevant for the design of preventive or rehabilitative approaches to address the decline of gait performance and mobility in older adults.

DATA AVAILABILITY STATEMENT

The raw data supporting the conclusions of this article will be made available by the authors, without undue reservation.

ETHICS STATEMENT

The studies involving human participants were reviewed and approved by the IRCCS Fondazione Santa Lucia (protocol n CE/PROG749). The patients/participants provided their written informed consent to participate in this study.

AUTHOR CONTRIBUTIONS

AD, YI, and FL contributed to the conception and design of the study. AD, FS-L, and GC contributed to data acquisition. AD and DZ organized the database. AD performed the statistical analysis and wrote the first draft of the manuscript. All authors contributed to manuscript revision, read, and approved the submitted version.

FUNDING

This work was supported by the Italian Ministry of Health (Ricerca corrente, IRCCS Fondazione Santa Lucia), the Italian Space Agency (grants I/006/06/0 and ASI-MARS-PRE DC-VUM - 2017-006), the H2020-779963 EUROBENCH FSTP-1 grant (sub-project PEPATO), and the Italian University Ministry (PRIN grant 2017CBF8NJ_005).

REFERENCES

Aagaard, P., Magnusson, P. S., Larsson, B., Kjaer, M., and Krustrup, P. (2007). Mechanical muscle function, morphology, and fiber type in lifelong trained elderly. *Med. Sci. Sports Exerc.* 39, 1989–1996. doi: 10.1249/mss.0b013e31814fb402

Anderson, D. E., and Madigan, M. L. (2014). Healthy older adults have insufficient hip range of motion and plantar flexor strength to walk like healthy young adults. *J. Biomech.* 47, 1104–1109. doi: 10.1016/j.jbiomech.2013.12.024

Alexander, N., Strutzenberger, G., Ameshofer, L. M., and Schwameder, H. (2017). Lower limb joint work and joint work contribution during downhill and uphill walking at different inclinations. *J. Biomech.* 61, 75–80. doi: 10.1016/j.jbiomech.2017.07.001

Arizono, N., Koreto, O., Iwai, Y., Hidaka, T., and Takeoka, O. (1984). Morphometric analysis of human neuromuscular junction in different ages. *Acta Pathol Jpn* 34, 1243–1249. doi: 10.1111/j.1440-1827.1984.tb00551.x

Berens, P. (2009). CircStat: a MATLAB toolbox for circular statistics. *J. Statist. Software* 31, 1–21.

Bianchi, L., Angelini, D., Orani, G. P., and Lacquaniti, F. (1998). Kinematic coordination in human gait: relation to mechanical energy cost. *J. Neurophysiol.* 79, 2155–2170. doi: 10.1152/jn.1998.79.4.2155

Bleyenheuft, C., and Detrembleur, C. (2012). Kinematic covariation in pediatric, adult and elderly subjects: is gait control influenced by age? *Clin. Biomechan.* 27, 568–572. doi: 10.1016/j.clinbiomech.2012.01.010

Borghese, N. A., Bianchi, L., and Lacquaniti, F. (1996). Kinematic determinants of human locomotion. *J. Physiol.* 494, 863–879.

Brooks, S. V., and Faulkner, J. A. (1988). Contractile properties of skeletal muscles from young, adult and aged mice. *J. Physiol.* 404, 71–82. doi: 10.1113/jphysiol.1988.sp017279

Cappellini, G., Ivanenko, Y. P., Dominici, N., Poppele, R. E., and Lacquaniti, F. (2010). Migration of motor pool activity in the spinal cord reflects body mechanics in human locomotion. *J. Neurophysiol.* 104, 3064–3073. doi: 10.1152/jn.00318.2010

DeVita, P., and Hortobagyi, T. (2000). Age causes a redistribution of joint torques and powers during gait. *J. Appl. Physiol.* 88, 1804–1811.

Dewolf, A. H., Ivanenko, Y., Zelik, K. E., Lacquaniti, F., and Willems, P. A. (2018). Kinematic patterns while walking on a slope at different speeds. *J Appl Physiol.* 125, 642–653. doi: 10.1152/japplphysiol.01020.2017

Dewolf, A. H., Ivanenko, Y. P., Lacquaniti, F., and Willems, P. A. (2017). Pendular energy transduction within the step during human walking on slopes at different speeds. *PLoS One* 12:e0186963. doi: 10.1371/journal.pone.0186963

Dewolf, A. H., Ivanenko, Y. P., Mesquita, R. M., Lacquaniti, F., and Willems, P. A. (2020a). Neuromechanical adjustments when walking with an aiding or hindering horizontal force. *Eur. J. Appl. Physiol.* 120, 91–106. doi: 10.1007/s00421-019-04251-4251

Dewolf, A. H., Mesquita, R. M., and Willems, P. A. (2020b). Intra-limb and muscular coordination during walking on slopes. *Eur. J. Appl. Physiol.* 120, 1841–1854. doi: 10.1007/s00421-020-04415-4414

Dewolf, A. H., Sylos-Labini, F., Cappellini, G., Lacquaniti, F., and Ivanenko, Y. (2020c). Emergence of different gaits in infancy: relationship between developing neural circuitries and changing biomechanics. *Front. Bioeng. Biotechnol.* 8:473. doi: 10.3389/fbioe.2020.00473

Dewolf, A. H., Ivanenko, Y. P., Zelik, K. E., Lacquaniti, F., and Willems, P. A. (2019a). Differential activation of lumbar and sacral motor pools during walking at different speeds and slopes. *J. Neurophysiol.* 122, 872–887. doi: 10.1152/jn.00167.2019

Dewolf, A. H., Meurisse, G. M., Schepens, B., and Willems, P. A. (2019b). Effect of walking speed on the intersegmental coordination of lower-limb segments in elderly adults. *Gait Posture* 70, 156–161. doi: 10.1016/j.gaitpost.2019.03.001

Dewolf, A. H., Sylos-Labini, F., Cappellini, G., Ivanenko, Y., and Lacquaniti, F. (2021). Age-related changes in the neuromuscular control of forward and backward locomotion. *PLoS One* 16:e0246372. doi: 10.1371/journal.pone.0246372

Franz, J. R. (2016). The age-associated reduction in propulsive power generation in walking. *Exerc. Sport Sci. Rev.* 44, 129–136. doi: 10.1249/JES.0000000000000086

Franz, J. R., and Kram, R. (2013). Advanced age affects the individual leg mechanics of level, uphill, and downhill walking. *J. Biomech.* 46, 535–540. doi: 10.1016/j.jbiomech.2012.09.032

Franz, J. R., and Kram, R. (2014). Advanced age and the mechanics of uphill walking: a joint-level, inverse dynamic analysis. *Gait Posture* 39, 135–140. doi: 10.1016/j.gaitpost.2013.06.012

Gueugnon, M., Stapley, P. J., Gouteron, A., Lecland, C., Morisset, C., Casillas, J.-M., et al. (2019). Age-Related adaptations of lower limb intersegmental coordination during walking. *Front. Bioeng. Biotechnol.* 7:173. doi: 10.3389/fbioe.2019.00173

Hafer, J. F., and Boyer, K. A. (2018). Age related differences in segment coordination and its variability during gait. *Gait Posture* 62, 92–98. doi: 10.1016/j.gaitpost.2018.02.021

Herssens, N., Verbecque, E., Hallemans, A., Vereeck, L., Van Rompaey, V., and Saeys, W. (2018). Do spatiotemporal parameters and gait variability differ across the lifespan of healthy adults? a systematic review. *Gait Posture* 64, 181–190. doi: 10.1016/j.gaitpost.2018.06.012

Hogan, N. (1984). Adaptive control of mechanical impedance by coactivation of antagonist muscles. *IEEE Trans. Automat. Contr.* 29, 681–690. doi: 10.1109/TAC.1984.1103644

Hong, S.-W., Leu, T.-H., Li, J.-D., Wang, T.-M., Ho, W.-P., and Lu, T.-W. (2014a). Influence of inclination angles on intra- and inter-limb load-sharing during uphill walking. *Gait Posture* 39, 29–34. doi: 10.1016/j.gaitpost.2013.05.023

Hong, S.-W., Wu, C.-H., Lu, T.-W., Hu, J.-S., Li, J.-D., Leu, T.-H., et al. (2014b). Biomechanical strategies and the loads in the lower limbs during downhill walking with different inclination angles. *Biomed. Eng. Appl. Basis Commun.* 26:1450071. doi: 10.4015/S1016237214500719

Hortobágyi, T., and DeVita, P. (2000). Muscle pre- and coactivity during downward stepping are associated with leg stiffness in aging. *J. Electromyogr. Kinesiol.* 10, 117–126. doi: 10.1016/s1050-6411(99)00026-27

Hortobágyi, T., Rider, P., Gruber, A. H., and DeVita, P. (2016). Age and muscle strength mediate the age-related biomechanical plasticity of gait. *Eur. J. Appl. Physiol.* 116, 805–814. doi: 10.1007/s00421-015-3312-3318

Ivanenko, Y. P., Dominici, N., Cappellini, G., Di Paolo, A., Giannini, C., Poppele, R. E., et al. (2013). Changes in the spinal segmental motor output for stepping during development from infant to adult. *J. Neurosci.* 33, 3025a–3036a.

Ivanenko, Y. P., Dominici, N., and Lacquaniti, F. (2007). Development of independent walking in toddlers. *Exerc. Sport Sci. Rev.* 35, 67–73. doi: 10.1249/JES.0b013e31803eafa8

Ivanenko, Y. P., Poppele, R. E., and Lacquaniti, F. (2006). Spinal cord maps of spatiotemporal alpha-motoneuron activation in humans walking at different speeds. *J. Neurophysiol.* 95, 602–618. doi: 10.1152/jn.00767.2005

Janshen, L., Santuz, A., Ekizos, A., and Arampatzis, A. (2017). Modular control during incline and level walking in humans. *J. Exp. Biol.* 220, 807–813. doi: 10.1242/jeb.148957

Kendall, F., McCreary, E., Provance, P., Rodgers, M., and Romani, W. (2005). *Muscles. Testing and Function with Posture and Pain*. Baltimore: Lippincott Williams and Wilkins.

Krupenevich, R. L., Clark, W. H., Ray, S. F., Takahashi, K. Z., Kashefsky, H. E., and Franz, J. R. (2021). Effects of age and locomotor demand on foot mechanics during walking. *J. Biomech.* 123:110499. doi: 10.1016/j.jbiomech.2021.110499

Laufer, Y. (2005). Effect of age on characteristics of forward and backward gait at preferred and accelerated walking speed. *J. Gerontol. A Biol. Sci. Med. Sci.* 60, 627–632. doi: 10.1093/gerona/60.5.627

Lay, A. N., Hass, C. J., and Gregor, R. J. (2006). The effects of sloped surfaces on locomotion: a kinematic and kinetic analysis. *J. Biomech.* 39, 1621–1628. doi: 10.1016/j.jbiomech.2005.05.005

Lexell, J. (1995). Human aging, muscle mass, and fiber type composition. *J. Gerontol. A Biol. Sci. Med. Sci.* 50 Spec No, 11–16. doi: 10.1093/gerona/50a.special_issue.11

Ling, S. M., Conwit, R. A., Ferrucci, L., and Metter, E. J. (2009). Age-Associated changes in motor unit physiology: observations from the baltimore longitudinal study of aging. *Arch. Phys. Med. Rehabil.* 90, 1237–1240. doi: 10.1016/j.apmr.2008.09.565

Martino, G., Ivanenko, Y., Serrao, M., Ranavolo, A., Draicchio, F., Rinaldi, M., et al. (2018). Differential changes in the spinal segmental locomotor output in hereditary spastic paraplegia. *Clin. Neurophysiol.* 129, 516–525. doi: 10.1016/j.clinph.2017.11.028

Martino, G., Ivanenko, Y. P., d'Avella, A., Serrao, M., Ranavolo, A., Draicchio, F., et al. (2015). Neuromuscular adjustments of gait associated with unstable conditions. *J. Neurophysiol.* 114, 2867–2882. doi: 10.1152/jn.00029.2015

Martino, G., Ivanenko, Y. P., Serrao, M., Ranavolo, A., d'Avella, A., Draicchio, F., et al. (2014). Locomotor patterns in cerebellar ataxia. *J. Neurophysiol.* 112, 2810–2821. doi: 10.1152/jn.00275.2014

McFadyen, B. J., and Winter, D. A. (1988). An integrated biomechanical analysis of normal stair ascent and descent. *J. Biomech.* 21, 733–744. doi: 10.1016/0021-9290(88)90282-90285

McGibbon, C. A. (2003). Toward a better understanding of gait changes with age and disablement: neuromuscular adaptation. *Exerc. Sport Sci. Rev.* 31, 102–108. doi: 10.1097/00003677-200304000-200304009

Meurisse, G. M., Bastien, G. J., and Schepens, B. (2019). The step-to-step transition mode: a potential indicator of first-fall risk in elderly adults? *PLoS One* 14:e0220791. doi: 10.1371/journal.pone.0220791

Mian, O. S., Thom, J. M., Ardigò, L. P., Narici, M. V., and Minetti, A. E. (2006). Metabolic cost, mechanical work, and efficiency during walking in young and older men. *Acta Physiol.* 186, 127–139. doi: 10.1111/j.1748-1716.2006.01522.x

Monaco, V., Ghionzoli, A., and Micera, S. (2010). Age-related modifications of muscle synergies and spinal cord activity during locomotion. *J. Neurophysiol.* 104, 2092–2102.

Monaco, V., Rinaldi, L. A., Macrì, G., and Micera, S. (2009). During walking elders increase efforts at proximal joints and keep low kinetics at the ankle. *Clin. Biomech.* 24, 493–498. doi: 10.1016/j.clinbiomech.2009.04.004

Montgomery, J. R., and Grabowski, A. M. (2018). The contributions of ankle, knee and hip joint work to individual leg work change during uphill and downhill walking over a range of speeds. *R Soc. Open Sci.* 5:180550. doi: 10.1098/rsos.180550

Noble, J. W., and Prentice, S. D. (2008). Intersegmental coordination while walking up inclined surfaces: age and ramp angle effects. *Exp. Brain Res.* 189, 249–255. doi: 10.1007/s00221-008-1464-z

Perry, M. C., Carville, S. F., Smith, I. C. H., Rutherford, O. M., and Newham, D. J. (2007). Strength, power output and symmetry of leg muscles: effect of age and history of falling. *Eur. J. Appl. Physiol.* 100, 553–561. doi: 10.1007/s00421-006-0247-240

Reeves, N. D., Spanjaard, M., Mohagheghi, A. A., Baltzopoulos, V., and Maganaris, C. N. (2009). Older adults employ alternative strategies to operate within their maximum capabilities when ascending stairs. *J. Electromyogr. Kinesiol.* 19, e57–e68. doi: 10.1016/j.jelekin.2007.09.009

Rosenberg, I. H. (2011). Sarcopenia: origins and clinical relevance. *Clin. Geriatr. Med* 27, 337–339. doi: 10.1016/j.cger.2011.03.003

Rozumalski, A., Steele, K. M., and Schwartz, M. H. (2017). Muscle synergies are similar when typically developing children walk on a treadmill at different speeds and slopes. *J. Biomech.* 64, 112–119. doi: 10.1016/j.jbiomech.2017.09.002

Saito, A., Tomita, A., Ando, R., Watanabe, K., and Akima, H. (2018). Similarity of muscle synergies extracted from the lower limb including the deep muscles between level and uphill treadmill walking. *Gait Posture* 59, 134–139. doi: 10.1016/j.gaitpost.2017.10.007

Samson, M. M., Crowe, A., de Vreede, P. L., Dessens, J. A. G., Duursma, S. A., and Verhaar, H. J. J. (2001). Differences in gait parameters at a preferred walking speed in healthy subjects due to age, height and body weight. *Aging Clin. Exp. Res.* 13, 16–21. doi: 10.1007/BF03351489

Santuz, A., Brüll, L., Ekizos, A., Schroll, A., Eckardt, N., Kibele, A., et al. (2020). Neuromotor dynamics of human locomotion in challenging settings. *iScience* 23:100796. doi: 10.1016/j.isci.2019.100796

Santuz, A., Ekizos, A., Eckardt, N., Kibele, A., and Arampatzis, A. (2018). Challenging human locomotion: stability and modular organisation in unsteady conditions. *Sci. Rep.* 8:2740. doi: 10.1038/s41598-018-21018-21014

Seidler, R. D., Bernard, J. A., Burutolu, T. B., Fling, B. W., Gordon, M. T., Gwin, J. T., et al. (2010). Motor control and aging: links to age-related brain structural, functional, and biochemical effects. *Neurosci. Biobehav. Rev.* 34, 721–733. doi: 10.1016/j.neubiorev.2009.10.005

Silder, A., Heiderscheit, B., and Thelen, D. G. (2008). Active and passive contributions to joint kinetics during walking in older adults. *J. Biomech.* 41, 1520–1527. doi: 10.1016/j.jbiomech.2008.02.016

Silverman, A. K., Neptune, R. R., Sinitski, E. H., and Wilken, J. M. (2014). Whole-body angular momentum during stair ascent and descent. *Gait Posture* 39, 1109–1114. doi: 10.1016/j.gaitpost.2014.01.025

Skinner, H. B., Barrack, R. L., and Cook, S. D. (1984). Age-related decline in proprioception. *Clin. Orthopaed. Related Res.* 184, 208–211.

Startzell, J. K., Owens, D. A., Mulfinger, L. M., and Cavanagh, P. R. (2000). Stair negotiation in older people: a review. *J. Am. Geriatr. Soc.* 48, 567–580. doi: 10.1111/j.1532-5415.2000.tb05006.x

Tomlinson, B. E., and Irving, D. (1977). The numbers of limb motor neurons in the human lumbosacral cord throughout life. *J. Neurol. Sci.* 34, 213–219.

Waanders, J. B., Murgia, A., Hortobágyi, T., DeVita, P., and Franz, J. R. (2020). How age and surface inclination affect joint moment strategies to accelerate and decelerate individual leg joints during walking. *J. Biomech.* 98:109440. doi: 10.1016/j.jbiomech.2019.109440

Williams, K., and Bird, M. (1992). The aging mover: a preliminary report on constraints to action. *Int. J. Aging Hum. Dev.* 34, 241–255. doi: 10.2190/93WR-P5N0-34FP-XGMF

Winter, D. A., Patla, A. E., Frank, J. S., and Walt, S. E. (1990). Biomechanical walking pattern changes in the fit and healthy elderly. *Phys. Ther.* 70, 340–347. doi: 10.1093/ptj/70.6.340

Conflict of Interest: The authors declare that the research was conducted in the absence of any commercial or financial relationships that could be construed as a potential conflict of interest.

frontiers in Human Neuroscience

ORIGINAL RESEARCH
published: 21 October 2021
doi: 10.3389/fnhum.2021.676242

Socio-Motor Improvisation in Schizophrenia: A Case-Control Study in a Sample of Stable Patients

Robin N. Salesse[1,2], Jean-François Casties[1], Delphine Capdevielle[1,3] and Stéphane Raffard[1,4]*

[1] University Department of Adult Psychiatry, Montpellier University Hospital, Montpellier, France, [2] CTIsuccess by Mooven, Contract Research Organisation, Montpellier, France, [3] INSERM U1061, Neuropsychiatrie Recherche Épidémiologique et Clinique, Université de Montpellier, Montpellier, France, [4] Epsylon Laboratory EA 4556, University Paul Valéry Montpellier 3, Montpellier, France

Improvising is essential for human development and is one of the most important characteristics of being human. However, how mental illness affects improvisation remains largely unknown. In this study we focused on socio-motor improvisation in individuals with schizophrenia, one of the more debilitating mental disorder. This represents the ability to improvise gestures during an interaction to promote sustained communication and shared attention. Using a novel paradigm called the mirror game and recently introduced to study joint improvisation, we recorded hand motions of two people mirroring each other. Comparing Schizophrenia patients and healthy controls skills during the game, we found that improvisation was impaired in schizophrenia patients. Patients also exhibited significantly higher difficulties to being synchronized with someone they follow but not when they were leaders of the joint improvisation game. Considering the correlation between socio-motor synchronization and socio-motor improvisation, these results suggest that synchronization does not only promote affiliation but also improvisation, being therefore an interesting key factor to enhance social skills in a clinical context. Moreover, socio-motor improvisation abnormalities were not associated with executive functioning, one traditional underpinning of improvisation. Altogether, our results suggest that even if both mental illness and improvisation differ from normal thinking and behavior, they are not two sides of the same coin, providing a direct evidence that being able to improvise in individual situations is fundamentally different than being able to improvise in a social context.

Keywords: psychiatry, embodiment, coordination dynamics, human bonding, mirror game

OPEN ACCESS

Edited by:
Nadia Dominici, Vrije Universiteit Amsterdam, Netherlands

Reviewed by:
Sebastian Walther, University of Bern, Switzerland
Pedro Sanchez, Osakidetza Basque Health Service, Spain

****Correspondence:***
Robin N. Salesse
salesse.robin@gmail.com

Specialty section:
This article was submitted to Motor Neuroscience, a section of the journal Frontiers in Human Neuroscience

Received: *04 March 2021*
Accepted: *06 August 2021*
Published: *21 October 2021*

Citation:
Salesse RN, Casties J-F, Capdevielle D and Raffard S (2021) Socio-Motor Improvisation in Schizophrenia: A Case-Control Study in a Sample of Stable Patients. Front. Hum. Neurosci. 15:676242. doi: 10.3389/fnhum.2021.676242

INTRODUCTION

Improvisation is commonly considered to be akin to insanity (Barrantes-Vidal, 2004). Famous so-called *mad genius* Syd Barrett, early lead singer, guitarist and principal songwriter behind the rock band *Pink Floyd*, or John Nash, the father of *game theory* and Nobel Prize in economics for "The pioneering analysis of equilibria in the theory of non-competitive games," are exceptional cases of improvisers diagnosed with schizophrenia. However, only a small group of people with schizophrenia are able to walk their impairment and benefit from it, the majority being left with

misunderstanding and stigmatization (Thornicroft et al., 2009), Social impairment is a major symptom shared by mental illnesses (Giacco et al., 2012; Kidd, 2013), affecting patients functioning, outcomes and quality of life. Abnormal, "bizarre" motor behaviors ("weird" posturing or aimless movements), and deficits in socio-motor synchronization ("the natural tendency to synchronize gestures during a social interaction"), were considered as characteristic of some individuals with schizophrenia, leading to a lack of rapport and feelings of connectedness with these patients (Bleuler, 1950; Varlet et al., 2012). Whereas socio-motor synchronization capture to what extend people act within the same timing, we hypothesize that socio-motor improvisation, the ability to improvise timely and new gestures during a social interaction, is a necessary property for promoting sustained communication and shared attention. We propose here to study this timely improvisation in individuals with schizophrenia through the scope of socio-motor improvisation and socio-motor synchronization.

Dance improvisation between multiple dancers is an excellent example of collaborative motor improvisation. New ideas do not appear simply from the internal processes of a single person but from the interaction within a group at the level of the minds, bodies and environment (Łucznik, 2015). Much human improvisation arises from activities that take place during social interactions. Encompassing behavioral outcomes in a social context, socio-motor improvisation refers to creative actions performed by two or more people during a social interaction (Noy et al., 2011; Gueugnon et al., 2016). It is fundamental here for a sake of understanding to remark that a successful improvisation in a collaborative context needs individuals to be connected, synchronized, at some point (Bernieri and Rosenthal, 1991; Noy et al., 2011). Socio- motor behavior constitutes a strong and necessary conveyor of social skills, synchrony playing a fundamental role during communicative non-verbal behaviors (Hove and Risen, 2009; Schmidt et al., 2012). Being synchronized is therefore also necessary to characterize this ability to create novelty together. Socio-motor improvisation and synchronization are the two sides of a same coin. Defined by Bernieri and Rosenthal (1991) as the smooth meshing in time of the simultaneous rhythmic activity of two people, synchrony predicts subsequent affiliation ratings (Hove and Risen, 2009), increases rapport (Bernieri, 1988) and cooperation (Wiltermuth and Heath, 2009) between individuals. Thus, socio-motor synchronization plays a fundamental role in enhancing connectedness, social rapport or cohesion in human interactions (Marsh et al., 2009; Chartrand and Lakin, 2013). Following Orth et al. (2017), rather than referring to behaviors that are uniquely generated by a cognitive system, socio-motor improvisation describes unfolding actions that are original because socio-motor improvisation relative to the individual or group, and functional because they support task success in terms of socio-motor synchronization (Hristovski et al., 2011).

Reducing the definition of improvisation to its *cognitive* dimension also affects schizophrenia studies and the understanding of this disorder, focusing on prototypical psychotic symptoms such as incoherent thinking, loss of contact with reality, hallucinations and cognitive deficits (Mier and Kirsch, 2015). Schizophrenia is a common psychotic illness and is considered one of the leading causes of disability in rich countries. Schizophrenia is often characterized by its psychotic symptoms and cognitive deficits, but social interaction deficits remain one of its most significant, defining, debilitating and tremendous features (Giacco et al., 2012; Kidd, 2013). Social interaction deficits affect patients' long-term functioning, outcomes and quality of life but are partially explained by clinical symptom severity (Schmidt et al., 2011). Recent interdisciplinary research highlighted the huge impact of implicit non-verbal motor behaviors on social exchanges, opening interesting ways to study and understand mental illnesses in their social context and complexity (Del-Monte et al., 2013; Lavelle et al., 2013, 2014). Many ecologically valid paradigms of gesture use demonstrates that patients with schizophrenia are truly impaired when imitating hand gestures, which is actually linked to social functioning and motor abnormalities (e.g., Matthews et al., 2013; Walther et al., 2015, 2016). Varlet et al. (2012) assessed non-verbal motor interaction comparing healthy and schizophrenia patients when performing socio-motor synchronization tasks. They showed that unintended synchronization was preserved while voluntary synchronization was impaired, interpreted as a potential effect of executive dysfunctioning. Confirming results were obtained using priming procedures (Raffard et al., 2015) and virtual social environments (Raffard et al., 2018) that positively affected unintended socio-motor synchronization in schizophrenia patients. Previous research on healthy subjects has shown that the emergence and stability of such unintended or intended synchronization is closely associated with affiliation, and social cohesion (Bernieri, 1988; Hove and Risen, 2009; Schmidt et al., 2011).

Studies regarding improvisation in mental illness have mainly focused their interest on cognition, representing to what extend executive abilities such as updating, shifting and inhibition (Benedek et al., 2014) are preserved in mental illnesses. However, one may consider improvisation in its social context, that is during joint interaction with others. Therefore, improvisation refers to an individual's ability to respond in a divergent, original or flexible manner to motor challenges induced by social interaction. Noy et al. (2011) introduced the mirror game as a paradigm for studying the dynamics of two people improvising motion together. Interestingly, the mirror game is based on an ambiguity between two contradictory instructions: socio-motor improvisation and socio-motor synchronization. Indeed, improvising implies the production of "various, complex and interesting" movements but risking being poorly synchronized due to the unpredictability of the motion performed. At the contrary but in a same time, being synchronized implies the production of highly predictable simultaneous and coordinated motion but obviously risking decreasing the quality and the level of the improvisation. Solving this trade-off between improvisation and synchronization in the mirror game reflects the core of our experimental protocol. In the present study, we combined, on the one hand, human movement paradigms specifically dedicated to study non-verbal bodily social interactions (Noy et al., 2011) and on the

other hand, well-known psychological measures of cognitive functioning associated with cognitive improvisation (Barrantes-Vidal, 2004). Hence, we investigated whether schizophrenia influences socio-motor improvisation. Due to impairments in voluntary but not unintended socio-motor synchronization tasks (Varlet et al., 2012), we expect that individuals with schizophrenia would perform poorly both in terms of socio-motor improvisation and socio-motor synchronization than healthy participants. Additionally, social science studies demonstrated that the motor system influences cognition, and that cognition also affects bodily actions, we therefore expected positive correlation between *cognitive* improvisation and socio-motor improvisation.

MATERIALS AND METHODS

Participants

We included 60 participants: 30 schizophrenia stable outpatients and 30 age-matched healthy participants (**Table 1**). Patients were recruited from the University Department of Adult Psychiatry and fulfilled the Diagnostic and Statistical Manual of Mental Disorders (American Psychiatric Association, 2000) criteria for schizophrenia. Diagnoses were established using the Structured Clinical Interview (SCID) for DSM–IV-TR. All patients received anti-psychotic medication. Exclusion criteria for both the clinical and non-clinical groups were: (a) known neurological disease, (b) Axe II diagnosis of developmental disorders or (c) substance abuse in the past month.

All participants were native French speakers with a minimal reading level validated using the National Adult Reading Test (f-NART, Mackinnon and Mulligan, 2005) and were able to perform the interaction task described below. All of the participants were adults with normal or corrected-to-normal vision. Age-matched healthy participants were recruited from a call for participation in the hospital's website and the community. They had no lifetime history of any psychosis diagnoses according to the SCID. Two healthy participants were discarded from the study because they dropped out before the end of the experiment for personal reasons. All participants provided written informed consent, prior to the experiment approved by the National Ethics Committee (CPP Sud-Méditerranée-III, Nîmes, France, #2013.04.05 and DA/2013-136) and conforming to the Declaration of Helsinki. Accordingly with identifying information policies, written informed consent for publication of identifying information/images was obtained. The thirty schizophrenia patients composed the Schizophrenia group, and the twenty-eight matched control participants composed the Control group.

Setup

We designed and built a custom hardware similar to the one designed by Noy et al. (2011) for recording dyadic motions in the mirror game (**Figure 1**). Players moved handles along parallel tracks 0.6 m long. Handle positions were measured by an optical encoder with a spatial resolution of 0.054 mm and were sampled at 100 Hz. Data were recorded on a computer using National Instruments LABVIEW 13.0 software.

Procedure

The experiment was completed in two visits. Visit 1 involved completing informed consent, clinical interviews and questionnaires. Visit 2 occurred approximately 1 or 2 days later. It consisted in a mirror game where participants and a confederate imitate each other in turns.

During visit 1, participants were rated with socio-demographic, psychological and psychopathology scales. Following recent recommendations from the social psychology literature (Doyen et al., 2012; Shanks et al., 2013), our participants were fully naive about the real goal of the experiment. To prevent any "un-blind experimenter effect," both the experimenter and the confederate were fully naive about the diagnosis of participants and were not informed about the group participants belonged to (schizophrenia or healthy controls). All participants were asked to inform their age, gender, Level of Education. All participants were right-handed as assessed by informal verbal inquiry. They were also rated with the Neurological Soft Signs Scale (Krebs et al., 2000) to assess subtle abnormalities in sensory-perceptual, motor functions directly associated with schizophrenia pathology (Gupta, 1995; Walther and Strik, 2012) or induced by neuroleptic medications (D'Agati et al., 2012). Social cognition was measured using the Autism spectrum quotient questionnaire (Baron-Cohen et al., 2001) and a social false-belief test (Desgranges et al., 2012) to evaluate theory of mind. It refers to the ability to infer mental states (e.g., beliefs, desires, intentions, imagination, emotions) that cause behavior within a social environment. Finally, participants were rated with the trail making test (Delis et al., 2001). TMT is a validated tool to assess cognitive flexibility and has been widely used to assess cognitive improvisation (Moritz et al., 2002; Laere et al., 2018). In the schizophrenia group, we administered the Positive and Negative Syndrome Scale (Kay et al., 1987) using the Structured Clinical Interview for the PANSS (SCI-PANSS). The degree of interactional deficits was assessed through the PANSS "poor rapport" item Q10 (Riehle et al., 2015). During visit 2, participants were asked to play a mirror game with a confederate. The confederate was an expert in playing the mirror game in order to prevent any edge effect due to insufficient socio-motor skills. Players sat facing each other on either side of the experimental apparatus (**Figures 1A,B**). They hold the handles comfortably with one or both hands depending on their preference. First, the game and the procedure were explained to the players). Participant were given the instruction to "imitate each other, create synchronized and interesting motions, and enjoy playing together" (detailed description is given in Noy et al., 2011), and were reminded that the purpose was a cooperation to enjoy creating motions together and not a competition. The experimenter was present in the room during the game to give the instructions but did not intervene during the game. Second, participants practiced three warm-up 15 s rounds (Participant leader, Confederate leader, and Joint improvisation) to get acquainted with the procedure. In participant leader and confederate leader conditions, one player was leading the motion

TABLE 1 | Socio-demographic description and mean, standard deviation, median and range of values are presented for the age, level of education, premorbid IQ (fNART), neurological soft signs (NSS), positive and negative symptom scale (PANSS), medication (chlorpromazine equivalent dose CPZE in mg/day), gender, trail making test (TMT A, TMT B, TMT B-A), global functioning (EGF), liebowitz social anxiety scale (LSAS anxiety, LSAS avoidance), social cognition and theory of mind (ToM15 false belief, ToM15 understanding).

	Schizophrenia patients (*N* = 30)				**Healthy controls (*N* = 28)**				**Statistics**		
	M	**SD**	**Med**	**Rg**	**M**	**SD**	**Med**	**Rg**			
Age	33.8	10.4	32.5	[18–58]	31.6	5.7	30.5	[24–49]	$U = 391.5$	$z = -0.44$	$p = 0.66$
Level of education	4.4	1.1	4	[3–6]	4.4	0.7	4	[3–6]	$U = 401.5$	$z = -0.31$	$p = 0.76$
fNart	22	7	22.0	[7–33]	23.3	4.3	23.5	[15–30]	$U = 369.5$	$z = -0.79$	$p = 0.43$
NSS	16.6	7	16.1	[6.9–34.5]	8.2	2.2	8	[4–12.7]	$U = 90.5$	$z = -5.02$	$\mathbf{p = 0.00}$
PANSS											
Positive	9.4	2.4	9	[7–15]							
Negative	15.1	7.1	13.0	[7–33]							
General psychopathology	27.2	5.6	27.5	[19–38]							
Total score	51.8	11	50.0	[35–75]							
PANSS-Q10	1.9	1.3	1	[1–5]							
CPZE	533	406	400	[150–2000]							
	N	%			N	%					
Gender/*Man*	28	93			25	89			$\chi^2(1, N) = 0.30$		$p = 0.58$
TMT A	35.5	11.7	34.0	[20–68]	27.8	7.6	26.5	[12–45]	$U = 252.0$	$z = -2.45$	$\mathbf{p = 0.01}$
TMT B	102	59.6	91.0	[34–300]	67.9	32.0	58	[34–195]	$U = 189.5$	$z = -3.45$	$\mathbf{p = 0.00}$
TMT B-A	66.5	55.7	52.0	[14–259]	40.1	30.5	32.5	[11–169]	$U = 224.5$	$z = -2.89$	$\mathbf{p = 0.00}$
EGF	43.8	8.1	42	[25–61]	79.3	8.7	80.5	[61–95]	$U = 0.5$	$z = 6.52$	$\mathbf{p = 0.00}$
LSAS anxiety	21.6	14.3	20	[0–58]	13.3	8	12.5	[1–36]	$U = 269.5$	$z = -2.33$	$\mathbf{p = 0.00}$
LSAS avoidance	17.5	11.8	20	[0–39]	9.3	7.3	7.5	[1–25]	$U = 238.5$	$z = -2.82$	$\mathbf{p = 0.02}$
Social cognition	21	5.1	22.0	[10–30]	16.5	4	17	[4–27]	$U = 210.5$	$z = -3.26$	$\mathbf{p = 0.00}$
ToM15 false belief	10.5	2.6	11	[4–14]	12.6	2	13	[6–15]	$U = 192.5$	$z = 3.53$	$\mathbf{p = 0.00}$
ToM understanding	13.7	1.7	14.0	[9–15]	14.4	0.9	15	[11–15]	$U = 340.5$	$z = 1.23$	$p = 0.22$

Group statistics are presented using appropriates non-parametric tests. Significant p values < 0.05 are represented in bold.

and the other was following. In joint-improvisation rounds, players moved together without a designated leader. Finally, they were asked to perform nine rounds of 60 s each. Rounds were separated with a 10 to 30 s pause to relax. According to the procedure proposed initially by Noy et al. (2011) rounds were counterbalanced in the following order: Participant leader, Confederate leader, Joint improvisation, Confederate leader, Joint improvisation, Participant leader, Joint improvisation, Participant leader, and Confederate leader.

Data Reduction

Two socio-motor variables were extracted from the mirror-game: socio-motor improvisation and socio-motor synchronization. Position signals were pre-processed with MathWorks MATLAB Software. Position signals were interpolated with a shape-preserving Piecewise Cubic Hermite Interpolating Polynomial (PCHIP) to correct small variations in the sampling rate (Kahaner et al., 1989) and filtered with a zero-phase forward and reverse digital second-order low-pass (10 Hz cut-off) Butterworth filter. Position time-series were then used to numerically estimate their corresponding velocity time-series using a fourth-order finite difference scheme (Słowiński et al., 2016). A detailed sample of time series is displayed in Appendix **Figure 1**. Time-series performed by participants were mostly non-stationary, multi-modal and multi-scale due to the nature of the task. Capturing socio-motor improvisation therefore implies a measure of the complexity of the signal. Whereas usual measures of complexity signals refer to the entropy such as the Shannon entropy, the non-stationarity of the time-series collected needed the use of multiscale entropy measures. According to Noy et al. (2011), socio-motor improvisation was computed with a wavelet-based complexity measure. This measure is based on a wavelet decomposition, a numerical approach decomposing signals in building blocks localized in space and frequency. Therefore, the wavelet complexity of a signal was defined as the inverse of the number of wavelets needed to describe 95% of the signal. Following Noy et al. (2011), the socio-motor improvisation measure was the compression ratio: the number of coefficients used to achieve the reconstruction normalized by the number of samples in the round. The higher this ratio, the more complex the signal, indicating a higher improvisation. Socio-motor synchronization was calculated with the index of synchronization provided by Rosenblum et al. (1996). This index takes into account fluctuations in coordination over short time scales, for example within a movement cycle. This index is based on the circular variance of the relative phase estimated with the Hilbert transform method. It is generally defined as 1 minus the circular variance. The variance is a measure of dispersion, of stability of a variable. A variance close to 0 indicates that all values are identical and

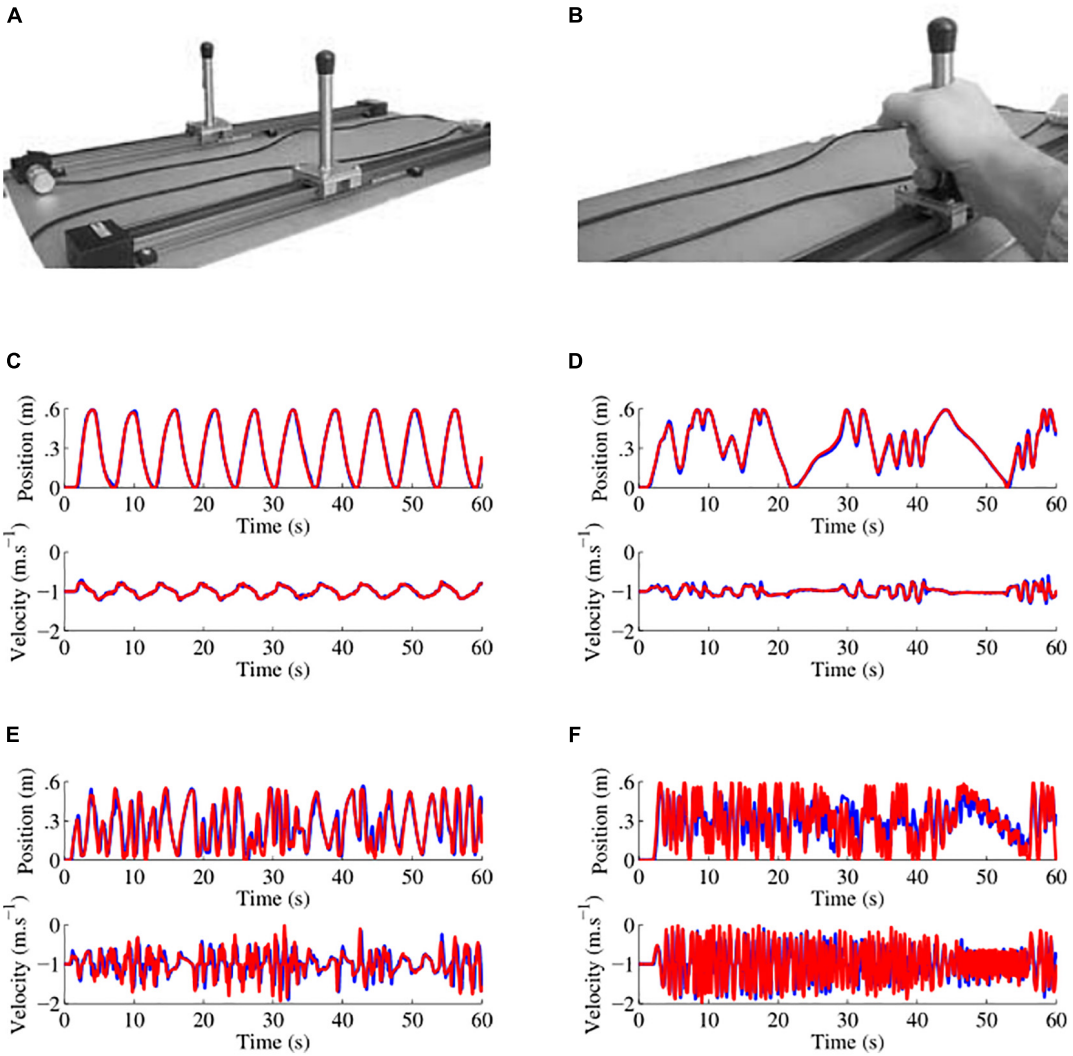

FIGURE 1 | Custom hardware apparatus and examples of data collected. **(A)** Picture of the apparatus used to play the mirror game, the motion of two players moving handles along 0.6 m tracks was sampled at 100 Hz with a spatial resolution of 0.054 mm. **(B)** Handles were held with one or two hands depending on participant preference. **(C–F)** Examples of position and velocity traces for four different players in the first round where the participant led the game. Here the leader is the red player. In **(C)** the traces are those of a schizophrenia patient with a socio-motor improvisation of 0.037 and a socio-motor synchronization of 0.998. In **(D)** the traces are those of another schizophrenia patient with a socio-motor improvisation of 0.040 and a socio-motor synchronization of 0.984. In **(E)** the traces are those of a healthy control with a socio-motor improvisation of 0.092 and a socio-motor synchronization of 0.867. In **(F)** the traces are those of another schizophrenia patient with a socio-motor improvisation of 0.108 and a socio-motor synchronization of 0.716.

a variance of 1 indicates a strong dispersion between values. The synchronization index thus provides a value between 0 (no synchronization) and 1 (perfect synchronization).

Statistical Analyses

Prior conducting statistical analyses, the three rounds in each condition were averaged according to the initial procedure proposed by Noy et al. (2011). Socio-motor improvisation and socio-motor synchronization were analyzed using two-way ANOVAs with Group (Schizophrenia vs. Healthy controls) as Group factor, with repeated measures on Conditions (Participant leader, Joint improvisation, Confederate leader). For all ANOVAs, Newman–Keuls *post hoc* tests were computed when the nature of the effects had to be specified. Size effects are reported using the partial eta squared η_p^2 (Bakeman, 2005) and interpreted according to Cohen's D (Cohen, 1988), where 0.02 corresponds to a small effect, 0.13 to a medium effect and 0.26 to a large effect. When necessary, alpha value of significance was corrected using the Bonferroni procedure. Questionnaires were separately compared for the schizophrenia and the control groups with a non-parametric U-Mann-Whitney test or a $\chi 2$ test for binary variables (e.g., gender). Pairwise comparisons between groups were performed using a *t*-test when necessary. The level of significance was set to $p < 0.05$ and was corrected using the Bonferroni procedure when necessary. Finally, we performed correlations to demonstrate the trade-off between

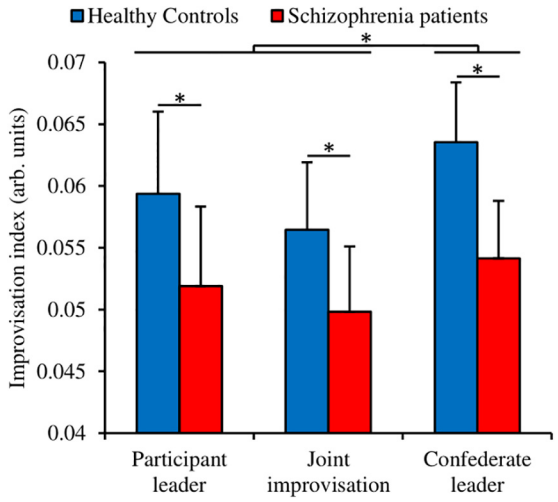

FIGURE 2 | Socio-motor improvisation extracted from the participants motion. Error bars correspond to the standard deviation around the mean. Star indicates significant *post hoc* differences.

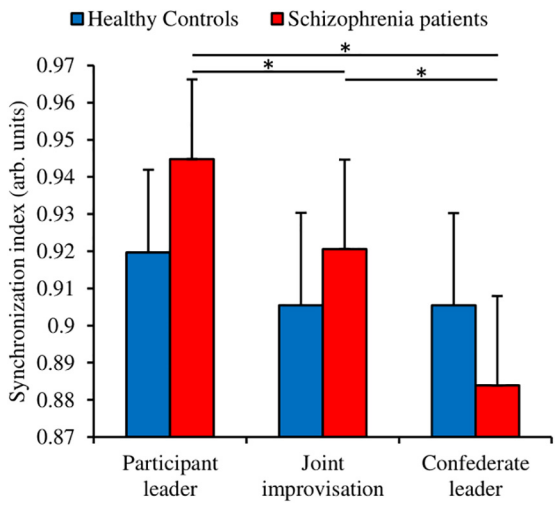

FIGURE 3 | Socio-motor synchronization index extracted from the participants motion. Error bars correspond to the standard deviation around the mean. Star indicates significant *post hoc* differences.

socio-motor improvisation and socio-motor synchronization, and the potential links between *cognitive* improvisation and socio-motor improvisation. The level of significance was lowered for multiple comparisons using the Bonferroni procedure, corresponding alpha values are reported in the captions.

RESULTS

Socio-Motor Performance

The mirror game allows capturing both socio-motor improvisation and socio-motor synchronization. Improvising implies the production of "various, complex and interesting" movements but risking being poorly synchronized. At the same time, being synchronous implies the production of simultaneous motion but risking decreasing the improvisation. Solving this trade-off between improvisation and synchronization in the mirror game reflects the core of our experimental protocol. Detailed kinematic characteristics are compared in Appendix **Figures 2**, **3**.

Improvisation Schizophrenia Patients Improvise Less Than Healthy Controls

We measured the socio-motor improvisation with a wavelet transform decomposition (Noy et al., 2011). We performed a Group (Schizophrenia patients; Healthy controls) × Condition (Participant leader; Joint improvisation; Confederate leader) ANOVA with repeated measures on the Condition factor (**Figure 2**). The analysis revealed a significant small to medium Group effect [$F(1,56) = 4.96$, $p = 0.030$, $\eta_p^2 = 0.081$] indicating that patients improvise less than healthy controls (respectively 0.052 vs. 0.060 in arbitrary units). The analysis also showed a significant small to medium Condition effect [$F(2,112) = 6.65$, $p = 0.002$, $\eta_p^2 = 0.106$]. The Newman-Keuls *post hoc* decomposition of this effect revealed that the Confederate leader condition exhibited a higher degree of improvisation than the two others conditions (Participant leader = 0.056; Joint improvisation = 0.053; Confederate leader = 0.059). The analysis failed to reveal a Group × Condition interaction [$F(2,112) = 0.44$, $p = 0.64$, $\eta_p^2 = 0.008$]. Altogether, these results suggest that healthy controls are more able to improvise than schizophrenia patients during socio-motor improvisation.

Synchronization Schizophrenia Patients Synchronize Better When Leading Than Following

We measured the socio-motor synchronization with the index of synchronization (Rosenblum et al., 1996). We performed a Group (Schizophrenia patients; Healthy controls) × Condition (Participant leader; Joint improvisation; Confederate leader) ANOVA with repeated measures on the Condition factor (**Figure 3**). The analysis failed to show a significant Group effect [$F(1,56) = 0.20$, $p = 0.656$, $\eta_p^2 = 0.004$]. However, the analysis revealed a significant medium to large Condition effect [$F(2,112) = 11.37$, $p = 0.0000$, $\eta_p^2 = 0.169$], and a significant small to medium Group × Condition interaction [$F(2,112) = 4.86$, $p = 0.009$, $\eta_p^2 = 0.080$]. The Newman-Keuls *post hoc* decomposition of this interaction revealed that the schizophrenia group performed better when leading the game rather than improvising or following. Nevertheless, healthy controls were not affected by the conditions, performing equally in the three situations.

Socio-Motor Improvisation Versus Socio-Motor Synchronization

We performed correlational analyses between socio-motor improvisation and the socio-motor for both groups (Schizophrenia patients, Healthy controls) in each of the three experimental conditions (Participant leader, Joint improvisation, Confederate leader). Results are represented in **Figure 4**. Socio-motor improvisation negatively correlates with socio-motor

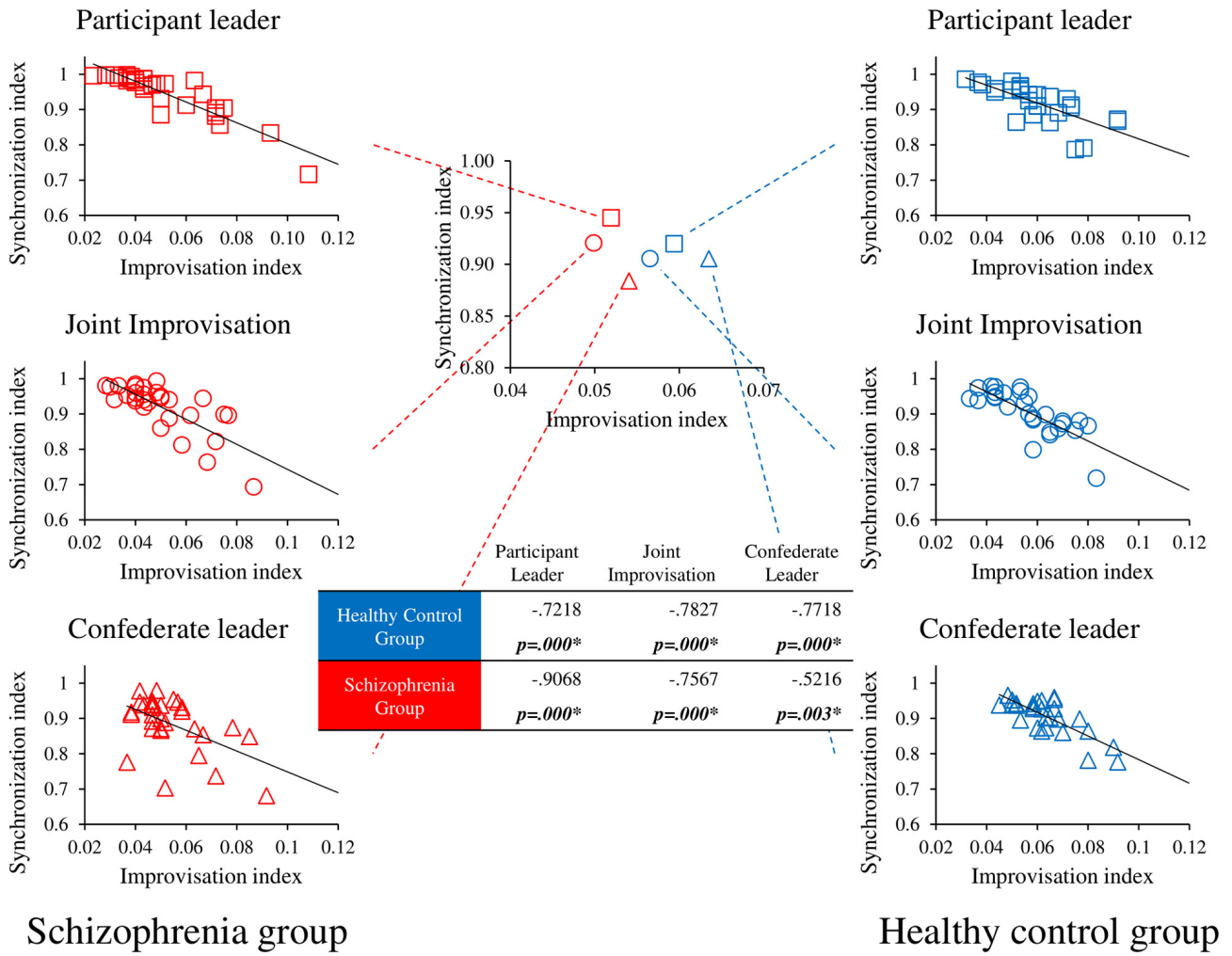

	Participant Leader	Joint Improvisation	Confederate Leader
Healthy Control Group	-.7218	-.7827	-.7718
	p*=.000	***p*=.000***	***p*=.000***
Schizophrenia Group	-.9068	-.7567	-.5216
	p*=.000	***p*=.000***	***p*=.003***

FIGURE 4 | Correlational analyses between socio-motor improvisation and socio-motor synchronization. *r* and *p* values are presented in the table for the correlation between Socio-motor improvisation and Socio-motor synchronization for each group in the three conditions. *p* values < 0.1 are represented in bold and * represents significant correlations <0.05. Central figure represents the improvisation-synchronization trade-off for each group in each condition whereas peripheral figures details correlations for each condition in the schizophrenia group on the left side and the healthy control group on the right side.

synchronization for both groups in all conditions, demonstrating the contradiction between improvising and being synchronized.

Correlational Analyses

Symptomatology and Socio-Motor Performance

To better understand the above-mentioned results, we conducted a correlational analysis between the PANSS and socio-motor variables (**Table 2**). The analyses failed to reveal any significant correlations.

Cognitive Creativity and Socio-Motor Variables

Finally, we explored whether the exhibited deficit on socio-motor improvisation might be explained by a general deficit in executive functions and cognitive creativity. Result showed that cognitive creativity (TMT), AQ, TOM15 (false-belief) and socio-motor improvisation are not correlated (Appendix **Table 1**).

DISCUSSION

Improvising is often considered a trait that everyone possesses to come up with new and useful ideas. Whereas psychology and neuroscience researchers are identifying thinking processes and brain regions involved in *cognitive* improvisation, little is known about motor improvisation during social interactions such as dance or sport (Memmert and Roth, 2007; Memmert et al., 2010). Indeed, leisure activities such as team sports, dance, music or theatre are often described as highly improvising demanding, particularly in terms of group improvisation (Hart et al., 2014). They imply processes such as improvisation but also synchronization and togetherness in order to reach a common collective goal. The analogy with daily lives is outstanding since not only ideas might need to be improvised, but behaviors in a social context also. Because mental illnesses involves both cognitive and socio-behavioral impairments, the

aim of this study was to focus on the ability to generate gestures during a social interaction, comparing healthy people with schizophrenia patients. Even if improvisation in motor actions does not pop-up in mind at first glance, it has been studied for decades in experimental psychology, human movement science and neuroscience under the capability of individuals to show original and functional motor actions as a fundamental aspect of skill, adaptability and flexibility (Seifert et al., 2016). From this perspective, socio-motor improvisation is obviously a cornerstone of social functioning. This originality in performing motor actions is observed at different levels: within individual, inter-individual and social levels. We assume that these levels are inter-dependent, social improvisation emerging from interactions observed at the individual level and between individuals. Therefore, our study proposes from a clinical perspective an understanding of how improvisation shapes social interactions and their deficits. We asked healthy controls and schizophrenia patients to play a mirror game with an expert player but naive about participants' diagnosis. The goal was to "imitate each other, create synchronized and interesting motions, and enjoy playing together." Participants role during the game was either leader, follower or uninstructed (Noy et al., 2011). We measured socio-motor improvisation, socio-motor synchronization and clinical variables.

Schizophrenia patients displayed impaired socio-motor improvisation compared to the healthy controls group in all conditions. Both groups exhibited, however, the same pattern of results, exhibiting a higher socio-motor improvisation when following an expert rather than leading or improvising. This result is perfectly in line with a recent research showing similar effects with sensibly lower values, presumably due to small differences in the apparatus used to capture the motion of the players (Brezis et al., 2017). Socio-motor improvisation being measured at the level of the dyad during a social game, patients were able to take advantage of the expert improvisational skill but to a lesser degree than healthy controls. This result is in line with the vast literature on social impairments in schizophrenia patients (Green et al., 2015; Owen et al., 2016) and more recently on imitation deficits (Matthews et al., 2013; Walther et al., 2015, 2016; Raffard et al., 2018).

Socio-motor synchronization revealed new and interesting results. Healthy controls performance was not significantly different in the three conditions whereas schizophrenia patients showed increasing socio-motor synchronization score as a function of their leading role in the game (Participant leader > Joint improvisation > Confederate leader). Even if the *post hoc* decomposition of this Group × Condition interaction failed to reveal a significant group difference in the Participant leader condition, it is unusual in the literature to observe such high level of socio-motor synchronization in schizophrenia patients (e.g., Kupper et al., 2010; Varlet et al., 2012; Raffard et al., 2015, 2018). Whereas most of studies using the mirror game studied dyads of novices or experts, one originality of our protocol was to face participants with an expert improviser (see Brezis et al., 2017 for a similar procedure). The inner goal of such a procedure was to ensure that changes in socio-motor improvisation and socio-motor synchronization could only be due to changes in participants' ability to reveal improvised and synchronized motions during the mirror game. We therefore performed a

TABLE 2 | Correlation between symptomatology and socio-motor variables for the schizophrenia group.

	Socio-motor creativity			Socio-motor synchronization		
	Participant Leader	Joint Improvisation	Confederate Leader	Participant Leader	Joint Improvisation	Confederate Leader
PANSS						
Positive	0.0992	0.1403	0.0791	−0.1352	−0.2614	−0.3526
	$p = 0.602$	$p = 0.460$	$p = 0.678$	$p = 0.476$	$p = 0.163$	$p = 0.056$
Negative	0.0365	−0.0389	−0.1277	0.0148	−0.1745	−0.3348
	$p = 0.848$	$p = 0.838$	$p = 0.501$	$p = 0.938$	$p = 0.357$	$p = 0.071$
General psychopathology	−0.2748	−0.2373	−0.2481	0.24	−0.1017	−0.1229
	$p = 0.142$	$p = 0.207$	$p = 0.186$	$p = 0.201$	$p = 0.593$	$p = 0.518$
Total score	−0.095	−0.1151	−0.1911	0.1021	−0.2215	−0.3552
	$p = 0.618$	$p = 0.545$	$p = 0.312$	$p = 0.591$	$p = 0.240$	$p = 0.054$
PANSS Q-10	0.1509	0.0728	−0.092	−0.1338	−0.2801	−0.3087
	$p = 0.426$	$p = 0.702$	$p = 0.629$	$p = 0.481$	$p = 0.134$	$p = 0.097$
NSS	0.3258	0.203	0.1764	−0.2478	0.0005	−0.2543
	$p = 0.079$	$p = 0.282$	$p = 0.351$	$p = 0.187$	$p = 0.998$	$p = 0.175$
CPZE	0.1195	0.1474	0.0057	−0.0733	−0.3582	−0.0688
	$p = 0.529$	$p = 0.437$	$p = 0.976$	$p = 0.700$	$p = 0.052$	$p = 0.718$

r and p values are presented for the correlation between PANSS total score and its sub-dimensions, neurological soft signs NSS, medication (Chlorpromazine equivalent dose CPZE) and socio-motor improvisation and synchronization for each condition. Bonferroni's adjustment for 6 comparisons lowers the alpha value from 0.05 to 0.0083.

correlational analysis between socio-motor improvisation and synchronization in order to better understand the trade-off between improvisation and synchronization. Results revealed that socio-motor improvisation negatively correlates with socio-motor synchronization for both groups in all conditions, demonstrating the contradiction between improvising and being synchronized. However, despite the evidence that healthy controls show higher socio-motor improvisation than schizophrenia patients, they synchronize equally in the three conditions whereas schizophrenia patients synchronize better when they are leaders rather than sharing the leadership or followers. First of all, these results explain why schizophrenia patients exhibit such high level of synchronization when they are leader in our protocol: because the degree of improvisation is significantly lower than in the control group. However, this low degree of improvisation is also the same in the Joint improvisation and Confederate leader conditions, without giving rise to high levels of synchronization. The second main result of this correlational analysis is thus to show that when the patients lead, the expert follow easily and the dyad socio-motor synchronization is high; however, when the expert leads, patients fail to follow easily, and the dyad socio-motor synchronization is low (**Figure 3**). Considering the negative correlation between socio-motor improvisation and synchronization, the astonishing good synchronization for schizophrenia patients leading the game is thus explained by the combination of a low degree of improvisation (motions highly predictable) and high skills of the expert as a follower.

Finally, executive measures that have been largely associated with flexibility and *cognitive* improvisation (Sass, 2001) were impaired in schizophrenia patients compared to healthy controls (**Table 1**). Our study also revealed neither a correlation between socio-motor improvisation and executive measures (Appendix **Table 1**) nor a correlation between socio-motor improvisation and symptomatology (**Table 2**). No significant correlations were found between neurological soft signs nor anti-psychotic treatments (mean dose of chlorpromazine equivalents). Socio-motor improvisation impairments are not secondary to cognitive functioning neurological soft signs, nor anti-psychotics treatments and thus can be considered as abnormalities mainly related to motor synchrony deficits. Altogether, the results show that socio-motor improvisation deficits in schizophrenia depends principally on synchronization skill ability. This might be interpreted as a dissociation between socio-motor improvisation and *cognitive* improvisation, i.e., that being able to improvise at the motor level in a social context does not depend on the cognitive ability to generate new ideas. Altogether, our results suggest that socio-motor improvisation and *cognitive* improvisation do not share the same underlying processes and provide a direct evidence that being able to improvise in individual situations is fundamentally different than being able to improvise in a social context. Therefore, our study explains why mental illness is associated with creativity in one-to-many situations ("creative minds," "mad genius") more than in collaborative situations such as brainstorming in a company or team activities.

LIMITS

The scale chosen to measure negative symptoms (PANSS) was outdated and could explain the lack of association between the severity of negative symptoms and performance in the socio-motor improvisation task. The use of more specific and sensitive scales for negative symptoms such as the Brief Negative Symptom Scale BNSS (Kirkpatrick et al., 2011) or the clinical Assessment Interview for Negative Symptoms (CAINS, Kring et al., 2013) could have been a better choice in a study that evaluated clinical constructs which are akin to and overlap with the concept of negative symptoms of schizophrenia. However, neither the CAINS nor the BNSS were validated in French at the time of our study. This is nevertheless an important limit of the present study.

Another limit of this study relates to the low symptom severity of the patients group. Indeed, contrary to several past studies demonstrating that patients with schizophrenia are truly impaired when imitating hand gestures, which was linked to social functioning, motor abnormalities (Matthews et al., 2013; Walther et al., 2015, 2016) and negative symptoms (Kupper et al., 2010; Lavelle et al., 2013). In the present study, the PANSS scores reflected a hardly symptomatic sample of patients with schizophrenia which could partly explain the lack of associations found in the present study between psychotic symptoms and the socio-motor improvisation task. Future studies including samples with higher levels of negative and motor symptoms are needed to further investigate the ecological validity of this task.

CONCLUSION

We defined socio-motor improvisation as an individual's ability to respond in a divergent, original or flexible manner to motor challenges induced by social interactions while being still socially efficient. Comparing Schizophrenia patients and healthy controls skills during the game, we found that patients were less able to improvise than healthy controls. We also showed that patients exhibited significantly higher difficulties to being synchronized with someone else when they were followers rather than leaders of the game. Interestingly, such impairments were not correlated with the usual *cognitive* improvisation. Altogether, our results suggest that socio-motor improvisation and *cognitive* improvisation do not share the same underlying processes and provide a direct evidence that being able to improvise in individual situations is fundamentally different than being able to improvise in a social context. Finally, the significant negative correlation exhibited by schizophrenia patients between socio-motor improvisation and socio-motor synchronization suggests that synchronization is an interesting key factor to enhance social skills such as social improvisation and flexibility in a clinical context.

DATA AVAILABILITY STATEMENT

The raw data supporting the conclusions of this article will be made available by the authors, without undue reservation.

ETHICS STATEMENT

The studies involving human participants were reviewed and approved by CPP Sud-Méditerranée-III, Nîmes, France, #2013.04.05 and DA/2013-13. The patients/participants provided their written informed consent to participate in this study.

AUTHOR CONTRIBUTIONS

RS, DC, and SR contributed to the acquisition of funding. RS proposed the original idea, designed the study, developed the technology for the data acquisition, performed the statistical analyses, and wrote the first draft. RS and J-FC recruited and assessed the participants. RS and SR prepared the final manuscript. All authors reviewed the manuscript.

FUNDING

This experiment was supported by an internal grant from the Montpellier University Hospital, #AOI-DM-UF9111.

SUPPLEMENTARY MATERIAL

The Supplementary Material for this article can be found online at: https://www.frontiersin.org/articles/10.3389/fnhum.2021.676242/full#supplementary-material

REFERENCES

American Psychiatric Association (2000). *Diagnostic and Statistical Manual of Mental Disorders – Text Revision*, 4th Edn. Washington, DC: American Psychiatric Association.

Bakeman, R. (2005). Recommended effect size statistics for repeated measures designs. *Behav. Res. Methods* 37, 379–384. doi: 10.3758/BF03192707

Baron-Cohen, S., Wheelwright, S., Skinner, R., Martin, J., and Clubley, E. (2001). The autism-spectrum quotient (AQ): evidence from asperger syndrome/high-functioning autism, malesand females, scientists and mathematicians. *J. Autism Dev. Disord.* 31, 5–17. doi: 10.1023/A:1005653411471

Barrantes-Vidal, N. (2004). Creativity & madness revisited from current psychological perspectives. *J. Conscious. Stud.* 11, 58–78.

Benedek, M., Jauk, E., Sommer, M., Arendasy, M., and Neubauer, A. C. (2014). Intelligence, creativity, and cognitive control: the common and differential involvement of executive functions in intelligence and creativity. *Intelligence* 46, 73–83. doi: 10.1016/j.intell.2014.05.007

Bernieri, F. J. (1988). Coordinated movement and rapport in teacher-student interactions. *J. Nonverbal Behav.* 12, 120–138. doi: 10.1007/BF00986930

Bernieri, F. J., and Rosenthal, R. (1991). *Interpersonal Coordination: Behavior Matching and Interactional Synchrony*. Paris: Editions de la Maison des Sciences de l'Homme.

Bleuler, E. (1950). *Dementia Praecox or the Group of Schizophrenias*. Oxford: International Universities Press.

Brezis, R.-S., Noy, L., Alony, T., Gotlieb, R., Cohen, R., Golland, Y., et al. (2017). Patterns of joint improvisation in adults with autism spectrum disorder. *Front. Psychol.* 8:1790. doi: 10.3389/fpsyg.2017.01790

Chartrand, T. L., and Lakin, J. L. (2013). The antecedents and consequences of human behavioral mimicry. *Annu. Rev. Psychol.* 64, 285–308. doi: 10.1146/annurev-psych-113011-143754

Cohen, J. (1988). *Statistical Power Analysis for the Behavioral Sciences*, 2nd Edn. Hillsdale, MI: Erlbaum Associates.

D'Agati, E., Casarelli, L., Pitzianti, M., and Pasini, A. (2012). Neuroleptic treatments and overflow movements in schizophrenia: are they independent? *Psychiatry Res.* 200, 970–976. doi: 10.1016/j.psychres.2012.07.049

Delis, D. C., Kaplan, E., and Kramer, J. H. (2001). *Delis-Kaplan Executive Functioning System: Examiner's Manual*. San Antonio, TX: The Psychological Corporation.

Del-Monte, J., Capdevielle, D., Varlet, M., Marin, L., Schmidt, R. C., Salesse, R. N., et al. (2013). Social motor coordination in unaffected relatives of schizophrenia patients: a potential intermediate phenotype. *Front. Behav. Neurosci.* 7:137. doi: 10.3389/fnbeh.2013.00137

Desgranges, B., Laisney, M., Bon, L., Duval, C., Mondou, A., Bejanin, A., et al. (2012). TOM-15: une épreuve de fausses croyances pour évaluer la théorie de l'esprit cognitive. *Rev. Neuropsychol.* 4, 216–220. doi: 10.3917/rne.043.0216

Doyen, S., Klein, O., Pichon, C. L., and Cleeremans, A. (2012). Behavioral priming: it's all in the mind, but whose mind? *PLoS One* 7:e29081. doi: 10.1371/journal.pone.0029081

Giacco, D., McCabe, R., Kallert, T., Hansson, L., Fiorillo, A., and Priebe, S. (2012). Friends and symptom dimensions in patients with psychosis: a pooled analysis. *PLoS One* 7:e50119. doi: 10.1371/journal.pone.0050119

Green, M. F., Horan, W. P., and Lee, J. (2015). Social cognition in schizophrenia. *Nat. Rev. Neurosci.* 16, 620–631. doi: 10.1038/nrn4005

Gueugnon, M., Salesse, R. N., Coste, A., Zhao, Z., Bardy, B. G., and Marin, L. (2016). The acquisition of socio-motor improvisation in the mirror game. *Hum. Mov. Sci.* 46, 117–128. doi: 10.1016/j.humov.2015.12.005

Gupta, S. (1995). Neurological soft signs in neuroleptic-naive and neuroleptic-treated schizophrenic patients and in normal comparison subjects. *Am. J. Psychiatry* 152, 191–196. doi: 10.1176/ajp.152.2.191

Hart, Y., Noy, L., Feniger-Schaal, R., Mayo, A. E., and Alon, U. (2014). Individuality and togetherness in joint improvised motion. *PLoS One* 9:e87213. doi: 10.1371/journal.pone.0087213

Hove, M. J., and Risen, J. L. (2009). It's all in the timing: interpersonal synchrony in-creases affiliation. *Soc. Cogn.* 27, 949–960. doi: 10.1521/soco.2009.27.6.949

Hristovski, R., Davids, K., Araujo, D., and Passos, P. (2011). Constraints-induced emergence of functional novelty in complex neurobiological systems: a basis for creativity in sport. *Nonlinear Dynamics Psychol. Life Sci.* 15, 175–206.

Kahaner, D., Moler, C., and Nash, S. (1989). *Numerical Methods and Software*. Prentice Hall: Englewood Cliffs, NJ, 1989.

Kay, S. R., Fiszbein, A., and Opler, L. A. (1987). The positive and negative syndrome scale (PANSS) for schizophrenia. *Schizophr. Bull.* 13, 261–276. doi: 10.1093/schbul/13.2.261

Kidd, S. A. (2013). From social experience to illness experience: reviewing the psychological mechanisms linking psychosis with social context. *Can. J. Psychiatry* 58, 52–58. doi: 10.1177/070674371305800110

Kirkpatrick, B., Strauss, G. P., Nguyen, L., Fischer, B. A., Daniel, D. G., Cienfuegos, A., et al. (2011). The brief negative symptom scale: psychometric properties. *Schizophr. Bull.* 37, 300–305. doi: 10.1093/schbul/sbq059

Krebs, M. O., Gut-Fayand, A., Bourdel, M., Dischamp, J., and Olié, J. (2000). Validation and factorial structure of a standardized neurological examination assessing neurological soft signs in schizophrenia. *Schizophr. Res.* 45, 245–260. doi: 10.1016/S0920-9964(99)00206-6

Kring, A. M., Gur, R. E., Blanchard, J. J., Horan, W. P., and Reise, S. P. (2013). The clinical assessment interview for negative symptoms (CAINS): final development and validation. *Am. J. Psychiatry* 170, 165–172. doi: 10.1176/appi.ajp.2012.12010109

Kupper, Z., Ramseyer, F., Hoffmann, H., Kalbermatten, S., and Tschacher, W. (2010). Video-based quantification of body movement during social interaction indicates the severity of negative symptoms in patients with schizophrenia. *Schizophr. Res.* 121, 90–100. doi: 10.1016/j.schres.2010.03.032

Laere, E., Tee, S. F., and Tang, P. Y. (2018). Assessment of cognition in schizophrenia using trail making test: a meta-analysis. *Psychiatry Investig.* 15, 945–955. doi: 10.30773/pi.2018.07.22

Lavelle, M., Healey, P. G., and McCabe, R. (2013). Nonverbal communication disrupted in interactions involving patients with schizophrenia? *Schizophr. Bull.* 39, 1150–1158. doi: 10.1093/schbul/sbs091

Lavelle, M., Healey, P. G., and McCabe, R. (2014). Nonverbal behavior during face-to-face social interaction in schizophrenia: a review. *J. Nerv. Ment. Dis.* 202, 47–54. doi: 10.1097/NMD.0000000000000031

Łucznik, K. (2015). Between minds and bodies: some insights about creativity from dance improvisation. *Technoetic Arts* 13, 301–308. doi: 10.1386/tear.13.3.301_1

Mackinnon, A., and Mulligan, R. (2005). The estimation of premorbid intelligence levels in French speakers. *Encephale* 31, 31–43.

Marsh, K. L., Richardson, M. J., and Schmidt, R. C. (2009). Social connection through joint action and interpersonal coordination. *Top. Cogn. Sci.* 1, 320–339. doi: 10.1111/j.1756-8765.2009.01022.x

Matthews, N., Gold, B. J., Sekuler, R., and Park, S. (2013). Gesture imitation in schizophrenia. *Schizophr. Bull.* 39, 94–101. doi: 10.1093/schbul/sbr062

Memmert, D., Baker, J., and Bertsch, C. (2010). Play and practice in the development of sport-specific creativity in team ball sports. *High Abil. Stud.* 21, 3–18. doi: 10.1080/13598139.2010.488083

Memmert, D., and Roth, K. (2007). The effects of non-specific and specific concepts on tactical creativity in team ball sports. *J. Sports Sci.* 25, 1423–1432. doi: 10.1080/02640410601129755

Mier, D., and Kirsch, P. (2015). "Social-cognitive deficits in schizophrenia," in *Social Behavior from Rodents to Humans*, eds M. Wöhr, and S. Krach (Cham: Springer), 397–409.

Moritz, S., Birkner, C., Kloss, M., Jahn, H., Hand, I., Haasen, C., et al. (2002). Executive functioning in obsessive–compulsive disorder, unipolar depression, and schizophrenia. *Arch. Clin. Neuropsychol.* 17, 477–483.

Noy, L., Dekel, E., and Alon, U. (2011). The mirror game as a paradigm for studying the dynamics of two people improvising motion together. *Proc. Natl. Acad. Sci. U.S.A.* 108, 20947–20952. doi: 10.1073/pnas.1108155108

Orth, D., van der Kamp, J., Memmert, D., and Savelsbergh, G. J. P. (2017). Creative motor actions as emerging from movement variability. *Front. Psychol.* 8:1903. doi: 10.3389/fpsyg.2017.01903

Owen, M. J., Sawa, A., and Mortensen, P. B. (2016). Schizophrenia. *Lancet* 388, 86–97. doi: 10.1016/S0140-6736(15)01121-6

Raffard, S., Salesse, R. N., Bortolon, C., Bardy, B. G., Henriques, J., Marin, L., et al. (2018). Using mimicry of body movements by a virtual agent to increase synchronization behavior and rapport in individuals with schizophrenia. *Sci. Rep.* 8:17356. doi: 10.1038/s41598-018-35813-6

Raffard, S., Salesse, R. N., Marin, L., Del-Monte, J., Schmidt, R. C., Varlet, M., et al. (2015). Social priming enhances interpersonal synchronization and feeling of connectedness towards schizophrenia patients. *Sci. Rep.* 5:8156. doi: 10.1038/srep08156

Riehle, M., Jung, E., Wiesjahn, M., Mehl, S., Rief, W., and Lincoln, T. M. (2015). What's in an item? Predicting social outcomes in schizophrenia spectrum disorders from the PANSS item "Poor Rapport". *Schizophr. Res.* 168, 593–594. doi: 10.1016/j.schres.2015.08.026

Rosenblum, M. G., Pikovsky, A. S., and Kurths, J. (1996). Phase synchronization of chaotic oscillators. *Phys. Rev. Lett.* 76, 1804–1807. doi: 10.1103/PhysRevLett.76.1804

Sass, L. A. (2001). Schizophrenia, modernism, and the "creative imagination": on creativity and psychopathology. *Creat. Res. J.* 13, 55–74. doi: 10.1207/S15326934CRJ1301_7

Schmidt, R. C., Morr, S., Fitzpatrick, P., and Richardson, M. J. (2012). Measuring the dynamics of interactional synchrony. *J. Nonverbal Behav.* 36, 263–279. doi: 10.1007/s10919-012-0138-5

Schmidt, S. J., Mueller, D. R., and Roder, V. (2011). Social cognition as a mediator variable between neurocognition and functional outcome in schizophrenia: empirical review and new results by structural equation modeling. *Schizophr. Bull.* 37(Suppl. 2), 41–54.

Seifert, L., Komar, J., Araújo, D., and Davids, K. (2016). Neurobiological degeneracy: a key property for functional adaptations of perception and action to constraints. *Neurosci. Biobehav. Rev.* 69, 159–165. doi: 10.1016/j.neubiorev.2016.08.006

Shanks, D. R., Newell, B. R., Lee, E. H., Balakrishnan, D., Ekelund, L., Cenac, Z., et al. (2013). Priming intelligent behavior: an elusive phenomenon. *PLoS One* 8:e56515. doi: 10.1371/journal.pone.0056515

Słowiński, P., Zhai, C., Alderisio, F., Salesse, R., Gueugnon, M., Marin, L., et al. (2016). Dynamic similarity promotes interpersonal coordination in joint action. *J. R. Soc. Interface* 13:20151093. doi: 10.1098/rsif.2015.1093

Thornicroft, G., Brohan, E., Rose, D., Sartorius, N., Leese, M., Indigo Study Group, et al. (2009). Global pattern of experienced and anticipated discrimination against people with schizophrenia: a cross-sectional survey. *Lancet* 373, 408–415. doi: 10.1016/S0140-6736(08)61817-6

Varlet, M., Marin, L., Raffard, S., Schmidt, R.C., Capdevielle, D., Boulenger, J.P., et al. (2012). Impairments of social motor coordination in schizophrenia. *PLoS One* 7:e29772. doi: 10.1371/journal.pone.0029772

Walther, S., Eisenhardt, S., Bohlhalter, S., Vanbellingen, T., Müri, R., Strik, W., et al. (2016). Gesture performance in schizophrenia predicts functional outcome after 6 months. *Schizophr. Bull.* 42, 1326–1333.

Walther, S., Stegmayer, K., Sulzbacher, J., Vanbellingen, T., Müri, R., Strik, W., et al. (2015). Nonverbal social communication and gesture control in schizophrenia. *Schizophr. Bull.* 41, 338–345.

Walther, S., and Strik, W. (2012). Motor symptoms and schizophrenia. *Neuropsychobiology* 66, 77–92. doi: 10.1159/000339456

Wiltermuth, S. S., and Heath, C. (2009). Synchrony and cooperation. *Psychol. Sci.* 20, 1–5.

Conflict of Interest: RS was employed by the company SAS Mooven while writing the last version of this manuscript without competing interests, or other interests that might be perceived to influence the results and discussion reported in this manuscript.

The remaining authors declare that the research was conducted in the absence of any commercial or financial relationships that could be construed as a potential conflict of interest.

frontiers in Human Neuroscience

ORIGINAL RESEARCH
published: 03 November 2021
doi: 10.3389/fnhum.2021.708969

Restricted Kinematics in Children With Autism in the Execution of Complex Oscillatory Arm Movements

Zhong Zhao[1], Xiaobin Zhang[2], Haiming Tang[1], Xinyao Hu[1], Xingda Qu[1], Jianping Lu[3] and Qiongling Peng[4]*

[1] Institute of Human Factors and Ergonomics, College of Mechatronics and Control Engineering, Shenzhen University, Shenzhen, China, [2] Shenzhen Guangming District Center for Disease Control and Prevention, Shenzhen, China, [3] Department of Child Psychiatry of Shenzhen Kangning Hospital, Shenzhen Mental Health Center, Shenzhen, China, [4] Developmental Behavioral Pediatric Department, Shenzhen Baoan Women's and Children's Hospital, Jinan University, Shenzhen, China

Restricted and repetitive behavior is a core symptom of autism spectrum disorder (ASD) characterized by features of restrictedness, repetition, rigidity, and invariance. Few studies have investigated how restrictedness is manifested in motor behavior. This study aimed to address this question by instructing participants to perform the utmost complex movement. Twenty children with ASD and 23 children with typical development (TD) performed one-dimensional, left-right arm oscillations by demonstrating varying amplitudes and frequencies. The entropy of amplitude and velocity was calculated as an index of kinematic complexity. Results showed that the velocity entropy, but not the amplitude entropy, was significantly lower in ASD than in TD ($p < 0.01$), suggesting restricted kinematics. Further analysis demonstrated that a significantly higher proportion of the velocity values was allocated at a low-speed level in the children with ASD ($p < 0.01$). A qualitative comparison of the complex movement with movement at preferred frequency suggested that the children with ASD might be less likely to shift away from the preferred movement. However, our study can be improved in terms of recruiting a larger sample of participants, measuring the level of motivation, and collecting both complex and preferred movements of the same participant.

Keywords: autism, restrictedness and repetitive behavior, movement complexity, entropy, behavioral assessment

OPEN ACCESS

Edited by:
Nadia Dominici, Vrije Universiteit Amsterdam, Netherlands

Reviewed by:
Piotr Słowiński, University of Exeter, United Kingdom
Antonio Parziale, University of Salerno, Italy

****Correspondence:***
Jianping Lu
szlujianping@126.com

Specialty section:
This article was submitted to Motor Neuroscience, a section of the journal Frontiers in Human Neuroscience

Received: *13 May 2021*
Accepted: *04 October 2021*
Published: *03 November 2021*

Citation:
Zhao Z, Zhang X, Tang H, Hu X, Qu X, Lu J and Peng Q (2021) Restricted Kinematics in Children With Autism in the Execution of Complex Oscillatory Arm Movements. Front. Hum. Neurosci. 15:708969. doi: 10.3389/fnhum.2021.708969

INTRODUCTION

Autism spectrum disorder (ASD) is a neurodevelopmental condition that greatly impairs the daily functionalities of affected individuals. According to the Diagnostic and Statistical Manual of Mental Disorders–5th Edition (DSM-V), restricted and repetitive behavior (RRB) is one of the two core symptoms of ASD (American Psychiatric and Association, 2013). People with autism spectrum disorder (ASD) exhibit a broad range of RRBs, such as repetitive motor activities and language, circumscribed interests, and adherence to specific routines (Kim and Lord, 2010).

Abbreviations: ASD, autism spectrum disorder; DSM-V, the Diagnostic and Statistical Manual of Mental Disorders–5th Edition; IMS, individual motor signature; LMEM, linear mixed-effect model; RBS-R, Repetitive Behavior Scale-Revised; RRB, restricted and repetitive behavior; TD, typical development.

The etiology of RRB remains unclear. It has been postulated that RRB might serve the purposes of reducing high arousal levels (Hutt et al., 1964; Repp et al., 1992) or deriving pleasure (Baron-Cohen, 1989; Klin et al., 2007). Notably, a sizable body of literature indicated that RRB could be the result of executive dysfunction (Turner, 1999; Lopez et al., 2005; D'Cruz et al., 2013). This hypothesis has received considerable support from studies that found a close relationship between the frontal lobe and RRB (Pierce and Courchesne, 2001; Shafritz et al., 2008), and between cognitive flexibility and RRB (Lopez et al., 2005; Tanimura et al., 2008). It was proposed that RRB may be derived from the inability to shift from preferred behaviors to new adaptive ones (Lopez et al., 2005; Corbett et al., 2009). People with ASD might be "locked into" a specific thought or behavior (Turner, 1999). Since RRB is an indispensable symptom of ASD, it is assumed that restricted kinematics (i.e., movement characterized by higher level of stereotypy, or lower degree of complexity) might be revealed in a wide variety of motor behaviors.

Despite motor deficits in people with ASD having been grossly documented, few studies have examined whether the restricted feature is manifested in motor behavior (Fournier et al., 2014; Li et al., 2019). The description of motor impairments in ASD could be dated back to the 1940s when Kanner reported the clumsy gait in children with ASD (Kanner, 1943). Many studies reported an association between ASD and abnormalities in postural control, gait patterns, and fine motor control (Esposito and Venuti, 2008; Fuentes et al., 2009; Fournier et al., 2014; Bojanek et al., 2020). Recently, a rigorous meta-analysis that compared the difference in motor coordination, arm movements, gait, and postural stability between individuals with ASD and those typically developing (TD) found that people with ASD present pronounced motor impairments across a wide range of behaviors (Fournier et al., 2010). However, whether and how the restricted feature is manifested in kinematics has been rarely reported.

Previous studies examining restricted kinematics in motor behavior have focused on the complexity of postural control and head movements in individuals with ASD (Fournier et al., 2014; Li et al., 2019; Zhao et al., 2021). For instance, Fournier et al. (2014) utilized multiscale entropy to quantify the complexity of postural control dynamics during quiet stance in children with ASD and age-matched TD children. Their results demonstrated that the children with ASD exhibited a reduced level of complexity both anteroposteriorly and mediolaterally, as observed in the center of pressure (COP) data (Fournier et al., 2014). Zhao et al. (2021) examined the level of head movement complexity in children with ASD during a face-to-face interaction and showed an elevated stereotypy in these children as compared with the TD peers. Noticeably, all these studies adopted unintentional tasks, in which participants were not instructed how to perform movements. It remains unexplored whether restricted kinematics could also be observed in individuals with ASD when they are deliberately instructed to perform the utmost complex movement.

The experimental design of this study was inspired by the research conducted by Słowiński et al. (2016), who investigated the existence of individual motor signature (IMS), a personalized motor feature that differentiates individuals. In the study of Słowiński et al. (2016), healthy participants were instructed to create one-dimensional, left-right oscillatory arm movement above a LeapMotion sensor. The movement of each participant was recorded three times, at least 1 week apart between two consecutive times. Although a complex movement was performed and the time series varied at different times, Słowiński et al. (2016) found that time-invariant and individual-specific kinematic properties were preserved in velocity distribution patterns, suggesting the existence of IMS. In light of this finding and given that ASD is characterized by stereotyped movement (Fournier et al., 2014; Li et al., 2019; Zhao et al., 2021), we were motivated to investigate whether restrictedness would be reflected in the movement of children with ASD when performing this particular motor task.

The significance of seeking restricted kinematics is of particular importance for obtaining objective behavioral markers of ASD. The current diagnosis of RRB in ASD heavily relies on the evaluation of an informant, which has been criticized as being laborious and having unreliable accuracy (Pyles et al., 1997). For example, the Autism Diagnostic Observation Schedule (ADOS) is considered a gold standard diagnostic instrument that requires significant clinical expertise. The length of the ADOS exam and shortage of trained clinicians significantly contributed to the delay in diagnosis (Shattuck et al., 2009). Data from the US reported that 13 months, on average, were required between the initial evaluation and confirmation of the diagnosis (Wiggins et al., 2006). Delayed diagnosis directly translates to postponed delivery of intervention programs, which negatively impacts the developmental outcomes of a child (Corsello, 2005). Therefore, a diagnostic tool that is both labor-saving and accurate is urgently called upon.

In this study, children with ASD and at least average non-verbal intellectual ability were recruited in order to ensure compliance with the experimental protocol. The instruction was to perform movements as complex as possible by demonstrating varying amplitudes and frequencies. Their movement was compared with that of TD participants.

We computed both the amplitude entropy and velocity entropy as indices of the kinematic complexity (the antonymous term for kinematic restrictedness). Entropy was originally introduced in the field of thermodynamics to denote the form of energy no longer available to do physical work (Clausius, 1867). It was later adapted to probability theory, information theory, and the theory of dynamical systems, where it is used to quantify the level of uncertainty, complexity, or irregularity (Shannon and Shannon, 1948; Kolmogorov, 1959). Entropy analysis has been previously performed to compute the complexity of movement in individuals with ASD, and a lower entropy value indicated a higher level of restrictedness/stereotypy (Fournier et al., 2014; Li et al., 2019; Zhao et al., 2021). In this study, we hypothesized that individuals with ASD would display more periodic movement patterns, and thus the entropy of amplitude and velocity would be significantly lower in ASD as compared with TD. In addition, we also examined the association between kinematic restrictedness and the RRB measured with the Repetitive Behavior Scale-Revised (RBS-R). A negative correlation between kinematic complexity and RBS-R scores was hypothesized.

MATERIALS AND METHODS

Participants

The participants of this study came from a larger research project dedicated to seeking behavioral markers of ASD from social interaction (Zhao et al., 2021) and restricted behavior. The estimated sample size of this study was 34 based on data from a previous study that investigated behavioral complexity (Fournier et al., 2014) by implementing power analysis (between-group t-test, $d = 1$, $\alpha = 0.05$, power = 0.8). Finally, 20 children with ASD and 23 children with TD were recruited, and the number of participants ($N = 43 > 34$) could provide sufficient power to register a statistical difference as the estimated sample. Children with ASD were recruited from the Department of Child Psychiatry in a first-class hospital. The diagnosis of ASD was confirmed with a series of rigorous procedures. The diagnosis was first made by a licensed psychiatrist with no less than 5 years of clinical experience by strictly following the DSM-IV criteria. Next, a senior psychiatrist further confirmed the diagnosis. A consultation with at least two additional senior psychiatrists would be involved if disagreement took place. The inclusion criteria were: (a) aged between 6 and 13 years old; (b) average non-verbal intellectual ability preselected by clinicians (IQ was subsequently tested by administering the Raven's Advance Progress Matrices as IQ $\geq$ 70); and (c) absence of clinical comorbidities such as schizophrenia or attention deficit hyperactivity disorder (ADHD). The TD participants were recruited from local communities if no physical or mental disorders were reported. None of the TD participants declared the existence of ASD/ADHD in first-degree relatives. A written informed consent approved by the ethics committee of a local university was given by the caregivers of the participants. The experimental protocol conformed to the Declaration of Helsinki. Subject demographics are presented in **Table 1**.

Apparatus

The experimental apparatus incorporated a computer (Lenovo Legion R720-15IKBN; Lenovo), a LeapMotion sensor (Leap Motion Inc.), two sticks, and a string (**Figure 1**). The LeapMotion sensor consists of two cameras and three infrared light-emitting diodes (LEDs, with a wavelength of 850 nm). It is a marker-less optical system that tracks the 3D movement of the palm and fingers of the users. Thanks to the low-cost and calibration-free characteristics of this device, this study utilized it to capture and save the spatial position of the center of the palm. The string was tied to the two sticks, and the distance between the sticks was 60 cm. Both the string and sticks allowed the participants to perform one-dimensional, left-right oscillatory movements. A solid box was offered to the participants to make sure that the dominant hand could move naturally and comfortably above the string.

TABLE 1 | Subject demographics and group comparisons.

	ASD	TD	Group comparison	p value
Sex (M:F)†	18:2	19:4	$\chi^2(1) = 0.487$	0.485
Age in months (Mean ± SD)‡	99 ± 24.6	110 ± 25.6	$t(41) = 1.48$	0.146
IQ (Mean ± SD)‡	102 ± 22.7	118 ± 15.5	$t(32.9) = 2.75$	0.012*

†*Chi-square test was performed.*
‡*Independent samples t-test was performed.*
**p < 0.05.*

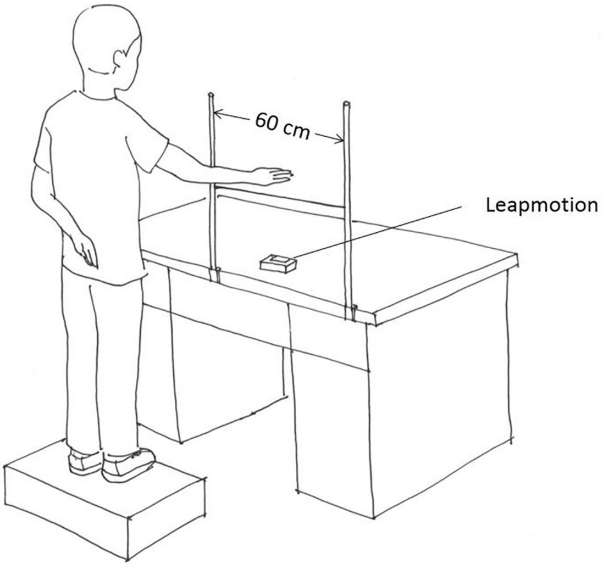

FIGURE 1 | Schematic illustration of the experimental setup.

Repetitive Behavior Scale-Revised (RBS-R)

This study employed the Chinese version of RBS-R, which is a 43-item questionnaire evaluating the impression of a caregiver on the RRBs of children with ASD (Bodfish et al., 2000). The original RBS-R incorporated six subscales: Stereotyped Behavior, Self-Injurious Behavior, Compulsive Behavior, Ritualistic Behavior, Sameness Behavior, and Restricted Behavior. Caregivers were required to rate each item on a 4-point Likert scale, ranging from 0 (behavior does not occur) to 3 (behavior occurs and is a severe problem). In order to validate the inner structure of the measured RRBs, Lam and Aman (2007) performed factor analysis to achieve a five-factor solution, which could be summarized as "stereotypic behavior," "self-injurious behavior," "compulsive behavior," "ritualistic/sameness behavior," and "restricted interests" (Lam and Aman, 2007). In this study, the RBS-R scores were calculated based on the findings of Lam et al., and correlations between kinematic complexity and RBS-R total, as well as subscale scores, were computed.

Experimental Procedure

The participants were required to perform continuous left-right oscillatory arm movements between the two sticks. The instruction was to perform a complex movements as possible. Prior to data collection, the experimenter behaviorally demonstrated that simple movement referred to periodic

movement with mono amplitude and frequency, and complex movement represented unpredictable movement with varying amplitude and frequency. The participants had practice trials to assure that they fully understood the instructions. In order to avoid falsely registering the movement of the subdominant hand, the participants were told to keep the subdominant hand behind their back. Three trials of a movement task were recorded with each trial lasting 60 s. The participants were required not to withdraw their hand out of the recording zone or to put the subdominant hand in it. If any experimental rule was violated (e.g., withdrawing the hand from the recording zone, stopping the hand from moving voluntarily), the trial would be stopped and reinitiated. A break of 2–5 min was arranged between two consecutive trials to avoid confounding effects caused by fatigue.

Data Analysis

The time series of the palm position was obtained as the raw data, which was further interpolated by means of the piecewise cubic Hermite interpolating polynomial method and filtered with a second-order low-pass Butterworth filter (5 Hz cut-off, **Figure 2A**). The first and the last 3 s were trimmed from the data analysis. Since the participants were required to perform complex oscillatory movements, each trial of movement was composed of multiple oscillations. This study focused on the difference in variation of oscillation amplitude and velocity between both groups of participants. The amplitude of a single oscillation was computed as the spatial distance between two consecutive endpoints (where velocity equaled 0). The set of amplitudes of a whole movement trial included the amplitude values of all single oscillations. Velocity (**Figure 2B**) was estimated by taking the first derivative of the position time series.

Before the calculation of entropy, we set the threshold range for amplitude and velocity values. Specifically, the threshold range for amplitude and velocity were set as 0–60 cm and -3 and 3 m/s, respectively. These threshold values were chosen empirically based on limits of the movement [e.g., the amplitude would not exceed 60 cm, since the maximum distance of the moving area was 60 cm, and it would be hard for the participants to move above 3 m/s in this experiment (Słowiński et al., 2016)]. Values out of these ranges were considered as noise, and they were discarded from further analysis. Subsequently, we used a normalized histogram with 101 equally distant bins (Słowiński et al., 2016) within the threshold range to compute the probability of each bin (**Figure 2C** illustrates two exemplary velocity distributions of a child with TD and a child with ASD), and calculated the Shannon entropy as:

$$\text{Entropy} = -\sum_{i=1}^{n} p(x_i) * \log\_2 p(x_i)$$

where $n = 101$; $p(x_i)$ = the probability of the ith bin.

Statistical Analysis

This study implemented linear mixed-effects models (LMEMs) to investigate whether group membership was a significant predictor of kinematic complexity. The dependent variables were amplitude entropy and velocity entropy. We entered "Group" and "Participant's sex" as fixed factors. The random factors were "Participants," "Age," "Participant's IQ," and "Order of the experimental trials." The lme4 (Bates et al., 2015) package for R (R Core Team, 2013) was used to perform LMEMs, and the statistical significance of fixed factors was determined using Type II Wald chi-square tests in the "car" package (Fox et al., 2013). Spearman's rank-order correlation tests were performed to compute correlations between kinematic complexity and RBS-R scores.

RESULTS

Kinematic Complexity

The results demonstrated that Group was a significant predictor of velocity entropy [$\chi^2(1) = 5.03$, $p = 0.02$]. Velocity entropy in the ASD group (M ± SD: 5.94 ± 0.44) was lower than that in the TD group (M ± SD: 6.09 ± 0.32). However, the results failed to show that Group was a significant predictor of amplitude entropy [$\chi^2(1) = 0.21$, $p = 0.65$] (**Figure 3**). In both LMEMs, the sex of the participant was not found to be a significant predictor for either amplitude entropy [$\chi^2(4) = 4.36$, $p = 0.36$] or velocity entropy [$\chi^2(4) = 8.08$, $p = 0.09$].

Reduced velocity entropy indicated lower variance in velocity distribution in the ASD group as compared with the TD group. In order to investigate how velocity values were distributed for both groups of participants, we divided the absolute velocity[1] into five equally divided segments between 0 and 3 m/s: Segment 1: 0–0.6 m/s; Segment 2:0.6–1.2 m/s; Segment 3: 1.2–1.8 m/s; Segment 4: 1.8–2.4 m/s; Segment 5: 2.4–3 m/s. The relative frequency of each segment (proportion of velocity values allocated in each segment) was calculated as the dependent variable. A two-way ANOVA was conducted with Group (ASD or TD) as the between-subjects factor, and Segment as the within-subjects factor. The results showed a Segment main effect [$F(4,164) = 58.36$, $p < 0.01$, $\eta_p^2 = 0.587$], and a Segment × Group interaction effect [$F(4,164) = 5.14$, $p < 0.05$,$\eta_p^2 = 0.111$]. Fisher's least significant difference (LSD) tests demonstrated that the ASD group had a significantly greater proportion of velocity values allocated in Segment 1 (0–0.6 m/s) ($p < 0.01$), but significantly less proportions in Segment 3 (1.2–1.8 m/s) ($p < 0.05$) and Segment 4 (1.8–2.4 m/s) ($p < 0.05$) (**Figure 4**). These results demonstrated that the reduced velocity entropy in ASD was due to the fact that the participants with ASD performed more low-speed movements.

Correlation Between Velocity Entropy and Repetitive Behavior Scale-Revised Scores

Spearman's rank-order correlation tests failed to show that velocity entropy was significantly correlated to RBS-R subscale scores or the total score (all $p > 0.05$). These results indicated that

[1]Given the fact that the velocity distribution was approximately symmetry around 0 for all participants, we only used the absolute values.

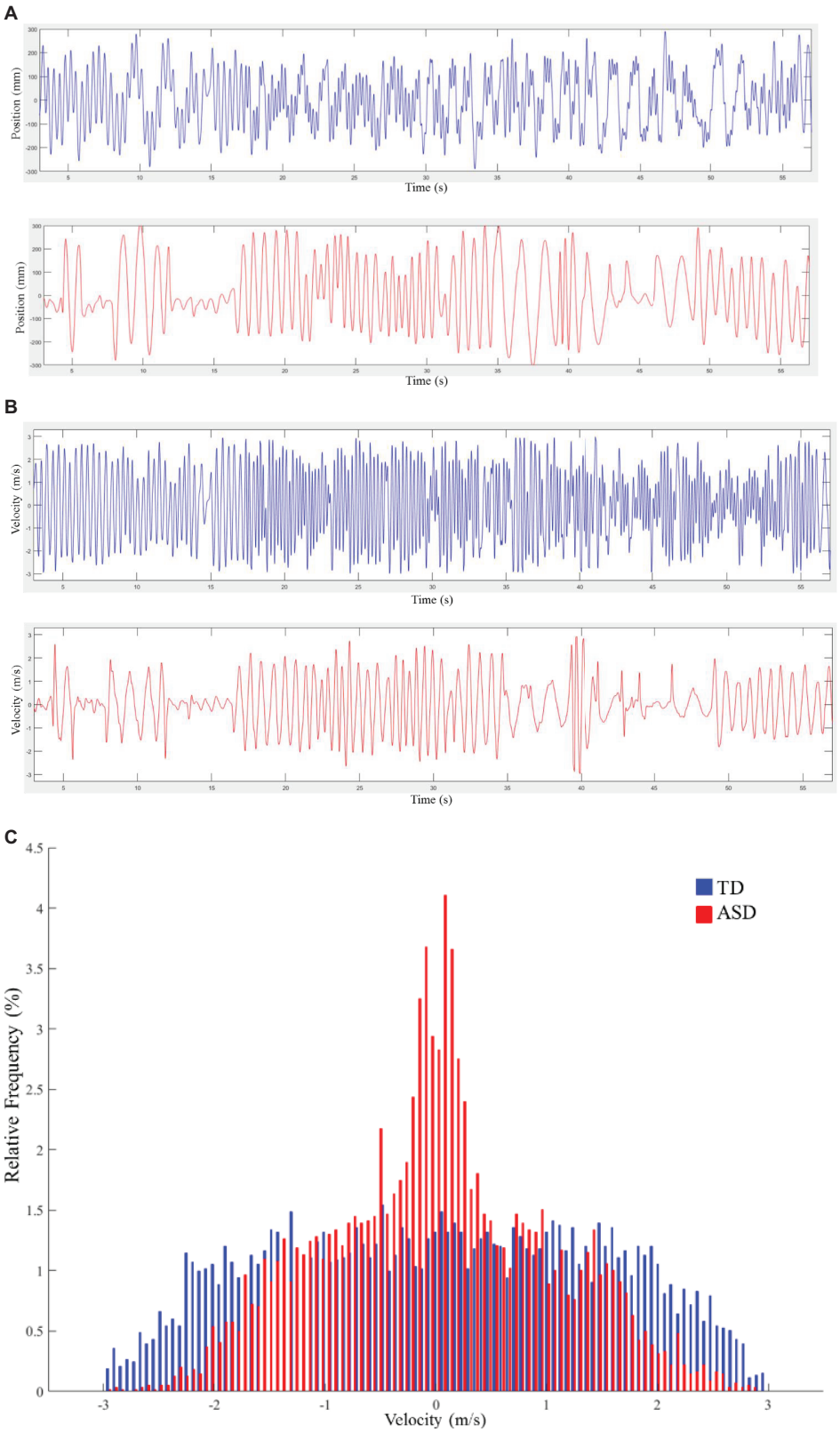

FIGURE 2 | (A) Exemplary samples of time series for the position. Typical development (TD) is plotted in blue, and autism spectrum disorder (ASD) is plotted in red. **(B)** Exemplary samples of time series for velocity. TD is plotted in blue, and ASD is plotted in red. **(C)** Velocity distributions for typical movement trials from a child with TD and a child with ASD. TD is plotted in blue, and ASD is plotted in red. Each bin in the graph represents the proportion of corresponding velocity values in the trial.

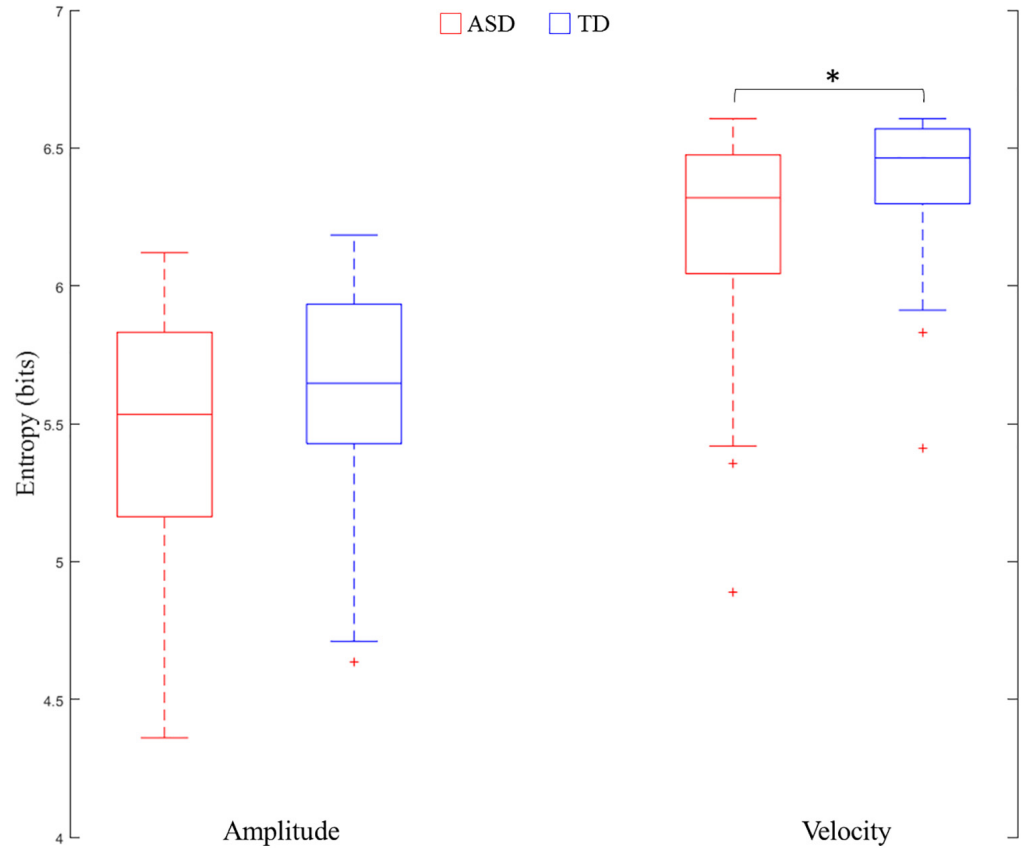

FIGURE 3 | Comparisons of entropy of amplitude and velocity between ASD and TD. * means $p < 0.05$.

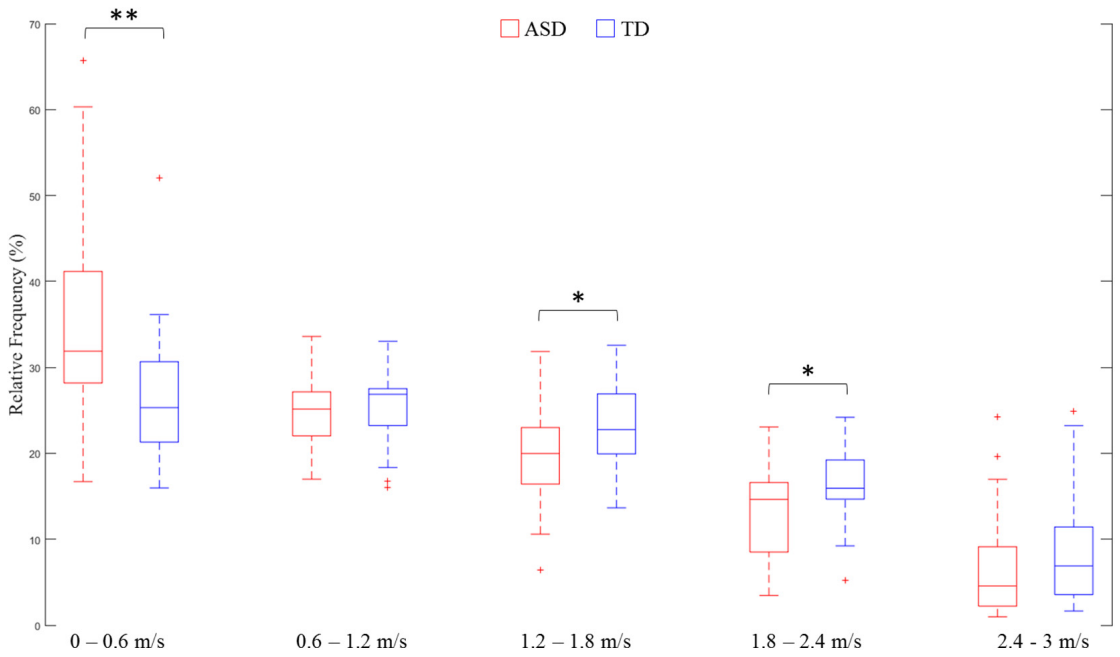

FIGURE 4 | Comparison of velocity distribution in each absolute velocity segment. ** means $p < 0.01$; * means $p < 0.05$.

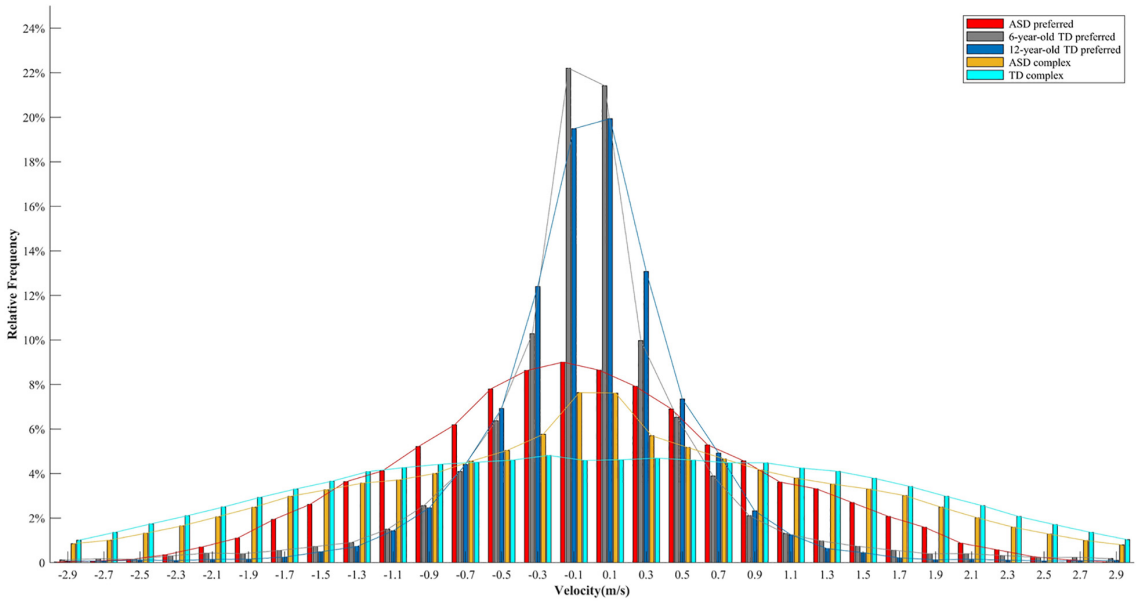

FIGURE 5 | Velocity distributions for the preferred movement in 6-year-old children with TD, 12-year-old children with TD, and children with ASD, and for the complex movement in children with ASD and children with TD. Each distribution includes velocity values of all the participants in a specific group.

velocity entropy might not be related to the RRBs of the children reported by caregivers.

DISCUSSION

This study investigated the existence of kinematic restrictedness in children with ASD and at least average non-verbal intelligence when performing volitional arm movements. The application of entropy analysis revealed a lower level of variance in the velocity distribution of participants with ASD, suggesting that children with ASD displayed a more restricted movement. Further analysis demonstrated that a higher proportion of velocity values was allocated at a low-speed level in children with ASD. Together with prior findings on restricted movement in individuals with ASD (Fournier et al., 2014; Li et al., 2019; Zhao et al., 2021), future studies on motor control in individuals with ASD are encouraged to examine the complexity of motor activity to complement conventional measures, such as the mean or peak of a given motor-related measure.

Why participants with ASD performed more low-speed movements? Previous studies demonstrated that individuals with ASD are less likely to shift away from their preferred response (Turner, 1999; Lopez et al., 2005; Corbett et al., 2009; D'Cruz et al., 2013). It was assumed that the greater proportion of low-speed movements might also be related to the incapacity of switching from one's preferred movement patterns in children with ASD. In this study, the participants were instructed to perform continuous oscillatory movements. Abundant research investigating the dynamics of continuous oscillatory movements has evidenced the existence of preferred frequency (Kay et al., 1987; Temprado et al., 1999), which typically refers to the movement rate at which the performer feels most comfortable and the least energy cost is needed (Holt et al., 1995; Temprado et al., 1999). In order to save energy, the preferred frequency would not be too fast, and velocity distribution would be characterized by the majority of values allocated around zero. This idea could be confirmed by data from two other experiments measuring the preferred frequency of children with TD and ASD. The first experiment included ten 6-year-old and eight 12-year-old children with TD, whereas the second experiment included five children with ASD aged between 7 and 12 years (M ± SD: 116.4 ± 23.2 months). Children with TD were healthy participants enrolled from nearby communities and reported no physical or mental disorders. Children with ASD were high-functioning individuals recruited from Shenzhen Kangning Hospital. The objective of these two experiments was to assess eye-hand coordination, and preferred frequency was measured at the beginning of these two experiments, with the same experimental setup as this study. In both experiments, the experimenter behaviorally demonstrated that preferred frequency represented the tempo of movement that was neither too fast nor too slow as if one could do it all day long (Schmidt et al., 1993; Temprado et al., 1999; Zhao et al., 2020). The participants had practice trials to ensure that they fully understood the instruction. The preferred movement was recorded for 30 s in the first experiment (in the TD group), and for 60 s in the second experiment (in the ASD group). To make the lengths of these two experiments equivalent, the movement of the first 30 s in the second experiment was selected to perform further data analysis. As shown in **Figure 5**, the majority of velocity values was allocated at a low-speed level (around 0) in the preferred movement for both children with ASD and TD. In addition, the velocity distribution between the

complex and the preferred movement in the children with ASD looked similar, but the difference in the TD group was much greater. In other words, **Figure 5** qualitatively illustrates that the participants with ASD are less likely to shift from their preferred movement patterns. Strictly speaking, however, the velocity distribution of complex movements should be compared with that of the preferred movement of the same individual. Only in this way the deviation from the preferred movement could be precisely calculated. Future studies that will explore restricted kinematics are encouraged to record the preferred movement of participants as a baseline to confirm whether lower velocity entropy could be explained by the incapacity of switching from preferred movement in children with ASD.

Limitations and Future Directions

The RBS-R scale was rated by caregivers to evaluate overt behavioral presentations of RRB in children with ASD. No significant correlation between velocity entropy and RBS-R scores seemed to indicate that velocity entropy was not related to the phenomenology of RRB. However, caution needs to be taken to make such a conclusion because of the fact that the sample size of this study was relatively small, and that Spearman's correlation analysis is a conservative test to reveal a significant correlation between these two variables. A larger sample of participants with ASD could be tested in the future to further examine whether velocity entropy is associated with behavioral presentations of RRB reported by caregivers.

In our experimental design, it was hard to rule out the possibility that the lower velocity entropy was caused by a lack of motivation in the participants with ASD, as the motivation level of both groups of participants was not measured. However, the result that only velocity entropy, and not amplitude entropy, was lower in ASD as compared with TD indicated that the participants with ASD were equally motivated to change oscillation amplitude in order to perform a complex movement as possible. However, it is still strongly recommended that future studies incorporate motivation measures in the experiment to verify whether motivation plays a major role.

Our study included children with at least average non-verbal IQ to ensure the compliance of participants with ASD with the instructions. Since ASD displays significant heterogeneity (Jacob et al., 2019), whether our findings could be generalized to the whole ASD population requires further investigation. The DSM-V criteria classify patients with ASD into three severity levels depending on the condition of social communication and RRBs (American Psychiatric and Association, 2013). Future studies could be conducted to investigate whether kinematic restrictedness could predict the level of RRBs by examining individuals with ASD but with different severity. If this holds true, kinematic restrictedness could be potentially used to quantify RRBs in ASD.

This study used a LeapMotion sensor to collect data. As compared with other motion capture systems (e.g., Vicon and Optotrack), LeapMotion exhibits a greater advantage in terms of portability and cost (Shafritz et al., 2008). In addition, the contactless and calibration-free characteristics might make this instrument particularly useful for individuals with ASD, since greater difficulty would be experienced when instructing these people to wear devices/markers or perform calibrations. However, previous studies have reported inconsistent findings regarding the accuracy of the LeapMotion sensor (Weichert et al., 2013; Guna et al., 2014; Niechwiej-Szwedo et al., 2018; Fazeli and Peng, 2021). Some studies reported the high accuracy of this instrument in data collection (Weichert et al., 2013; Guna et al., 2014). For instance, Weichert et al. (2013) evaluated the accuracy and repeatability of the LeapMotion sensor in both static and dynamic tasks using an industrial robot with a reference pen. An average error of 0.2 mm in static tasks and 1.2 mm in dynamic tasks was reported for the LeapMotion sensor (Weichert et al., 2013). As a comparison, a greater error has been reported in other studies. For example, Niechwiej-Szwedo et al. (2018) examined the accuracy of the LeapMotion sensor during the performance of visually guided upper limb movements. Their results showed that the spatial and temporal errors were between 2–5 cm and 40 ± 44 ms, respectively. The average error in peak velocity was 0.024 ± 0.103 m/s (Niechwiej-Szwedo et al., 2018). In this study, our results showed that significant group differences existed across a wide range of the velocity spectrum ([0, 0.6] and [1.2, 2.4] m/s), which is much larger than the error in velocity reported by Niechwiej-Szwedo et al. (2018). Thus, it is assumed that the general pattern of our results might not be severely affected by the error of LeapMotion in data collection. However, strictly speaking, the accuracy of LeapMotion in our experiment should be validated by comparing it with other precise reference systems for motion capture. Future studies that will use LeapMotion in both research and practice might take into account the accuracy of this instrument.

The participants performed arm oscillations without having the hand constrained. In other words, their hands could move freely in different directions. Previous studies have mainly focused on investigating restricted kinematics in unintentional movements (Fournier et al., 2014; Li et al., 2019; Zhao et al., 2021). As the objective and the innovation of this study, we only explored restricted kinematics in volitional movements. In our experiment, the participants were particularly instructed to perform hand oscillations in the left-right direction. This suggests that the left-right direction captured the volitional movement and that movements on other dimensions could be viewed as unintentional. Thus, only movements in the left-right direction were analyzed in this study. All these relevant studies including ours suggest that restrictedness might widely exist in the kinematics of people with ASD. This information is useful for researchers to seek behavioral markers of ASD. Future studies might consider exploring restrictedness in various motor tasks with individuals with ASD.

CONCLUSION

Consistent with the findings on restrictedness in postural control strategy and head movement (Fournier et al., 2014; Li et al., 2019; Zhao et al., 2021), our study demonstrated the existence of kinematic restrictedness in children with ASD when performing volitional complex arm movements. The exploration of restricted

kinematics underlies the possibility of developing an objective and automatic assessment of RRBs in ASD. However, our study could be improved in terms of recruiting a larger sample of participants, measuring the level of motivation, and collecting both complex and preferred movements of the same participant.

DATA AVAILABILITY STATEMENT

The datasets presented in this article are not readily available because participants did not give consent to share data. Requests to access the datasets should be directed to the corresponding author.

ETHICS STATEMENT

The studies involving human participants were reviewed and approved by the Institutional Review Board of Shenzhen University. Written informed consent to participate in this study was provided by the participants' legal guardian/next of kin.

AUTHOR CONTRIBUTIONS

ZZ, XZ, and JL were involved in the experimental design and recruitment of participants. ZZ, HT, and XH analyzed the movement data and performed statistics. ZZ, XZ, XQ, and QP drafted and revised the manuscript. All authors contributed to the article and approved the submitted version.

FUNDING

This study was financially supported by the National Natural Science Foundation of China (No. 82171539), the SZU funding project (No. 860-000002110259), the Shenzhen Science and Technology Innovation Commission of (Nos. JCYJ20190808115205498 and JCYJ20180305164359668), Sanming Project of Medicine in Shenzhen (No. SZSM201612079), Key Realm R&D Program of Guangdong Province (No. 2019B030335001), Shenzhen Key Medical Discipline Construction Fund (No. SZXK042), and Shenzhen Double Chain Grant [2018]256.

ACKNOWLEDGMENTS

The authors would like to thank Xianpeng Zhang, Zeming Huang, Chuang Luo, and Jian Cai for data collection, and Dongsheng Peng for conducting part of the data analysis.

REFERENCES

American Psychiatric and Association (2013). *Diagnostic and Statistical Manual of Mental Disorders*, 5th Edn. Arlington, VA: American Psychiatric Publishing. doi: 10.1176/appi.books.9780890425596

Baron-Cohen, S. (1989). Do autistic children have obsessions and compulsions? *Br. J. Clin. Psychol.* 28, 193–200. doi: 10.1111/j.2044-8260.1989.tb01369.x

Bates, D., Mächler, M., Bolker, B. M., and Walker, S. C. (2015). Fitting linear mixed-effects models using lme4. *J. Stat. Softw.* 67, 1–48. doi: 10.18637/jss.v067.i01

Bodfish, J. W., Symons, F. J., Parker, D. E., and Lewis, M. H. (2000). Varieties of repetitive behavior in autism: comparisons to mental retardation. *J. Autism Dev. Disord.* 30, 237–243. doi: 10.1023/A:1005596502855

Bojanek, E. K., Wang, Z., White, S. P., and Mosconi, M. W. (2020). Postural control processes during standing and step initiation in autism spectrum disorder. *J. Neurodev. Disord.* 12:1. doi: 10.1186/s11689-019-9305-x

Clausius, R. (1867). *The Mechanical Theory of Heat - with its Applications to the Steam Engine and to Physical Properties of Bodies*. London: John van Voorst.

Corbett, B. A., Constantine, L. J., Hendren, R., Rocke, D., and Ozonoff, S. (2009). Examining executive functioning in children with autism spectrum disorder, attention deficit hyperactivity disorder and typical development. *Psychiatry Res.* 166, 210–222. doi: 10.1016/j.psychres.2008.02.005

Corsello, C. M. (2005). Early intervention in autism. *Infants Young Children* 18, 74–85. doi: 10.1097/00001163-200504000-00002

D'Cruz, A.-M., Ragozzino, M. E., Mosconi, M. W., Shrestha, S., Cook, E. H., and Sweeney, J. A. (2013). Reduced behavioral flexibility in autism spectrum disorders. *Neuropsychology* 27, 152–160. doi: 10.1037/a0031721

Esposito, G., and Venuti, P. (2008). Analysis of toddlers' gait after six months of independent walking to identify autism: a preliminary study. *Percept. Mot. Skill* 106, 259–269. doi: 10.2466/pms.106.1.259-269

Fazeli, H. R., and Peng, Q. (2021). Estimation of spatial-temporal hand motion parameters in rehabilitation using a low-cost noncontact measurement system. *Med. Eng. Phys.* 90, 43–53. doi: 10.1016/j.medengphy.2021.02.005

Fournier, K. A., Amano, S., Radonovich, K. J., Bleser, T. M., and Hass, C. J. (2014). Decreased dynamical complexity during quiet stance in children with autism spectrum disorders. *Gait Posture* 39, 420–423. doi: 10.1016/j.gaitpost.2013.08.016

Fournier, K. A., Hass, C. J., Naik, S. K., Lodha, N., and Cauraugh, J. H. (2010). Motor coordination in autism spectrum disorders: a synthesis and meta-analysis. *J. Autism. Dev. Disord.* 40, 1227–1240. doi: 10.1007/s10803-010-0981-3

Fox, J., Friendly, M., and Weisberg, S. (2013). Hypothesis tests for multivariate linear models using the car package. *R J.* 5, 39–52. doi: 10.32614/RJ-2013-004

Fuentes, C. T., Mostofsky, S. H., and Bastian, A. J. (2009). Children with autism show specific handwriting impairments. *Neurology* 73, 1532–1537. doi: 10.1212/WNL.0b013e3181c0d48c

Guna, J., Jakus, G., PogacNik, M., Toma, I. S., and Sodnik, J. (2014). An analysis of the precision and reliability of the leap motion sensor and its suitability for static and dynamic tracking. *Sensors* 14, 3702–3720. doi: 10.3390/s140203702

Holt, K. G., Jeng, S. F., Ratcliffe, R., and Hamill, J. (1995). Energetic cost and stability during human walking at the preferred stride frequency. *J. Mot. Behav.* 27, 164–178. doi: 10.1080/00222895.1995.9941708

Hutt, C., Hutt, S. J., Lee, D., and Ounsted, C. (1964). Arousal and childhood autism. *Nature* 204, 908–909. doi: 10.1038/204908a0

Jacob, S., Wolff, J. J., Steinbach, M. S., Doyle, C. B., Kumar, V., and Elison, J. T. (2019). Neurodevelopmental heterogeneity and computational approaches for understanding autism. *Transl. Psychiatry* 9:63. doi: 10.1038/s41398-019-0390-0

Kanner, L. (1943). Autistic disturbances of affective contact. *Nervous Child* 2, 217–250.

Kay, B. A., Kelso, J. A., Saltzman, E. L., and Schöner, G. (1987). Space–time behavior of single and bimanual rhythmical movements: data and limit cycle model. *J. Exp. Psychol. Hum. Percept. Perform.* 13, 178–192. doi: 10.1037/0096-1523.13.2.178

Kim, S. H., and Lord, C. (2010). Restricted and repetitive behaviors in toddlers and preschoolers with autism spectrum disorders based on the Autism Diagnostic Observation Schedule (ADOS). *Autism Res.* 3, 162–173. doi: 10.1002/aur.142

Klin, A., Danovitch, J. H., Merz, A. B., and Volkmar, F. R. (2007). Circumscribed interests in higher functioning individuals with autism spectrum disorders: an

exploratory study. *Res. Pract. Persons Severe Disabl.* 32, 89–100. doi: 10.2511/rpsd.32.2.89

Kolmogorov, A. N. (1959). Entropy per unit time as a metric invariant of automorphism. *Doklady Akademii Nauk Sssr* 124, 754–755.

Lam, K. S., and Aman, M. G. (2007). The repetitive behavior scale-revised: independent validation in individuals with autism spectrum disorders. *J. Autism Dev. Disord.* 37, 855–866. doi: 10.1007/s10803-006-0213-z

Li, Y., Mache, M. A., and Todd, T. A. (2019). Complexity of center of pressure in postural control for children with autism spectrum disorders was partially compromised. *J. Appl. Biomech.* 35, 190–195. doi: 10.1123/jab.2018-0042

Lopez, B. R., Lincoln, A. J., Ozonoff, S., and Lai, Z. (2005). Examining the relationship between executive functions and restricted, repetitive symptoms of autistic disorder. *J. Autism Dev. Disord.* 35, 445–460. doi: 10.1007/s10803-005-5035-x

Niechwiej-Szwedo, E., Gonzalez, D., Nouredanesh, M., and Tung, J. (2018). Evaluation of the leap motion controller during the performance of visually-guided upper limb movements. *PLoS One* 13:e0193639. doi: 10.1371/journal.pone.0193639

Pierce, K., and Courchesne, E. (2001). Evidence for a cerebellar role in reduced exploration and stereotyped behavior in autism. *Biol. Psychiatry* 49, 655–664. doi: 10.1016/S0006-3223(00)01008-8

Pyles, D. A., Riordan, M. M., and Bailey, J. S. (1997). The stereotypy analysis: an instrument for examining environmental variables associated with differential rates of stereotypic behavior. *Res. Dev. Disabil.* 18, 11–38. doi: 10.1016/S0891-4222(96)00034-0

R Core Team (2013). *R: a Language and Environment for Statistical Computing*. Vienna: R foundation for statistical computing.

Repp, A. C., Karsh, K. G., Deitz, D. E. D., and Singh, N. N. (1992). A study of the homeostatic level of stereotypy and other motor movements of persons with mental handicaps. *J. Intellect. Disabil. Res.* 36, 61–75. doi: 10.1111/j.1365-2788.1992.tb00471.x

Schmidt, R. C., Shaw, B. K., and Turvey, M. T. (1993). Coupling dynamics in interlimb coordination. *J. Exp. Psychol. Hum. Percept. Perform.* 19, 397–415. doi: 10.1037/0096-1523.19.2.397

Shafritz, K. M., Dichter, G. S., Baranek, G. T., and Belger, A. (2008). The neural circuitry mediating shifts in behavioral response and cognitive set in Autism. *Biol. Psychiatry* 63, 974–980. doi: 10.1016/j.biopsych.2007.06.028

Shannon, C. E., and Shannon, C. E. (1948). A mathematical theory of communication. *Bell Syst. Technical J.* 5, 3–55. doi: 10.1002/j.1538-7305.1948.tb01338.x

Shattuck, P. T., Durkin, M., Maenner, M., Newschaffer, C., Mandell, D. S., Wiggins, L., et al. (2009). Timing of identification among children with an autism spectrum disorder: findings from a population-based surveillance study. *J. Am. Acad. Child Adolesc. Psychiatry* 48, 474–483. doi: 10.1097/CHI.0b013e31819b3848

Słowiński, P., Zhai, C., Alderisio, F., Salesse, R., Gueugnon, M., Marin, L., et al. (2016). Dynamic similarity promotes interpersonal coordination in joint action. *J. R. Soc. Interface* 13:20151093. doi: 10.1098/rsif.2015.1093

Tanimura, Y., Yang, M. C., and Lewis, M. H. (2008). Procedural learning and cognitive flexibility in a mouse model of restricted, repetitive behaviour. *Behav. Brain Res.* 189, 250–256. doi: 10.1016/j.bbr.2008.01.001

Temprado, J. J., Zanone, P. G., Monno, A., and Laurent, M. (1999). Attentional load associated with performing and stabilizing preferred bimanual patterns. *J. Exp. Psychol. Hum. Percept. Perform.* 25, 1579–1594. doi: 10.1037/0096-1523.25.6.1579

Turner, M. (1999). Annotation: repetitive behaviour in autism: a review of psychological research. *J. Child Psychol. Psychiatry* 40, 839–849. doi: 10.1111/1469-7610.00502

Weichert, F., Bachmann, D., Rudak, B., and Fisseler, D. (2013). Analysis of the accuracy and robustness of the leap motion controller. *Sensors* 13, 6380–6393. doi: 10.3390/s130506380

Wiggins, L. D., Baio, J., and Rice, C. (2006). Examination of the time between first evaluation and first autism spectrum diagnosis in a population-based sample. *J. Dev. Behav. Pediatr.* 27, S79–S87. doi: 10.1097/00004703-200604002-00005

Zhao, Z., Salesse, R. N., Qu, X., Marin, L., Gueugnon, M., and Bardy, B. G. (2020). Influence of perceived emotion and gender on social motor coordination. *Br. J. Psychol.* 111, 536–555. doi: 10.1111/bjop.12419

Zhao, Z., Zhu, Z., Zhang, X., Tang, H., Xing, J., Hu, X., et al. (2021). Atypical head movement during face-to-face interaction in children with autism spectrum disorder. *Autism Res.* 14, 1197–1208. doi: 10.1002/aur.2478

Conflict of Interest: The authors declare that the research was conducted in the absence of any commercial or financial relationships that could be construed as a potential conflict of interest.

frontiers in Human Neuroscience

REVIEW
published: 17 January 2022
doi: 10.3389/fnhum.2021.789467

Rhythm and Music-Based Interventions in Motor Rehabilitation: Current Evidence and Future Perspectives

*Thenille Braun Janzen[1], Yuko Koshimori[2,3], Nicole M. Richard[2,4] and Michael H. Thaut[2,5]**

[1] Center of Mathematics, Computing and Cognition, Universidade Federal do ABC, São Bernardo do Campo, Brazil, [2] Music and Health Science Research Collaboratory, Faculty of Music, University of Toronto, Toronto, ON, Canada, [3] Brain Health Imaging Centre, CAMH, Toronto, ON, Canada, [4] Faculty of Music, Belmont University, Nashville, TN, United States, [5] Rehabilitation Sciences Institute, University of Toronto, Toronto, ON, Canada

Research in basic and clinical neuroscience of music conducted over the past decades has begun to uncover music's high potential as a tool for rehabilitation. Advances in our understanding of how music engages parallel brain networks underpinning sensory and motor processes, arousal, reward, and affective regulation, have laid a sound neuroscientific foundation for the development of theory-driven music interventions that have been systematically tested in clinical settings. Of particular significance in the context of motor rehabilitation is the notion that musical rhythms can entrain movement patterns in patients with movement-related disorders, serving as a continuous time reference that can help regulate movement timing and pace. To date, a significant number of clinical and experimental studies have tested the application of rhythm- and music-based interventions to improve motor functions following central nervous injury and/or degeneration. The goal of this review is to appraise the current state of knowledge on the effectiveness of music and rhythm to modulate movement spatiotemporal patterns and restore motor function. By organizing and providing a critical appraisal of a large body of research, we hope to provide a revised framework for future research on the effectiveness of rhythm- and music-based interventions to restore and (re)train motor function.

Keywords: Rhythmic Auditory Stimulation, music-based interventions, Neurologic Music Therapy (NMT), rehabilitation, movement, gait, upper extremities, auditory-motor entrainment

OPEN ACCESS

Edited by:
Nadia Dominici, VU Amsterdam, Netherlands

Reviewed by:
Joon-Ho Shin, National Rehabilitation Center, South Korea
Valérie Cochen De Cock, Beau-Soleil Clinic, France

***Correspondence:**
Michael H. Thaut
michael.thaut@utoronto.ca

Specialty section:
This article was submitted to Motor Neuroscience, a section of the journal Frontiers in Human Neuroscience

Received: *05 October 2021*
Accepted: *27 December 2021*
Published: *17 January 2022*

Citation:
Braun Janzen T, Koshimori Y, Richard NM and Thaut MH (2022) Rhythm and Music-Based Interventions in Motor Rehabilitation: Current Evidence and Future Perspectives. Front. Hum. Neurosci. 15:789467. doi: 10.3389/fnhum.2021.789467

INTRODUCTION

Brain and clinical research conducted over the past 25 years have provided a new understanding of the capabilities of music to engage and shape non-musical perceptual, cognitive, language, and motor functions to effectively support brain recovery processes (Thaut, 2010; Koshimori and Thaut, 2018, 2019; Altenmüller and James, 2020; Thaut and Koshimori, 2020; Chatterjee et al., 2021). In the context of motor rehabilitation, the finding that musical rhythm entrains movement in patients with neurological disorders opened new frontiers for the use of rhythm and music as a continuous

time reference to prime the motor system and re-program the execution of movement patterns (Thaut et al., 1996, 2015).

Music is a potent driving force for movement. Synchronization of body movements to external rhythmic auditory stimuli, such as music or a metronome, is possible because the regular and predictable rhythmic structure of the music is readily and precisely detected by the auditory system, inducing entrainment of neuronal activity in auditory and motor regions of the brain involved in rhythm perception and movement production (Thaut et al., 2015; Damm et al., 2020). Growing experimental evidence of the effect of rhythmic entrainment on movement spatiotemporal patterns and the current advances of the neural underpinnings of auditory-motor coupling have informed the development of theory-driven interventions that have been tested in a large number of studies.

In this paper, we review recent studies focusing on four evidence-based interventions using rhythm and active music playing to improve motor functions following central nervous injury and/or degeneration: respectively, Rhythmic Auditory Stimulation, and Music-supported Therapy, Therapeutic Instrumental Music Performance, and Patterned Sensory Enhancement (**Table 1**). This paper aims to provide a critical narrative review of the current literature on the effects of rhythm- and music-based interventions for motor rehabilitation in a wide range of clinical populations (e.g., Parkinson's Disease, stroke, cerebral palsy, traumatic brain injury, and multiple sclerosis) as well as aging. Additionally, considering that evidenced-based practices are built on ongoing fundamental brain research and theories, we briefly overview recent neurophysiological and neuroimaging evidence of the potential mechanisms underlying the effectiveness of rhythm and music in shaping movement timing and control. To finalize, we highlight research questions and methodological concerns that should be on the agenda for future research. By organizing and providing a critical appraisal of a large body of research, we hope to provide a revised framework for future research on the effectiveness of rhythm- and music-based interventions to restore and (re)train motor function.

CLINICAL APPLICATIONS

Rhythmic Auditory Stimulation

The presentation of rhythmic auditory cues as means to facilitate movement and promote sustained functional changes in patients with motor impairment has been extensively investigated (reviewed in Sihvonen et al., 2017; Ghai et al., 2018a; Ghai and Ghai, 2019; Schaffert et al., 2019). Rhythmic Auditory Stimulation (RAS) is a Neurologic Music Therapy (NMT) rehabilitation technique that involves the presentation of auditory rhythmic cues in the form of repetitive isochronous pulses (e.g., metronome clicks) or metrically accentuated music with an embedded metronome to promote auditory-motor entrainment of intrinsically rhythmic movements (Thaut and Hoemberg, 2014; Thaut et al., 2015). Typically, rhythmic cues are matched to the individual's preferred cadence and, once the movement is entrained to the external cues, the rhythm is gradually increased or decreased by 5–10% over baseline (Thaut et al., 1996; Nombela et al., 2013).

A series of seminal research studies conducted in the 1990s demonstrated that auditory rhythms prime the motor system by providing anticipatory time cues that allow movement planning and preparation, thus helping to regulate walking timing and pace in healthy older adults as well as in individuals with Parkinson's Disease (Thaut et al., 1996; McIntosh et al., 1997), stroke (Thaut et al., 1993, 1997; Prassas et al., 1997), traumatic brain injury (Hurt et al., 1998) and cerebral palsy (Thaut et al., 1998). These findings have been replicated in an increasing number of studies, building a robust body of experimental and clinical evidence on the application of RAS as a rehabilitation tool for gait disorders in Parkinson's Disease (Ghai et al., 2018a), stroke (Ghai and Ghai, 2019), traumatic brain and spinal cord injury (Magee et al., 2017), multiple sclerosis (Ghai and Ghai, 2018), cerebral palsy (Ghai et al., 2018b), and older adults (Ghai et al., 2018c). As the scope of this paper does not allow for a thorough description of all clinical research published to date – many of which have already been examined in past systematic reviews and meta-analyses – in the following sections we highlight findings that have been consistently reported across studies and focus the review on articles published in English in the past 5 years (**Supplementary Table 1**). Our goal is to underline points of consensus in the literature and call attention to areas of research that are yet to be fully explored (**Table 2**).

Parkinson's Disease

Parkinson's Disease (PD) is characterized primarily by a dysfunctional basal ganglia system that results in motor impairments including rigidity, bradykinesia, and/or resting tremor in the early disease stage. In advanced PD, recurrent falls, postural impairment, unstable balance, and freezing of gait (FOG) are often observed in addition to gait dysfunctions such as reduced gait velocity and stride length, increased cadence, and irregular timing of walking pace (Morris et al., 1994, 2001; Luquin et al., 2017). Typically, the primary treatment for motor symptoms in PD includes pharmacological interventions, such as dopamine replacement therapy (Oakes et al., 2004; Fasano et al., 2012). However, motor symptoms observed in more advanced cases tend to have limited responses to conventional therapies (Luquin et al., 2017).

Recent meta-analyses and systematic reviews agree that RAS is an effective tool to improve spatiotemporal gait parameters, enhancing gait velocity and stride length, and reducing gait cadence (reviewed in Spaulding et al., 2013; Rocha et al., 2014; Ghai et al., 2018a; Zhou et al., 2021). Studies repeatedly show that, in the presence of auditory rhythmic cues, PD patients typically walk faster and with increased step length. According to Ghai et al. (2018a), a clinical dosage of three to five 20–40 min-sessions per week is most effective for this population.

More recently, there is growing evidence that RAS training is effective to improve motor function such as balance, FOG, motor performance, and recurrence of falls. A recent randomized control trial (RCT) included 154 participants with early to mid-stage PD (H&Y 1–3) who were assigned to three different interventions: multimodal balance training with RAS

TABLE 1 | Description of interventions.

Intervention	Description
Rhythmic Auditory Stimulation (RAS) (Thaut et al., 1996)	RAS is a Neurologic Music Therapy rhythm-based rehabilitation technique designed to facilitate the rehabilitation of intrinsically rhythmic movements through rhythmic auditory cues, such as metronome beats or music with embedded metronome. The rhythmic cues are first matched to each patient's preferred gait cadence and gradually increased/decreased 5–10% to encourage rhythmic entrainment.
Music-supported Therapy (MST) (Schneider et al., 2007)	MST is based on music playing as a rehabilitation tool to train fine and gross movement of the paretic upper extremity. Training sessions consist of playing an electronic keyboard and/or drum pads where exercises involve melodic sequences that vary in the number of tones, movement velocity, and type of movement. Exercises progressively increase in difficulty until patients learn to play songs.
Therapeutic Instrumental Music Performance (TIMP) (Thaut and Hoemberg, 2014)	TIMP is a Neurologic Music Therapy technique that involves playing musical instruments to exercise and stimulate functional movement patterns. In this technique, musical instruments such as drums or keyboard are not played in a traditional manner but are rather placed in strategic locations relative to the patient's body to train range of motion, endurance, strength, functional hand movements, finger dexterity, and limb coordination. Training exercises involve a strong rhythmic component whereby metronome or music are used to provide rhythmic cues to facilitate auditory-motor entrainment. Cueing frequency is initially matched to the patient's comfort level and gradually decreased/increased depending on the therapy goal.
Patterned Sensory Enhancement (PSE) (Thaut and Hoemberg, 2014)	PSE is a Neurologic Music Therapy technique that takes advantage of the rhythmic, melodic, harmonic, and dynamic-acoustical elements of music to provide temporal, spatial, and force cues. This technique uses musical patterns to structure and regulate movement patterns and can be applied to movements that are not rhythmical by nature (e.g., arm and hand movements, functional movement sequences such as dressing or sit-to-stand transfers).

TABLE 2 | Current state of knowledge: summary of current findings on the therapeutic effects of rhythm- and music-based interventions (RAS, MST, TIMP, and PSE) on motor rehabilitation.

	Main Findings
Rhythmic Auditory Stimulation (RAS)	∘ There is consistent evidence supporting the use of RAS for gait training in PD and sub-acute stroke, with repeated reports of significant improvements in gait spatiotemporal parameters (velocity, cadence, stride length). ∘ Recent studies with PD patients suggest positive effects on balance, freezing of gait, overall motor functioning, fear of fall, and number of falls. ∘ Emerging findings indicate that RAS optimizes conventional therapies, such as Deep Brain Stimulation, treadmill training, and motor imagery. ∘ However, there is a paucity of randomized controlled studies on the effectiveness of RAS for the treatment of gait impairments in acute stages of stroke, TBI, MS, CP, dementia or Alzheimer's Disease, and older adults. Limited research is available on the effectiveness of RAS for the treatment of gait impairment in children.
Music-supported Therapy (MST)	∘ There is a strong body of research on the effectiveness of MST to improve functional movements of the paretic upper extremity in sub-acute and chronic stroke. However, there are no clinical studies in other populations. ∘ Further research is needed to better determine optimal MST treatment intensity and duration depending on the stroke stage. ∘ In relation to the application of music practice (e.g., piano/keyboard lessons, drumming), there is currently little research evidence on the effectiveness of active music playing to improve motor function in CP, TBI, MS, and older adults.
Therapeutic Instrumental Music Performance (TIMP)	∘ There is emerging evidence on the benefits of TIMP for upper extremity rehabilitation in stroke, with preliminary results suggesting significant improvements in fine and gross motor function. ∘ Recent studies indicate the feasibility of TIMP-based interventions for CP and PD; however, little is yet known about the potential application in other populations.
Patterned Sensory Enhancement (PSE)	∘ There is growing evidence of the benefits of rhythmically cued PSE exercises to improve upper extremity function in stroke, with recent findings showing associations between improved function and better regulation of muscle activation patterns of the paretic limb. ∘ Initial findings also demonstrate the effectiveness of PSE training for gross motor capacity for sit-to-stand movements in CP. No studies are yet available on other clinical populations.

and without RAS, and an educational program as a control intervention (Capato et al., 2020a). The training consisted of two 45-min weekly sessions over 5 weeks. RAS was presented using a metronome with varying speeds depending on the type of exercise. Results indicated that both active interventions provided significant improvement on balance at post-training compared to baseline and to control. However, balance improvement was greater for the RAS group compared to the group that received training without rhythmic cues. Another notable benefit of the RAS-assisted balance training was that only the RAS group showed a carry-over effect at a 6-month follow-up compared to the baseline measurement. This same multimodal balance training with and without RAS was implemented with more severe cases of PD (H&Y 4) (Capato et al., 2020b). Similarly, the results indicated positive effects from both active interventions in improving balance, however, the beneficial effects were maintained only in the RAS group at the 6-month follow-up.

Rhythmic auditory cueing has been shown to effectively improve FOG (Capato et al., 2020a; Horin et al., 2020; Naro et al., 2020; for a review of earlier studies, see Ginis et al., 2018). Capato et al. (2020a) reported that the benefits of treadmill training with RAS were observed in PD patients with and without FOG. It has also been demonstrated that RAS-assisted interventions reduce the scores of MD-UPDRS III (Bailey et al., 2018; Calabrò et al., 2019; Naro et al., 2020). Importantly, the benefits of RAS training on the MD-UPDRS III were retained at a 6-month follow-up (Capato et al., 2020a) and at a 1-month follow-up in more severe PD (Capato et al., 2020b), results which were not observed in the active control groups without RAS. Interestingly,

emerging evidence also suggests that RAS training complements the effects of conventional therapies for PD, including deep brain stimulation, by significantly enhancing gait velocity and stability when these interventions are combined (Gooßes et al., 2020; Naro et al., 2020).

Recent evidence also suggests that RAS-assisted gait training significantly reduces patients' overall fear of falling (Thaut et al., 2019; Capato et al., 2020b; Naro et al., 2020; Cochen De Cock et al., 2021) and the number of falls (Thaut et al., 2019). Using a randomized withdrawal/discontinuation design, a recent study investigated the effect of RAS on incidences of falls in 47 participants with moderate to severe stages of PD (H&Y 3 and 4) with a history of falls (Thaut et al., 2019). One group ($n = 25$) trained daily with RAS for 24 weeks, while the other group ($n = 22$) undertook the same training but discontinued the protocol between weeks 8 and 16 and then resumed the training for the last 8 weeks of the intervention. During the training, participants walked for 30 min in a home-based environment with a metronome click embedded in folk and classical instrumental music with a strong 2/4 tempo. The first 8 weeks of training significantly reduced the number of falls in both groups. Discontinuation of the RAS training between weeks 8 and 16 resulted in a significant increase in incidences of falls in the control group. Moreover, once RAS training resumed, the number of falls decreased again in the control group.

The effects of auditory cueing on stride length variability, on the other hand, have shown inconsistent results. Some studies report improvements (Dalla Bella et al., 2017; Chang et al., 2019; Erra et al., 2019; Park et al., 2021) while others report that external auditory rhythm increases stride variability (Harrison et al., 2019; Lirani-Silva et al., 2019; Horin et al., 2020). This inconsistency in the results may be partly due to the selected rhythm cadence. Studies reporting beneficial effects typically employ individualized optimal tempi based on participant's preferred cadence (e.g., ±10% of preferred cadence), whereas studies reporting negative effects on stride length variability used tempi of preferred cadence (Harrison et al., 2019; Lirani-Silva et al., 2019; Horin et al., 2020). These findings indicate that it is important to optimize RAS cadence individually to investigate the effects of external auditory cueing on stride length variability. These mixed results may also be associated with significant baseline differences in stride length variability among study participants and with patients' rhythmic abilities and musical training (Dalla Bella et al., 2017; Cochen De Cock et al., 2018). Further research on this topic is warranted.

Stroke

Impairments in motor function such as decreased postural stability, gait dysfunctions, and impaired upper-limb function are common consequences of stroke (Langhorne et al., 2009). Over the years, a considerable body of literature has investigated the effectiveness of RAS for lower limb rehabilitation in stroke (reviewed in Nascimento et al., 2015; Magee et al., 2017; Ghai and Ghai, 2019; le Perf et al., 2019). Clinical research on sub-acute and chronic stroke patients have consistently shown beneficial effects of RAS training on gait spatiotemporal parameters, with significant improvements in gait velocity, stride length, cadence, and postural stability (Nascimento et al., 2015; Magee et al., 2017; Ghai and Ghai, 2019). Overall, it has been suggested that maximum benefits are observed with training protocols consisting of 20- to 40-min sessions repeated three to five times a week (Ghai and Ghai, 2019).

Findings from recent RCTs suggest that RAS training also optimizes the effects of other therapeutic strategies for post-stroke gait (Lee et al., 2018; Mainka et al., 2018; Wang et al., 2021). For instance, Mainka et al. (2018) randomly allocated 35 stroke patients to three groups: treadmill training with or without RAS and therapy based on the Bobath approach. All groups received 4 weeks of intervention in addition to conventional therapy. Rhythmic cues consisted of metronome-embedded music adjusted to each patients' cadence. Post-treatment assessments revealed that gait velocity and cadence improved more in patients in the RAS training compared to the other therapeutic groups. This finding adds to existing evidence of the beneficial effects of combining RAS with other adjunct therapeutic strategies for gait (for further discussion, see Ghai and Ghai, 2019).

The vast majority of studies addressing the effectiveness of RAS on gait focuses on the sub-acute and chronic stages of stroke (Ghai and Ghai, 2019, for review of earlier studies). The first 2 weeks post-stroke is generally defined as the acute stage of stroke, whereas the sub-acute stage refers to 3–11 weeks post-stroke, the early chronic stage comprises 12–24 weeks post-stroke and more than 24 weeks after the stroke is classified as the chronic stage of stroke (Rehme et al., 2012). Recently, Gonzalez-Hoelling et al. (2021) examined the effects of RAS gait training in patients after 4–21 days from stroke onset. Of the 55 participants, 28 in-patients were assigned to a rehabilitation program consisting of conventional therapy combined with RAS gait training conducted for 90 min, three times a week. The duration of the intervention varied according to the patient's hospitalization duration, with participants completing between three and 34 sessions (average of 14 sessions). The study indicated that, at discharge, all patients improved significantly in measures of gait, balance, and walking ability, with no significant differences between conventional therapy combined with RAS training. The authors noted, however, that patients in the combined-RAS training showed more improvement in functional ambulation, walking ability, and independent walking than participants in the conventional rehabilitation program. Nevertheless, Gonzalez-Hoelling and colleagues reported that all patients in the RAS-training group were unable to walk at the baseline assessment and that some patients did not tolerate the additional therapy sessions required for the RAS training, which may have limited the gains in the RAS group. In previous RAS studies with individuals in early post-stroke (Thaut et al., 1997, 2007), only patients who were able to complete five stride cycles with handheld assistance were enrolled in the program. For instance, in Thaut et al. (2007), 43 patients within 21 days of stroke onset received RAS gait training for 30 min, five times a week, for 3 weeks, while another group of acute stroke patients ($n = 35$) received an active control therapy based on Bobath therapy for the same duration. RAS training consisted of music with an embedded metronome matched to each patient's baseline

cadence, with rhythm frequency increased by 5%. Study findings demonstrated higher gains for patients in the RAS training than the control group in measures of gait velocity, stride length, cadence, and gait symmetry after 3 weeks of intervention (Thaut et al., 2007). Taken together, these studies suggest that patients' motor function at enrollment need to be carefully considered for an appropriate adherence to the protocol, ensuring that the duration of the training, task difficulty, and cueing frequency is adjusted according to each individual's cognitive and motor capacity as well as the clinical stage. Moreover, it has also been shown that patients' rhythm abilities may significantly interact with the strength of the response to rhythmic cueing (Crosby et al., 2020). Further research is warranted to better determine the earliest stage at which RAS training would be feasible and effective in stroke.

Other Clinical Applications

The effect of auditory-motor entrainment on gait performance in PD and stroke is well-documented and the clinical evidence of its effectiveness for gait training is robust. In the past years, there has been growing interest in the application of RAS as a motor rehabilitation technique in other neurological conditions where gait and postural stability are affected, including traumatic brain injury, multiple sclerosis, cerebral palsy, Alzheimer's disease, as well as in aging (Thaut and Abiru, 2010; Magee et al., 2017; Sihvonen et al., 2017).

Impairments in gait are common after traumatic brain injury (TBI) resulting in reduced walking speed, stride length, and cadence, as well as increased step-to-step variability and abnormal muscle activation patterns of lower extremity muscles (Williams et al., 2010; Acuña et al., 2018; Galea et al., 2018). To date, few clinical studies have examined the feasibility and effectiveness of RAS training for gait rehabilitation in this population (Hurt et al., 1998; Goldshtrom et al., 2010; Kim et al., 2016; Sheridan et al., 2021; Thompson et al., 2021). In the first study to examine the effects of RAS training in TBI (Hurt et al., 1998), a 5-week home RAS gait training was provided to five community-dwelling adults with post-TBI (experiment 2). All patients in the study were able to walk independently or with an assistive device without physical assistance from the therapist. RAS consisted of metronome pulses embedded in rhythmically accented music set at 5% over each patient's fast walk cadence. Post-test assessments indicated a significant improvement in speed, stride length, and cadence of preferred pace gait after 5 weeks of RAS training (Hurt et al., 1998). Recent case reports and feasibility studies have further examined the potential of RAS training in this population (Sheridan et al., 2021; Thompson et al., 2021). For instance, in Thompson et al. (2021), 10 individuals 1–20 years post-TBI were enrolled in a RAS gait program consisting of daily 30-min training for 2 weeks, totaling 10 treatment sessions. The study pointed to the feasibility of RAS for gait training with those individuals who were able to ambulate for 30 min without assistive devices and reported positive trends toward changes in gait parameters such as velocity, step length, cadence, and 10-min walk speed, with sustained improvements at a 1-week follow-up assessment. More research is needed to build a stronger body of clinical evidence of the potential applications of RAS in TBI gait rehabilitation.

There is increasing research on the potential for RAS to help address gait and postural dysfunctions in multiple sclerosis (MS) (reviewed in Ghai and Ghai, 2018; Vinciguerra et al., 2019; Lopes and Keppers, 2021). MS is a chronic demyelinating disease of the central nervous system affecting sensory, motor, and cognitive functioning (Benedetti et al., 1999; Comber et al., 2017; Oreja-Guevara et al., 2019). Recent studies have shown that persons with MS with mild to moderate motor impairments are able to synchronize their steps to music or a metronome at a range of different tempi (Moumdjian et al., 2019a,b), however, higher gait synchronization is found when the auditory rhythm is set at +8 and +10% of preferred cadence (Moumdjian et al., 2020). Clinical studies have successfully implemented RAS in gait rehabilitation in this clinical population. In Shahraki et al. (2017), 18 patients were randomly allocated to two groups: one group performed gait training with RAS at +10% of preferred cadence for 3 weeks, with 30-min sessions three times a week, while the control group performed similar gait exercises without RAS. The results of the study suggested significant differences between groups, with higher gains in stride length, stride time, cadence, and gait speed in RAS training compared to conventional gait intervention. RAS training also has been shown to complement the effects of other therapeutic strategies, such as motor imagery (Seebacher et al., 2017, 2019) and treadmill training (Maggio et al., 2021). Motor imagery combined with rhythmic cueing was investigated in a large RCT with 112 persons with MS (Seebacher et al., 2017). Participants in the RAS-combined home-based training were asked to kinesthetically imagine the execution of a movement with music or metronome-induced rhythmic auditory cueing for 17 min, six times a week, for a total of 4 weeks. Findings indicated that music- and metronome-cued motor imagery significantly improved gait spatiotemporal parameters compared to control, with positive effects on walking speed and the 6-min walking test, suggesting reduced physical fatigue. Further, results also showed significant improvements in quality of life, pain, physical and mental health in persons with MS after metronome/music-cued motor imagery intervention compared to the control intervention (Seebacher et al., 2017). In a subsequent study, Seebacher et al. (2019) reported that providing additional verbal cues increases the effectiveness of music-cued mental imagery training for individuals with mild to moderate MS. The beneficial effects of gait therapy combined with RAS have also been shown (Maggio et al., 2021). Ten persons with MS were assigned to an intervention consisting of 30 min of treadmill training with RAS conducted three times per week for a total of 8 weeks, while 10 patients received conventional overground gait training for the same amount of time. Post-intervention assessments indicated significant changes from baseline in measures of static and dynamic balance, gait velocity, and mobility for the RAS-combined intervention. Furthermore, results pointed to significant improvements in non-motor aspects, including mood, perception of quality of life, as well as physical and mental health for patients in the RAS training group (Maggio et al., 2021).

To date, there is limited research on the effects of RAS gait training for individuals with cerebral palsy (CP)

(Ghai et al., 2018b, for further review). CP is a developmental disorder characterized by pre/postnatal brain damage and is considered the most common cause of physical disability in childhood, often affecting gait function including shorter step length, increased step variability, poor dynamic gait stability, and slower gait velocity compared to typically developing children at the same age (Katz-Leurer et al., 2009; Pakula et al., 2009; Kurz et al., 2012). Recently, an experimental study investigating the association between rhythm perception and gait characteristics in children with CP and typically developing children reported no significant differences in rhythm perception abilities between groups, also finding that children in both groups successfully synchronized their steps to a metronome 7.5% faster or slower than preferred cadence (Schweizer et al., 2020). Initial research findings indeed reported positive effects of RAS on gait training for children and adolescents with CP (Thaut et al., 1998; Kwak, 2007; Baram and Lenger, 2012). However, no clinical studies on the effects of RAS have been conducted in this pediatric population in the past 5 years, revealing an area yet to be fully explored.

Rhythmic Auditory Stimulation gait training has been examined to some extent in adults with spastic CP (Kim et al., 2011, 2012, 2020; Varsamis et al., 2012; Efraimidou et al., 2016), where deficits in independent walking, bilateral control, as well as pain and fatigue are often associated with a decline in mobility in the adult population. In a series of clinical studies, Kim and colleagues reported that a 3-week RAS training improved functional gait in measures such as cadence, stride length, and gait velocity, also promoting significant kinematic changes of the pelvic and hip movement (Kim et al., 2011, 2012). More recently, Kim et al. (2020) examined whether the musical properties of the rhythmic cues would influence the effectiveness of the training. A total of 13 young adults with diplegic CP received 30 min of RAS training, three times per week for 4 weeks. The rhythmic cues for one group consisted of simple chord progressions emphasizing the metronome tempo, whereas the cues presented to the second group included more complex chord progressions and a melodic structure along with the metronome. Analysis of spatiotemporal and kinematic gait parameters revealed significant improvements in both groups in measures of cadence, velocity, stride length, as well as changes in the minimal flexion angle of the hip joint and increased hip extension at terminal stance. These findings thus corroborate the evidence that the predictable rhythmic structure of the auditory cues is the primary driving agent of change in gait parameters. Nevertheless, the study reported group differences in the range of the ankle motion, with more improvement in maximal ankle plantar flexion in the pre-swing phase in the complex chord group compared to simple chord cues. The authors suggested that musically complex cues may facilitate engagement and enhance the drive to move. Indeed, Thaut et al. (1997) proposed that the musical texture of the cues provide additional timing information that may facilitate detection, anticipation, and synchronization to the rhythmic cues. Further research with biomechanical measures would be of interest to better understand how specific parameters of the acoustic cues can facilitate auditory-motor entrainment.

Gait disturbances, postural instability as well as increased risk of falls are frequently observed in mild to moderate dementia and Alzheimer's disease (AD) as a function of the severity of cognitive impairments (IJmker and Lamoth, 2012; Allali et al., 2016; Castrillo et al., 2016; Kikkert et al., 2016). Wittwer et al. (2013) examined the immediate effects of RAS on gait in a study involving 30 older adults with mild to moderately severe AD who were able to ambulate for 100 m on a level surface without a gait aid. Participants were required to walk over an electronic walkway and synchronize their steps either to music or a metronome matched to each individual's baseline cadence. Assessments of gait spatiotemporal parameters under each condition revealed deleterious effects on gait with a significant decrease in gait velocity and greater stride length variability when walking in time with both types of auditory cues compared to baseline. As discussed earlier, significantly increased gait variability at baseline and the chosen cueing frequency may influence the response to RAS gait training. The authors also raised the possibility that people with dementia may require more practice and longer intervention periods to produce positive benefits on gait parameters (see also Clair and O'Konski, 2006). In a subsequent intervention study, Wittwer et al. (2020) examined the feasibility of a home-based RAS gait training to address movement-related deficits in early AD. Eleven community-dwelling older adults living with AD and able to ambulate were enrolled in an intervention consisting of eight 45-min gait training sessions delivered at home over 4 weeks. Rhythmic cues involved music with a clear temporal structure and progressively modified tempo ($\pm$10% preferred cadence). Post-intervention assessments indicated a significant increase in gait velocity associated with improved stride length after the intervention. Moreover, findings also demonstrated that the home-based gait training was associated with high levels of safety, compliance, adherence, and satisfaction, opening the possibility for further investigation on the effects of RAS gait training for people with AD.

Rhythmic cueing has also been investigated in healthy older adults (reviewed in Ghai et al., 2018c; Thaut and Koshimori, 2020). According to a recent meta-analysis and systematic review, RAS significantly enhances spatiotemporal gait parameters such as gait velocity, cadence, and stride length in older adults ($\geq$60 years old) (Ghai et al., 2018c). However, most studies to date only concern the immediate effects of rhythmic auditory entrainment on gait. The direct effect of rhythmic cueing was the primary focus in recent studies showing positive effects on gait variability (Vitorio et al., 2018) and dynamical postural stability in healthy older adults (Minino et al., 2021). Only one clinical RCT has been conducted to examine the effects of RAS gait training for community-dwelling older adults (Trombetti et al., 2011). In this study, 134 adults were randomly allocated to a music-based intervention or a delayed intervention control group. The intervention consisted of 1-h weekly sessions conducted over a 6-month period whereby participants performed a variety of multitasking exercises, such as walking in synchrony with piano music with changes in rhythmic structure. Assessments conducted after 6 months of training revealed improvements

in gait performance under single- and dual-task conditions, enhanced balance, and a significant reduction in the number of falls and the risk of falling. Moreover, positive benefits persisted after 6 months of intervention (Trombetti et al., 2011). Considering that decreased gait function and balance in aging are important predictors of falls, more research is needed to better understand the effectiveness of RAS intervention on aging gait.

Music-Based Interventions

Music-based interventions have emerged as a promising therapeutic approach for the restoration of upper extremity functional abilities in several neurologic conditions. In the past years, an increasing number of clinical studies have assessed the potential rehabilitative effects of music-based interventions involving active music playing to address fine and gross upper extremity motor deficits, with particular focus on stroke (Zhang et al., 2016; Grau-Sánchez et al., 2020, for review) and cerebral palsy (Alves-Pinto et al., 2016). In the following sections, we review clinical evidence published in the past 5 years on the effects of three music-based interventions for the rehabilitation of discrete and non-rhythmic movements, namely Music-supported Therapy (Schneider et al., 2007), Therapeutic Instrumental Music Performance (TIMP) (Thaut, 2005; Thaut and Hoemberg, 2014), and Patterned Sensory Enhancement (PSE) (Thaut et al., 1991; Thaut and Hoemberg, 2014; **Table 1**). We begin by examining recent literature on stroke and cerebral palsy, which have been at the forefront of research on this topic, followed by an overview of current findings concerning other clinical populations, including Parkinson's Disease, traumatic brain injury, multiple sclerosis, and aging (**Supplementary Table 2**).

Stroke

Motor deficits of the upper extremity are common in patients with stroke and have a relevant impact on patients' activities of daily living, independence, and quality of life (Morris et al., 2013). Motor function recovery for this population relies primarily on motor rehabilitation (Langhorne et al., 2011), thus music-based therapies have received ample research attention in the past years (for discussion, see Thaut and McIntosh, 2014; Zhang et al., 2016; Moumdjian et al., 2017; Chen, 2018; Altenmüller and James, 2020; Grau-Sánchez et al., 2020; Huang et al., 2021).

One of the most investigated music-based interventions to treat upper limb hemiparesis after stroke is Music-supported Therapy (MST) (Schneider et al., 2007; Rodriguez-Fornells et al., 2012; reviewed in Grau-Sánchez et al., 2020). This intervention involves playing a keyboard and/or electronic drum using motor sequences of increasing difficulty to train fine and gross motor skills, respectively. The therapeutic technique is based on the premise that playing musical instruments is an enjoyable activity involving complex and coordinated movements that require auditory-motor coupling and integration through real-time multisensory information (Schneider et al., 2007; Rodriguez-Fornells et al., 2012; Ripollés et al., 2016). Initial clinical research suggested that a rehabilitation regimen consisting of fifteen 30-min sessions of active music playing completed over a period of 3 to 4 weeks, in addition to conventional therapy, is effective to improve upper extremity movement parameters such as speed, precision, and smoothness (Schneider et al., 2007, 2010; Altenmüller et al., 2009). These results have been replicated in a growing body of research showing that this intervention protocol significantly improves functional movements of the paretic upper extremity in subacute as well as in chronic stroke (Chong et al., 2017; Grau-Sánchez et al., 2017, 2018; Fujioka et al., 2018; Ghai et al., 2021; for review of earlier studies, see Grau-Sánchez et al., 2020).

Recently, studies examining the progression and retention of motor gains with music-supported therapy have shown that movement velocity, accuracy, and force are rapidly improved within the first training sessions involving simple movement sequences on the piano (Grau-Sánchez et al., 2017). However, functional gains and transfer to everyday tasks are observed after at least 4 weeks of intervention and are even more noticeable after a second training period, thus suggesting progressive improvements (Grau-Sánchez et al., 2018, 2020). Importantly, recent intervention protocols have indicated that treatment intensity and duration may need to be increased to promote effective motor recovery for patients in the chronic stage of stroke (Grau-Sánchez et al., 2021).

When comparing the effectiveness of music-supported therapy with conventional therapy, a recent RCT has shown that active music playing promotes the same retention of gains as standard rehabilitation programs when the amount of extra therapy received by the control group is the same as the intervention group. Specifically, Grau-Sánchez et al. (2018) randomly assigned 40 subacute stroke patients to two treatment groups: one group received 30-min sessions of music-supported therapy five times per week in addition to their standard rehabilitation program, while the control group received the same amount of additional conventional therapy. Assessments conducted after 4 weeks of intervention and at a 3-month follow-up indicated that both training protocols promoted improvements in motor function and no significant differences between treatment groups were observed at follow-up. Thus, these findings indicate that music-supported therapy is as effective as standard rehabilitation therapy to enhance the motor function and movement kinematics of the paretic upper extremity in the subacute stage of stroke.

There is also increasing research on the potential application of TIMP for upper limb rehabilitation in stroke. TIMP is an NMT technique for sensorimotor training that involves active music playing as a means to train gross or fine motor skills (Thaut and Hoemberg, 2014). Unlike Music-supported Therapy, in this protocol, musical instruments are not played in a conventional way but are rather used as a source of visual, tactile, and auditory feedback as they are positioned in strategic locations relative to the patient's body to train therapeutic meaningful movements that are transferable to real-world applications, such as trunk rotation, shoulder flexion/extension, elbow flexion/extension, forearm supination/pronation, hand grasp and release, finger individuation, and reaching movements. This intervention has been investigated in recent feasibility and randomized pilot studies with subacute and chronic stroke

patients (Raghavan et al., 2016; Street et al., 2018, 2019, 2020; Haire et al., 2021a). In Raghavan et al. (2016), 13 chronic stroke patients completed 45-min group music-based therapy, twice a week, over 6 weeks. The intervention was led by a music therapist and an occupational therapist and included a range of therapeutic meaningful exercises using percussion instruments, piano, and drums to train gross and fine motor skills of the paretic upper extremity. Assessments conducted post-intervention indicated significant improvements from baseline in motor impairment (Fugl-Meyer Test), sensory deficits (Two-point Discrimination test), disability (Modified Ranking Scale), and overall well-being. Importantly, a follow-up assessment suggested retention of gains after 1 year of treatment completion (Raghavan et al., 2016). Haire et al. (2021a) recently examined the effects of a TIMP-based intervention consisting of nine sessions for 30 community-dwelling individuals with sustained unilateral stroke. The study included three groups where active TIMP exercises were combined with mental imagery with and without metronome cueing. The findings indicated significant gains in paretic arm control after 3 weeks of intervention as measured by the Fugl-Meyer and Wolf Motor Function tests.

The feasibility of a TIMP home-based intervention was examined in a study with 10 subacute stroke patients (Street et al., 2018). Analysis of structured interviews indicated that a 6-week intervention for arm rehabilitation was considered highly motivating, with high tolerance and adherence to treatment, as well as non-fatiguing. However, analysis of quantitative data provided inconclusive results. The authors argued that outcome measures, clinical stage, case severity, treatment length, and dosage, should be individually considered to better adjust the intervention to each individual's capacity (Street et al., 2018, 2019). In a subsequent study, the authors provided further considerations on the feasibility of TIMP intervention in different home environments and the adaptability of the exercises for portable electronic devices (iPad) based on two patient cases (Street et al., 2019). Study results indicated significant improvements in motor function after 12 sessions and retention of gains particularly for the patient with less severe impairments at baseline.

Patterned Sensory Enhancement is another NMT intervention that uses rhythmic, melodic, and harmonic elements of music to provide temporal, spatial, and dynamic information about the movement (Thaut et al., 2002). In this technique, a music therapist plays a musical instrument to provide cues to facilitate the timing, force, duration, and direction of movements that are typically discrete and non-rhythmic in nature (Thaut et al., 1991; Thaut and Hoemberg, 2014). Research has shown that cueing cyclical reaching movements of the paretic arm in chronic stroke promotes a significant reduction in trajectory variability and normalizes the velocity and acceleration profiles of arm movement (Thaut et al., 2002). Recent meta-analyses and systematic reviews have indicated that rhythmically cued exercises are indeed effective to improve upper extremity function in stroke (reviewed in Ghai, 2018; le Perf et al., 2019). Clinical evidence supports the use of rhythmic cueing to enhance arm function post-stroke, with significant changes in outcome measures such as the Fugl-Meyer upper extremity assessment, Action arm reaching test, Wolf motor function test, Nine-hole peg test, Stroke impact scale, and elbow range of motion (Ghai, 2018). Optimum training dosage for upper extremity seems to involve 30 min to 1-h training sessions for a minimum of three times a week (Ghai, 2018).

Recent RCTs have provided further evidence of the effects of rhythmically cued PSE training in the recovery of upper limb function. In a recent study (Tian et al., 2020), 15 stroke patients received 30 min of training in addition to conventional therapy, while patients in the control group received 30 min of additional conventional therapy, 5 days per week, for a total of 4 weeks. The training consisted of presenting a metronome with gradually increasing frequency during the performance of gross motor function tasks, such as shoulder flexion/extension or abduction/adduction, elbow flexion/extension, arm-reaching, and grasping tasks. Post-intervention assessments indicated that patients in both groups improved from baseline, however, patients in the rhythmic cued training showed more improvement in motor function assessments including the Fugl-Meyer upper extremity assessment, the Wolf motor function test, and the Barthel Index. Moreover, surface electromyography recordings of the affected biceps and triceps revealed a significant reduction in the co-activation interval of the agonist and antagonist after cued training, particularly during elbow extension movements, which was not observed after conventional therapy. This finding suggests that rhythmically cued training helped regulate the activation pattern of agonist and antagonist muscles of the affected arm, facilitating task-oriented movements of the hemiparetic upper extremity (Tian et al., 2020). Another study examined the immediate effects of different types of auditory cueing on paretic shoulder movements after stroke (Kang et al., 2020). A group of 16 chronic stroke patients performed upper limb movements, such as shoulder abduction, holding, and adduction, in three different cueing conditions: monotonic rhythmic cues (metronome); melodic cues where changes in pitch contour reflected different movement kinematics; and no auditory cueing. Analysis of movement kinematics using inertial measurement units indicated that the musical properties of the rhythmic cues influenced the execution of paretic shoulder movements particularly during the holding phase. Overall, the findings suggested that presenting pitch contour embedded in isochronous rhythm enhanced movement positioning, decreased movement variability, and improved endurance, thus indicating that pitch information may provide additional or more salient information regarding movement spatial location (Kang et al., 2020). These findings seem to be specific to the holding phase of shoulder movement and further research is of interest to better understand how ascending and descending pitch information may affect other kinematic phases of upper limb movements.

It is also worth noting that studies examining music-based interventions for stroke often report non-motor benefits, including improved language skills (Grau-Sánchez et al., 2018), as well as increased quality of life and positive emotions (Fujioka et al., 2018; Grau-Sánchez et al., 2018; Street et al., 2020). A recent study by Haire et al. (2021b) reported significant non-motor benefits in an intervention based on TIMP for stroke patients.

The study protocol involved nine sessions administered over 3 weeks to 30 stroke patients. Post-intervention assessments indicated a positive impact on affect and mood for participants in all groups, while the intervention combined with mental imagery resulted in increased mental flexibility, as measured with the Trail Making Test – part B (Haire et al., 2021b). Given the consistency of findings reporting non-motor benefits of RAS across studies, further research would be of interest to better understand the mechanisms underlying these positive cognitive effects.

Cerebral Palsy

Motor function and posture disorders resulting from brain damage during the development of the nervous system are common impairments that may also be accompanied by sensory, cognitive, and behavioral deficits that are predominantly addressed with rehabilitation (Boyd et al., 2001; Rosenbaum et al., 2007).

Initial clinical evidence has emerged on the effects of active musical instrument playing (i.e., piano or keyboard) to improve manual dexterity, finger, and hand motor function for persons with CP (Chong et al., 2013; Lampe et al., 2015; Alves-Pinto et al., 2016). Alves-Pinto et al. (2017) studied the effects of piano training on sensorimotor skills of a group of 16 individuals with CP (age range: 11–52 years) and a group of six typically developing youth (age range: 7–17 years). All participants received 2 h of piano lessons weekly with a piano teacher for a total of 4 weeks. Assessments using MIDI data indicated a trend toward an improvement in movement variability of keypresses for individuals with CP, however, these changes did not reach statistical significance. The authors argued that the number of sessions offered in the intervention may have not been sufficient to promote significant benefits. Another point to observe is that the primary outcome measure in this study was not a standardized and validated test to clinically evaluate hand/finger motor function, thus it may have not adequately captured possible outcome changes. More recently, Alves-Pinto et al. (2021) examined whether music instrument playing would induce changes in the brain as a result of neuroplastic processes. A single participant (16 years old) with unilateral spastic CP underwent 18 months of individualized piano training with a professional piano teacher. The post-intervention assessment revealed no significant changes in manual function as measured with the Box and Block Test and the Hand Grip assessment. Nevertheless, brain imaging examining white matter structure suggested potential changes in sensorimotor pathways after the intervention. Further research is greatly needed to better determine the best intervention protocol (dosage and duration) and the outcome measures most suitable to assess the effectiveness of active musical instrument playing as a rehabilitation tool in this population.

Recent studies have investigated the effectiveness of TIMP for motor rehabilitation of children and adolescents with CP. In Marrades-Caballero et al. (2018), 18 children and youth with severe bilateral CP aged between 4 and 16 years were randomized to standard physiotherapy treatment (control) while the second group received TIMP intervention in addition to usual care. Results suggested significant motor function improvements from baseline during the first phase of the study in measures of arm and hand positioning for participants who received TIMP while no significant change was observed for those in the control group. Further, these improvements remained stable in a follow-up assessment conducted 16 weeks after treatment was completed. Dogruoz Karatekin and Icagasioglu (2021) reported significant functional gains and improved grip strength, selective strength of the fingers, gross and fine hand motor skills after 3 months of TIMP-based piano intervention in nine adolescents with CP. These findings show promising evidence of the potential of this music-based therapy.

There is also preliminary evidence of the effects of PSE on gross motor capacity and functional strength in children with spastic CP (Peng et al., 2011; Wang et al., 2013), however recent research is limited. Peng et al. (2011) studied the immediate effects of PSE to improve muscle power and movement control during loaded sit-to-stand. It was observed that children who practiced sit-to-stands in the PSE condition presented shorter movement time, improved smoothness of center-of-mass trajectory, and increased extensor power of lower extremities compared to those practicing with no music. A subsequent randomized controlled study was developed to investigate the effects of a 6-week home-based PSE exercise program (Wang et al., 2013). Thirty-six children aged 5 to 13 with spastic diplegia were divided into two groups: a PSE group or a control group where exercises were performed without music. The study results indicated that both groups improved in measures of the Gross Motor Function Measure. However, children who exercised with PSE music presented significantly higher improvements in gross motor capacity than those who practiced without music. Moreover, gains were preserved at a 3-month follow-up (Wang et al., 2013). These findings thus indicate that auditory entrainment might act as guidance thereby improving critical gross motor skills for sit-to-stand movements. Further research would be of interest to examine the feasibility of PSE intervention for upper extremity function in this population.

Other Clinical Applications

Interventions involving active music playing for upper extremity rehabilitation have been extensively implemented in clinical practice (Hurt-Thaut, 2008; Altenmüller and Schlaug, 2015). However, the number of clinical trials examining the effectiveness of these techniques in fine/gross motor function is surprisingly limited and does not seem to reflect the broad use of these therapeutic techniques in the clinical context.

Fine motor disability in PD has recently gained more attention from clinicians and researchers, and preliminary findings suggest that music-based interventions may be particularly well-suited to help address these motor deficits. In a recent case study, Buard et al. (2019b) examined the effects of a TIMP-based protocol consisting of 15 sessions of bimanual exercises using a keyboard, castanets, and other percussion instruments to address fine motor skills in three PD patients. Assessments conducted pre- and post-intervention indicated significant improvements in overall motor function – as shown by a reduction in MD-UPDRS III scores – and increased fine motor skills. Additionally, neuroimaging results revealed significant increase in cortical beta-band activity

and stronger functional connectivity between auditory and motor areas of the brain after 5 weeks of music-based intervention. Piano training has been implemented to address deficits in executive functions in older adults with PD (Bugos et al., 2021). Forty-five PD patients were allocated to a waitlist control group or group piano training consisting of finger dexterity exercises and learning simple piano melodies over 10 days. Cognitive assessments indicated significant improvements in the Stroop test after the training, however, no significant changes were observed in other cognitive measures such as verbal fluency (D-KEFS Verbal Fluency subtest), processing speed and cognitive flexibility (Trail Making Test – Part B, Coding and Symbol Search). No assessment of hand/finger motor function was performed as the study focused on non-motor symptoms of PD. Thus, the effectiveness and clinical guidelines for the application of active music playing for upper extremity rehabilitation in PD are yet to be determined.

Two recent studies investigated the effects of piano training on cognitive functioning in patients with TBI, however, little is yet known about its effectiveness on motor function (reviewed in Mollica et al., 2021). In Vik et al. (2018), an 8-week intervention program based on piano training was implemented for young adults ($n = 7$) with mild TBI. Although motor function was not systematically evaluated, results revealed improvements in measures of verbal learning and significant changes in brain activity in frontal regions during a music listening test (see also Vik et al., 2019). Similar results were reported in a recent RCT (Siponkoski et al., 2020), where 39 patients with moderate to severe TBI received two weekly individual sessions of 60 min duration consisting of learning to play songs on the piano and playing sequences of musical rhythms and musical exercises on the drum. Results indicated significant enhancement in executive function after 3 months of intervention, with carry-over effects at a 3-month post-intervention follow-up. In addition, brain imaging results suggested increased gray matter volume in prefrontal areas, which were correlated with cognitive improvements after the intervention (Siponkoski et al., 2020). On the other hand, no significant changes were observed in upper extremity motor functions. The authors suggested that the intervention targeted primarily cognitive function and that the study inclusion criteria focused on cognitive but not motor deficits, which may have interacted with the effectiveness of the intervention on motor-related outcomes.

The effects of piano playing for upper extremity rehabilitation in MS have been investigated in one RCT (Gatti et al., 2015). Nineteen hospitalized adults were randomly allocated into two groups: one group received 30 min of daily upper-limb rehabilitation based on keyboard music exercises for 3 weeks, while the second group received the same intervention but with the auditory feedback provided by the keyboard turned off. Post-intervention assessments of hand function indicated significant time effects for all outcome measures, however, the change in hand dexterity was significantly greater in the group who received auditory feedback than in the control group. This finding corroborates the results reported in a similar study with stroke patients (Tong et al., 2015) and highlights the key role of auditory-motor coupling to engage multisensory and motor networks during active music playing to promote neurologic recovery.

Clinical research on the application of music-based interventions specifically targeting fine and/or gross upper limb skills in elderly people is limited. Kim et al. (2017) assessed age-related changes in gross motor function with bimanual drumming tasks. Older adults with and without mild dementia performed tasks involving simultaneous or alternated bimanual movements in synchrony with a metronome. Findings revealed significant correlations between synchronization errors committed during bimanual tapping and older adults' performance on cognitive tasks involving executive control and cognitive flexibility. Specifically, the group of adults with mild dementia presented greater synchronization errors and increased variability compared to healthy older adults and a control group of younger adults. In a subsequent study, Kim and Yoo (2020) examined the effects of a dual-task intervention for healthy older adults. Ten adults completed an 8-week intervention involving dual-task exercises such as walking or tapping in synchrony with metronome cues while playing percussion musical instruments with different rhythmic patterns or rhythmically chanting/singing. Assessments conducted pre/post-intervention evaluating gait during dual tasking showed that the intervention group exhibited decreased step length and increased step frequency after training, whereas participants who did not receive the intervention presented opposite gait patterns with increased walking speed and stride length. For the authors, this finding suggests that participants in the intervention group used a compensatory strategy to guarantee safety during cognitively demanding tasks such as walking while playing a musical instrument. Results also demonstrated a significant improvement in tasks requiring executive control of attention for participants in the intervention group, suggesting that the protocol may be effective in improving cognitive processing and gait control, which are critical to prevent falls in this population.

While research on music-based interventions for motor rehabilitation of older adults is scarce, there is growing evidence of the effectiveness of short-term musical training for cognitive rehabilitation in this population (Bugos et al., 2007; Seinfeld et al., 2013; Bugos, 2019; MacRitchie et al., 2020). Although a thorough review of the effectiveness of music-based intervention in cognitive rehabilitation is beyond the scope of this paper (for further discussion, see Hegde, 2014; Sihvonen et al., 2017; Fusar-Poli et al., 2018; Koshimori and Thaut, 2019; Schneider et al., 2019; Mollica et al., 2021), it is of note that recent intervention studies have shown significant improvements in cognitive function in healthy older adults involved in piano training programs (Bugos and Kochar, 2017; Degé and Kerkovius, 2018; Bugos, 2019; Zendel et al., 2019; MacRitchie et al., 2020; Guo et al., 2021; Worschech et al., 2021). For instance, in MacRitchie et al. (2020), 15 older adults (aged 65 years or older) participated in a piano training program consisting of ten 60-min group lessons involving learning to play simple melodies and ensemble playing tasks. Pre/post assessments included the Trail Making Test, the Jebsen Taylor hand function tests, and a visuomotor synchronization task. Results revealed significant gains in visuomotor skills as

indicated by improved scores in Part A of the Trail Making Test after the 10-week intervention. However, no significant changes were observed in measures of fine motor skills. These findings indicate that a short-term intervention may be sufficient to promote positive benefits in cognitive functioning, whereas transfer of skills into general fine motor function may require longer interventions for healthy older adults (MacRitchie et al., 2020). Investigating this hypothesis is crucial to help structure standardized therapeutic protocols for specific treatment targets in this population.

UNDERLYING MECHANISMS

Rhythm- and music-based interventions are complex multimodal rehabilitation techniques that involve multiple active therapeutic elements, varied therapeutic contexts (i.e., individual or group treatments), and treatment plans or musical exercises that are developed to target specific goals, challenges, or symptoms. Thus, all these elements can potentially contribute to the positive changes promoted by music interventions (Sihvonen et al., 2017; Altenmüller and Stewart, 2020; Brancatisano et al., 2020; Grau-Sánchez et al., 2020). The neural mechanisms underlying the motor benefits reviewed here have only started to be uncovered by experimental, neuroimaging, and neurophysiological research conducted in the past years (reviewed in Koshimori and Thaut, 2018; Damm et al., 2020). In the context of motor rehabilitation, there is converging evidence of the capacity for rhythm and music to induce neural entrainment of widely distributed auditory, sensorimotor, and motor networks of brain (Damm et al., 2020), to modulate the dopaminergic mesolimbic system (Koshimori and Thaut, 2018; Damm et al., 2020) – which is notably involved in rhythm perception, reward-based motivated learning, and affective regulation – and to promote structural and functional neuroplastic changes through active engagement with music (Altenmüller and Schlaug, 2015). In the following sections, we briefly overview current neuroimaging and neurophysiological evidence supporting the potential implications of these mechanisms on the effects of rhythm- and music-based intervention.

Auditory-Motor Entrainment: The Role of Beta-Band Modulations

Research evidence suggests that the ability to synchronize bodily movements to external rhythmic stimuli is based on neural entrainment, whereby the repetitive firing of neurons in the brain synchronizes to the rhythm of temporally predictable events (Lakatos et al., 2019). Electrophysiological studies have shown that auditory rhythms induce entrainment in the auditory cortex as the periodicity of the neural response in the auditory system closely matches the frequency of the auditory beat (Nozaradan et al., 2011, 2012; Fujioka et al., 2012a; Nozaradan, 2014; Doelling and Poeppel, 2015; Crasta et al., 2018; Doelling et al., 2019; Bouvet et al., 2020). Moreover, the rhythmic neuronal firing remains phase-locked to the stimulus frequency even when a beat is omitted or after stimulus discontinuation, allowing individuals to predict and anticipate when the next beat will occur (Lakatos et al., 2013; Tal et al., 2017; Nobre and van Ede, 2018).

The predictability of auditory rhythms primes the motor system into a state of readiness to move and provides precise anticipatory time cues whereby movement planning and execution occurs (Thaut et al., 2015; Crasta et al., 2018). For instance, it has been shown that merely listening to auditory rhythms or music engages brain structures involved in the encoding of temporal stimuli and in movement control, such as the premotor cortex, supplementary motor area, basal ganglia, and cerebellum (Grahn and Brett, 2007; Chen et al., 2008a; Bengtsson et al., 2009; Grahn and Rowe, 2009; Fujioka et al., 2012a; Konoike et al., 2012; Merchant et al., 2015). Importantly, neuroimaging research has revealed that auditory and motor cortices are interconnected through widely distributed and hierarchically organized neural networks involving cortical, subcortical, brain stem, and cerebellar regions (Chen et al., 2006, 2008a,b; Schmahmann et al., 2007; Helmich et al., 2010; Fernández-Miranda et al., 2015; for reviews: Petter et al., 2016; Janzen and Thaut, 2019).

It has been proposed that the functional and anatomical connections between auditory and motor-related areas allow entrainment induced by periodic auditory stimuli to modulate the activity of a distributed network of motor and sensory structures (Buzsáki, 2009; Large et al., 2015; Thaut et al., 2015; for review, see Damm et al., 2020). Psychophysical and brain imaging investigations into rhythmic auditory-motor entrainment have shown extremely fast and temporally precise auditory projections into the motor system, entraining motor responses even below thresholds of conscious awareness and engaging complex corticocerebellar networks (Thaut et al., 1999, 2009; Roberts et al., 2000; Stephan et al., 2002; Thaut and Kenyon, 2003). A series of neurophysiological studies have shown temporally correlated modulations between auditory and motor areas, primarily in beta oscillations bands, supporting the hypothesis of coupling between auditory and motor areas through neuronal entrainment by external rhythms (Fujioka et al., 2012a,b; Ross et al., 2017; Crasta et al., 2018; Buard et al., 2019a). It has been suggested that beta-band oscillations (10–30 Hz) may indeed reflect auditory-to-motor neural coupling. In cortical sensory areas, brain oscillatory rhythms in the beta frequency range are linked to rhythm perception and reflect motor-related sensory cues (Snyder and Large, 2005; Fujioka et al., 2009, 2015; Saleh et al., 2010). Moreover, beta modulation is also associated with a range of motor behaviors (Foffani et al., 2005; Gilbertson et al., 2005; Androulidakis et al., 2007) and anticipation (Saleh et al., 2010; Jenkinson and Brown, 2011; van Ede et al., 2014; Fujioka et al., 2015; Crasta et al., 2018).

Beta modulation following rhythm- and music-based interventions have been reported in recent clinical studies (Altenmüller et al., 2009; Fujioka et al., 2012b; Buard et al., 2019b; Calabrò et al., 2019; Naro et al., 2020). A parallel-group RCT combined with electroencephalography (EEG) demonstrated that 25 participants with PD who received an 8-week treadmill gait training with RAS showed a stronger EEG power increase related to specific periods of the gait cycle and greater improvement of fronto-centroparietal/temporal

connectivity in alpha and beta-bands compared to the patients who received the training without RAS (Calabrò et al., 2019). In addition, increases in the fronto-centroparietal and fronto-temporal beta connectivity were significantly correlated with improvement in functional gait assessment. The authors suggest that this extensive oscillatory recruitment may reflect the engagement of compensatory/adaptive mechanisms involving different cortical areas as well as the cerebellum that bypass or compensate deficient basal ganglia-thalamo-cortical loops in PD (discussed in Nombela et al., 2013; Koshimori and Thaut, 2018; Damm et al., 2020).

There is also evidence that external rhythms may facilitate residual activation of the basal ganglia-cortical circuitry. Studies with PD patients implanted with neurostimulators in the subthalamic nucleus (STN) further demonstrated that rhythmic auditory cues modulate the amplitude of beta oscillations of the STN during motor performance (Fischer et al., 2018; Naro et al., 2020). Naro et al. (2020) reported that patients with deep brain stimulation exhibited stronger remodulation of sensorimotor beta oscillations with gait cycle after a motor training program consisting of RAS combined with conventional physiotherapy than patients without deep brain stimulation, thus suggesting that the combination of these interventions potentiated the restoration of altered beta-band response profiles in PD.

Importantly, growing research evidence indicate that improvements in fine and gross manual skills following Music-supported Therapy (MST) are associated with modulation of beta-band frequency and stronger EEG coherence in broader cortical areas (Altenmüller et al., 2009; Fujioka et al., 2012b; Buard et al., 2019b; Ghai et al., 2021). For instance, in Altenmüller et al. (2009), 32 stroke patients who significantly improved fine and gross manual skills following 3 weeks of MST training showed more pronounced event-related desynchronization (ERD) in beta-band frequency before movement onset, which was not observed in a patient control group. Findings also showed stronger beta-band intra- and interhemispheric coherence between frontal and parietal areas compared to the control group during self-paced movements using the index finger and the whole arm (Altenmüller et al., 2009). An association between better rehabilitation outcomes and greater ERD have also been reported in recent studies (Fujioka et al., 2012b; Buard et al., 2019b; Ghai et al., 2021). In a recent case series, Ghai et al. (2021) examined neurophysiological changes induced by a 3-week intensive piano training in two participants after stroke. Using magnetoencephalography, the study reported changes in functional connectivity between the auditory and motor cortex in the affected hemisphere with increased alpha and beta-band coherence while listening passively to a trained musical piece. These neurophysiological changes were accompanied by improvements in manual dexterity (Ghai et al., 2021). However, these findings must be interpreted with caution as none of these neuroimaging studies involved a patient control group that engaged in a comparable active control intervention. Thus, further research would be of interest to better understand the mechanisms underlying changes in connectivity within auditory-motor networks induced by actively engaging in music playing.

The Dopaminergic System: From Reward to Rhythm Perception and Production

Neuroimaging findings have suggested that the midbrain-striatal dopaminergic system may play an important role in the effects of rhythm- and music-based interventions. It is well-known that pleasant music modulates the activity in the reward-motivation brain networks and stimulates dopamine release in the striatum system (Blood and Zatorre, 2001; Salimpoor et al., 2011; Koelsch, 2014; Ferreri et al., 2019), which may explain mood-enhancing effects and improvements in quality of life after engaging in positive and rewarding experiences associated with music interventions (for review, see Sihvonen et al., 2017; Brancatisano et al., 2020; Grau-Sánchez et al., 2020; Chatterjee et al., 2021).

However, dopaminergic activity also plays an important role in rhythm perception and production (Grahn and Brett, 2007), rhythmic motor control (Miller et al., 2013; Braunlich et al., 2019; Koshimori et al., 2019), and prediction error (Friston et al., 2017; Ramakrishnana et al., 2017; Sarno et al., 2017), thus suggesting that the dopaminergic system is key to understanding auditory-motor interactions. Considering that music extensively modulates anatomical and functional connectivity between auditory areas and striatum, examining dopaminergic responses and changes in frontostriatal networks induced by music and rhythm is of interest.

Indeed, only few studies to date have investigated dopaminergic function using PET and dopamine radioligands (Salimpoor et al., 2011; Koshimori et al., 2019). In a recent study, Koshimori et al. (2019) employed [^{11}C]-(+)-PHNO-PET to measure RAS-induced dopaminergic responses in the basal ganglia of eight healthy young adults during a finger-tapping task with and without RAS. Results indicated significantly greater dopamine responses in the left ventral striatum during non-RAS finger tapping compared to RAS. This result suggests that, in healthy younger adults, performing a task without auditory rhythmic cues required more motivational/attentional efforts directed toward motor timing control. This study thus demonstrated that rhythmic cues modulated dopaminergic responses in the basal ganglia, opening new avenues for further investigations into whether RAS may be able to modulate residual dopaminergic function and/or restore basal ganglia-thalamo-cortical network in PD.

Neuroplasticity

It has been well-documented that music training and learning promote significant functional and structural changes in the brain, particularly in motor regions (Münte et al., 2002; Altenmüller and Schlaug, 2015). For instance, Pascual-Leone (2001) demonstrated that learning to play short sequences on the piano significantly changes the cortical representation of flexor and extensor finger muscles in the primary motor cortex. Considering that active music-based interventions involve motor skill acquisition, sensorimotor integration, multimodal stimulation, and extensive practice, it is hypothesized that similar

activity-dependent neuroplastic changes are promoted by short periods of intervention (Altenmüller and Stewart, 2020; Grau-Sánchez et al., 2020).

There is indeed growing evidence of the direct association between neuroplasticity and functional recovery after rhythm- and music-based interventions (del Olmo et al., 2006; Amengual et al., 2013; Grau-Sánchez et al., 2013; Ripollés et al., 2016). For instance, in Ripollés et al. (2016), fMRI data of 14 chronic stroke participants indicated that improvement in fine and gross manual dexterity following MST was associated with enhanced connectivity in a network involving the precentral gyrus, supplementary motor area, inferior frontal gyrus and primary auditory cortex in the affected hemisphere as well as in the primary auditory cortex in the non-affected hemisphere when compared to healthy participants during a listening task contrasting trained/familiar music to untrained/unfamiliar music. Two experimental studies using Transcranial Magnetic Stimulation (TMS) to evaluate changes in sensorimotor representations have shown that gains in motor performance after MST training were associated with an increase in excitability of the motor system and cortical motor map reorganization in the affected hemisphere in subacute and chronic stroke patients (Amengual et al., 2013; Grau-Sánchez et al., 2013).

Emerging evidence in other clinical populations has indicated reestablishment of functional connectivity between auditory and motor regions after rhythm- and music-based intervention. Results from a neuroimaging study with 10 with neurodevelopmental disorders showed stronger endogenous connectivity from the left primary motor cortex to the right cerebellum after 18 months of piano training compared to a control patient group who did not receive any training (Alves-Pinto et al., 2015). Functional changes in cerebellar circuits were also reported in a study using PET to examine neural changes post-RAS intervention (del Olmo et al., 2006). Results demonstrated that PD patients with H&Y 1–2.5 stages exhibited an increase in the resting glucose metabolism measured by [^{18}F]-FDG PET in the right cerebellum and increased activity in the right parietal (BA39) and temporal lobes compared to the brain function before the intervention. Moreover, these functional changes were accompanied with normalized finger tapping performance and gait, suggesting that RAS training strengthened corticocerebellar activity, which may be associated with compensatory/adaptive responses.

Collectively, these early findings suggest that rhythm- and music-based interventions can promote cortical reorganization and functional changes through neuroplasticity. However, these findings must be interpreted with caution as these neuroimaging studies did not involve a patient control group that engaged in a comparable active control intervention. Further research is needed to uncover the specific underlying neural mechanisms by which activity-induced plasticity is generated and to better understand whether music and rhythm modulate the residual neural resources in brain areas altered by aging or neurological disorders and/or engage unaffected brain areas to compensate for impair function. These findings will help refine the current intervention protocols and generate new hypotheses.

FUTURE PERSPECTIVES

Research conducted in the past decades has significantly contributed to a better understanding of how and why rhythm- and music-based interventions can be effective tools in motor rehabilitation. Nevertheless, there are several questions yet to be explored and methodological limitations that need to be addressed in future research.

Most research efforts to date have been devoted to investigating the effects of auditory rhythms on motor function in Parkinson's disease and stroke, with findings consistently supporting the use of rhythmic auditory cues to enhance motor performance in these conditions. On the other hand, there is a paucity of high-quality randomized clinical trials with other populations, including (but not limited to) traumatic brain injury, children with cerebral palsy, Alzheimer's disease, and older adults. The studies reviewed here provide promising behavioral evidence and lay the foundation upon which new research can be developed to better understand the effects of rhythmic auditory cueing on gait, posture, balance, and upper extremity function. Further research is critical to determine standardized protocols (cueing frequency, treatment intensity and duration, and best clinical stage) tailored to these neurological conditions. Protocol inconsistencies in relation to types and frequencies of RAS, instructions given to participants, and differences in participants' clinical characteristics at baseline also seem to be at the root of some of the conflicting results reported.

There is increasing interest in the application of active music playing interventions to improve upper-limb functionality, manual dexterity, and fine motor skills, and growing evidence indicates that musical training is beneficial for motor rehabilitation. Research on subacute stroke has been at the forefront, as revealed by the significant number of publications in the past years, whereas the effects of music interventions to address upper-limb function in other clinical populations (e.g., traumatic brain injury, multiple sclerosis) and aging is still in the initial stages. Questions regarding the feasibility of home-based training programs, optimal training intensity and duration, best clinical stage, and the long-term sustainability of improvements should be systematically investigated. It is also important to note that many studies involving musical training (i.e., piano training) did not involve a trained music therapist to administer the intervention. Although the studies reviewed here showed beneficial effects regardless of the involvement of a dedicated music therapist, it is important to better understand the role of the therapeutic relationship between patient and therapist on the outcomes and the ethical implications of the administration of music-based treatments for individuals with neurological conditions.

In order to improve the quality of evidence, randomized controlled trials with larger samples, stratification of patients based on spared cognitive, rhythm abilities, and baseline

function, as well as appropriate standardized outcomes measures are needed. One of the crucial methodological aspects that should be addressed in future research is the inclusion of active non-musical control conditions with similar motivational, mood, and emotion-inducing qualities. Particular attention should be given to ensure that experimental and control groups are similar in relation to training intensity. More information on retention of gains with long-term follow-up assessments is also necessary. Combining behavioral assessments with other objective outcome measures, including biomechanical measures (e.g., motion capture, electromyography), is key to better understanding the effects of auditory rhythms and different parameters of auditory feedback on movement kinematics and muscular activity.

Music and rhythm interventions in motor rehabilitation need to be grounded within a neurobiological understanding of the underlying mechanisms, and for that, neuroimaging studies play an important role. More neurophysiology studies are needed to determine how RAS-induced entrainment modulates brain oscillatory activity in non-auditory areas in clinical populations. Neuroimaging research is also essential to better understand the mechanisms underlying the effects of auditory rhythmic cueing on other motor-related symptoms, such as balance and freezing of gait. One hypothesis is that these beneficial effects may be partly mediated by modulation of brain activity in the pedunculopontine nucleus (PPN) (Thevathasan et al., 2012a,b; Molina et al., 2020; He et al., 2021). This subcortical region has important connections with the subthalamic nucleus, basal ganglia, and inferior colliculus, and may be able to modulate activity in dopaminergic networks (Koshimori and Thaut, 2018). Studies examining the dopaminergic function and dopamine radioligands using PET as well as with individuals undergoing neuromodulation to treat PD could shed new light on subcortical mechanisms underlying rhythm- and music-based interventions. Neuroimaging research has great potential to promote active crosstalk between basic and applied research, for instance, allowing a better understanding of how rhythm-based intervention may be extended to remediate cognitive, speech and language deficits in populations where timing and rhythm disorders are part of core symptoms of neurodevelopmental disorders, such as speech and language impairments, developmental stuttering, and autism spectrum disorder (Falk et al., 2015; Janzen and Thaut, 2018; Ladányi et al., 2020; Lense et al., 2021).

To date, brain plasticity induced by rhythm- and music-based interventions have been mostly demonstrated by comparing brain activity pre- and post-intervention. However, the recent advent of portable neuroimaging technologies that are less sensitive to motion artifacts such as Functional Near Infrared Spectroscopy (fNIRS) can provide valuable insight into brain function in freely moving participants in ecological settings (Balardin et al., 2017). Recent studies have implemented fNIRS to investigate the neural correlates associated with cued rhythmic movements in healthy young and older adults during short-term RAS training (Vitorio et al., 2018; Curzel et al., 2021). Overall, these studies demonstrated the feasibility of this neuroimaging technology to monitor brain activity during walking (Vitorio et al., 2018) and drumming to rhythmic auditory cues (Curzel et al., 2021), opening new possibilities for monitoring the relationships between neural plasticity and behavioral improvement during interventions.

Finally, another important item on the research agenda is increasing the availability of music interventions in hospitals, communities, and home settings. Recent advances in mobile technologies whereby motor behaviors can be monitored via dedicated sensors may be instrumental to implementing assistive rehabilitation strategies via apps, serious games, or touchscreen musical instruments on tablets (Dalla Bella, 2018). For instance, a recent open-label clinical trial demonstrated the beneficial effects of a 1-month (30 min/day, 5 days) gait training with auditory rhythm in a home setting with 45 patients with moderate PD via the use of a smartphone application combined with ankle-worn sensors (Cochen De Cock et al., 2021). Street et al. (2020) discussed the potential use of touchscreen devices (iPad) in acute stroke rehabilitation as tools to enhance treatment dosage and engagement. More recently, the potential benefits and challenges of adapting in-person therapeutic sessions to remote music therapy services have been examined, with recommendations for the implementation of telehealth into routine care (Cole et al., 2021). Further research to investigate how technology can be incorporated into clinical practice in music-based motor rehabilitation would be of interest.

CONCLUSION

The effectiveness of rhythm- and music-based interventions in motor rehabilitation has been investigated in a growing number of studies. Converging research evidence indicates that musical rhythm is a powerful tool capable of modulating the activity of multiple brain networks and inducing neural plasticity, with great potential for supporting or recovering motor functioning. While the effect of rhythmic auditory cueing on gait performance is well-documented in PD and stroke and the clinical evidence of its effectiveness for gait training in these populations is robust, the effects of RAS on gait training in other populations (e.g., traumatic brain injury, children with cerebral palsy, and older adults) is yet to be fully examined. Similarly, Music-supported Therapy has been systematically examined in subacute stroke and there is growing evidence of its positive benefits to recover functional movement of the paretic upper extremity. Nevertheless, the understanding of the effects of active music playing for rehabilitation of fine and gross motor function in other neurological conditions is in its initial stages.

Recent neuroimaging and neurophysiological research have started the journey toward a sound neuroscientific basis for rhythm- and music-based interventions, providing a better understanding of how the brain responds to the periodicity of auditory rhythmic patterns and how movements can be shaped by rhythm. A full understanding of the mechanisms underlying the wide range of therapeutic benefits of rhythm-based musical interventions is on the research agenda for the years to come.

The body of knowledge reviewed here provides evidence of the feasibility and effectiveness of the application of rhythm and music to restore motor function in a wide variety of clinical

settings. The research gaps highlighted in this article clearly demonstrate that this area of research has a large potential yet to be fully explored.

AUTHOR CONTRIBUTIONS

All authors listed have made a substantial, direct, and intellectual contribution to the work, and approved it for publication.

SUPPLEMENTARY MATERIAL

The Supplementary Material for this article can be found online at: https://www.frontiersin.org/articles/10.3389/fnhum.2021.789467/full#supplementary-material

Supplementary Table 1 | Summary of studies published in the past 5 years investigating the application of Rhythmic Auditory Stimulation for gait rehabilitation.

Supplementary Table 2 | Summary of studies published in the past 5 years investigating the application of music-based interventions for motor rehabilitation.

REFERENCES

Acuña, S. A., Tyler, M. E., Danilov, Y. P., and Thelen, D. G. (2018). Abnormal muscle activation patterns are associated with chronic gait deficits following traumatic brain injury. *Gait Posture* 62, 510–517. doi: 10.1016/j.gaitpost.2018.04.012

Allali, G., Annweiler, C., Blumen, H. M., Callisaya, M. L., de Cock, A. M., Kressig, R. W., et al. (2016). Gait phenotype from mild cognitive impairment to moderate dementia: results from the GOOD initiative. *Eur. J. Neurol.* 23, 527–541. doi: 10.1111/ene.12882

Altenmüller, E., and James, C. (2020). "The impact of music interventions on motor rehabilitation following stroke in elderly," in *Music and the Aging Brain*, eds L. Cuddy, S. Belleville, and A. Mussard (Amsterdam: Elsevier), 407–432. doi: 10.1016/b978-0-12-817422-7.00016-x

Altenmüller, E., Marco-Pallares, J., Münte, T. F., and Schneider, S. (2009). Neural reorganization underlies improvement in stroke-induced motor dysfunction by music-supported therapy. *Ann. N. Y. Acad. Sci.* 1169, 395–405. doi: 10.1111/j.1749-6632.2009.04580.x

Altenmüller, E., and Schlaug, G. (2015). Apollo's gift: new aspects of neurologic music therapy. *Prog. Brain Res.* 217, 237–252. doi: 10.1016/bs.pbr.2014.11.029

Altenmüller, E., and Stewart, L. (2020). *Oxford Textbook of Neurorehabilitation*. Oxford: Oxford University Press. doi: 10.1093/med/9780198824954.001.0001

Alves-Pinto, A., Ehrlich, S., Cheng, G., Turova, V., Blumenstein, T., and Lampe, R. (2017). Effects of short-term piano training on measures of finger tapping, somatosensory perception and motor-related brain activity in patients with cerebral palsy. *Neuropsychiatr. Dis. Treat.* 13, 2705–2718. doi: 10.2147/NDT.S145104

Alves-Pinto, A., Emch, M., and Lampe, R. (2021). Effects of Piano Training in Unilateral Cerebral Palsy Using Probabilistic and Deterministic Tractography: a Case Report. *Front. Hum. Neurosci.* 15:622082. doi: 10.3389/fnhum.2021.622082

Alves-Pinto, A., Turova, V., Blumenstein, T., and Lampe, R. (2016). The Case for Musical Instrument Training in Cerebral Palsy for Neurorehabilitation. *Neural Plast.* 2016:1072301. doi: 10.1155/2016/1072301

Alves-Pinto, A., Turova, V., Blumenstein, T., Thienel, A., Wohlschläger, A., and Lampe, R. (2015). FMRI assessment of neuroplasticity in youths with neurodevelopmental-associated motor disorders after piano training. *Eur. J. Paediatr. Neurol.* 19, 15–28. doi: 10.1016/j.ejpn.2014.09.002

Amengual, J. L., Rojo, N., Veciana de las Heras, M., Marco-Pallarés, J., Grau-Sánchez, J., Schneider, S., et al. (2013). Sensorimotor Plasticity after Music-Supported Therapy in Chronic Stroke Patients Revealed by Transcranial Magnetic Stimulation. *PLoS One* 8:e61883. doi: 10.1371/journal.pone.0061883

Androulidakis, A. G., Doyle, L. M. F., Yarrow, K., Litvak, V., Gilbertson, T. P., and Brown, P. (2007). Anticipatory changes in beta synchrony in the human corticospinal system and associated improvements in task performance. *Eur. J. Neurosci.* 25, 3758–3765. doi: 10.1111/j.1460-9568.2007.05620.x

Bailey, C. A., Corona, F., Murgia, M., Pili, R., Pau, M., and Côté, J. N. (2018). Electromyographical gait characteristics in Parkinson's disease: effects of combined physical therapy and rhythmic auditory stimulation. *Front. Neurol.* 9:211. doi: 10.3389/fneur.2018.00211

Balardin, J. B., Zimeo Morais, G. A., Furucho, R. A., Trambaiolli, L., Vanzella, P., Biazoli, C., et al. (2017). Imaging Brain Function with Functional Near-Infrared Spectroscopy in Unconstrained Environments. *Front. Hum. Neurosci.* 11:258. doi: 10.3389/fnhum.2017.00258

Baram, Y., and Lenger, R. (2012). Gait improvement in patients with cerebral palsy by visual and auditory feedback. *Neuromodulation* 15, 48–52. doi: 10.1111/j.1525-1403.2011.00412.x

Benedetti, M. G., Piperno, R., Simoncini, L., Bonato, P., Tonini, A., and Giannini, S. (1999). Gait abnormalities in minimally impaired multiple sclerosis patients. *Mult. Scler.* 5, 363–368. doi: 10.1177/135245859900500510

Bengtsson, S. L., Ullén, F., Henrik Ehrsson, H., Hashimoto, T., Kito, T., Naito, E., et al. (2009). Listening to rhythms activates motor and premotor cortices. *Cortex* 45, 62–71. doi: 10.1016/j.cortex.2008.07.002

Blood, A. J., and Zatorre, R. J. (2001). Intensely pleasurable responses to music correlate with activity in brain regions implicated in reward and emotion. *Proc. Natl. Acad. Sci. U. S. A.* 98, 11818–11823. doi: 10.1073/pnas.191355898

Bouvet, C. J., Bardy, B. G., Keller, P. E., Bella, S. D., Nozaradan, S., and Varlet, M. (2020). Accent-induced modulation of neural and movement patterns during spontaneous synchronization to auditory rhythms. *J. Cogn. Neurosci.* 32, 2260–2271. doi: 10.1162/jocn_a_01605

Boyd, R. N., Morris, M. E., and Graham, H. K. (2001). Management of upper limb dysfunction in children with cerebral palsy: a systematic review. *Eur. J. Neurol.* 8, 150–166. doi: 10.1046/j.1468-1331.2001.00048.x

Brancatisano, O., Baird, A., and Thompson, W. F. (2020). Why is music therapeutic for neurological disorders? The Therapeutic Music Capacities Model. *Neurosci. Biobehav. Rev.* 112, 600–615. doi: 10.1016/j.neubiorev.2020.02.008

Braunlich, K., Seger, C. A., Jentink, K. G., Buard, I., Kluger, B. M., and Thaut, M. H. (2019). Rhythmic auditory cues shape neural network recruitment in Parkinson's disease during repetitive motor behavior. *Eur. J. Neurosci.* 49, 849–858. doi: 10.1111/ejn.14227

Buard, I., Dewispelaere, W. B., Thaut, M., and Kluger, B. M. (2019b). Preliminary neurophysiological evidence of altered cortical activity and connectivity with neurologic music therapy in Parkinson's disease. *Front. Neurosci.* 13:105. doi: 10.3389/fnins.2019.00105

Buard, I., Dewispelaere, W. B., Teale, P., Rojas, D. C., Kronberg, E., Thaut, M. H., et al. (2019a). Auditory entrainment of motor responses in older adults with and without Parkinson's disease: an MEG study. *Neurosci. Lett.* 708:134331. doi: 10.1016/j.neulet.2019.134331

Bugos, J., and Kochar, S. (2017). Efficacy of a short-term intense piano training program for cognitive aging: a pilot study. *Music. Sci.* 21, 137–150. doi: 10.1177/1029864917690020

Bugos, J. A. (2019). The Effects of Bimanual Coordination in Music Interventions on Executive Functions in Aging Adults. *Front. Integr. Neurosci.* 13:68. doi: 10.3389/FNINT.2019.00068/BIBTEX

Bugos, J. A., Lesiuk, T., and Nathani, S. (2021). Piano training enhances Stroop performance and musical self-efficacy in older adults with Parkinson's disease. *Psychol. Music* 49, 615–630. doi: 10.1177/0305735619888571

Bugos, J. A., Perlstein, W. M., McCrae, C. S., Brophy, T. S., and Bedenbaugh, P. H. (2007). Individualized piano instruction enhances executive functioning and working memory in older adults. *Aging Ment. Health* 11, 464–471. doi: 10.1080/13607860601086504

Buzsáki, G. (2009). *Rhythms of the Brain*. Oxford: Oxford University Press. doi: 10.1093/acprof:oso/9780195301069.001.0001

Calabrò, R. S., Naro, A., Filoni, S., Pullia, M., Billeri, L., Tomasello, P., et al. (2019). Walking to your right music: a randomized controlled trial on the novel use of treadmill plus music in Parkinson's disease. *J. Neuroeng. Rehabil.* 16:68. doi: 10.1186/s12984-019-0533-9

Capato, T. T. C., de Vries, N. M., Inthout, J., Barbosa, E. R., Nonnekes, J., and Bloem, B. R. (2020a). Multimodal Balance Training Supported by Rhythmical Auditory Stimuli in Parkinson's Disease: a Randomized Clinical Trial. *J. Parkinsons Dis.* 10, 333–346. doi: 10.3233/JPD-191752

Capato, T. T. C., Nonnekes, J., de Vries, N. M., IntHout, J., Barbosa, E. R., and Bloem, B. R. (2020b). Effects of multimodal balance training supported by rhythmical auditory stimuli in people with advanced stages of Parkinson's disease: a pilot randomized clinical trial. *J. Neurol. Sci.* 418:117086. doi: 10.1016/j.jns.2020.117086

Castrillo, A., Olmos, L. M. G., Rodríguez, F., and Duarte, J. (2016). Gait Disorder in a Cohort of Patients with Mild and Moderate Alzheimer's Disease. *Am. J. Alzheimers Dis.Dement.* 31, 257–262. doi: 10.1177/1533317515603113

Chang, H. Y., Lee, Y. Y., Wu, R. M., Yang, Y. R., and Luh, J. J. (2019). Effects of rhythmic auditory cueing on stepping in place in patients with Parkinson's disease. *Medicine* 98:e17874. doi: 10.1097/MD.0000000000017874

Chatterjee, D., Hegde, S., and Thaut, M. (2021). Neural plasticity: the substratum of music-based interventions in neurorehabilitation. *NeuroRehabilitation* 48, 155–166. doi: 10.3233/NRE-208011

Chen, J. L. (2018). Music-supported therapy for stroke motor recovery: theoretical and practical considerations. *Ann. N. Y. Acad. Sci.* 1423, 57–65. doi: 10.1111/nyas.13726

Chen, J. L., Penhune, V. B., and Zatorre, R. J. (2008a). Listening to musical rhythms recruits motor regions of the brain. *Cereb. Cortex* 18, 2844–2854. doi: 10.1093/cercor/bhn042

Chen, J. L., Penhune, V. B., and Zatorre, R. J. (2008b). Moving on time: brain network for auditory-motor synchronization is modulated by rhythm complexity and musical training. *J. Cogn. Neurosci.* 20, 226–239. doi: 10.1162/jocn.2008.20018

Chen, J. L., Zatorre, R. J., and Penhune, V. B. (2006). Interactions between auditory and dorsal premotor cortex during synchronization to musical rhythms. *NeuroImage* 32, 1771–1781. doi: 10.1016/j.neuroimage.2006.04.207

Chong, H. J., Cho, S.-R., Jeong, E., and Kim, S. J. (2013). Finger exercise with keyboard playing in adults with cerebral palsy: a preliminary study. *J. Exerc. Rehabil.* 9, 420–425. doi: 10.12965/jer.130050

Chong, H. J., Han, S. J., and Kim, S. J. (2017). Keyboard playing as a hand exercise for patients with subacute stroke. *Music Ther. Perspect.* 35, 144–150. doi: 10.1093/mtp/miw023

Clair, A. A., and O'Konski, M. (2006). The effect of Rhythmic Auditory Stimulation (RAS) on gait characteristics of cadence, velocity, and stride length in persons with late stage dementia. *J. Music Ther.* 43, 154–163. doi: 10.1093/jmt/43.2.154

Cochen De Cock, V., Dotov, D., Damm, L., Lacombe, S., Ihalainen, P., Picot, M. C., et al. (2021). BeatWalk: personalized Music-Based Gait Rehabilitation in Parkinson's Disease. *Front. Psychol.* 12:655121. doi: 10.3389/fpsyg.2021.655121

Cochen De Cock, V., Dotov, D. G., Ihalainen, P., Bégel, V., Galtier, F., Lebrun, C., et al. (2018). Rhythmic abilities and musical training in Parkinson's disease: do they help? *Npj Parkinsons Dis.* 4:8. doi: 10.1038/s41531-018-0043-7

Cole, L. P., Henechowicz, T. L., Kang, K., Pranjić, M., Richard, N. M., Tian, G. L. J., et al. (2021). Neurologic Music Therapy via Telehealth: a Survey of Clinician Experiences, Trends, and Recommendations During the COVID-19 Pandemic. *Front. Neurosci.* 15:347. doi: 10.3389/fnins.2021.648489

Comber, L., Galvin, R., and Coote, S. (2017). Gait deficits in people with multiple sclerosis: a systematic review and meta-analysis. *Gait Posture* 51, 25–35. doi: 10.1016/j.gaitpost.2016.09.026

Crasta, J. E., Thaut, M. H., Anderson, C. W., Davies, P. L., and Gavin, W. J. (2018). Auditory Priming Improves Neural Synchronization in Auditory-Motor Entrainment. *Neuropsychologia* 117, 102–112. doi: 10.1016/j.neuropsychologia.2018.05.017

Crosby, L. D., Wong, J. S., Chen, J. L., Grahn, J., and Patterson, K. K. (2020). An Initial Investigation of the Responsiveness of Temporal Gait Asymmetry to Rhythmic Auditory Stimulation and the Relationship to Rhythm Ability Following Stroke. *Front. Neurol.* 11:517028. doi: 10.3389/fneur.2020.517028

Curzel, F., Brigadoi, S., and Cutini, S. (2021). fNIRS & e-drum: an ecological approach to monitor hemodynamic and behavioural effects of rhythmic auditory cueing training. *Brain Cogn.* 151:105753. doi: 10.1016/j.bandc.2021.105753

Dalla Bella, S. (2018). Music and movement: towards a translational approach. *Neurophysiol. Clin.* 48, 377–386. doi: 10.1016/J.NEUCLI.2018.10.067

Dalla Bella, S., Benoit, C.-E., Farrugia, N., Keller, P. E., Obrig, H., Mainka, S., et al. (2017). Gait improvement via rhythmic stimulation in Parkinson's disease is linked to rhythmic skills. *Sci. Rep.* 7:42005. doi: 10.1038/srep42005

Damm, L., Varoqui, D., de Cock, V. C., Dalla Bella, S., and Bardy, B. (2020). Why do we move to the beat? A multi-scale approach, from physical principles to brain dynamics. *Neurosci. Biobehav. Rev.* 112, 553–584. doi: 10.1016/j.neubiorev.2019.12.024

Degé, F., and Kerkovius, K. (2018). The effects of drumming on working memory in older adults. *Ann. N. Y. Acad. Sci.* 1423, 242–250. doi: 10.1111/nyas.13685

del Olmo, M. F., Arias, P., Furio, M. C., Pozo, M. A., and Cudeiro, J. (2006). Evaluation of the effect of training using auditory stimulation on rhythmic movement in Parkinsonian patients-a combined motor and [18F]-FDG PET study. *Parkinson. Relat. Disord.* 12, 155–164. doi: 10.1016/j.parkreldis.2005.11.002

Doelling, K. B., Assaneo, M. F., Bevilacqua, D., Pesaran, B., and Poeppel, D. (2019). An oscillator model better predicts cortical entrainment to music. *Proc. Natl. Acad. Sci. U. S. A.* 116, 10113–10121. doi: 10.1073/PNAS.1816414116

Doelling, K. B., and Poeppel, D. (2015). Cortical entrainment to music and its modulation by expertise. *Proc. Natl. Acad. Sci. U. S. A.* 112, E6233–E6242. doi: 10.1073/PNAS.1508431112

Dogruoz Karatekin, B., and Icagasioglu, A. (2021). The effect of therapeutic instrumental music performance method on upper extremity functions in adolescent cerebral palsy. *Acta Neurol. Belg.* 1:3. doi: 10.1007/s13760-021-01618-0

Efraimidou, V., Tsimaras, V., Proios, M., Christoulas, K., Giagazoglou, P., Sidiropoulou, M., et al. (2016). The effect of a music and movement program on gait, balance and psychological parameters of adults with cerebral palsy. *J. Phys. Educ. Sport* 16, 1357–1364. doi: 10.7752/jpes.2016.04217

Erra, C., Mileti, I., Germanotta, M., Petracca, M., Imbimbo, I., de Biase, A., et al. (2019). Immediate effects of rhythmic auditory stimulation on gait kinematics in Parkinson's disease ON/OFF medication. *Clin. Neurophysiol.* 130, 1789–1797. doi: 10.1016/j.clinph.2019.07.013

Falk, S., Müller, T., and Dalla Bella, S. (2015). Non-verbal sensorimotor timing deficits in children and adolescents who stutter. *Front. Psychol.* 6:847. doi: 10.3389/fpsyg.2015.00847

Fasano, A., Daniele, A., and Albanese, A. (2012). Treatment of motor and non-motor features of Parkinson's disease with deep brain stimulation. *Lancet Neurol.* 11, 429–442. doi: 10.1016/S1474-4422(12)70049-2

Fernández-Miranda, J. C., Wang, Y., Pathak, S., Stefaneau, L., Verstynen, T., and Yeh, F. C. (2015). Asymmetry, connectivity, and segmentation of the arcuate fascicle in the human brain. *Brain Struct. Funct.* 220, 1665–1680. doi: 10.1007/s00429-014-0751-7

Ferreri, L., Mas-Herrero, E., Zatorre, R. J., Ripollés, P., Gomez-Andres, A., Alicart, H., et al. (2019). Dopamine modulates the reward experiences elicited by music. *Proc. Natl. Acad. Sci. U. S. A.* 116, 3793–3798. doi: 10.1073/PNAS.1811878116

Fischer, P., Chen, C. C., Chang, Y.-J., Yeh, C.-H., Pogosyan, A., Herz, D. M., et al. (2018). Alternating Modulation of Subthalamic Nucleus Beta Oscillations during Stepping. *J. Neurosci.* 38, 5111–5121. doi: 10.1523/JNEUROSCI.3596-17.2018

Foffani, G., Bianchi, A. M., Baselli, G., and Priori, A. (2005). Movement-related frequency modulation of beta oscillatory activity in the human subthalamic nucleus. *J. Physiol.* 568, 699–711. doi: 10.1113/jphysiol.2005.089722

Friston, K. J., Parr, T., and de Vries, B. (2017). The graphical brain: belief propagation and active inference. *Netw. Neurosci.* 1, 381–414. doi: 10.1162/netn_a_00018

Fujioka, T., Dawson, D. R., Wright, R., Honjo, K., Chen, J. L., Chen, J. J., et al. (2018). The effects of music-supported therapy on motor, cognitive, and psychosocial functions in chronic stroke. *Ann. N. Y. Acad. Sci.* 1423, 264–274. doi: 10.1111/nyas.13706

Fujioka, T., Ross, B., and Trainor, L. J. (2015). Beta-Band Oscillations Represent Auditory Beat and Its Metrical Hierarchy in Perception and Imagery. *J. Neurosci.* 35, 15187–15198. doi: 10.1523/JNEUROSCI.2397-15.2015

Fujioka, T., Trainor, L. J., Large, E. W., and Ross, B. (2009). Beta and gamma rhythms in human auditory cortex during musical beat processing. *Ann. N. Y. Acad. Sci.* 1169, 89–92. doi: 10.1111/j.1749-6632.2009.04779.x

Fujioka, T., Trainor, L. J., Large, E. W., and Ross, B. (2012a). Internalized Timing of Isochronous Sounds Is Represented in Neuromagnetic Beta Oscillations. *J. Neurosci.* 32, 1791–1802. doi: 10.1523/JNEUROSCI.4107-11.2012

Fujioka, T., Ween, J. E., Jamali, S., Stuss, D. T., and Ross, B. (2012b). Changes in neuromagnetic beta-band oscillation after music-supported stroke rehabilitation. *Ann. N. Y. Acad. Sci.* 1252, 294–304. doi: 10.1111/j.1749-6632.2011.06436.x

Fusar-Poli, L., Bieleninik, Ł, Brondino, N., Chen, X. J., and Gold, C. (2018). The effect of music therapy on cognitive functions in patients with dementia: a systematic review and meta-analysis. *Aging Ment. Health* 22, 1097–1106. doi: 10.1080/13607863.2017.1348474

Galea, O. A., Cottrell, M. A., Treleaven, J. M., and O'Leary, S. P. (2018). Sensorimotor and Physiological Indicators of Impairment in Mild Traumatic Brain Injury: a Meta-Analysis. *Neurorehabil. Neural Repair* 32, 115–128. doi: 10.1177/1545968318760728

Gatti, R., Tettamanti, A., Lambiase, S., Rossi, P., and Comola, M. (2015). Improving Hand Functional Use in Subjects with Multiple Sclerosis Using a Musical Keyboard: a Randomized Controlled Trial. *Physiother. Res. Int.* 20, 100–107. doi: 10.1002/pri.1600

Ghai, S. (2018). Effects of real-time (sonification) and rhythmic auditory stimuli on recovering arm function post stroke: a systematic review and meta-analysis. *Front. Neurol.* 9:488. doi: 10.3389/fneur.2018.00488

Ghai, S., and Ghai, I. (2018). Effects of rhythmic auditory cueing in gait rehabilitation for multiple sclerosis: a mini systematic review and meta-analysis. *Front. Neurol.* 9:386. doi: 10.3389/fneur.2018.00386

Ghai, S., and Ghai, I. (2019). Effects of (music-based) rhythmic auditory cueing training on gait and posture post-stroke: a systematic review & dose-response meta-analysis. *Sci. Rep.* 9:2183. doi: 10.1038/s41598-019-38723-3

Ghai, S., Ghai, I., Schmitz, G., and Effenberg, A. O. (2018a). Effect of rhythmic auditory cueing on parkinsonian gait: a systematic review and meta-analysis. *Sci. Rep.* 8:506. doi: 10.1038/s41598-017-16232-5

Ghai, S., Ghai, I., and Effenberg, A. O. (2018b). Effect of rhythmic auditory cueing on gait in cerebral palsy: a systematic review and meta-analysis. *Neuropsychiatr. Dis. Treat.* 14, 43–59. doi: 10.2147/NDT.S148053

Ghai, S., Ghai, I., and Effenberg, A. O. (2018c). Effect of rhythmic auditory cueing on aging gait: a systematic review and meta-analysis. *Aging Dis.* 9, 901–923. doi: 10.14336/AD.2017.1031

Ghai, S., Maso, F. D., Ogourtsova, T., Porxas, A. X., Villeneuve, M., Penhune, V., et al. (2021). Neurophysiological changes induced by music-supported therapy for recovering upper extremity function after stroke: a case series. *Brain Sci.* 11:666. doi: 10.3390/brainsci11050666

Gilbertson, T., Lalo, E., Doyle, L., di Lazzaro, V., Cioni, B., and Brown, P. (2005). Existing motor state is favored at the expense of new movement during 13-35 Hz oscillatory synchrony in the human corticospinal system. *J. Neurosci.* 25, 7771–7779. doi: 10.1523/JNEUROSCI.1762-05.2005

Ginis, P., Nackaerts, E., Nieuwboer, A., and Heremans, E. (2018). Cueing for people with Parkinson's disease with freezing of gait: a narrative review of the state-of-the-art and novel perspectives. *Ann. Phys. Rehabil. Med.* 61, 407–413. doi: 10.1016/j.rehab.2017.08.002

Goldshtrom, Y., Knorr, G., and Goldshtrom, I. (2010). Rhythmic exercises in rehabilitation of TBI patients: a case report. *J. Bodyw. Mov. Ther.* 14, 336–345. doi: 10.1016/j.jbmt.2009.06.002

Gonzalez-Hoelling, S., Bertran-Noguer, C., Reig-Garcia, G., and Suñer-Soler, R. (2021). Effects of a music-based rhythmic auditory stimulation on gait and balance in subacute stroke. *Int. J. Environ. Res. Public Health* 18:2032. doi: 10.3390/ijerph18042032

Gooßes, M., Saliger, J., Folkerts, A.-K., Nielsen, J., Zierer, J., Schmoll, P., et al. (2020). Feasibility of Music-Assisted Treadmill Training in Parkinson's Disease Patients With and Without Deep Brain Stimulation: insights From an Ongoing Pilot Randomized Controlled Trial. *Front. Neurol.* 11:790. doi: 10.3389/fneur.2020.00790

Grahn, J. A., and Brett, M. (2007). Rhythm and Beat Perception in Motor Areas of the Brain. *J. Cogn. Neurosci.* 19, 893–906. doi: 10.1162/jocn.2007.19.5.893

Grahn, J. A., and Rowe, J. B. (2009). Feeling the Beat: premotor and Striatal Interactions in Musicians and Nonmusicians during Beat Perception. *J. Neurosci.* 29, 7540–7548. doi: 10.1523/JNEUROSCI.2018-08.2009

Grau-Sánchez, J., Amengual, J. L., Rojo, N., Veciana de las Heras, M., Montero, J., Rubio, F., et al. (2013). Plasticity in the sensorimotor cortex induced by Music-supported therapy in stroke patients: a TMS study. *Front. Hum. Neurosci.* 7:494. doi: 10.3389/fnhum.2013.00494

Grau-Sánchez, J., Duarte, E., Ramos-Escobar, N., Sierpowska, J., Rueda, N., Redón, S., et al. (2018). Music-supported therapy in the rehabilitation of subacute stroke patients: a randomized controlled trial. *Ann. N. Y. Acad. Sci.* 1423, 318–328. doi: 10.1111/nyas.13590

Grau-Sánchez, J., Münte, T. F., Altenmüller, E., Duarte, E., and Rodríguez-Fornells, A. (2020). Potential benefits of music playing in stroke upper limb motor rehabilitation. *Neurosci. Biobehav. Rev.* 112, 585–599. doi: 10.1016/j.neubiorev.2020.02.027

Grau-Sánchez, J., Ramos, N., Duarte, E., Särkämö, T., and Rodríguez-Fornells, A. (2017). Time course of motor gains induced by music-supported therapy after stroke: an exploratory case study. *Neuropsychology* 31, 624–635. doi: 10.1037/neu0000355

Grau-Sánchez, J., Segura, E., Sanchez-Pinsach, D., Raghavan, P., Münte, T. F., Palumbo, A. M., et al. (2021). Enriched Music-supported Therapy for chronic stroke patients: a study protocol of a randomised controlled trial. *BMC Neurol.* 21:19. doi: 10.1186/s12883-020-02019-1

Guo, X., Yamashita, M., Suzuki, M., Ohsawa, C., Asano, K., Abe, N., et al. (2021). Musical instrument training program improves verbal memory and neural efficiency in novice older adults. *Hum. Brain Mapp.* 42, 1359–1375. doi: 10.1002/hbm.25298

Haire, C. M., Tremblay, L., Vuong, V., Patterson, K. K., Chen, J. L., Burdette, J. H., et al. (2021a). Therapeutic Instrumental Music Training and Motor Imagery in Post-Stroke Upper-Extremity Rehabilitation: a Randomized-Controlled Pilot Study. *Arch. Rehabil. Res. Clin. Transl.* 3:100162. doi: 10.1016/j.arrct.2021.100162

Haire, C. M., Vuong, V., Tremblay, L., Patterson, K. K., Chen, J. L., and Thaut, M. H. (2021b). Effects of therapeutic instrumental music performance and motor imagery on chronic post-stroke cognition and affect: a randomized controlled trial. *NeuroRehabilitation* 48, 195–208. doi: 10.3233/NRE-208014

Harrison, E. C., Horin, A. P., and Earhart, G. M. (2019). Mental Singing Reduces Gait Variability More Than Music Listening for Healthy Older Adults and People with Parkinson Disease. *J. Neurol. Phys. Ther.* 43, 204–211. doi: 10.1097/NPT.0000000000000288

He, S., Deli, A., Fischer, P., Wiest, C., Huang, Y., Martin, S., et al. (2021). Gait-phase modulates alpha and beta oscillations in the pedunculopontine nucleus. *bioRxiv* [Preprint]. doi: 10.1101/2021.03.05.434086

Hegde, S. (2014). Music-based cognitive remediation therapy for patients with traumatic brain injury. *Front. Neurol.* 5:34. doi: 10.3389/fneur.2014.00034

Helmich, R. C., Derikx, L. C., Bakker, M., Scheeringa, R., Bloem, B. R., and Toni, I. (2010). Spatial Remapping of Cortico-striatal Connectivity in Parkinson's Disease. *Cereb. Cortex* 20, 1175–1186. doi: 10.1093/CERCOR/BHP178

Horin, A. P., Harrison, E. C., Rawson, K. S., and Earhart, G. M. (2020). People with Parkinson disease with and without freezing of gait respond similarly to external and self-generated cues. *Gait Posture* 82, 161–166. doi: 10.1016/j.gaitpost.2020.09.005

Huang, W. H., Dou, Z. L., Jin, H. M., Cui, Y., Li, X., and Zeng, Q. (2021). The Effectiveness of Music Therapy on Hand Function in Patients With Stroke: a Systematic Review of Randomized Controlled Trials. *Front. Neurol.* 12:624. doi: 10.3389/fneur.2021.641023

Hurt, C. P., Rice, R. R., McIntosh, G. C., and Thaut, M. H. (1998). Rhythmic Auditory Stimulation in Gait Training for Patients with Traumatic Brain Injury. *J. Music Ther.* 35, 228–241. doi: 10.1093/jmt/35.4.228

Hurt-Thaut, C. (2008). "Clinical practice in music therapy," in *The Oxford Handbook of Music Psychology*, eds S. Hallam, I. Cross, and M. H. Thaut (Oxford: Oxford University Press), 819–836. doi: 10.1093/oxfordhb/9780199298457.013.0047

IJmker, T., and Lamoth, C. J. C. (2012). Gait and cognition: the relationship between gait stability and variability with executive function in persons with and without dementia. *Gait Posture* 35, 126–130. doi: 10.1016/j.gaitpost.2011.08.022

Janzen, T. B., and Thaut, M. H. (2018). Rethinking the role of music in the neurodevelopment of autism spectrum disorder. *Music Sci.* 1, 1–18. doi: 10.1177/2059204318769639

Janzen, T. B., and Thaut, M. H. (2019). "Cerebral Organization of Music Processing," in *Cerebral Organization of Music*, eds M. H. Thaut and D. A. Hodges (New York: Oxford University Press), doi: 10.1093/oxfordhb/9780198804123.013.6

Jenkinson, N., and Brown, P. (2011). New insights into the relationship between dopamine, beta oscillations and motor function. *Trends Neurosci.* 34, 611–618. doi: 10.1016/J.TINS.2011.09.003

Kang, S., Shin, J. H., Kim, I. Y., Lee, J., Lee, J. Y., and Jeong, E. (2020). Patterns of enhancement in paretic shoulder kinematics after stroke with musical cueing. *Sci. Rep.* 10:18109. doi: 10.1038/s41598-020-75143-0

Katz-Leurer, M., Rotem, H., Keren, O., and Meyer, S. (2009). Balance abilities and gait characteristics in post-traumatic brain injury, cerebral palsy and typically developed children. *Dev. Neurorehabil.* 12, 100–105. doi: 10.1080/17518420902800928

Kikkert, L. H. J., Vuillerme, N., van Campen, J. P., Hortobágyi, T., and Lamoth, C. J. (2016). Walking ability to predict future cognitive decline in old adults: a scoping review. *Ageing Res. Rev.* 27, 1–14. doi: 10.1016/j.arr.2016.02.001

Kim, S. J., Cho, S. R., and Yoo, G. E. (2017). Age-related changes in bimanual instrument playing with rhythmic cueing. *Front. Psychol.* 8:1569. doi: 10.3389/fpsyg.2017.01569

Kim, S. J., Kwak, E. E., Park, E. S., and Cho, S. R. (2012). Differential effects of rhythmic auditory stimulation and neurodevelopmental treatment/Bobath on gait patterns in adults with cerebral palsy: a randomized controlled trial. *Clin. Rehabil.* 26, 904–914. doi: 10.1177/0269215511434648

Kim, S. J., Kwak, E. E., Park, E. S., Lee, D. S., Kim, K. J., Song, J. E., et al. (2011). Changes in gait patterns with rhythmic auditory stimulation in adults with cerebral palsy. *NeuroRehabilitation* 29, 233–241. doi: 10.3233/NRE-2011-0698

Kim, S. J., Shin, Y. K., Yoo, G. E., Chong, H. J., and Cho, S. R. (2016). Changes in gait patterns induced by rhythmic auditory stimulation for adolescents with acquired brain injury. *Ann. N. Y. Acad. Sci.* 1385, 53–62. doi: 10.1111/nyas.13294

Kim, S. J., and Yoo, G. E. (2020). Rhythm-Motor Dual Task Intervention for Fall Prevention in Healthy Older Adults. *Front. Psychol.* 10:3027. doi: 10.3389/fpsyg.2019.03027

Kim, S. J., Yoo, G. E., Shin, Y. K., and Cho, S. R. (2020). Gait training for adults with cerebral palsy following harmonic modification in rhythmic auditory stimulation. *Ann. N. Y. Acad. Sci.* 1473, 11–19. doi: 10.1111/nyas.14306

Koelsch, S. (2014). Brain correlates of music-evoked emotions. *Nat. Rev. Neurosci.* 15, 170–180. doi: 10.1038/nrn3666

Konoike, N., Kotozaki, Y., Miyachi, S., Miyauchi, C. M., Yomogida, Y., Akimoto, Y., et al. (2012). Rhythm information represented in the fronto-parieto-cerebellar motor system. *NeuroImage* 63, 328–338. doi: 10.1016/j.neuroimage.2012.07.002

Koshimori, Y., Strafella, A. P., Valli, M., Sharma, V., Cho, S. S., Houle, S., et al. (2019). Motor synchronization to rhythmic auditory stimulation (RAS) attenuates dopaminergic responses in ventral striatum in young healthy adults: [11C]-(+)-PHNO PET study. *Front. Neurosci.* 13:106. doi: 10.3389/fnins.2019.00106

Koshimori, Y., and Thaut, M. H. (2018). Future perspectives on neural mechanisms underlying rhythm and music based neurorehabilitation in Parkinson's disease. *Ageing Res. Rev.* 47, 133–139. doi: 10.1016/j.arr.2018.07.001

Koshimori, Y., and Thaut, M. H. (2019). New Perspectives on Music in Rehabilitation of Executive and Attention Functions. *Front. Neurosci.* 13:1245. doi: 10.3389/fnins.2019.01245

Kurz, M. J., Arpin, D. J., and Corr, B. (2012). Differences in the dynamic gait stability of children with cerebral palsy and typically developing children. *Gait Posture* 36, 600–604. doi: 10.1016/j.gaitpost.2012.05.029

Kwak, E. E. (2007). Effect of Rhythmic Auditory Stimulation on Gait Performance in Children with Spastic Cerebral Palsy. *J. Music Ther.* 44, 198–216. doi: 10.1093/jmt/44.3.198

Ladányi, E., Persici, V., Fiveash, A., Tillmann, B., and Gordon, R. L. (2020). Is atypical rhythm a risk factor for developmental speech and language disorders?. *Wiley Interdiscip. Rev. Cogn. Sci.* 11:e1528. doi: 10.1002/WCS.1528

Lakatos, P., Gross, J., and Thut, G. (2019). A New Unifying Account of the Roles of Neuronal Entrainment. *Curr. Biol.* 29, R890–R905. doi: 10.1016/j.cub.2019.07.075

Lakatos, P., Musacchia, G., O'Connel, M. N., Falchier, A. Y., Javitt, D. C., and Schroeder, C. E. (2013). The Spectrotemporal Filter Mechanism of Auditory Selective Attention. *Neuron* 77, 750–761. doi: 10.1016/j.neuron.2012.11.034

Lampe, R., Thienel, A., Mitternacht, J., Blumenstein, T., Turova, V., and Alves-Pinto, A. (2015). Piano training in youths with hand motor impairments after damage to the developing brain. *Neuropsychiatr. Dis. Treat.* 11, 1929–1938. doi: 10.2147/NDT.S84090

Langhorne, P., Bernhardt, J., and Kwakkel, G. (2011). Stroke rehabilitation. *Lancet* 377, 1693–1702. doi: 10.1016/S0140-6736(11)60325-5

Langhorne, P., Coupar, F., and Pollock, A. (2009). Motor recovery after stroke: a systematic review. *Lancet Neurol.* 8, 741–754. doi: 10.1016/S1474-4422(09)70150-4

Large, E. W., Herrera, J. A., and Velasco, M. J. (2015). Neural networks for beat perception in musical rhythm. *Front. Syst. Neurosci.* 9:159. doi: 10.3389/fnsys.2015.00159

le Perf, G., Donguy, A. L., and Thebault, G. (2019). Nuanced effects of music interventions on rehabilitation outcomes after stroke: a systematic review. *Top. Stroke Rehabil.* 26, 473–484. doi: 10.1080/10749357.2019.1623518

Lee, S., Lee, K., and Song, C. (2018). Gait training with bilateral rhythmic auditory stimulation in stroke patients: a randomized controlled trial. *Brain Sci.* 8:164. doi: 10.3390/brainsci8090164

Lense, M. D., Ladányi, E., Rabinowitch, T.-C., Trainor, L., and Gordon, R. (2021). Rhythm and timing as vulnerabilities in neurodevelopmental disorders. *Philos. Trans. R. Soc. B Biol. Sci.* 376:20200327. doi: 10.1098/rstb.2020.0327

Leow, L. A., Waclawik, K., and Grahn, J. A. (2018). The role of attention and intention in synchronization to music: effects on gait. *Exp. Brain Res.* 236, 99–115. doi: 10.1007/s00221-017-5110-5

Lirani-Silva, E., Lord, S., Moat, D., Rochester, L., and Morris, R. (2019). Auditory Cueing for Gait Impairment in Persons with Parkinson Disease: a Pilot Study of Changes in Response with Disease Progression. *J. Neurol. Phys. Ther.* 43, 50–55. doi: 10.1097/NPT.0000000000000250

Lopes, J., and Keppers, I. I. (2021). Music-based therapy in rehabilitation of people with multiple sclerosis: a systematic review of clinical trials. *Arq. Neuropsiquiatr.* 79, 527–535. doi: 10.1590/0004-282X-ANP-2020-0374

Luquin, M.-R., Kulisevsky, J., Martinez-Martin, P., Mir, P., and Tolosa, E. S. (2017). Consensus on the Definition of Advanced Parkinson's Disease: a Neurologists-Based Delphi Study (CEPA Study). *Parkinsons Dis.* 2017:4047392. doi: 10.1155/2017/4047392

MacRitchie, J., Breaden, M., Milne, A. J., and McIntyre, S. (2020). Cognitive, Motor and Social Factors of Music Instrument Training Programs for Older Adults' Improved Wellbeing. *Front. Psychol.* 10:2868. doi: 10.3389/fpsyg.2019.02868

Magee, W. L., Clark, I., Tamplin, J., and Bradt, J. (2017). Music interventions for acquired brain injury. *Cochrane Database Syst. Rev.* 1:CD006787. doi: 10.1002/14651858.CD006787.pub3

Maggio, M. G., Tripoli, D., Porcari, B., Manuli, A., Filoni, S., Naro, A., et al. (2021). How may patients with MS benefit from using music assisted therapy? A case-control feasability study investigating motor outcomes and beyond. *Mult. Scler. Relat. Disord.* 48:102713. doi: 10.1016/j.msard.2020.102713

Mainka, S., Wissel, J., Völler, H., and Evers, S. (2018). The use of rhythmic auditory stimulation to optimize treadmill training for stroke patients: a randomized controlled trial. *Front. Neurol.* 9:755. doi: 10.3389/fneur.2018.00755

Marrades-Caballero, E., Santonja-Medina, C. S., Sanz-Mengibar, J. M., and Santonja-Medina, F. (2018). Neurologic music therapy in upper-limb rehabilitation in children with severe bilateral cerebral palsy: a randomized controlled trial. *Eur. J. Phys. Rehabil. Med.* 54, 866–872. doi: 10.23736/S1973-9087.18.04996-1

McIntosh, G. C., Brown, S. H., Rice, R. R., and Thaut, M. H. (1997). Rhythmic auditory-motor facilitation of gait patterns in patients with Parkinson's disease. *J. Neurol. Neurosurg. Psychiatry* 62, 22–26. doi: 10.1136/jnnp.62.1.22

Merchant, H., Grahn, J., Trainor, L., Rohrmeier, M., and Fitch, W. T. (2015). Finding the beat: a neural perspective across humans and non-human primates. *Philos. Trans. R. Soc. B Biol. Sci.* 370:20140093. doi: 10.1098/rstb.2014.0093

Miller, N. S., Kwak, Y., Bohnen, N. I., Müller, M. L. T. M., Dayalu, P., and Seidler, R. D. (2013). The pattern of striatal dopaminergic denervation explains sensorimotor synchronization accuracy in Parkinson's disease. *Behav. Brain Res.* 257, 100–110. doi: 10.1016/j.bbr.2013.09.032

Minino, R., Troisi Lopez, E., Sorrentino, P., Rucco, R., Lardone, A., Pesoli, M., et al. (2021). The effects of different frequencies of rhythmic acoustic stimulation on gait stability in healthy elderly individuals: a pilot study. *Sci. Rep.* 11:19530 . doi: 10.1038/s41598-021-98953-2

Molina, R., Hass, C. J., Sowalsky, K., Schmitt, A. C., Opri, E., Roper, J. A., et al. (2020). Neurophysiological Correlates of Gait in the Human Basal Ganglia and the PPN Region in Parkinson's Disease. *Front. Hum. Neurosci.* 14:194. doi: 10.3389/FNHUM.2020.00194

Mollica, A., Thaut, M., and Burke, M. J. (2021). Proposing Music-based Interventions for the Treatment of Traumatic Brain Injury Symptoms: current Evidence and Future Directions. *Can. J. Psychiatry* 66, 707–709. doi: 10.1177/07067437211007811

Morris, J. H., van Wijck, F., Joice, S., and Donaghy, M. (2013). Predicting health related quality of life 6 months after stroke: the role of anxiety and upper limb dysfunction. *Disabil. Rehabil.* 35, 291–299. doi: 10.3109/09638288.2012.691942

Morris, M. E., Huxham, F., McGinley, J., Dodd, K., and Iansek, R. (2001). The biomechanics and motor control of gait in Parkinson disease. *Clin. Biomech.* 16, 459–470. doi: 10.1016/S0268-0033(01)00035-3

Morris, M. E., Iansek, R., Matyas, T. A., and Summers, J. J. (1994). The pathogenesis of gait hypokinesia in parkinson's disease. *Brain* 117, 1169–1181. doi: 10.1093/brain/117.5.1169

Moumdjian, L., Maes, P. J., Dalla Bella, S., Decker, L. M., Moens, B., Feys, P., et al. (2020). Detrended fluctuation analysis of gait dynamics when entraining to music and metronomes at different tempi in persons with multiple sclerosis. *Sci. Rep.* 10:12934. doi: 10.1038/s41598-020-69667-8

Moumdjian, L., Moens, B., Maes, P. J., van Nieuwenhoven, J., van Wijmeersch, B., Leman, M., et al. (2019a). Walking to Music and Metronome at Various Tempi in Persons With Multiple Sclerosis: a Basis for Rehabilitation. *Neurorehabil. Neural Repair* 33, 464–475. doi: 10.1177/1545968319847962

Moumdjian, L., Moens, B., Vanzeir, E., de Klerck, B., Feys, P., and Leman, M. (2019b). A model of different cognitive processes during spontaneous and intentional coupling to music in multiple sclerosis. *Ann. N. Y. Acad. Sci.* 1445, 27–38. doi: 10.1111/nyas.14023

Moumdjian, L., Sarkamo, T., Leone, C., Leman, M., and Feys, P. (2017). Effectiveness of music-based interventions on motricity or cognitive functioning in neurological populations: a systematic review. *Eur. J. Phys. Rehabil. Med.* 53, 466–482. doi: 10.23736/S1973-9087.16.04429-4

Münte, T. F., Altenmüller, E., and Jäncke, L. (2002). The musician's brain as a model of neuroplasticity. *Nat. Rev. Neurosci.* 3, 473–478. doi: 10.1038/nrn843

Naro, A., Pignolo, L., Sorbera, C., Latella, D., Billeri, L., Manuli, A., et al. (2020). A Case-Controlled Pilot Study on Rhythmic Auditory Stimulation-Assisted Gait Training and Conventional Physiotherapy in Patients With Parkinson's Disease Submitted to Deep Brain Stimulation. *Front. Neurol.* 11:794. doi: 10.3389/fneur.2020.00794

Nascimento, L. R., de Oliveira, C. Q., Ada, L., Michaelsen, S. M., and Teixeira-Salmela, L. F. (2015). Walking training with cueing of cadence improves walking speed and stride length after stroke more than walking training alone: a systematic review. *J. Physiother.* 61, 10–15. doi: 10.1016/j.jphys.2014.11.015

Nobre, A. C., and van Ede, F. (2018). Anticipated moments: temporal structure in attention. *Nat. Rev. Neurosci.* 19, 34–48. doi: 10.1038/nrn.2017.141

Nombela, C., Hughes, L. E., Owen, A. M., and Grahn, J. A. (2013). Into the groove: can rhythm influence Parkinson's disease?. *Neurosci. Biobehav. Rev.* 37, 2564–2570. doi: 10.1016/j.neubiorev.2013.08.003

Nozaradan, S. (2014). Exploring how musical rhythm entrains brain activity with electroencephalogram frequency-tagging. *Philos. Trans. R. Soc. B Biol. Sci.* 369:20130393. doi: 10.1098/rstb.2013.0393

Nozaradan, S., Peretz, I., Missal, M., and Mouraux, A. (2011). Tagging the Neuronal Entrainment to Beat and Meter. *J. Neurosci.* 31, 10234–10240. doi: 10.1523/JNEUROSCI.0411-11.2011

Nozaradan, S., Peretz, I., and Mouraux, A. (2012). Selective Neuronal Entrainment to the Beat and Meter Embedded in a Musical Rhythm. *J. Neurosci.* 32, 17572–17581. doi: 10.1523/JNEUROSCI.3203-12.2012

Oakes, D., Shoulson, I., Kieburtz, K., Rudolph, A., Lang, A., Western Hos-pital, T., et al. (2004). Levodopa and the Progression of Parkinson's Disease. *N. Engl. J. Med.* 351, 2498–2508. doi: 10.1056/NEJMoa033447

Oreja-Guevara, C., Blanco, T. A., Ruiz, L. B., Pérez, M. ÁH., Meca-Lallana, V., and Ramió-Torrentà, L. (2019). Cognitive dysfunctions and assessments in multiple sclerosis. *Front. Neurol.* 10:581. doi: 10.3389/fneur.2019.00581

Pakula, A. T., van Naarden Braun, K., and Yeargin-Allsopp, M. (2009). Cerebral Palsy: classification and Epidemiology. *Phys. Med. Rehabil. Clin. N. Am.* 20, 425–452. doi: 10.1016/j.pmr.2009.06.001

Park, K. S., Hass, C. J., and Janelle, C. M. (2021). Familiarity with music influences stride amplitude and variability during rhythmically-cued walking in individuals with Parkinson's disease. *Gait Posture* 87, 101–109. doi: 10.1016/j.gaitpost.2021.04.028

Pascual-Leone, A. (2001). The Brain That Plays Music and Is Changed by It. *Ann. N. Y. Acad. Sci.* 930, 315–329. doi: 10.1111/j.1749-6632.2001.tb05741.x

Peng, Y. C., Lu, T. W., Wang, T. H., Chen, Y. L., Liao, H. F., Lin, K. H., et al. (2011). Immediate effects of therapeutic music on loaded sit-to-stand movement in children with spastic diplegia. *Gait Posture* 33, 274–278. doi: 10.1016/j.gaitpost.2010.11.020

Petter, E. A., Lusk, N. A., Hesslow, G., and Meck, W. H. (2016). Interactive roles of the cerebellum and striatum in sub-second and supra-second timing: support for an initiation, continuation, adjustment, and termination (ICAT) model of temporal processing. *Neurosci. Biobehav. Rev.* 71, 739–755. doi: 10.1016/j.neubiorev.2016.10.015

Prassas, S., Thaut, M., McIntosh, G., and Rice, R. (1997). Effect of auditory rhythmic cuing on gait kinematic parameters of stroke patients. *Gait Posture* 6, 218–223. doi: 10.1016/S0966-6362(97)00010-6

Raghavan, P., Geller, D., Guerrero, N., Aluru, V., Eimicke, J. P., Teresi, J. A., et al. (2016). Music Upper Limb Therapy—Integrated: an enriched collaborative approach for stroke rehabilitation. *Front. Hum. Neurosci.* 10:498. doi: 10.3389/fnhum.2016.00498

Ramakrishnana, A., Byunb, Y. W., Rand, K., Pedersen, C. E., Lebedev, M. A., and Nicolelis, M. A. L. (2017). Cortical neurons multiplex reward-related signals along with sensory and motor information. *Proc. Natl. Acad. Sci. U. S. A.* 114, E4841–E4850. doi: 10.1073/pnas.1703668114

Rehme, A. K., Eickhoff, S. B., Rottschy, C., Fink, G. R., and Grefkes, C. (2012). Activation likelihood estimation meta-analysis of motor-related neural activity after stroke. *NeuroImage* 59, 2771–2782. doi: 10.1016/j.neuroimage.2011.10.023

Ripollés, P., Rojo, N., Grau-Sánchez, J., Amengual, J. L., Càmara, E., Marco-Pallarés, J., et al. (2016). Music supported therapy promotes motor plasticity in individuals with chronic stroke. *Brain Imaging Behav.* 10, 1289–1307. doi: 10.1007/s11682-015-9498-x

Roberts, S., Eykholt, R., and Thaut, M. H. (2000). Analysis of correlations and search for evidence of deterministic chaos in rhythmic motor control by the human brain. *Phys. Rev. E Stat. Phys. Plasmas Fluids Relat. Interdiscip. Topics* 62, 2597–2607. doi: 10.1103/PhysRevE.62.2597

Rocha, P. A., Porfírio, G. M., Ferraz, H. B., and Trevisani, V. F. M. (2014). Effects of external cues on gait parameters of Parkinson's disease patients: a systematic review. *Clini. Neurol. Neurosurg.* 124, 127–134. doi: 10.1016/j.clineuro.2014.06.026

Rodriguez-Fornells, A., Rojo, N., Amengual, J. L., Ripollés, P., Altenmüller, E., and Münte, T. F. (2012). The involvement of audio-motor coupling in the music-supported therapy applied to stroke patients. *Ann. N. Y. Acad. Sci.* 1252, 282–293. doi: 10.1111/j.1749-6632.2011.06425.x

Rosenbaum, P., Paneth, N., Leviton, A., Goldstein, M., and Bax, M. (2007). A report: the definition and classification of cerebral palsy April 2006. *Dev. Med. Child Neurol.* 49, 8–14. doi: 10.1111/j.1469-8749.2007.tb12610.x

Ross, B., Barat, M., and Fujioka, T. (2017). Sound-Making Actions Lead to Immediate Plastic Changes of Neuromagnetic Evoked Responses and Induced β-Band Oscillations during Perception. *J. Neurosci.* 37, 5948–5959. doi: 10.1523/JNEUROSCI.3613-16.2017

Saleh, M., Reimer, J., Penn, R., Ojakangas, C. L., and Hatsopoulos, N. G. (2010). Fast and Slow Oscillations in Human Primary Motor Cortex Predict Oncoming Behaviorally Relevant Cues. *Neuron* 65, 461–471. doi: 10.1016/j.neuron.2010.02.001

Salimpoor, V. N., Benovoy, M., Larcher, K., Dagher, A., and Zatorre, R. J. (2011). Anatomically distinct dopamine release during anticipation and experience of peak emotion to music. *Nat. Neurosci.* 14, 257–264. doi: 10.1038/nn.2726

Sarno, S., de Lafuente, V., Romo, R., and Parga, N. (2017). Dopamine reward prediction error signal codes the temporal evaluation of a perceptual decision report. *Proc. Natl. Acad. Sci. U. S. A.* 114, E10494–E10503. doi: 10.1073/pnas.1712479114

Schaffert, N., Braun Janzen, T., Mattes, K., and Thaut, M. H. (2019). A Review on the Relationship Between Sound and Movement in Sports and Rehabilitation. *Front. Psychol.* 10:244. doi: 10.3389/fpsyg.2019.00244

Schmahmann, J. D., Pandya, D. N., Wang, R., Dai, G., D'Arceuil, H. E., de Crespigny, A. J., et al. (2007). Association fibre pathways of the brain: parallel observations from diffusion spectrum imaging and autoradiography. *Brain* 130, 630–653. doi: 10.1093/BRAIN/AWL359

Schneider, C. E., Hunter, E. G., and Bardach, S. H. (2019). Potential Cognitive Benefits From Playing Music Among Cognitively Intact Older Adults: a Scoping Review. *J. Appl. Gerontol.* 38, 1763–1783. doi: 10.1177/0733464817751198

Schneider, S., Münte, T., Rodriguez-Fornells, A., Sailer, M., and Altenmüller, E. (2010). Music-supported training is more efficient than functional motor training for recovery of fine motor skills in stroke patients. *Music Percept.* 27, 271–280. doi: 10.1525/mp.2010.27.4.271

Schneider, S., Schönle, P. W., Altenmüller, E., and Münte, T. F. (2007). Using musical instruments to improve motor skill recovery following a stroke. *J. Neurol.* 254, 1339–1346. doi: 10.1007/s00415-006-0523-2

Schweizer, M., Eylon, S., and Katz-Leurer, M. (2020). The correlation between rhythm perception and gait characteristics at different rhythms among children with cerebral palsy and typically developing children. *Gait Posture* 82, 83–89. doi: 10.1016/j.gaitpost.2020.08.120

Seebacher, B., Kuisma, R., Glynn, A., and Berger, T. (2017). The effect of rhythmic-cued motor imagery on walking, fatigue and quality of life in people with multiple sclerosis: a randomised controlled trial. *Mult. Scler.* 23, 286–296. doi: 10.1177/1352458516644058

Seebacher, B., Kuisma, R., Glynn, A., and Berger, T. (2019). Effects and mechanisms of differently cued and non-cued motor imagery in people with multiple sclerosis: a randomised controlled trial. *Mult. Scler. J.* 25, 1593–1604. doi: 10.1177/1352458518795332

Seinfeld, S., Figueroa, H., Ortiz-Gil, J., and Sanchez-Vives, M. V. (2013). Effects of music learning and piano practice on cognitive function, mood and quality of life in older adults. *Front. Psychol.* 4:810. doi: 10.3389/fpsyg.2013.00810

Shahraki, M., Sohrabi, M., Taheri Torbati, H. R., Nikkhah, K., and NaeimiKia, M. (2017). Effect of rhythmic auditory stimulation on gait kinematic parameters of patients with multiple sclerosis. *J. Med. Life* 10, 33–37.

Sheridan, C., Thaut, C., Brooks, D., and Patterson, K. K. (2021). Feasibility of a rhythmic auditory stimulation gait training program in community-dwelling adults after TBI: a case report. *NeuroRehabilitation* 48, 221–230. doi: 10.3233/NRE-208016

Sihvonen, A. J., Särkämö, T., Leo, V., Tervaniemi, M., Altenmüller, E., and Soinila, S. (2017). Music-based interventions in neurological rehabilitation. *Lancet Neurol.* 16, 648–660. doi: 10.1016/S1474-4422(17)30168-0

Siponkoski, S.-T., Martínez-Molina, N., Kuusela, L., Laitinen, S., Holma, M., Ahlfors, M., et al. (2020). Music Therapy Enhances Executive Functions and Prefrontal Structural Neuroplasticity after Traumatic Brain Injury: evidence from a Randomized Controlled Trial. *J. Neurotrauma* 37, 618–634. doi: 10.1089/neu.2019.6413

Snyder, J. S., and Large, E. W. (2005). Gamma-band activity reflects the metric structure of rhythmic tone sequences. *Cogn. Brain Res.* 24, 117–126. doi: 10.1016/J.COGBRAINRES.2004.12.014

Spaulding, S. J., Barber, B., Colby, M., Cormack, B., Mick, T., and Jenkins, M. E. (2013). Cueing and Gait Improvement Among People With Parkinson's Disease: a Meta-Analysis. *Arch. Phys. Med. Rehabil.* 94, 562–570. doi: 10.1016/j.apmr.2012.10.026

Stephan, K. M., Thaut, M. H., Wunderlich, G., Schicks, W., Tian, B., Tellmann, L., et al. (2002). Conscious and subconscious sensorimotor synchronization-Prefrontal cortex and the influence of awareness. *Neuroimage* 15, 345–352. doi: 10.1006/nimg.2001.0929

Street, A., Zhang, J., Pethers, S., Bond, K., Wiffen, L., and Palmer, H. (2020). Neurologic music therapy in multidisciplinary acute stroke rehabilitation: could it be feasible and helpful?. *Top. Stroke Rehabil.* 27, 541–552. doi: 10.1080/10749357.2020.1729585

Street, A. J., Fachner, J., and Magee, W. L. (2019). Upper limb rehabilitation in chronic stroke using neurologic music therapy: two contrasting case studies to inform on treatment delivery and patient suitability. *Nord. J. Music Ther.* 28, 382–404. doi: 10.1080/08098131.2019.1606848

Street, A. J., Magee, W. L., Bateman, A., Parker, M., Odell-Miller, H., and Fachner, J. (2018). Home-based neurologic music therapy for arm hemiparesis following stroke: results from a pilot, feasibility randomized controlled trial. *Clin. Rehabil.* 32, 18–28. doi: 10.1177/0269215517717060

Tal, I., Large, E. W., Rabinovitch, E., Wei, Y., Schroeder, C. E., Poeppel, D., et al. (2017). Neural entrainment to the beat: the "missing-pulse" phenomenon. *J. Neurosci.* 37, 6331–6341. doi: 10.1523/JNEUROSCI.2500-16.2017

Thaut, M., and Koshimori, Y. (2020). "Neurorehabilitation in aging through neurologic music therapy,"in Music and the Aging Brain, eds L. L. Cuddy, and S. Belleville, (Amsterdam: Elsevier), 351–382. doi: 10.1016/b978-0-12-817422-7.00014-6

Thaut, M., McIntosh, G. C., and Rice, R. R. (1997). Rhythmic facilitation of gait training in hemiparetic stroke rehabilitation. *J. Neurol. Sci.* 151, 207–212. doi: 10.1016/S0022-510X(97)00146-9

Thaut, M., Schleiffers, S., and Davis, W. (1991). Analysis of emg activity in biceps and triceps muscle in an upper extremity gross motor task under the influence of auditory rhythm. *J. Music Ther.* 28, 64–88. doi: 10.1093/jmt/28.2.64

Thaut, M. H. (2005). *Rhythm, Music, and the Brain: Scientific Foundations and Clinical Applications*. New York: Routledge, doi: 10.4324/9780203958827

Thaut, M. H. (2010). Neurologic music therapy in cognitive rehabilitation. *Music Percept.* 27, 281–285. doi: 10.1525/mp.2010.27.4.281

Thaut, M. H., and Abiru, M. (2010). Rhythmic auditory stimulation in rehabilitation of movement disorders: a review of current research. *Music Percept.* 27, 263–269. doi: 10.1525/mp.2010.27.4.263

Thaut, M. H., and Hoemberg, V. (eds) (2014). *Handbook of Neurologic Music Therapy*. New York: Oxford University Press.

Thaut, M. H., Hurt, C. P., Dragan, D., and McIntosh, G. C. (1998). Rhythmic entrainment of gait patterns in children with cerebral palsy. *Dev. Med. Child Neurol.* 40:15.

Thaut, M. H., and Kenyon, G. P. (2003). Rapid motor adaptations to subliminal frequency shifts during syncopated rhythmic sensorimotor synchronization. *Hum. Mov. Sci.* 22, 321–338. doi: 10.1016/S0167-9457(03)00048-4

Thaut, M. H., Kenyon, G. P., Hurt, C. P., McIntosh, G. C., and Hoemberg, V. (2002). Kinematic optimization of spatiotemporal patterns in paretic arm training with stroke patients. *Neuropsychologia* 40, 1073–1081. doi: 10.1016/S0028-3932(01)00141-5

Thaut, M. H., Kenyon, G. P., Schauer, M. L., and McIntosh, G. C. (1999). The connection between rhythmicity and brain function. *IEEE Eng. Med. Biol. Mag.* 18, 101–108. doi: 10.1109/51.752991

Thaut, M. H., Leins, A. K., Rice, R. R., Argstatter, H., Kenyon, G. P., McIntosh, G. C., et al. (2007). Rhythmic auditory stimulation improves gait more than NDT/Bobath training in near-ambulatory patients early poststroke: a single-blind, randomized trial. *Neurorehabil. Neural Repair* 21, 455–459. doi: 10.1177/1545968307300523

Thaut, M. H., and McIntosh, G. C. (2014). Neurologic Music Therapy in Stroke Rehabilitation. *Curr. Phys. Med. Rehabil. Rep.* 2, 106–113. doi: 10.1007/s40141-014-0049-y

Thaut, M. H., McIntosh, G. C., and Hoemberg, V. (2015). Neurobiological foundations of neurologic music therapy: rhythmic entrainment and the motor system. *Front. Psychol.* 5:1185. doi: 10.3389/fpsyg.2015.01185

Thaut, M. H., McIntosh, G. C., Prassas, S. G., and Rice, R. R. (1993). Effect of Rythmic Auditory curing on Temporal Stride Parameters and EMG Patterns in Hemiparetic Gait of Stroke Patients. *J. Neurol Rehabil.* 7, 9–16.

Thaut, M. H., McIntosh, G. C., Rice, R. R., Miller, R. A., Rathbun, J., and Brault, J. M. (1996). Rhythmic auditory stimulation in gait training for Parkinson's disease patients. *Mov. Disord.* 11, 193–200. doi: 10.1002/mds.870110213

Thaut, M. H., Rice, R. R., Braun Janzen, T., Hurt-Thaut, C. P., and McIntosh, G. C. (2019). Rhythmic auditory stimulation for reduction of falls in Parkinson's disease: a randomized controlled study. *Clin. Rehabil.* 33, 34–43. doi: 10.1177/0269215518788615

Thaut, M. H., Stephan, K. M., Wunderlich, G., Schicks, W., Tellmann, L., Herzog, H., et al. (2009). Distinct cortico-cerebellar activations in rhythmic auditory motor synchronization. *Cortex* 45, 44–53. doi: 10.1016/j.cortex.2007.09.009

Thevathasan, W., Cole, M. H., Graepel, C. L., Hyam, J. A., Jenkinson, N., Brittain, J.-S., et al. (2012a). A spatiotemporal analysis of gait freezing and the impact of pedunculopontine nucleus stimulation. *Brain* 135, 1446–1454. doi: 10.1093/BRAIN/AWS039

Thevathasan, W., Pogosyan, A., Hyam, J. A., Jenkinson, N., Foltynie, T., Limousin, P., et al. (2012b). Alpha oscillations in the pedunculopontine nucleus correlate

with gait performance in parkinsonism. *Brain* 135, 148–160. doi: 10.1093/BRAIN/AWR315

Thompson, S., Hays, K., Weintraub, A., Ketchum, J. M., and Kowalski, R. G. (2021). Rhythmic Auditory Stimulation and Gait Training in Traumatic Brain Injury: a Pilot Study. *J. Music Ther.* 58, 70–94. doi: 10.1093/jmt/thaa016

Tian, R., Zhang, B., and Zhu, Y. (2020). Rhythmic Auditory Stimulation as an Adjuvant Therapy Improved Post-stroke Motor Functions of the Upper Extremity: a Randomized Controlled Pilot Study. *Front. Neurosci.* 14:649. doi: 10.3389/fnins.2020.00649

Tong, Y., Forreider, B., Sun, X., Geng, X., Zhang, W., Du, H., et al. (2015). Music-supported therapy (MST) in improving post-stroke patients' upper-limb motor function: a randomised controlled pilot study. *Neurol. Res.* 37, 434–440. doi: 10.1179/1743132815Y.0000000034

Trombetti, A., Hars, M., Herrmann, F. R., Kressig, R. W., Ferrari, S., and Rizzoli, R. (2011). Effect of music-based multitask training on gait, balance, and fall risk in elderly people: a randomized controlled trial. *Arch. Intern. Med.* 171, 525–533. doi: 10.1001/archinternmed.2010.446

van Ede, F., Szebényi, S., and Maris, E. (2014). Attentional modulations of somatosensory alpha, beta and gamma oscillations dissociate between anticipation and stimulus processing. *Neuroimage* 97, 134–141. doi: 10.1016/J.NEUROIMAGE.2014.04.047

Varsamis, P., Staikopoulos, K., and Kartasidou, L. (2012). Effect Of Rhythmic Auditory Stimulation On Controlling Stepping Cadence Of Individuals With Mental Retardation And Cerebral Palsy. *Int. J. Spec. Educ.* 27, 68–75.

Vik, B. M. D., Skeie, G. O., and Specht, K. (2019). Neuroplastic effects in patients with traumatic brain injury after music-supported therapy. *Front. Hum. Neurosci.* 13:177. doi: 10.3389/fnhum.2019.00177

Vik, B. M. D., Skeie, G. O., Vikane, E., and Specht, K. (2018). Effects of music production on cortical plasticity within cognitive rehabilitation of patients with mild traumatic brain injury. *Brain Inj.* 32, 634–643. doi: 10.1080/02699052.2018.1431842

Vinciguerra, C., de Stefano, N., and Federico, A. (2019). Exploring the role of music therapy in multiple sclerosis: brief updates from research to clinical practice. *Neurol. Sci.* 40, 2277–2285. doi: 10.1007/s10072-019-04007-x

Vitorio, R., Stuart, S., Gobbi, L. T. B., Rochester, L., Alcock, L., and Pantall, A. (2018). Reduced Gait Variability and Enhanced Brain Activity in Older Adults With Auditory Cues: a Functional Near-Infrared Spectroscopy Study. *Neurorehabil. Neural Repair* 32, 976–987. doi: 10.1177/1545968318805159

Wang, T. H., Peng, Y. C., Chen, Y. L., Lu, T. W., Liao, H. F., Tang, P. F., et al. (2013). A home-based program using patterned sensory enhancement improves resistancance exercise effects for children with cerebral palsy: a randomized controlled trial. *Neurorehabil. Neural Repair* 27, 684–694. doi: 10.1177/1545968313491001

Wang, Y., Pan, W.-Y., Li, F., Ge, J.-S., Zhang, X., Luo, X., et al. (2021). Effect of Rhythm of Music Therapy on Gait in Patients with Stroke. *J. Stroke Cerebrovasc. Dis.* 30:105544. doi: 10.1016/j.jstrokecerebrovasdis.2020.105544

Williams, G., Galna, B., Morris, M. E., and Olver, J. (2010). Spatiotemporal deficits and kinematic classification of gait following a traumatic brain injury: a systematic review. *J. Head Trauma Rehabil.* 25, 366–374. doi: 10.1097/HTR.0b013e3181cd3600

Wittwer, J. E., Webster, K. E., and Hill, K. (2013). Effect of Rhythmic Auditory Cueing on Gait in People With Alzheimer Disease. *Arch. Phys. Med. Rehabil.* 94, 718–724. doi: 10.1016/j.apmr.2012.11.009

Wittwer, J. E., Winbolt, M., and Morris, M. E. (2020). Home-Based Gait Training Using Rhythmic Auditory Cues in Alzheimer's Disease: feasibility and Outcomes. *Front. Med.* 6:335. doi: 10.3389/fmed.2019.00335

Worschech, F., Marie, D., Jünemann, K., Sinke, C., Krüger, T. H. C., Großbach, M., et al. (2021). Improved Speech in Noise Perception in the Elderly After 6 Months of Musical Instruction. *Front. Neurosci.* 15:840. doi: 10.3389/fnins.2021.696240

Zendel, B. R., West, G. L., Belleville, S., and Peretz, I. (2019). Musical training improves the ability to understand speech-in-noise in older adults. *Neurobiol. Aging* 81, 102–115. doi: 10.1016/j.neurobiolaging.2019.05.015

Zhang, Y., Cai, J., Zhang, Y., Ren, T., Zhao, M., and Zhao, Q. (2016). Improvement in Stroke-induced Motor Dysfunction by Music-supported Therapy: a Systematic Review and Meta-Analysis. *Sci. Rep.* 6:38521. doi: 10.1038/srep38521

Zhou, Z., Zhou, R., Wei, W., Luan, R., and Li, K. (2021). Effects of music-based movement therapy on motor function, balance, gait, mental health, and quality of life for patients with Parkinson's disease: a systematic review and meta-analysis. *Clin. Rehabil.* 35, 937–951. doi: 10.1177/0269215521990526

Conflict of Interest: The authors declare that the research was conducted in the absence of any commercial or financial relationships that could be construed as a potential conflict of interest.

Publisher's Note: All claims expressed in this article are solely those of the authors and do not necessarily represent those of their affiliated organizations, or those of the publisher, the editors and the reviewers. Any product that may be evaluated in this article, or claim that may be made by its manufacturer, is not guaranteed or endorsed by the publisher.

frontiers in Human Neuroscience

MINI REVIEW
published: 17 January 2022
doi: 10.3389/fnhum.2021.787157

The Control of Movements via Motor Gamma Oscillations

*José Luis Ulloa**

Programa de Investigación Asociativa (PIA) en Ciencias Cognitivas, Centro de Investigación en Ciencias Cognitivas (CICC), Facultad de Psicología, Universidad de Talca, Talca, Chile

The ability to perform movements is vital for our daily life. Our actions are embedded in a complex environment where we need to deal efficiently in the face of unforeseen events. Neural oscillations play an important role in basic sensorimotor processes related to the execution and preparation of movements. In this review, I will describe the state of the art regarding the role of motor gamma oscillations in the control of movements. Experimental evidence from electrophysiological studies has shown that motor gamma oscillations accomplish a range of functions in motor control beyond merely signaling the execution of movements. However, these additional aspects associated with motor gamma oscillation remain to be fully clarified. Future work on different spatial, temporal and spectral scales is required to further understand the implications of gamma oscillations in motor control.

Keywords: neural oscillations, gamma, movement, motor cognition, conflict

OPEN ACCESS

Edited by:
Marco Iosa,
Sapienza University of Rome, Italy

Reviewed by:
Junichi Ushiyama,
Keio University Shonan Fujisawa Campus, Japan
Tony W. Wilson,
Boys Town National Research Hospital, United States

***Correspondence:**
José Luis Ulloa
joseluisulloafulgeri@gmail.com

Specialty section:
This article was submitted to Motor Neuroscience, a section of the journal Frontiers in Human Neuroscience

Received: *30 September 2021*
Accepted: *22 December 2021*
Published: *17 January 2022*

Citation:
Ulloa JL (2022) The Control of Movements via Motor Gamma Oscillations. Front. Hum. Neurosci. 15:787157. doi: 10.3389/fnhum.2021.787157

THE NEURAL ORGANIZATION OF MOVEMENTS

Human cognition is embedded in our interactions with others and with the environment (Varela et al., 2016; Rossi et al., 2019). From this point of view, to understand cognition is critical to understand how action and motor functions are realized within the nervous system. The impact of actions on our minds has been historically neglected, but now it has been acknowledged that even simple movements can modulate cognitive functions (Leisman et al., 2016). The motor system constitutes all those processes involving the movement of the muscles and the neural systems advocated to the control of the muscles. The motor system is tightly interconnected with other neural systems to organize movements. A quintessential example of this interaction occurs between perception and action systems (Prinz, 1997; Jeannerod, 2006). Perception and action are linked even at the lowest level of organization in the motor system, with feedforward and feedback loops being essential for motor control. The function of basic units in the motor system directly commanding the muscles depends on feedback from the muscles and from information in tendons and joints (Poppele and Bosco, 2003; Windhorst, 2007). This reciprocal interaction is replicated in higher levels of organization of the motor system. The brain circuits associated with movements converge on the primary motor cortex (M1 or Brodmann area 4) and signals are sent through the spinal cord to the muscles so motor commands are executed. However, previous to M1 activity the smooth unfolding of actions is programmed and organized in motor-related brain areas such as the premotor cortex (PMC, lateral part of the Brodmann area 6), the supplementary motor area (SMA, medial part of the Brodmann area 6) and the prefrontal cortex (PFC). The SMA forms a circuit loop with the PFC to organize voluntary actions devised in the PFC, while the PMC forms a circuit loop with parietal cortices and seems to be more reactive to externally evoked movements (Donoghue and Sanes, 1994). This network of brain regions extends to other subcortical areas such as the thalamus, the basal ganglia and the cerebellum, which contribute to the fine tuning of motor parameters in iterative loops that affect the ongoing activity of the muscles (Rosenbaum, 2010).

Connections with high-level centers such as the PFC are supposed to feed with action "intentions" and "goals." It is thus important to understand how these brain signals are transmitted to regions downstream in the motor system. In addition, human movements are not realized in a vacuum. Actions are created and modulated by a rich context, with motor programs being regulated and monitored at distinct levels of the motor system (Haggard, 2008). These distinct levels where action processing occurs have been investigated with modern brain imaging techniques. Among these methods, the electrophysiological techniques are useful for identifying and characterizing brain rhythms associated with action processing.

THE NEURAL DYNAMICS OF MOVEMENTS

Time-resolved electrophysiological techniques allow us to capture the macroscopic neural dynamics of the nervous system. This means we can precisely describe the sequence of neural activations that occur across multiple regions in the brain as humans or other animals engage in an activity or remain at rest. Rhythmic brain activity is associated with many perceptual and cognitive processes contributing to both low to high-level functions in humans (Varela et al., 2001; Buzsaki, 2006; Hari and Puce, 2017). In the motor system, the coding of movements has been shown to rely on the collective activity of a population of neurons (a population code; Georgopoulos et al., 1982, 1983). Likewise, rhythmic brain activity also seems to play an important – albeit not fully understood – role in the organization of movements (see van Wijk et al., 2012; Cheyne, 2013 for excellent reviews). Many studies investigating movement production have been focused on well-known neural oscillations in the alpha (10–12 Hz) and beta (13–30 Hz) band ranges. There is consistent evidence that execution of movements induces a decrease in alpha (Pfurtscheller, 1981; Salmelin and Hari, 1994; Cochin et al., 1999; Muthukumaraswamy et al., 2004; Neuper et al., 2006; Koelewijn et al., 2008) and beta (Cheyne et al., 2008; Gaetz et al., 2010; Wilson et al., 2010, 2014) oscillatory activity in sensorimotor cortices. Beta activity is characterized by building up well before the onset of movements, persisting and waning during the movement and being followed by a strong re-synchronization after movement end (beta rebound; Jurkiewicz et al., 2006; Engel and Fries, 2010; Zaepffel et al., 2013). More recently, gamma oscillatory activity (above 40 Hz) has attracted attention by its putative role in motor control. Gamma oscillations have been widely studied in vision and attention research, where they have shown a crucial role in integrating visual information (Gray and Singer, 1989; Tallon-Baudry et al., 1997). Based on these studies, it has been proposed that gamma oscillations may be a general cortical activity that integrates events among separated areas of the cortex for a variety of cognitive processes (Bressler, 1990; Fries, 2005). Based on recent works, researchers have started to uncover the functions of gamma oscillations in the motor system. In the following sections, I will outline distinct aspects of motor gamma oscillations, including local and long-range activity involved in simple and complex movements. The reader can also consult a summary table at the end of the manuscript that I have prepared with methodological details and main findings.

MOTOR GAMMA OSCILLATIONS

Overview

In a seminal study using electrocorticography (ECoG) Crone et al. (1998) identified two kinds of motor gamma responses. A motor gamma centered in the 35–50 Hz range that started with the motor response and remains active during the duration of the movement and a motor gamma activity centered in the 75–100 Hz range that started slightly before the motor response and was transient. This latter neural activity was somatotopically organized and was more circumscribed at contralateral sides than alpha or beta oscillations. Follow-up studies have confirmed these findings for a wide range of gamma frequency bands using again ECoG (Pfurtscheller et al., 2003; Leuthardt et al., 2004; Ball et al., 2008; Darvas et al., 2010), but also using magnetoencephalography (MEG; Dalal et al., 2007; Cheyne et al., 2008; Tecchio et al., 2008; Muthukumaraswamy, 2010; Wilson et al., 2010; Trevarrow et al., 2019; Spooner et al., 2021; Wiesman et al., 2021), scalp electroencephalography (EEG; Pfurtscheller et al., 1993; Ball et al., 2008; Darvas et al., 2010; Herz et al., 2012; Oliveira et al., 2019; Djalovski et al., 2021) and stereo EEG (Brovelli et al., 2005; Szurhaj et al., 2005). The detected gamma activities in EEG tend to be in the low frequency band range near 40 to 60 Hz because of the filtering properties of the scalp, cortical orientations of neuronal populations and other factors that limit the detection of fast rhythms in EEG (Nunez and Srinivasan, 2006). The range of frequencies in which motor gamma has been found is quite variable, analogous to what happens in gamma oscillations in other domains (Uhlhaas et al., 2011). In the motor domain, gamma oscillations have been reported for ranges between 75–100 Hz (Crone et al., 1998), 65–90 Hz (Dalal et al., 2007), 59–84 Hz (Ball et al., 2008), 81–101 Hz (Darvas et al., 2010), 60–90 Hz (Muthukumaraswamy, 2010; Grent-'t-Jong et al., 2013), 64–84 Hz (Wiesman et al., 2020), and 72–84 Hz (Spooner et al., 2021), to name a few. In intracranial EEG studies, the range of motor gamma is even broader, covering a 60–200 Hz range (Brovelli et al., 2005). These distinct frequency ranges may also reflect distinct forms of gamma oscillations in the high frequency range (Uhlhaas et al., 2011). To date, there is no clear understanding of the functional significance of distinct gamma types. To develop a full picture of gamma oscillations, efforts should be done to systematically and precisely describe the frequency range in which motor gamma oscillations occur.

Motor gamma oscillations have been observed for simple movements, including finger movements, tongue protrusions, eye-winking, fist-clenching and foot movements (Pfurtscheller and Neuper, 1992; Crone et al., 1998; Pfurtscheller et al., 2003; Miller et al., 2007; Cheyne et al., 2008), but they have been also observed for more elaborated representations of actions such as motor imagery (Miller et al., 2010; Grosse-Wentrup et al., 2011), mirroring of movements (Butorina et al., 2014), walking and cycling movements (Gwin et al., 2011; Seeber et al., 2016) and

interpersonal interaction (Djalovski et al., 2021). Motor gamma oscillations seem also to change during human development. It has been reported that gamma oscillations associated with motor processing are very variable in frequency for very young children, with frequency ranges varying between 35–45 and 70–80 Hz (Cheyne et al., 2014). This variability seems to settle in 70–80 Hz in children, adolescents and adults (Gaetz et al., 2010). In addition, the power of motor gamma oscillations has been reported to change from childhood to adolescence, with decreases of gamma oscillations at the M1 (Trevarrow et al., 2019) and the SMA (Wilson et al., 2010). One interpretation of these findings is that, as the nervous system matures, motor control becomes more localized and efficient (Wilson et al., 2010). The reported decrease of gamma oscillations in adolescence contrast with another study showing an increase of motor gamma power from childhood to adolescence and weaker motor gamma in adults relative to adolescents (Gaetz et al., 2010). There is also evidence that lateralization of motor gamma activity is modulated during adolescence (Huo et al., 2011), meaning that the strong lateralization of motor gamma oscillations is the product of a developmental trajectory. Overall, these studies highlight the pervasive nature of gamma oscillations in distinct forms of motor processing and its changes during development.

Local Gamma Activity

It has been often remarked that brain oscillations at the lower end of the spectrum tend to engage large areas, while those oscillations at higher frequencies are localized in restricted cortical areas (Lopes da Silva, 2013). Local motor gamma activity has been generally found in M1 (Crone et al., 1998; Cheyne et al., 2008; Darvas et al., 2010; Muthukumaraswamy, 2010), but also from accessory motor regions in the SMA (Szurhaj et al., 2005; Ball et al., 2008; Wilson et al., 2010; Tamás et al., 2018), the PMC (Brovelli et al., 2005; Gaetz et al., 2013; Dürschmid et al., 2014; Wiesman et al., 2020) and regions closer to the frontal cortex (Gaetz et al., 2013; Grent-'t-Jong et al., 2013). In addition, it has been widely recognized that M1 receives inputs from subcortical areas such as the thalamus, the cerebellum, and the basal ganglia. The basal ganglia is a set of interconnected nuclei in the forebrain that exerts an inhibitory influence on several motor systems (Nambu et al., 2002). Motor gamma activity has been also found in the basal ganglia, in particular in the globus pallidus (GB) and the subthalamic nucleus (STN; Alegre et al., 2005; Brücke et al., 2008). This broad motor gamma network is potentially critical for the organization of movements. However, the relationship between gamma oscillations arising from cortical and subcortical regions is still poorly understood. Hints of a possible relationship have been suggested. A study designed to compare motor gamma activity evoked for upper and lower limbs found that the peak frequency of gamma was slightly higher, and consistent within individuals, for both right and left fingers and elbows relative to foot movements (Cheyne et al., 2008; Cheyne and Ferrari, 2013). These individual gamma "fingerprints" led the authors to speculate that gamma activity detected at cortical sites may have a common origin and that source could be at the level of cortico-subcortical networks. Overall, findings from studies focusing on local neural activity show that gamma oscillations are distributed across several cortical and subcortical structures.

The nature of gamma oscillations is an ongoing mystery. Unlike neural oscillations in the low frequency range, like alpha and beta, motor gamma oscillations have been described as prokinetic, i.e., to promote movements. The increase of gamma oscillatory activity has been found to occur very close to triggering of movements (Crone et al., 1998; Pfurtscheller et al., 2003; Cheyne et al., 2008; Darvas et al., 2010; Muthukumaraswamy, 2010; but see also Muthukumaraswamy, 2010 for modulations at the movement end). This temporal feature suggests a role of gamma oscillations in the driving of movements, but the evidence is not clear. Some authors have suggested that motor gamma activity is associated with the processing of sensory reafferences (from the muscles) in sensory and motor cortical centers (Szurhaj et al., 2005). This view holds that motor gamma oscillations bind sensorimotor information and facilitate movement. In this sense, gamma oscillations should be strongly related to the processing of sensory information. However, in a MEG study, Muthukumaraswamy (2010) shows that motor gamma occurred equally well for both self-paced and evoked movements but not for passive movements. In this same study, the author also showed that motor gamma activity peaked only at the beginning of a sequence of repetitive movements and remained silent during the execution period. The short-lived behavior of motor gamma oscillations has been observed in other studies (Cheyne et al., 2008; Gaetz et al., 2013; Wiesman et al., 2020). Thus, motor gamma oscillations are tightly locked to the initiation of voluntary movements and they don't seem to be a direct consequence of sensory feedback produced by movements. Using a mirror illusion effect, a study supports this idea. The illusion of a moving hand can be evoked through the reflection (in a mirror) of the movement of the opposite hand. Using this paradigm (Butorina et al., 2014) demonstrated an increase of motor gamma in a mirror manipulation. The increase of motor gamma oscillations in this illusion suggest that gamma activity is independent of proprioceptive feedback. It is worth noting, however, that gamma activity evoked during this illusion was less strong than the activity evoked for the actual movements. More studies will be required to clarify the contribution of sensory feedback to motor gamma activity. A role of motor gamma oscillations in the control of movements should also involve the coding of basic motor parameters. There is evidence that gamma oscillations are associated with the coding of motor parameters like force and direction. Muthukumaraswamy (2010) showed that greater motor gamma power at M1 was associated with greater force of movements. In addition, ECoG studies have shown that motor gamma power at the M1 could be used for decoding the direction of movements (Leuthardt et al., 2004; Ball et al., 2009; Yanagisawa et al., 2012). Interestingly, there are also studies showing that subcortical gamma activity is involved in the coding of basic of motor parameters associated with movements. Gamma activity at the STN is greater when greater force is required (Tan et al., 2013; Alhourani et al., 2020) and it is associated with larger (Brucke et al., 2012; Lofredi et al., 2018) and faster movements (Brucke et al., 2012; Joundi et al., 2012). Altogether, the current evidence highlight some

of the characteristics of motor gamma oscillations: its close connection (at least temporally) with movement initiation and its contribution to the coding of some basic motor properties. However, recent works have acknowledged a more sophisticated role of motor gamma oscillations in the processing of actions.

In real life, movements need to be performed under challenging conditions or might entail rapid adjustments. Cognitive control describes the ability to generate, maintain and adjust strategies directed to specific goals, which altogether allows the emergence of flexible behavior (Botvinick et al., 2001). A key question in cognitive neuroscience has been how cognitive control is carried out in the brain. Distinct lines of research have emphasized the idea that cognitive control, and more generally, executive functions, are commanded by the PFC (Toba et al., 2020). In this line, electrophysiological evidence shows that these prefrontal operations involve theta (Cohen et al., 2008; Nigbur et al., 2011; Gulbinaite et al., 2014) and gamma (Jensen et al., 2007; Roux et al., 2012) oscillatory responses. However, emergent evidence suggests that gamma oscillations at M1 (Isabella et al., 2015; Heinrichs-Graham et al., 2018; Spooner et al., 2021), motor regions like the PMC (Gaetz et al., 2013; Wiesman et al., 2020) and medial frontal regions (Grent-'t-Jong et al., 2013) contribute to the neural processing of movements in the context of interference or conflict. These studies are based on cognitive psychology paradigms where participants are required to perform movements under conditions of interference and require the inhibition of responses. These studies have shown that motor gamma responses increase during interference in an Eriksen flanker (Grent-'t-Jong et al., 2013; Heinrichs-Graham et al., 2018; Spooner et al., 2021). In this task, participants respond to a central letter or object flanked by distractor stimuli that evoke an alternative response (Eriksen and Eriksen, 1974). In an incompatible or interference condition, a conflict is generated because a target attribute is presented alongside a distractor. To succeed in this task, participants have to focus on suppressing an automatic tendency to respond to the irrelevant dimension. Interestingly, in distinct versions of this task, there have been selective changes either in power (Grent-'t-Jong et al., 2013; Spooner et al., 2021) or the frequency (Heinrichs-Graham et al., 2018) of gamma oscillations. These differences could be due to differences in the experimental setting, such as the use of distinct button responses systems and the involvement of a different number of fingers. It is likely that our understanding of the impact of gamma oscillations in this type of motor responses will improve with more studies that incorporate distinct spectral metrics (power, frequency and phase). Motor gamma responses have been also studied in a modified Go/No-Go task where a switch condition is included (Isabella et al., 2015). In the Go/No-Go task, participants must perform speeded responses in Go trials and must refrain from responding on No-Go trials (Logan et al., 2014). In the No-Go condition, a response inhibition is used to cancel an intended movement. Conversely, in a switch condition, participants are asked to perform a distinct movement. In the study of Isabella et al. inhibition to stop was reflected in increased theta power and inhibition to switch was reflected in increased gamma power. These findings show a complementary roles of theta and gamma oscillations in the inhibition of responses (Isabella et al., 2015). Gamma activity is also modulated by contextual information. In another MEG study, participants were asked to perform a repetitive bimanual response in response to visual stimuli. For a given hand, the context was uncertain because in 20% of the trials a signal indicated that no movement has to be performed. For the other hand, the context was certain because there was never a stop signal and movements has to be executed every time (Wiesman et al., 2021). When contralateral responses of each hand were compared to each other the authors found increased motor gamma power for movements performed in the uncertain relative to the certain context. The engagement of motor gamma oscillations in this situation speak of mechanisms oriented to process the dynamic and uncertain conditions of our environment. These findings converge with other studies that show the responsiveness of motor gamma activity to environmental cues, such as in attentional capture (Spooner et al., 2020). This responsiveness to dynamical environmental demands highlights the adaptive functions that motor gamma oscillations have and its potential implications for our interactions with our surrounding environment. Lastly, it is worth mentioning that subcortical gamma activity has been also observed in experimental situations where participants are required to inhibit responses. There is robust evidence of the involvement of the basal ganglia in motor control. A basal ganglia circuit involves close interactions with cortical and other subcortical regions and is important for fine adjustment of movements and the inhibition of responses. This circuit has two main pathways. A direct pathway has been associated with facilitation of movement preparation, while an indirect pathway has been associated with the suppression of movement preparation (Chakravarthy, 2013). In this basal ganglia circuit the STN operate as a break within the indirect pathway. In addition, there is a hyperdirect pathway (a faster route than the aforementioned pathways) where frontal (IFG, PFC) and motor (preSMA) regions are connected directly with the STN (Swann et al., 2012; Chen et al., 2020). This pathway seems to be important for the inhibition of automatic responses. In these studies, the inhibition of responses can be assessed with a Stop signal task. In this task, a participants had to respond to a visual stimulus (go cue) and in a set of trials this go cue is followed by a stop signal. The task is to stop the ongoing response to the cue (Bari and Robbins, 2013). Recent work has demonstrated that gamma activity at the STN is modulated during inhibitory responses (Ray et al., 2012; Alegre et al., 2013; Fischer et al., 2017). Altogether the evidence reviewed above suggest that local gamma activity at cortical and subcortical areas is important for distinct types of movements and for the inhibition of responses. Beyond local activity, gamma oscillations have been also hypothesized to carry information in structures far away apart.

Brain-Muscle Coupling

Researchers have been dealing for long time to understand how motor commands are transmitted from the cortex to the muscles. Axons from the neurons in high-level processing areas of the motor system descend through the spinal cord and reach the neurons that connect directly with the muscles (Rosenbaum, 2010). In the spinal cord, alpha neurons connecting with the muscles form what has been called motor units. Each motor unit

is composed of a motor neuron and all the muscles this motor neuron innervates (Rosenbaum, 2010). The electrical activity of the muscles indirectly reflects the activity of spinal alpha neurons (and thus of motor units) and is measured by electromyography (EMG). The study of muscular activity originated from early investigations by Hans Piper, who detected a muscular 40 Hz activity using a stethoscope. This rhythm is called the Piper rhythm in his honor. In a seminal study in humans, Conway et al. (1995) demonstrated that brain signals show brain-muscle coupling (as coherence) in the beta range when participants are asked to perform isometric contractions with weak force. Isometric contractions are static compressions of the muscle and occur without movement. Later studies showed that a contraction entailing force may lead to a decrease of beta coherence (Kilner et al., 1999) and a predominance of coherence in the gamma range (∼40 Hz; Brown et al., 1998; Mima et al., 1999; Li et al., 2020). Gamma brain-muscle coupling is produced also for slow movements (Salenius et al., 1996; Marsden et al., 2000), repeated maximal contractions (Brown et al., 1998) and isotonic movements (for lower limb movements; Gwin and Ferris, 2012). Unlike isometric contractions, isotonic movements are associated with changes in the muscle's length. Some studies pinpoint to some distinctions in the brain muscle-coupling in the gamma or beta range. For instance, Omlor et al. (2007) showed that gamma coupling occurs in complex or dynamic movements, while beta is predominant for movements with a stable motor output. It has been also hypothesized that gamma coupling could be important for the correct prediction of errors in fast force transitions (Mehrkanoon et al., 2014). Finally, local gamma activity seems to be independent of brain-muscle coupling. Muthukumaraswamy (2011) showed that for simple and repetitive movements, cortical gamma increase was paralleled by an increase of brain-muscle coupling, but for static force production there is a burst of gamma activity without an increase in brain-muscle coupling. These findings suggest different functional processes reflected in brain-muscle coupling and cortical activity.

There is a more general issue that involves the synchronic nature of brain-muscle coupling. Some studies have found instantaneous (or zero delay) synchronization in brain-muscle coupling (Conway et al., 1995; Halliday et al., 1998). In the motor system, a mechanism that could induce zero delay synchronization could involve afferent feedback from the muscles. There is evidence supporting this notion. For instance, ischemia-induced deafferentation (producing lack afferent feedback) dampen brain-muscle coupling (Pohja and Salenius, 2003). Conversely, it has been shown that affecting spindle activity in the muscles does not change the Piper rhythm (Hagbarth et al., 1983) or the brain-muscle coupling (Mima et al., 2000). In addition, there are studies reporting a delay between brain and the muscle signals in brain-muscle coupling (Salenius et al., 1997; Brown et al., 1998; Mima et al., 2000). This lag occurs in a direction where the motor cortex is activated first and drives the activity of the muscle. The sources of the leading activity in the brain have been shown to follow a somatotopic organization and to be at the M1 (Gross et al., 2005), although the SMA may also contribute (Salenius et al., 1997; Hari and Salenius, 1999). It has been also reported a 15 ms longer delay in brain-muscle coupling for lower relative to upper limb movements (Mima et al., 2000). These differences have been in part explained as differences in the conduction distance between the cortex and the muscle. The practical importance of brain-muscle coupling to motor behavior is still discussed. Some studies have shown an increased brain-muscle gamma coupling with increased readiness to respond in simple reaction time experiments (Schoffelen et al., 2005, 2011). There remain several aspects of motor-muscle coupling about which relatively little is known.

Brain–Brain Coupling

It is currently acknowledged that neural functions derive from some specialization of brain areas. However, the modern view maintains that cognitive functions emerge from the cooperative participation of groups of brain regions or networks (Sporns, 2011). While local neural activity covers an area of ∼1 cm through monosynaptic connections, large-scale activity is said to occur between neural assemblies that are over 1 cm apart and involve polysynaptic pathways (Varela et al., 2001). Long-range interactions involve a complex configuration of connections between distinct nodes that are difficult to understand. This is further complicated by the fact that connectivity measures show limitations because of the probability of spurious synchronization. The exact functional significance of brain–brain coupling has not been demarcated, but it is assumed that the co-activation of brain regions during a task reflects the relevance of a given neuronal ensemble for the cognitive process under study. In the motor domain, brain regions related to action processing are thought to act in concert so precise and smooth movement are brought about. Studies of connectivity have been propelled by former functional magnetic resonance and positron emission tomography that defined the key nodes associated with the motor brain network. For instance, simple finger movements involved a lateralized motor network comprising regions like the M1, PMC and the SMA (Catalan, 1998; Diciotti et al., 2007). Electrophysiological studies have investigated the oscillatory coupling between these regions (e.g., Gerloff, 1998; Gross et al., 2005). For instance, Gross et al. (2005) investigated with MEG the connectivity across several frequency bands for a set of unimanual and bimanual movements. This study showed that left M1-right M1 coupling was greater for bimanual relative to unimanual movements. In addition, it was shown that changes in gamma M1-SMA coupling and gamma brain-muscle coupling occurred for movements with distinct complexity. This basic core motor network has been naturally extended to other regions, like the PFC and posterior parietal cortex. For instance, it has been shown that distinct types of finger movements involve distinct gamma connectivity profiles between primary sensorimotor cortices with the SMA and the PFC (Tamás et al., 2018). Differences in patterns of connectivity has been also disclosed with dynamic causal modeling. In an EEG study, it has been shown that isometric contractions of the forearm involve gamma coupling between the M1 and SMA, while repetitive finger movements involve an additional coupling between the PMC and both the M1 and SMA (Herz et al., 2012). Again, subcortical regions have been seen to contribute to motor control and to code basic motor parameters. For instance, it has been

shown increased cortico-subcortical coupling between the M1 and STN for increased force (Alhourani et al., 2020) and velocity (Fischer et al., 2020) in manual responses. Gamma coupling has been also seen in responses associated with inhibition. For instance, an ECoG showed increased gamma coupling between the preSMA and right inferior frontal gyrus (IFG) for responses that required a stopping response (Swann et al., 2012).

Brain–brain coupling can also occur across different frequency bands. Typically, activities in the lower frequency band modulate the amplitude, frequency, or phase of the higher frequency signal. This cross-frequency coupling (CFC) has been linked to several cognitive processes and has been shown to be altered in pathological states (Canolty and Knight, 2010). A form of CFC, phase-amplitude coupling (PAC) has been typically found between theta and gamma, where the phase of theta activity modulates the amplitude of gamma activity (Lisman and Jensen, 2013). Theta-gamma coupling has been also shown in the motor domain. A study involving a variety of distinct tasks (a serial response, auditory motor coordination and Go/No-Go task) revealed that an increase theta-gamma PAC coupling is associated with an increment in motor performance (Dürschmid et al., 2014). These effects reflect a role of motor gamma oscillations in association with theta rhythms in motor learning. PAC coupling has been also shown to be involved in inhibition of responses. In an MEG study, participants were asked to perform a social approach-avoidance task where they have to avoid or approach emotional displays using a joystick (Bramson et al., 2018). The authors observed that theta power at the PFC was modulated by the congruence conditions, with increased theta activity in the incongruent relative to the congruent condition. Cognitive control exerted by the PFC was further qualified by PAC between PFC theta and M1 motor gamma. This is, the increase of gamma activity during emotional action control was modulated by the PFC. Even more, in a transcranial alternating current stimulation (tACS) study, emotional control was elicited by increasing this PFC-M1 theta-gamma coupling (Bramson et al., 2020). Other studies have characterized theta-gamma coupling and found that is modulated by sensory modulations. Somatosensory entrainment reduced theta-gamma PAC in simple fingers movements in a visual response paradigm (Spooner et al., 2021). The evidence presented support the idea that gamma activity occurs locally and in large-scale interactions. From a functional point of view, motor gamma encodes certain basic motor parameters and seems to play a role in inhibitory responses. More evidence still needs to be gathered to fully understand the role of gamma oscillations in movements. Another important aspect of gamma is its biological substrates. This is important since it has been observed that disturbances in the generation of gamma oscillations have been associated with some neurological and psychiatric conditions.

Neurobiological Mechanisms and Physiopathology

Neural oscillations correspond to rhythmic fluctuations in the excitability of populations of neurons occurring at distinct spatial and temporal scales (Varela et al., 2001; Buzsaki, 2006). The mechanisms that give rise to oscillations involve the interactions between inhibitory interneurons, based on aminobutyric acid (GABA)ergic neurotransmission, and excitatory pyramidal cells, based on glutamatergic neurotransmission. An alternating cycle between excitatory and inhibitory states emerges when excitatory pyramidal cells get activated and stimulate interneurons which then inhibit the excitatory cells. The following decrease in inhibition allows the excitation period to start again (Buzsáki and Wang, 2012). Both excitatory and inhibitory mechanisms are important for the generation of neural oscillations, particularly in the gamma band. Excitatory mechanisms led by α-amino-3-hydroxy-5-methyl-4-isoxazolepropionic acid (AMPA) and N-methyl-D-aspartate (NMDA) neurotransmission is critical for the generation of gamma oscillations (Fuchs et al., 2001; Carlén et al., 2012). Similarly, the inhibitory features of parvalbumin-expressing GABAergic interneurons are a key element in the generation of gamma oscillations (Sohal et al., 2009). The role of GABA neurotransmission has been investigated with MEG and pharmacological interventions. Some studies have shown that modulations of GABA neurotransmission are more directly associated with changes in beta rather than gamma oscillations in the motor cortex (Gaetz et al., 2011; Hall et al., 2011; Muthukumaraswamy et al., 2013). However, enhancing gamma activity with transcranial magnetic stimulation (TMS) has been associated with changes in GABA levels (Nowak et al., 2017). Different outcomes from these studies could be related to distinct methods to measure GABA and to differences in the used paradigms. For instance, while Nowak et al. (2017) applied a Go/No-Go task, the aforementioned studies use simple reaction time paradigms. Besides neurotransmission, gamma oscillations also emerge as a result of network properties, such as mutual inhibition, mutual excitation and recurrent inhibition (Uhlhaas et al., 2011). These properties define models where gamma oscillations arise from locally generated excitations or inhibitions within an ensemble, or could result from increased input (Sedley and Cunningham, 2013). The current evidence highlights the importance of neurotransmission systems and network properties for the emergence of gamma oscillations. In line with a role of excitatory and inhibitory states in the normal brain functioning, unbalanced neurotransmission and alterations of oscillatory activity have been associated with neuropsychiatric and neurological disorders.

Schizophrenia is a complex neuropsychiatric disorder characterized by delusions, hallucinations, apathy and a loss of social motivation. It has been shown that patients with schizophrenia have aberrant gamma oscillations in perceptual (Uhlhaas et al., 2006) and executive (Cho et al., 2006) functions. More recently, it has been also shown that these patients exhibit motor disturbances and these alterations may involve changes in motor oscillations. Compared with healthy individuals, early onset schizophrenic patients show a reduction of gamma oscillatory responses in M1 and the cerebellum in a finger movement paradigm (Wilson et al., 2011). These findings suggest that alterations of gamma activity span distinct cognitive domains and may reflect a general dysfunction of gamma oscillatory activity. This notion converges with the idea of an altered neurotransmission balance in schizophrenia

(Gaspar et al., 2009). Autism spectrum disorder (ASD) is a neurodevelopmental disorder characterized by deficits in social communication, restricted interests, and repetitive behaviors (American Psychiatric Association, 2013). In a series of studies with MEG and a game-like motor task An et al. (2018, 2021) investigated the neural responses associated with finger presses in normal and ASD children. These studies showed a decrease in gamma peak activity (An et al., 2018) and decreased beta-gamma ipsilateral PAC activity (An et al., 2021) in M1 of ASD children in comparison with healthy participants. Once again, these modulations of motor gamma oscillations may reflect an unbalance in the excitatory and inhibitory neurotransmission systems. Indeed, these neurotransmissions anomalies have been hypothesized to be a core aspect of ASD (Rubenstein and Merzenich, 2003). Lastly, Parkinson's disease is a neurodegenerative disorder leading to tremor, bradykinesia, stiffness, and difficulty with walking, balance, and coordination. PD is characterized by a loss of nigrostriatal dopaminergic neurons and thus dopamine replacement has been used as a pharmacological treatment (Lang and Lozano, 1998a). A more recent therapy is based on deep brain stimulation (DBS) of the STN and has been shown to decrease motor disturbances in PD (Lang and Lozano, 1998b). Interestingly, improvement of motor functions seems to be related to a decrease of beta oscillations (which are over activated in the disorder) and an increase of motor gamma oscillations (Brown et al., 2001). These findings highlight the complementary roles of beta and gamma oscillations during health and a how an alteration of the oscillatory activities might underlie pathological conditions.

Gamma oscillations are modulated by alterations in the normal functioning of the nervous system that compromise the production of movements. A stroke occurs when the blood supply to a brain region is impeded (possibly by an obstruction or a rupture of the vasculature). Stroke can lead to sensory deficits problems to produce or understand speech and is associated with impairments in motor functions. It has been shown that patients with stroke have decreased brain-muscle gamma coupling than healthy controls during the realization of movements (Fang et al., 2009; Rossiter et al., 2013). Interestingly, peripheral nerve stimulation therapy in patients with stroke shows decreased M1 gamma activity and these effects are related to an improvement in motor symptoms (Wilson et al., 2011). These effects are said to result from a more efficient local processing in the motor cortex after therapy. Cerebral palsy (CP) is a common motor disability in children that affects the ability to move and maintain the balance of the body. Studies show an aberrant gamma response in children with CP compared with healthy individuals, either with an increase (Guo et al., 2012; Short et al., 2020) or decrease (Kurz et al., 2014; Hoffman et al., 2019) of gamma activity. The reported gamma abnormalities in CP span distinct gamma ranges, with intervals between 38 and 56 Hz to interval between 70 and 200 Hz. However, studies differ in disorder specificities, brain recording methods, as well as in using distinct experimental manipulations, including walking (Short et al., 2020), simple bodily responses (Kurz et al., 2014), response inhibition (Hoffman et al., 2019) and electric stimulation (Guo et al., 2012). Overall, these cases support the view that abnormalities in motor gamma oscillations are implicated in neuropsychiatric and neurological disorders.

FUTURE DIRECTIONS

I have tried to summarize our current understanding of the role of motor gamma oscillations in the control of movements. There are many aspects of motor gamma oscillations that need to be clarified in future studies. Still, the current evidence suggests that motor gamma oscillations accomplish a role beyond mere movement initiation. Local and long-range motor gamma activity serves as a core mechanism to organize distinct forms of motor processing. The impact of gamma motor oscillations probably relies on the extensive network of brain regions that include cortical, subcortical and spinal cord activity (indirectly reflected in the EMG measurement). The current challenge is to put all this in one or several models of motor control. There are many open questions and future directions that need to be taken. Research in this domain will be enriched with longitudinal studies, which will allow us to have a better grasp of the development trajectory of motor oscillations and whether and how these changes are contingent with changes in motor milestones in human beings (see Stephen et al., 2021 for an example). This endeavor will be only approachable within an interdisciplinary and collaborative framework. This is also important because "movement" data can take a variety of forms. A better interpretation of these data requires the collaboration between scientists from distinct disciplines. In this same line, it is necessary to replicate findings for a set of well-defined experimental paradigms with well-characterized movements. There are many types of movements reported in the literature. Both simple and complex types of movements should be systematically studied and can become potential markers for the use in clinical as well as more fundamental research on motor control. Gamma oscillations involve a wide range of brain regions beyond being confined to cortical regions. The versatility of gamma oscillations in the organization of movements is probably because of this wide network activity. A multi-scale approach to understanding brain connections that occur at distinct levels of processing will be essential. It is important to understand the specific contribution of each node in the sensorimotor gamma network, including primary sensorimotor cortices, as well the PMC, the SMA, and other regions, such as the parietal cortex and the PFC. The contribution of subcortical regions such as the thalamus, cerebellum, and basal ganglia needs to be integrated in the often cortico-centered models of motor control. There is robust evidence that the basal ganglia exerts an important influence on the organization of simple and complex responses. It is necessary to understand how the activity of the PFC influences downstream motor pathways. The ability to prepare actions and predict the consequences of our actions rely in a complex organization likely commanded by the PFC. In this line, new ideas about cognition and brain function suggest that the brain could operate as a Bayesian inference machine (Friston, 2010). In this framework, predictions derived from the internal models are confronted with new sensory information from the environment (a sensory

consequence of a movement) and the comparisons between these signals update an internal model which subsequently can alter motor activity. Recent evidence suggest that neural oscillations associated with motor control in the beta (Tan et al., 2016) and gamma (Wiesman et al., 2021) range are sensitive to certainty of events in the external environment.

There are methodological aspects that deserve more attention. We need to better understand the role of different frequency gamma ranges and why there is such a frequency diversity in which gamma responses are found. One of the difficulties in the study of motor, and more generally, gamma oscillations, is its frequency variability. Using a diversity of neural metrics, future studies should aim to categorize the diversity of frequency ranges of gamma responses found in distinct brain areas. It is possible that the integrative properties endowed by gamma oscillations operate at distinct spatio-temporo-spectral dimensions. In addition, future studies will need to expand analyses methods to consider the complexity and non-linear nature of local and long-range brain activity. The inherent complexity of brain networks has not been fully explored, and can make up another dimension in which motor parameters are coded. We need also consider the social context in which movements are carried out. In models of motor control, it is necessary to incorporate the fact that the actions are carried out in a social context associated with social inter-actions. These interactions shape our experience and our perceptual processes. Future lines of research should be concerned with evaluating actions in both laboratory contexts and real contexts outside the laboratory. Flexible and adaptive behavior is grounded in our ability to perform actions, and this adaptive behavior varies according to the contingencies we encounter in our social daily life. Lastly, gamma oscillations are not the only oscillations involved in motor processing. In fact, it is intriguing that so many distinct oscillatory responses contribute to the processing of motor information in the nervous system. This attests to the importance of actions for human beings. The science of movements has become one of the most exciting challenges in neuroscience emerging these recent years. The evolution of this field has benefited from recent advances in experimental psychology, cognitive neuroscience and computational modeling, which altogether have dramatically sped up our understanding of movements. A collective effort will be instrumental to fully understand the role of motor gamma oscillations in human movements.

AUTHOR CONTRIBUTIONS

The author made substantial contributions to the discussion of content, wrote the article and edited the manuscript before submission.

FUNDING

JU was supported by ANID/CONICYT FONDECYT Iniciación 11190673 and by the Programa de Investigación Asociativa (PIA) en Ciencias Cognitivas (RU-158-2019), Research Center on Cognitive Sciences (CICC), Faculty of Psychology, Universidad de Talca, Chile.

SUPPLEMENTARY MATERIAL

The Supplementary Material for this article can be found online at: https://www.frontiersin.org/articles/10.3389/fnhum.2021.787157/full#supplementary-material

Supplementary Table 1 | Summary of the studies associated with motor gamma oscillations included in the revision. The table depicts the reference; the method; the task or type of movement executed; the number of participants (N); the body part concerned with the movement; the frequency band range; the area or electrodes where gamma activity was found and the main findings. In "N" two or more numbers indicate distinct set of participants. In clinical studies "p" stand for patient and "h" stand for healthy participant. In "Frequency" the numbers indicate the frequency range (minimum maximum). Two or more numbers indicate distinct frequency ranges reported. STN, subthalamic nucleus; GP, globus pallidus; PAC, phase-amplitude coupling; IFG, inferior frontal gyrus; PFC, prefrontal cortex; M1, primary motor cortex; PMC, premotor cortex; SMA, supplementary motor cortex; DBS, deep brain stimulation; EEG, electroencephalography; MEG, magnetoencephalography; ECoG, electrocorticography; CMC, cortico-muscular coherence.

REFERENCES

Alegre, M., Alonso-Frech, F., Rodríguez-Oroz, M. C., Guridi, J., Zamarbide, I., Valencia, M., et al. (2005). Movement-related changes in oscillatory activity in the human subthalamic nucleus: Ipsilateral vs. contralateral movements. *Eur. J. Neurosci.* 22, 2315–2324. doi: 10.1111/j.1460-9568.2005.04409.x

Alegre, M., Lopez-Azcarate, J., Obeso, I., Wilkinson, L., Rodriguez-Oroz, M. C., Valencia, M., et al. (2013). The subthalamic nucleus is involved in successful inhibition in the stop-signal task: a local field potential study in Parkinson's disease. *Exp. Neurol.* 239, 1–12. doi: 10.1016/j.expneurol.2012.08.027

Alhourani, A., Korzeniewska, A., Wozny, T. A., Lipski, W. J., Kondylis, E. D., Ghuman, A. S., et al. (2020). Subthalamic nucleus activity influences sensory and motor cortex during force transduction. *Cereb. Cortex* 30, 2615–2626. doi: 10.1093/cercor/bhz264

American Psychiatric Association (2013). in *Diagnostic and Statistical Manual of Mental Disorders: DSM-5*, 5th Edn, ed. American Psychiatric Association Arlington, TX: American Psychiatric Association.

An, K., Ikeda, T., Hasegawa, C., Yoshimura, Y., Tanaka, S., Saito, D. N., et al. (2021). Aberrant brain oscillatory coupling from the primary motor cortex in children with autism spectrum disorders. *NeuroImage* 29:102560. doi: 10.1016/j.nicl.2021.102560

An, K., Ikeda, T., Yoshimura, Y., Hasegawa, C., Saito, D. N., Kumazaki, H., et al. (2018). Altered gamma oscillations during motor control in children with autism spectrum disorder. *J. Neurosci.* 38, 7878–7886. doi: 10.1523/JNEUROSCI.1229-18.2018

Ball, T., Demandt, E., Mutschler, I., Neitzel, E., Mehring, C., Vogt, K., et al. (2008). Movement related activity in the high gamma range of the human EEG. *NeuroImage* 41, 302–310. doi: 10.1016/j.neuroimage.2008.02.032

Ball, T., Schulze-Bonhage, A., Aertsen, A., and Mehring, C. (2009). Differential representation of arm movement direction in relation to cortical anatomy and function. *J. Neural Eng.* 6:016006. doi: 10.1088/1741-2560/6/1/016006

Bari, A., and Robbins, T. W. (2013). Inhibition and impulsivity: behavioral and neural basis of response control. *Prog. Neurobiol.* 108, 44–79. doi: 10.1016/j.pneurobio.2013.06.005

Botvinick, M., Braver, T. S., Barch, D. M., Carter, C. S., and Cohen, J. D. (2001). Conflict monitoring and cognitive control. *Psychol. Rev.* 108, 624–652. doi: 10.1037/0033-295X.108.3.624

Bramson, B., den Ouden, H. E., Toni, I., and Roelofs, K. (2020). Improving emotional-action control by targeting long-range phase-amplitude neuronal coupling. *ELife* 9:e59600. doi: 10.7554/eLife.59600

Bramson, B., Jensen, O., Toni, I., and Roelofs, K. (2018). Cortical oscillatory mechanisms supporting the control of human social–emotional actions. *J. Neurosci.* 38, 5739–5749. doi: 10.1523/JNEUROSCI.3382-17.2018

Bressler, S. L. (1990). The gamma wave: a cortical information carrier? *Trends Neurosci.* 13, 161–162. doi: 10.1016/0166-2236(90)90039-D

Brovelli, A., Lachaux, J.-P., Kahane, P., and Boussaoud, D. (2005). High gamma frequency oscillatory activity dissociates attention from intention in the human premotor cortex. *NeuroImage* 28, 154–164. doi: 10.1016/j.neuroimage.2005.05.045

Brown, P., Oliviero, A., Mazzone, P., Insola, A., Tonali, P., and Di Lazzaro, V. (2001). Dopamine dependency of oscillations between subthalamic nucleus and pallidum in Parkinson's disease. *J. Neurosci.* 21, 1033–1038. doi: 10.1523/JNEUROSCI.21-03-01033.2001

Brown, P., Salenius, S., Rothwell, J. C., and Hari, R. (1998). Cortical correlate of the piper rhythm in humans. *J. Neurophysiol.* 80, 2911–2917. doi: 10.1152/jn.1998.80.6.2911

Brucke, C., Huebl, J., Schonecker, T., Neumann, W.-J., Yarrow, K., Kupsch, A., et al. (2012). Scaling of movement is related to Pallidal oscillations in patients with dystonia. *J. Neurosci.* 32, 1008–1019. doi: 10.1523/JNEUROSCI.3860-11.2012

Brücke, C., Kempf, F., Kupsch, A., Schneider, G.-H., Krauss, J. K., Aziz, T., et al. (2008). Movement-related synchronization of gamma activity is lateralized in patients with dystonia: movement-related gamma in dystonia. *Eur. J. Neurosci.* 27, 2322–2329. doi: 10.1111/j.1460-9568.2008.06203.x

Butorina, A., Prokofyev, A., Nazarova, M., Litvak, V., and Stroganova, T. (2014). The mirror illusion induces high gamma oscillations in the absence of movement. *NeuroImage* 103, 181–191. doi: 10.1016/j.neuroimage.2014.09.024

Buzsaki, G. (2006). *Rhythms of the Brain*. New York, NY: Oxford University Press.

Buzsáki, G., and Wang, X.-J. (2012). Mechanisms of gamma oscillations. *Annu. Rev. Neurosci.* 35, 203–225. doi: 10.1146/annurev-neuro-062111-150444

Canolty, R. T., and Knight, R. T. (2010). The functional role of cross-frequency coupling. *Trends Cogn. Sci.* 14, 506–515. doi: 10.1016/j.tics.2010.09.001

Carlén, M., Meletis, K., Siegle, J. H., Cardin, J. A., Futai, K., Vierling-Claassen, D., et al. (2012). A critical role for NMDA receptors in parvalbumin interneurons for gamma rhythm induction and behavior. *Mol. Psychiatry* 17, 537–548. doi: 10.1038/mp.2011.31

Catalan, M. (1998). The functional neuroanatomy of simple and complex sequential finger movements: a PET study. *Brain* 121, 253–264. doi: 10.1093/brain/121.2.253

Chakravarthy, V. S. (2013). "A model of the neural substrates for exploratory dynamics in basal ganglia," in *Progress in Brain Research*, Vol. 202, eds V. S. C. Pammi and N. Srinivasan (Amsterdam: Elsevier), 389–414. doi: 10.1016/B978-0-444-62604-2.00020-4

Chen, W., de Hemptinne, C., Miller, A. M., Leibbrand, M., Little, S. J., Lim, D. A., et al. (2020). Prefrontal-Subthalamic hyperdirect pathway modulates movement inhibition in humans. *Neuron* 106, 579–588.e3. doi: 10.1016/j.neuron.2020.02.012

Cheyne, D. (2013). MEG studies of sensorimotor rhythms: a review. *Exp. Neurol.* 245, 27–39. doi: 10.1016/j.expneurol.2012.08.030

Cheyne, D., and Ferrari, P. (2013). MEG studies of motor cortex gamma oscillations: evidence for a gamma "fingerprint" in the brain? *Front. Hum. Neurosci.* 7:575. doi: 10.3389/fnhum.2013.00575

Cheyne, D., Bells, S., Ferrari, P., Gaetz, W., and Bostan, A. C. (2008). Self-paced movements induce high-frequency gamma oscillations in primary motor cortex. *NeuroImage* 42, 332–342. doi: 10.1016/j.neuroimage.2008.04.178

Cheyne, D., Jobst, C., Tesan, G., Crain, S., and Johnson, B. (2014). Movement-related neuromagnetic fields in preschool age children: movement-Related Brain Activity in Preschool Children. *Hum. Brain Mapp.* 35, 4858–4875. doi: 10.1002/hbm.22518

Cho, R. Y., Konecky, R. O., and Carter, C. S. (2006). Impairments in frontal cortical synchrony and cognitive control in schizophrenia. *Proc. Natl. Acad. Sci. U.S.A.* 103, 19878–19883. doi: 10.1073/pnas.0609440103

Cochin, S., Barthelemy, C., Roux, S., and Martineau, J. (1999). Observation and execution of movement: similarities demonstrated by quantified electroencephalography. *Eur. J. Neurosci.* 11, 1839–1842. doi: 10.1046/j.1460-9568.1999.00598.x

Cohen, M. X., Ridderinkhof, K. R., Haupt, S., Elger, C. E., and Fell, J. (2008). Medial frontal cortex and response conflict: evidence from human intracranial EEG and medial frontal cortex lesion. *Brain Res.* 1238, 127–142. doi: 10.1016/j.brainres.2008.07.114

Conway, B. A., Halliday, D. M., Farmer, S. F., Shahani, U., Maas, P., Weir, A. I., et al. (1995). Synchronization between motor cortex and spinal motoneuronal pool during the performance of a maintained motor task in man. *J. Physiol.* 489, 917–924. doi: 10.1113/jphysiol.1995.sp021104

Crone, N. E., Miglioretti, D. L., Gordon, B., Sieracki, J. M., Wilson, M. T., Uematsu, S., et al. (1998). Functional mapping of human sensorimotor cortex with electrocorticographic spectral analysis. I. Alpha and beta event-related desynchronization. *Brain A J. Neurol.* 121(Pt. 12), 2271–2299. doi: 10.1093/brain/121.12.2271

Dalal, S. S., Guggisberg, A. G., Edwards, E., Sekihara, K., Findlay, A. M., Canolty, R. T., et al. (2007). "Spatial localization of cortical time-frequency dynamics," in *Proceedings of the 2007 29th Annual International Conference of the IEEE Engineering in Medicine and Biology Society*, (Piscataway, NJ: IEEE), 4941–4944. doi: 10.1109/IEMBS.2007.4353449

Darvas, F., Scherer, R., Ojemann, J. G., Rao, R. P., Miller, K. J., and Sorensen, L. B. (2010). High gamma mapping using EEG. *NeuroImage* 49, 930–938. doi: 10.1016/j.neuroimage.2009.08.041

Diciotti, S., Gavazzi, C., Della Nave, R., Boni, E., Ginestroni, A., Paoli, L., et al. (2007). Self-paced frequency of a simple motor task and brain activation. *NeuroImage* 38, 402–412. doi: 10.1016/j.neuroimage.2007.07.045

Djalovski, A., Dumas, G., Kinreich, S., and Feldman, R. (2021). Human attachments shape interbrain synchrony toward efficient performance of social goals. *NeuroImage* 226:117600. doi: 10.1016/j.neuroimage.2020.117600

Donoghue, J. P., and Sanes, J. N. (1994). Motor areas of the cerebral cortex. *J. Clin. Neurophysiol.* 11, 382–396.

Dürschmid, S., Quandt, F., Krämer, U. M., Hinrichs, H., Heinze, H.-J., Schulz, R., et al. (2014). Oscillatory dynamics track motor performance improvement in human cortex. *PLoS One* 9:e89576. doi: 10.1371/journal.pone.0089576

Engel, A. K., and Fries, P. (2010). Beta-band oscillations—Signalling the status quo? *Curr. Opin. Neurobiol.* 20, 156–165. doi: 10.1016/j.conb.2010.02.015

Eriksen, B. A., and Eriksen, C. W. (1974). Effects of noise letters upon the identification of a target letter in a nonsearch task. *Percept. Psychophys.* 16, 143–149. doi: 10.3758/BF03203267

Fang, Y., Daly, J. J., Sun, J., Hvorat, K., Fredrickson, E., Pundik, S., et al. (2009). Functional corticomuscular connection during reaching is weakened following stroke. *Clin. Neurophysiol.* 120, 994–1002. doi: 10.1016/j.clinph.2009.02.173

Fischer, P., Lipski, W. J., Neumann, W.-J., Turner, R. S., Fries, P., Brown, P., et al. (2020). Movement-related coupling of human subthalamic nucleus spikes to cortical gamma. *ELife* 9:e51956. doi: 10.7554/eLife.51956

Fischer, P., Pogosyan, A., Herz, D. M., Cheeran, B., Green, A. L., Fitzgerald, J., et al. (2017). Subthalamic nucleus gamma activity increases not only during movement but also during movement inhibition. *ELife* 6:e23947. doi: 10.7554/eLife.23947

Fries, P. (2005). A mechanism for cognitive dynamics: neuronal communication through neuronal coherence. *Trends Cogn. Sci.* 9, 474–480. doi: 10.1016/j.tics.2005.08.011

Friston, K. (2010). The free-energy principle: a unified brain theory? *Nat. Rev. Neurosci.* 11, 127–138. doi: 10.1038/nrn2787

Fuchs, E. C., Doheny, H., Faulkner, H., Caputi, A., Traub, R. D., Bibbig, A., et al. (2001). Genetically altered AMPA-type glutamate receptor kinetics in interneurons disrupt long-range synchrony of gamma oscillation. *Proc. Natl. Acad. Sci. U.S.A.* 98, 3571–3576. doi: 10.1073/pnas.051631898

Gaetz, W., Edgar, J. C., Wang, D. J., and Roberts, T. P. L. (2011). Relating MEG measured motor cortical oscillations to resting γ-Aminobutyric acid (GABA) concentration. *NeuroImage* 55, 616–621. doi: 10.1016/j.neuroimage.2010.12.077

Gaetz, W., Liu, C., Zhu, H., Bloy, L., and Roberts, T. P. L. (2013). Evidence for a motor gamma-band network governing response interference. *NeuroImage* 74, 245–253. doi: 10.1016/j.neuroimage.2013.02.013

Gaetz, W., MacDonald, M., Cheyne, D., and Snead, O. C. (2010). Neuromagnetic imaging of movement-related cortical oscillations in children and adults: age predicts post-movement beta rebound. *NeuroImage* 51, 792–807. doi: 10.1016/j.neuroimage.2010.01.077

Gaspar, P. A., Bustamante, M. L., Silva, H., and Aboitiz, F. (2009). Molecular mechanisms underlying glutamatergic dysfunction in schizophrenia: therapeutic implications. *J. Neurochem.* 111, 891–900. doi: 10.1111/j.1471-4159.2009.06325.x

Georgopoulos, A. P., Caminiti, R., Kalaska, J. F., and Massey, J. T. (1983). "Spatial coding of movement: a hypothesis concerning the coding of movement direction by motor cortical populations," in *Neural Coding of Motor Performance*, Vol. 7, eds J. Massion, J. Paillard, W. Schultz, and M. Wiesendanger (Berlin: Springer), 327–336. doi: 10.1007/978-3-642-68915-4_34

Georgopoulos, A. P., Kalaska, J., Caminiti, R., and Massey, J. (1982). On the relations between the direction of two-dimensional arm movements and cell discharge in primate motor cortex. *J. Neurosci.* 2, 1527–1537. doi: 10.1523/JNEUROSCI.02-11-01527.1982

Gerloff, C. (1998). Functional coupling and regional activation of human cortical motor areas during simple, internally paced and externally paced finger movements. *Brain* 121, 1513–1531. doi: 10.1093/brain/121.8.1513

Gray, C. M., and Singer, W. (1989). Stimulus-specific neuronal oscillations in orientation columns of cat visual cortex. *Proc. Natl. Acad. Sci. U.S.A.* 86, 1698–1702. doi: 10.1073/pnas.86.5.1698

Grent-'t-Jong, T., Oostenveld, R., Jensen, O., Medendorp, W. P., and Praamstra, P. (2013). Oscillatory dynamics of response competition in human sensorimotor cortex. *NeuroImage* 83, 27–34. doi: 10.1016/j.neuroimage.2013.06.051

Gross, J., Pollok, B., Dirks, M., Timmermann, L., Butz, M., and Schnitzler, A. (2005). Task-dependent oscillations during unimanual and bimanual movements in the human primary motor cortex and SMA studied with magnetoencephalography. *NeuroImage* 26, 91–98. doi: 10.1016/j.neuroimage.2005.01.025

Grosse-Wentrup, M., Schölkopf, B., and Hill, J. (2011). Causal influence of gamma oscillations on the sensorimotor rhythm. *NeuroImage* 56, 837–842. doi: 10.1016/j.neuroimage.2010.04.265

Gulbinaite, R., van Rijn, H., and Cohen, M. X. (2014). Fronto-parietal network oscillations reveal relationship between working memory capacity and cognitive control. *Front. Hum. Neurosci.* 8:761. doi: 10.3389/fnhum.2014.00761

Guo, X., Xiang, J., Mun-Bryce, S., Bryce, M., Huang, S., Huo, X., et al. (2012). Aberrant high-gamma oscillations in the somatosensory cortex of children with cerebral palsy: a meg study. *Brain Dev.* 34, 576–583. doi: 10.1016/j.braindev.2011.09.012

Gwin, J. T., and Ferris, D. P. (2012). Beta- and gamma-range human lower limb corticomuscular coherence. *Front. Hum. Neurosci.* 6:258. doi: 10.3389/fnhum.2012.00258

Gwin, J. T., Gramann, K., Makeig, S., and Ferris, D. P. (2011). Electrocortical activity is coupled to gait cycle phase during treadmill walking. *NeuroImage* 54, 1289–1296. doi: 10.1016/j.neuroimage.2010.08.066

Hagbarth, K.-E., Jessop, J., Eklund, G., and Wallin, E. U. (1983). The Piper rhythm-a phenomenon related to muscle resonance characteristics? *Acta Physiol. Scand.* 117, 263–271. doi: 10.1111/j.1748-1716.1983.tb07205.x

Haggard, P. (2008). Human volition: towards a neuroscience of will. *Nat. Rev. Neurosci.* 9, 934–946. doi: 10.1038/nrn2497

Hall, S. D., Stanford, I. M., Yamawaki, N., McAllister, C. J., Rönnqvist, K. C., Woodhall, G. L., et al. (2011). The role of GABAergic modulation in motor function related neuronal network activity. *NeuroImage* 56, 1506–1510. doi: 10.1016/j.neuroimage.2011.02.025

Halliday, D. M., Conway, B. A., Farmer, S. F., and Rosenberg, J. R. (1998). Using electroencephalography to study functional coupling between cortical activity and electromyograms during voluntary contractions in humans. *Neurosci. Lett.* 241, 5–8. doi: 10.1016/S0304-3940(97)00964-6

Hari, R., and Puce, A. (2017). *MEG-EEG Primer*. New York, NY: Oxford University Press.

Hari, R., and Salenius, S. (1999). Rhythmical corticomotor communication. *Neuroreport* 10, R1–R10.

Heinrichs-Graham, E., Hoburg, J. M., and Wilson, T. W. (2018). The peak frequency of motor-related gamma oscillations is modulated by response competition. *NeuroImage* 165, 27–34. doi: 10.1016/j.neuroimage.2017.09.059

Herz, D. M., Christensen, M. S., Reck, C., Florin, E., Barbe, M. T., Stahlhut, C., et al. (2012). Task-specific modulation of effective connectivity during two simple unimanual motor tasks: a 122-channel EEG study. *NeuroImage* 59, 3187–3193. doi: 10.1016/j.neuroimage.2011.11.042

Hoffman, R. M., Wilson, T. W., and Kurz, M. J. (2019). Hand motor actions of children with cerebral palsy are associated with abnormal sensorimotor cortical oscillations. *Neurorehabil. Neural Repair* 33, 1018–1028. doi: 10.1177/1545968319883880

Huo, X., Wang, Y., Kotecha, R., Kirtman, E. G., Fujiwara, H., Hemasilpin, N., et al. (2011). High gamma oscillations of sensorimotor cortex during unilateral movement in the developing brain: a MEG study. *Brain Topogr.* 23, 375–384. doi: 10.1007/s10548-010-0151-0

Isabella, S., Ferrari, P., Jobst, C., Cheyne, J. A., and Cheyne, D. (2015). Complementary roles of cortical oscillations in automatic and controlled processing during rapid serial tasks. *NeuroImage* 118, 268–281. doi: 10.1016/j.neuroimage.2015.05.081

Jeannerod, M. (2006). *Motor Cognition: What Actions Tell the Self*. Oxford: Oxford University Press.

Jensen, O., Kaiser, J., and Lachaux, J.-P. (2007). Human gamma-frequency oscillations associated with attention and memory. *Trends Neurosci.* 30, 317–324. doi: 10.1016/j.tins.2007.05.001

Joundi, R. A., Brittain, J.-S., Green, A. L., Aziz, T. Z., Brown, P., and Jenkinson, N. (2012). Oscillatory activity in the subthalamic nucleus during arm reaching in Parkinson's disease. *Exp. Neurol.* 236, 319–326. doi: 10.1016/j.expneurol.2012.05.013

Jurkiewicz, M. T., Gaetz, W. C., Bostan, A. C., and Cheyne, D. (2006). Post-movement beta rebound is generated in motor cortex: evidence from neuromagnetic recordings. *NeuroImage* 32, 1281–1289. doi: 10.1016/j.neuroimage.2006.06.005

Kilner, J. M., Baker, S. N., Salenius, S., Jousmäki, V., Hari, R., and Lemon, R. N. (1999). Task-dependent modulation of 15-30 Hz coherence between rectified EMGs from human hand and forearm muscles. *J. Physiol.* 516, 559–570. doi: 10.1111/j.1469-7793.1999.0559v.x

Koelewijn, T., van Schie, H. T., Bekkering, H., Oostenveld, R., and Jensen, O. (2008). Motor-cortical beta oscillations are modulated by correctness of observed action. *NeuroImage* 40, 767–775. doi: 10.1016/j.neuroimage.2007.12.018

Kurz, M. J., Becker, K. M., Heinrichs-Graham, E., and Wilson, T. W. (2014). Neurophysiological abnormalities in the sensorimotor cortices during the motor planning and movement execution stages of children with cerebral palsy. *Dev. Med. Child Neurol.* 56, 1072–1077. doi: 10.1111/dmcn.12513

Lang, A. E., and Lozano, A. M. (1998a). Parkinson's disease. *N. Engl. J. Med.* 339, 1044–1053. doi: 10.1056/NEJM199810083391506

Lang, A. E., and Lozano, A. M. (1998b). Parkinson's disease. *N. Engl. J. Med.* 339, 1130–1143. doi: 10.1056/NEJM199810153391607

Leisman, G., Moustafa, A., and Shafir, T. (2016). Thinking, walking, talking: integratory motor and cognitive brain function. *Front. Public Health* 4:94. doi: 10.3389/fpubh.2016.00094

Leuthardt, E. C., Schalk, G., Wolpaw, J. R., Ojemann, J. G., and Moran, D. W. (2004). A brain–computer interface using electrocorticographic signals in humans. *J. Neural Eng.* 1, 63–71. doi: 10.1088/1741-2560/1/2/001

Li, S., Fan, M., Yu, H., and Gao, L. (2020). Gamma frequency band shift of contralateral corticomuscular synchronous oscillations with force strength for hand movement tasks. *NeuroReport* 31, 338–345. doi: 10.1097/WNR.0000000000001409

Lisman, J. E., and Jensen, O. (2013). The theta-gamma neural code. *Neuron* 77, 1002–1016. doi: 10.1016/j.neuron.2013.03.007

Lofredi, R., Neumann, W.-J., Bock, A., Horn, A., Huebl, J., Siegert, S., et al. (2018). Dopamine-dependent scaling of subthalamic gamma bursts with movement velocity in patients with Parkinson's disease. *ELife* 7:e31895. doi: 10.7554/eLife.31895

Logan, G. D., Van Zandt, T., Verbruggen, F., and Wagenmakers, E.-J. (2014). On the ability to inhibit thought and action: general and special theories of an act of control. *Psychol. Rev.* 121, 66–95. doi: 10.1037/a0035230

Lopes da Silva, F. (2013). EEG and MEG: relevance to neuroscience. *Neuron* 80, 1112–1128. doi: 10.1016/j.neuron.2013.10.017

Marsden, J. F., Werhahn, K. J., Ashby, P., Rothwell, J., Noachtar, S., and Brown, P. (2000). Organization of cortical activities related to movement in humans. *J. Neurosci.* 20, 2307–2314. doi: 10.1523/JNEUROSCI.20-06-02307.2000

Mehrkanoon, S., Breakspear, M., and Boonstra, T. W. (2014). The reorganization of corticomuscular coherence during a transition between sensorimotor states. *NeuroImage* 100, 692–702. doi: 10.1016/j.neuroimage.2014.06.050

Miller, K. J., Leuthardt, E. C., Schalk, G., Rao, R. P. N., Anderson, N. R., Moran, D. W., et al. (2007). Spectral changes in cortical surface potentials during motor movement. *J. Neurosci.* 27, 2424–2432. doi: 10.1523/JNEUROSCI.3886-06.2007

Miller, K. J., Schalk, G., Fetz, E. E., den Nijs, M., Ojemann, J. G., and Rao, R. P. N. (2010). Cortical activity during motor execution, motor imagery, and imagery-based online feedback. *Proc. Natl. Acad. Sci. U.S.A.* 107, 4430–4435. doi: 10.1073/pnas.0913697107

Mima, T., Simpkins, N., Oluwatimilehin, T., and Hallett, M. (1999). Force level modulates human cortical oscillatory activities. *Neurosci. Lett.* 275, 77–80. doi: 10.1016/S0304-3940(99)00734-X

Mima, T., Steger, J., Schulman, A. E., Gerloff, C., and Hallett, M. (2000). Electroencephalographic measurement of motor cortex control of muscle activity in humans. *Clin. Neurophysiol.* 111, 326–337. doi: 10.1016/S1388-2457(99)00229-1

Muthukumaraswamy, S. D. (2010). Functional properties of human primary motor cortex gamma oscillations. *J. Neurophysiol.* 104, 2873–2885. doi: 10.1152/jn.00607.2010

Muthukumaraswamy, S. D. (2011). Temporal dynamics of primary motor cortex gamma oscillation amplitude and piper corticomuscular coherence changes during motor control. *Exp. Brain Res.* 212, 623–633. doi: 10.1007/s00221-011-2775-z

Muthukumaraswamy, S. D., Johnson, B. W., and McNair, N. A. (2004). Mu rhythm modulation during observation of an object-directed grasp. *Brain Res. Cogn. Brain Res.* 19, 195–201. doi: 10.1016/j.cogbrainres.2003.12.001

Muthukumaraswamy, S. D., Myers, J. F. M., Wilson, S. J., Nutt, D. J., Lingford-Hughes, A., Singh, K. D., et al. (2013). The effects of elevated endogenous GABA levels on movement-related network oscillations. *NeuroImage* 66, 36–41. doi: 10.1016/j.neuroimage.2012.10.054

Nambu, A., Tokuno, H., and Takada, M. (2002). Functional significance of the cortico–subthalamo–pallidal 'hyperdirect' pathway. *Neurosci. Res.* 43, 111–117. doi: 10.1016/S0168-0102(02)00027-5

Neuper, C., Wörtz, M., and Pfurtscheller, G. (2006). "ERD/ERS patterns reflecting sensorimotor activation and deactivation," in *Progress in Brain Research*, Vol. 159, eds C. Neuper and W. Klimesch (Amsterdam: Elsevier), 211–222. doi: 10.1016/S0079-6123(06)59014-4

Nigbur, R., Ivanova, G., and Stürmer, B. (2011). Theta power as a marker for cognitive interference. *Clin. Neurophysiol.* 122, 2185–2194. doi: 10.1016/j.clinph.2011.03.030

Nowak, M., Hinson, E., van Ede, F., Pogosyan, A., Guerra, A., Quinn, A., et al. (2017). Driving human motor cortical oscillations leads to behaviorally relevant changes in local GABA A inhibition: a tACS-TMS study. *J. Neurosci.* 37, 4481–4492. doi: 10.1523/JNEUROSCI.0098-17.2017

Nunez, P. L., and Srinivasan, R. (2006). *Electric Fields of the Brain: The Neurophysics of EEG*, 2nd Edn. New York, NY: Oxford University Press.

Oliveira, A. S., Andersen, C. Ø, Grimstrup, C. B., Pretzmann, F., Mortensen, N. H., Castro, M. N., et al. (2019). A software for testing and training visuo-motor coordination for upper limb control. *J. Neurosci. Methods* 324:108310. doi: 10.1016/j.jneumeth.2019.06.002

Omlor, W., Patino, L., Hepp-Reymond, M.-C., and Kristeva, R. (2007). Gamma-range corticomuscular coherence during dynamic force output. *NeuroImage* 34, 1191–1198. doi: 10.1016/j.neuroimage.2006.10.018

Pfurtscheller, G. (1981). Central beta rhythm during sensorimotor activities in man. *Electroencephalogr. Clin. Neurophysiol.* 51, 253–264. doi: 10.1016/0013-4694(81)90139-5

Pfurtscheller, G., and Neuper, C. (1992). Simultaneous EEG 10 Hz desynchronization and 40 Hz synchronization during finger movements. *NeuroReport* 3, 1057–1060. doi: 10.1097/00001756-199212000-00006

Pfurtscheller, G., Graimann, B., Huggins, J. E., Levine, S. P., and Schuh, L. A. (2003). Spatiotemporal patterns of beta desynchronization and gamma synchronization in corticographic data during self-paced movement. *Clin. Neurophysiol.* 114, 1226–1236. doi: 10.1016/S1388-2457(03)00067-1

Pfurtscheller, G., Neuper, C., and Kalcher, J. (1993). 40-Hz oscillations during motor behavior in man. *Neurosci. Lett.* 164, 179–182. doi: 10.1016/0304-3940(93)90886-P

Pohja, M., and Salenius, S. (2003). Modulation of cortex-muscle oscillatory interaction by ischaemia-induced deafferentation. *NeuroReport* 14, 321–324. doi: 10.1097/00001756-200303030-00005

Poppele, R., and Bosco, G. (2003). Sophisticated spinal contributions to motor control. *Trends Neurosci.* 26, 269–276. doi: 10.1016/S0166-2236(03)00073-0

Prinz, W. (1997). Perception and action planning. *Eur. J. Cogn. Psychol.* 9, 129–154. doi: 10.1080/713752551

Ray, N. J., Brittain, J.-S., Holland, P., Joundi, R. A., Stein, J. F., Aziz, T. Z., et al. (2012). The role of the subthalamic nucleus in response inhibition: evidence from local field potential recordings in the human subthalamic nucleus. *NeuroImage* 60, 271–278. doi: 10.1016/j.neuroimage.2011.12.035

Rosenbaum, D. A. (2010). *Human Motor Control*, 2nd Edn. Burlington, MA: Elsevier Inc.

Rossi, A., Grasso-Cladera, A., Luarte, N., Riillo, A., and Parada, F. J. (2019). The brain/body-in-the-world system is cognitive science's study object for the twenty-first century / El sistema cerebro/cuerpo-en-el-mundo es el objeto de estudio de la ciencia cognitiva en el siglo XXI. *Estudios Psicol.* 40, 363–395. doi: 10.1080/02109395.2019.1596704

Rossiter, H. E., Eaves, C., Davis, E., Boudrias, M.-H., Park, C., Farmer, S., et al. (2013). Changes in the location of cortico-muscular coherence following stroke. *NeuroImage* 2, 50–55. doi: 10.1016/j.nicl.2012.11.002

Roux, F., Wibral, M., Mohr, H. M., Singer, W., and Uhlhaas, P. J. (2012). Gamma-Band activity in human prefrontal cortex codes for the number of relevant items maintained in working memory. *J. Neurosci.* 32, 12411–12420. doi: 10.1523/JNEUROSCI.0421-12.2012

Rubenstein, J. L. R., and Merzenich, M. M. (2003). Model of autism: increased ratio of excitation/inhibition in key neural systems: model of autism. *Genes Brain Behav.* 2, 255–267. doi: 10.1034/j.1601-183X.2003.00037.x

Salenius, S., Portin, K., Kajola, M., Salmelin, R., and Hari, R. (1997). Cortical control of human motoneuron firing during isometric contraction. *J. Neurophysiol.* 77, 3401–3405. doi: 10.1152/jn.1997.77.6.3401

Salenius, S., Salmelin, R., Neuper, C., Pfurtscheller, G., and Hari, R. (1996). Human cortical 40 Hz rhythm is closely related to EMG rhythmicity. *Neurosci. Lett.* 213, 75–78. doi: 10.1016/0304-3940(96)12796-8

Salmelin, R., and Hari, R. (1994). Spatiotemporal characteristics of sensorimotor neuromagnetic rhythms related to thumb movement. *Neuroscience* 60, 537–550. doi: 10.1016/0306-4522(94)90263-1

Schoffelen, J.-M., Oostenveld, R., and Fries, P. (2005). Neuronal coherence as a mechanism of effective corticospinal interaction. *Science* 308, 111–113. doi: 10.1126/science.1107027

Schoffelen, J.-M., Poort, J., Oostenveld, R., and Fries, P. (2011). Selective movement preparation is subserved by selective increases in corticomuscular gamma-band coherence. *J. Neurosci.* 31, 6750–6758. doi: 10.1523/JNEUROSCI.4882-10.2011

Sedley, W., and Cunningham, M. O. (2013). Do cortical gamma oscillations promote or suppress perception? An under-asked question with an over-assumed answer. *Front. Hum. Neurosci.* 7:595. doi: 10.3389/fnhum.2013.00595

Seeber, M., Scherer, R., and Müller-Putz, G. R. (2016). EEG oscillations are modulated in different behavior-related networks during rhythmic finger movements. *J. Neurosci.* 36, 11671–11681. doi: 10.1523/JNEUROSCI.1739-16.2016

Short, M. R., Damiano, D. L., Kim, Y., and Bulea, T. C. (2020). Children with unilateral cerebral palsy utilize more cortical resources for similar motor output during treadmill gait. *Front. Hum. Neurosci.* 14:36. doi: 10.3389/fnhum.2020.00036

Sohal, V. S., Zhang, F., Yizhar, O., and Deisseroth, K. (2009). Parvalbumin neurons and gamma rhythms enhance cortical circuit performance. *Nature* 459, 698–702. doi: 10.1038/nature07991

Spooner, R. K., Wiesman, A. I., Wilson, T. W., (2021). Peripheral somatosensory entrainment modulates the cross-frequency coupling of movement-related theta-gamma oscillations. *Brain Connect.* brain.2021.0003. doi: 10.1089/brain.2021.0003

Spooner, R. K., Wiesman, A. I, Proskovec, A. L., Heinrichs-Graham, E., and Wilson, T. W. (2020). Prefrontal theta modulates sensorimotor gamma networks during the reorienting of attention. *Hum. Brain Mapp.* 41, 520–529. doi: 10.1002/hbm.24819

Sporns, O. (2011). *Networks of the Brain*. Cambridge, MA: MIT Press.

Stephen, J. M., Solis, I., Janowich, J., Stern, M., Frenzel, M. R., Eastman, J. A., et al. (2021). The developmental chronnecto-genomics (Dev-CoG) study: a multimodal study on the developing brain. *NeuroImage* 225:117438. doi: 10.1016/j.neuroimage.2020.117438

Swann, N. C., Cai, W., Conner, C. R., Pieters, T. A., Claffey, M. P., George, J. S., et al. (2012). Roles for the pre-supplementary motor area and the right inferior frontal gyrus in stopping action: electrophysiological responses and functional and structural connectivity. *NeuroImage* 59, 2860–2870. doi: 10.1016/j.neuroimage.2011.09.049

Szurhaj, W., Bourriez, J.-L., Kahane, P., Chauvel, P., Mauguière, F., and Derambure, P. (2005). Intracerebral study of gamma rhythm reactivity in the sensorimotor cortex. *Eur. J. Neurosci.* 21, 1223–1235. doi: 10.1111/j.1460-9568.2005.03966.x

Tallon-Baudry, C., Bertrand, O., Delpuech, C., and Pernier, J. (1997). Oscillatory γ-Band (30–70 Hz) activity induced by a visual search task in humans. *J. Neurosci.* 17, 722–734. doi: 10.1523/JNEUROSCI.17-02-00722.1997

Tamás, G., Chirumamilla, V. C., Anwar, A. R., Raethjen, J., Deuschl, G., Groppa, S., et al. (2018). Primary sensorimotor cortex drives the common cortical network for gamma synchronization in voluntary hand movements. *Front. Hum. Neurosci.* 12:130. doi: 10.3389/fnhum.2018.00130

Tan, H., Pogosyan, A., Anzak, A., Ashkan, K., Bogdanovic, M., Green, A. L., et al. (2013). Complementary roles of different oscillatory activities in the subthalamic nucleus in coding motor effort in Parkinsonism. *Exp. Neurol.* 248, 187–195. doi: 10.1016/j.expneurol.2013.06.010

Tan, H., Wade, C., and Brown, P. (2016). Post-Movement beta activity in sensorimotor cortex indexes confidence in the estimations from internal models. *J. Neurosci.* 36, 1516–1528. doi: 10.1523/JNEUROSCI.3204-15.2016

Tecchio, F., Zappasodi, F., Porcaro, C., Barbati, G., Assenza, G., Salustri, C., et al. (2008). High-gamma band activity of primary hand cortical areas: a sensorimotor feedback efficiency index. *NeuroImage* 40, 256–264. doi: 10.1016/j.neuroimage.2007.11.038

Toba, M. N., Malkinson, T. S., Howells, H., Mackie, M. A., and Spagna, A. (2020). Same or different? A multi-method review on the relationships between processes underlying executive control. *PsyArXiv* [Preprint]. doi: 10.31234/osf.io/6zcvn

Trevarrow, M. P., Kurz, M. J., McDermott, T. J., Wiesman, A. I., Mills, M. S., Wang, Y.-P., et al. (2019). The developmental trajectory of sensorimotor cortical oscillations. *NeuroImage* 184, 455–461. doi: 10.1016/j.neuroimage.2018.09.018

Uhlhaas, P., Linden, D. E. J., Singer, W., Haenschel, C., Lindner, M., Maurer, K., et al. (2006). Dysfunctional long-range coordination of neural activity during gestalt perception in schizophrenia. *J. Neurosci.* 26, 8168–8175. doi: 10.1523/JNEUROSCI.2002-06.2006

Uhlhaas, P., Pipa, G., Neuenschwander, S., Wibral, M., and Singer, W. (2011). A new look at gamma? High- (>60 Hz) γ-band activity in cortical networks: function, mechanisms and impairment. *Prog. Biophys. Mol. Biol.* 105, 14–28. doi: 10.1016/j.pbiomolbio.2010.10.004

van Wijk, B. C. M., Beek, P. J., and Daffertshofer, A. (2012). Neural synchrony within the motor system: what have we learned so far? *Front. Hum. Neurosci.* 6:252. doi: 10.3389/fnhum.2012.00252

Varela, F., Lachaux, J.-P., Rodriguez, E., and Martinerie, J. (2001). The brainweb: phase synchronization and large-scale integration. *Nat. Rev. Neurosci.* 2, 229–239. doi: 10.1038/35067550

Varela, F., Thompson, E., and Rosch, E. (2016). *The Embodied Mind: Cognitive Science and Human Experience*, revised Edn. Cambridge, MA: MIT Press.

Wiesman, A. I., Christopher-Hayes, N. J., Eastman, J. A., Heinrichs-Graham, E., and Wilson, T. W. (2021). Response certainty during bimanual movements reduces gamma oscillations in primary motor cortex. *NeuroImage* 224:117448. doi: 10.1016/j.neuroimage.2020.117448

Wiesman, A. I., Koshy, S. M., Heinrichs-Graham, E., and Wilson, T. W. (2020). Beta and gamma oscillations index cognitive interference effects across a distributed motor network. *NeuroImage* 213:116747. doi: 10.1016/j.neuroimage.2020.116747

Wilson, T. W., Slason, E., Asherin, R., Kronberg, E., Teale, P. D., Reite, M. L., et al. (2011). Abnormal gamma and beta MEG activity during finger movements in early-onset psychosis. *Dev. Neuropsychol.* 36, 596–613. doi: 10.1080/87565641.2011.555573

Wilson, T. W., Heinrichs-Graham, E., and Becker, K. M. (2014). Circadian modulation of motor-related beta oscillatory responses. *NeuroImage* 102, 531–539. doi: 10.1016/j.neuroimage.2014.08.013

Wilson, T. W., Slason, E., Asherin, R., Kronberg, E., Reite, M. L., Teale, P. D., et al. (2010). An extended motor network generates beta and gamma oscillatory perturbations during development. *Brain Cogn.* 73, 75–84. doi: 10.1016/j.bandc.2010.03.001

Windhorst, U. (2007). Muscle proprioceptive feedback and spinal networks. *Brain Res. Bull.* 73, 155–202. doi: 10.1016/j.brainresbull.2007.03.010

Yanagisawa, T., Hirata, M., Saitoh, Y., Kishima, H., Matsushita, K., Goto, T., et al. (2012). Electrocorticographic control of a prosthetic arm in paralyzed patients. *Ann. Neurol.* 71, 353–361. doi: 10.1002/ana.22613

Zaepffel, M., Trachel, R., Kilavik, B. E., and Brochier, T. (2013). Modulations of EEG beta power during planning and execution of grasping movements. *PLoS One* 8:e60060. doi: 10.1371/journal.pone.0060060

Conflict of Interest: The author declares that the research was conducted in the absence of any commercial or financial relationships that could be construed as a potential conflict of interest.

Publisher's Note: All claims expressed in this article are solely those of the authors and do not necessarily represent those of their affiliated organizations, or those of the publisher, the editors and the reviewers. Any product that may be evaluated in this article, or claim that may be made by its manufacturer, is not guaranteed or endorsed by the publisher.

Advantages of publishing in Frontiers

OPEN ACCESS
Articles are free to read for greatest visibility and readership

FAST PUBLICATION
Around 90 days from submission to decision

HIGH QUALITY PEER-REVIEW
Rigorous, collaborative, and constructive peer-review

TRANSPARENT PEER-REVIEW
Editors and reviewers acknowledged by name on published articles

Frontiers
Avenue du Tribunal-Fédéral 34
1005 Lausanne | Switzerland

Visit us: www.frontiersin.org
Contact us: frontiersin.org/about/contact

REPRODUCIBILITY OF RESEARCH
Support open data and methods to enhance research reproducibility

DIGITAL PUBLISHING
Articles designed for optimal readership across devices

FOLLOW US
@frontiersin

IMPACT METRICS
Advanced article metrics track visibility across digital media

EXTENSIVE PROMOTION
Marketing and promotion of impactful research

LOOP RESEARCH NETWORK
Our network increases your article's readership